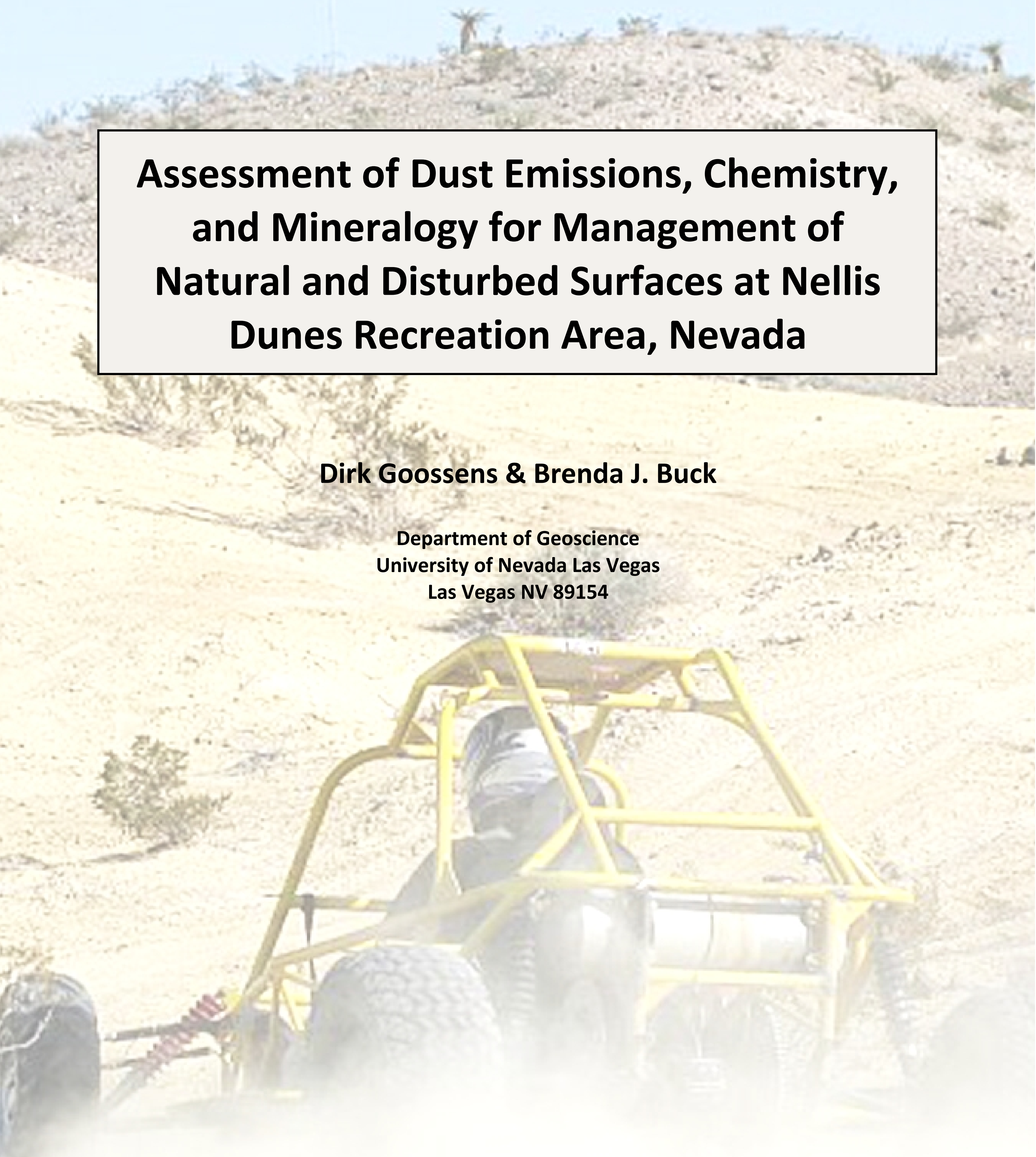

Assessment of Dust Emissions, Chemistry, and Mineralogy for Management of Natural and Disturbed Surfaces at Nellis Dunes Recreation Area, Nevada

Dirk Goossens & Brenda J. Buck

Department of Geoscience
University of Nevada Las Vegas
Las Vegas NV 89154

Final Report to Bureau of Land Management for Task Agreement Number FAA010017: Assessing Factors Contributing to Dust Emissions from Public Lands On Air Quality in Areas of Clark County, Nevada
January 2011

Cover photo:

Driving a dune buggy in the Nellis Dunes Recreation Area
(courtesy: Rhonda Fairchild)

Assessment of Dust Emissions, Chemistry, and Mineralogy for Management of Natural and Disturbed Surfaces at Nellis Dunes Recreation Area, Nevada

Dirk Goossens & Brenda J. Buck

Department of Geoscience
University of Nevada Las Vegas
Las Vegas NV 89154

Final Report to Bureau of Land Management for Task Agreement Number FAA010017: Assessing Factors Contributing to Dust Emissions from Public Lands On Air Quality in Areas of Clark County, Nevada
January 2011

Table of Contents

Chapter 1

INTRODUCTION

Brenda Buck[1] and Dirk Goossens[1]

[1]*Department of Geoscience, University of Nevada Las Vegas*

RATIONALE FOR STUDY

Like many places in the southwestern USA, poor air quality is a concern for the Las Vegas Valley in southern Nevada. The southernmost county in Nevada, Clark County, is designated as being in serious non-attainment for PM10 (Fig. 1). The Environmental Protection Agency (EPA) created a PM10 standard for air quality in 1987, and later added a PM2.5 standard as well. These standards replaced the older Total Suspended Particulate (TSP) standard.

The PM10 standard measures the concentration of airborne particles with a diameter of 10 µm or less, and was implemented because research has shown that these smaller particles can have serious health implications. The smaller the particle, the deeper it can penetrate into the lung (Plumlee et al., 2006), therefore PM2.5 (particulates less than 2.5 µm) are thought to be even more hazardous. Exposure to particulate matter is associated with an increased risk of cardiovascular and respiratory morbidity, asthma, lung cancer, inflammation and increased mortality (e.g. Dockery et al., 1993; Besancenot et al., 1997; Peters et al., 1997; Lambert et al., 1999; Donaldson et al., 2000; Ichinose et al., 2005; Griffin and Kellogg 2004; Chow et al., 2006; Laden et al., 2006; Wang et al., 2008; Hildebrandt et al., 2009; Laing et al., 2010; Soto-Martinez and Sly, 2010). These health effects are particularly strong for children, older adults and those with asthma (Sacks et al., 2010). Additional known health hazards with respect to inhaled dust are asbestosis, silicosis, mesothelioma, valley fever, meningitis, and inhalation of heavy metals that can cause cancer, hypertension, cardiovascular disease, kidney damage, diminished intellectual capacity in children and skeletal damage (e.g. Korenyi-Both et al., 1992; Jinadu 1995; Athar et al 1998; Järup, 2003; Komatsu et al., 2003; Sultan et al., 2005; Otsuki et al., 2007; Constantopoulos, 2008; Roggli et al., 2010).

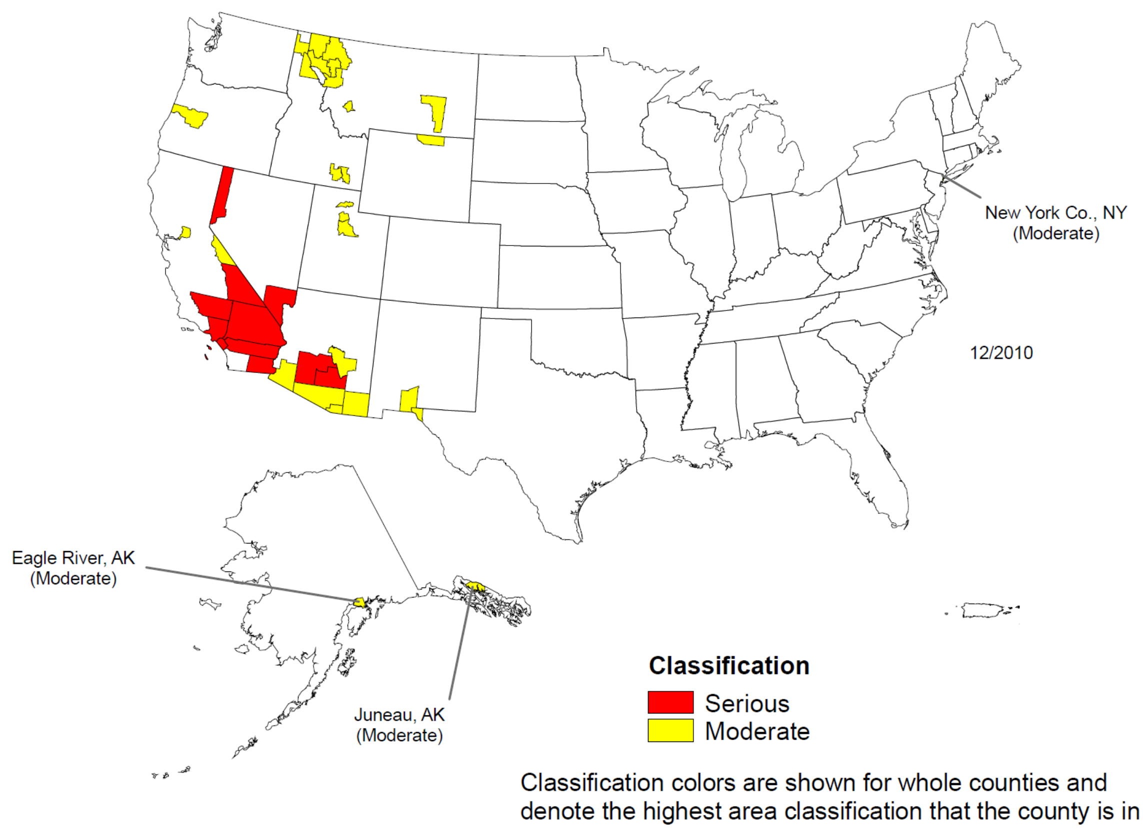

Fig. 1: Counties designated as non-attainment for PM10. Clark County, southern Nevada is in serious non-attainment. (From EPA 2010: http://www.epa.gov/oaqps001/greenbk/mappm10.html)

Nationally, the largest single source of both PM10 and PM2.5 is road dust (Fig. 2) (EPA, 2005). Because of the health concerns associated with particulate matter, and because human activities, especially those that stir up dust, are known to impact air quality, this study was designed to assess dust emissions from the Nellis Dunes Recreational Area (NDRA). The NDRA is managed by the Bureau of Land Management (BLM) and lies in the northeastern portion of the Las Vegas Valley, Clark County. The NDRA is located approximately 8 km from the margin of the conurbation Las Vegas - North Las Vegas - Henderson and is the only location in Clark County that is freely accessible to the public for off-road driving. For over 40 years, NDRA has been heavily used for ORV recreation. Off-road vehicle (ORV) driving is one of the most prevalent and fastest growing recreational activities on public lands worldwide (Cordell, 2004; Cordell et al., 2008; Outdoor World Directory, 2010). Southern Nevada is no exception – the number of off-road drivers has quadrupled in the last few years (Spivey, 2008). In 2008, the BLM estimated that the number of off-road-drivers at NDRA was over 300,000, which is over 15% of the population (Goossens and Buck, 2009). Prior to this study, the contributions of ORV activity to dust emissions were not known at this site.

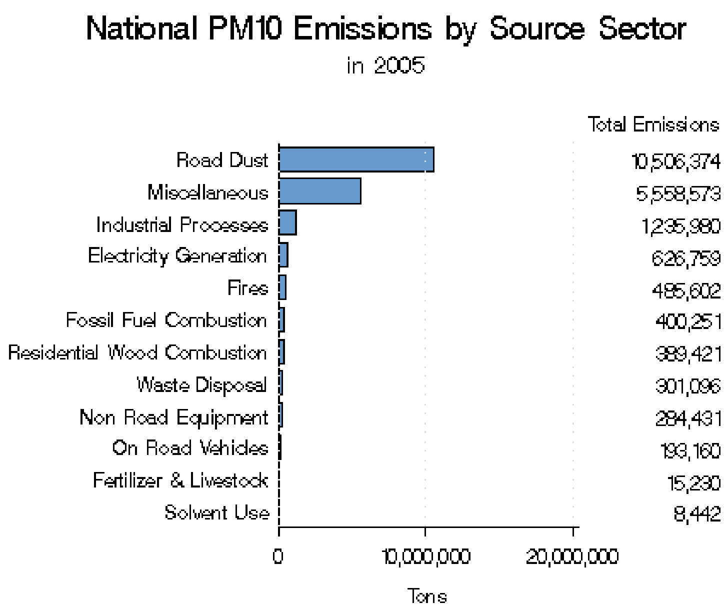

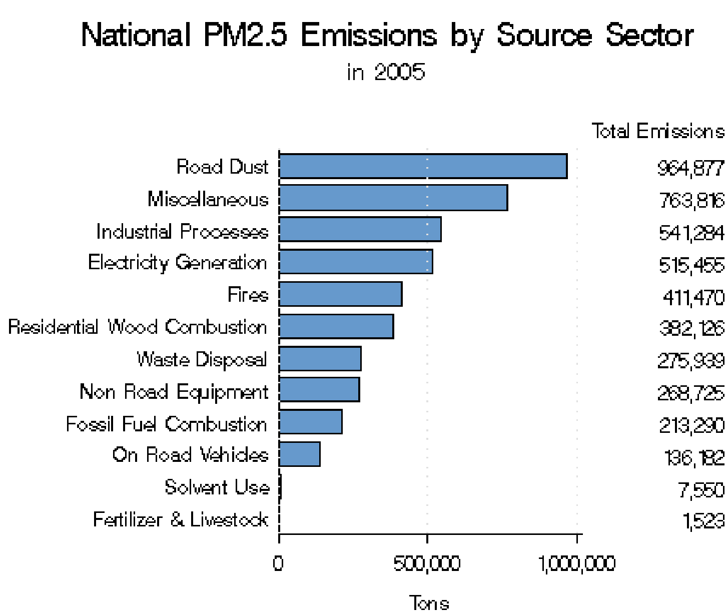

Fig. 2: National sources of PM10 and PM2.5 Emissions
(From EPA 2005:http://www.epa.gov/air/emissions/pm.htm)

Wind erosion, especially in arid regions such as southern Nevada, is a well-known mechanism for producing dust emissions (Shao, 2008). Sand particles and sand-sized aggregates of silt and clay are easily eroded by the wind and liberate substantial amounts of dust upon impact on the ground. In deserts, most dust production by wind erosion has been associated with the presence of sand-sized grains although aerodynamic emissions of dust not initiated by sand movement have been reported as well (Cole and Kerch, 1990). Prior to this study, it was known that wind erosion plays an important role at NDRA because of the presence of the active sand dunes for which the site is named. However, it was not known how much wind erosion contributes to dust emissions at the site, or what interactions, if any, occur between wind erosion and ORV activities.

With increasing use of NDRA for ORV recreational activities, increasing population growth in the Las Vegas Valley, and a need to improve air quality here and in other similar desert locations in the southwestern USA, data were needed to better understand the processes controlling dust emissions for land use management decisions. A thorough understanding of these processes requires detailed field and laboratory data collection combined with surficial maps that link processes to specific types of land surface characteristics. This research project linked aerial data (surficial maps) with dust emissions generated by ORV activities and natural wind processes, with chemical and mineralogical data, and with an *in vivo* toxicological study.

This report describes the results of this research, which includes: (1) a map of the different surfaces at NDRA and how their characteristics relate to dust emissions, (2) a study of how ORV emissions vary with vehicle type, speed, and across different surface types (3) a study of how dust emissions vary between surfaces disturbed by ORV activities and undisturbed surfaces, (4) an assessment of wind erosion and its contribution to dust emission in the Nellis Dunes area, (5) an assessment of total emissions (wind and ORV-generated), (6) an assessment of PM10 concentrations in the area, (7) characterization of the mineralogy of the different surface types as sources for dust, (8) characterization of the chemical composition of soils and dust, (9) an assessment of the arsenic content in soils and dust, (10) the results of an *in vivo* experiment conducted in mice to examine the toxicological and histopathological effects following exposure to dust samples from three surface types in the Nellis Dunes area, and (11) land management recommendations based on these data.

Each topic is presented as a separate chapter in this report. Each chapter describes the problem, explains the methodologies, discusses the results, summarizes the conclusions and provides bibliographical references. Therefore, each chapter can be read independently although references to other chapters may appear. An overall summary of the main results of the entire project is given in section 2 of Chapter 12 (Land Management Recommendations for the Nellis Dunes Recreation Area), pp. 234-249 in this report.

Portions of this research have been published in peer-reviewed scientific journals and are available upon request. Contact Brenda Buck (buckb@unlv.nevada.edu) or Dirk Goossens (Dirk.Goossens@ees.kuleuven.be) for reprints.

References

Akhter, M.S., Madany, I.M., 1993. Heavy metals in street and house dust in Bahrain. Water Air Soil Pollution 66, 111-119.

Besancenot, J.P., Boko, M., Oke, P.C., 1997. Weather conditions and cerebrospinal meningitis in Benin (Gulf of Guinea, West Africa). European Journal of Epidemiology 13, 807-815.

Chow, J., Watson, J., Mauderly, J., Costa, D., Wyzga, R., Vedal, S., Hidy, G., Altshuler, S., Marrack, D., Heuss, J., Wolff, G., Pope, C., Dockery, D., 2006. Health effects of fine particulate air pollution: lines that connect. Journal of the Air and Waste Management Association 56, 1368-1380.

Cole, C.F., Kerch, R.L., 1990. Air quality measurement. In: Kennedy, B.A. (ed): Surface Mining (2nd edition). Society for Mining, Metallurgy, and Exploration, Inc., Baltimore, pp. 841-859.

Constantopoulos, S., 2008, Environmental mesothelioma associated with tremolite asbestos: Lessons from the experiences of Turkey, Greece, Corsica, New Caldonia and Cyprus. Regulatory Toxicology and Pharmacology 52, S110-S115.

Cordell, H. K., 2004. Outdoor recreation for 21st Century America. Venture Publishing Inc., State College, PA.

Cordell, H.K., Betz, C.J., Green, G.T., Stephens, B., 2008. Off-Highway Vehicle Recreation in the United States and its Regions and States: A National Report from the National Survey on Recreation and the Environment (NSRE). USDA Forest Service's Southern Research Station, Internet Research Report Series, http://www.fs.fed.us/recreation/programs/ohv/IrisRec1rpt.pdf.

Dockery, D.W., Pope, C.A., Xu, X., Spengler, J.D., Ware, J.H., Fay, M.E., Ferris, B.G. Jr., Speizer, F.E., 1993. An association between air pollution and mortality in six U.S. cities. The New England Journal of Medicine 329, 1753-1759. http://www.nejm.org/toc/nejm/329/24/.

Donaldson, K., Gilmour, M., MacNee, W.. 2000. Asthma and PM10. Respiratory Research 1, 12-15.

EPA, 2005. National Summary of Particulate Matter Emissions. http://www.epa.gov/air/emissions/pm.htm.

EPA, 2010. Counties designated nonattainment for PM10. http://www.epa.gov/oaqps001/greenbk/mappm10.html.

Goossens, D., Buck, B., 2009. Dust dynamics in off-road vehicle trails: measurements on 16 arid soil types, Nevada, USA. Journal of Environmental Management 90, 3458-3469.

Griffin, D.W., Kellogg, C.A., 2004. Dust storms and their impact on ocean and human health: Dust in Earth’s atmosphere. EcoHealth 1, 284-295.

Hildebrandt, K., Ruckerl, R., Koenig, W., Schneider, A., Pitz, M., Heinrich, J., Marder, V., Frampton, M., Oberdorster, G., Wichmann, H., Peters, A., 2009. Short-term effects of air pollution: a panel study of blood markers in patients with chronic pulmonary disease, Particle and Fibre Toxicology 6, 25:1-13. doi:10.1186/1743-8977-6-25

Ichinose, T., Nishikawa, M., Takano, H., Sera, N., Sadakane, K., Mori, I., Yanagisawa, R., Odae, T., Tamura, H., Hiyoshi, K., Quan, H., Tomura, S., Shibamoto, T., 2005. Pulmonary toxicity induced by intratracheal instillation of Asian yellow dust (Kosa) in mice. Environmental Toxicology and Pharmacology 20, 48–56.

Järup, L., 2003. Impact of environmental pollution on heath: balancing risk. British Medical Bulletin 68, 167-182.

Jinadu, B.A., 1995. Valley Fever Task Force Report on the Control of Coccidioides imitis. Kern County Health Department, Bakersfield, CA.

Komatsu, K., Vaz, V., McRill, C., Colman, T., Comrie, A., Sigel, K., Clark, T., Phelan, M., Hajjeh, R., Park, B., 2003. Increase in coccidioidomycosis – Arizona, 1998-2001. Journal of the American Medical Association 289, 1500-1502.

Korenyi-Both,A.L., Korenyi-Both, A.L., Molnar, A.C., Fidelus-Gort, R., 1992. Al Eskan disease/ Desert Storm pneumonitis. Military Medicine 157, 452-462.

Laden, F., Schwartz, J., Speizer, F., Dockery, D., 2006. Reduction in fine particulate air pollution and mortality: extended follow-up of the Harvard six cities study. American Journal of Respiratory and Critical Care Medicine 173, 667-672.

Laing, S., Wang, G., Briazova, T., Zhang, C., Wang, A., Zheng, Z., Gow, A., Chen, A., Rajagopalan, S., Chen, L., Sun, Q., Zhang, K., 2010. Airborne particulate matter selectively activates endoplasmic reticulum stress response in the lung and liver tissues. Am. J. Physiol. Cell Physiol. 299, C736-C749.

Lambert, A.L., Dong, W., Winsett, D.W., Selgrade, M.K., Gilmour, M.I., 1999. Residual oil fly ash exposure enhances allergic sensitization to house dust mite. Toxicology and Applied Pharmacology 158, 269-277.

Otsuki, T., Maeda, M., Murakami, S., Hayashi, H., Miura, Y., Kusaka, M., Nakano, T., Fukuoka, K., Kishimoto, T., Hyodoh, F., Ueki, A., Nishimura, Y., 2007. Immunological effects of silica and asbestos. Cellular and Molecular Immunology 4, 261-268.

Peters, A., Wichmann, H., Tuch, T., Heinrich, J., Heyder, J., 1997. Respiratory effects are associated with the number of ultrafine particles. American Journal of Respiratory and Critical Care Medicine 155, 1376-1383.

Plumlee, G., Morman, S., Ziegler, T., 2006. The toxicological geochemistry of earth materials: an overview of processes and the interdisciplinary methods used to understand them. Reviews in Mineralogy & Geochemistry 64, 5-57.

Roggli, V., Gibbs, A., Attanoos, R., Churg, A., Popper, H., Cagle, P., Corrin, B., Franks, T., Galateau-Salle, F., Galvin, J., Hasleton, P., Henderson, D., Honma, K., 2010. Pathology of Asbestosis – an update of the diagnostic criteria. Archives of Pathology and Laboratory Medicine 134, 462-480.

Sacks, J., Stanek, L., Luben, T., Johns, D., Buckley, B., Brown, J., Ross, M., 2010. Particulate matter induced health effects: who's susceptible? Environmental Health Perspectives, doi: 10.1289/ehp.1002255.

Shao, Y., 2008. Physics and Modelling of Wind Erosion (2nd Ed.). Springer Science + Business Media B.V., Dordrecht.

Soto-Martinez, M., and Sly, P., 2010. Review Series: What goes around, comes around: childhood influences on later lung health? Relationship between environmental exposures in children and adult lung disease: The case for outdoor exposures. Chronic Respiratory Disease 7, 173-186.

Spivey, S., 2008. Off-road fans, critics face off. Las Vegas Review-Journal, Monday, March 17, 2008, 10B.

Sultan, B., Labadi, K., Guegan, J.F., Janicot, S., 2005. Climate drives the meningitis epidemics onset in West Africa. PLoS Med 2, 43-49.

Wang, K., You, D., Balakrishna, S., Ripple, M., Ahlert, T., Fahmy, B., Becnel1, D., Daly, M., Subra, W., McElduff, J.S., Lomax, L.G., Troxclair, D., Cormier, S.A., 2008. Sediment from hurricane Katrina: potential to produce pulmonary dysfunction in mice. International Journal of Clinical and Experimental Medicine 1, 130-144.

Chapter 2

PHYSICAL SETTINGS OF THE NELLIS DUNES RECREATION AREA

Brett McLaurin[1], Dirk Goossens[2] and Brenda Buck[2]

[1]*Department of Geography and Geosciences, Bloomsburg University of Pennsylvania*
[2]*Department of Geoscience, University of Nevada Las Vegas*

1. Location

The Nellis Dunes Recreation Area (NDRA) is located about 8 km from the northeastern margin of the conurbation Las Vegas - North Las Vegas - Henderson, in the northeastern portion of the Las Vegas Valley referred to as the Nellis Basin (Beard et al., 2007) (Fig. 1). It lies west of the Gale Hills at the southern end of the Dry Lake Range and has a more or less triangular shape with N-S, W-E and SW-NE sides of 8.0, 7.8 and 9.0 km respectively, and a small additional rectangle 2.4 km x 1.6 km in the SE. It encompasses an area of approximately 37 km^2.

2. Physical settings: an overview

2.1 Topography

The Las Vegas Valley is located in the Great Basin region of the Basin and Range physiographic province of the USA. It is an intermountain valley, surrounded by generally N-S-trending mountain ranges between 450 and 2100 m above the valley floor in the N and E, and up to 3000 m above the valley floor in the west. Nellis Dunes Recreation Area is located on the eastern side of the valley, in between the Sheep Range

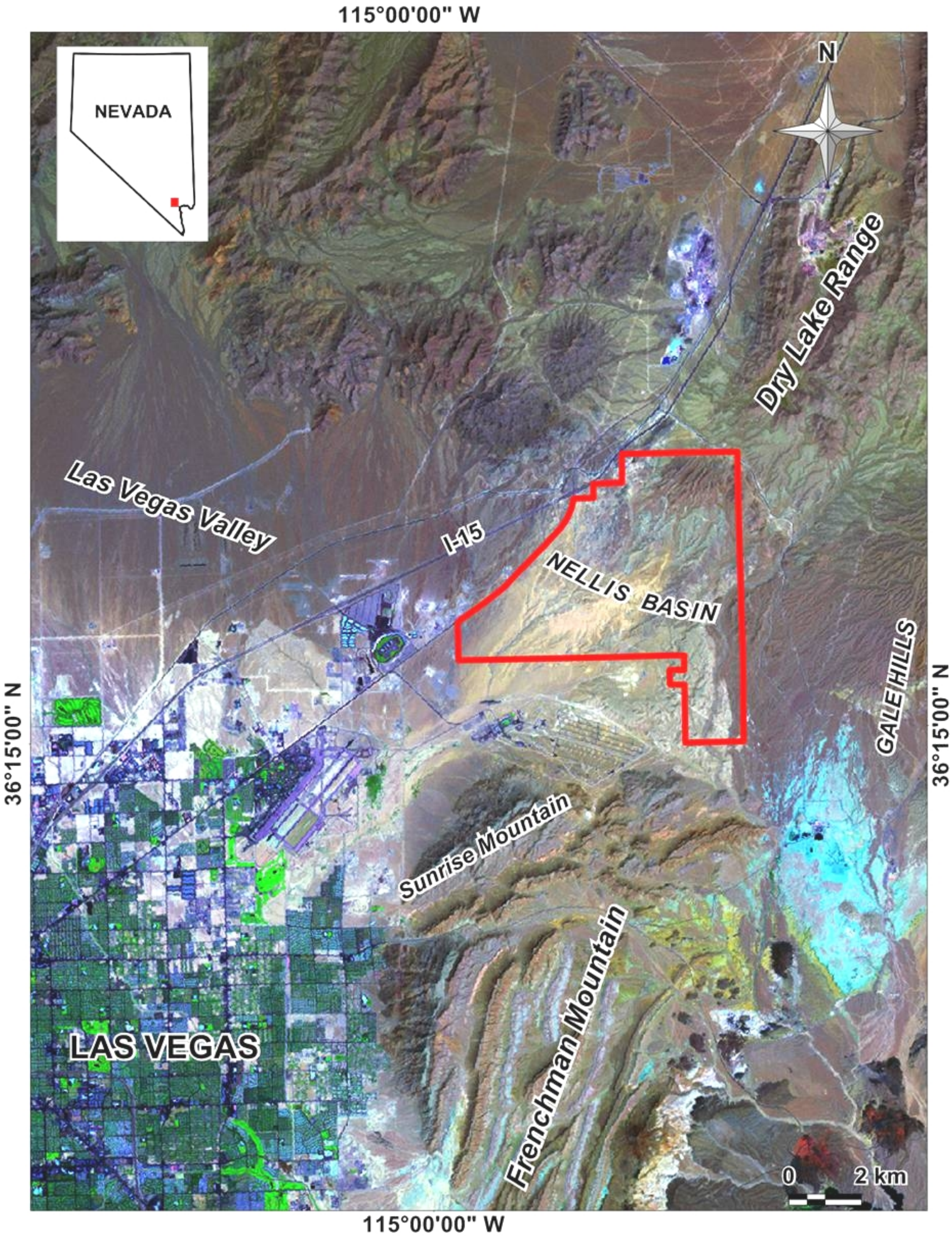

Fig. 1: Landsat band combination 7, 4, 1 showing the location of the study area relative to geographic features in the northeastern part of the Las Vegas Valley. The Nellis Dunes Recreation Area is outlined in red and occupies the Nellis Basin.

(to the N) and the Sunrise and Frenchmen Mountains (to the S), on a surface generally tilting from the NE to the SW. A detailed topographic map of the area is shown in Fig. 2. The southwestern and southeastern parts of the area are generally flat, tilting slightly to the SW. The central part shows a more complex topography, with various SW-NE-oriented valleys separated by elongated ridges and (especially in the NW) plateaus. The incision of these valleys is more prominent in the south (25-35 m) than in the north (usually about 15-20 m). In the northeastern corner the area becomes slightly mountainous, with several SW-NE ridges separating narrow valleys up to 50 m deep (Fig. 2). These ridges culminate at about 60-80 m above the surrounding landscape. Their altitude is around 850 m a.s.l., whereas the lowermost parts of Nellis Dunes Recreation Area (SW and SE corners) are situated at about 605 m a.s.l.

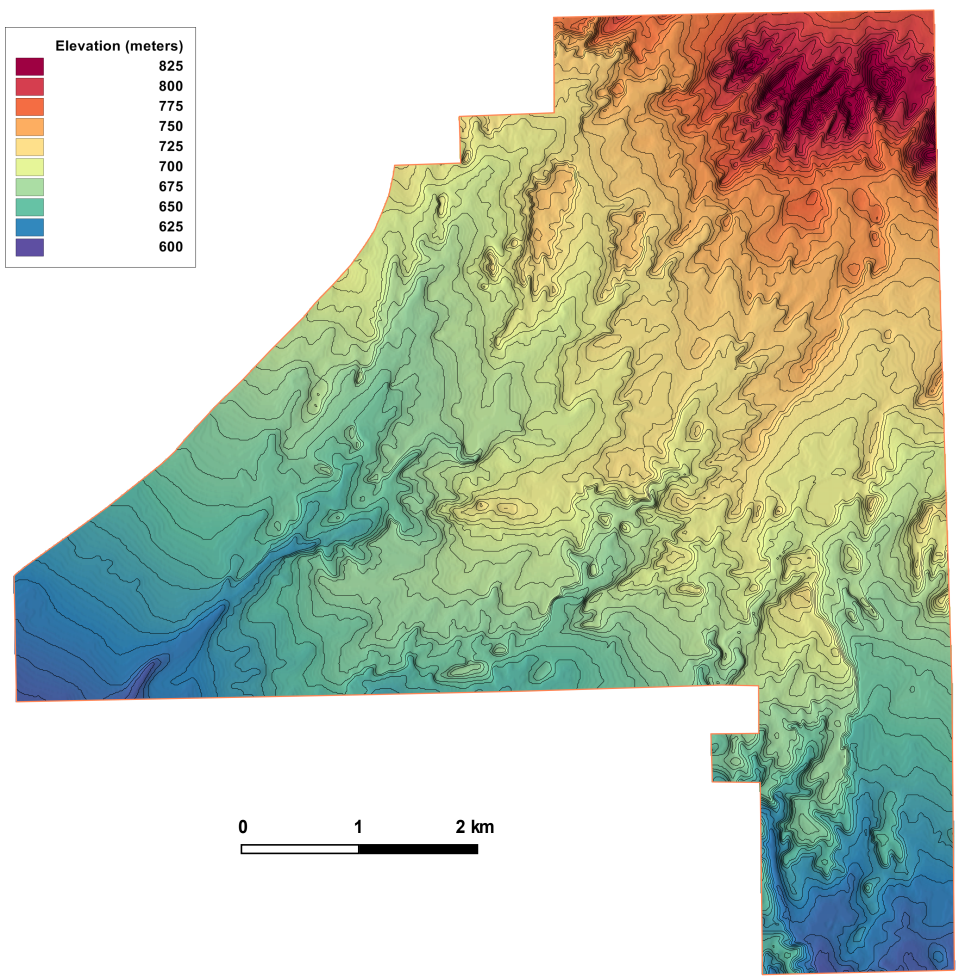

Fig. 2: Topographic map of the Nellis Dunes Recreation Area.

2.2 Geology

Nellis Dunes Recreation Area is mainly composed of incised fan remnants and exposed late Tertiary and Quaternary sediments (Fig. 3). The oldest rock units in the NDRA occur in the mountains in the northeast. They belong to the faulted and folded Ordovician Pogonip Formation, Eureka Quartzite, and Ely Springs Dolomite (Beard et al., 2007). The

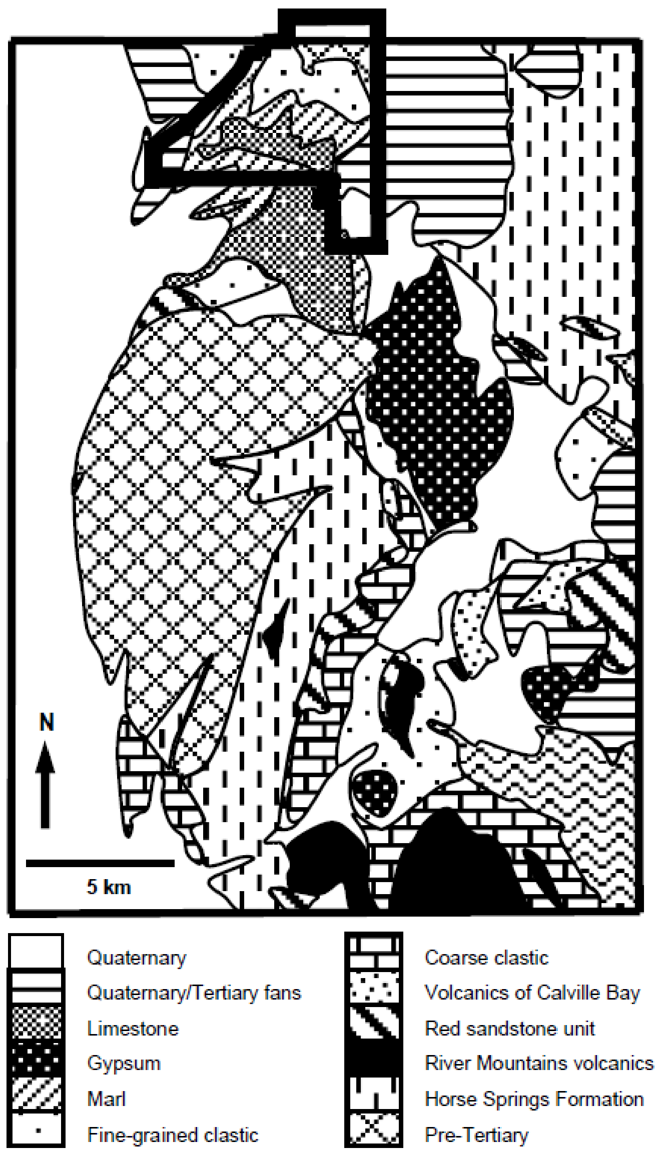

Fig. 3: Simplified geologic map of the area east of Las Vegas. NDRA is indicated by the black contour in the north. (Modified from Castor and Faulds, 2001)

largest block of exposed bedrock, representing the highest elevations, belongs to the Permian Bird Spring Formation. Overlying the Paleozoic carbonates are Neogene units (10-15 Ma) assigned to the Muddy Creek Formation (Beard et al., 2007). They consist of 2-50 m thick limestone that overlies, and is partially interbedded with, a marl sequence as much as 10 m thick. The marl locally contains rock fragments of limestone, and thin gypsite layers (Castor and Faulds, 2001). A fine-grained sandy sequence underlies the limestone and marl. In the western areas, east of the I-15 interstate highway, Muddy Creek lithologies include conglomerate, sandstone, shale, and gypsum. Quaternary to late Tertiary alluvial fan remnants and inset fans are found throughout the field area. In the northern portion of the NDRA these remnants with associated resistant petrocalcic horizons cap isolated mesas. The center of the southern portion of the NDRA is characterized by an extended zone of dune sands, which cover the Tertiary deposits. Although much of the sand is generally only a few dm thick, many highly active reversing dunes (oriented NW-SE) are present. These ridges can be up to 250 m long and are separated by areas of thin sand or silty-rocky subsoil. The belt with sand dunes covers 9% of the NDRA.

2.3 Soils

Soil development is negligible in the areas of bedrock exposure (these include the badlands of exposed Muddy Creek Formation) and active sand dunes. In these regions the surficial characteristics are controlled by the underlying geology or dune sand characteristics. In the remaining areas (primarily the fan remnants), the soils are characterized by thin (0-10 cm), platy, alkaline, A and Av (vesicular) horizons containing low amounts of organic matter. Vesicular A (Av) horizons are almost always associated with desert pavements. Well-developed soils occur primarily in the southeast and southwestern portions of the field area. They contain pedogenic accumulations of calcium carbonate at depth (~15 to >100 cm), forming calcic and petrocalcic horizons. In many areas (especially in the western portion of the NDRA) the surface horizons are eroded exposing the calcic or petrocalcic horizons at the surface. In these areas, much of the surface gravels can be composed of broken fragments of the petrocalcic horizons. Pedogenic gypsum and other salt minerals are negligible or absent. Soils in the study area are classified as Typic Haplocalcids, Calcic Petrocalcids and Typic Torriorthents.

2.4 Climate

Nellis Dunes Recreation Area is located in the northeastern part of the Mojave Desert and is thus characterized by an arid climate. Summers are hot and dry, with temperatures over 40 °C, whereas winters are mild, with an average daily maximum in January around

13.5 °C. Average annual temperature is 19.5 °C (Lazaro et al., 2004). Precipitation is low, partly because of the rain shadow created by the Sierra Nevada Range and the Spring Mountains west of Las Vegas, which protect the area from large western synoptic systems (BLM, 2004). Average annual precipitation is 105 mm, but may vary substantially between years. Monthly average precipitation ranges from 2 mm in June to 14 mm in February. Scattered thunderstorms typically occur at the end of July and the beginning of August.

Average annual wind speed (at 10 m standard height) at Nellis Air Force Base, which borders to the south of the NDRA, is 3.3 m s^{-1}, and average annual gust speed, 11.0 m s^{-1} (Goossens and Buck, 2011). Gusts can be up to 25 m s^{-1}.

More details are shown in Fig. 4. The figure displays data on wind speed recorded during the wind erosion measurements phase of the project (December 2007 - December 2008). Data refer to a height of 20 m and were measured from a wind tower erected in the southwest corner of the NDRA. Wind speed was highest in April, decreased systematically until December, and then stayed more or less constant until March. This pattern applies to both the day-time (8:00 - 20:00) and night-time (20:00 - 8:00) winds. Winds were stronger during the day hours, and the difference between day and night remained more or less constant between January and August but decreased considerably from September to December. There were nearly no differences in monthly average wind speed between day and night in November and December. In March 2008 daily wind speeds were abnormally low.

Data on wind direction are displayed in Fig. 5. There is a distinct bi-modal regime: in the late spring through early autumn, winds blow mainly from the S and SW whereas in the late autumn through early spring they blow opposite, predominantly from the NE-E. However, they can blow from any direction at any time.

The bi-modal wind regime with two nearly opposing wind directions is reflected by the NW-SE oriented reversing dunes in the NDRA, which are oriented perpendicular to the two dominant wind directions.

3. Surface units prone to dust emission

The aim of the project was to study dust emissions caused by natural processes (wind erosion) and human activities (of-road vehicular activity or ORV) in the Nellis Dunes Recreation area. Besides meteorological and human factors the occurrence and intensity of the emissions is almost exclusively determined by the type and characteristics of the surfaces on which emission takes place. Defining, mapping and analysis of the different types of surfaces that occur in the NDRA is thus the first necessary step in studying dust

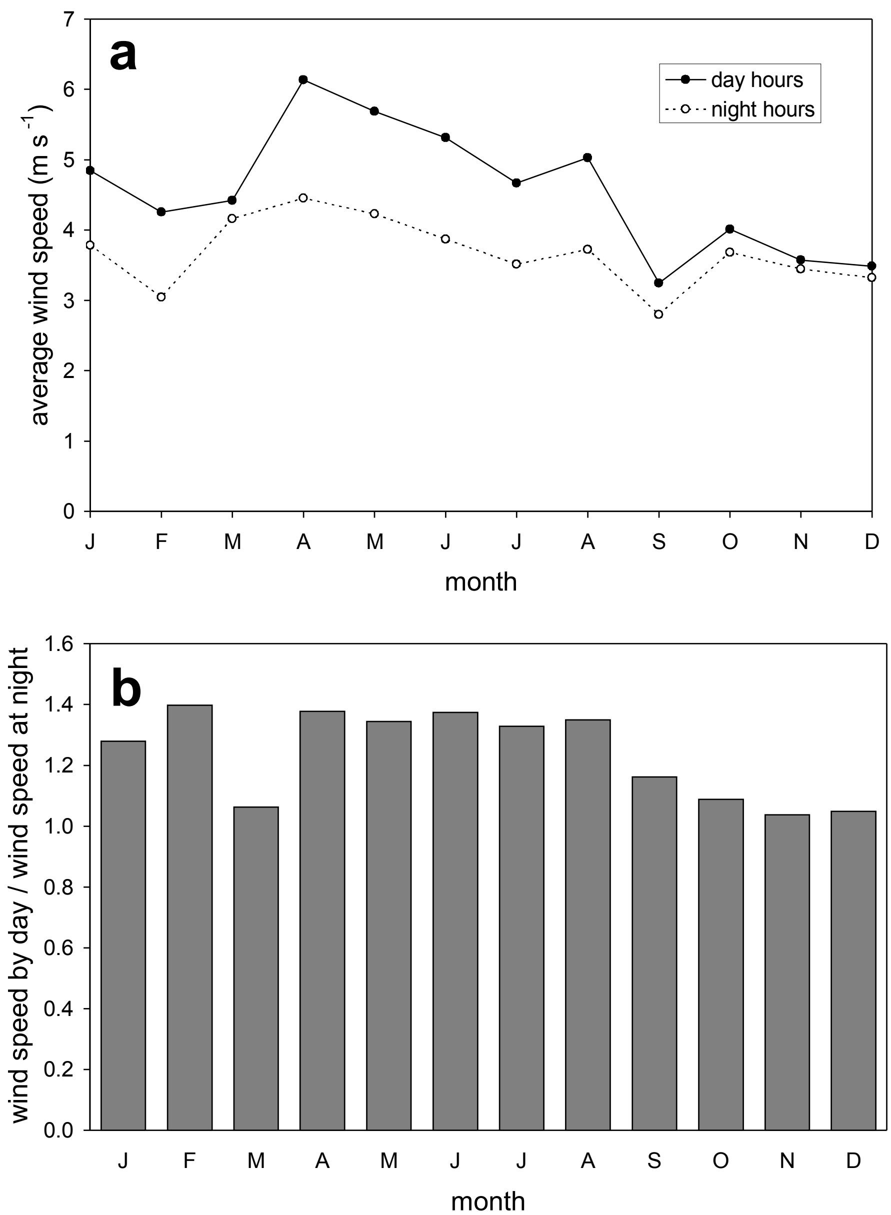

Fig. 4: Wind speed regime at NDRA. (a) average wind speed (at 20 m); (b) ratio of wind speed by day to wind speed at night.

emissions in the Nellis Dunes area. This section describes the criteria used to select the surface units, lists and describes the 17 surface units selected, and provides a detailed map of the NDRA displaying the occurrence of the surface units in the study area. A map with the ORV trails is also presented.

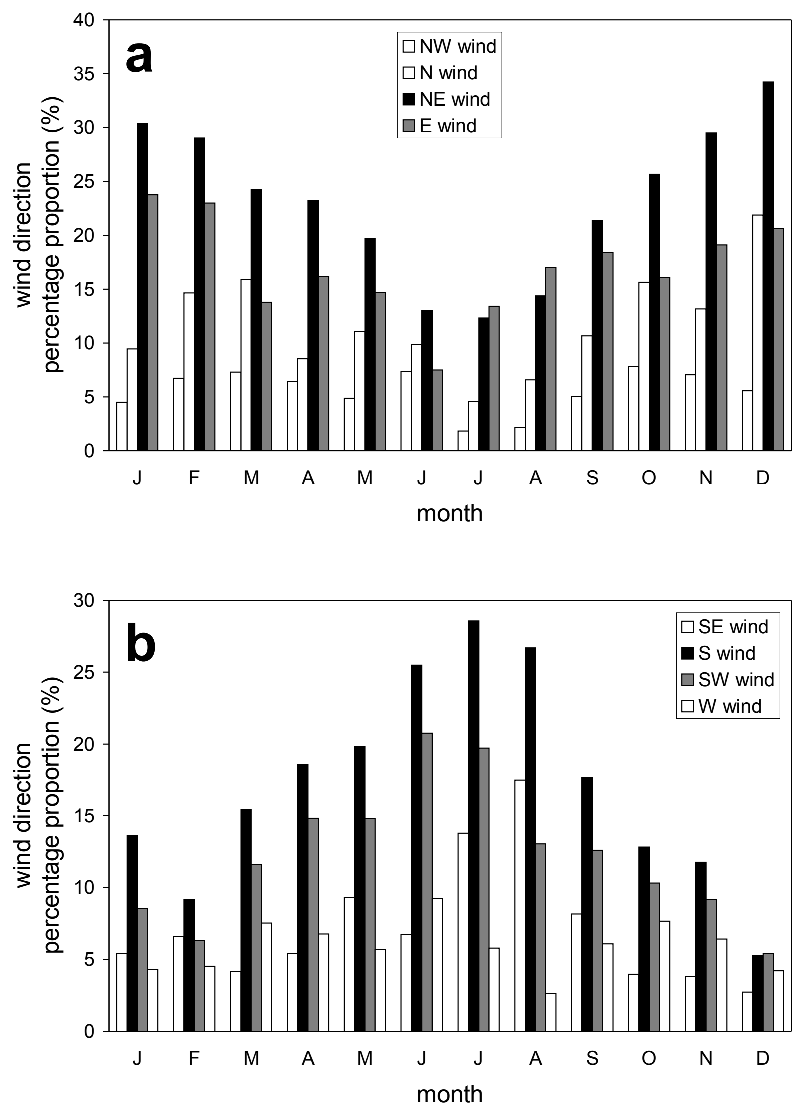

Fig. 5: Bi-seasonal regime of wind direction at NDRA. (a) N-NE sector; (b) S-SW sector. Percentages are based on 24-h data.

3.1 Criteria

The identification of the surface units is primarily based on their potential to emit dust. Therefore, dust emission units do not necessarily need to correspond with geologic, geomorphic, or pedologic units, although direct or indirect relationships with such units usually exist. The type of surface, combined with the composition of the subsoil, usually determines the vulnerability of a unit to emit dust. The criteria for selecting emission units are thus mainly based on the following observations: presence and amount of rock fragments, presence and amount of crusts, presence and amount of vegetation, textural composition of the top layer (sand, silt, and clay), and sometimes, though not always, topographic position and geomorphic setting. These characteristics are relatively stable over time, making them useful tools for selecting and defining surface units for the purpose of studying dust emission. Other factors such as rainfall and, at the local scale, disturbance caused by animal activity, also affect the emission of dust but are more variable in time and space and thus less recommended as selection tools. In NDRA there is no grazing and animal disturbance of the top layer is very small to negligible. Furthermore NDRA is quite small (37 km^2), and rainfall is distributed nearly homogeneously over the area. Rainfall and animal disturbance are thus not relevant criteria to define dust-emission surface units in NDRA. However, NDRA is extensively used for ORV recreation, and therefore areas that are highly disturbed due to human activity are included in the mapping criteria.

3.2 The 17 surface units selected for this study

Seventeen surface types were identified in the Nellis Dunes Recreation Area based on textural composition, surface crusts, rock cover, and vegetation. They can be grouped into four major classes:

(1) *Sands and sand-affected areas:* active or stabilized sands, with or without rock fragments and/or vegetation;

(2) *Silt and clay areas:* loose and slightly stabilized silt and clay deposits, with or without rock fragments;

(3) *Rock-covered areas:* stabilized silty or sandy silt deposits with rock fragments on top, desert pavements over a silty sublayer (Av horizon), bedrock, and/or petrocalcic horizons;

(4) *Drainage areas:* active drainages in sand and silt areas, and gravelly drainages.

In this study, sand is defined as the fraction 63–2000 μm, silt as the fraction 2–63 μm, and clay as the fraction <2 μm.

The distribution of the surface units as a proportion of the total area of the NDRA is illustrated in Figure 6. A detailed description of each unit is given below, and a summary, for quick reference purposes, is provided in Table 1. Quantitative information for each unit is shown in Table 2. Photographs of the units, grouped by class are shown in Figures 7–10.

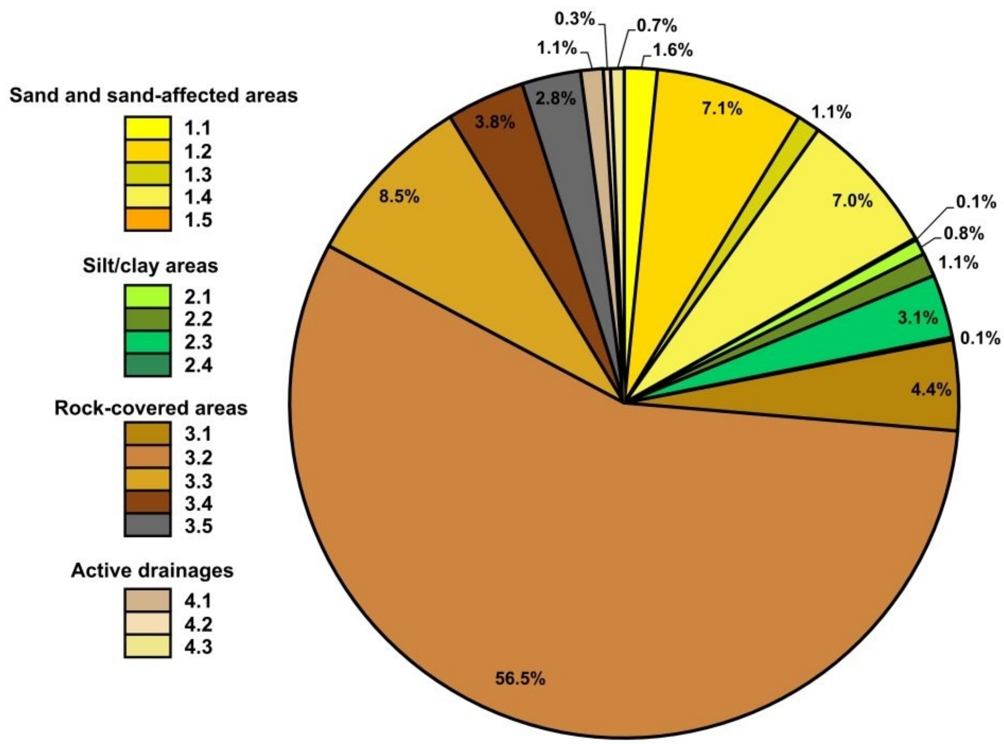

Fig. 6: Chart illustrating the areal proportions of the 17 surface types within the Nellis Dunes Recreation Area.

3.2.1 Sand and sand-affected areas

Surface Unit 1.1: Dunes with no vegetation. Active sand dunes and sand sheets with no vegetation occur mostly, though not exclusively, as prominent ridges. The depth of the active sand layer varies from a few decimeters to several meters. Sparse rock fragments and underlying petrocalcic horizons may locally outcrop where the sand layer is thin. Surface crusts are absent.

Surface Unit 1.2: Dunes with vegetation. Dune sands with sparse shrubs. The sand is active and there is no surface crust. Small coppice dunes may be present. Rock fragments may occur on the surface, but rock cover is low (<5%) and does not affect the deflation.

Surface Unit 1.3: Disturbed sand surfaces. Mixture of loose and active sand, rock fragments and underlying bedrock. This unit typically occurs in areas where shallow (<2-3 cm) sands cover a substratum of petrocalcic horizons and/or bedrock and disturbance by human activity is high.

Table 1: Overview and characteristics of the 17 surface units in the Nellis Dunes Recreation Area

Map unit	Description	Rock fragments	Surface crust	Vegetation
Sand and sand-affected areas				
1.1	Active dunes without vegetation. Decimeter to several meters thick.	Sparse; may have exposed petrocalcic horizons	Absent	Absent
1.2	Active dunes with vegetation. Coppice dunes <50 cm may be present.	Sparse; <5% rock cover	Absent	Isolated shrubs
1.3	Anthropogenic disturbed sand surfaces. Typically <2-3 cm thick loosse sands overlying petrocalcic horizons or bedrock.	Common, mixed with 2-3 cm thick loose sand overlying bedrock	Absent	Absent
1.4	Patchy, shallow (1-3 cm thick), loose sand overlying silty/rocky subsoil	Common, not interlocking, rocks in subsoil are exposed at surface	Absent	Isolated shrubs
1.5	Very fine sand and coarse silt outcrops. Commonly badlands.	Absent	Physical	Mostly absent
Silt/clay areas				
2.1	Silt/clay outcrops with biological crust	Sparse, <3-4% rock cover	Biologic	Isolated shrubs
2.2	Silt/clay outcrops with gravel	Common, <15%, not interlocking	Physical	Usually absent
2.3	Aggregated silt deposits, commonly badlands, aggregates <5 mm diameter	Absent	Physical, patchy distribution	Absent
2.4	Anthropogenic disturbed silt surfaces	Variable, not interlocking	Absent	Absent
Rock-covered areas				
3.1	Well-developed desert pavements with underlying silty Av horizon	Abundant: tightly interlocking rock fragments, nearly 100% surface cover	Physical between rock fragments	Rare, isolated shrubs
3.2	Rock-covered surface with silt/clay	Many: 60-80%, poorly interlocking	Physical and biological between rock fragments	Common, shrubs (10-15%)
3.3	Rock-covered surface with sandy loam	Many: 60-80%, poorly interlocking	Physical and biological between rock fragments	Common, shrubs (10-15%)
3.4	Rock-covered with encrusted sand and biological crusts	Common: 20-30%, poorly interlocking	Biological, continuous	Common, shrubs (10%)
3.5	Bedrock and/or exposed petrocalcic horizons	Continuous rock outcrop	Absent	Rare shrubs
Active drainages				
4.1	Gravelly drainages, without fine sediment	Abundant: 90-100%, non-interlocking gravel clasts	Absent	Absent
4.2	Gravel and sand drainages	Abundant: 70-80% with sand mixture	Absent	Absent
4.3	Gravel and silt/clay drainages	Common: 30-60%, poorly interlocking, with silt mixture	Physical	Common, shrubs (10-30%)

Surface Unit 1.4: Patchy layers of sand over silty or rocky subsoil. These surfaces constitute a thin layer of loose sand (1-3 cm) covering the subsoil. Many underlying clasts are exposed at the surface. There is no surface crust; the sand is active, and small dunes may locally occur.

Surface Unit 1.5: Outcrops of a mixture of very fine sand and coarse silt. These outcrops may occur in badlands and on steep slopes, but also on plateaus. In NDRA, they typically have a yellow color. These surfaces are almost free of vegetation and are usually stabilized by a silty sandy crust.

Table 2: Information on texture, rock cover, surface crust, surface resistance and vegetation for the 17 surface units in the Nellis Dunes Recreation Area

Surface unit	Soil texture										Rock fragments			Surface crust	Surface resistance		Vegetation
	>2000 μm (%)	1000–2000 μm (%)	710–1000 μm (%)	500–710 μm (%)	250–500 μm (%)	180–250 μm (%)	105–180 μm (%)	63–105 μm (%)	<63 μm (%)	Median grain diameter (fraction < 500 μm) (μm)	Rock cover (on surface)		Rock content (>2 mm in upper 15 mm) (%)	Presence	Normal resistance (kg* cm^{-2})	Tangential resistance (kg* cm^{-2})	Vegetation cover (%)
											total area (%)	non-vegetated area only (%)					
sands and sand-affected surfaces																	
1.1	0.01	0.01	0.01	0.03	12.03	58.77	26.97	2.12	0.07	209.98	0.0	0.0	0.01	no	0.136	0.051	0.5
1.2	13.86	0.61	0.23	0.17	4.06	21.14	48.32	10.50	0.88	181.50	4.3	4.6	13.86	no	0.143	0.134	8.7
1.3	49.74	2.76	0.99	8.75	3.01	4.10	24.25	5.15	1.08	178.45	54.6	54.9	49.74	no	0.159	0.171	0.5
1.4	40.84	0.60	0.16	0.22	0.44	2.01	45.42	8.43	1.44	153.21	23.6	28.3	40.84	no	0.149	0.244	18.3
1.5	10.77	6.70	2.14	1.70	7.58	9.03	46.69	11.77	2.35	152.20	4.3	4.3	10.77	yes	0.615	0.710	1.0
silt/clay surfaces																	
2.1	19.62	2.46	1.19	1.69	7.97	13.35	18.02	26.20	8.63	155.94	3.4	4.1	19.62	yes	0.210	0.780	16.8
2.2	24.45	5.86	3.70	3.96	9.81	7.47	15.13	15.29	10.95	52.35	11.3	11.6	24.45	yes	0.207	0.689	2.1
2.3	31.85	18.67	9.31	10.21	14.34	4.45	4.56	3.09	3.02	122.54	2.7	2.7	31.85[c]	yes	0.117	0.364	0.0
2.4	42.31	1.65	1.17	1.76	8.79	12.79	21.21	7.40	2.88	192.97	31.7	31.9	42.31	yes	1.112	1.940	0.5
rock-covered surfaces																	
3.1	74.40	1.80	1.26	0.88	2.97	2.95	8.19	5.77	1.47	117.26	94.9	97.8	74.40	no[a]	NA[a]	NA[a]	3.0
3.2	46.68	5.01	2.30	1.97	5.15	5.32	20.38	9.24	3.31	135.91	64.4	75.6	46.68	yes	1.109	1.451	14.4
3.3	32.29	1.63	0.55	0.50	1.12	2.07	41.07	18.37	2.34	139.98	32.6	40.1	32.29	yes	1.152	0.969	18.4
3.4	20.81	2.73	0.83	1.19	6.33	9.38	38.43	16.90	2.90	156.68	22.6	25.1	20.81	yes	0.218	0.560	10.1
3.5	99.99	0.00	0.00	0.00	0.00	0.00	0.00	0.00	0.00	84.79	94.3	98.5	99.99	no[b]	NA[b]	NA[b]	4.4
drainage surfaces																	
4.1	94.77	1.24	0.38	0.36	1.11	0.55	1.25	0.25	0.07	211.10	97.9	97.9	94.77	no[a]	NA[a]	NA[a]	0.0
4.2	63.93	4.50	1.24	1.10	6.43	10.02	9.82	2.17	0.56	229.08	76.0	76.0	63.93	no	0.085	0.127	0.0
4.3	60.54	6.27	2.45	2.37	11.42	9.44	5.10	1.40	0.64	202.23	35.8	47.0	60.54	yes	1.452	1.219	21.4

[a] Desert pavement.
[b] Bedrock.
[c] Particles >2 mm consist of aggregates of silt.

3.2.2 Silt and clay areas

Surface Unit 2.1: Silt and clay with crust. These surfaces usually occur near drainage channels in silt areas. The sediment is predominantly composed of silt and commonly shows a continuous cyanobacterial crust. Some vegetation (isolated shrubs) is typical. A few scattered rock fragments (<3-4%) may occur, but they remain sparse.

Surface Unit 2.2: Silt and clay with gravel. Mixture of silt and gravel, but with considerably more (>85% in weight) silt than gravel on the surface. A surface crust may be present, although many areas are not encrusted. These surfaces do not occur in drainage areas but are typically located on hill slopes and plateau escarpments.

Surface Unit 2.3: Aggregated silt deposits. Silt and clay surfaces where the particles are bound in aggregates up to 5 mm in diameter. The percentage of free particles is low. A surface crust is common, but the crust may be disturbed or even absent. These surfaces are entirely devoid of vegetation, and their erosion produces badlands-style topography.

Surface Unit 2.4: Disturbed silt surfaces. Mixture of noncrusted silt and rock fragments overlying bedrock. They occur in areas where the surface has been disturbed by human activity and are the silt equivalent of surface unit 1.3.

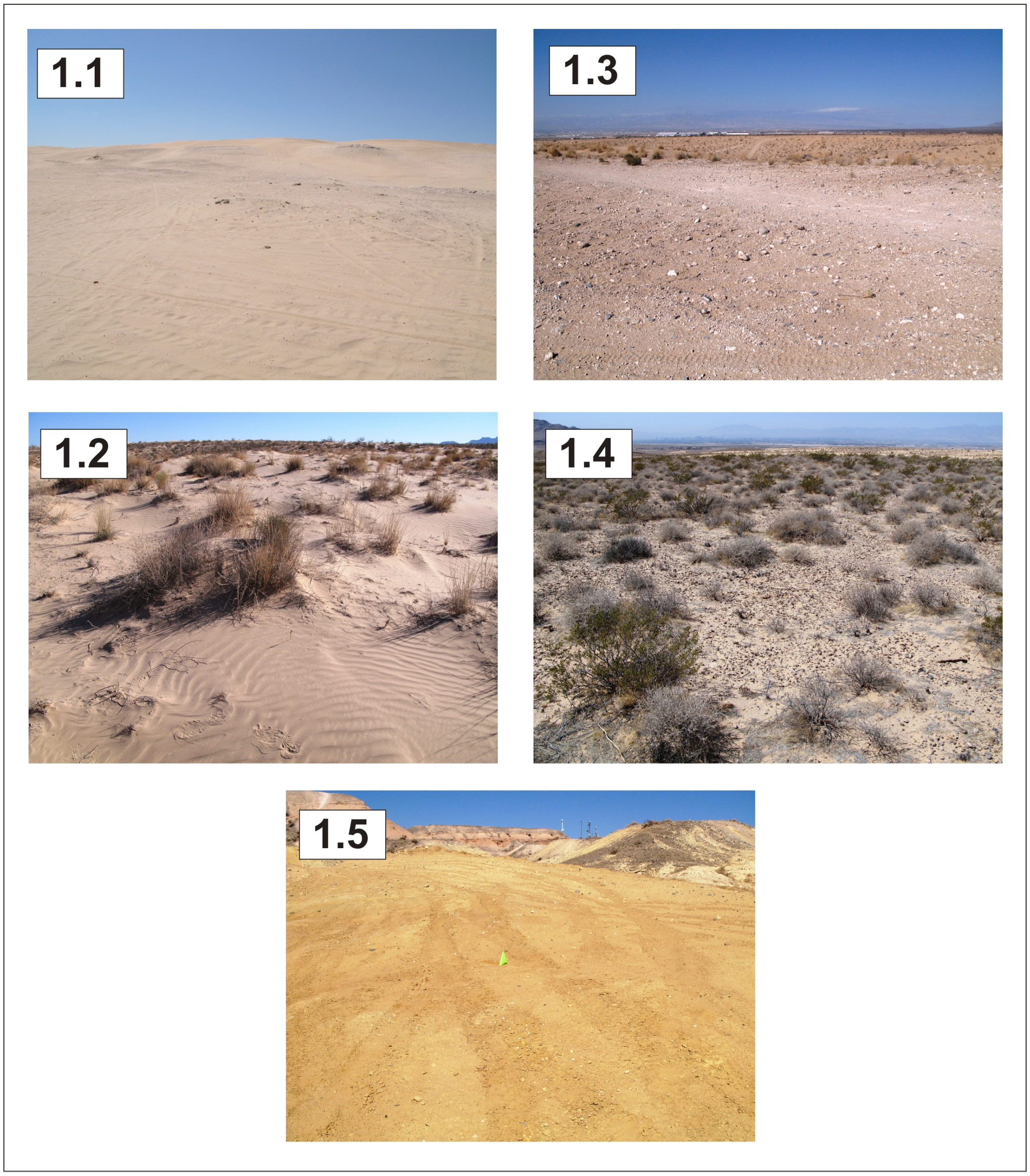

Fig. 7: Photograph of sand and sand-affected area surface units. 1.1: Dunes with no vegetation; 1.2: Dunes with vegetation; 1.3: Disturbed sand surfaces; 1.4: Patchy layers of sand over silty or rocky subsoil; 1.5: Very fine sand and coarse silt.

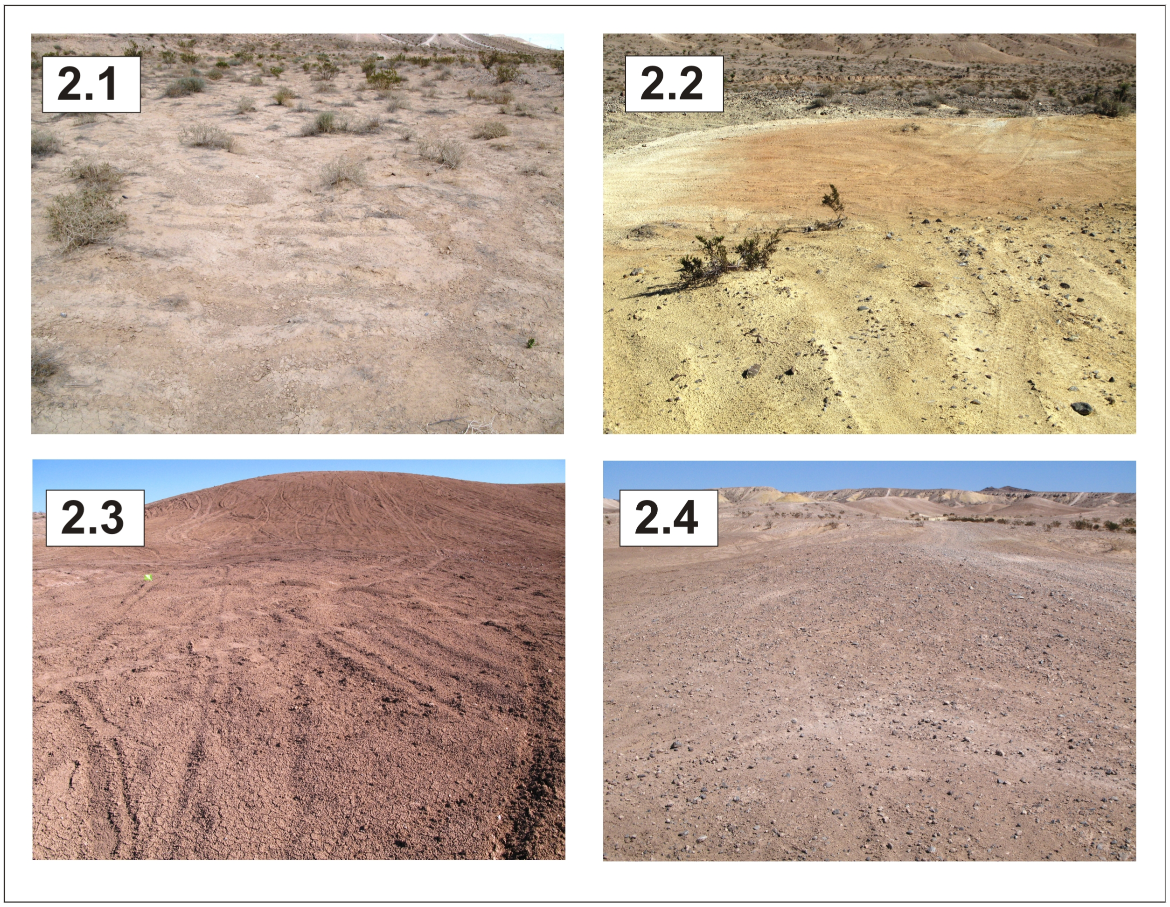

Fig. 8: Photograph of silt and clay area surface units. 2.1: Silt and clay with crust; 2.2: Silt and clay with gravel; 2.3: Aggregated silt deposits; 2.4: Disturbed silt surfaces.

3.2.3 Rock-covered areas

Surface Unit 3.1: Desert pavements. Well-developed and mature desert pavements over a (usually silty) subsoil (Av horizon). The rock fragments are partially embedded in the silt, and rock cover density is close to 100%. Vegetation (shrubs) may locally occur, but most desert pavements are devoid of any vegetation.

Surface Unit 3.2: Rock-covered surfaces with silt and clay zones. The top layer is composed of silt with some very fine sand and contains many rock fragments (cover percentage: 60-80%). Pavements are less well developed as compared to unit 3.1. The areas in between the rock fragments show a continuous and permanent surface crust.

Vegetation (shrubs) typically covers 10-15% of the surface. These surfaces occur anywhere in the landscape and are the dominant surface unit in the Nellis Dunes Recreation Area.

Surface Unit 3.3: Rock-covered surfaces with sandy loam. These surfaces resemble surface unit 3.2, but the top layer contains small amounts of sand. The sand has been blown in from nearby sand areas. In the Nellis Dunes field, they typically occur in silt areas located close to the sand dunes. Vegetation (shrubs) typically covers 10-15% of the surface.

Surface Unit 3.4: Rock-covered surfaces with encrusted sand. This type of surface is similar to the 3.2 and 3.3 surfaces but is largely composed of sand, with small amounts of silt. It is covered by a continuous cyanobacterial crust. This crust is much weaker than the silt crusts of surface units 3.2 and 3.3. Vegetation (shrubs) is common and covers approximately 10% of the surface.

Surface Unit 3.5: Bedrock and/or petrocalcic horizons. Outcrops of bedrock and exposed petrocalcic horizons. The percentage of rock cover is close to 100%. Silt may have accumulated only near a few sparse shrubs and in deep cracks. Outcropping bedrock is commonly Paleozoic and Neogene carbonates.

3.2.4 Active drainages

Surface Unit 4.1: Gravelly drainages. Active drainages with almost pure gravel. In the NDRA these surfaces typically occur in the channels of the major drainages. The gravel is almost free of sand, silt, and clay, and its cover percentage is close to 100%.

Surface Unit 4.2: Gravel and sand drainages. Active drainages with a mixture of gravel and sand. They occur in sand areas, in particular within the smaller sized valleys, and also in the upstream zone of the larger drainages where there is insufficient water to wash the sand. Vegetation is usually absent.

Surface Unit 4.3: Gravel and silt and clay drainages. Active drainages with a mixture of silt and gravel. They are the silt equivalent of surface unit 4.2 except that many of them have considerable vegetation (usually shrubs). Silt and gravel drainages without vegetation also occur, especially in first-order channels in badlands.

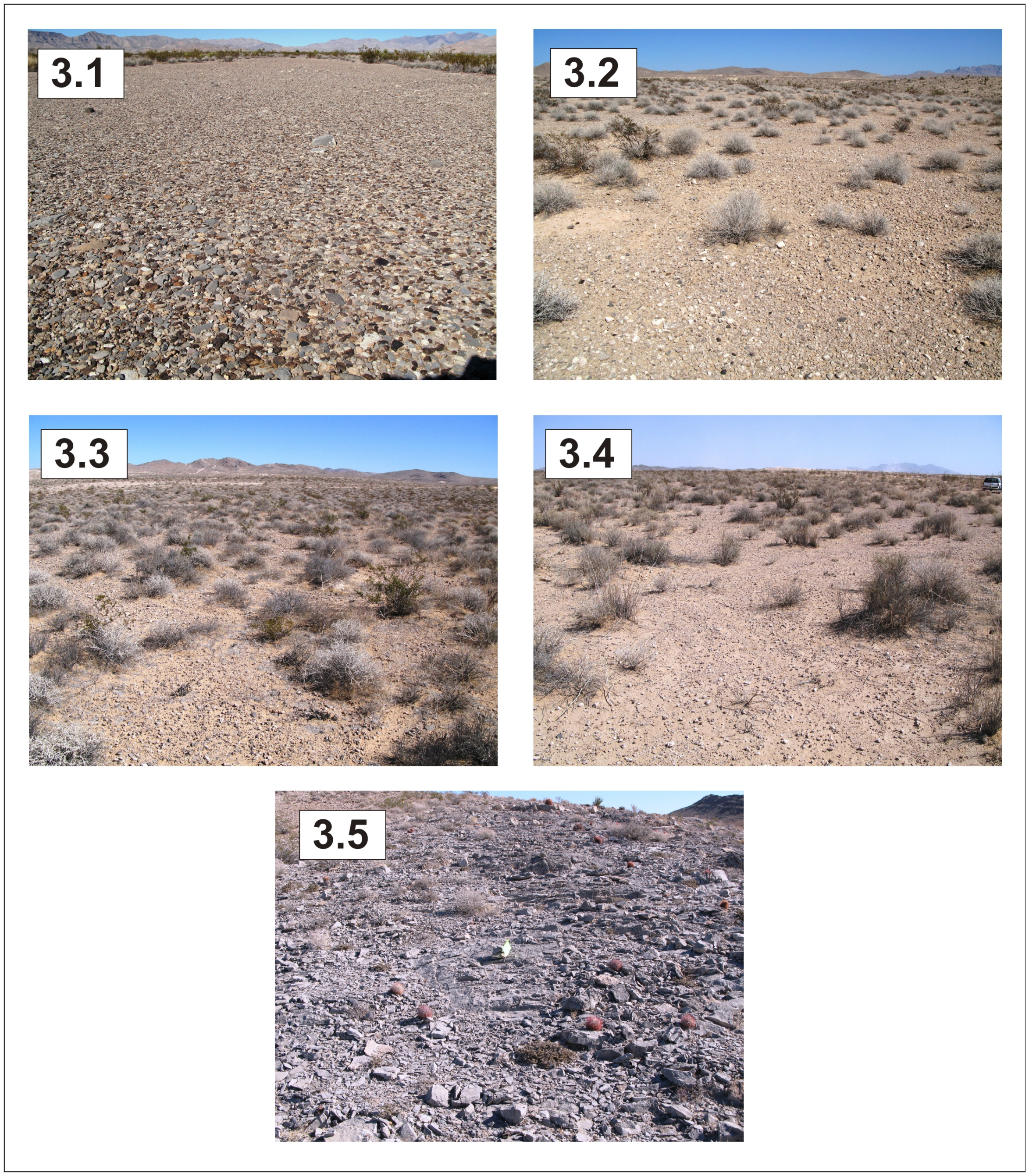

Fig. 9: Photograph of rock-covered area surface types. 3.1: Desert pavements; 3.2: Rock-covered surfaces with silt and clay zones; 3.3: Rock-covered surfaces with sandy loam; 3.4: Rock-covered surfaces with encrusted sand; 3.5: Bedrock and/or petrocalcic horizons.

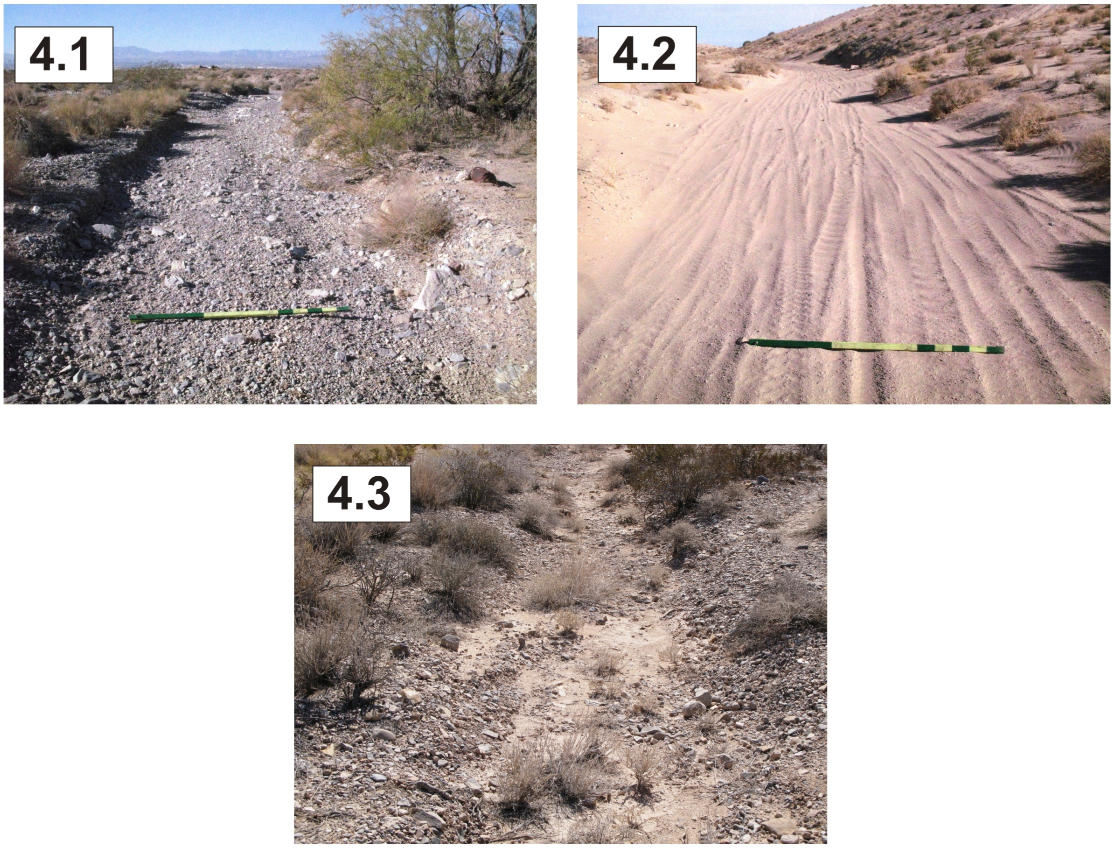

Fig. 10: Photograph of active drainage areas. 4.1: Gravelly drainages; 4.2: Gravel and sand drainages; 4.3: Gravel and silt and clay drainages.

3.3 Creation of a surface units map

3.3.1 Methodology

Mapping of the NDRA began with the designation of the 17 surface units described above. Apart from the grain-size characteristics, mineralogical composition and distribution of the surface mineralogy was also examined using the shortwave infrared (SWIR) and the thermal infrared (TIR) bands of the ASTER (Advanced Spaceborne Thermal Emission and Reflection Radiometer) instrument. This imagery was acquired on 6 July 2000 and obtained from Land Processes Distributed Active Archive Center (https://lpdaac.usgs.gov/) supported by NASA (National Aeronautics and Space Administration) and the U.S. Geological Survey. The SWIR component of ASTER has a 30-m spatial resolution that covers the spectral range of 1.6 to 2.4 µm over six bands. The TIR component covers the spectral range of 8.1 to 11.7 µm over five bands with a spatial resolution of 90 m. Analysis of the study area using the ASTER imagery focused on using the SWIR and TIR bands to isolate the occurrence of individual minerals and their relationship to mapped surface units. Calculation of a quartz (Rockwell and Hofstra, 2008) and carbonate index (Ninomiya et al., 2005) using bands 10-13 and bands 13-14, respectively, created images that defined the occurrences of these types of minerals. ASTER bands 8, 6, and 4 were combined to produce a SWIR image that was then further processed using a decorrelation stretch to enhance the differences between the individual bands (Mather, 2004).

The quartz and carbonate indices derived from the ASTER imagery are useful for characterization of surface mineralogy over large areas, but they do not provide the needed spatial detail for constructing a dust emission potential map at the scales involved. Thus, construction of the surface units map involved the use of high-resolution, Quickbird satellite imagery and field reconnaissance. The Quickbird imagery consists of two products. The first is a 0.6-m resolution panchromatic band and the second is a 2.4-m resolution multispectral product consisting of three visible bands and a near-infrared (0.45-0.90 µm) band. Field mapping, using the Quickbird imagery as a base, was accomplished through use of a ruggedized field computer with a global positioning system (GPS) attachment. This setup allowed field locations and unit contacts to be mapped with a high degree of accuracy. The contacts were then compiled using the Manifold GIS mapping package to produce the final surface units map. Developing the map in GIS allows creation of a georeferenced product that can be combined with other types of geographic information such as topography or aerial photography.

3.3.2 Distribution of the surface units over the NDRA

3.3.2.1 Remote sensing data

ASTER multispectral satellite imagery using band combinations 8-6-4 from the SWIR and the quartz and carbonate indices from the TIR bands were examined for the study area. The quartz index indicates quartz sand in the central and western parts of the study area (bright areas in Fig. 11a). The carbonate index (bright areas in Fig. 11b) shows that the concentration of carbonates is confined to the eastern parts of the study area. The ASTER band combination that provides the best surface unit determination is the 8-6-4 SWIR combination (Fig. 12). Here, the sandy areas underlain by units 1.1, 1.2, and 1.4 are shown in yellow (Fig. 12; area A), denoting the quartz composition of the sands. The main belt of dune sands is well defined, stretching from the southwest into the central

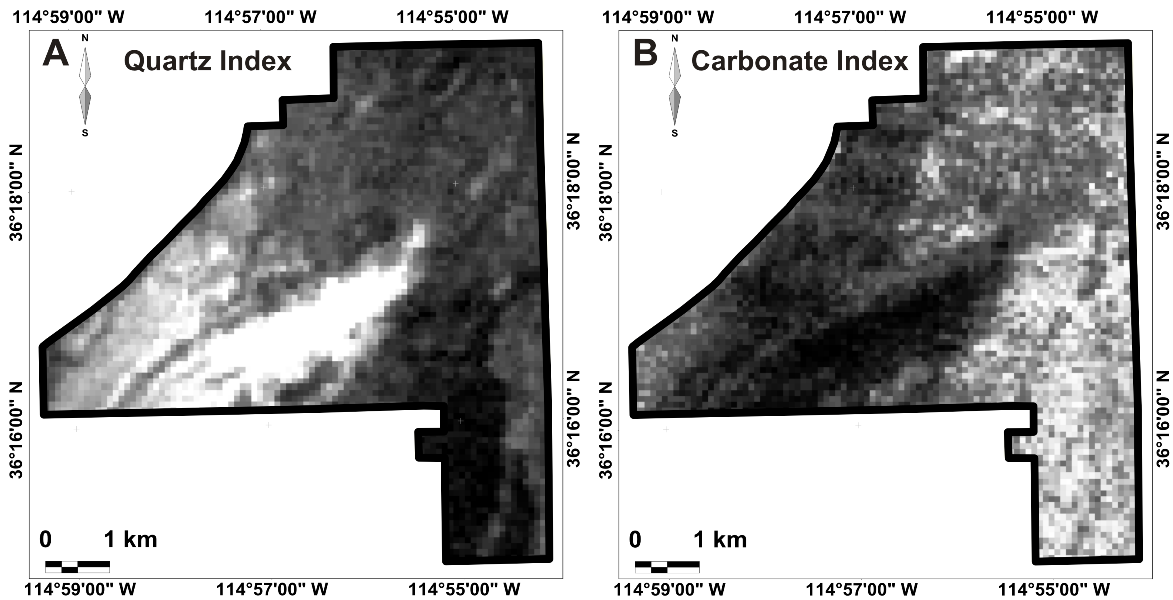

Fig. 11: Results of band mathematics calculations and ratios using ASTER (Advanced Spaceborne Thermal Emission Reflection Radiometer) thermal infrared bands. (a) Quartz index with brighter areas showing the occurrence of quartz. The bright areas in the center of the image denote the location of the main dune field. (b) Carbonate index with brighter areas indicate the occurrence of carbonates. The carbonate signature in the southeast portion of the study area reflects outcropping of limestone units within the Muddy Creek Formation.

portion of the map areas. Sandy areas also lie to the west (Fig. 12; area B), where they are separated from the main belt by a deeply incised wash (Fig. 12; area C). The sandy zones are more sparse and isolated in area B compared to those in area A. Silty units, such as 2.3, are the light purple areas (Fig. 12; area D) that occur primarily in the northwest. These units are capped by thin gypsum layers that are shown in darker purple (Fig. 12; area E). Paleozoic carbonates of the Bird Spring Formation occur in the northern part of the NDRA (Fig.12; area F), whereas the better expressed carbonate signature derived from limestone clasts of the Muddy Creek Formation (Beard et al., 2007) occur in the south and eastern part of the NDRA (Fig. 12; area G).

3.3.2.2 The surface units map

Detailed mapping of surface units using a Quickbird imagery base indicates that the overall distribution of surficial units in the NDRA follows a northeast-southwest trend (Fig. 13). This orientation is particularly evident in the western part of the study area, where a rough zonation of rock-covered surfaces (3.x units) progresses from silty clay zones (3.2) to sand-encrusted areas (3.4). The sandy dune areas (1.1 and 1.2) are often rimmed by a thin layer of patchy sand (1.4). This type of zonation is most evident in those areas where there is significant sand present.

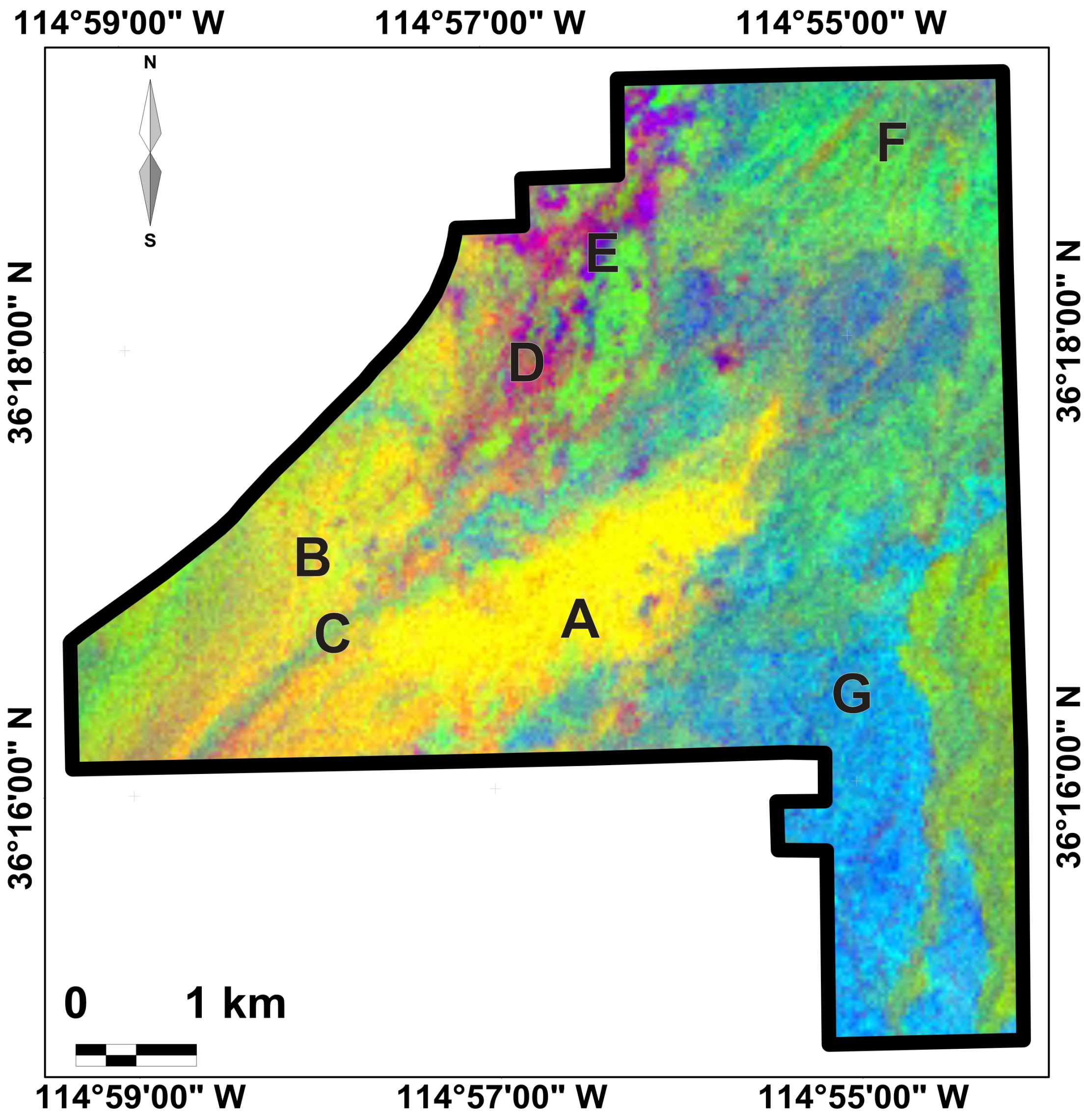

Fig. 12: Advanced Spaceborne Thermal Emission Reflection Radiometer (ASTER) shortwave infrared image of bands 8-6-4 with a decorrelation stretch applied. A and B: Quartz-rich sandy areas; C: Wash separating sandy areas; D: Muddy deposits representing unit 2.3; E: Gypsum layers capping ridge tops; F: Paleozoic carbonates of the Bird Spring Formation; G: Carbonate of the lower Muddy Creek Formation.

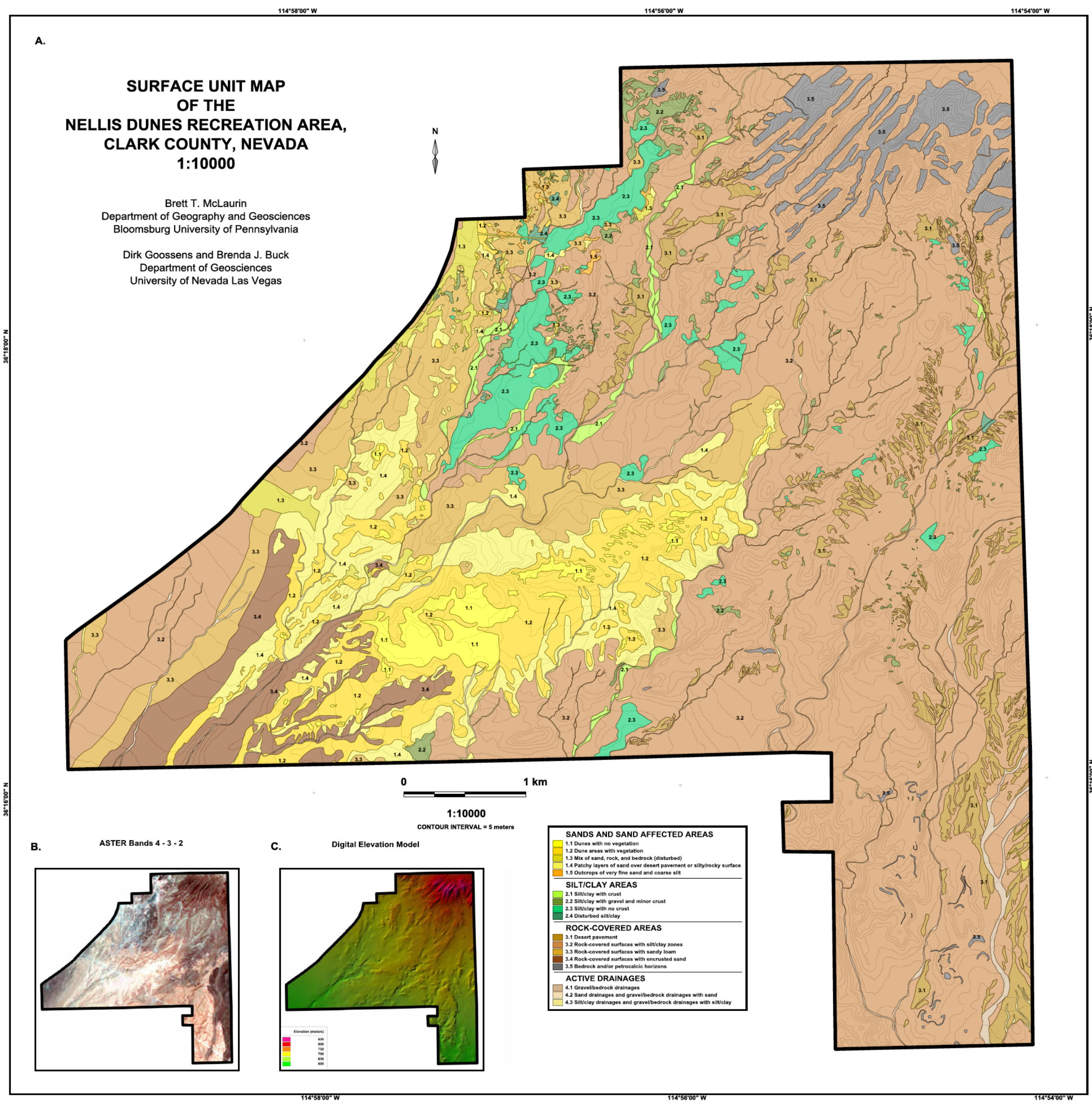

Fig. 13: (a) Surface unit map of the Nellis Dunes Recreation Area; (b) Advanced Spaceborne Thermal Emission Reflection Radiometer (ASTER) composite image with band combination 4-3-2; (c) Digital elevation model compiled from the U.S. Geological Survey 10-m resolution digital elevation models of the Apex and Frenchman Mountain quadrangles.

The central part of the sand dune area is characterized by slightly meandering, NW-SE-oriented ridges of reversing dunes indicating that sand transport alternates from two opposing directions (NE and SW). Smaller, more amorphous sand accumulations occur in the areas in between the reversing dunes. Their morphology changes through time reflecting the most recent direction of sand transport. The abrupt changes from sand-dominated units to rock-covered surfaces with silt and clay zones (3.2) are often partitioned by deeply incised drainages such as those that mark the eastern edge of the dune field in the south-central portion of the study area. Sand that is transported from the west becomes trapped within the drainages, which prevent much of the sand from entering the areas to the east.

The surficial units in the northwestern part of the NDRA are primarily controlled by the lithologies of the underlying Muddy Creek Formation. Although some sand is present (3.3 and 1.5), the most significant unit is the aggregated silt deposit (2.3). This unit contains no vegetation and is characterized by badland-style topography. These areas contain some of the highest density of vehicular trackways. The northeast-southwest orientation of this unit follows underlying mudstone of the Muddy Creek Formation from which this surface unit is derived. West and east of the main belt of unit 2.3, yellow sand units (1.5) occur stratigraphically above the 2.3 units. These are, in turn, overlain by the more resistant Muddy Creek limestone and gypsum or more commonly, petrocalcic horizons that cap isolated mesas and are preserved as topographic highs.

East of these areas where there are significant sand and silt units, the landscape is dominated by relict and inset alluvial fan geomorphic surfaces (e.g., Peterson, 1981; Bull, 1991); especially common are the rock-covered surfaces with silt and clay (3.2). These large expanses are occasionally interrupted by finer grained silt units (2.2 and 2.3) and well-developed desert pavements (3.1) along the flanks of drainages. The desert pavements are easily identifiable from the Quickbird imagery and appear as elongated areas that are darker in color and have a smoother surface texture with little vegetation. The desert pavement surfaces occur in areas east of the main silt occurrences.

Bedrock and/or petrocalcic units (3.5) occur as three outcropping types. They are (1) petrocalcic horizons, (2) Paleozoic limestone, and (3) Neogene limestone of the Muddy Creek Formation. Petrocalcic horizons exposed at the surface are often of limited lateral extent and represent areas of soil erosion. These occur along the tops and sides of all of the highest, and oldest, geomorphic surfaces. Many of these zones occur in the western part of the study area, but most of them are below the resolution of mapping. Paleozoic limestone of the Permian Bird Spring Formation forms hills in the northern part of the NDRA. South of this area isolated outcrops occur where the surficial material is thin. Limestone layers in the south-central and southeastern parts of the NDRA are different from the gray-black limestone, characteristic of the Paleozoic strata in the north. These units are relatively flat-lying and consist of white to grayish, laminated limestone and are part of the Muddy Creek Formation. The outcrop occurs as thin ledges that are separated by zones of map unit 3.2 (rock-covered surfaces with silt and clay).

Some of the map units correspond well with specific geomorphic surfaces or to bedrock formations, while others do not. Units that correspond to exposed bedrock are 1.5, 2.2, 2.3, and 3.5. The active drainages (4.1, 4.2, and 4.3), correspond to Q4 surfaces of Bull (1991). In most Quaternary maps, only unit 1.1 would be defined as an active, aeolian geomorphic surface (e.g., Qe of House et al., 2010) because of the dune forms and thickness of the aeolian sand. The other units in this study with active but thin, aeolian sands (1.2, 1.4, and 3.4) overlie a wide variety of inset or relict alluvial fan surfaces that correspond to Q1-Q3 of Bull (1991) or Qea of House et al. (2010). Unit 3.1 is defined by well-developed desert pavements and is found on early Holocene-latest Pleistocene inset fans, corresponding to Q3 surfaces of Bull (1991) and Qay1 of House et al. (2010). The remaining units cross a broad spectrum of geomorphic surfaces. The most extensive unit, 3.2, is found on a wide variety of geomorphic landforms that have poorly developed desert pavements, reflecting a combination of processes including young surfaces where desert pavements have not fully developed, to very old surfaces where they have degraded (House et al., 2010). These include Pliocene ballenas with exposed and fragmented stage 6 petrocalcic horizons (Gile et al., 1966; Peterson, 1981; House et al., 2010), middle-early Pleistocene fan remnants, early Holocene-latest Pleistocene and late-middle Holocene inset fans, and colluvial slopes of bedrock outcrops (Peterson, 1981; House et al., 2010). Although unit 3.3 is mostly present on middle to early Pleistocene fan remnants, its distribution is primarily controlled by proximity to local sand sources and not geomorphic position. Unit 2.1 occurs on latest and middle Holocene inset fans and inside active drainages along bars, where biological soil crust formation is favored (Williams et al., 2010). Disturbed surfaces (1.3 and 2.4) can occur on any geomorphic surface.

3.4 The ORV trails in the Nellis Dunes Recreation Area

3.4.1 Mapping methodology

Since the goal of the project involved, among other issues, addressing the impact of off-road vehicles on the various surface types, it was important to determine the location, width, and length of the unpaved tracks that exist throughout the NDRA. Trackway depth was not recorded because the extreme variability and density of the tracks made collecting those data impractical. Using the highest resolution Quickbird imagery (0.6 m), track centerlines were digitized and the widths measured. A structured query language (SQL) statement using a geospatial buffer extension was executed that converted the centerlines into polygons of the appropriate width. These polygons were then intersected with the surface units map to determine the area of surface units covered by ORV tracks.

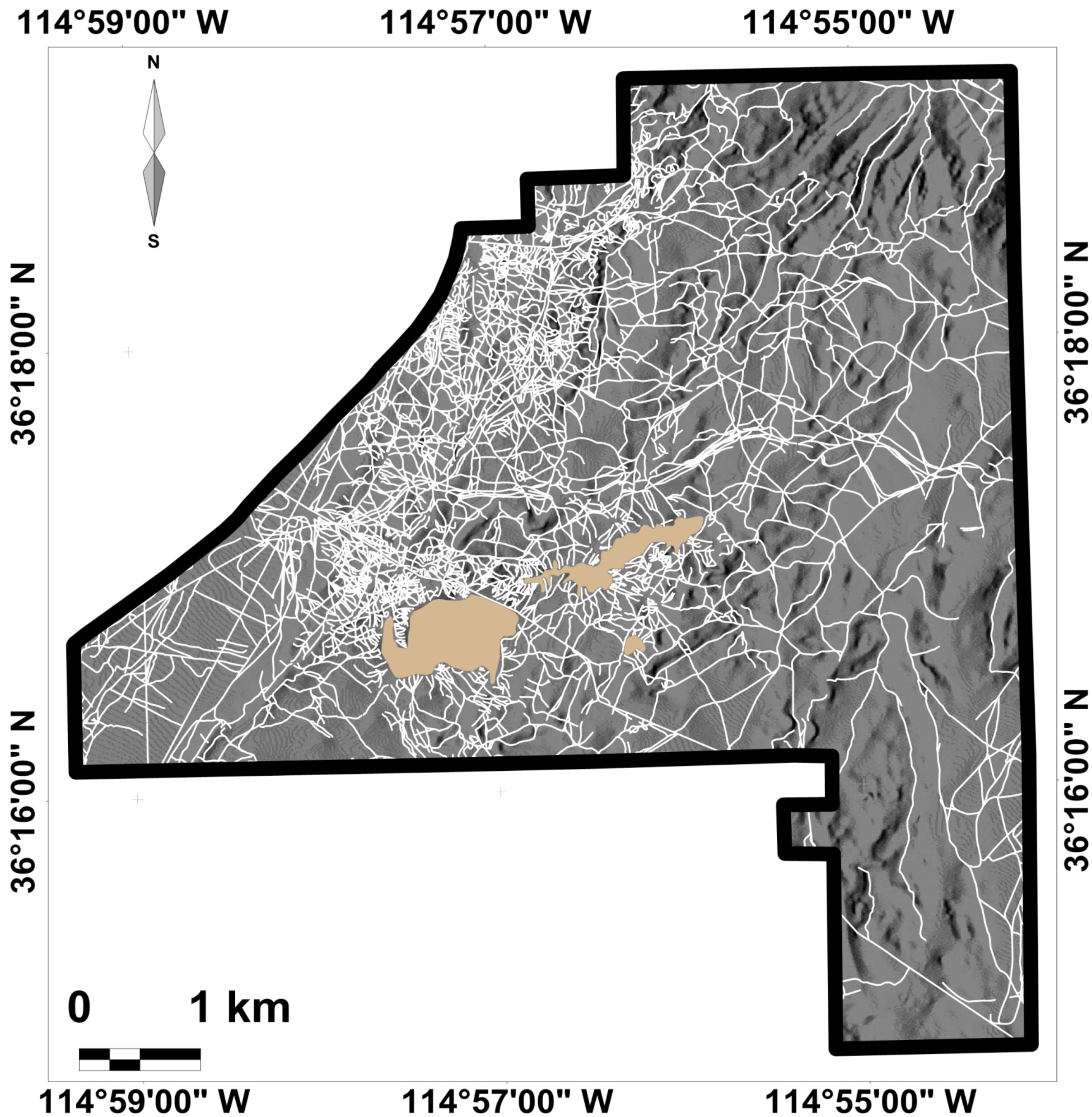

Fig. 14: Location of the tracks in the Nellis Dunes Recreation Area. Areas underlain by sandy units often show abrupt termination of tracks, especially within the more active dunes (unit 1.1 and, to a lesser extent, unit 1.2). The movement of windblown sand buries any trackways generated from off-road driving. These areas are delineated by the brown shading.

3.4.2 Distribution and density

The density of tracks can be expressed either as the total length of tracks within each mapping unit or by using a metric that calculates the length of trackway (km) within a particular surface unit to the total surface area of that unit (km^2). This metric is a derivation of the road density, as described by Forman et al. (2003), which is frequently used as a method to assess the impact of roads on environments. The definition of road density is the length of road (km) divided by the total area (km^2) and is expressed as km/km^2. However, for this study, we are concerned with the trackway density within each surface unit. Thus, we utilize the length of track within each surface unit and divide it by the surface area of each surface unit to calculate the trackway density (km/km^2).

The locations of the various tracks in the Nellis Dunes Recreation Area are shown in Fig. 14. It should be noted that track locations are particularly variable in those areas underlain by the sandy units 1.1 and 1.2 due to their temporary nature. Windblown sand in these active dune areas often covers tracks; hence many trackways appear to abruptly terminate within these sandy zones. In Figure 14, these areas are delineated by brown shading.

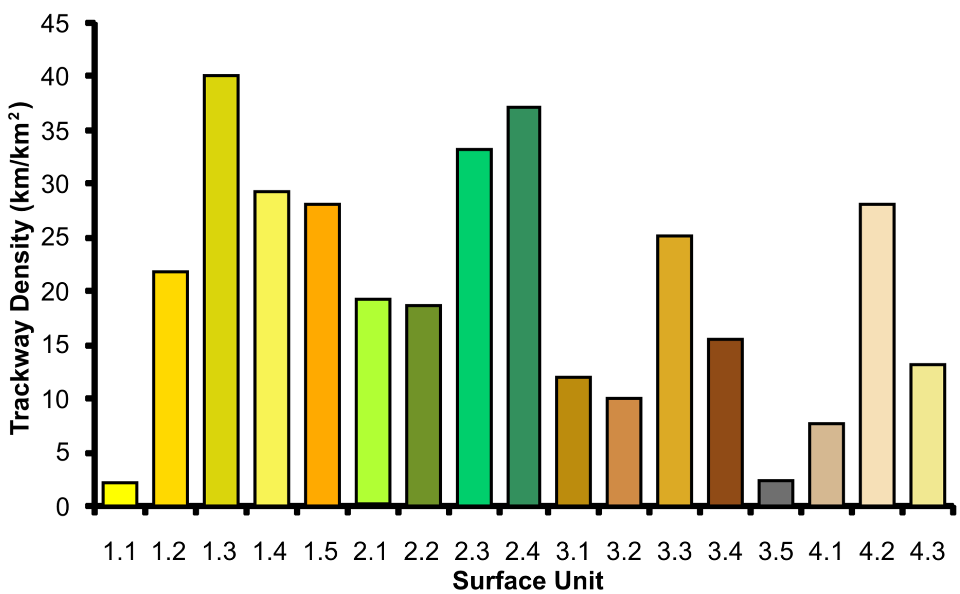

Fig. 15: Graph illustrating the trackway density for each surface unit, which reflects the density of permanent trackway within each unit. The trackway density (km/km2) is calculated by dividing the length of track with each unit (km) by the total surface area covered by the unit (km2). Most trackways generated in unit 1.1 (active dunes with no vegetation) are only temporary due to their rapid burial with windblown sand and are thus not well represented by this figure.

The trackway density in all 17 units is shown in Figure 15. The units with the lowest trackway density are 1.1 (2.2 km/km^2) and 3.5 (2.3 km/km^2). The sand dunes of unit 1.1, as stated previously, do not preserve trackways very well due to being quickly covered by windblown sand. Thus, the actual trackway density and utilization of this unit for ORV activity is certainly higher. Bedrock and outcropping petrocalcic horizons (unit 3.5) have low values for track density, since it is difficult for ORV activity to leave trackways in this type of material. However, tracks can occasionally be traced across these areas where a thin layer of sediment covers the rock surface. The highest trackway density units are 1.3 (40.2 km/km^2) and 2.4 (36.9 km/km^2), which is expected because surface disturbance is part of their definition (see section 3.2). The units with the next highest density of trackways are 2.3 (33.1 km/km^2) and 1.4 (29.4 km/km^2). The 2.3 unit is silty and devoid of any vegetation and rocks and thus very easy to drive; hence it is used by all drivers (including the less experienced ones), which explains the high density of trackways. The 1.4 unit is sandier and often borders areas adjacent to the sand dune units of 1.1 and 1.2. The high trackway density of 28.1 km/km^2 for unit 4.2 (gravelly and sandy drainages) reflects the popularity of these washes as trackways, particularly in those areas close to the main dune field.

References

Beard, L.S., Anderson, R.E., Block, D.L., Bohannon, R.G., Brady, R.J., Castor, S.B., Duebendorfer, E.M., Faulds, J.E., Felger, T.J., Howard, K.A., Kuntz, M.A., Williams, V.S., 2007. Preliminary geologic map of the Lake Mead 30′ × 60′ quadrangle, Clark County, Nevada, and Mohave County, Arizona. U.S. Geological Survey Open-File Report 2007-1010, scale 1:100,000, 3 sheets.

BLM, 2004. Las Vegas Valley Disposal Boundary, Final Environmental Impact Statement and Record of Decision, Chapter 3: Affected Environment. Las Vegas Bureau of Land Management, Las Vegas, Nevada.

Bull, W.B., 1991. Geomorphic Response to Climate Change. Oxford University Press, New York.

Castor, S.B., Faulds, J.E., 2001. Post-6 Ma limestone along the southeastern part of the Las Vegas Valley shear zone, southern Nevada. In: Young, A., Spamer, E.E. (Eds.), Colorado River. Origin and Evolution. Grand Canyon Association, Grand Canyon, Arizona, 77-79.

Forman, R.T.T., Sperling, D., Bissonette, J.A., Clevenger, A.P., Cutshall, C.D., Dale, V.H., Fahrig, L., France, R., Goldman, C.R., Heanue, K., Jones, J.A., Swanson, F.J., Turrentine, T., Winter, T.C., 2003. Road ecology: Science and Solutions. Island Press, Washington.

Gile, L.H., Peterson, F.F., Grossman, R.B., 1966. Morphological and genetic sequences of carbonate accumulation in desert soils. Soil Science 101, 347–360.

Goossens, D., Buck, B., 2011. Effects of wind erosion, off-road vehicular activity, atmospheric conditions and the proximity of a metropolitan area on PM10 characteristics in a recreational site. Atmospheric Environment 45, 94-107.

House, P.K., Buck, B.J., Ramelli, A.R., 2010. Geologic assessment of piedmont and playa flood hazards in the Ivanpah Valley area, Clark County, Nevada. Nevada Bureau of Mines and Geology, Report 53. http://www.nbmg.unr.edu/Pubs/r/r53/index.html. (online only)

Lazaro, M.A., Chang, Y-S., Kuiper, J.A., Kotamarti, V.R., James, D.E., Brazao, R., Pulugurtha, S., 2004. Cumulative Las Vegas Valley Air Quality Modeling Assessment of ongoing Bureau of Land Management (BLM) Federal Land Disposition Actions within the BLM Disposal Boundary. Report prepared for the Bureau of Land Management (BLM), University of Chicago and University of Nevada Las Vegas.

Mather, P.M., 2004. Computer processing of remotely-sensed images: An introduction (third edition). Wiley, Chichester.

Ninomiya, Y., Fu, B., Cudahy, T.J., 2005. Detecting lithology with Advanced Spaceborne Thermal Emission Reflection Radiometer (ASTER) multispectral thermal infrared “radiance-at-sensor” data. Remote Sensing of Environment 99, 127–139.

Peterson, F.F., 1981. Landforms of the Basin and Range Province defined for soil survey. Nevada Agricultural Experiment Station Technical Bulletin 28. University of Nevada, Reno.

Rockwell, B.W., Hofstra, A.H., 2008. Identification of quartz and carbonate minerals across northern Nevada using ASTER thermal infrared emissivity data - Implications for geologic mapping and mineral resource investigations in well-studied and frontier areas. Geosphere 4, 218–246.

Williams, A., Buck, B., Soukup, D., Merkler, D., 2010. Geomorphic controls of biological soil crust distribution, Mojave Desert (USA). Proceedings 19th World Congress of Soil Science, Soil Solutions for a Changing World, 1-6 August 2010, Brisbane, Australia. Published on CD-ROM.

Chapter 3

DUST EMISSION BY OFF-ROAD DRIVING: FIELD EXPERIMENTS

Dirk Goossens and Brenda Buck

Department of Geoscience, University of Nevada Las Vegas

1. The worldwide increase in ORV activities and its impacts

Off-road vehicle (ORV) driving is one of the most prevalent and fastest growing leisure activities on public lands worldwide (Cordell, 2004; Cordell et al., 2008). For example, in western Australia the sales of off-road motorcycles and quad bikes (four-wheelers) increased by 67% between 2004 and 2008 (DSR, 2009). In Montana (USA) the number of registered ORV drivers doubled between 2002 and 2007 (Sylvester, 2009). In southern Nevada (USA) the number of off-road drivers has quadrupled in only the last few years (Spivey, 2008). In 2008, the Bureau of Land Management in Las Vegas estimated that the number of off-road drivers in the city had increased to more than 300,000, which is over 15% of the population (Goossens and Buck, 2009a). Elsewhere in the world ORV activity is also increasing, on all continents (Outdoor World Directory, 2010).

Damage to the land from ORV driving is extensive. ORV driving is one of the most destructive types of land use disturbing the top soil, vegetation and even local ecosystems (Adkinson, 1991; Kutiel et al., 2000; Wiedmer, 2002). Also, it creates noise, produces large amounts of exhaust-gases and emits significant quantities of soil dust, especially when the soil is dry (Goossens and Buck, 2009a). Surfaces disturbed may require decades or even centuries to become more or less restored, if recovery is at all possible (Wilshire and Nakata, 1976).

Considering the damage it is not surprising that the first studies investigating the consequences of off-road driving appeared more than 40 years ago. These studies primarily focused on the effects off-road vehicles exert on the soil itself. The increased compaction of the soil due to ORV driving has been described in detail (Liddle and Greig-Smith, 1975; Wilshire and Nakata, 1976; Sparrow et al., 1978; Voorhees et al., 1978; Wilshire et al., 1978; Anderson et al., 1990; Smith and Dickson, 1990; Adkinson, 1991). Webb et al. (1978), Wilshire et al. (1978) and Griggs and Walsh (1981) investigated how off-road driving affects the soil temperature regime. Other soil parameters studied include organic matter content and pH (Wilshire et al., 1978; Kutiel et al., 2000), soil nitrogen (Belnap, 2002), and hydrologic parameters such as infiltration (Wilshire et al., 1978; Eckert et al., 1979; NPSNM, 2008) and soil water content (Liddle and Greig-Smith, 1975).

Effects on vegetation have been studied as well. A consequent decrease in frequency, cover, abundance, vigor, and maximum height of the vegetation along ORV trails has been observed (Sparrow et al., 1978; Adkinson, 1991; Kutiel et al., 2000; NPSNM, 2008). A review of the literature on the effect on biological productivity was provided by Wilshire et al. in 1978. Effects on the fauna were studied by McEwen (1978), Anderson et al. (1990) and Schlacher and Thompson (2007), and effects on stream environments, such as rivers and washes, by TCAFS (2002) and Wiedmer (2002). Also, soil erosion in and near ORV trails has been examined (Fish et al., 1981; Tinsley and Fish, 1985; Tuttle and Griggs, 1987).

Emissions of soil dust created by ORV activity were hardly studied before the early 1990s but received much attention since then: Moosmüller et al., 1998; Gillies et al., 1999, 2005; Kuhns et al., 2003; Goossens and Buck, 2009b; to cite only a few studies. Most studies focused on direct measurements of ORV emission but others also considered wind erosion in disturbed ORV trails (Goossens and Buck, 2009a) or characterized and mapped surface types in terms of dust production (Bacon et al., 2008; McLaurin et al., in press).

Dust emissions created by ORV activities require special attention because ORV driving is a non-selective process. This means that components that normally stay fixed in the soil may become released and inhaled. This is a special concern if ORV-driven substrata contain chemical or mineral substances, or organisms harmful to the human body. Moreover, the risk of inhaling harmful substances is not limited to the drivers themselves: passive visitors to ORV sites will also be affected, as will residents of downwind located areas. For evident reasons the risk is highest in the area of production, i.e. the ORV site, because of the higher airborne concentrations. The risk in downwind zones is more difficult to predict as it depends on the degree of dilution as the dust blows towards these areas, which is affected by the meteorological conditions and the degree of roughness of the earth's surface.

Because of the very high number of visitors to the Nellis Dunes Recreation Area, emission of dust caused by ORV activity is of special concern at this site. Previous research (Moosmüller et al., 1998; Gillies et al., 1999, 2005; Kuhns et al., 2003) has shown that accurate predictions of emissions caused by driving on unpaved surfaces are very difficult because the emissions strongly depend on the type of surface driven, the type of vehicle used, the driving speed, and other factors. The large number of surface types in the NDRA, and the highly heterogeneous distribution, especially in the most intensively driven western part of the area, complicate accurate predictions based on previous data. A separate study investigating the emissions on each surface type was thus necessary, for each type of vehicle used in the Nellis Dunes Recreation Area. This chapter describes the results of these measurements.

Apart from the emissions generated during the driving itself, ORV also disturbs the topsoil. The structure of the top layer in ORV trails is very different compared to the original surface in which the trail has been created. ORV trails are much more sensitive to wind erosion than undisturbed surfaces, which are often characterized by physical or biological surface crusts or by a natural protection of surficial rock fragments. This difference is significant in areas rich in silt and clay (such as in the entire eastern part of the NDRA) because in these areas dust production by wind erosion is nearly exclusively restricted to the ORV trails. The difference in dust emission potential between ORV trails and undisturbed terrain is studied in Chapter 4 of this report.

2. The ORV experiment: procedure

2.1 Vehicle types tested

Three types of vehicle were tested in the experiment: the four-wheeler (quad), the dune buggy, and the dirt bike (motorcycle). These vehicles are by far the most commonly used ORV vehicles in the Nellis Dunes Recreation Area; observations during the numerous visits to the site during the project indicated that they should represent nearly 99% of all off-road vehicles driving in the area. Fig. 1 shows a photograph of each vehicle. All vehicles used in the test were equipped with standard type tires. Tire tread was not considered as a parameter in this study.

2.2 Locations

Experiments were performed on 16 of the 17 surface types occurring in the Nellis Dunes area. Surface type 3.5 (bedrock) was not tested because (1) these surfaces contain negligible emittable dust, and (2) in NDRA there is almost no driving on this unit because these surfaces are too rough to be driven and are also usually located on very steep slopes. It is safe to state that, at least in NDRA, the 3.5 units produce negligible ORV-generated dust.

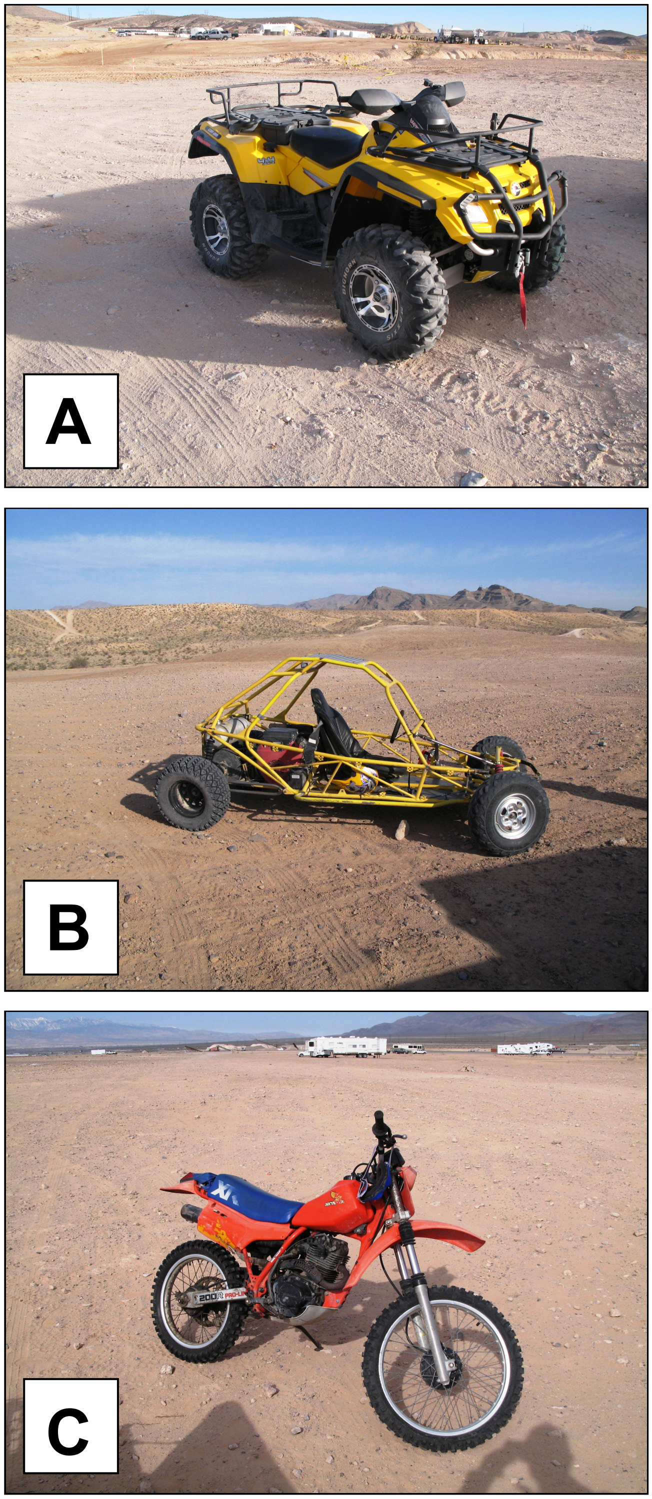

Fig. 1: The three vehicle types tested. A: 4-wheeler (quad); B: dune buggy; C: dirt bike (motorcycle)

Much attention was paid to seeking adequate experimental locations, to ensure reliable as well as representative data. A track long enough to attain high speeds was selected on each surface unit. For safety reasons, and also to ensure homogeneous emissions near the measurement spot, only straight sections without curves were selected. Fig. 2 shows the locations of the sites.

All experiments were performed on dry soils. Moisture content was always very close to zero: relative humidity in the region is extremely low, evaporation rates very high, and no rains occurred during at least 3 weeks prior to the measurements.

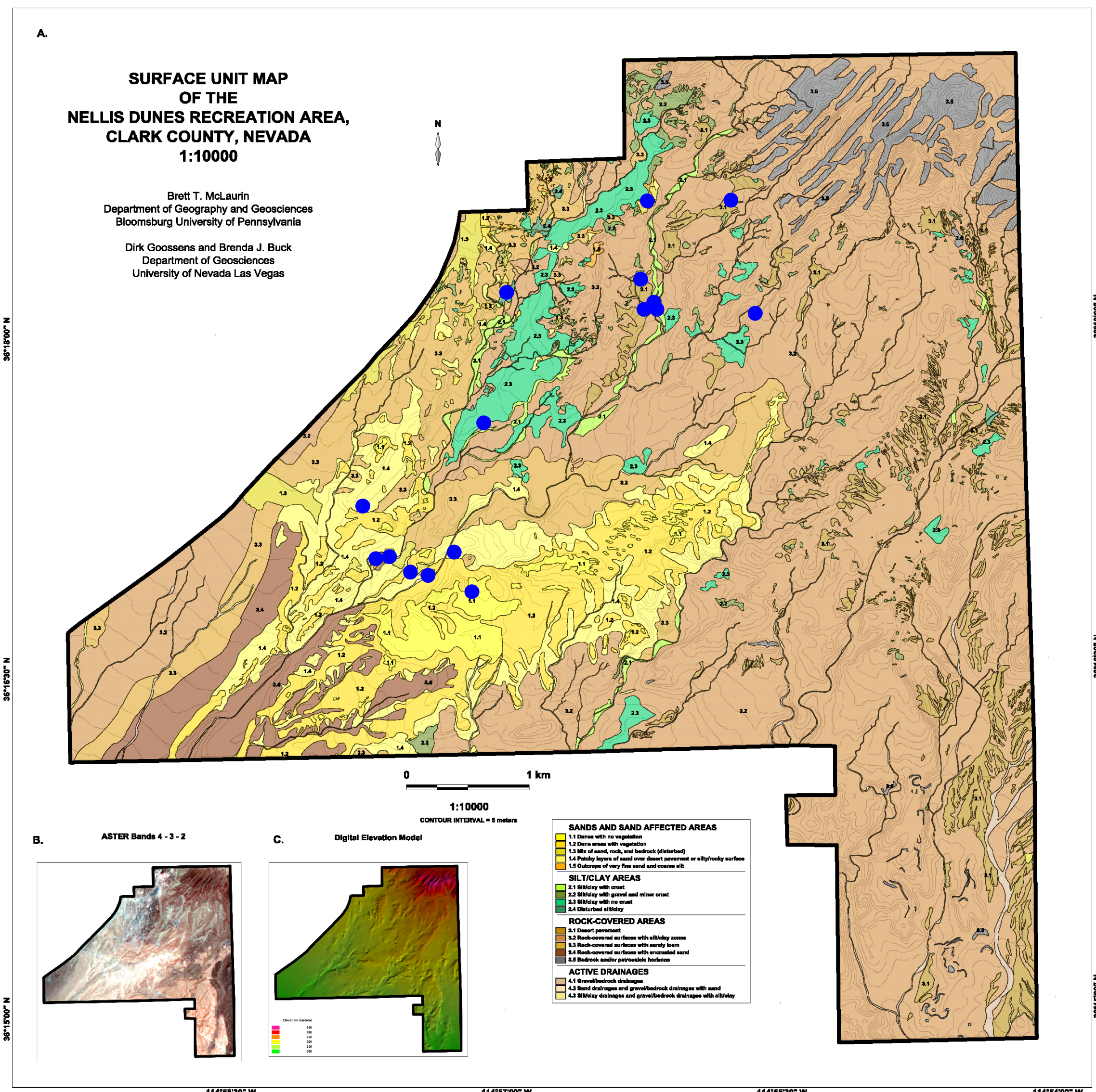

Fig. 2: Location of the ORV-experiment sites (blue dots)

2.3 Field procedure

Big Spring Number Eight (BSNE) samplers (Fryrear 1986; see Fig. 3) were used to collect the dust. We used BSNE samplers because of their relatively large inlet area (10 cm^2), and also because efficiency of the BSNE is known for various grain size fractions (Goossens and Offer, 2000; Goossens et al., 2000; Sharratt et al., 2007). All data were corrected for the efficiency of the traps.

Fig. 3: Pole with four Big Spring Number Eight (BSNE) samplers

Two vertical poles with 4 BSNEs each were erected 1.5 m from the centre line of the track (Fig. 4). BSNEs were installed at the following heights: 0.25 m, 0.50 m, 0.75 m and 1.00 m. Drivers were asked to drive at approximately 1 m from the poles. Observations during the runs revealed that the height of the dust cloud was always between 1.0 and 1.5 m near the poles; dust clouds were thus adequately sampled during the experiment.

Fig. 4: Photo of the set-up of dust poles and dust traps during a dirt bike run

Measurements were done on days when the wind blew perpendicular to the road. During 95% of the runs the two poles were installed on the same side of the road to ensure adequate collection. A few cases occurred where the wind speed was so low that the dust was emitted to both sides of the road; if that happened one of the poles was put on the other side of the road, or if that was not possible, the amounts of dust recorded by the traps were doubled. Careful observations were made of the wind during each run to determine the correction, and all results were later corrected for low wind speed conditions (but this was only necessary for a few tests).

Dirt bikes are normally being driven at higher speeds than 4-wheelers and dune buggies. To ensure representative results it was decided to select the driving speeds according to the type of vehicle. Three speeds were selected for each vehicle at each location, and although the drivers were able to drive with the same speeds on most locations there were a few cases where they had to drive somewhat slower for safety reasons. A portable electronic Schwinn speedometer (Pacific Cycle Inc., Madison, WI, USA) was attached to each vehicle to measure the exact speed during each run. For the dirt bike the speeds averaged 32, 43 and 56 km h^{-1}; for the 4-wheeler: 28, 36 and 48 km h^{-1}; and for the dune buggy: 24, 32 and 40 km h^{-1}.

Between 22 and 30 runs were made for each combination of driving speed, vehicle and surface type. Altogether 3684 runs were made, 144 experiments in total. For safety reasons (very rough and mountainous terrain), and also because of the absence of loose sediment on the surface, no measurements were carried out on surface unit 3.5 (bedrock), as stated earlier. This does not really pose a problem for this study because the emission will be virtually equal to zero on these surfaces.

After each experiment clean BSNEs were installed on the poles. Used BSNEs were immediately stored in a closed box to prevent subsequent contamination of the traps.

2.4 Laboratory procedure

After each field test all BSNEs were taken to a closed laboratory for dust collection. Samples were collected with a brush, and with great care to not affect the grain size distribution. All samples were weighed with an analytical Ohaus Explorer balance (Ohaus Corporation, Pine Brook, NJ, USA). Precision of the measurements was 0.0001 g.

To determine the proportion of individual grain size fractions all samples were analyzed with a Malvern Mastersizer 2000 grain size analyzer (Malvern Instruments Ltd., Malvern, UK). Emissions were calculated for grain size fractions between 2.5 µm and 100 µm. No calculations were made for particles >100 µm since, in the current study, we are only interested in the emission of suspendable particles.

2.5 Calculation of the emission

Two possibilities exist to calculate the emission. The most common procedure is to calculate the emission as a flux, i.e. mass of sediment emitted per unit surface and per unit time (expressed in, for example, kg m^{-2} s^{-1}). However, in the case of off-road driving this option is not very useful because the area of road surface prone to emission depends on the number of wheels of the vehicle, the width of the wheels, and the surface structure of the wheels and the road: only where the wheels effectively touch the road direct emission will occur. Additionally, the problem is more complex because the intersurfaces can also experience emission due to the turbulence created by the driving vehicle. This makes it difficult to determine the exact size of the emission surface and, thus, of the emission flux. A much better option for off-road driving is to calculate the emission in terms of emitted mass per unit length (for example, kg of dust emitted per driven km). If the total length of a run is known, the total mass of dust emitted during that run can be calculated. Of course, for adequate estimations the emission rates should be known for various driving speeds, and information is needed on the speed (and its variation) during a run.

In this study emission is presented as emitted mass per unit length. The calculation procedure is as follows:

First, the amount of dust passing through the dust cloud is calculated at the height of each trap. By dividing the mass of dust caught by a trap through the trap's inlet area (10 cm^2 for a BSNE), and after correction for the trap's efficiency, the total transport (in g cm^{-2}) at each trap height is calculated. Next, the total mass transported through a vertical strip 1 cm wide and parallel to the road is calculated by vertically integrating the dust profile from the road surface (i.e., at zero height) to the top of the cloud. In the case of aeolian transport of particles <100 μm the horizontal transport flux (*Fh*) usually decays with height (z) according to the function $Fh = az^b$, where coefficient a and exponent b are determined empirically (Buschiazzo and Zobeck, 2005). The vertical transport profile in the dust cloud during the Nellis Dunes experiments showed a similar decay for all experiments. However, for mathematical reasons no calculations of the profile down to $z = 0$ are possible when the power function above is used. Therefore the profile was described with a 4th order polynomial (for several experiments a 3rd order polynomial already gave an optimum fit). All curve fittings were carefully inspected in a graph before calculating any transport to ensure adequate fits.

The result of the calculation is the mass of dust transported through a 1-cm wide strip parallel to the road and with a height equal to the height of the cloud (very close to 1.5 m at the location of the poles in almost all experiments). Since there is no dust above the upper edge of the cloud, this corresponds to the total mass of dust emitted per unit length driven by the vehicle.

3. The ORV experiment: results

3.1 PM10 emissions

For each combination of vehicle and surface type emission data are available for 4 speeds: the 3 speeds tested during the experiments and zero emission at zero driving speed (recall that no wind erosion occurred during the measurements). Since the emission progressively increased with the driving speed, speed-emission curves could be constructed for all experiments. Fig. 5 shows the curves for the 51 combinations of vehicle and surface type for PM10. In order to not overload the graphs and keep the pictures readable the individual data points are not shown, but it should be emphasized that they are very close to the curves shown. For example, for the 4-wheeler graph (upper graph in Fig. 5) the correlation coefficient R is >0.95 for 16 of the 17 curves (even >0.98 for 14 of the curves), and its lowest value is still 0.89 (surface unit 1.2). The other graphs show similar correlations.

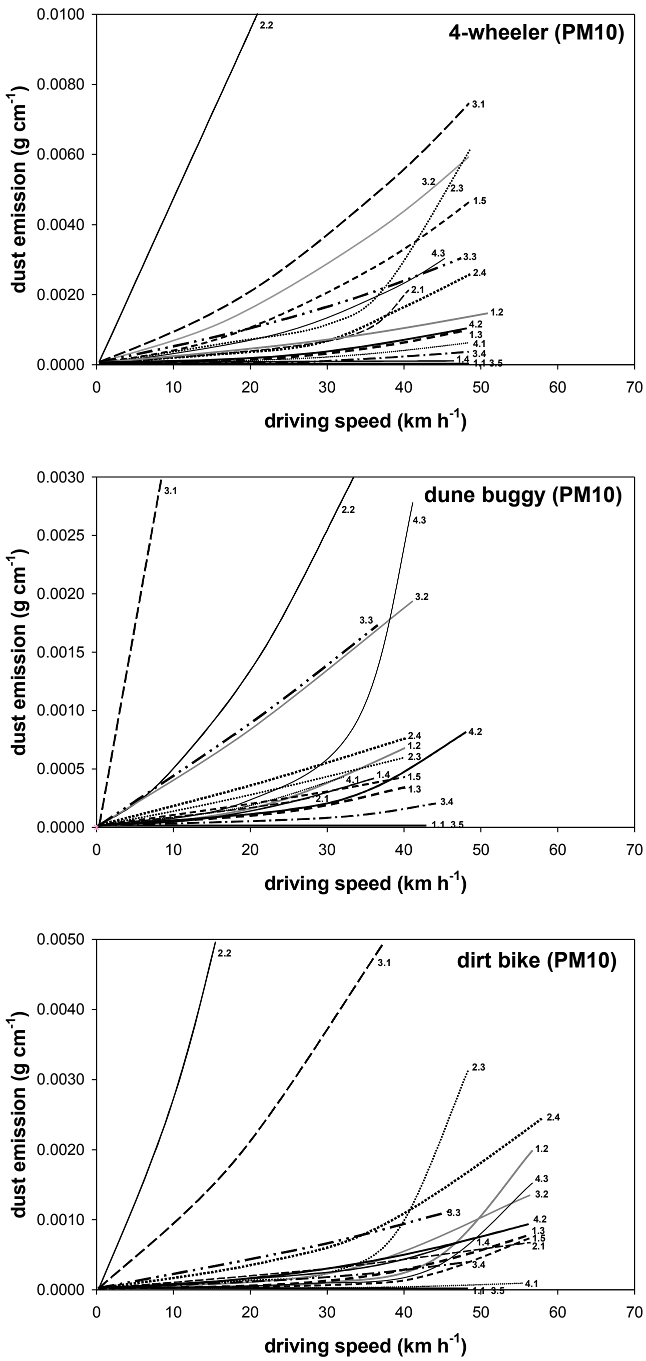

Fig. 5: Basic emission curves for PM10

Although the shape and position of individual curves vary with vehicle and surface type the general trends in the figure are evident: highest emissions were always measured on surface units 2.2 (silt/clay with gravel) and 3.1 (desert pavements) whereas lowest emissions occurred on the uncrusted (or only weakly crusted) sandy surfaces (1.1, 1.2, 1.3, 1.4, 3.4) and the gravel and bedrock surfaces (3.5, 4.1). The thin surficial stone layer of the desert pavements (3.1) did not provide much protection against off-road driving. The silty surfaces (except 2.2 and 3.1) showed intermediate emission values.

To facilitate interpretations the data of Fig. 5 are replotted in Fig. 6, for the silty and sandy surfaces separately and also for the ensemble of all surface units. In addition, the emission values were calculated for identical driving speeds for all vehicles. Interpolation was used to calculate the emission at each particular speed. No data are shown for the dune buggy at driving speeds >40 km h^{-1} because the dune buggy was unable to reach such speeds during the experiments.

Fig. 6 shows that, on average, PM10 emission increased exponentially with the driving speed. As could be expected, the silty surfaces produced much more dust than the sandy surfaces. Also, emission varied considerably with the type of vehicle. Most PM10 was emitted by the 4-wheeler whereas, on average, the dune buggy and the dirt bike emitted almost equal amounts of PM10 despite the fact that the dune buggy has twice as many wheels than the dirt bike.

Fig. 7 shows the speed-emission curves for the 17 surface units separately. Although it is relatively easy to recognize the general trend (highest emission: 4-wheeler; intermediate emission: dune buggy; lowest emission: dirt bike) substantial differences occur for individual surface units, both with respect to the relative order of the vehicles and the rate of increase of emission with driving speed. These differences do not appear to be systematically related to a specific type of surface or vehicle but may occur anywhere in the data set (see Fig. 7), which makes it difficult to interpret.

In Fig. 8 the data of Fig. 7 are replotted for the silty and sandy surfaces separately, and also for the ensemble of all surface units. Similar to Fig. 6 the data were recalculated to identical driving speeds to facilitate comparisons. The general trend is clear: most PM10 was emitted by the 4-wheeler, at all driving speeds. On average the dune buggy produced slightly more PM10 than the dirt bike, but from a driving speed of around 35 km h^{-1} the dirt bike seems to produce more PM10 than the dune buggy. This increased production is only discernable on silty surfaces; it does not seem to occur on sandy surfaces.

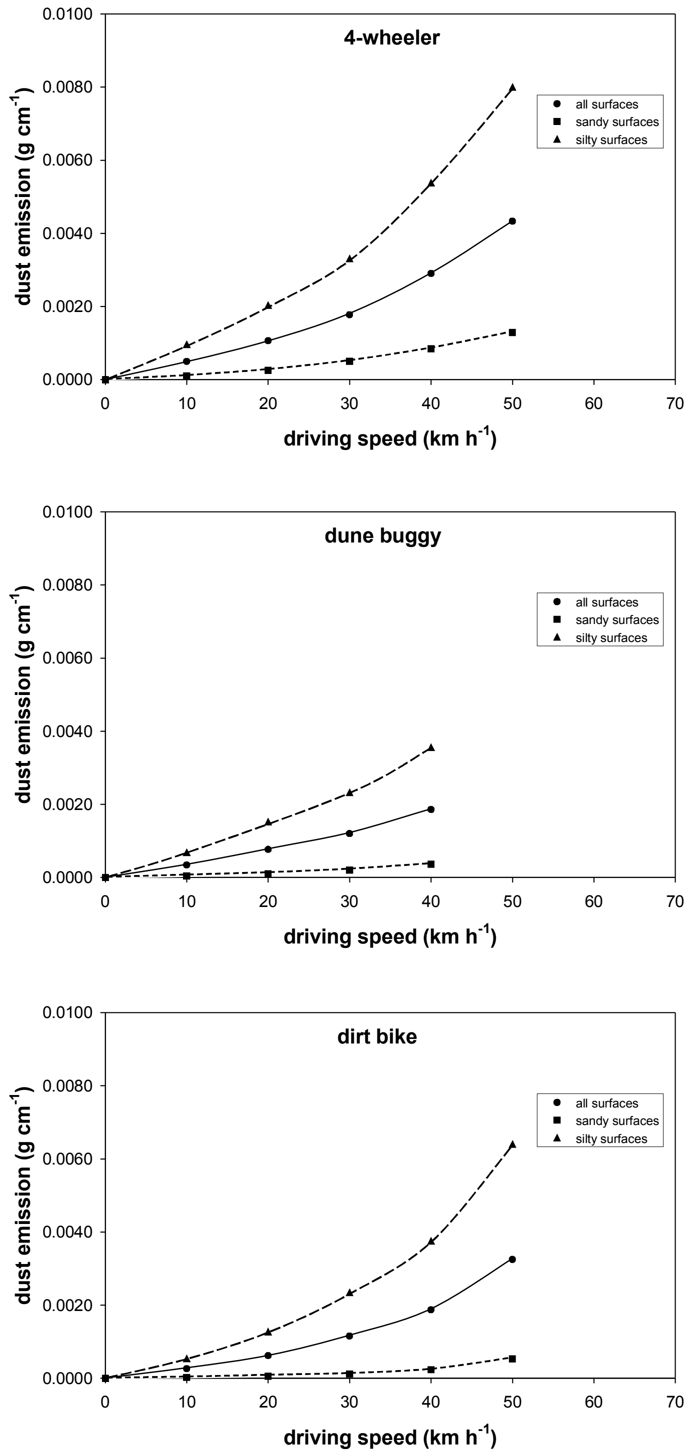

Fig. 6: PM10 emission curves, grouped for the major surface classes

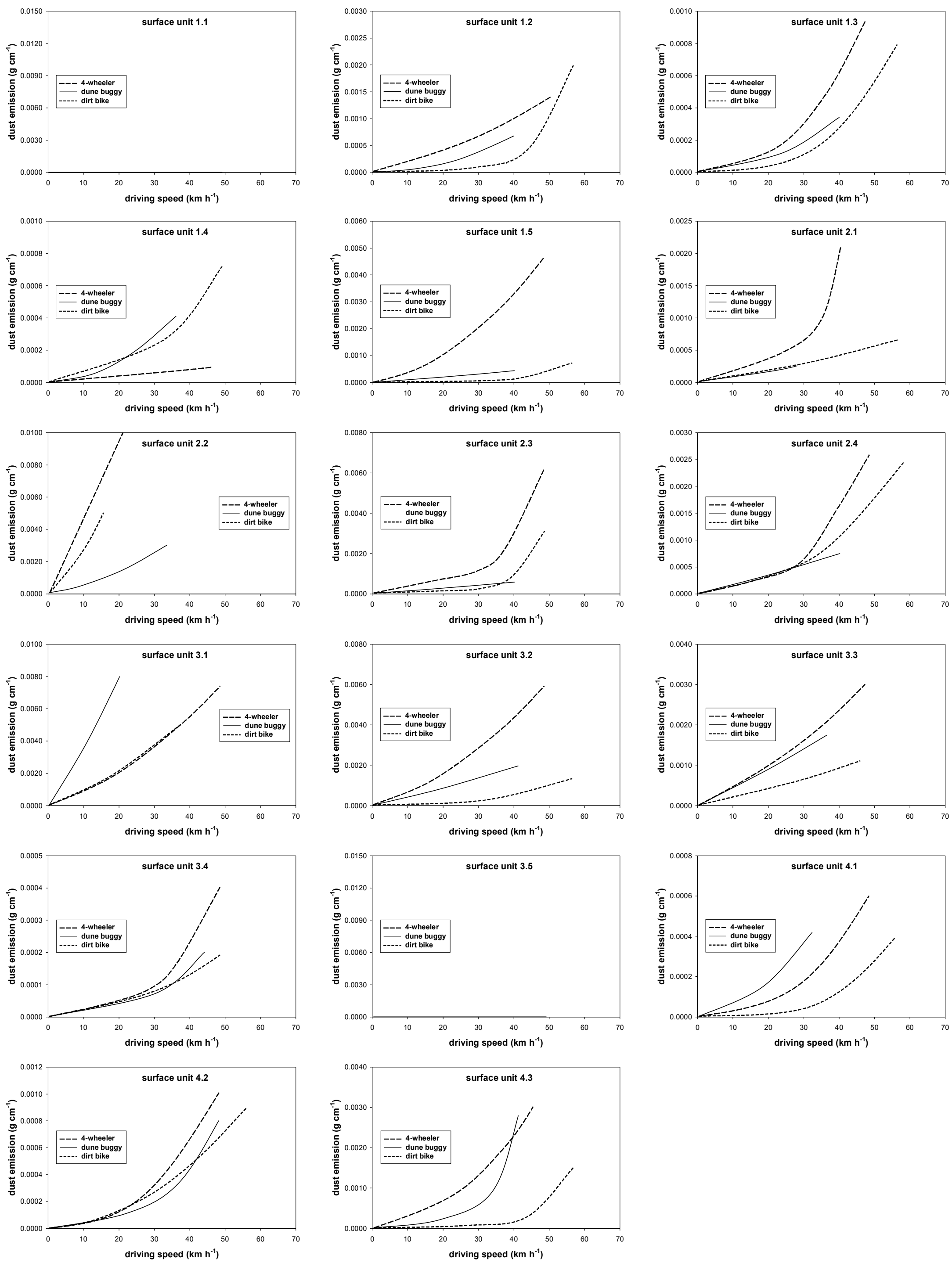

Fig. 7: PM10 emission curves for the individual surface types

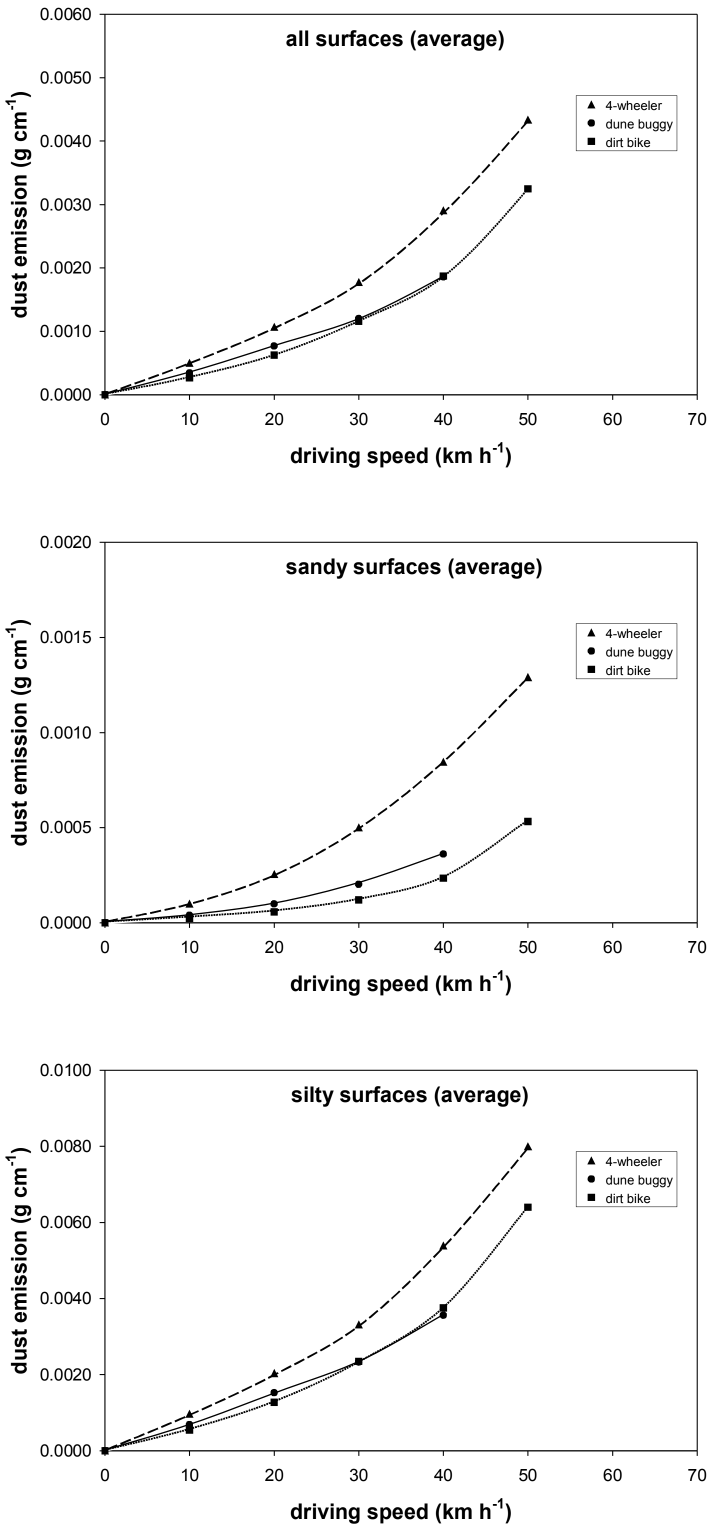

Fig. 8: PM10 emission curves, grouped for the 3 vehicles tested

3.2 TSP emissions

Fig. 9 shows the speed-emission curves for all 51 combinations of vehicle and surface type, for the fraction <60 µm (defined in this study as TSP, or total suspendable particles). We used the 60-µm limit as a cut-off for TSP because it corresponds to the maximum size of those grains that will still be transported in short-term suspension during average conditions of wind speed and turbulence (Pye and Tsoar, 1990). It also nearly coincides with the upper diameter of silt (52 µm or 63 µm, depending on which criterion is used).

The general trends already observed in Fig. 5 also appear in Fig. 9: most dust was produced by surface units 2.2 (silt/clay with gravel) and 3.1 (desert pavements) whereas the sandy surfaces produced the least amounts of dust. Differences between the PM10 and TSP patterns exist for various surface units: a striking example are the 4.3 surfaces (silty drainages), which proportionally emit much more TSP than PM10. Less significant differences can be detected for several other surface units.

Averaging the data for the two major surface groups (silty and sandy surfaces) leads to TSP patterns that are similar to those for PM10 (Fig. 10). Not surprisingly silty surfaces produce much more TSP than sandy surfaces, for all 3 vehicles tested.

Plotting the speed-emission curves for individual surface units shows similar patterns as for PM10 (Fig. 11, and compare to Fig. 7). Differences do occur: examples are the dune buggy on surface unit 3.3 (rock-covered surfaces with sandy loam), and the 4-wheeler on surface unit 3.4 (rock-covered surfaces with encrusted sand). Also here, differences in the mutual behavior of the vehicles do not seem to be systematically correlated to surface type, as for PM10.

Replotting the data for the silt and sand classes (Fig. 12) leads to similar conclusions as for PM10. Most dust is produced by the 4-wheeler whereas, on average for all surface types, the dune buggy and the dirt bike produce almost equal amounts of dust. However, on sandy surfaces the dune buggy proportionally emits much more TSP than PM10 compared to the other vehicles. No such trend was found for the silty surfaces.

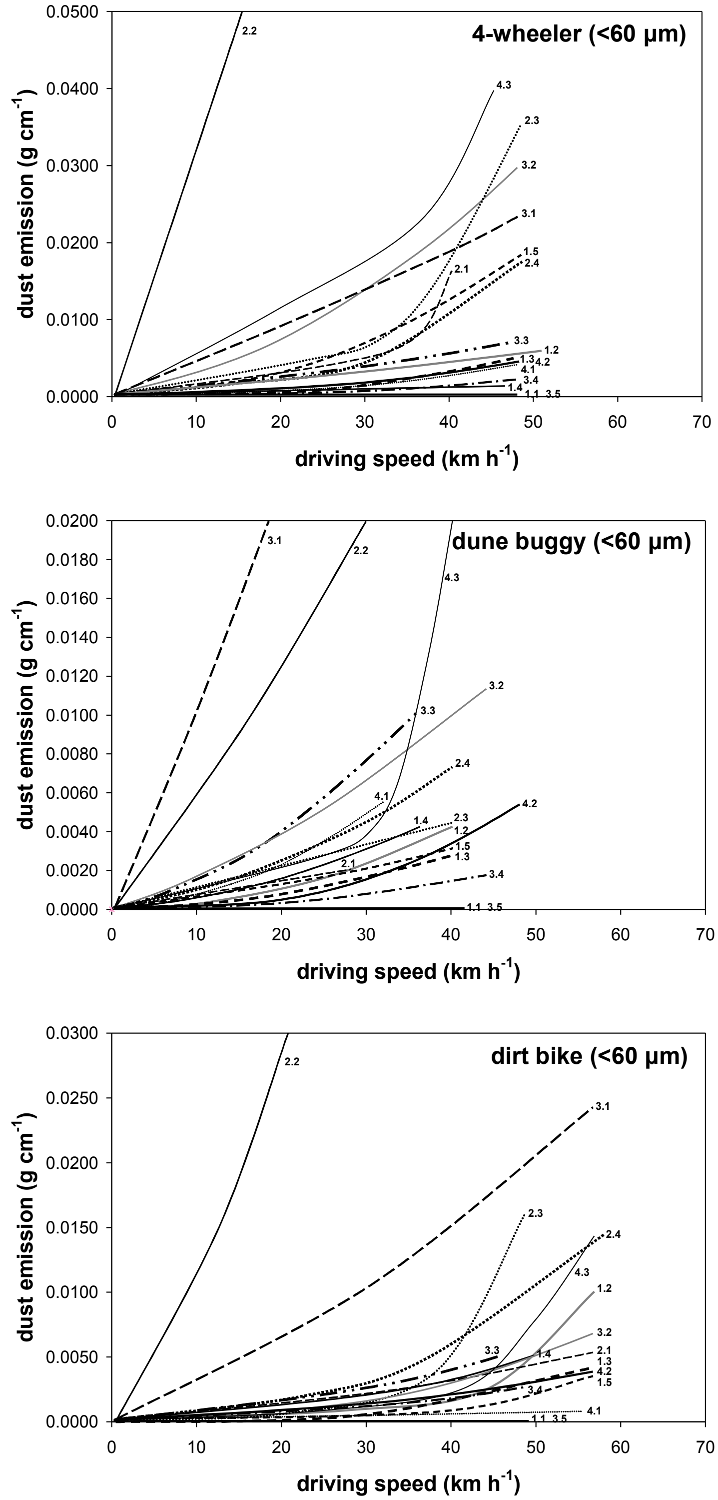

Fig. 9: Basic emission curves for TSP

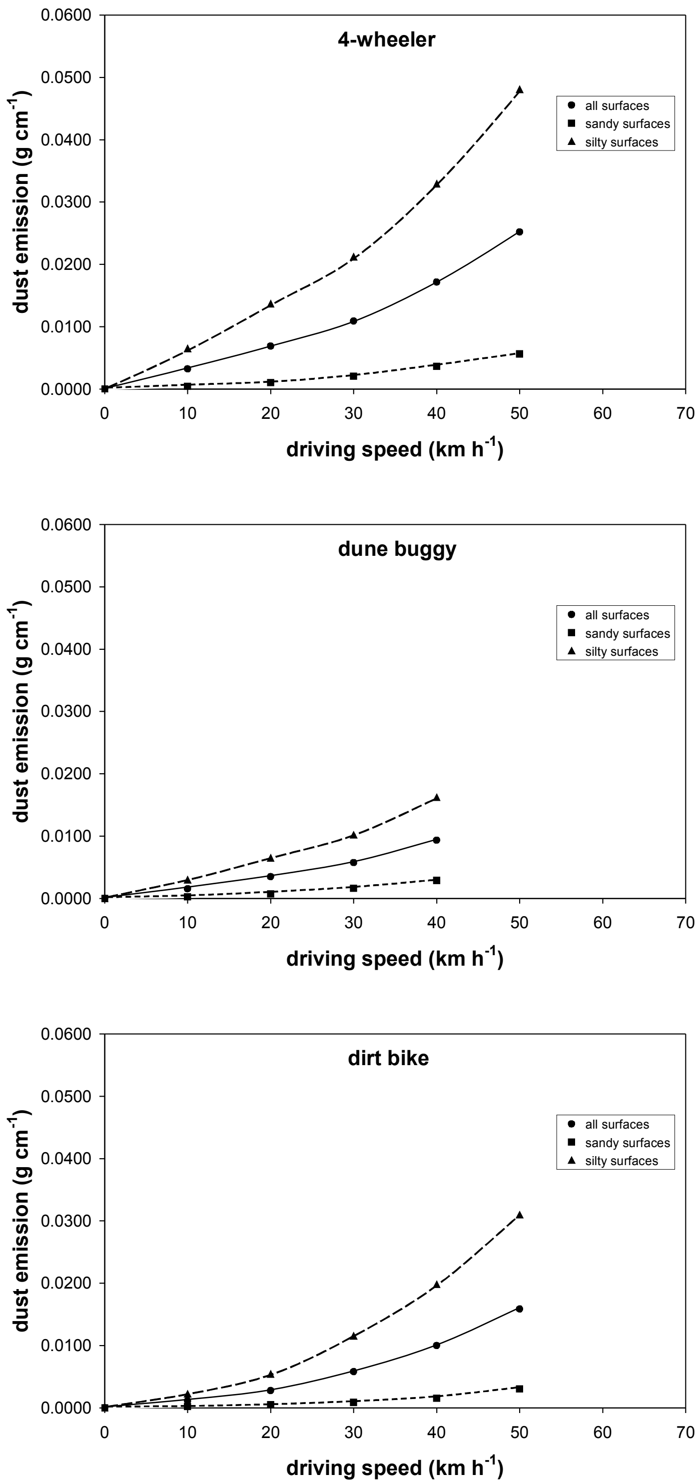

Fig. 10: TSP emission curves, grouped for the major surface classes

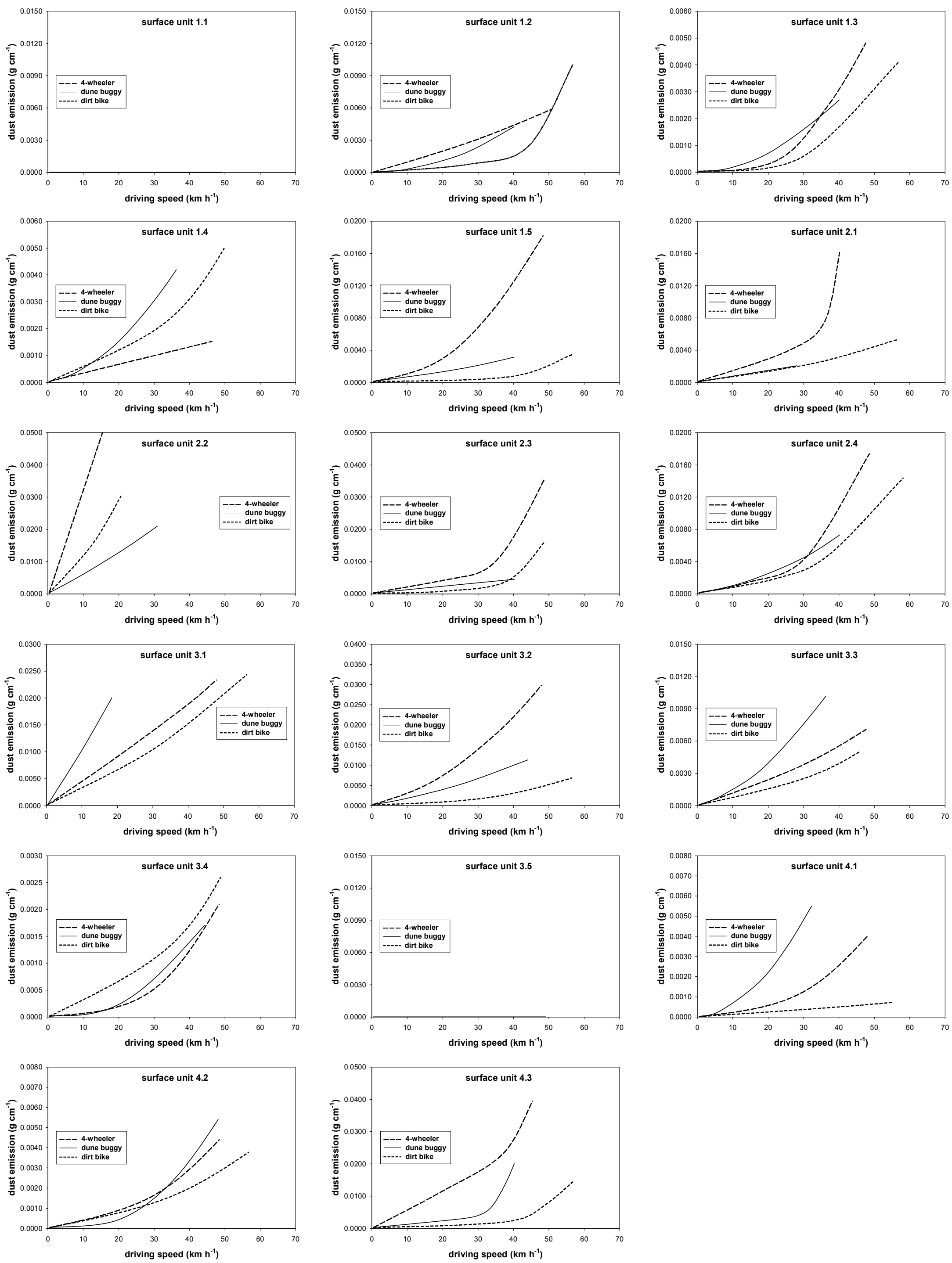

Fig. 11: TSP emission curves for the individual surface types

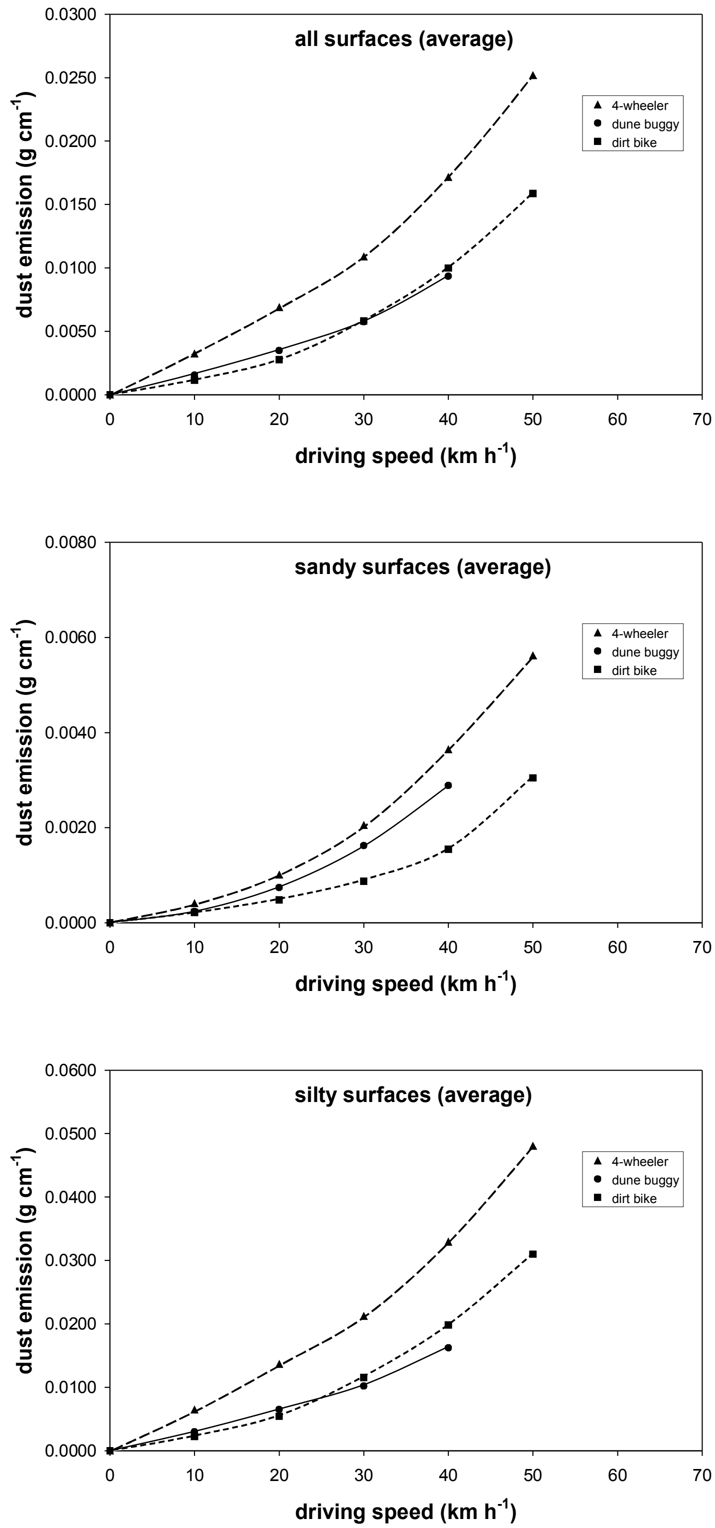

Fig. 12: TSP emission curves, grouped for the 3 vehicles tested

3.3 Discussion

The data show that the amount of dust emitted by off-road vehicles strongly varies depending on which type of vehicle is driving with what speed over what type of surface. This is quite understandable if we consider how the emissions are produced. Most unpaved roads consist of a graded and compacted roadbed usually created from the parent soil material (Gillies et al., 2005). The rolling wheels of the vehicle impart a force to the surface that pulverizes the roadbed material and ejects particles from the shearing force as well as by the turbulent vehicle waves (Nicholson et al., 1989). Previous studies have shown that the emission rate primarily depends on the vehicle speed (Nicholson et al., 1989; Etyemezian et al., 2003a, 2003b), the fine particle content of the road (Cowherd et al., 1990; MRI, 2001), the vehicle weight (US EPA, 1996, 2003; MRI, 2001), and the soil moisture content (Gillies et al., 2005). This is reflected by the 1995 US EPA AP-42 guidance document, where the emission is quantified as

$$EF = 0.161 \cdot s \cdot S \cdot W^{0.7} \cdot w^{0.5} \cdot \left(\frac{365 - p}{365} \right)$$

where EF is the emission factor (g/vehicle kilometer traveled), s the silt content of the road material (%), S the vehicle speed (m s^{-1}), W the weight of the vehicle (Mg), w the number of wheels, and p the number of days per year with measurable precipitation (>0.25 mm). However, later versions (US EPA, 1999) no longer included the vehicle speed as a parameter in estimating emission factors for unpaved roads (Etyemezian et al., 2003b).

Vehicle speed *is* an important parameter, however, as is clearly demonstrated by the Nellis Dunes experiment. In most cases (combinations of vehicle type and surface unit) the increase of emission with vehicle speed was exponential, similar to what has been found in other studies (e.g. Hussein et al., 2008; Etyemezian et al., 2003b). In a few cases the relationship was linear, as suggested by the US EPA (1995) formula. Linear relationships have also been reported by Gillies et al. (2005) and Hussein et al. (2008). The Nellis Dunes experiment did not show correlations between the type of increase (linear or exponential) and the surface or vehicle type.

The effects of wheel and tire parameters (such as wheel diameter, wheel width and tire tread) on dust emission have not yet been adequately quantified and these parameters do not appear in the emission equations currently in use. This study did not consider these parameters, but all vehicles used were equipped with standard-sized wheels and tires.

The large number of surface types tested in this study permit checking of the proposed relationship between emission and silt content of the road material. Samples were taken from the roads at the same locations where the emissions had been measured. The silt content (<60 µm) was determined with the Malvern Mastersizer 2000 instrument after the non-erodible fractions (>500 µm) had been removed by sieving. Plotting the emission (TSP) as a function of the silt percentage a more or less linear relationship is observed (Fig. 13), but there is considerable spread in the data. This is reflected by the coefficient of determination R^2, which, for the data in Fig. 13, equals only 0.43. The data in Fig. 13 are for the average driving speeds of the distinct vehicles. Looking at the R^2 values for individual speeds we find that the relationship between TSP emission and the silt content of the road becomes better as the driving speed increases. The R^2 values are: 0.27 (10 km h^{-1}), 0.30 (20 km h^{-1}), 0.34 (30 km h^{-1}), and 0.47 (40 km h^{-1}). No R^2 could be calculated for a speed of 50 km h^{-1} because the dune buggy was unable to attain this speed over the surface types tested. Therefore, driving speed is a crucial parameter in off-road driving and formulae calculating the emission *must* include it.

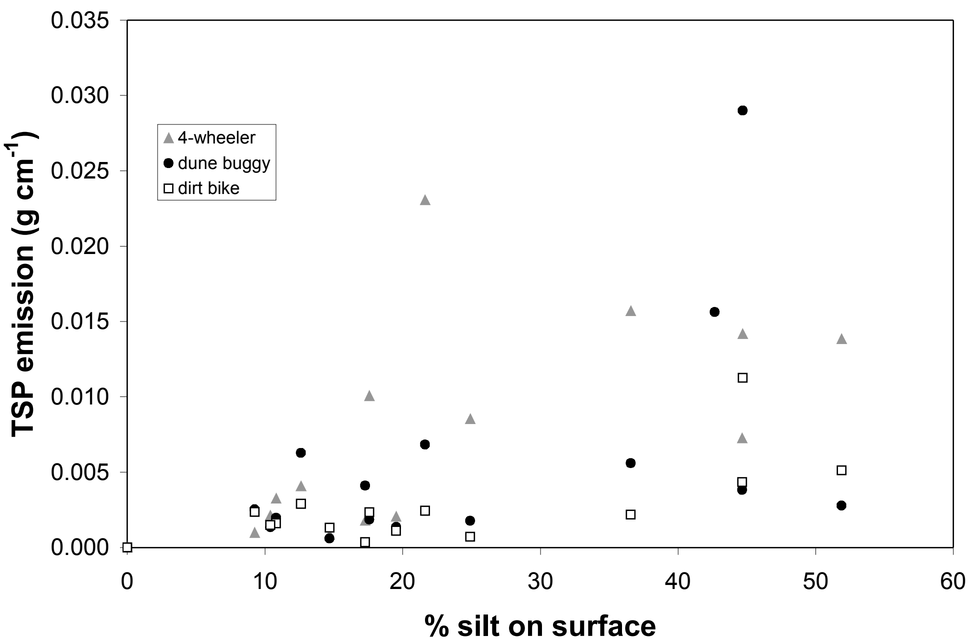

Fig. 13: Relationship between TSP emission rate and silt content of the road surface. Data points of the 4-wheeler and dirt bike for surface unit 2.2 are out of the vertical range and do not appear in the picture.

The proportion of PM10 in the emitted TSP does not seem to vary with the driving speed, regardless of which soil class (silt or sand) or vehicle type is considered (Fig. 14). The graphs on the left of Fig. 14 also show that the proportion of PM10 in the total dust production is almost identical for the dune buggy and the dirt bike. This is unlike the 4-wheeler, for which the dust emitted contains a greater proportion of PM10 compared to the two other vehicles when driving over sandy surfaces, but a lower proportion of PM10 when driving over silty surfaces. As an average for *all* surfaces tested the proportion of PM10 in dust emitted by a 4-wheeler is slightly lower than in dust emitted by a dune buggy or a dirt bike. A replot of the data for each distinct vehicle (Fig. 14, right) leads to the same conclusions. In general, for the surface units tested in the Nellis Dunes experiment the proportion of PM10 in the TSP is between 15 and 25%, slightly varying with vehicle and surface type, but not with driving speed.

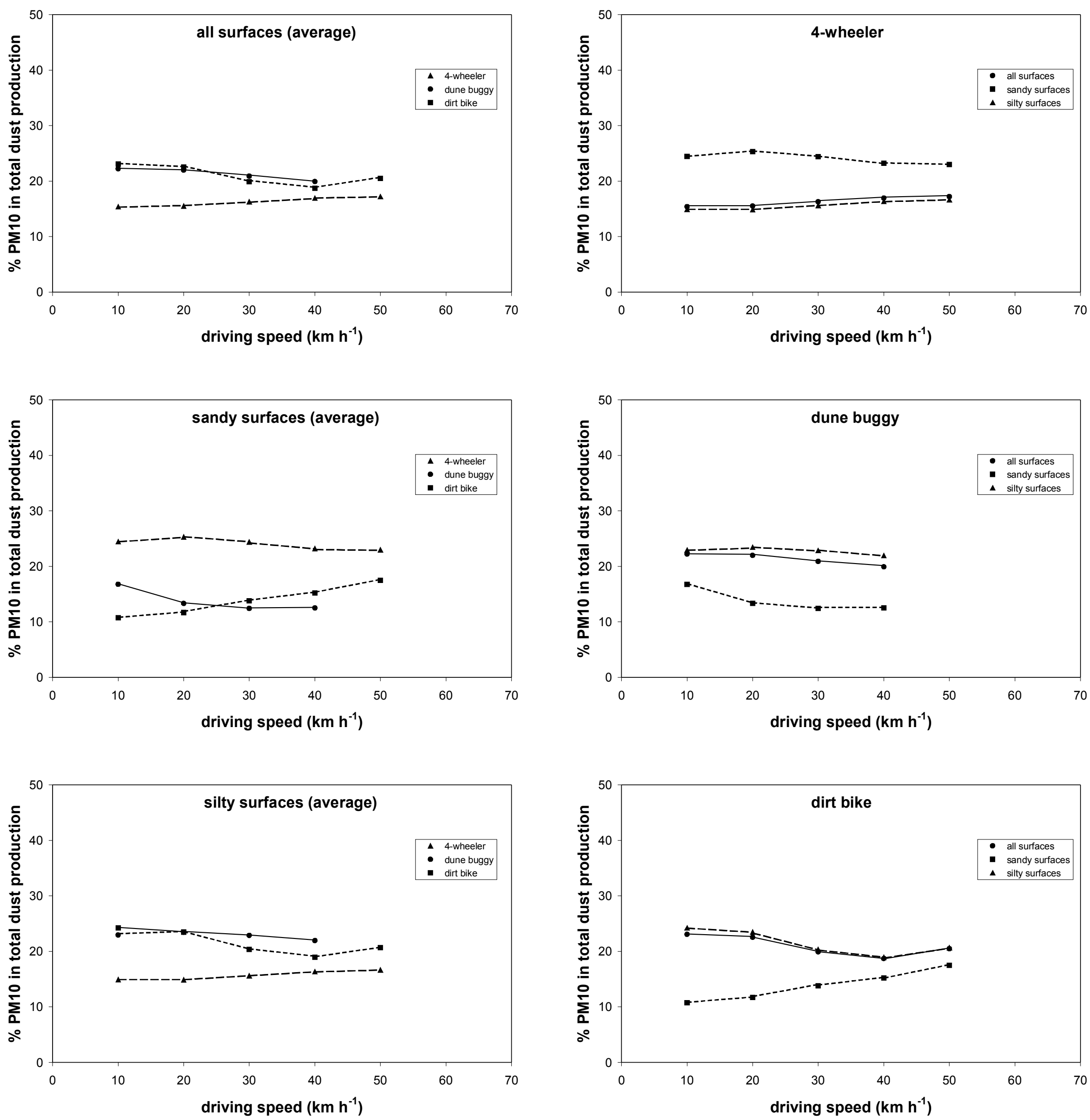

Fig. 14: Proportion of PM10 in TSP

Fig. 15 shows the (average) median grain diameter (*D50)* of the emitted dust. As mentioned earlier, for safety and practical reasons it was not possible to drive with the same speeds over all surface units. Therefore, to be able to calculate average curves (such as in Fig. 15) the raw *D50* data were first plotted in a graph to check how *D50* varied with the driving speed. This was done for all surface units, and for all 3 vehicles. The data showed that *D50* did not vary substantially with the driving speed, and for those cases where a (slight) relationship was observed the relationship was almost linear. To reconstruct the *D50* for standard speeds (3 for each vehicle, see Fig. 15) we thus used linear interpolation (or, in a few cases, extrapolation).

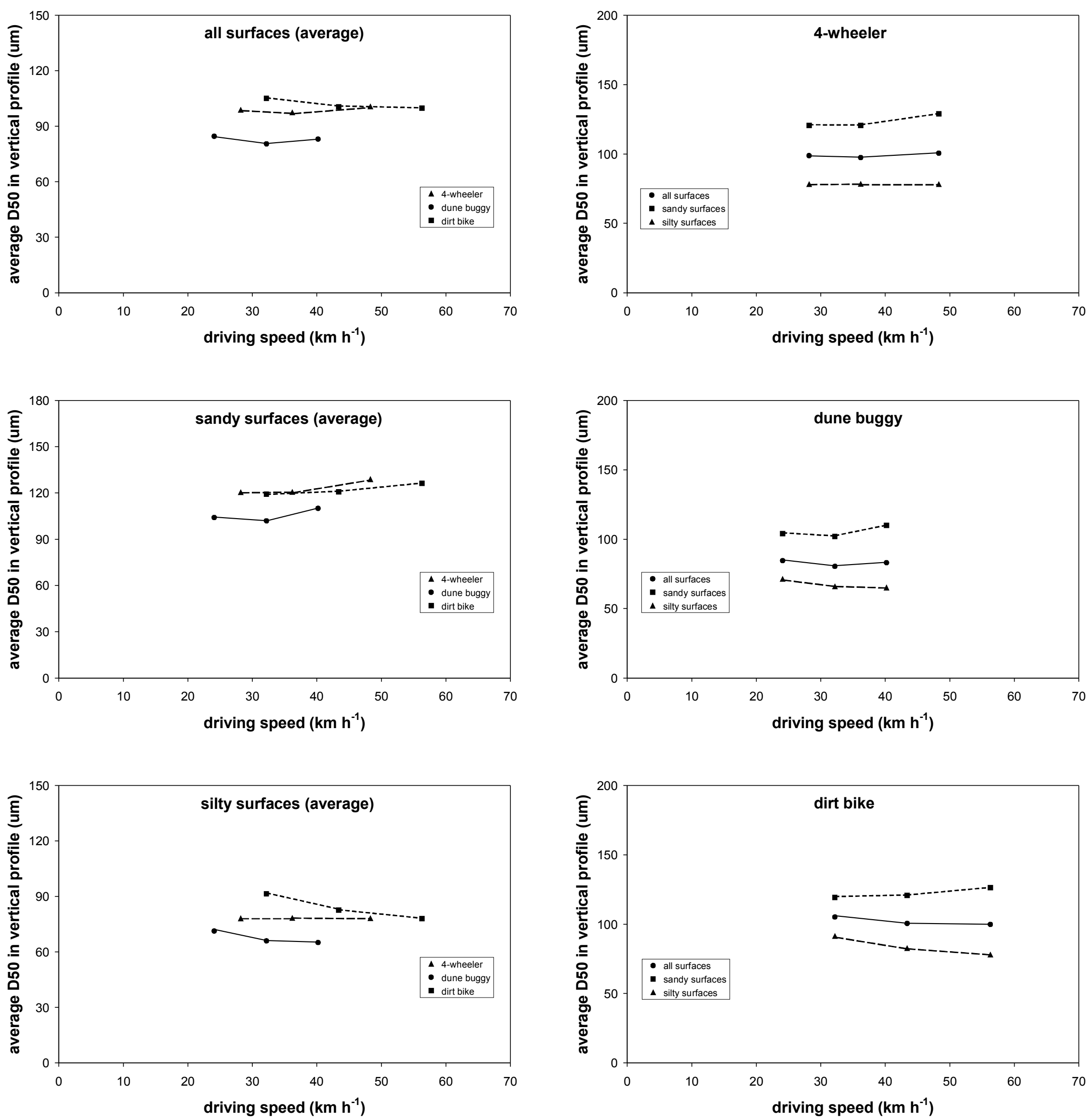

Fig. 15: Average median grain diameter (D50) of emitted dust as a function of driving speed

From this data, two conclusions can be derived. First, the average median grain diameter in the dust cloud remains almost constant as a function of the driving speed. A slight increase in grain size (coarser dust) with speed occurs for sand surfaces, but for silt surfaces a slight decrease in grain size occurs (Fig. 15, left). Secondly, the dust emitted by a dune buggy is finer than that emitted by a 4-wheeler or a dirt bike regardless over which class of soil (sand or silt) the vehicle is driving. The 4-wheeler and dirt bike emit dust with nearly the same grain size. Replotting the data for the distinct vehicles (Fig. 15, right) shows these relationships.

Continuous off-road driving in a trail leads to a progressive coarsening of the top layer in the trail. Fig. 16 compares the average grain size (represented by the median grain diameter, D_{50}) of sediment emitted during off-road driving to that of the topsoil in the trail. The figure shows that except for the aggregated silt deposits (unit 2.3), the sediment in the trails is consistently coarser than the one emitted (which means that the trails become coarser with time). Also, the speed of coarsening is a clear function of the type of surface. Trails in drainages coarsen the most rapidly, and trails on sandy surfaces coarsen faster than trails on silty surfaces (see Fig. 16). Note that surface unit 2.3 is composed primarily of silt aggregates up to >5 mm in diameter, which are pulverized during off-road driving. Therefore, a value above unity in Fig. 16 is normal.

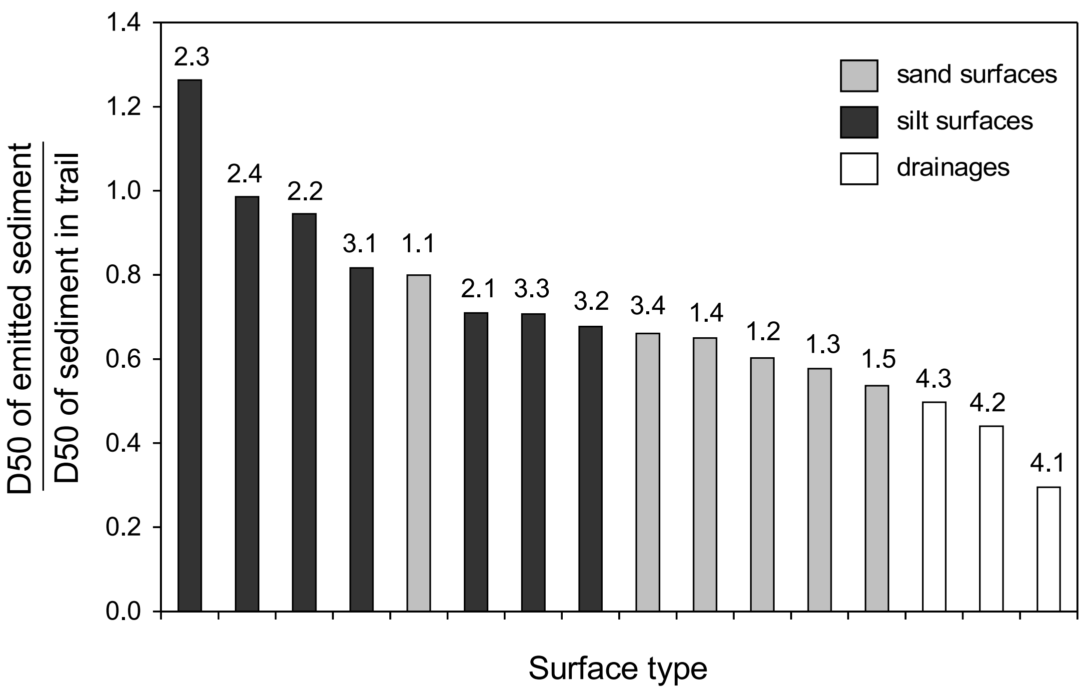

Fig. 16: Ratio of median grain diameter (D50) in ORV-emitted sediment to the median grain diameter in the trail, for the various surface units investigated

Table 1: Proportion of PM10 in emitted dust compared to the parent sediment (average for all vehicle types and driving speeds tested)

surface unit	PM10 content in total sediment (%)		PM10 in emitted sediment / PM10 on road surface
	road surface	emitted sediment	
1.1	0.00	0.00	NA
1.2	4.23	2.32	0.55
1.3	5.92	2.78	0.47
1.4	3.72	1.77	0.48
1.5	7.64	6.76	0.88
2.1	4.78	3.41	0.71
2.2	11.05	6.12	0.55
2.3	13.08	6.63	0.51
2.4	8.27	6.39	0.77
3.1	24.45	8.67	0.35
3.2	14.37	7.61	0.53
3.3	6.46	4.03	0.62
3.4	5.04	2.56	0.51
3.5	NA	NA	NA
4.1	5.51	3.62	0.66
4.2	4.04	3.68	0.91
4.3	5.17	3.49	0.67
		average (= E-factor):	*0.57*

Columns 2 and 3 in Table 1 show the PM10 content on the road and in the emitted dust, respectively. As could be expected, roads with higher PM10 produce PM10-rich dust. However, the PM10 content is always lower in the emitted dust compared to the parent soil (see right column in Table 1). The average value for all surface units (called in this study the E-factor, see Table 1) is only 0.57, or 57%. Therefore, off-road driving emits PM10 less efficiently than it emits the coarser fractions.

The Nellis Dunes data allow one to check for which grain size fraction(s) emission is most efficient. Calculating the E-factor for various grain size classes and displaying the results in a histogram (Fig. 17) we see that emission due to off-road driving is most efficient at a grain size of approximately 60 µm. This value is only slightly smaller than that for wind erosion, which is situated around 80 µm (Bagnold, 1941; Horikawa and Shen, 1960; Iversen and White, 1982). The E-factor drops below unity from a grain size of approximately 25 µm – i.e. for grains <25 µm the emission process is not very efficient

(Fig. 17). Particle and interparticle forces (cohesion and adhesion) hamper the removal of the grains from the road surface.

It should be recalled that all numbers given above were derived for air-dry surfaces; for moist surfaces they will be substantially higher.

4. ORV scenarios for Nellis Dunes Recreation Area

Several scenarios were investigated to study how emissions change when vehicles perform realistic drives over the various surface units occurring in the Nellis Dunes Recreation Area. These scenarios do net yet intend to calculate the real amounts of emission effectively produced in the NDRA. Instead, they aim to check how the composition of a run (proportion of surface units within a run) affects the emissions. The real amounts of ORV dust produced annually in the NDRA are studied in Chapter 6.

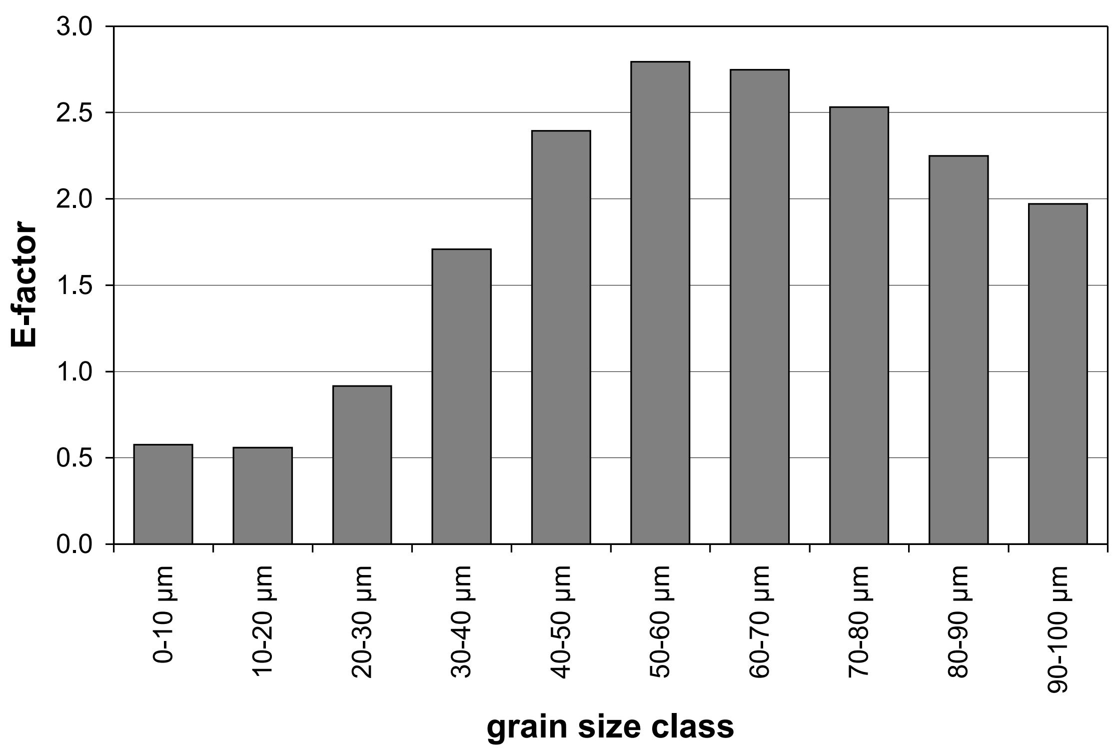

Fig. 17: E-factor for various grain size classes of road dust

When driving off-road, drivers usually drive their vehicles over various types of surfaces. Also, they constantly change their speed due to local factors such as topography, curves in the road, local obstacles, etc. To get an idea of the amounts of dust produced during a realistic drive, various routes were selected in the Nellis Dunes Recreation Area and the emission was calculated for typical drives along these routes. The following scenarios were calculated:

- Scenario 1: drive through a sandy area
- Scenario 2: drive through a silty area
- Scenario 3: drive through drainages
- Scenario 4: drive through mixed terrain

These trajectories are plotted on a simplified surface unit map (Fig. 18). Detailed information for each route is given in Table 2. For each scenario the emission was calculated for both PM10 and TSP, for all 3 vehicles tested, and for 5 driving speeds varying from 10 to 50 km h^{-1} (10 to 40 km h^{-1} for the dune buggy).

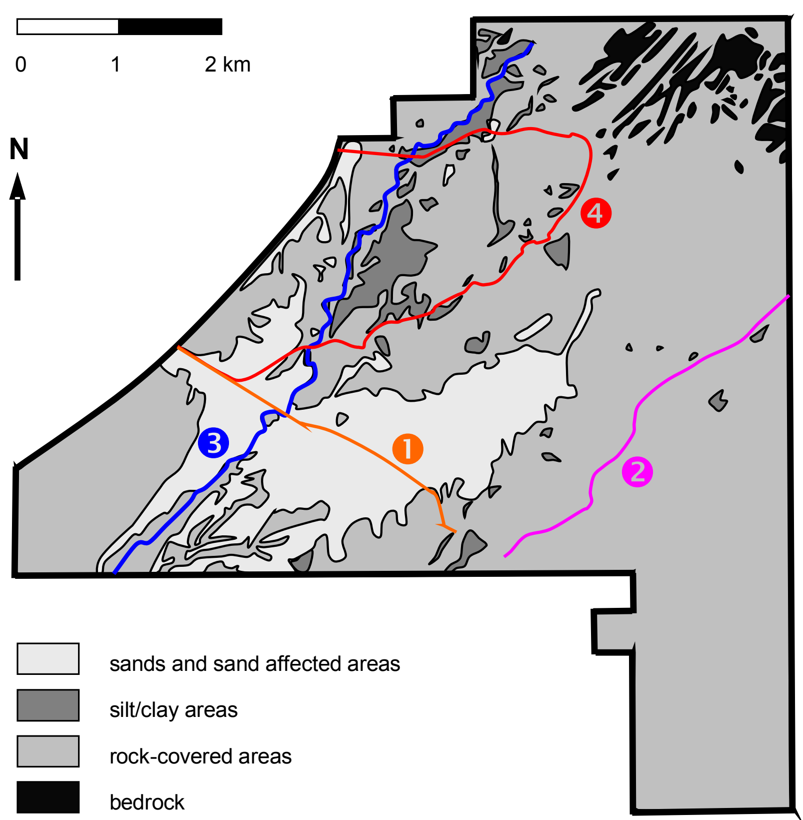

Fig. 18: Trajectories of the 4 driving scenarios, superimposed on a simplified surface map of the NDRA. 1: Scenario 1 (sandy area); 2: Scenario 2 (silty area); 3: Scenario 3 (drainages); 4: Scenario 4 (mixed terrain).

Table 2: Characteristics of the driving scenarios tested

scenario 1: sand area		
surface unit	distance driven	
	meters	% in drive
1.1	225	6.62
1.2	1157	34.03
1.3	714	21.00
1.4	925	27.21
3.2	343	10.09
4.2	29	0.85
4.3	7	0.21
total drive:	*3400*	*100.00*

scenario 2: silt area		
surface unit	distance driven	
	meters	% in drive
2.2	11	0.27
3.1	264	6.43
3.2	3654	88.97
4.1	57	1.39
4.3	121	2.95
total drive:	*4107*	*100.00*

scenario 3: drainage area		
surface unit	distance driven	
	meters	% in drive
4.1	4070	51.95
4.2	1590	20.29
4.3	2175	27.76
total drive:	*7835*	*100.00*

scenario 4: mixed area		
surface unit	distance driven	
	meters	% in drive
1.2	125	1.50
1.3	889	10.67
1.4	429	5.15
1.5	154	1.85
2.1	164	1.97
2.3	1239	14.88
2.4	146	1.75
3.1	157	1.89
3.2	3654	43.88
3.3	861	10.34
4.1	321	3.85
4.2	7	0.08
4.3	182	2.19
total drive:	*8328*	*100.00*

PM10 emissions for these scenarios are presented in Fig. 19. The main conclusions are: (1) in all 4 scenarios the largest amounts of PM10 are produced by the 4-wheeler, followed by the dune buggy and the dirt bike; (2) the faster the vehicles are driving, the more PM10 they will emit; (3) typical amounts of PM10 emitted are as follows: for drives in sand areas: 30-40 g km^{-1}; for drives in silt areas: 150-200 g km^{-1} (100 g km^{-1} for dirt bikes); for drives through drainages: 30-40 g km^{-1}; and for drives in mixed terrain: 60-100 g km^{-1}.

Similar curves were calculated for TSP (Fig. 20). The results are similar to those for PM10, although some slight differences can be observed for the dune buggy in the sand and drainage areas. The typical amounts of TSP emitted are: for drives in sand areas, about 200 g km^{-1}; for drives in silt areas, 600-700 g km^{-1} (1000-2000 g km^{-1} for 4-wheelers); for drives through drainages, 300-400 g km^{-1} (100-200 g km^{-1} for dirt bikes); and for drives in mixed terrain, 300-500 g km^{-1} (500-800 g km^{-1} for 4-wheelers).

Although these numbers are based on simulations, they give a good idea of the order of magnitude that can be expected for the various regions in the Nellis Dunes Recreation Area.

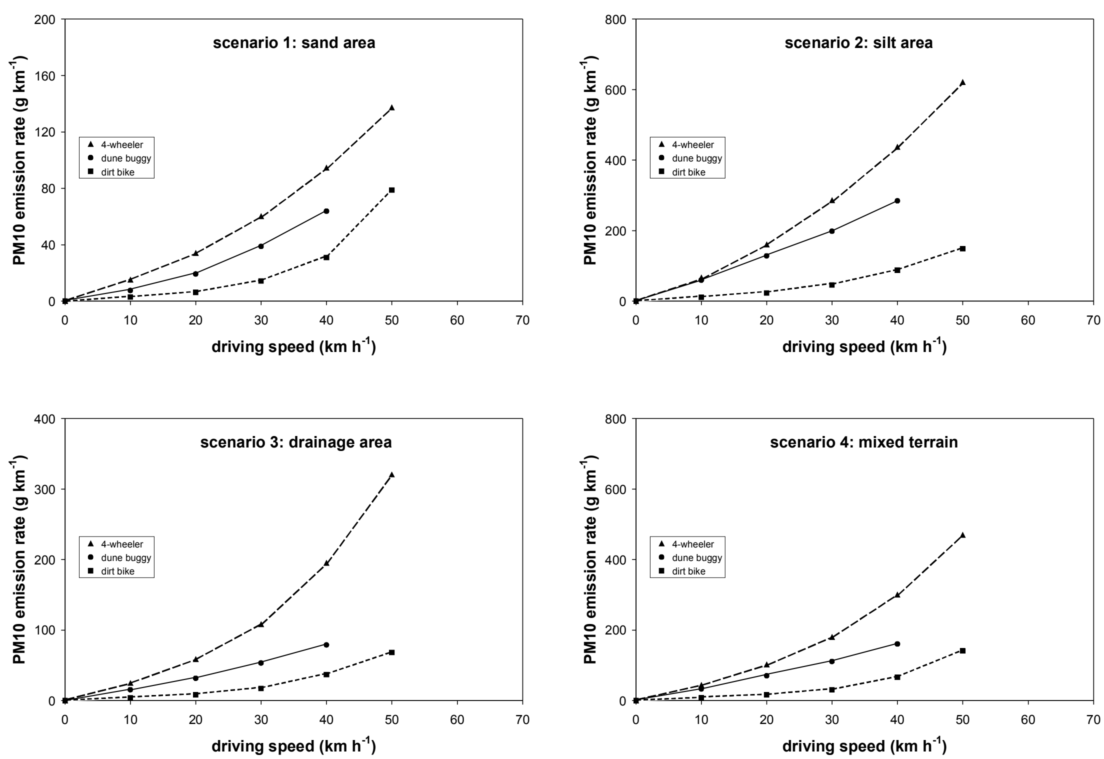

Fig. 19: PM10 emission rates for the 4 scenarios tested

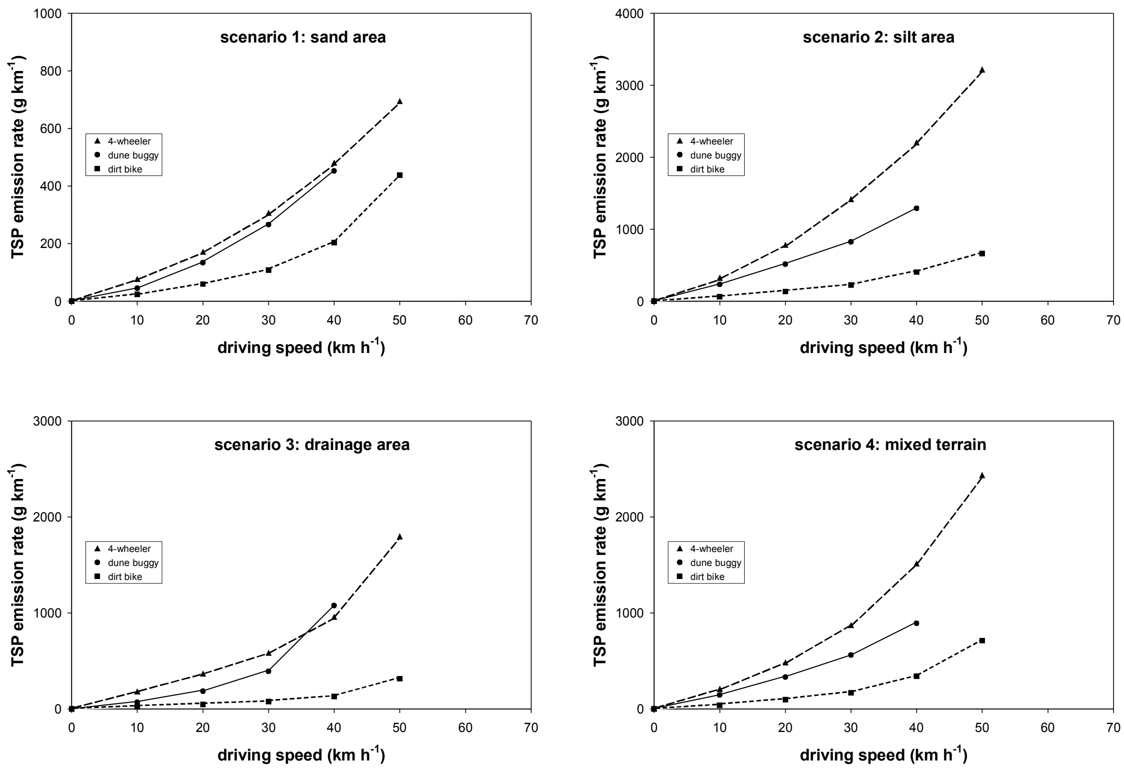

Fig. 20: TSP emission rates for the 4 scenarios tested

5. The ORV experiment: summary of conclusions

The experiments in the Nellis Dunes area show that off-road driving emits significant amounts of dust. This is true for PM10 dust as well as for coarser dust. However, the amounts emitted vary greatly with the type of sediment and the characteristics of the surface over which the vehicle is driving, the type of ORV vehicle, and the speed of driving.

For evident reasons sandy soils produce less dust than silty soils. However the high internal variability within mapped units (rock content, presence of vegetation, contamination of the top layer with locally blown in sediment, etc.) can also significantly affect emission rates. Using only a single soil parameter (such as the percentage of silt, as in the 1995 US EPA AP-42 formula) is thus insufficient to describe the effect of soil on dust emission.

At NDRA the highest PM10 emissions were always measured on surface units 2.2 (silt/clay with gravel) and 3.1 (desert pavements) whereas lowest emissions occurred on the uncrusted (or only weakly crusted) sandy surfaces (1.1, 1.2, 1.3, 1.4, 3.4) and the gravel and bedrock surfaces (3.5, 4.1). The thin surficial stone layer of the desert pavements (3.1) did not provide much protection against off-road driving. The silty surfaces (except 2.2 and 3.1) showed intermediate emission values.

As already reported in many previous studies the emission rates strongly depend on the driving speed. At NDRA, in general, PM10 and TSP emission increased exponentially with the driving speed. However, systematic correlations between the normalized rate of increase of emission with speed and surface type were not found. Similar surfaces can show different rates, which makes it difficult to model the emissions. Therefore, it is critical to collect field measurements for specific locations in order to obtain adequate data in each particular case.

Of the three types of vehicles tested, the 4-wheeler produced the largest amounts of dust, followed by the dune buggy and the dirt bike. It may be worth recalling that in many areas the dirt bike is able to drive faster than the dune buggy (and, sometimes, the 4-wheeler). Also, the dust emitted by a dune buggy is somewhat finer than that emitted by a 4-wheeler or a dirt bike.

Dust emitted by off-road driving is finer than the parent sediment on the road surface. Off-road driving thus results in a progressive coarsening of the top layer on the road.

Removal of particles by off-road driving is most efficient for grain sizes around 60 µm. For particles <25 µm the efficiency (in physical terms) of the process becomes very low: cohesion and adhesion forces hamper emission of the grains. These numbers were derived for air-dry surfaces; for moist surfaces they will be substantially higher. It should be noted, however, that the finest particles (PM10) have the greatest impact on human health.

Realistic emission rates for off-road driving on dry surfaces in the Nellis Dunes Recreation Area with 4-wheelers, dune buggies and dirt bikes are: drives in sandy areas, 30-40 g km^{-1} (PM10) and 150-250 g km^{-1} (TSP); drives in silty areas, 100-200 g km^{-1} (PM10) and 600-2000 g km^{-1} (TSP); drives in drainages, 30-40 g km^{-1} (PM10) and 100-400 g km^{-1} (TSP); and drives in mixed terrain, 60-100 g km^{-1} (PM10) and 300-800 g km^{-1} (TSP).

For information on the annual amounts of dust effectively produced in NDRA by ORV activity the reader is referred to Chapter 6 of this report.

Acknowledgements

Randy Jordan (Sun Buggy Fun Rentals, Las Vegas) provided a dune buggy, a dirt bike and several of the drivers. The 4-wheeler was provided by Shelly Kingsley, and another dirt bike by Brian Wilson. Brett McLaurin (Bloomsburg University, USA) assisted in constructing the map of the soil units. We also thank the following persons who assisted in the field experiments: Lars Bangen, Rob Davis, Rhonda Fairchild, Janice Morton, Michelle Stropky, Yuanxin Teng and Amanda Williams.

References

Adkinson, G.P., 1991**.** Ecological Impacts of Trail Use in Three Indiana Nature preserves. M.Sc. Thesis, The School of Graduate Studies, Department of Life Sciences, Indiana State University, Terre Haute, IN, USA.

Anderson, E., Mason, P., Holmes, E., 1990. Mt**.** Blue Experimental ATV Trail. Annual Report 1989, Unity College, Unity, ME, USA.

Bacon, S.N., McDonald, E.V., Baker, S.E., Caldwell, T.G., Stullenbarger, G., 2008. Desert terrain characterization of landforms and surface materials within vehicle test courses at U.S. Army Yuma Proving Ground, USA. Journal of Terramechanics 45, 167–183.

Bagnold, R.A., 1941. The Physics of Blown Sand and Desert Dunes. Methuen, London.

Belnap, J., 2002**.** Impacts of off-road vehicles on nitrogen cycles in biological soil crusts: resistance in different U.S. deserts. Journal of Arid Environments 52, 155-165.

Buschiazzo, D.E., Zobeck, T.M., 2005. Airborne horizontal mass flux calculated with different equations. Proc. 2005 ASAE Annual Meeting, Tampa, Florida, USA, Paper No. 052049.

Cordell, H. K., 2004. Outdoor recreation for 21st Century America. Venture Publishing Inc., State College, PA.

Cordell, H.K., Betz, C.J., Green, G.T., Stephens, B., 2008. Off-Highway Vehicle Recreation in the United States and its Regions and States: A National Report from the National Survey on Recreation and the Environment (NSRE). USDA Forest Service's Southern Research Station, Internet Research Report Series, http://www.fs.fed.us/recreation/programs/ohv/IrisRec1rpt.pdf.

Cowherd, C., Englehart, P., Muleski, G.E., Kinsey, J.S., Rosbury, K.D., 1990. Control of Fugitive and Hazardous Dusts. Noyes Data Corp., Park Ridge, New Jersey.

DSR, 2009. Off-road vehicle regional land use planning study. Western Australia Department of Sport and Recreation, http://www.dsr.wa.gov.au/3292.

Eckert, R.E. Jr., Wood, M.K., Blackburn, W.H., Peterson, E.F., 1979**.** Impacts of off-road vehicles on the infiltration and sediment production of two desert soils. Journal of Range Management 32, 394-397.

Etyemezian, V., Kuhns, H., Gillies, J., Chow, J., Hendrickson, K., McGown, M., Pitchford, M., 2003a. Vehicle-based road dust emission measurement: III - effect of speed, traffic volume, location, and season on PM10 road dust emission in the Treasure Valley, ID. Atmospheric Environment 37, 4583-4593.

Etyemezian, V., Kuhns, H., Gillies, J., Green, M., Pitchford, M., Watson, J., 2003b. Vehicle-based road dust emission measurement: I - methods and calibration. Atmospheric Environment 37, 4559-4571.

Fish, E.B., Borthers, G.L., Lewis, R.B., 1981. Erosional impacts of trails in Guadalupe Mountains National Park, Texas. Landscape Planning 8, 387-398.

Fryrear, D.W., 1986. A field dust sampler. Journal of Soil and Water Conservation 41, 117-120.

Gillies, J.A., Watson, J.G., Rogers, C.F., DuBois, J.C., Chow, J.C., Langston, R., Sweet, J., 1999. Long term efficiencies of dust suppressants to reduce PM10 emissions from unpaved roads. The Journal of the Air and Waste Management Association 49, 3-16.

Gillies, J.A., Etyemezian, V., Kuhns, H., Nikolic, D., Gillette, D.A., 2005. Effect of vehicle characteristics on unpaved road dust emissions. Atmospheric Environment 39, 2341-2347.

Goossens, D., Buck, B., 2009a. Dust dynamics in off-road vehicle trails: measurements on 16 arid soil types, Nevada, USA. Journal of Environmental Management 90, 3458-3469.

Goossens, D., Buck, B., 2009b. Dust emission by off-road driving: experiments on 17 arid soil types, Nevada, USA. Geomorphology107, 118-138.

Goossens, D., Offer, Z.Y., 2000. Wind tunnel and field calibration of six aeolian dust samplers. Atmospheric Environment 34, 1043-1057.

Goossens, D., Offer, Z.Y., London, G., 2000. Wind tunnel and field calibration of five aeolian sand traps. Geomorphology 35, 233-252.

Griggs, G., Walsh, B.L., 1981. The impact, control, and mitigation of off-road vehicle activity in Hungry Valley, California. Environmental Geology 3, 229-243.

Horikawa, K., Shen, H.W., 1960. Sand Movement by Wind Action. United States Army, Corps of Engineers, Beach Erosion Board, Technical Memorandum TM-119.

Hussein, T., Johansson, C., Karlsson, H., Hansson, H-C., 2008. Factors affecting non-tailpipe aerosol particle emissions from paved roads: on-road measurements in Stockholm, Sweden. Atmospheric Environment 42, 688-702.

Iversen, J.D., White, B.R., 1982. Saltation threshold on Earth, Mars and Venus. Sedimentology 29, 111-119.

Kuhns, H., Etyemezian, V., Green, M., Hendrickson, K., McGown, M., Barton, K., Pitchford, M., 2003. Vehicle-based road dust emission measurement: II - Effect of precipitation, wintertime road sanding, and street sweepers on inferred PM10 emission potentials from paved and unpaved roads. Atmospheric Environment 37, 4573-4582.

Kutiel, P., Eden, E., Zhevelev, Y., 2000. Effect of experimental trampling and off-road motorcycle traffic on soil and vegetation of stabilized coastal dunes, Israel. Environmental Conservation 27, 14-23.

Liddle, M.J., Greig-Smith, P., 1975. A survey of tracks and paths in a sand dune ecosystem. I. Soils. Journal of Applied Ecology 12, 893-908.

McEwen, D.N., 1978. Turkey Bay off-road vehicle area at land between the Lakes: an example of new opportunities for managers and riders. Southern Illinois University, Department of Recreation, Research Report No. 1, 1-28.

McLaurin, B.T., Goossens, D., Buck, B., in press. Combining surface mapping and process data to assess, predict, and manage dust emissions from natural and disturbed land surfaces. Geosphere.

Moosmüller, H., Gillies, J.A., Rogers, C.F., DuBois, D.W., Chow, J.C.,Watson, J.G., Langston, R., 1998. Particulate emission rates for unpaved shoulders along a paved road. Journal of the Air and Waste Management Association 48, 398-407.

MRI (Midwest Research Institute), 2001. Revisions to AP-42 Section 13.2.2 "Unpaved Roads". Technical Memorandum prepared for the US EPA, Research Triangle Park, NC, Midwest Research Institute, Kansas City, MO.

Nicholson, K.W., Branson, J.R., Geiss, P., Cannel, R.J., 1989. The effects of vehicle activity on particle resuspension. Journal of Aerosol Science 20, 1425-1428.

NPSNM, 2008. Impacts of off-road vehicles on native vegetation. Native Plant Society of New Mexico (NPSNM), http://www.npsnm.unm.edu/pdfs/npsnm_orv.pdf.

Outdoor World Directory, 2010. Off Road Resource web sites. http://www.agsites.net/links/offroadresource.html.

Pye, K., Tsoar, H., 1990. Aeolian Sand and Sand Dunes. Unwin Hyman, London.

Schlacher, T.A., Thompson, L.M.C., 2007. Exposure of fauna to off-road vehicle (ORV) traffic on sandy beaches. Coastal Management 35, 567-583.

Sharrat, B., Feng, G., Wendling, L., 2007. Loss of soil and PM10 from agricultural fields associated with high winds on the Columbia Plateau. Earth Surface Processes and Landforms 32, 621-630.

Smith, D.L.O., Dickson, J.W., 1990**.** Contributions of vehicle weight and ground pressure to soil compaction. Journal of Agricultural Engineering Research 46, 13-29.

Sparrow, S.D., Wooding, F.J., Whiting, E.H., 1978**.** Effects of off-road vehicle traffic on soils and vegetation in the Denali Highway region of Alaska**.** Journal of Soil and Water Conservation 33, 20-27.

Spivey, S., 2008. Off-road fans, critics face off. Las Vegas Review-Journal, Monday, March 17, 2008, 10B.

Sylvester, J.T., 2009. Montana Off-Highway Vehicles 2008. Bureau of Business and Economic Research, University of Montana-Missoula.

TCAFS, 2002**.** Off-Road Vehicles and Their Impact on Stream Environments: A Policy Statement from the Texas Chapter of the American Fisheries Society. Texas Chapter of the American Fisheries Society (TCAFS), http://www.sdafs.org/tcafs/content/orvpol.htm.

Tinsley, B.E., Fish, E.B., 1985**.** Evaluation of trail erosion in Guadalupe Mountains National Park, Texas**.** Landscape Planning 12, 29-47.

Tuttle, M., Griggs, G., 1987**.** Soil erosion and management recommendations at three state vehicular recreation areas, California. Environmental Geological Water Science 10, 111-123.

US EPA, 1995. User's Guide for the Industrial Source Complex (ISC3) Dispersion Models. Vol. II: Description of Model Algorithms. US Environmental Protection

Agency, Office of Air Quality Planning and Standards: Emissions, Monitoring, and Analysis Division, Research Triangle Park, North Carolina, USA.
US EPA, 1996. Compilation of Air Pollutant Emission Factors. Vol. 1: Stationary Point and Area Sources. US EPA Office of Air and Radiation, Office of Air Quality Planning and Standards, Research Triangle Park, North Carolina, USA.
US EPA, 1999. Compilation of Air Pollutant Emission Factors. Vol. I: Stationary Point and Area Sources, Report No. AP-42. US Environmental Protection Agency, Research Triangle Park, North Carolina, USA.
US EPA, 2003. AP-42, Fifth Edition. Vol. 1: Miscellaneous Sources, Chapter 13. US Environmental Protection Agency, Research Triangle Park, North Carolina, USA.
Voorhees, W.B., Senst, C.G., Nelson, W.W., 1978. Compaction and soil structure modifications by wheel traffic in the northern corn belt. Soil Science Society of America Journal 42, 344-349.
Webb, R.H., Ragland, H.C., Godwin, W.H., Jenkins, O., 1978. Environmental effects of soil property changes with off-road vehicle use. Environmental Management 2, 219-233.
Wiedmer, M., 2002. Lower Kenai peninsula summer off-road vehicle trail stream crossings. Alaska Department of Fish and Game, Habitat and Restoration Division Technical Reports, Report 02-02, Anchorage, AK, USA.
Wilshire, H.G., Nakata, J.K., 1976. Off-road vehicle effects on California's Mojave desert. California Geology 29, 123-132.
Wilshire, H.G., Nakata, J.K., Shipley, S., Prestegaard, K., 1978. Impacts of vehicles on natural terrain at seven sites in the San Francisco Bay area. Environmental Geology 2, 295-319.

Chapter 4

DUST DYNAMICS IN OFF-ROAD VEHICLE TRAILS

Dirk Goossens and Brenda Buck

Department of Geoscience, University of Nevada Las Vegas

1. Description of the problem

ORV driving is one of the most destructive types of land use disturbing the top soil, vegetation and even local ecosystems (Adkinson, 1991; Kutiel et al., 2000; Wiedmer, 2002). Surfaces disturbed by ORV driving may require decades or even centuries to become more or less restored, if recovery is at all possible (Wilshire and Nakata, 1976). With respect to air quality two aspects of ORV driving should be considered: the production of exhaust gases, and the emission of significant quantities of soil dust, especially when the soil is dry (Goossens and Buck, 2009). The Nellis Dunes project focuses on the latter aspect.

Emissions of soil dust created by ORV activity were hardly studied before the early 1990s but received much attention since then: Moosmüller et al., 1998; Gillies et al., 1999, 2005; Kuhns et al., 2003; Goossens and Buck, 2009; to cite only a few studies. However, all these studies focused on direct measurements of the emission, or on suppressing emissions. They did not investigate the dust-dynamic properties of the soil in the trails. ORV driving significantly disturbs the topsoil. The structure of the top layer in ORV trails is thus very different compared to the original surface on which the trail has been created. ORV trails are much more sensitive to wind erosion than undisturbed surfaces, which are often characterized by surface crusts or by a natural protection of surficial rock fragments. This difference is significant in areas rich in silt and clay (such as the entire eastern part of the NDRA) because in these areas dust production by wind erosion is nearly exclusively restricted to the ORV trails.

ORV trails cover a significant proportion of the NDRA. The total length of the trails is 537 km, and the surface occupied by the trails is 233 ha. This is 6.4 % of the total surface of NDRA. However, measurements performed between December 2007 and December 2008 (see Chapter 5 in this report) indicated that 15.4 % of all dust produced by wind erosion in NDRA during this period was produced in the trails. This already points to the much higher dust production capacity of ORV trails compared to undisturbed terrain. A comparative study of dust dynamics in and outside ORV trails is thus necessary.

One reason why such comparative studies are currently lacking is that until recently, portable field wind tunnels were required to measure *in situ* dust production. Although very useful, field wind tunnels have important limitations. For an adequate simulation of the boundary layer a minimum fetch length is required, which means that the tunnel should be at least a few meters long. This may hamper access to difficult sites (Sweeney et al., 2008). Also, the local topography should be flat enough to allow appropriate installation of the tunnel. Due to the tunnel's size it is also not possible to test very small surfaces, which may be a handicap in the case of highly differentiated terrain. Another handicap is that repeating measurements on the same soil requires a move of the complete tunnel, which often is very laborious. Additional problems are the dismantling, transportation and reassembling of the tunnel between the measuring sites, and the cost of labor required to operate the instrument.

The recent development of the Portable In Situ Wind Erosion Laboratory or PI-SWERL (Etyemezian et al., 2007) permits much faster, more accurate, simple, and less disturbing measurements of dust emissions on field plots than portable wind tunnels can offer. In this project we used the PI-SWERL to investigate the dust-dynamic properties in ORV trails for 16 of the 17 surface types occurring in the Nellis Dunes Recreation Area. For a detailed description of the units we refer to Chapter 2. Only surface unit 3.5 (bedrock) was not examined because these surfaces contain negligible emittable dust and because there is almost no driving on this unit because of their steep and rough slopes.

The objectives of the study were to check whether there are differences in dust dynamics between the trails and the corresponding undisturbed soil, and to examine how the emission properties change when new trails are created on undisturbed terrain. The hypothesis is that dust dynamics should strongly depend on surface type. The measurements also aimed to provide information for adequate management of ORV areas and ORV driving in general. These aspect are discussed in Chapter 12 of this report.

2. The PI-SWERL experiment: procedure

2.1 Locations

Experiments were performed on 16 of the 17 surface types occurring in the Nellis Dunes area. Surface type 3.5 (bedrock) was not tested, as explained before. However, it is safe to state that, at least in NDRA, the 3.5 units produce negligible ORV-generated dust. Measurements were carried out at 32 locations, two for each surface unit. Fig. 1 shows the location of the sites.

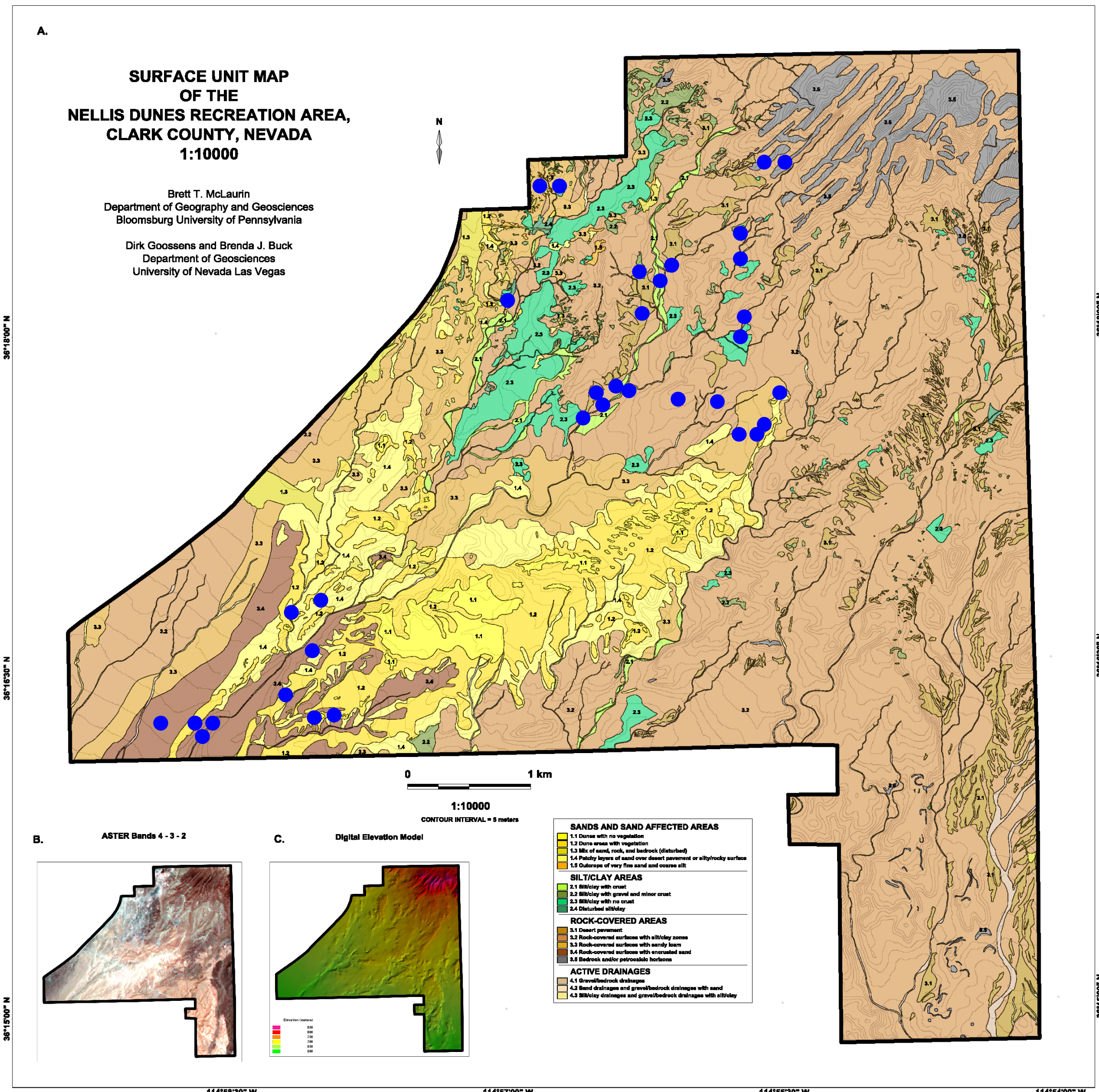

Fig. 1: Location of the PI-SWERL experimental sites (blue dots)

All measurements were performed on dry soils. Moisture content was always very close to zero: relative humidity in the region is extremely low, evaporation rates very high, and no rains occurred during at least 3 weeks prior to the measurements.

On each site PI-SWERL measurements were done in a frequently used trail (as indicated by the abundance of recently created tire tracks) and on undisturbed terrain well outside, but sufficiently close to the trail to ensure identical properties of the original topsoil. Zones outside trails that were obviously affected by off-road driving (i.e., areas covered by a thin layer of sediment deposited after its emission from the trail) were carefully avoided.

2.2 The Portable In Situ Wind Erosion Laboratory

The Portable In Situ Wind Erosion Laboratory (PI-SWERL) was developed at the Division of Atmospheric Sciences, Desert Research Institute, Las Vegas, Nevada, USA. Detailed descriptions of the instrument are provided in papers by Etyemezian et al. (2007) and Sweeney et al. (2008); a brief summary follows below.

The PI-SWERL mainly consists of an open-bottomed cylindrical chamber 0.25 m high and 0.57 m in diameter (Fig. 2, right), which is placed on the surface to be tested. A shallow foam between the chamber and the surface ensures a hermetic closure of the system. A 0.51 m diameter flat annular ring with a width of 0.06 m hangs parallel to and 0.05-0.06 m above the soil surface within the chamber. While in operation, the rotating ring creates a velocity gradient between its flat-bottom and the ground, inducing a shear stress on the surface. This shear stress is proportional with the rotational speed of the

Fig. 2: Photograph of the PI-SWERL (right), with computer, battery and control box mounted on carriage (left)

ring, which is controlled by a computer and expressed in revolutions per minute (RPM). Comparative tests with the portable field wind tunnel of the Wind Erosion Research Laboratory, University of Guelph (Guelph, Ontario, Canada) provided calibrations between the PI-SWERL's RPM and the friction velocity u_* (J. King, DRI Las Vegas, pers. com., 2008).

Clean air blows into the chamber via a filtered inlet. During a test the concentration of the emitted dust is measured in the chamber with a DustTrak aerosol monitor, model 8520 (TSI Inc., St. Paul, Michigan, USA). The DustTrak only measures the PM10 fraction (particles <10 μm in diameter). All results described in this report thus refer to that fraction; not to total dust. This puts some restrictions on this study although PM10 generally is considered the most harmful fraction of airborne dust (Carvacho et al., 2006). The dust-laden air leaves the chamber via an outlet near the top of the chamber.

Two types of runs were done in this study:

- *RAMP test*. The chamber was first cleaned by a clean air flush during 60 s while the annular blade was not rotating. After 60 s the rotational speed of the blade was steadily increased during 180 s until an RPM of 3000 had been reached, after which the power to the motor was cut off and the chamber was flushed during an additional 30 s. Fig. 3A shows the typical dust concentration curve during such a test. Measuring the concentration at sufficiently short time intervals (1 s in the figure, which was also the value used in this study) the deflation threshold, i.e. the critical wind condition (here expressed in RPM) at which erosion starts, can be directly derived from the curve after checking for the corresponding RPM (or u_*) in the data file.

- *STEP test*. A series of consecutive measurements with different RPMs were conducted (Fig. 3B). The chamber was first cleaned by a clean air flush during 60 s. Then the blade started rotating at a first speed (RPM) for 90 s, after which the speed rapidly increased (usually within seconds) to a second value (RPM). This second step lasted for 120 s. The procedure was repeated two more times, with time durations of 150 s (third RPM) and 180 s (fourth RPM), after which the power was cut off and the chamber was flushed for 60 more seconds. Fig. 3B shows the typical dust concentration curve during a STEP test. In general, for most surfaces the PM10 concentration peaks shortly after a new RPM has been reached and then decays more or less asymptotically to a lower value (not necessarily zero) although some surfaces may show different curves (see later in this chapter). The data recorded during a test allow one to calculate the mass of emitted PM10 during and after each step; dividing the mass flux through the area prone to erosion underneath the chamber (0.26 m^2) and through the total emission time then provides the emission flux (μg m^{-2} s^{-1}). Of course, the emission fluxes measured depend on the size of each step (difference in RPM). To obtain a unique emission curve for each surface unit the emission flux can be plotted as a function of the friction velocity (see inset in upper left corner in Fig. 3B).

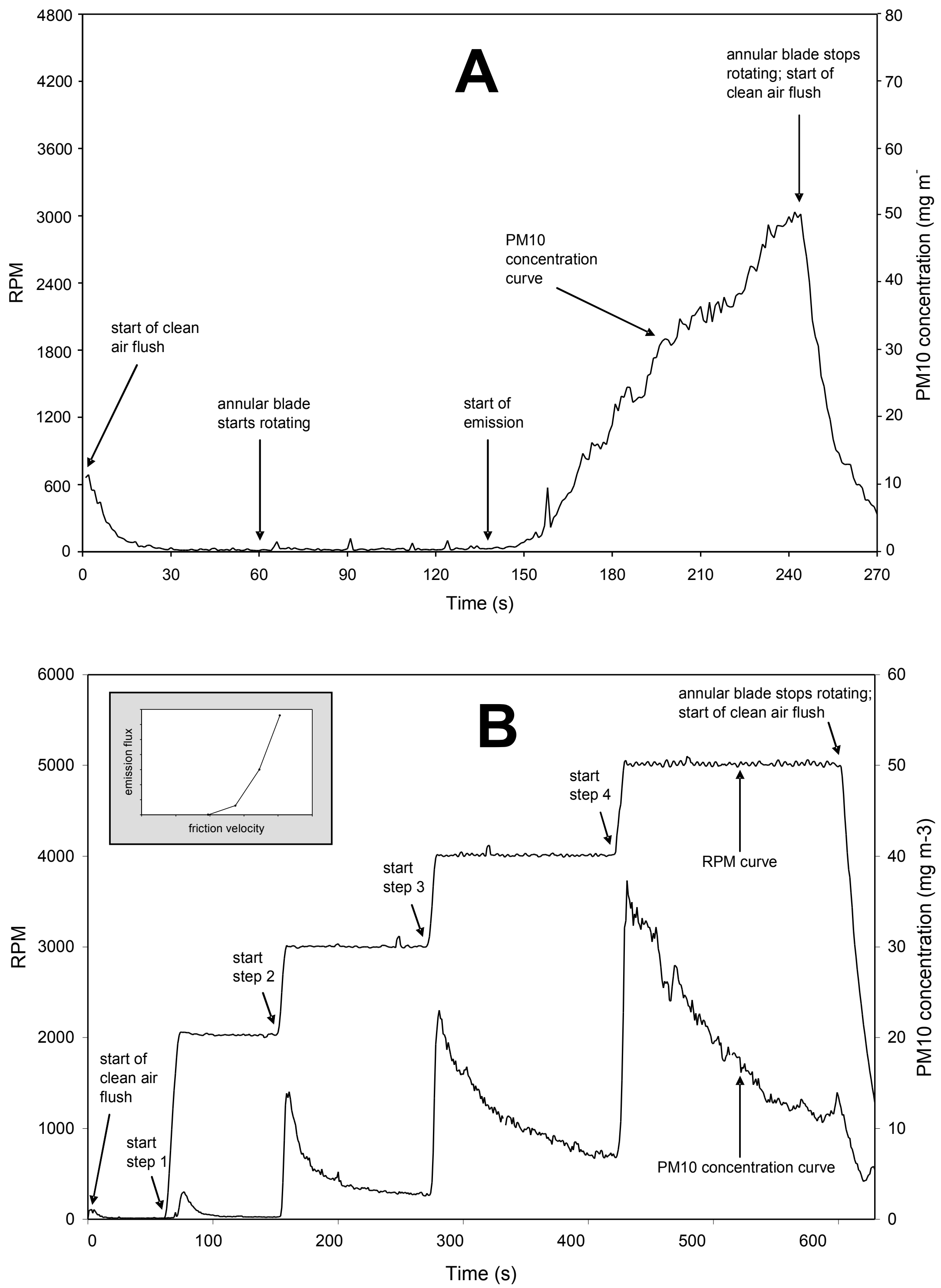

Fig. 3: Typical PI-SWERL emission curves. A: RAMP test; B: STEP test.

2.3 Field procedure

RAMP tests were conducted on all surface units except unit 3.5 (bare bedrock), as described before. For the remaining sites two RAMP tests and two STEP tests were carried out in a trail and outside the trail, at nearly the same spot to avoid any bias caused by differences in the parent soil. Four RAMP tests and four STEP tests were thus carried out for each surface unit, and the average result was calculated. Results of the repetitions were very comparable, indicating that the data are consistent and reliable.

A total of four steps were used during each STEP test. For most surfaces the following RPMs were generated: 2000, 2500, 3000 and 4000. Extra RPMs of 1000, 1800 and 2250 were used for highly erodible surfaces. One experiment with an RPM of 5000 was conducted for surface type 4.3 (silt and clay drainages).

Surface resistance measurements were also made at all sites to interpret the emissions. Normal resistance was measured with a penetrometer Model 29-3729 (Ele International, Loveland, CO, USA), and tangential resistance, with a torvane (Durham Geo Slope Indicator, Stone Mountain, GA, USA). Between 20 and 25 measurements were made on each spot with each instrument, and the average values were calculated.

The PM10 content in the trails as well as on the corresponding parent soil was measured at all PI-SWERL spots by collecting sediment from the top layer (3 samples) and measuring the grain size distribution with a Malvern Mastersizer S laser particle size analyzer (Malvern Instruments Ltd., Malvern, UK). All measurements were done with a dry sampling unit (not in water) to ensure analyzing the original sediment.

3. The PI-SWERL experiment: results and discussion

3.1 Deflation threshold

The deflation threshold is the threshold friction velocity at which erosion starts. The ratio of the deflation threshold in a trail to the threshold on the undisturbed parent surface is shown in Fig. 4. The data in the figure are the average of the four RAMP tests carried out for each surface unit. For all sand surfaces (units 1.1, 1.2, 1.3, 1.4, 1.5 and 3.4) the deflation threshold is higher in ORV trails compared to undisturbed terrain. This is particularly true for pure sands (1.5, 1.4, 1.2, 1.1). For sands contaminated by silt (3.4) or anthropogenically disturbed (1.3) the difference is smaller, but still noticeable. This means that for sandy surfaces, wind erosion is more difficult in the ORV trails than on undisturbed soils. In contrast, silt surfaces show an opposite trend: the deflation threshold is higher on the parent soil. The difference is small when some sand is still present (3.3) but becomes pronounced for pure silts (2.3, 2.2, 3.2, 3.1, 2.1). Within the silt group the ratio is lowest for the disturbed silts (2.4), similar to the disturbed sands (1.3). This means that for silty surfaces, ORV activity significantly increases the potential for wind erosion on these surfaces. Drainages show the lowest ratios. Note the granulometric trend within the drainage group: the more silt, the lower the ratio of the deflation thresholds becomes (Fig. 4).

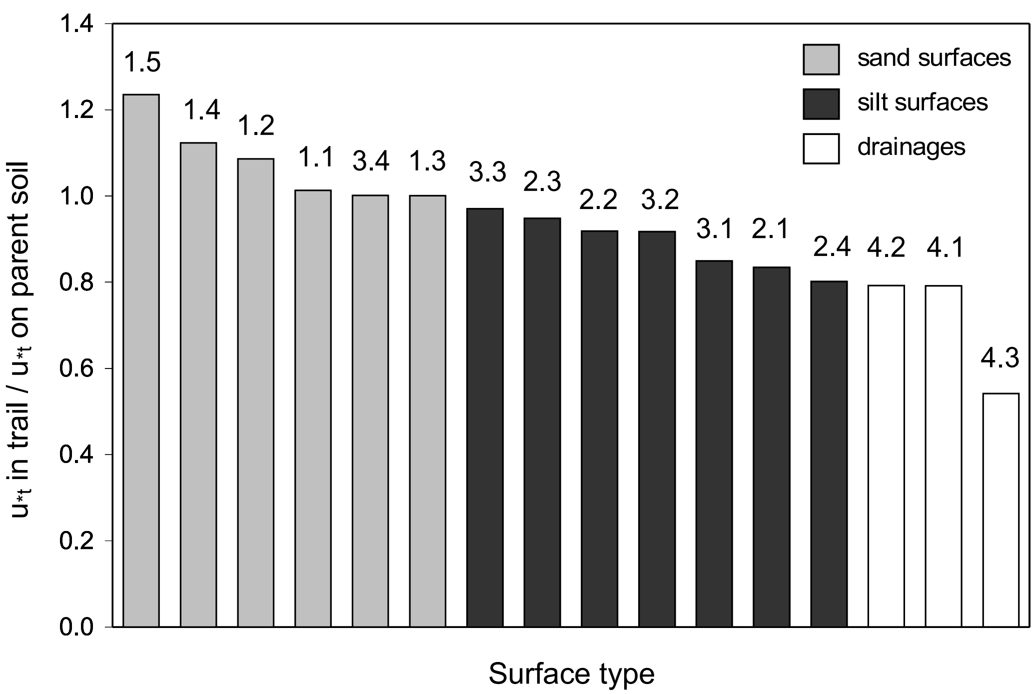

Fig. 4: Ratio of deflation threshold (threshold friction velocity) u_{*t} in a trail to the deflation threshold on undisturbed terrain, for the various surface units investigated

Creating new ORV trails is thus most risky in drainages. This does not necessarily imply that drainages will produce most dust, but wind erosion is expected to start earlier in newly created trails in these areas compared to the other surface units tested (provided all other conditions are identical). Silty surfaces not located in drainages also show a risk, though less than in drainages. Interesting, also in terms of management, is that sand surfaces show an opposite trend: creating new ORV trails in sand lowers the deflation threshold, which means that wind erosion will start later in the trails compared to undisturbed terrain. As such, ORV driving may help reduce wind erosion in these areas, but on the other hand it also produces dust even during periods of low wind when no wind erosion occurs (Goossens and Buck, 2009). Also, the incisions created by the trails may promote wind erosion at spots where they cause the streamlines to converge. The protective effect of ORV driving would thus be highest on large and flat sand sheets instead of in areas with complex dune topography.

The reason why ORV trails in sand show a higher deflation threshold than on corresponding undisturbed terrain is most probably the increased compaction of the topsoil. Compaction is also expected to occur on silt surfaces, but here ORV driving creates, in addition to compaction, a fresh top layer of loose material not occurring on the original undisturbed soil. This top layer was visible on almost every trail in the silty part of the Nellis Dunes area. In contrast, most undisturbed silt surfaces are characterized by a physical or biological surface crust, that in places is very strong. Sand surfaces usually do not contain a surface crust, especially if they are kept active, such as in the dunes (units 1.1, 1.2, 1.4) or in zones disturbed by people or cattle (unit 1.3). These surfaces always have a layer of loose sediment on top, and compaction due to ORV activity may increase their resistance to wind erosion. On silt surfaces the loose top layer created by ORV vehicles is very vulnerable to wind erosion, especially if the soil has stayed dry for a while, as is common in desert environments.

Compared to the other sand units, the sandy drainages (4.2) show a much higher risk for increased emissions when becoming disturbed by ORV driving (Fig. 4). The reason for this is that periodic water flow in these drainages concentrates dissolved calcium carbonate, which then forms a surface crust through evaporation. Samples viewed under a microscope showed micrite-sized calcite crystals cementing sand grains. Such crusts are known to reach up to 7 mm in thickness with a dry rupture resistance that varies from moderately hard to very hard (Schoeneberger et al., 2002). When this crust is disturbed by off-road vehicles, the cement bonds are broken making these drainages particularly vulnerable to wind erosion.

3.2 Emission fluxes

The emission flux in a trail is compared with the emission flux on undisturbed parent soil in Fig. 5. These fluxes represent the potential emission, i.e. the emission in optimum soil and atmospheric conditions. They do not necessarily predict the actual emission that will occur at a given point of time because meteorological and soil conditions vary in time. However, comparing the potential emissions of trails with those of undisturbed terrain gives a very good indication of how ORV driving affects the capacity of the top layer to produce dust, and it is one of the most reliable parameters than can be used especially if the conditions tested represent good averages.

The results show that the potential emission of PM10 is always higher in the trails compared to undisturbed terrain: the ratio shown in the ordinate in Fig. 5 is <1 for all surface types. Therefore, off-road driving does increase the potential of a soil to emit

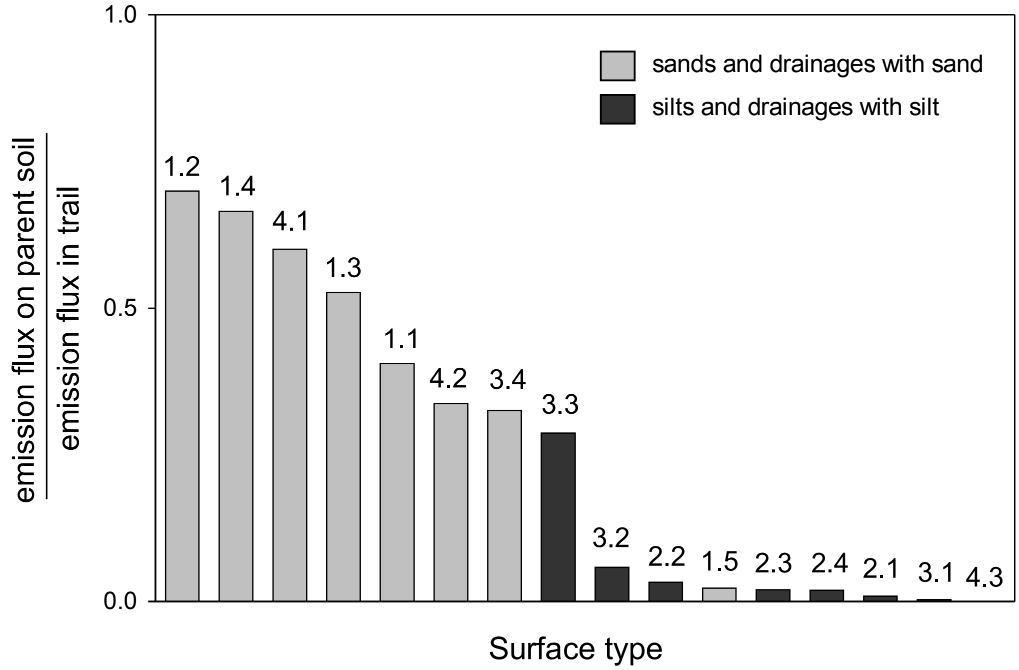

Fig. 5: Ratio of emission flux on undisturbed terrain to the emission flux in a trail, for the various surface units investigated

dust. This is particularly important during episodes of strong winds as, in relative terms, much more dust may be emitted from the trails compared to undisturbed soil despite the usually much larger surface area of the latter. Observations made in the Nellis Dunes Recreation Area during periods of strong winds confirm that most local dust clouds are initiated on trails rather than on undisturbed terrain, at least outside the proper sand dunes (surface units 1.1 and 1.2). Secondly, a clear difference can be seen between those surface units where the local erodible sediment is sand and the units where the local erodible sediment is silt. All units with sand except 1.5 (outcrops of very fine sand and coarse silt) are located on the left in the figure whereas all units with silt are located on the right. The potential to emit extra PM10 when a new trail is created is thus much higher on silt (or silty) surfaces than on sand (or sandy) surfaces. Silty surfaces clearly constitute a much higher risk for increased emissions when new ORV trails are created. The high risk of unit 1.5 is partly explained by the silt content and partly by the strong surface crust characterizing the undisturbed soil. In contrast to all the other sandy units, undisturbed areas of unit 1.5 have a strong surface crust and do not contain a top layer of loose, uncompacted sediment.

Compaction and/or the presence of crusts thus play a significant role in dust emission when new ORV trails are being created. When comparing the relationship between the potential PM10 emission flux on the undisturbed parent surfaces to the surface resistance on the same spots, the data show that 0.3 kg* cm^{-2} is a critical threshold with respect to

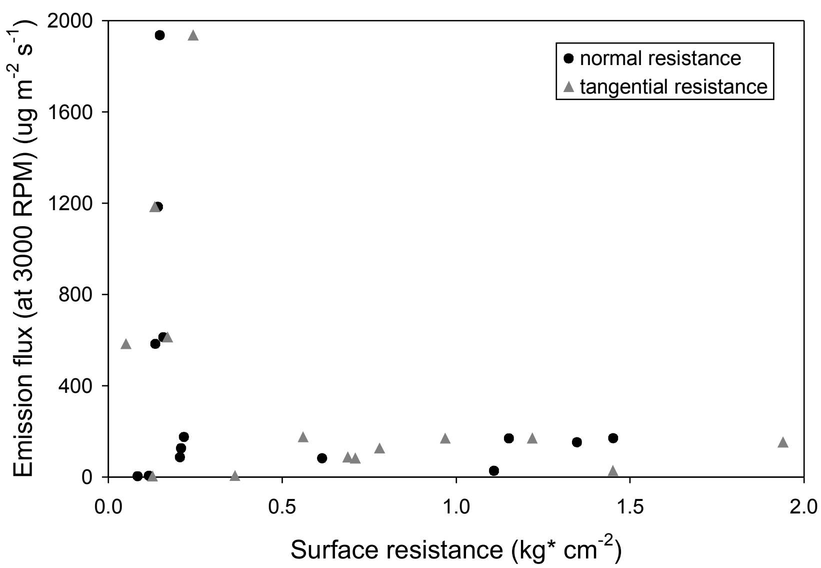

Fig. 6: Relationship between surface resistance and PM10 emission flux. Normal resistance was measured with a penetrometer, and tangential resistance, with a torvane.

PM10 emission (Fig. 6). Strong emission only occurs when the surface resistance remains below this threshold, and no significant emissions are to be expected once the threshold is exceeded. However, this threshold was measured on dry soils and thus will be greater when the soil is moist or wet.

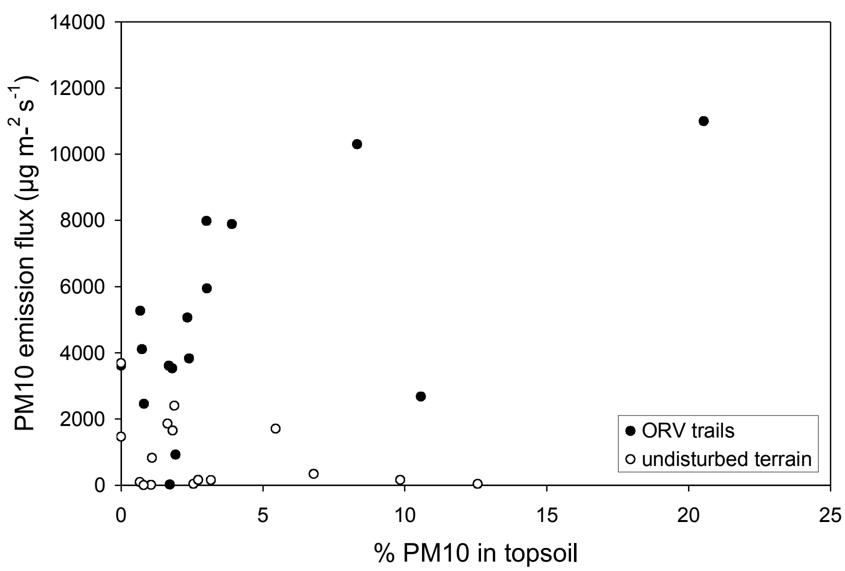

Fig. 7: Relationship between PM10 emission flux (at 3000 RPM) and the PM10 content in the topsoil. Black dots: ORV trails; open circles: undisturbed terrain.

Apart from surface resistance the emission flux also depends on the quantity of PM10 available in the soil. Fig. 7 compares the emission flux with the percentage of PM10 in the top layer (upper 2-3 cm), in the ORV trails (black dots) and on the corresponding parent terrain (open circles). As could be expected, in the trails high PM10 emission fluxes generally occur over surfaces with a high PM10 content, but a large degree of spread in the data is also noted. Outside the trails, on undisturbed surfaces, no such relationship is discernable: a high PM10 content in the topsoil does not lead to high emission fluxes. In fact, all emission fluxes measured over undisturbed surfaces remained very low, usually below 2000 µg m^{-2} s^{-1}.

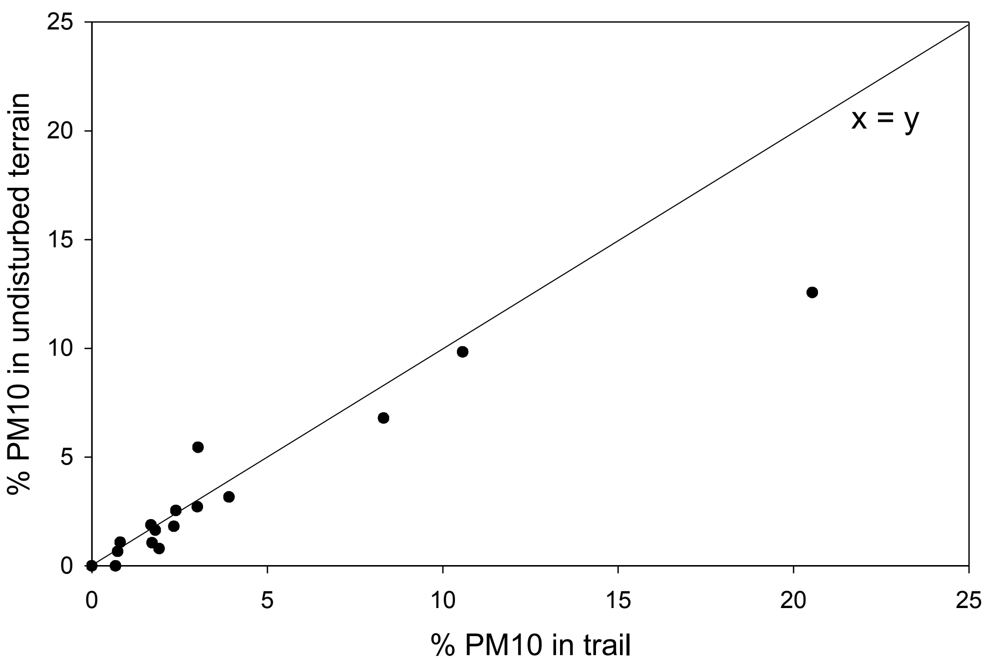

Fig. 8: PM10 content in the trails compared to the PM10 content in undisturbed terrain

This indicates that much of the PM10 in the top layer of undisturbed soils is stabilized and not directly available for emission. This is certainly true for the silt units, which all show a surface crust except the disturbed silts of unit 2.4. Frequent off-road driving breaks the interparticle bonds, at least partially, liberating the PM10 grains and allowing them to become available for emission. Fig. 8 shows that the PM10 content is only very slightly higher in the trails than in the undisturbed soil. Despite the almost identical amount of PM10 potentially available in the top layer, the PM10 particles in the trails are much more vulnerable to emission because ORV activity has disrupted the protective surface crusts.

3.3 Coarsening of the top layer

Continuous off-road driving in a trail leads to a progressive coarsening of the top layer in the trail (see also Chapter 3 in this report). Fig. 9 compares the average grain size (represented by the median grain diameter, D_{50}) of sediment emitted during off-road driving to that of the topsoil in the trail. Except for the aggregated silt deposits (unit 2.3) the sediment in the trails is consistently coarser than the sediment emitted. This indicates that the trails become coarser with time. Also, the speed of coarsening is a clear function of the type of surface. Trails in drainages coarsen the most rapidly, and trails on sandy surfaces coarsen faster than trails on silty surfaces (see Fig. 9). Note that surface unit 2.3 is composed primarily of silt aggregates up to >5 mm in diameter, which are pulverized during off-road driving. Therefore, a value above unity in Fig. 9 is normal.

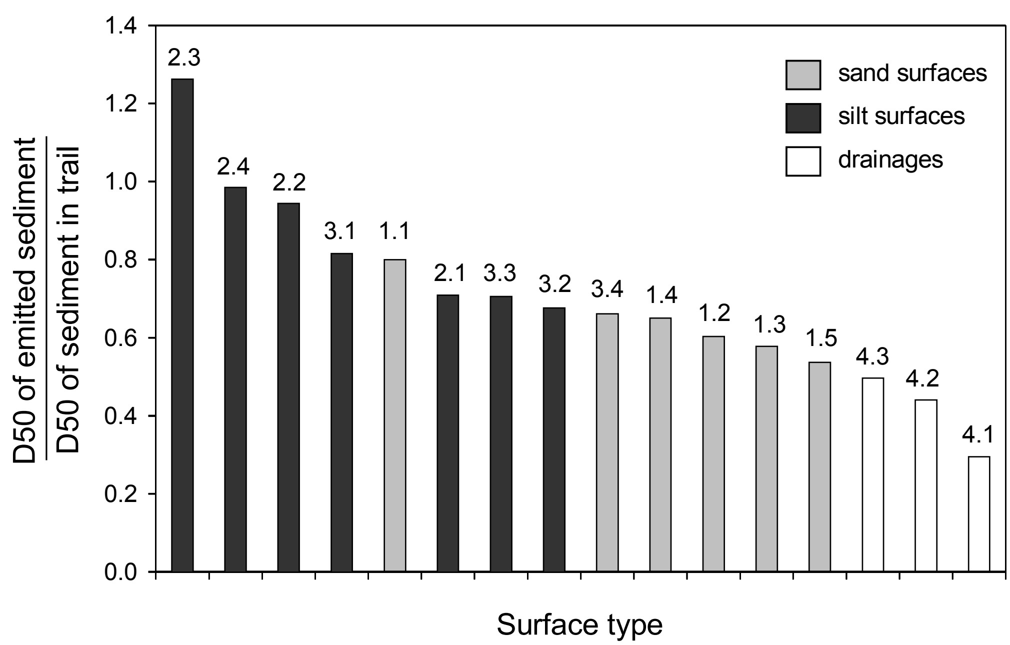

Fig. 9: Ratio of median grain diameter (D50) in ORV-emitted sediment to the median grain diameter in the trail, for the various surface units investigated

The progressive coarsening of the top layer in a trail implies that the deflation threshold in the trail would also increase with time, at least when the median diameter of the top layer is over about 80 µm (the grain size with minimum critical shear velocity for wind erosion, see Pye and Tsoar (1990) for a summary of some literature). All surface units tested in this study have a median grain diameter >80 µm in the trails except the silty units 2.2, 2.3 and 2.4, where the value is slightly below 80 µm (unit 2.2: 73 µm; unit 2.3: 57 µm; unit 2.4: 71 µm). Apart from these three units off-road driving would thus result in a gradually increasing deflation threshold in the trails and, thus, a diminishing risk for wind erosion. However, as stated earlier, other factors such as changes in the topography of the trail, or the supply of new erodible particles from deeper layers, may override this process.

3.4 Dust emission potential

The potential of a soil to supply sediment for emission is a critical parameter. According to Macpherson et al. (2008) surfaces can be classified as "active" or "suppressed". A surface is active when, during emission, an increase of the wind speed (or, more general, an increased shear on the bed) results in a higher emission. Suppressed surfaces show no discernable response in dust emissions to increases in wind speed, suggesting that an initial depletion of loose fine material from these surfaces limits subsequent emissions (Macpherson et al., 2008). For example, the surface shown in Fig. 3B is clearly active: each step increase in wind velocity (or, in the figure, in RPM) results in a new emission peak higher than the previous one. Suppressed surfaces would show no substantial differences between consecutive peaks, and the peaks would also be rather low.

The Nellis Dunes data allow us to calculate the emission behavior of the 16 surfaces tested. Fig. 10A shows the evolution of the peaks during the PI-SWERL tests, for the undisturbed surfaces. The figure indicates that, except for surface unit 4.3 (gravel and silt and clay drainages), all surfaces are active. Also, the rate of increase of a peak with increasing RPM is systematically higher for the surfaces with sand compared to those with silt or gravel. Hence, despite that all surfaces except 4.3 are active those composed of silt and/or gravel are clearly characterized by a higher supply limitation (for PM10) than those consisting of sand.

To investigate how the emission behavior changes when off-road vehicles create new trails, the evolution of the PI-SWERL peaks in the trails were plotted in Fig. 10B. The "activity" of the top layer has increased considerably: all curves show higher peak values compared to Fig. 10A. Therefore, more PM10 is available for emission in the top layer in the trails compared to undisturbed terrain; the PM10 reservoir in the trails is larger than in the original soil. However, Fig. 10B also shows that the clear distinction between the surface units with sand and those with silt and/or gravel, typical for undisturbed terrain, no longer exists in the trails. This is further illustrated in Fig. 10C, which shows the difference between the diagrams of Figs. 10A and 10B. The position of the curves is random; no clear distinction can be made between the trails in sand and those in silt and/or gravel.

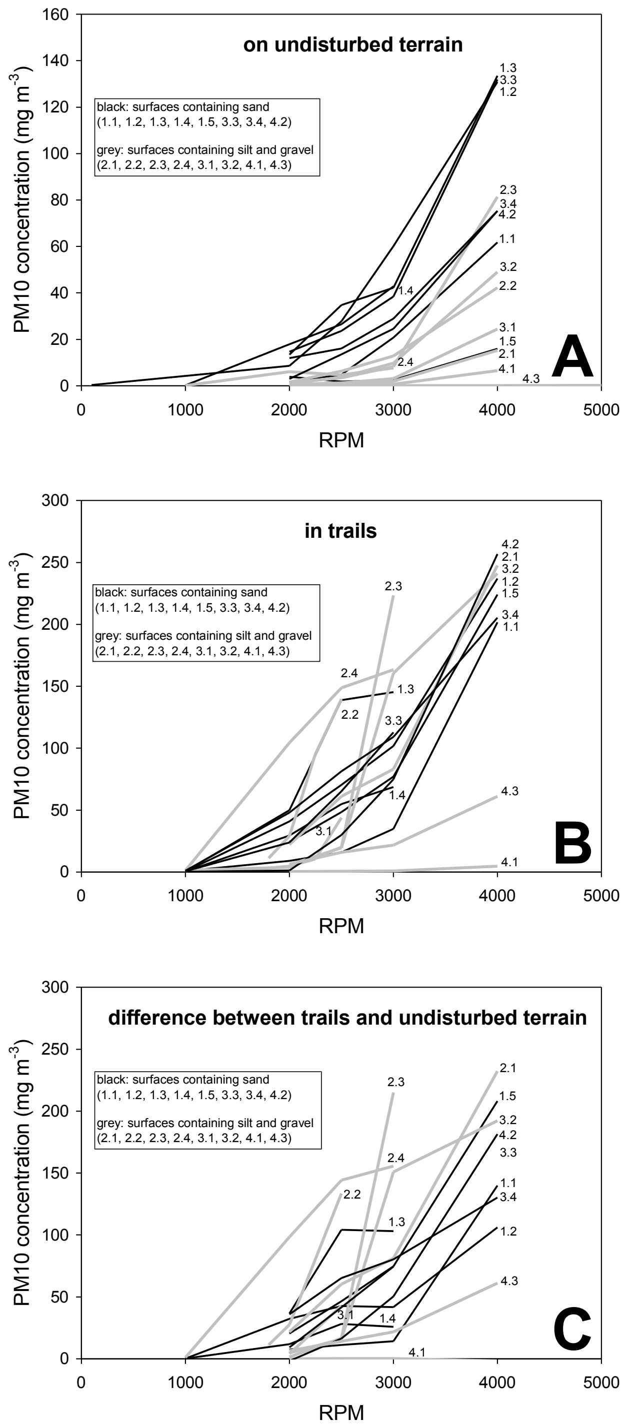

Fig. 10: Peak value in the PI-SWERL emission curve as a function of rotational speed of the blade (RPM). A: undisturbed terrain; B: ORV trails; C: difference between the diagrams 10A and 10B. Vertical scale in the A-figure has been exaggerated compared to the B- and C-figures to improve legibility.

However, it would be incorrect to conclude that the supply limitation in an ORV trail is not correlated to the type of surface, as suggested by Figs. 10B and 10C. Instead of looking at the evolution of the emission peak, as proposed by Macpherson et al. (2008), we study the evolution of the PM10 concentration after the peak has been reached. To ensure adequate comparisons of all surface types the data should first be normalized. This is done by recalculating the concentrations relative to the preceding peak. The procedure is repeated after each increase in RPM, for all 16 surface units. Four data sets are thus available for each unit, one for each RPM. Figs. 11 A and B show the average of these 4 sets, for the undisturbed surfaces and the trails respectively. Looking at Fig. 11A three observations can be made: (1) all normalized concentrations are below unity except for the two active sand dune units (1.1 and 1.2); (2) all curves show a descending trend except those of the same two units; (3) all units with sand are located in the upper part of the diagram whereas those with silt are located in the lower part. We conclude that the PM10 reservoir in the top layer of undisturbed desert surfaces is supply-limited, except for active sand dunes, which continue to produce significant amounts of PM10 well after an increase of the shear stress has occurred. Therefore, at least in relative terms, sand dunes would constitute a higher risk than silty surfaces, which suffer from serious supply limitations. The real risk of both surface groups is more difficult to evaluate because the total amount of PM10 emitted over time depends on both the peak and the post-peak emission, and the former is definitely higher for the silty surfaces.

Examining the data for the trails (Fig. 11B) the trends described previously are still discernable but less clear: for several units the position and slope of the curve has changed, the distinction between the sand and silt units is less pronounced, and only unit 1.1 still shows an increase with time. Therefore, ORV driving does affect the reservoir of emission-available PM10 in the top layer. To investigate how ORV driving affects the PM10 reservoir, we calculate the difference between Figs. 11B and 11A (see Fig. 11C). The trends are very pronounced: (1) all pure sand curves except unit 1.5 are below the zero line; (2) all silt curves are above the zero line; (3) gravel beds (unit 4.1) are exactly on the zero line, indicating that the composition of these surfaces does not change during off-road driving because this surface does not contain wind-erodible material; (4) gravelly substrata with wind-erodible material are close to the zero line but still located above (silt: 2.4, 3.2, 3.3, 4.3) or below it (sand: 1.3, 4.2). The position of the 1.5 curve (very fine sand and coarse silt) presumably is explained by the presence of coarse silt in this unit.

It can be concluded that changes in supply limitation due to the creation of ORV trails definitely are correlated to the type of surface, contrary to what Macpherson et al.'s (2008) approach suggests. Creating a new trail on sand surfaces increases the supply limitation of the top layer: the capacity of the reservoir of emission-available PM10 particles is reduced. Creating a new trail on silty surfaces has the opposite effect: the supply limitation will decrease and the capacity of the reservoir will increase. Creating a new trail on gravelly surfaces will slightly reduce (gravel with sand) or slightly increase (gravel with silt) the reservoir, or keep the reservoir unchanged (pure gravel without

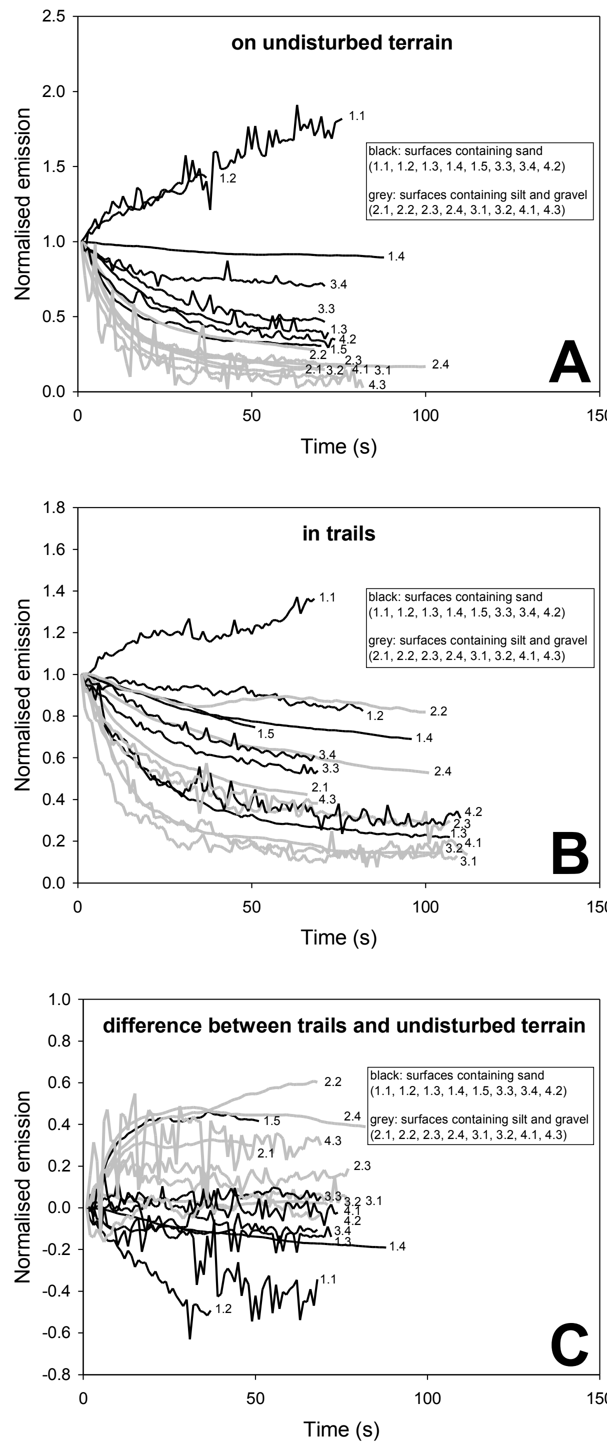

Fig. 11: Normalized emissions after the peak value in the PI-SWERL emission curve has been reached. A: undisturbed terrain; B: ORV trails; C: difference between the diagrams 11A and 11B. Note different vertical scales to improve legibility.

wind-erodible material). These results are likely best explained by compaction during ORV driving. Driving over loose sand surfaces compacts the soil, increases the shear resistance, and sticks the particles together. On undisturbed silt surfaces the particles are already behaving in a cohesive manner (in both the subsoil and surface crust); driving over these surfaces destroys the crust and creates a layer of very loose material highly susceptible to emission. Driving over gravel compacts the surface but has no impact on the emission of PM10 because no substantial PM10 reservoir is present.

All data and conclusions presented herein were obtained with, or are based on, the PI-SWERL. This instrument provides a point measurement of dust emission potential. However, the significance of such point measurements are not restricted to the measured spots themselves but are applicable to a broader area, particularly in sandy areas or in areas affected by blown-in sand. It is well known that saltation, i.e. the transport of sand sized particles, is a critical contributor to dust emissions (Gillette, 1977; Shao et al., 1993; Alfaro and Gomes, 2001). Sand particles mobilized from a disturbed landscape, for example an ORV trail, may create a cascade of emissions from undisturbed landscapes, even landscapes not directly adjacent to the trail. The strength of the top layer is a crucial factor in this process. Surfaces with a loose top layer, such as the sandy units 1.1, 1.2, 1.3 and 1.4, are very vulnerable to such emissions whereas most silt surfaces (units 2.1, 2.2, 2.3) and rock-covered silts (units 3.1, 3.2, 3.3, 3.4) suffer much less from cascade emissions because of their surface crust, their rock cover, or both. Depending on the type of surface ORV trails may thus affect the emission of dust at different scales.

4. The PI-SWERL experiment: summary of conclusions

The creation of new ORV trails in undisturbed terrain strongly affects the emission behavior of the soil. While ORV activity itself always results in seriously increased emissions, adequate management in ORV regions also requires that attention is paid to the effect ORV driving exerts on natural emission, i.e., wind erosion. Depending on the climatological conditions, vegetation cover and the intensity of ORV activities wind erosion may or may not be greater than the direct emissions produced by the vehicles.

ORV driving decreases the deflation threshold (the critical wind condition at which wind erosion starts) on silty surfaces and in drainages, but increases the threshold on sandy surfaces. Wind erosion is thus expected to start earlier in the trails on silty surfaces and in drainages and later on sandy surfaces. However, local factors, especially irregularities in the local topography due to incisions in and by the trails, also affect the deflation threshold.

The potential PM10 production (quantified by means of the emission flux) is significantly higher in ORV trails than on undisturbed terrain. ORV trails thus constitute a higher risk of increased emissions than undisturbed terrain. This is especially true for trails developed in silty surfaces, and less so for those in sand.

Compaction and the amount of PM10 in the top layer are key factors with respect to dust production in an ORV trail. On sandy surfaces ORV driving increases the degree of compaction in the top layer, making the surface less PM10 productive. In contrast, on silty surfaces ORV driving results in the creation of a loose surficial layer of fine sediment, thus increasing emissions despite the increased compaction of the deeper soil. Although the PM10 content is similar in both ORV trails and in undisturbed terrain, the emissions are significantly higher in the trails. In the trails high emissions are usually associated with a high PM10 content in the top layer. This differs from the undisturbed terrain, where emissions remain small regardless of the percentage of PM10 in the top layer.

Continued ORV driving in a trail results in a gradual coarsening of the top layer. The speed of coarsening is higher in trails in sand than in trails in silt. Trails in drainages coarsen even more rapidly.

The creation of a new ORV trail on a surface affects the degree of supply limitation in the top layer and, thus, the emission regime of the latter ("active" *versus* "suppressed"). However, the effect is a function of whether the trail is created on a sandy surface, a silty surface or on gravel. On sands, trail formation increases the supply limitation of the top layer; the capacity of the reservoir of emission-available PM10 is reduced. On silt the supply limitation decreases; the capacity of the PM10 reservoir increases. On gravel the reservoir does not change appreciably when new ORV trails are created. Compaction and the related binding of the grains explain this difference in behavior.

Acknowledgements

We thank V. Etyemezian, G. Nikolich and J. King (Desert Research Institute, Las Vegas, NV, USA) for providing the PI-SWERL instrument and for assistance during some of the PI-SWERL measurements.

References

Adkinson, G.P., 1991. Ecological Impacts of Trail Use in Three Indiana Nature preserves. M.Sc. Thesis, The School of Graduate Studies, Department of Life Sciences, Indiana State University, Terre Haute, IN, USA.

Alfaro, S.C., Gomes, L., 2001. Modeling mineral aerosol production by wind erosion: Emission intensities and aerosol distributions in source areas. Journal of Geophysical Research 106, D16, 18075-18084.

Carvacho, O.F., Ashbaugh, L.L., Flocchini, R.G., 2006. Elemental composition of PM10 and PM2.5 in ambient air downwind of agricultural operations in California's San Joaquin Valley. In: Brebbia, C.A., Conti, M.E., Tiezzi, E. (Eds.), Management of Natural Resources, Sustainable Development and Ecological Hazards (The Ravage of the Planet 2006). Witpress.com, Southampton, doi: 10.2495/RAV060681.

Etyemezian, V., Nikolich, G., Ahonen, S., Pitchford, M., Sweeney, M., Purcell, R., Gillies, J., Kuhns, H., 2007. The Portable In Situ Wind Erosion Laboratory (PI-SWERL): A new method to measure PM10 windblown dust properties and potential for emissions. Atmospheric Environment 41, 3789-3796.

Gillette, D.A., 1977. Fine particle emissions due to wind erosion. Transactions of the American Society of Agricultural Engineers 29, 890-897.

Gillies, J.A., Watson, J.G., Rogers, C.F., DuBois, J.C., Chow, J.C., Langston, R., Sweet, J., 1999. Long term efficiencies of dust suppressants to reduce PM10 emissions from unpaved roads. The Journal of the Air and Waste Management Association 49, 3-16.

Gillies, J.A., Etyemezian, V., Kuhns, H., Nikolic, D., Gillette, D.A., 2005. Effect of vehicle characteristics on unpaved road dust emissions. Atmospheric Environment 39, 2341-2347.

Goossens, D., Buck, B., 2009. Dust emission by off-road driving: experiments on 17 arid soil types, Nevada, USA. Geomorphology 107, 118-138.

Kuhns, H., Etyemezian, V., Green, M., Hendrickson, K., McGown, M., Barton, K., Pitchford, M., 2003. Vehicle-based road dust emission measurement: II - Effect of precipitation, wintertime road sanding, and street sweepers on inferred PM10 emission potentials from paved and unpaved roads. Atmospheric Environment 37, 4573-4582.

Kutiel, P., Eden, E., Zhevelev, Y., 2000. Effect of experimental trampling and off-road motorcycle traffic on soil and vegetation of stabilized coastal dunes, Israel. Environmental Conservation 27, 14-23.

Macpherson, T., Nickling, W.G., Gillies, J.A., Etyemezian, V., 2008. Dust emissions from undisturbed and disturbed supply-limited desert surfaces. Journal of Geophysical Research 113, F02S04, doi: 10.1029/2007/JF000800.

Moosmüller, H., Gillies, J.A., Rogers, C.F., DuBois, D.W., Chow, J.C.,Watson, J.G., Langston, R., 1998. Particulate emission rates for unpaved shoulders along a paved road. Journal of the Air and Waste Management Association 48, 398-407.

Pye, K., Tsoar, H., 1990. Aeolian Sand and Sand Dunes. Unwin Hyman, London.

Schoeneberger, P.J., Wysocki, D.A., Benham, E.C., Broderson, W.D. (Eds.), 2002. Field Book for Describing and Sampling Soils, Version 2.0. Natural Resources Conservation Service, National Soil Survey Center, Lincoln, NE, USA.

Shao, Y., Raupach, M.R., Findlater, P.A., 1993. Effect of saltation bombardment on the entrainment of dust by wind. Journal of Geophysical Research 98, 12719-12726.

Sweeney, M., Etyemezian, V., Macpherson, T., Nickling, W., Gillies, J., Nikolich, G., McDonald, E., 2008. Comparison of PI-SWERL with dust emission measurements from a straight-line field wind tunnel. Journal of Geophysical Research 113, F01012, doi: 10.1029/2007JF000830.

Wiedmer, M., 2002**.** Lower Kenai peninsula summer off-road vehicle trail stream crossings. Alaska Department of Fish and Game, Habitat and Restoration Division Technical Reports, Report 02-02, Anchorage, AK, USA.

Wilshire, H.G., Nakata, J.K., 1976. Off-road vehicle effects on California's Mojave desert. California Geology 29, 123-132.

Chapter 5

EMISSION AND DEPOSITION OF DUST BY WIND IN THE NELLIS DUNES RECREATION AREA

Dirk Goossens and Brenda Buck

Department of Geoscience, University of Nevada Las Vegas

1. Gross emission, net emission and gross deposition

This chapter describes the emission of dust generated by wind erosion in the Nellis Dunes Recreation Area (NDRA). Emissions were measured at 68 locations ("dust stations") installed on all 17 surface units that occur in the area. For practical applications and management issues it is essentially net emission (the difference in sediment mass, on the Earth's surface, before and after a time interval within which aeolian activity has taken place) that is of concern. Net emission is what is commonly referred to as "emission". However, the measurements carried out also allowed us to calculate two other, often neglected parameters of aeolian dust dynamics: gross emission and gross deposition. Gross emission is the total mass of sediment effectively worn away from the Earth's surface after a given time interval. Gross deposition, in its turn, is the total mass of sediment effectively depositing on the Earth's surface. Net emission is the difference between gross emission and gross deposition. Because during a wind erosion event some of the sediment emitted is replaced by freshly deposited sediment eroded upwind, net emission is always less then gross emission. Net emission is the final effect of the aeolian activity that took place. If it is positive then the sediment layer on the surface becomes thinner; if it is negative then the surface is nourished with sediment and the sediment layer thickens. In this perspective, net emission is the equivalent of negative accumulation.

A detailed, more fundamental study of gross emission, net emission and gross deposition based on the results of the Nellis Dunes measurements can be found in a scientific paper published in the journal Earth Surface Processes and Landforms (Goossens and Buck, 2010). A copy of that paper has been attached to this report (see Appendix B). In the current chapter we present the original data of the measurements, for this is what is needed to evaluate the role of wind erosion in the global dust production in NDRA. Readers interested in the more fundamental approach are referred to the published paper.

2. Dust dynamics by wind in the Nellis Dunes Recreation Area: methodology

2.1 Selection of dust stations

Dust dynamics were measured on all 17 surface units that occur in the Nellis Dunes area. Four dust stations were selected for each surface unit, 68 stations in total. For practical reasons (ability to collect all samples on a same day, which is necessary to compare stations and exclude effects caused by variations in atmospheric conditions) the stations were installed in 34 groups of two stations each. In each group the stations were installed in the same neighborhood, between 5 and 20 m from each other. There was no interference between the stations and each station can be considered an independent site, measuring its own dust dynamics. All data were calculated for each station individually, and the average result of the four stations installed on a same surface unit was calculated later. Data for the individual stations remain available and can be provided upon request.

Since the purpose of the measurements was to measure dust dynamics by wind erosion only, a special effort was made to install the stations in areas well away from zones of intense recreational use. This prevents local off-road vehicular activity (ORV) from affecting the results. Dust emitted by ORV activity has already been significantly diluted when arriving at a dust station, and its vertical concentration gradient will be close to zero because the medium-sized and coarse particles will have been removed from the cloud during transport. Because of the zero concentration gradient ORV-supplied dust does not affect the calculation of the local emission caused by wind erosion (see section 2.4 for more details).

The locations of the stations are shown in Fig. 1. The scale of the map does not allow showing the position of the two individual stations installed in a same neighborhood, therefore only the 34 neighborhoods are marked on the map.

2.2 Dust collection and analysis

Each dust station consisted of a 2-m long, 2-cm diameter metal pole to which 4 BSNE sediment samplers (Fryrear, 1986) were attached (Fig. 2). Airborne sediment was collected at the following heights: 25 cm, 50 cm, 75 cm and 100 cm. No collections were performed at higher levels because the focus of the study was on erosion and deposition at or near ground level. BSNE samplers were used because (1) this type of sampler is widely used worldwide; (2) its efficiency for collecting particles has been determined over a wide particle range, from less than 10 µm up to 287 µm (Shao et al., 1993; Goossens and Offer, 2000; Goossens et al., 2000; Sharratt et al., 2007). Samples were collected over periods of 2 weeks each, from 19 December 2007 to 16 December 2008. Twenty-six periods were thus sampled. Two-week samplings were the minimum to collect enough dust for subsequent grain size and chemical analysis.

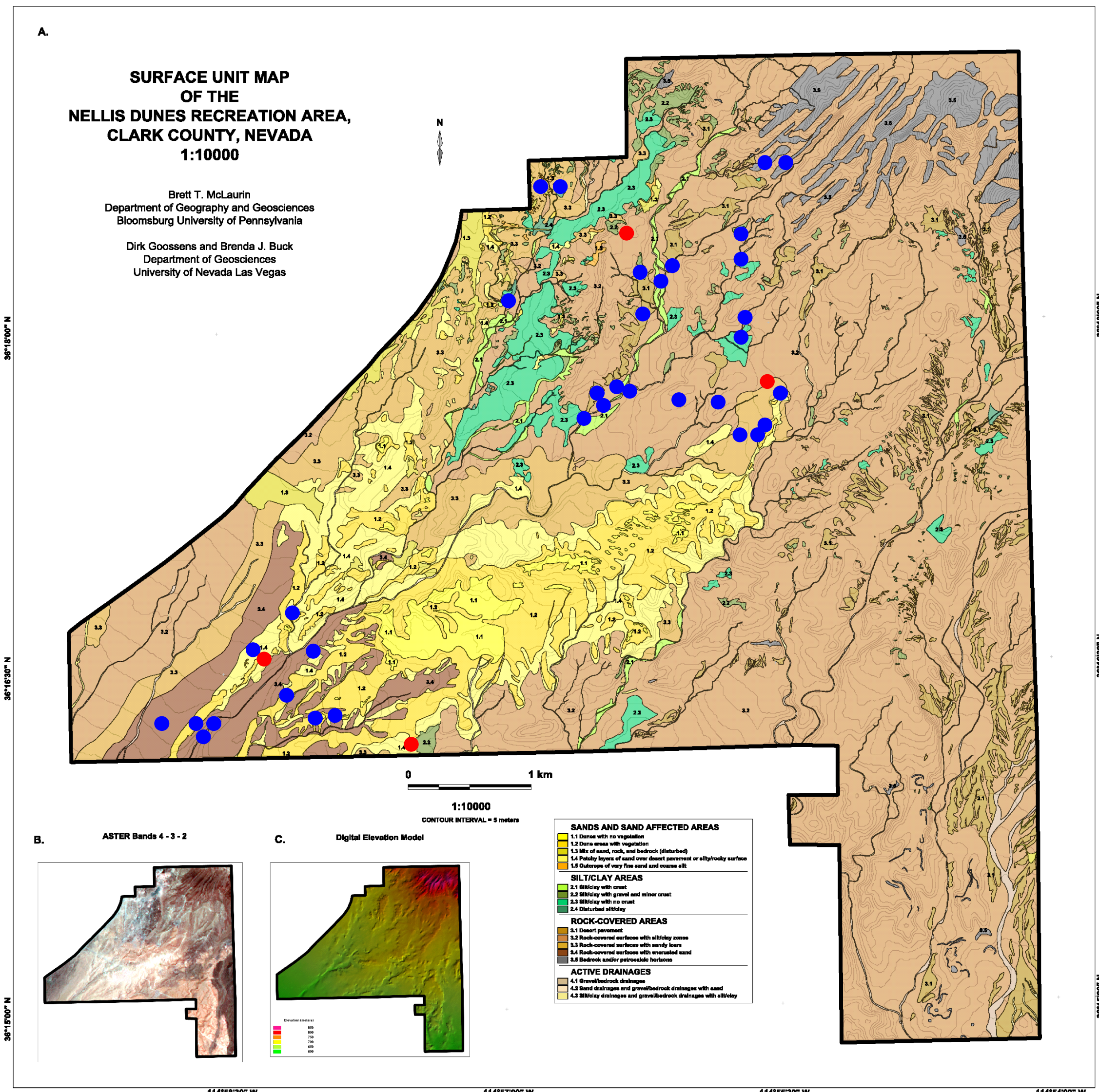

Fig. 1: Location of the wind erosion measurement sites (blue) and wind towers (red). Two dust stations were installed at each site.

Fig. 2: Dust station with four BSNE dust collectors

After each period new, fresh samplers were installed and the used ones brought to the laboratory. Sediment was collected with a brush. Samples were weighed to a precision of 0.0001 g and subsequently analyzed for grain size distribution using a Malvern Mastersizer 2000 laser particle size analyzer (Malvern Instruments Ltd., Malvern, UK) in the Environmental Soil Analytical Laboratory at UNLV. Samples were initially analyzed in a water solution, but additional dry analyses were performed with a Malvern Mastersizer S instrument to determine the degree of dispersion during wet analysis. Some dispersion also occurred in a few samplers themselves during (rare) cases of rainfall during the measurements. All data were corrected for such dispersion using the information provided by the dry analyses.

Corrections for insplash of particles into the BSNEs during heavy rainfall were also performed. Comparisons of the mass of sediment collected at a same level and at identical airborne concentrations for splash and non-splash episodes showed that significant insplash only occurred in the lowermost two BSNEs; the uppermost two BSNEs were not significantly affected. Splash corrections were only necessary for a minority of collection periods.

2.3 Wind measurements

Three 20-m wind towers (Fig. 3) and one 10-m wind tower were erected in the Nellis Dunes area. Each cluster of dust stations contained at least one wind tower (see Fig. 1). Wind speed, wind direction and temperature data were collected as 1-h averages between 19 December 2007 and 16 October 2008 and as 10-min averages from 16 October 2008 to 16 December 2008. Data from the nearby Nellis Air Force Base meteorological station, which borders on the test field, were used to fill data gaps. Such gaps were filled only after careful calibration between the wind towers and the Nellis Air Force Base station.

Additional wind measurements were performed at all dust stations with a portable 3-m long wind tower containing 4 anemometers (heights: 56 cm, 121 cm, 202 cm and 259 cm) to determine the roughness length (z_0) and the wind profile near each pole (Fig. 4). In total, 396 periods of 10 min each were sampled with the portable tower. Wind speeds at all catcher levels (25 cm, 50 cm, 75 cm and 100 cm) were then calculated and linked to the data collected from the 4 wind towers. From this information it is possible to calculate the wind speeds and friction velocities required to determine erosion, for wind erosion only occurs at winds strong enough to create a neutral atmospheric boundary layer in the lowermost meters near the ground (see Turner, 1994). Under such circumstances the wind profile is logarithmic and there is no need for stability corrections. Since there was at least one wind tower close by each dust station and wind speed was measured at relatively high altitudes from each tower, and because the roughness length is known at each station, wind data can be reconstructed at all stations using the wind profile (logarithmic, as explained above) and the tower data. Comparing data collected by the portable tower to those reconstructed by the method explained above (Fig. 5) confirms the reliability of the technique.

2.4 Calculation of net emission

Various methods exist to calculate net erosion (emission) of soil dust. A review is given in a recent book by Shao (2008). Emission calculations based on airborne dust concentration data generally are more reliable than calculations based on airborne dust transport data because they are more direct; therefore we selected the former option to calculate net erosion in the Nellis Dunes area.

Fig. 3: 20-m wind tower with anemometer and wind vane

Fig. 4: Portable wind towers with four anemometers

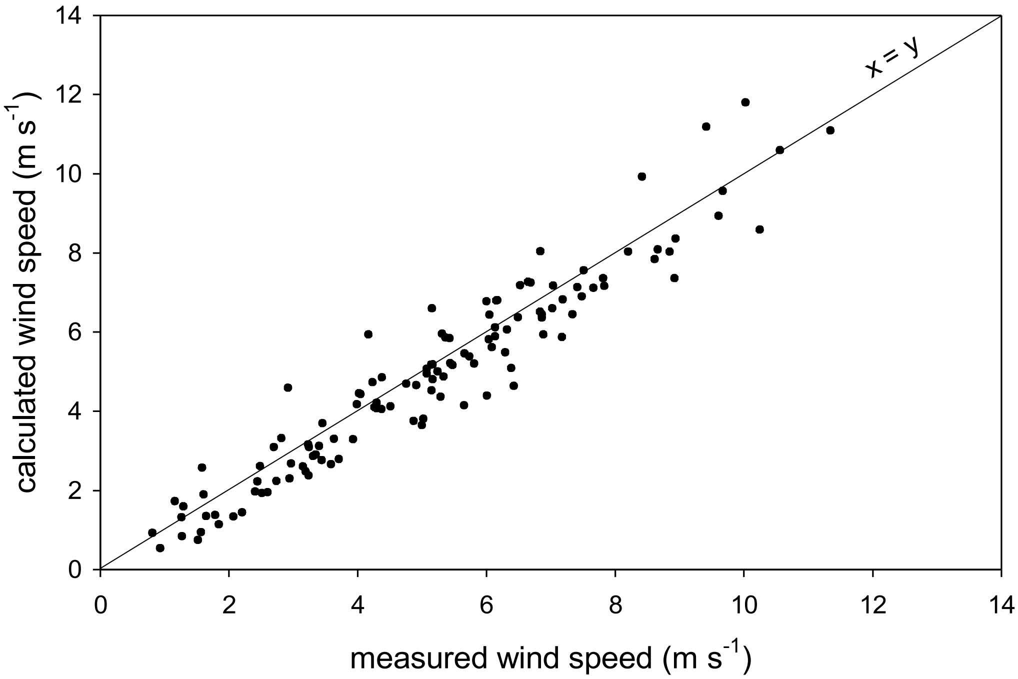

Fig. 5: Calculated *versus* measured wind speeds. Duration of test periods varied from 20 to 40 minutes. Each test period consisted of individual intervals of 10 minutes; 396 10-min intervals were measured in total.

Methods based on airborne concentration use vertical particle exchange to calculate vertical dust flux. Because this flux is affected by both the upward and downward movements of particles it always is an average flux; while in transport particles experience the effects of both velocity components. Also, they experience, simultaneously with the turbulent forces, the effect of gravity. Thus, numerical values of vertical dust flux collected from experiments always refer to net vertical flux; there is no need to add an extra term for deposition for the effect of deposition is already included in the experimentally recorded number.

Vertical dust flux can be calculated with Gillette's (1977) gradient method:

$$F = \frac{k \cdot u_* \cdot (C_1 - C_2)}{\ln(z_2 / z_1)} \tag{1}$$

where F = vertical dust flux, k = von Karman constant (0.4), u_* = friction velocity, and C_1 and C_2 = airborne dust concentrations at heights z_1 and z_2, respectively. This formula calculates the average vertical flux between heights z_1 and z_2; it does not calculate the erosion at ground level nor does it provide information on how the flux varies within the vertical layer bordered by z_1 and z_2. The latter problem can be solved by integrating the original exchange formula for neutral atmospheric conditions (neutral because we apply it to episodes with active wind erosion), $F = -k \cdot u_* \cdot z \cdot \frac{\partial C}{\partial z}$, accepting that C varies with z as a power function $C = a \cdot z^b$ (see e.g. Nickling, 1978; Buschiazzo and Zobeck, 2005), where a and b are numerical constants. This leads to:

$$F = -k \cdot u_* \cdot a \cdot b \cdot z^b \tag{2}$$

This expression, which was first proposed by Goossens et al. (2001), allows calculating vertical dust flux at any arbitrary height z in the constant shear stress layer. For b>0, F is negative and the flux is directed downward; for b<0, F is positive and the flux is directed upward.

For calculating the flux at ground level, the best option is to construct the vertical flux profile and extrapolate it to zero level (Goossens et al., 2001; Hoffmann et al., 2008) for neither Gillette's gradient method and Goossens et al.'s integration methods provides a mathematical solution for $z = 0$. To do this, several options exist: (1) calculate the vertical flux for several separate layers using the gradient method, adjust each flux value to the average height of the corresponding layer, and extrapolate the profile to zero level (modified Gillette 1977 method); (2) use the gradient technique, but the vertical fluxes are calculated for layers bordered by the highest catcher (top) and each subsequent catcher underneath (bottom); the flux is then calculated as the average vertical flux for these layers (see Hoffmann et al., 2008); (3) calculate the vertical flux at a large number of elevations using the integration method and extrapolating the profile to zero level (Goossens et al., 2001); (4) calculate the vertical flux at only those elevations where the catchers are installed and extrapolate the profile to zero level. Comparative tests showed that the first and last option lead to similar results whereas those from the second option result in under-estimation and the third option results in an overestimation of the emission (Fig. 6). The first option has the disadvantage that it sometimes results in negative erosion results and that small experimental error in the measurements (which is inevitable) has major effects on the final result. Option 4 does not suffer from these problems and also exclusively uses original data; therefore this option was selected to calculate net erosion in the Nellis Dunes experiment.

All extrapolations were done by fitting a third order polynomial through the data points, which gave a variation coefficient $R^2 > 0.99$ for all stations. Visual inspections of the profiles were made to confirm the extrapolations.

The airborne dust concentrations C_z, necessary to calculate erosion, were calculated by dividing the horizontal transport flux F_h measured by the BSNEs by the wind speed (at each appropriate elevation). Average values were used for each 2-week period because all horizontal flux data are 2-week averages. All data were corrected for the efficiency of the BSNE using information from the calibration studies by Shao et al. (1993) and Goossens and Offer (2000).

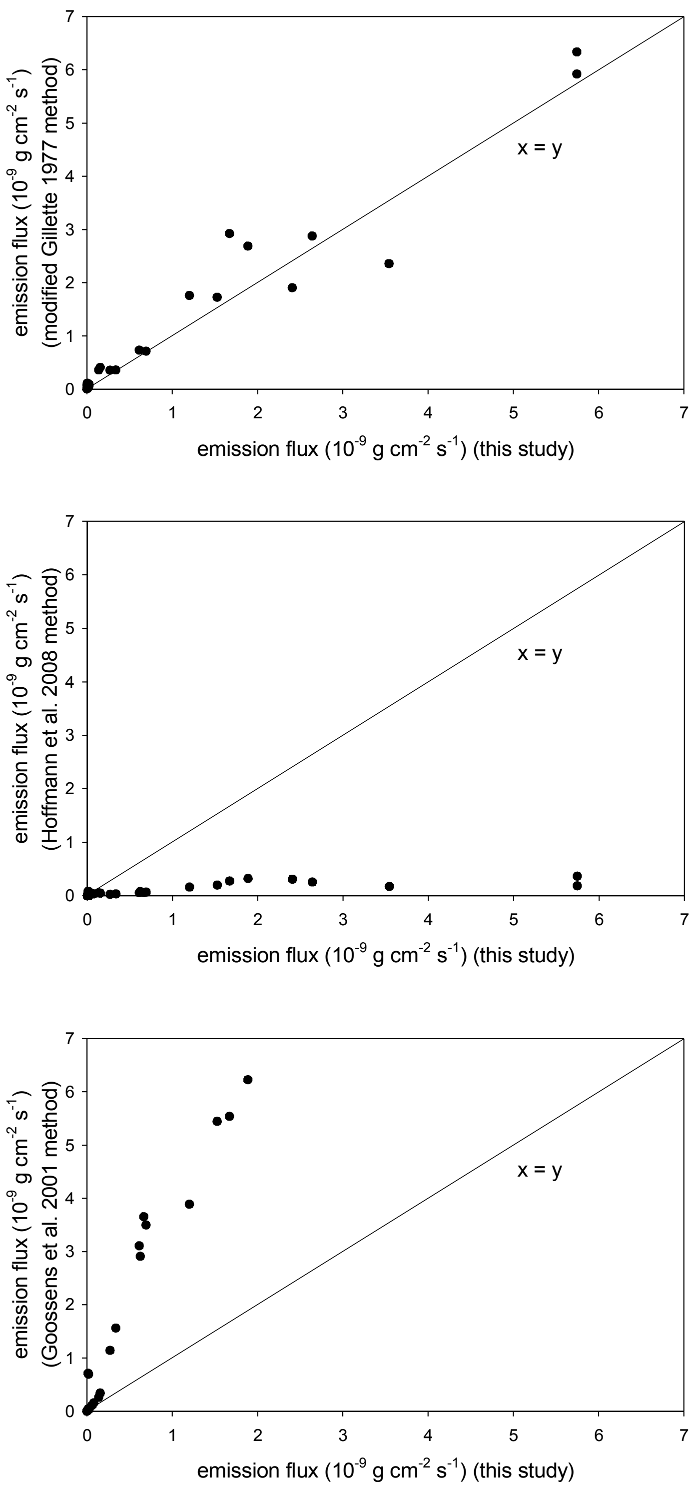

Fig. 6: Comparison of methods for extrapolating vertical dust flux to ground level. See text for explanation of each method.

The value of u_* in eq. (2) refers to the average friction velocity of the episodes of wind erosion; not the average u_* of all 14 days in each 2-week period. To determine the episodes of wind erosion we measured the deflation threshold (critical friction velocity at which wind erosion starts) with a Portable In Situ Wind Erosion Laboratory (PI-SWERL, see Chapter 4 of this report), at all dust stations. At least 4 measurements were done for each surface unit and the average deflation threshold was then calculated. To calculate the value of u_* in eq. (2), all 1-hour data from the 362-day long experiment were investigated and average friction velocities were calculated for each 2-week period by retaining only those u_* values that exceeded the deflation threshold. As 1-hour periods are still quite long for averaging friction velocities for the purpose of erosion calculations, we repeated the analysis for the period 16 October 2008 - 16 December 2008 for which 10-min data could be collected. Calculating the average friction velocities for 2-week intervals with these two options resulted in a difference of less than 3%, at all dust stations. Therefore, 1-hour data could be used for calculating u_* in eq. (2).

2.5 Calculation of gross deposition

Various techniques exist to calculate gross deposition. An overview, including comparisons between techniques, can be found in the study by Goossens and Rajot (2008). No direct measurements of dust deposition were performed in NDRA because (1) direct measurements of deposition at ground level usually suffer from local disturbances; (2) the proportion of dust in sediment deposited in sand areas (for instance, the sand dune units 1.1 and 1.2 in NDRA, see Chapter 2 for a description of the units) often is below the detection level of most grain size analyzers; and (3) the collection efficiency of dust deposition samplers heavily depends on wind speed and grain size, which affects the size distribution of collected dust (Goossens, 2007). Instead, dust deposition was calculated from the BSNE data using the inferential technique. This technique calculates deposition F_D as the product of airborne dust concentration C and the velocity of deposition v_d:

$$F_D = C \cdot v_d \tag{3}$$

In addition, comparative studies (e.g. Goossens and Rajot, 2008) showed that applying this technique to BSNE collections leads to deposition quantities identical to those measured with deposition catchers properly corrected for efficiency.

The velocity of deposition v_d, which is a function of particle size and shape and also depends on u_* and z_0, can be derived from standard graphs (see e.g. Sehmel, 1980), or it can be calculated from theoretical models (Sehmel and Hodgson, 1978; Slinn and Slinn, 1980; Slinn, 1983; Pleim et al., 1984; Venkatram and Pleim, 1999). Because these models assume that particles are spherical, which is a too simplified presumption for natural dust (see Goossens, 2007 or Goossens and Rajot, 2008 for examples), we used Dietrich's (1982) formula to calculate v_d. This formula includes a term for flattening

(*CSF*) and rounding (*P*) of grains and thus allows including particle shape in the calculations. For most types of soil-derived aeolian dust *CSF* and *P* are close to 0.70 and 3.45, respectively (Goossens, 2005); for the Nellis Dunes dust we used values of 0.69 and 3.47, which were derived from microscopic analysis of several dust samples. Strictly speaking Dietrich's formula does not calculate v_d but v_∞, the terminal settling velocity. For quartz grains in air and friction velocities below approximately 50 cm s^{-1} (typical values for the Nellis Dunes experiment reported here) the difference between v_d and v_∞ remains negligibly small once particles are coarser than 10 µm (see Sehmel, 1980). As the errors associated with particle shape are much larger than the difference between v_d and v_∞, Dietrich's approach was used. Comparisons of v_∞ and v_d calculated with Dietrich's and Slinn and Slinn's (1980) equations show that for (spherical, since Slinn and Slinn's formula applies to spheres) grains up to 50 µm the data are almost identical, and that for coarser grains the differences remain acceptable (Goossens and Rajot, 2008).

Velocities of deposition were initially calculated for 10 grain size fractions: 0-10 µm, 10-20 µm, 20-30 µm, 30-40 µm, 40-50 µm, 50-60 µm, 60-70 µm, 70-80 µm, 80-90 µm and 90-100 µm. Values for the mean particle size in each class (5 µm for the fraction 0-10 µm, 15 µm for the fraction 10-20 µm, etc.) were used when calculating deposition. In this report we regrouped the data into 3 classes: <20 µm, 20-60 µm and 60-100 µm. These 3 classes were selected based on the mode of transport of the particles: long-term suspension (<20 µm; particles can travel tens to hundreds of km after being released), short-term suspension (20-60 µm; particles usually travel several km to several tens of km after being released), and modified saltation (60-100 µm; particles usually travel several tens to at maximum several hundreds of m before settling to the surface again). Particles >100 µm were not considered in this study because most of these particles are transported in saltation, stay close to the surface, and do not create specific health problems.

To obtain gross (i.e., real) deposition, all data need to be recalculated to a perfectly absorbent surface. For aeolian deposition, water most probably is the best option currently available (Breuning-Madsen and Awadzi, 2005; Gigliotti et al., 2005; Goossens, 2005; Sow et al., 2006); therefore all deposition fluxes were recalculated to a water surface using the conversion factors provided by Goossens' (2005) study. Field measurements on dust deposition in SW Niger by Goossens and Rajot (2008) showed that this approach leads to very reliable results.

Gross deposition values were calculated at all 4 levels where BSNEs were installed (25, 50, 75 and 100 cm). To determine gross deposition at ground level, vertical deposition profiles were calculated and extrapolated to zero level. As with net erosion, a third order polynomial provided an excellent fit at all dust stations.

Note that the same dataset (concentrations measured with the BSNEs) is used for the calculations of gross deposition and net emission; this reduces the effect of experimental uncertainties when these two processes are compared.

2.6 Calculation of gross emission

Because net emission simply is the difference between gross emission and gross deposition, gross emission can be calculated as the sum of net emission and gross deposition:

$$E = e + S \tag{4}$$

where E = gross emission, e = net emission and S = gross deposition. Note that, once sediment has been emitted, S can eventually become superior to E if sediment emitted upstream is settling at a rate higher than the local erosion rate. If this happens, e is negative, which simply means that the surface is accumulating sediment.

3. Dust dynamics by wind in the Nellis Dunes Recreation Area: results and discussion

3.1 Role of surface units

3.1.1 Emission rates

The emission rates (in g cm^{-2} s^{-1}) for gross emission (E), gross deposition (S) and net emission (e) are displayed in Fig. 7 for the three grain size fractions investigated: <20 µm (sediment prone to long-term suspension), 20-60 µm (sediment prone to short-term suspension) and 60-100 µm (sediment prone to modified saltation). In general the patterns are very similar for E, S and e. This is understandable for E and S, for if lots of grains are released from the surface then many grains are available for sedimentation. The agreement between the patterns of E and e is less evident than it may look at first sight, especially because e is so much smaller than E and S. For the sediment fraction <20 µm the ratio e/E is still 0.553 (or 55.5 %); for the fraction 20-60 µm it is only 0.012 (or 1.2 %), and for the fraction 60-100 µm, 0.002 (or 0.2 %). This shows that the coarser the sediment is, the more hidden sediment dynamics takes place on the Earth's surface. We call it hidden because it is not recorded by classic wind erosion measurements, which only record the final (net) result. Many more grains are moving over the surface that can be derived from net emission measurements; most grains have just been displaced over the surface after the event has ceased without having been evacuated. For the <20 µm fraction gross emission is 1.8 times greater than the net emission. For the fraction 20-60 µm it is 82 times greater, and for the fraction 60-100 µm, it is 460 times greater. Net emission is thus very different from gross emission.

Looking at the differences between the surface units, we see that the most active units (highest emission and sedimentation rates) are the sand substrata of units 1.1 to 1.5, and also, though somewhat less, the rock-covered sands of unit 3.4. Silt and drainage areas are much less active, at least in terms of mass. These conclusions apply to all 3 grain size classes but the dominance of the sand dunes (units 1.1 and 1.2) is particularly clear for dust transported in modified saltation (60-100 µm). For medium-sized silt (20-60 µm) the sandy drainages of unit 4.2 also show high aeolian activity.

The data for net emission are summarized in Table 1. All numbers are positive, which means that all 17 surface units in the Nellis Dunes area are net-emissive: there is always more emission than deposition; all units are characterized by a negative sedimentation

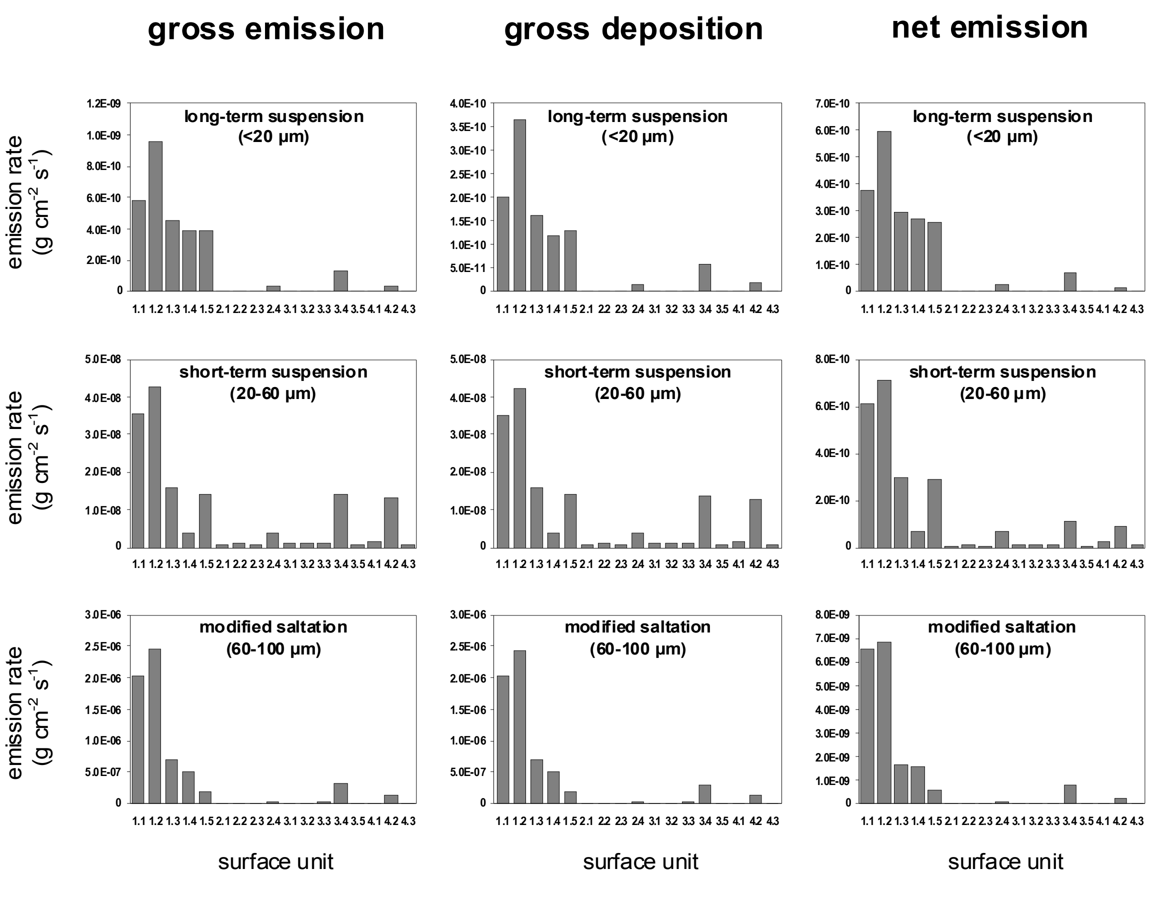

Fig. 7: Emission rates for gross emission, gross deposition and net emission for sediment prone to long-term suspension (<20 µm), short-term suspension (20-60 µm) and modified saltation (60-100 µm).

Table 1: Net emission rates for dust emission by wind erosion for the 17 surface units, for sediment prone to long-term suspension (<20 µm), short-term suspension (20-60 µm) and modified saltation (60-100 µm).

surface unit	net emission rate by wind erosion (g m^{-2} $year^{-1}$)		
	<20 µm (long-term suspension)	20-60 µm (short-term suspension)	60-100 µm (modified saltation)
1.1	118.32	193.44	2059.51
1.2	188.37	224.44	2169.64
1.3	92.94	92.90	506.17
1.4	85.32	22.83	484.21
1.5	81.84	92.75	184.79
2.1	0.23	1.52	2.56
2.2	1.03	4.23	3.34
2.3	0.60	1.70	1.21
2.4	7.96	21.19	24.33
3.1	0.60	3.54	3.98
3.2	0.31	3.09	4.28
3.3	0.48	3.03	7.85
3.4	23.58	36.10	242.02
3.5	0.17	1.56	1.50
4.1	1.70	8.66	6.76
4.2	5.74	29.22	57.53
4.3	0.48	2.74	3.46
sandy surfaces	113.36	125.27	1080.86
silty surfaces	2.46	7.16	7.86
rock-covered surfaces	5.03	9.46	51.93
drainages	2.64	13.54	22.59

balance. The large differences between the units are obvious from the table. The most emissive units (in terms of mass) are the sand substrata (units 1.x), followed by the rock-covered substrata (units 3.x) and the drainages (units 4.x). Silt substrata (units 2.x) are the least emissive. The high emission rates of the sand surfaces during natural wind conditions are explained by the loose and cohesionless structure of the top layer and the many saltating sand grains, which act as an initiator for releasing finer particles (Shao, 2008). Rock-covered silt substrata are less homogeneous than rock-free silts, the rock fragments increase the degree of turbulence near the ground promoting emission, and biological activity near and underneath the clasts produces loose aggregates vulnerable to emission. Drainages, finally, are more cohesive that their dry equivalent due to the precipitation of soluble carbonates and salts imported from surrounding regions during runoff. These substances bind the grains once the water has evaporated, creating protective crusts or cements.

3.1.2 Annual emissions by wind erosion in NDRA

The data in section 3.1.1 show the emission (or sedimentation) rates, i.e. the vulnerability of the surface units to the parameter (emission or sedimentation) in question. The current section investigates the effective productivity of the units. Effective productivity does not only depend on the emission and deposition rates, but is also determined by the areal extent of the units. Units with a high emission rate may be marginal suppliers of dust if they cover only small surfaces, and units with relatively low emission rates may still produce significant amounts if they are very abundant. This section investigates which units are the greatest suppliers of dust when wind erosion takes places in the Nellis Dunes Recreation Area.

The absolute amounts of dust gross emitted, gross deposited and net emitted annually in the Nellis Dunes area (in tons per year) are displayed in Fig. 8 for the three grain size fractions investigated (<20 µm, 20-60 µm and 60-100 µm). As with the emission rates the patterns are very similar for *E*, *S* and *e* for each fraction. The parameter of most interest for management purposes is net emission, and this parameter is described in more detail below.

During natural wind erosion by far most dust in NDRA is (net) emitted in the loose, uncompacted sand units 1.1 to 1.4. The most productive areas are the partly vegetated sand dunes (unit 1.2). The unvegetated dunes (1.1) produce significantly less dust, not only because they cover an area more than 4 times smaller that the partly vegetated dunes but also because they are more active and have lost a significant portion of their fine particles over time, leading to a much lower dust content in the top layer compared to the vegetated dunes that are less frequently prone to wind erosion (Fig. 9). All silt units, though very rich in dust, do not significantly contribute to net dust production in NDRA during wind erosion because their top layer is stabilized by surface crusts and/or rock cover. Even unit 3.2 (rock-covered silt and clay), which is by far the most abundant unit and covers more than 56 % of the NDRA, does not contribute significantly to the dust load in the Nellis Dunes area. Only for medium-sized dust (20-60 µm) is this unit a significant supplier of dust (Fig. 8). Unit 3.4, which is very similar to unit 3.2 except that it contains much more sand, produces even more dust than unit 3.2 despite it is 15 times less abundant and is commonly characterized by a cyanobacterial crust. The other sand unit characterized by a surface crust (unit 1.5, mixture of sand and fine silt) is not an important supplier of dust during natural wind erosion in the NDRA because of its very limited occurrence (only 0.1 % of the surface of NDRA).

The amounts of dust (net) emitted annually in NDRA are shown in Table 2. The large differences between the units are prominent. An interesting observation is that the numbers for the <20 µm and 20-60 µm fractions are almost identical (859 ton and 935 ton respectively) despite the much larger particles of the latter fraction. If all grains would be perfectly spherical, then it can be calculated that the number of <20 µm particles net

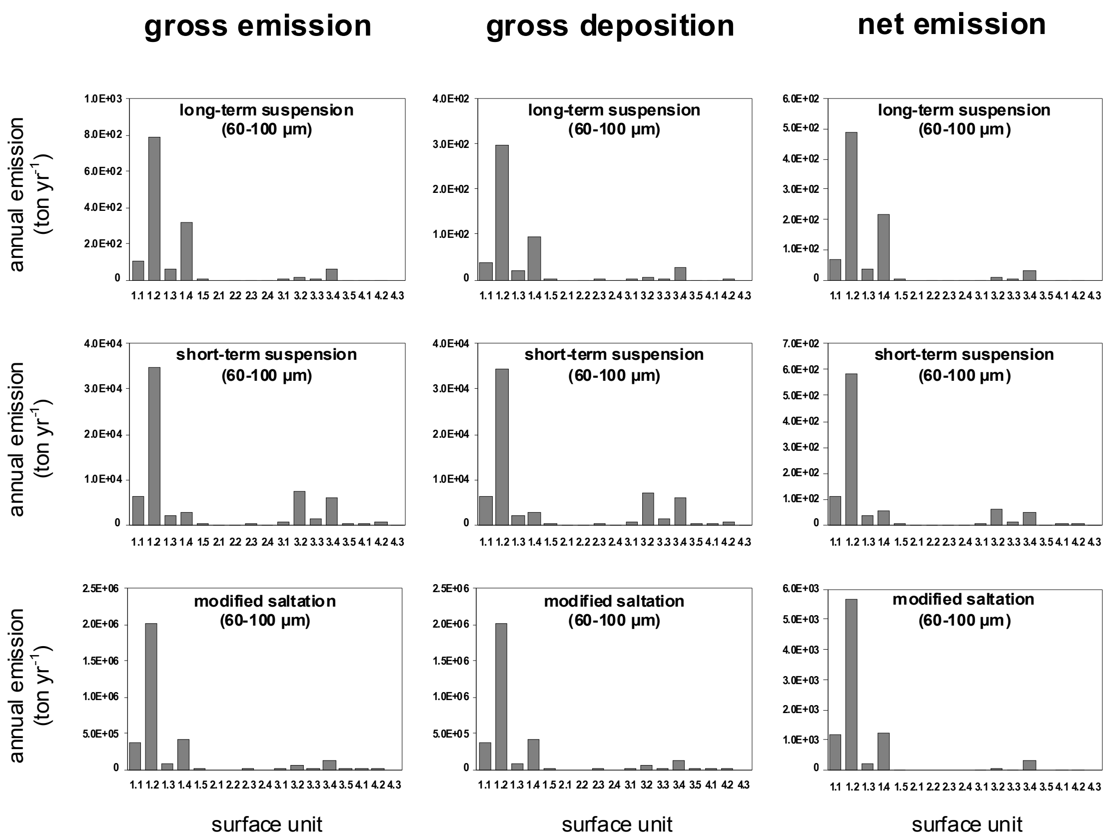

Fig. 8: Annual amounts of dust gross emitted, gross deposited and net emitted in the Nellis Dunes area in 2008, for sediment prone to long-term suspension (<20 µm), short-term suspension (20-60 µm) and modified saltation (60-100 µm).

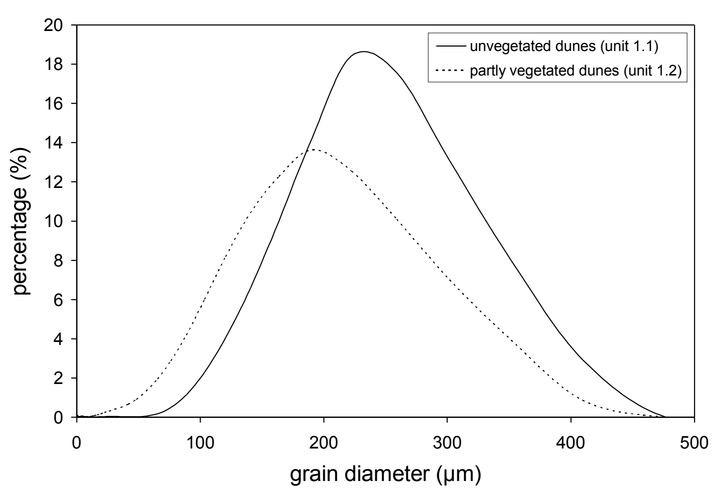

Fig. 9: Grain size distribution of the top soil (upper cm) in unvegetated and partly vegetated dunes at NDRA

Table 2: Annual amounts of dust net emitted in NDRA by wind erosion for the 17 surface units, for sediment prone to long-term suspension (<20 µm), short-term suspension (20-60 µm) and modified saltation (60-100 µm).

surface unit	emission amounts (ton yr^{-1})		
	<20 µm (long-term suspension)	20-60 µm (short-term suspension)	60-100 µm (modified saltation)
1.1	68.02	111.21	1184.00
1.2	489.10	582.76	5633.40
1.3	37.08	37.07	201.98
1.4	217.24	58.12	1232.83
1.5	3.02	3.42	6.82
2.1	0.06	0.42	0.70
2.2	0.43	1.75	1.38
2.3	0.66	1.89	1.34
2.4	0.35	0.93	1.07
3.1	0.95	5.63	6.33
3.2	6.28	63.52	87.99
3.3	1.49	9.38	24.29
3.4	32.35	49.53	332.04
3.5	0.18	1.61	1.55
4.1	0.65	3.32	2.59
4.2	0.72	3.68	7.24
4.3	0.11	0.65	0.83
NDRA	858.70	934.87	8726.38

emitted in NDRA is 59 times larger than the number of net emitted 20-60 µm particles. The number of net emitted 60-100 µm particles is almost identical as for 20-60 µm particles (only 1.17 times higher). Therefore, on an annual basis, most particles net emitted by wind in NDRA are evacuated in long-term suspension.

3.2 Seasonal patterns

3.2.1 Net emission

The seasonal evolution of (net) emission in NDRA is shown in Fig. 10 for each of the four categories of surface units: sandy surfaces (units 1.1 to 1.5), silty surfaces (units 2.1 to 2.4), rock-covered surfaces (units 3.1 to 3.5) and drainages (units 4.1 to 4.3). Because the emission values can strongly differ within the same surface group, it is necessary to normalize the data; otherwise the patterns for the most active units would obscure those

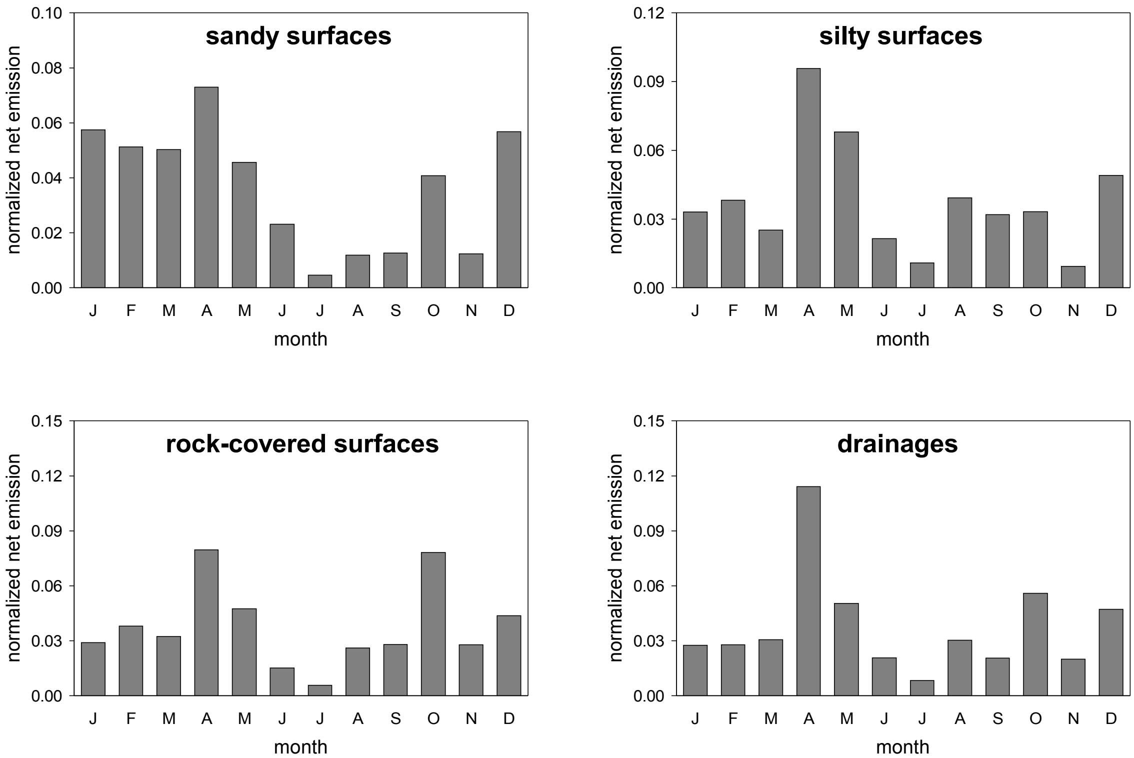

Fig. 10: Seasonal evolution of net emission in NDRA for the four categories of surfaces: sandy surfaces (units 1.1 to 1.5), silty surfaces (units 2.1 to 2.4), rock-covered surfaces (units 3.1 to 3.5), and drainages (units 4.1 to 4.3). Data are for total suspendable dust (0-60 µm).

of the slightly active units. All data were normalized by setting the annual average net emission equal to unity for all surface units. This does not affect the shape of the diagrams.

The patterns for the various size fractions were almost identical; in Fig. 10 we show the data for the total suspendable dust fraction (0-60 µm) as an example.

There is a clear difference between the sandy surfaces on the one hand and the three other types of surfaces on the other. The silty, rocky and drainage surfaces shown identical patterns with the highest net emission in the spring (April-May) and the lowest emission in summer (June-July). In the remaining months net emissions are fairly constant (the high value in October was caused by an only 1-h long, but very heavy storm on October 5). The sandy surfaces behave differently in that they are also highly emissive in the winter months (December-March) when the other surfaces are relatively stable. The contrast between winter-spring and summer-fall is much more pronounced for surfaces containing sand than for other surface types. The effect of the October 5 storm is clearly visible in the sand diagram but does not affect the general trend.

Although the diagrams are still somewhat irregular due to the relatively short duration (only one year) of the measurements we can still make the following important observations: the most dust in NDRA emitted by natural wind erosion occurs in the spring (and winter for sandy surfaces) whereas the smallest emissions occur in the summer, especially in the period June-July.

<u>3.2.2 Evacuation rate</u>

The rate at which sediment is evacuated during wind erosion can be quantified by the ratio of gross deposition to gross emission, *S*/*E*. For example, if *S*/*E* = 0.90 then 90 % of the eroding particle mass is replaced with freshly settling grains eroded upwind; 10 % of the mass is not replaced and will be evacuated from the spot in question. Especially the finest particle fractions, which are transported in long-term suspension and do not rapidly return to the surface, can be expected susceptible to evacuation.

Fig. 11 shows how the evacuation of dust from NDRA varies throughout the year for each of the four categories of surfaces. Here too the data were normalized to allow displaying all surface groups in a single diagram. The pictures for the various size fractions were nearly identical; we show the data for the total suspendable dust fraction (0-60 µm) as an example.

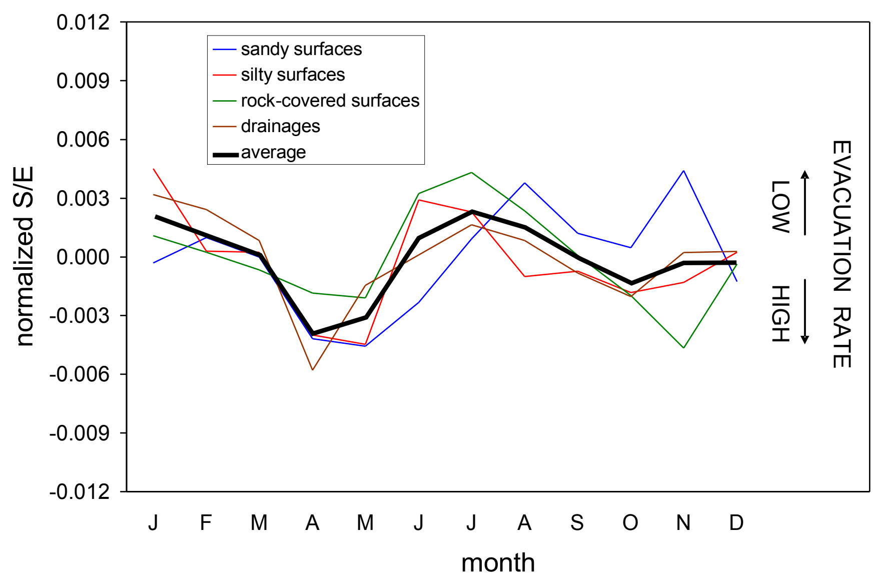

Fig. 11: Seasonal evolution of dust evacuation rate in NDRA for the four categories of surfaces: sandy surfaces (units 1.1 to 1.5), silty surfaces (units 2.1 to 2.4), rock-covered surfaces (units 3.1 to 3.5), and drainages (units 4.1 to 4.3). Data are for total suspendable dust (0-60 µm).

The evacuation rate is highest (low *S/E*) in spring (April-May) and in the fall (October), and lowest (high *S/E*) in summer (June-August) and in winter (January-February). To better interpret this pattern we calculated the evacuation rate as a function of dust activity. In NDRA dust transport is highest from mid April to mid May, lowest from mid July to mid February, and intermediate in the remaining months (Fig. 12A). Plotting *S/E* for each of these three periods separately (Fig. 12B) we see that the stronger the dust activity, the higher (low *S/E*) the evacuation becomes. During active periods dust emitted will settle less easily to the surface again; it will remain better suspended in the atmosphere and more easily evacuated from the Nellis Dunes area. This behavior is directly correlated to the wind speed (see Fig. 12C), for the stronger the wind blows the higher dust activity is and the higher the upward velocity fluctuations of the wind vector become, keeping the particles better aloft.

3.2.3 Grain size

To get an idea of the seasonal evolution of the size of the dust emitted from NDRA we calculated the median grain diameter (D50) of the airborne sediment and plotted it in Fig. 13A. Here too the temporal evolutions were very similar for all grain size fractions; Fig. 13A shows the curves for the total suspendable dust fraction (0-60 µm) as an example. Airborne dust was coarsest in winter (December-February) and then became finer until November. Local peaks of somewhat coarser dust do occur, but do not mask the general trend. However, the most important conclusion is that dust emitted from sand areas is considerably finer than dust emitted from silty areas, and certainly finer than dust emitted from rock-covered areas and drainages (Fig 13A). The difference is substantial: the annual average median grain diameters are 33 µm (sand areas), 38 µm (silt areas), 41 µm (rock-covered areas) and 40 µm (drainages). Two mechanisms may explain this behavior. First, the sand areas are much more active than the other areas. Over time they have lost a significant proportion of their most erodible fractions and in contrast to the other units, which can replace these fractions from underlying silty reservoirs, replacement of coarse silt (the most erodible fraction) is difficult. Therefore, in the total suspendable fraction, the proportion of coarse silt is smaller in the dunes and the median grain diameter of the suspendable dust will be lower. Secondly, in sand areas most dust emission is caused by impacting saltating grains. Fine particles that would normally not be released because they are sticking to other grains may now become emitted upon impact, resulting in a smaller median grain diameter in the cloud of emitted grains.

There is a tendency for the emitted dust to be somewhat coarser during periods of higher emission. To illustrate this we plotted the median grain diameter (for the total suspendable fraction, as before) as a function of the net emission rate (Fig. 13B). Although not very spectacular the trend is easily discernable in the diagram. High net emissions are associated with high wind speeds, which facilitate the emission of coarser grains.

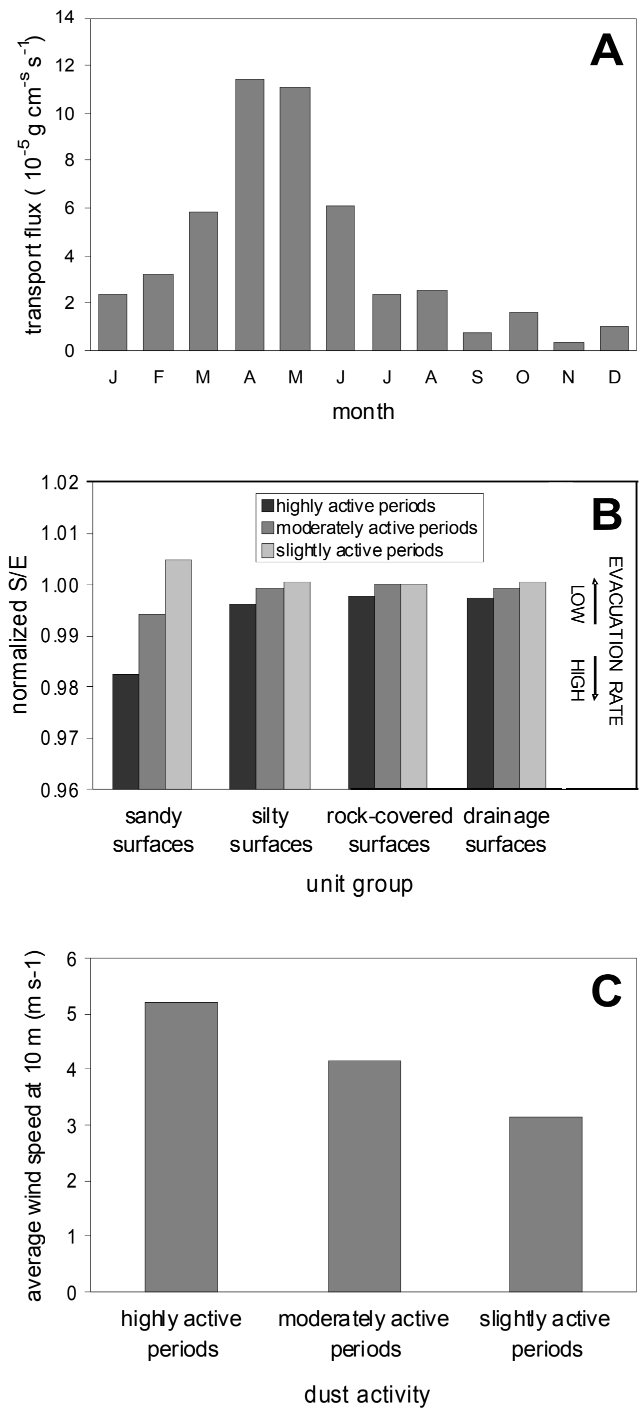

Fig. 12: Dust evacuation rate as a function of dust activity. (A) dust transport at NDRA; (B) normalized evacuation rate for highly active, moderately active and slightly active periods, for the four categories of surfaces; (C) average wind speed at 10 m. See text for criteria. Data are for total suspendable dust (0-60 µm).

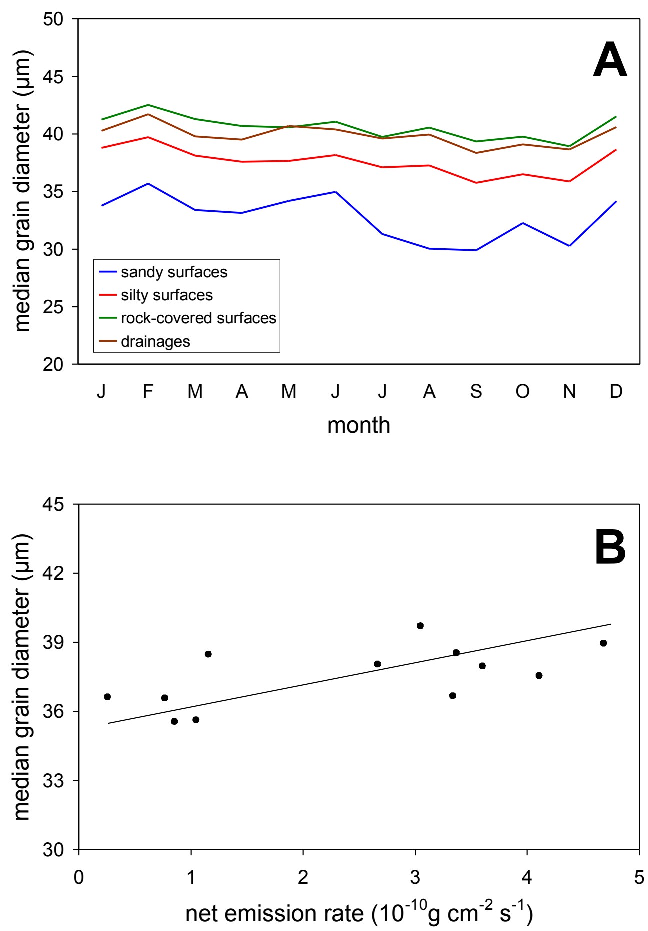

Fig. 13: Grain size of airborne dust at NDRA. (A) seasonal evolution of the median grain diameter for total suspendable dust (0-60 µm), average for the four sampling heights of 25 cm, 50 cm, 75 cm and 100 cm; (B) median grain diameter for total suspendable dust as a function of the net emission rate.

4. Summary of conclusions

All 17 surface units in the Nellis Dunes area are net-emissive: there is always more emission than deposition. All units are thus characterized by a negative sedimentation balance.

The units most vulnerable to dust emission during natural wind erosion are the sand substrata, followed by the rock-covered substrata and the drainages. Silt substrata with no or only sparse rock fragments are the least emissive surfaces. The high emission rates of the sand substrata are explained by the loose and cohesionless structure of the top layer and the many saltating sand grains, which act as an initiator for releasing finer particles. Rock-covered silt substrata are less homogeneous than rock-free silts; the rock fragments increase the degree of turbulence near the ground promoting emission, and biological activity near and underneath the clasts produces loose aggregates vulnerable to emission. Drainages, finally, are more cohesive due to the precipitation of soluble carbonates and salts imported from surrounding regions during runoff. These substances bind the grains once the water has evaporated, creating protective crusts or cements.

During wind erosion by far most dust in NDRA is emitted from the loose, uncompacted sand units 1.1 to 1.4. The most productive areas are the partly vegetated sand dunes (unit 1.2). The unvegetated dunes (unit 1.1) produce significantly less dust. All silt units, though very rich in dust, do not significantly contribute to net dust production in NDRA during wind erosion because their top layer is stabilized by surface crusts and/or rock cover. Unit 1.5 (mixture of sand and fine silt) is not an important supplier of dust in the NDRA because of its very limited occurrence (only 0.1 % of the surface of NDRA) and because it is characterized by a physical surface crust.

The silty, rocky and drainage surfaces produce most dust in the spring (April-May) and much less dust in summer (June-July). The sandy surfaces behave differently in that they are also highly emissive in the winter months (December-March) when the other surfaces are relatively stable. The contrast between winter-spring and summer-fall is much more pronounced for surfaces containing sand than for other surface types.

In NDRA most dust transport from natural wind erosion takes place from mid April to mid May. Dust transport is low from mid July to mid February, and intermediate in the remaining months. The evacuation rate is highest in spring (April-May) and in the fall (October), and lowest in summer (June-August) and in winter (January-February).

Periods of high evacuation rates are associated with periods of high dust activity. During active periods the emitted dust settles less easily to the surface, remains better suspended in the atmosphere and is more easily evacuated from the Nellis Dunes area. This behavior is directly correlated to the wind speed. The stronger the wind blows, the higher dust activity is and the higher the upward velocity fluctuations of the wind vector become keeping the particles better aloft.

Airborne dust in NDRA is coarsest in winter (December-February) and gets finer until November. Dust emitted from sand areas is considerably finer than dust emitted from silty areas, and even finer than dust emitted from rock-covered areas and drainages. One reason is that the sand areas are much more active than the other areas. Over time they have lost a significant proportion of their most erodible fractions (coarse silt) and in contrast to the other units, which can replace these fractions from underlying silty reservoirs, replacement of coarse silt is difficult. This results into a smaller median grain diameter in the dunes. A second reason is that in sand areas most dust emission is caused by impacting saltating grains. Fine particles that would normally not be released because they are sticking to other grains may now become emitted upon impact, resulting in a smaller median grain diameter in the cloud of emitted grains.

Dust emitted from NDRA is coarsest during periods of strong wind erosion. High net emissions are associated with high wind speeds, which facilitate the emission of coarser grains.

Acknowledgement

D. Pepper and U. Rangegowda (College of Engineering, University of Nevada Las Vegas, Las Vegas, NV, USA) and X. Wang (Purdue University Calumet, Hammond, IN, USA) organized the collection of wind data from the wind towers and performed the initial processing of the wind records. V. Etyemezian and G. Nikolich (Desert Research Institute, Las Vegas, NV, USA) provided the portable wind tower and processed the raw data. Wind data from the Nellis Air Force Base meteorological station were provided by M. EmelyPoynter (Nellis Air Force Base, Las Vegas, NV, USA).

References

Breuning-Madsen, H., Awadzi, T.W., 2005. Harmattan dust deposition and particle size in Ghana. Catena 63, 23-38.

Buschiazzo, D.E., Zobeck, T.M., 2005. Airborne horizontal mass flux calculated with different equations. Proc. 2005 ASAE Annual Meeting, Tampa, Florida, USA, Paper No. 052049.

Dietrich, W.E., 1982. Settling velocity of natural particles. Water Resources Research 18**,** 1615-1626.

Fryrear, D.W., 1986. A field dust sampler. Journal of Soil and Water Conservation 41**,** 117–120.

Gigliotti, C.L., Totten, L.A., Offenberg, J.H., Dachs, J., Nelson, E.D., Reinfelder, J., Eisenreich, S.J., 2005. Atmospheric concentrations and deposition of polycyclic aromatic hydrocarbons to the mid Atlantic east coast region. Environmental Science & Technology 39**,** 5550-5559.

Gillette, D.A., 1977. Fine particulate emissions due to wind erosion. Transactions of the ASAE 20, 890-897.

Goossens, D., 2005. Quantification of the dry aeolian deposition of dust on horizontal surfaces: an experimental comparison of theory and measurements. Sedimentology 52, 859-873.

Goossens, D., 2007. Bias in grain size distribution of deposited atmospheric dust due to the collection of particles in sediment catchers. Catena 70, 16-24.

Goossens, D., Buck, B., 2010. Gross erosion, net erosion and gross deposition of dust by wind: field data from 17 desert surfaces. Earth Surface Processes and Landforms, doi: 10.1002/esp.2080.

Goossens, D., Offer, Z.Y., 2000. Wind tunnel and field calibration of six aeolian dust samplers. Atmospheric Environment 34, 1043-1057.

Goossens, D., Rajot, J.L., 2008. Techniques to measure the dry aeolian deposition of dust in arid and semi-arid landscapes: a comparative study in West Niger. Earth Surface Processes and Landforms 33, 178-195.

Goossens, D., Gross, J., Spaan, W., 2001. Aeolian dust dynamics in agricultural land areas in Lower Saxony, Germany. Earth Surface Processes and Landforms 26, 701-720.

Goossens, D., Offer, Z.Y., London, G., 2000. Wind tunnel and field calibration of five aeolian sand traps. Geomorphology 35, 233-252.

Hoffmann, C., Funk, R., Li, Y., Sommer, M., 2008. Effect of grazing on wind driven carbon and nitrogen ratios in the grasslands of Inner Mongolia. Catena 75, 182-190.

Nickling, W.G., 1978. Eolian sediment transport during dust storms: Slims River Valley, Yukon Territory. Canadian Journal of Earth Sciences 15, 1069-1084.

Pleim, J.E., Venkatram, A., Yamartino, R., 1984. ADOM/TADAP Model Development Program, vol. 4: The Dry Deposition Module. Ontario Ministry of Environment, Rexdale.

Sehmel, G.A., 1980. Particle and gas dry deposition: a review. Atmospheric Environment 14, 983-1011.

Sehmel, G.A., Hodgson, W.H., 1978. A Model for Predicting Dry Deposition of Particles and Gases to Environmental Surfaces. DOE Report PNL-SA-6721, Pacific Northwest Laboratories, Richland, WA.

Shao, Y., 2008. Physics and Modelling of Wind Erosion (2nd Ed.). Springer Science + Business Media B.V., Dordrecht.

Shao, Y., McTainsh, G.H., Leys, J.F., Raupach, M.R., 1993. Efficiencies of sediment samplers for wind erosion measurement. Australian Journal of Soil Research 31, 519-532.

Sharratt, B., Feng, G., Wendling, L., 2007. Loss of soil and PM10 from agricultural fields associated with high winds on the Columbia Plateau. Earth Surface Processes and Landforms 32, 621-630.

Slinn, W.G.N., 1983. Air-to-sea transfer of particles. In: Liss, P.S., Slinn, W.G.N. (Eds.), Air–Sea Exchange of Gases and Particles. NATO ASI Series, Reidel, Dordrecht, 299-405.

Slinn, S.A., Slinn, W.G.N., 1980. Predictions for particle deposition on natural waters. Atmospheric Environment 14, 1013-1016.

Sow, M., Goossens, D., Rajot, J.L., 2006. Calibration of the MDCO dust collector and of four versions of the inverted frisbee dust deposition sampler. Geomorphology 82, 360-375.

Turner, D.B., 1994. Workbook of Atmospheric Dispersion Estimates: An Introduction to Dispersion Modeling. Lewis Publishers, Boca Raton.

Venkatram, A., Pleim, J., 1999. The electrical analogy does not apply to modeling dry deposition of particles. Atmospheric Environment 33, 3075-3076.

Chapter 6

TOTAL DUST PRODUCTION IN THE NELLIS DUNES RECREATION AREA: CONTRIBUTIONS OF THE NATURAL AND ANTHROPOGENIC EMISSIONS

Dirk Goossens and Brenda Buck

Department of Geoscience, University of Nevada Las Vegas

1. Introduction

Two types of processes contribute to dust emission in the Nellis Dunes Recreation Area (NDRA): wind erosion and off-road vehicular activity (ORV). Emission rates as well as annual dust production were studied in the Chapters 5 and 3 of this report for wind erosion and ORV respectively, for all 17 surfaces types in the NDRA. Emission rates quantify the vulnerability of each surface and its capacity to produce dust. In contrast, annual dust production quantifies the effective productivity, which depends on the emission rate and the areal extent of the specific surface unit. This chapter studies the total dust production in NDRA. We investigated the contributions of wind erosion and ORV activity to the total emissions, and examined the differences between the two types of processes. We also investigated the emissions for various grain size classes of dust. Separating between grain size classes is important because (1) grain size directly determines the transport mode, determining the size of the area affected by the emissions; (2) health risks related to airborne dust strongly depend on the size of the particles (Tiittanen et al., 1999).

2. Methodology

2.1 Dust production by wind erosion

Dust production by wind erosion was measured at 68 experimental stations, four stations on each surface unit. The procedure is described in detail in Chapter 5 of this report. In short, BSNE sediment traps (Fryrear, 1986) were used to collect dust at 4 altimetric levels: 25 cm, 50 cm, 75 cm and 100 cm. Emissions were calculated from the horizontal transport flux data using particle exchange theory. Samples were collected over periods of 2 weeks each, from 19 December 2007 to 16 December 2008. Twenty-six periods were thus sampled. Two-week samplings were the minimum to collect enough dust for subsequent grain size and chemical analysis. After having determined the total weight of each sample, sediment was analyzed for grain size distribution using a Malvern Mastersizer 2000 laser particle size analyzer (Malvern Instruments Ltd., Malvern, UK) at the Environmental Soil Analytical Laboratory at UNLV.

For this study we grouped the data into 3 classes: <20 µm, 20-60 µm and 60-100 µm. These 3 classes were selected based on the mode of transport of the particles: long-term suspension (<20 µm; particles can travel tens to hundreds of km after being released), short-term suspension (20-60 µm; particles usually travel several km to several tens of km after being released), and modified saltation (60-100 µm; particles usually travel several tens to at maximum several hundreds of meters before settling to the surface again). The threshold values of 20, 60 and 100 µm were selected according to the criteria proposed by Pye and Tsoar (1990). Analysis of previously collected wind erosion data from NDRA (Goossens and Buck, 2010) showed that these criteria are applicable to the dust released in the Nellis Dunes area. PM10 (particles <10 µm) was also measured, but in this study they are a subcomponent of the PM20 fraction and are not separated into another class because that size fraction is not transported in any specific special way. Also, particles >100 µm were not considered because most of these particles are transported in saltation, remain close to the surface, and do not create specific health problems.

Apart from the real dust emissions, potential dust emissions were also measured at all stations using a Portable In-Situ Wind Erosion Laboratory (PI-SWERL). Potential emissions represent emissions during optimal conditions of soil and atmosphere during wind erosion and give an indication of the maximum emission possible during such conditions. The procedure is described in detail in Chapter 4 of this report. Because the PI-SWERL only measures PM10 and the current chapter considers other size fractions, absolute PI-SWERL emission data will only be presented in exceptional cases, but normalized PI-SWERL data will be used in combination with real emissions when examining relationships between soil properties and emission.

2.2 Dust production by off-road vehicular activity

Dust production during ORV activity was measured on all surface units except unit 3.5 because (1) this unit is composed of bedrock and hardly contains dust particles; (2) in NDRA there is no driving on this unit because these surfaces are generally too rough and too steep to be driven upon. It is safe to state that, at least in NDRA, the 3.5 units do not produce ORV-generated dust. The procedure followed is described in detail in Chapter 3. In short, experiments were performed with three types of vehicles: dirt bikes (motorcycles), dune buggies, and 4-wheelers (quads). Dust was collected with BSNE samplers installed along the experimental transects. All samples were analyzed with the Mastersizer 2000 instrument to determine grain size distribution, and emissions were calculated for the same 3 classes mentioned before: <20 µm, 20-60 µm and 60-100 µm. Experiments were performed at different driving speeds varying from 24 km h^{-1} to 56 km h^{-1}, and data were calculated for 6 standard speeds: 0, 10, 20, 30, 40 and 50 km h^{-1}. Greater speeds were not possible because of safety reasons (too rough terrain).

The original emission data are expressed in mass of sediment emitted per unit length (grams of dust emitted per driven cm), but to compare these emissions to those created by wind erosion they were recalculated to tons ha^{-1} yr^{-1}. This was possible because the length and width of all ORV trails in NDRA could be mapped from detailed aerial photographs, allowing calculation of the surface area of each trail. We then calculated the emissions based on the following criteria: (1) NDRA is visited by 300,000 visitors per year; (2) visits are made with an "average" vehicle (average of a dirt bike, dune buggy and 4-wheeler, which altogether represent approximately 99% of the vehicles used at NDRA); (3) average length of a run is 10 km; (4) the proportion of a surface unit in a run equals the proportion of that unit in the total track length within NDRA. Criterion (1) is an estimate based on a survey carried out by the Las Vegas office of the Bureau of Land Management in 2004 (BLM, 2004), which mentions a number of 285,000 visitors. Criterion (2) is a reasonable assumption as there is no real preference in type of vehicle used at NDRA. The number in criterion (3) may look somewhat low when compared to other ORV areas. For example, in a study carried out in Montana, USA, Sylvester (2009) reported run lengths of between 15 and 20 miles (24 and 32 km). However, at NDRA many tracks are very rough (resulting in low driving speeds), and the density of tracks also is very high (which means drivers make many turns, resulting in a limited daily average driving speed and, thus, in a limited number of km driven). The number of 10 km per run is a good average at NDRA. The assumption in criterion (4) is justified because it can be expected that the more popular a unit is to ORV drivers (which also means: the higher the proportion of that unit will be in a run), the more tracks will be driven in that unit over time, and therefore the higher the track density will become within that unit.

Although we are confident that 300,000 visitors per year and 10 km run length are representative numbers for NDRA the data for ORV emission can always easily be recalculated should new numbers on visitors or run lengths become available.

3. Results

3.1 Emission rates and amounts

Rates for total dust emission (wind erosion + ORV) are shown in Fig. 1 for each of the three grain size fractions investigated in this chapter. The data for wind erosion can be read in the upper diagrams of 0 km h^{-1} (no driving); those for ORV-generated emissions are shown in Fig. 2.

For wind erosion, the highest emission rates occur in the active sand substrata of units 1.1 to 1.5, and although somewhat less, the rock-covered sands of unit 3.4. Silt and drainage areas are much less emissive. These conclusions apply to all 3 grain size classes but the dominance of the sand dunes (units 1.1 and 1.2) is particularly noticeable for dust transported in modified saltation.

The high emission rates of the sand surfaces are explained by the saltating sand grains, which act as an initiator for releasing finer particles (Shao, 2008).

The patterns for ORV-generated dust emission are notably different (Fig. 2). The highest emission rates occur in the silt and rock-covered silt units, and especially unit 2.2 (silt and clay with gravel). This pattern applies to all driving speeds although it becomes better visible as driving speed increases. There are no differences between the three grain size fractions except that, for coarse dust (60-100 µm), the sand units 1.1 to 1.5 show emission rates comparable to those of most silt and silt/rock units. Also note that unvegetated dunes (unit 1.1) behave differently compared to the partly vegetated dunes (unit 1.2) in that they do not produce any (or almost any) dust during ORV driving (Fig. 2).

For total emission there are no substantial differences between the two suspension fractions (<20 µm and 20-60 µm) except that the sand substrata produce a little more dust in the finest fraction (Fig. 1). This is entirely caused by wind erosion and not by ORV activity (Fig. 2). However the emission pattern is entirely different for coarse dust: here, the sand dunes (1.1 and 1.2) are by far the most emissive units although the units 1.3, 1.4 and 1.5 also contain substantial amounts of 60-100 µm dust in the top soil.

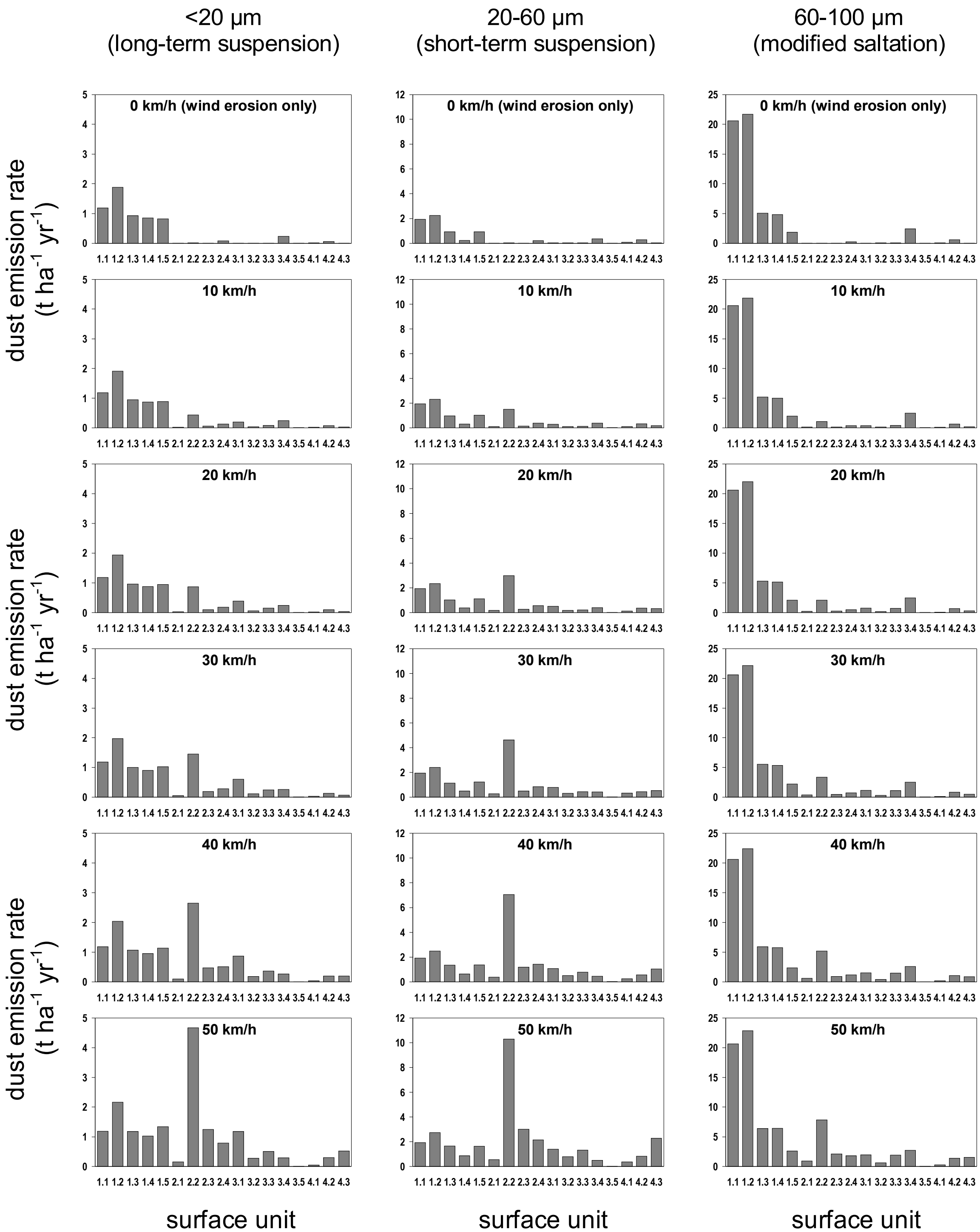

Fig. 1: Rates for total dust emission (wind erosion + ORV) at Nellis Dunes Recreation Area. Data for ORV are based on the criteria described in section 2.2.

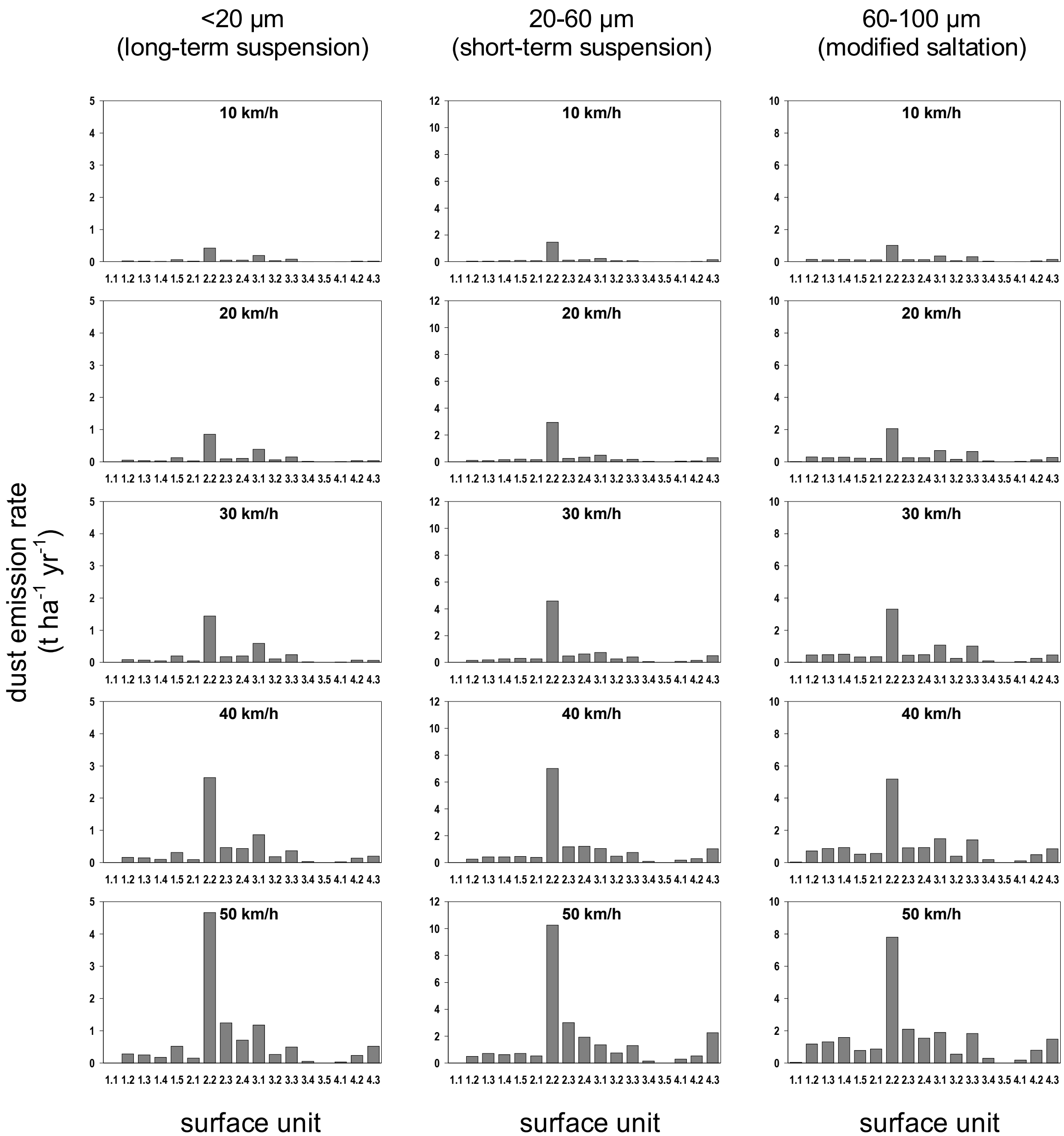

Fig. 2: Rates for ORV-generated dust emissions at Nellis Dunes Recreation Area. Data are based on the criteria described in section 2.2.

How is dust production distributed over the NDRA? To answer this question we calculated the total annual emissions for all 17 surface units (Figs. 3 and 4). The numbers refer to the year 2008 (more correctly: the period 19 December 2007 to 16 December 2008).

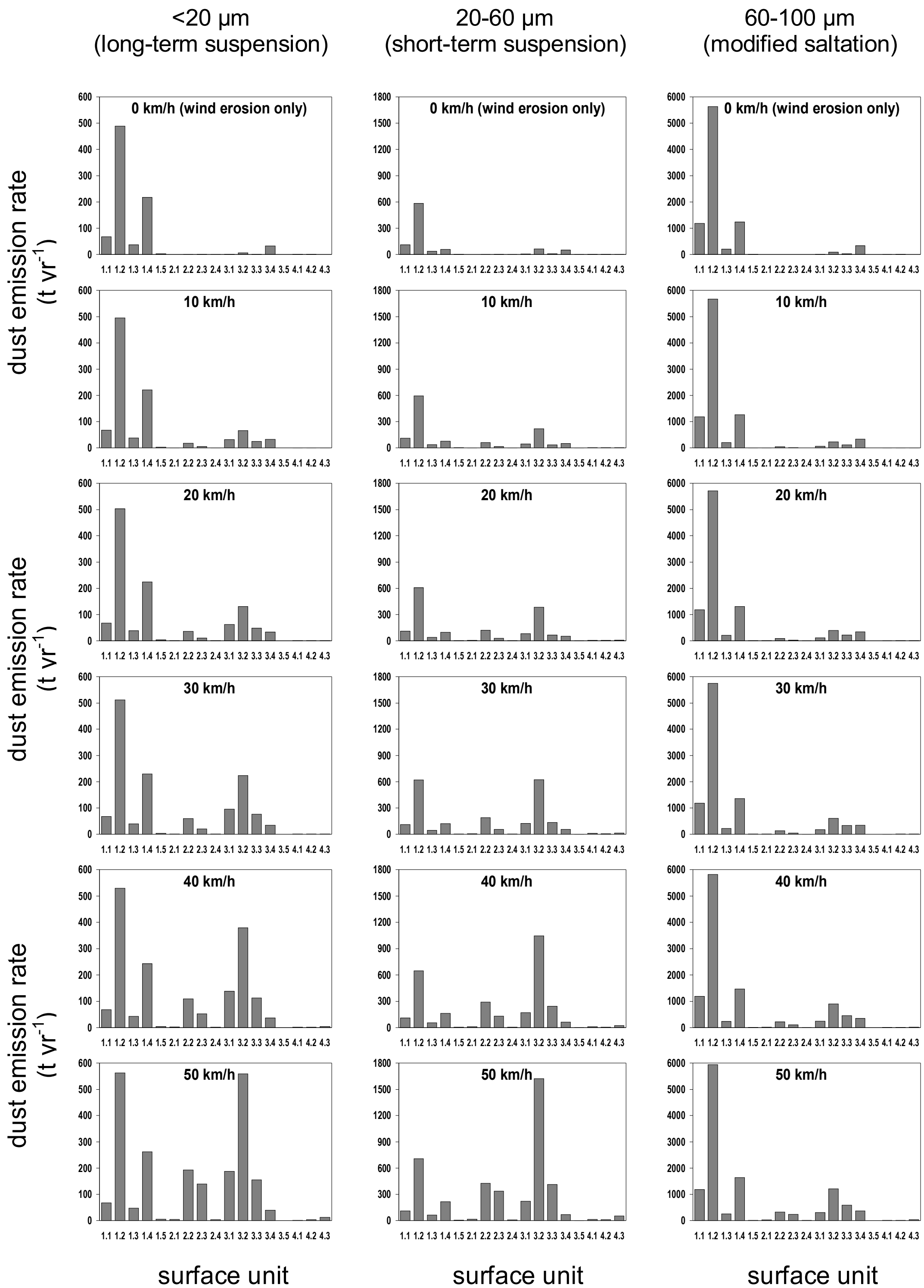

Fig. 3: Annual dust emission (wind erosion + ORV) at Nellis Dunes Recreation Area. Data for ORV are based on the criteria described in section 2.2.

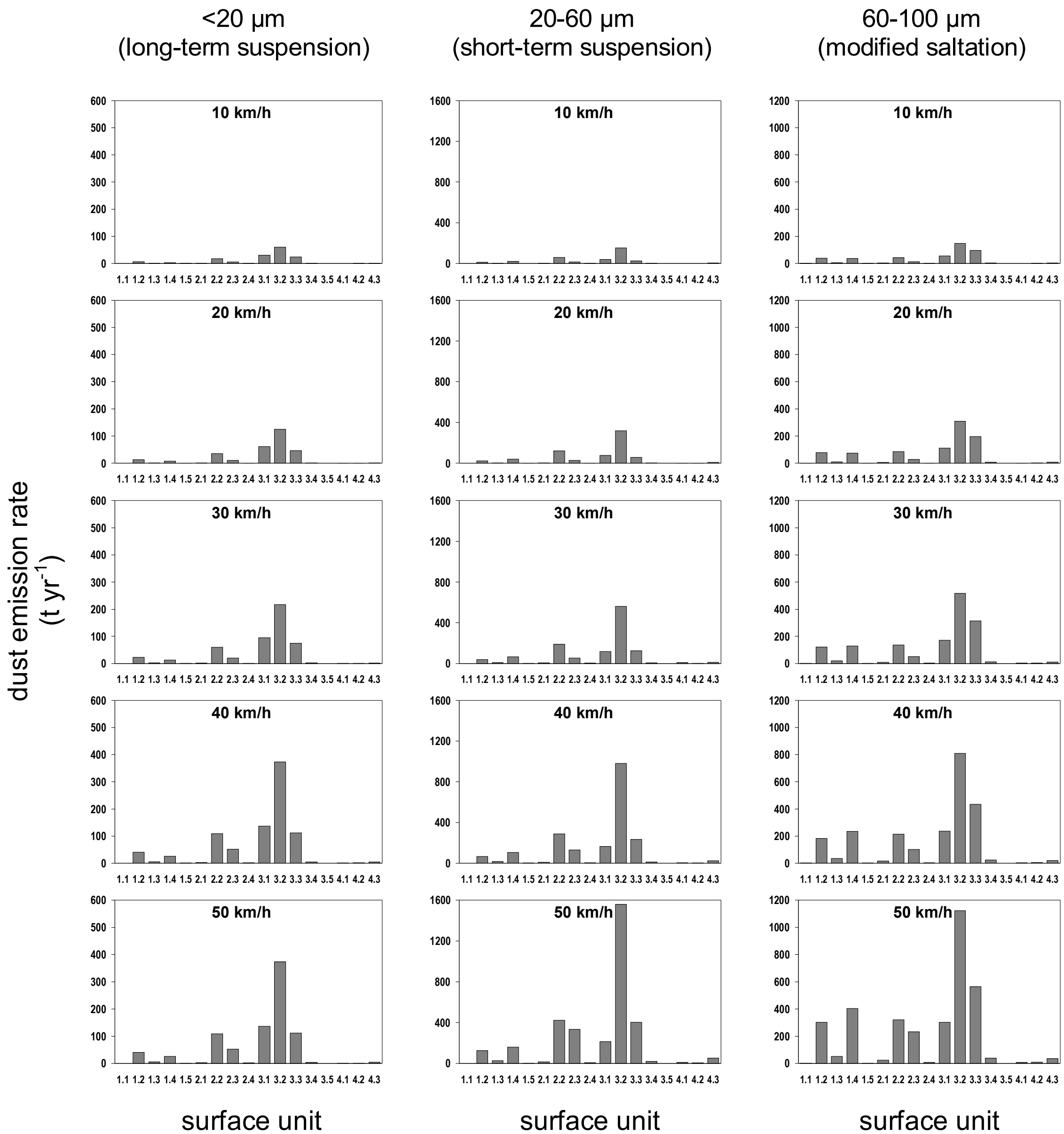

Fig. 4: Annual dust emissions generated by ORV driving at Nellis Dunes Recreation Area. Data are based on the criteria described in section 2.2.

During wind erosion (Fig. 3, upper diagrams 0 km h^{-1}) by far the most dust in NDRA was produced in the loose, uncompacted sand units 1.1 to 1.4. The most productive areas were the partly vegetated sand dunes (unit 1.2). The unvegetated dunes (1.1) produced significantly less dust, most probably because they are more active and have lost a significant portion of their fine particles over time, leading to a much lower dust content in the top layer compared to the vegetated dunes that are less frequently prone to wind erosion (Fig. 5). All silt units, although very rich in dust, do not significantly contribute to dust production in NDRA during wind erosion because their top layer is stabilized by surface crusts and/or rock cover.

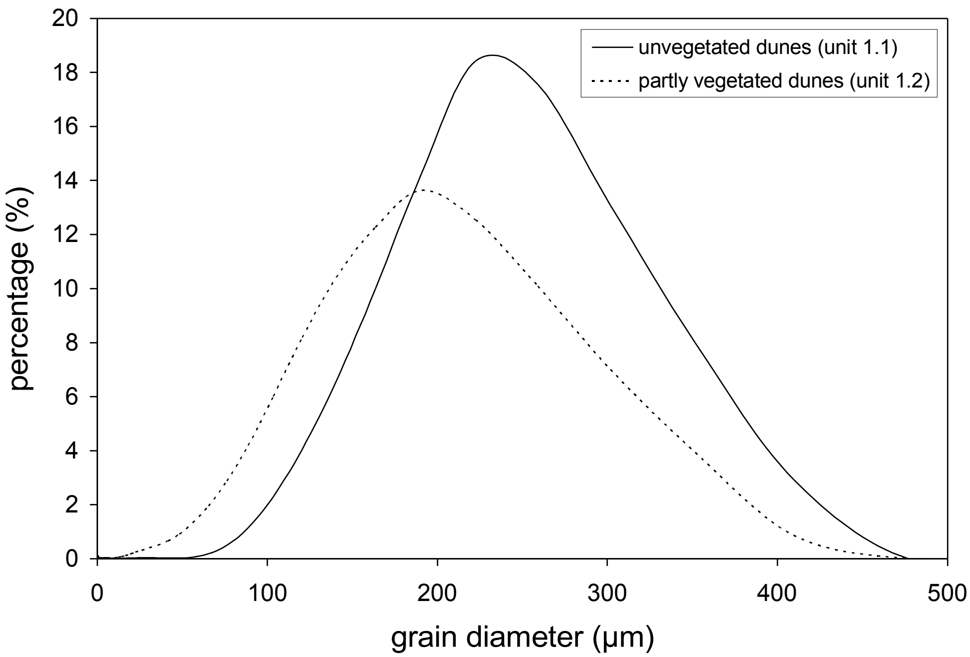

Fig. 5: Grain size distribution of the top soil (upper cm) in unvegetated and partly vegetated dunes at NDRA

The pattern is entirely different for ORV-produced dust emissions (Fig. 4). Here, most dust is produced in the silt and silt/rock areas, with the exclusion of the units 2.1 (silt and clay with crust) and 2.4 (disturbed silt surfaces). No differences occur between the two suspension fractions, but for coarser dust the vegetated sand dunes (1.2) and the patchy layers of loose dune sand (1.4) also are important sources of dust.

Looking at the total dust production in NDRA (wind erosion + ORV, Fig. 3) we see that at low driving speeds, it is mainly the sandy substrata that produce the most dust. With increasing driving speed, the silt and rock-covered silt areas become important sources. For the two suspension fractions (<20 µm and 20-60 µm) the contributions to dust production of the silt areas are equal or exceed those of the sand areas from a driving speed of approximately 30-40 km h^{-1}. In contrast, for coarse dust, the sand areas remain the dominant supplier of dust up to a driving speed of at least 50 km h^{-1}.

In terms of mass, most dust emitted in NDRA is transported in modified saltation (Fig. 6). If only wind erosion occurs, almost equal amounts of dust are transported in long-term suspension and short-term suspension despite the larger grain size (and, thus, mass per particle) of the latter. Therefore, during wind erosion, much more fine particles are released than coarse dust. If ORV driving occurs, more mass is transported in the coarse compared to the fine fractions, and the difference increases with increasing driving speed.

The right vertical scale in Fig. 6 shows the emission rates (in tons ha^{-1} yr^{-1}). For wind erosion (ORV driving speed = 0 km h^{-1}) the emission rates for long-term and short-term suspension are each 0.4 tons ha^{-1} yr^{-1}, therefore 0.8 tons ha^{-1} yr^{-1} for the total suspendable fraction. These numbers refer to the average for all 17 surface units. However, significant differences occur between individual units: from almost 2 tons ha^{-1} yr^{-1} for the vegetated sand dunes of unit 1.2 to less than 0.002 tons ha^{-1} yr^{-1} for the bedrock areas of unit 3.5 (values apply to the total suspendable fraction). When there is also ORV activity the emission rates markedly increase: at 50 km h^{-1} the rates are already 0.6 tons ha^{-1} yr^{-1} (long-term suspension) and 1.2 tons ha^{-1} yr^{-1} (short-term suspension). For dust transported in modified saltation the emission rates are 2.4 tons ha^{-1} yr^{-1} for pure wind erosion (no ORV driving), and 3.3 tons ha^{-1} yr^{-1} for a driving speed of 50 km h^{-1} (total emission).

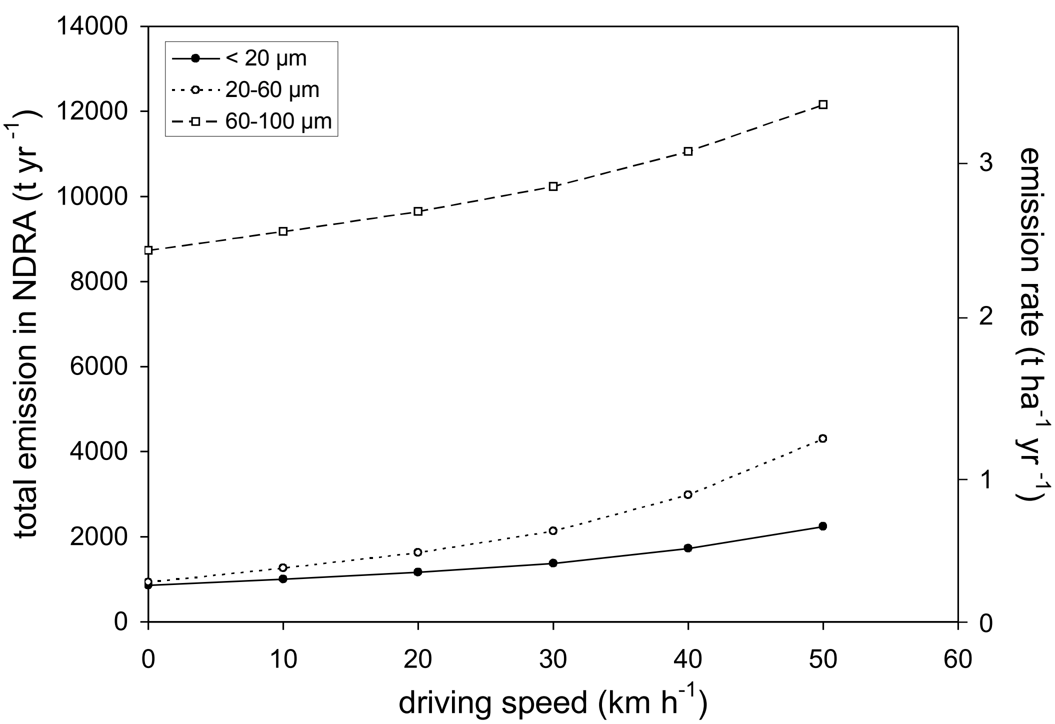

Fig. 6: Total annual emissions (left scale) and emission rates (right scale) in NDRA for the three grain size classes studied. Data for ORV are based on the criteria described in section 2.2.

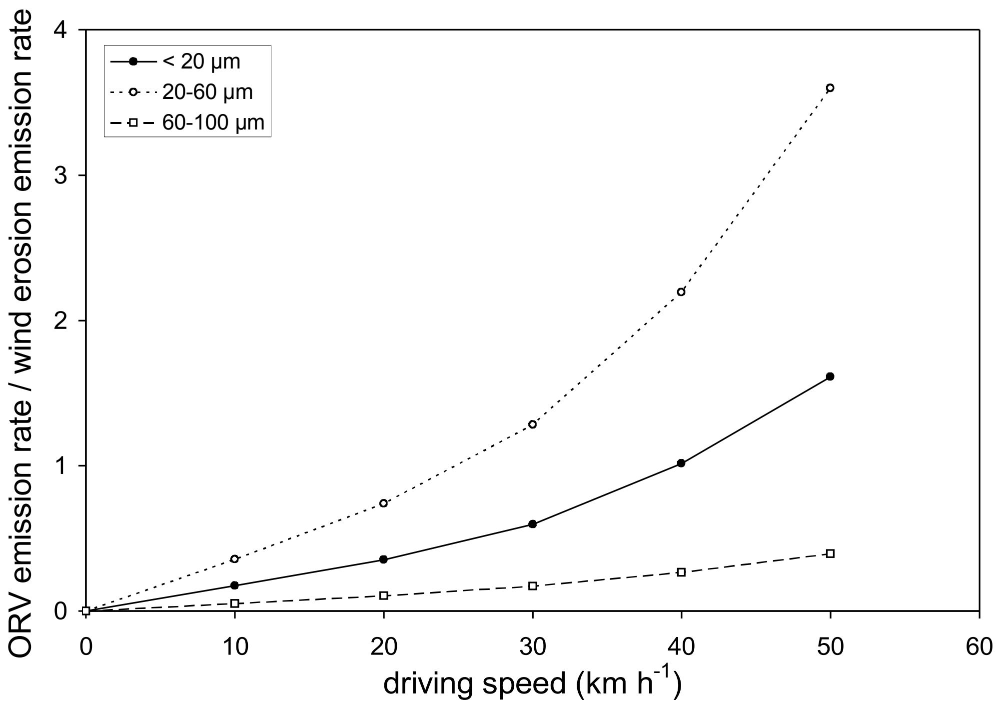

Fig. 7: Relative importance of ORV driving and wind erosion in dust production at NDRA. Numbers refer to emission rates; not to total annual dust production. Data for ORV are based on the criteria described in section 2.2.

Driving speed is thus a very important factor in dust production. In Fig. 7 we can read at which driving speed more dust is produced annually (in NDRA) by ORV than by wind erosion. For dust transported in long-term suspension (< 20 µm) the average critical speed is 40 km h^{-1}. For dust transported in short-term suspension (20-60 µm) it is considerably lower, only 25 km h^{-1}. For dust transported in modified saltation (60-100 µm) the critical speed is 88 km h^{-1}. Therefore, for the coarsest fraction ORV does not contribute substantially to the emissions because there are almost no areas in NDRA where it is possible to drive >80 km h^{-1}. On most spots 40 km h^{-1} is not a problem, and 25 km h^{-1} is far below the average driving speed at NDRA. Therefore, ORV driving at NDRA mainly contributes to the production of short-term suspendable dust and also, though to a somewhat lesser extent, to the production of long-term suspendable dust.

The driving speeds cited above apply to conditions where the 4 assumptions (criteria) described in section 2.2 are met. They also are averages for the 17 surface units investigated and as such are representative for NDRA as a whole. Important differences exist for individual units however (see Table 1): in the sand areas the critical driving speeds are (very) much higher than in silt and rock-covered silt areas. In the latter, even driving at very low speeds produces more dust than wind erosion does.

Table 1: Critical driving speed from which dust production by ORV exceeds dust production by wind erosion

Surface unit	Critical driving speed (km h^{-1})		
	<20 µm	20-60 µm	60-100 µm
sand surfaces			
1.1	NA	NA	NA
1.2	92	76	126
1.3	89	60	102
1.4	80	28	133
1.5	57	60	69
silt surfaces			
2.1	<10	<10	<10
2.2	<10	<10	<10
2.3	<10	<10	<10
2.4	15	13	19
rock-covered surfaces			
3.1	<10	<10	<10
3.2	<10	<10	<10
3.3	<10	<10	<10
3.4	75	70	113
3.5	NA	NA	NA
drainages			
4.1	37	30	34
4.2	26	43	44
4.3	<10	<10	<10

NA: dust production by ORV = 0, or insufficient data available

Finally, the data allow calculation of the susceptibility of a surface to disturbance by ORV driving. Susceptibility is here defined in terms of increased dust emission when pristine land is disturbed by ORV activity. It can be quantified by the ratio $E_{tracks}/E_{undisturbed\ terrain}$, where E_{tracks} is the emission rate (expressed in, for example, tons ha^{-1} yr^{-1}) in ORV trails and $E_{undisturbed\ terrain}$ is the emission rate on undisturbed pristine land. In Fig. 8 we plotted the ratio for all 17 surface units occurring in NDRA. All data are annual averages and are thus sufficiently representative because they include all variations (mostly seasonal) occurring over time. They were obtained with the PI-SWERL instrument and therefore refer to the PM10 fraction. The units most susceptible to ORV disturbance are the silt units and also most, though not all, rock-covered silt units. By far the most vulnerable type of surface is the desert pavement of unit 3.1. Also, silty drainages (unit 4.3) show a high risk. Sand surfaces, on the other hand, do not

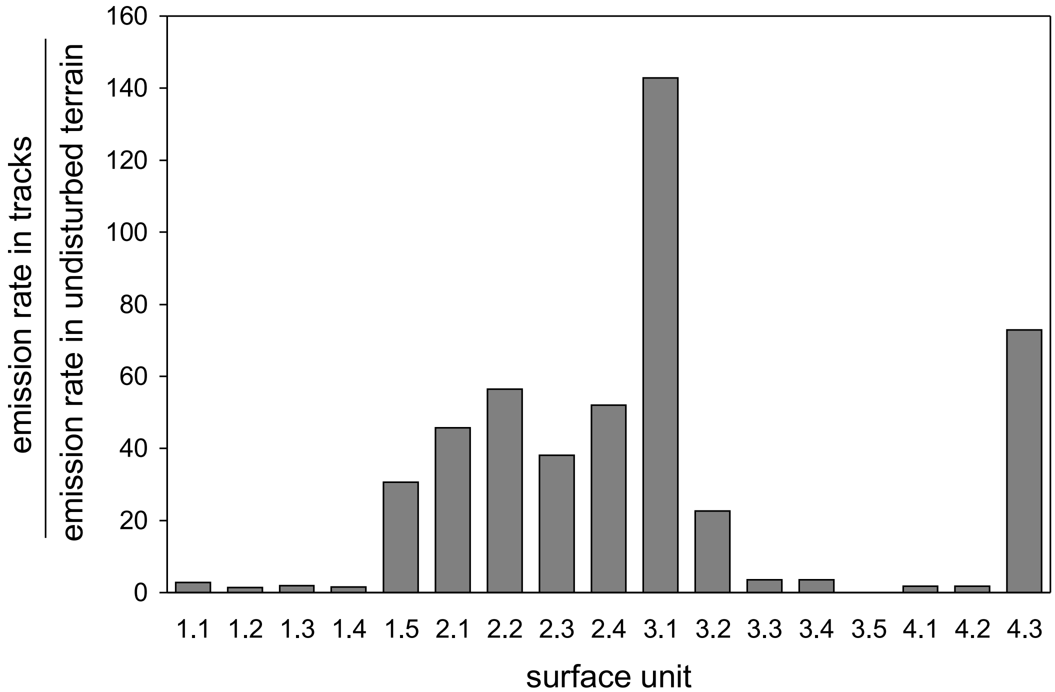

Fig. 8: Susceptibility of the 17 surface types in NDRA to disturbance by ORV activity

constitute an important risk when disturbed by ORV activity. Therefore, from a management point of view, considering dust emissions only, new ORV trails are acceptable in sandy areas but should be avoided in silty areas including silty drainages.

3.2 Relationships with surface properties

Apart from meteorological conditions (for wind erosion) and driving characteristics including the type of vehicle (for ORV-generated emissions), dust production is mainly determined by the properties of the emission surface. In this study the following surface characteristics were investigated: texture (percentage silt, sand and clay), rock fragments (rock cover, rock content of the top layer), surface resistance (crustal strength) and vegetation (cover density).

Relationships between the percentages of silt/sand/clay and dust emission rate are shown in Fig. 9. All data are for the total suspendable fraction (0-60 µm). Two types of data are shown for wind erosion: real emissions and potential emissions. Real emissions refer to the emissions measured by the BSNEs whereas potential emissions refer to the emissions measured by the PI-SWERL. To plot both types of emission in a single diagram the data were normalized (see vertical scales).

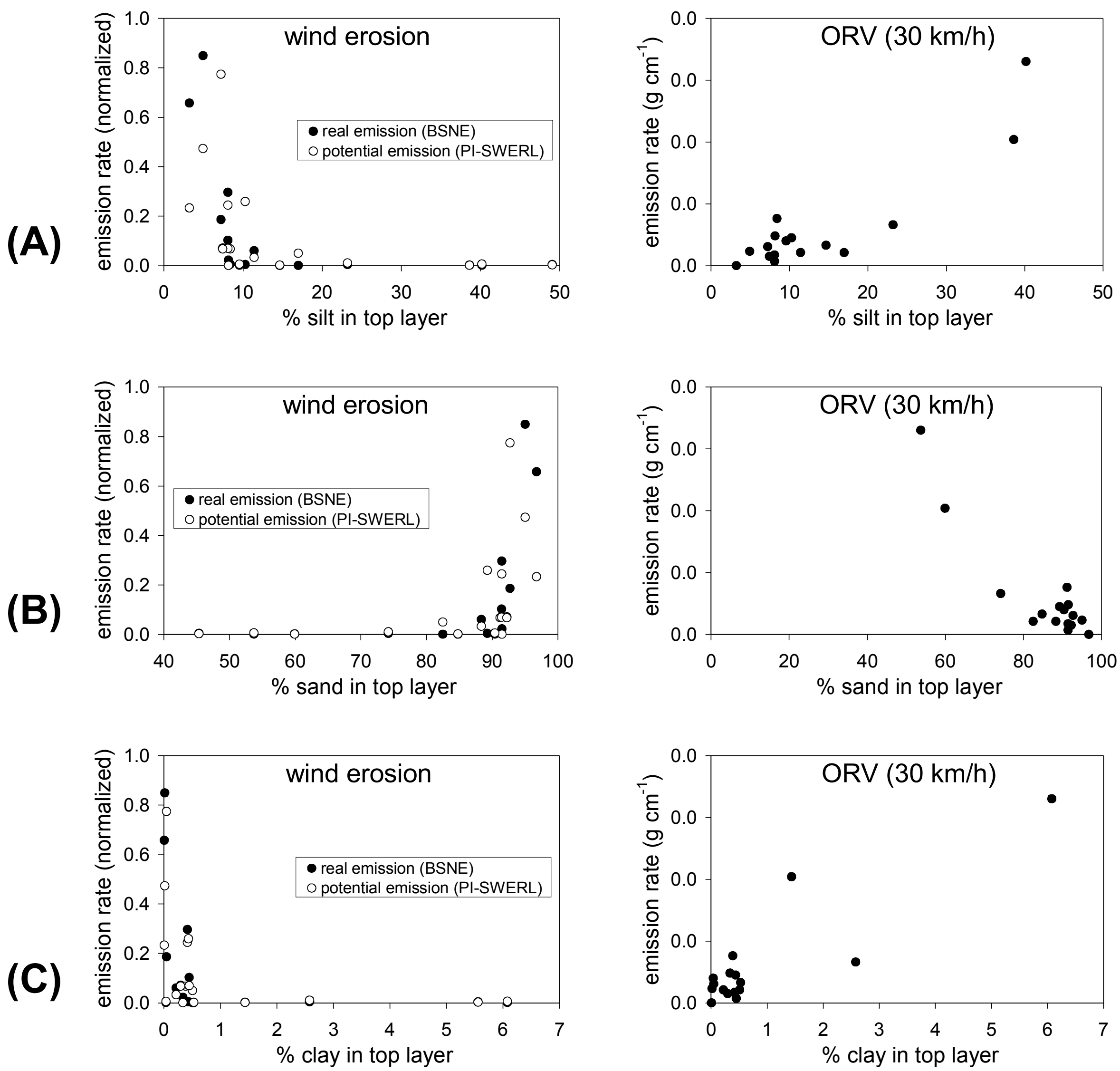

Fig. 9: Relationship between dust emission rate and soil texture. Left: wind erosion; right: ORV driving. (A) emission rate and silt content; (B) emission rate and sand content; (C) emission rate and clay content.

A very strong relationship exists between dust production and texture for wind erosion (see left-hand diagrams in Fig. 9). For wind erosion, dust production increases with decreasing silt content, increasing sand content and decreasing clay content. Nearly no dust is emitted when the silt content is >11%, the sand content is <90% or the clay content is >0.5%. This points to the strong stabilizing effect of the finest particles in the soil (silt and clay) and the role of saltation as a dust-emitting mechanism (sand). During ORV driving (see right-hand diagrams in Fig. 9; all data refer to an average driving speed of 30 km h-1) emissions also correlate to soil texture but the relationships are inverse.

Most dust is emitted when the top soil is rich in silt and clay, and poor in sand. Therefore, during ORV driving it is mainly the dust reservoir in the top soil that determines whether or not a surface is productive. Contrary to wind erosion, factors affecting the physical binding forces of the particles are not key-factors in ORV dust production.

This is further confirmed when comparing dust production to surface resistance defined here as crust strength (see upper diagrams in Fig. 10). Crust strength was measured on all 17 surface types with a penetrometer (normal resistance) and a torvane (tangential resistance). For dust produced by wind erosion (left diagram) emission becomes unimportant once surface resistance is larger than 3×10^4 Pa. In contrast, during ORV driving (right diagram), dust is produced at any condition of resistance. The reason is that the vehicles' tires destroy any existing crust while driving over the surface and also break most of the aggregates in the top layer; no effect of surface resistance on dust production should therefore be expected.

Does rock cover play a role in dust emissions? For wind erosion, high emissions only occur at low rock cover percentages whereas low emissions may occur at any rock cover percentage (Fig. 10B). What the data show is that the maximum emission decreases with the percentage of rock cover. Similar trends can be seen for the rock content in the top layer (we sampled the upper 5 cm): again, maximum emission decreases with the rock content (Fig. 10C). In contrast, for ORV-generated emissions (right column in Fig. 10) no relationships exist between dust production and either rock cover or rock content. Therefore, rocks on and in the soil protect the soil from dust emission during wind erosion, but do not provide any protection during ORV driving.

When vegetation cover (in NDRA: shrubs) is compared to either wind-produced or ORV-produced dust we find no relationships (Fig. 10D). Therefore, vegetation is not a key factor in dust production, at least in NDRA and for the type and densities of vegetation investigated in this study.

It can be concluded that soil texture, the presence of rocks and the presence of surface crusts all affect the emission of dust during wind erosion whereas during ORV driving only texture plays a role. ORV driving is very destructive to the top soil and neutralizes any protective effects soil parameters may have on dust emission. Only texture still plays a role because it determines the size of the reservoir of dust available for emission. In addition to texture, for ORV-produced dust important factors are the type of vehicle and the speed of driving in determining how much dust will be produced.

4. Summary of conclusions

Perhaps the most important conclusion of this chapter is that off-road vehicular activity can produce dust emissions comparable to those created by wind erosion. For the Nellis Dunes area as a whole, the annual amounts generated by wind erosion are 859 ton

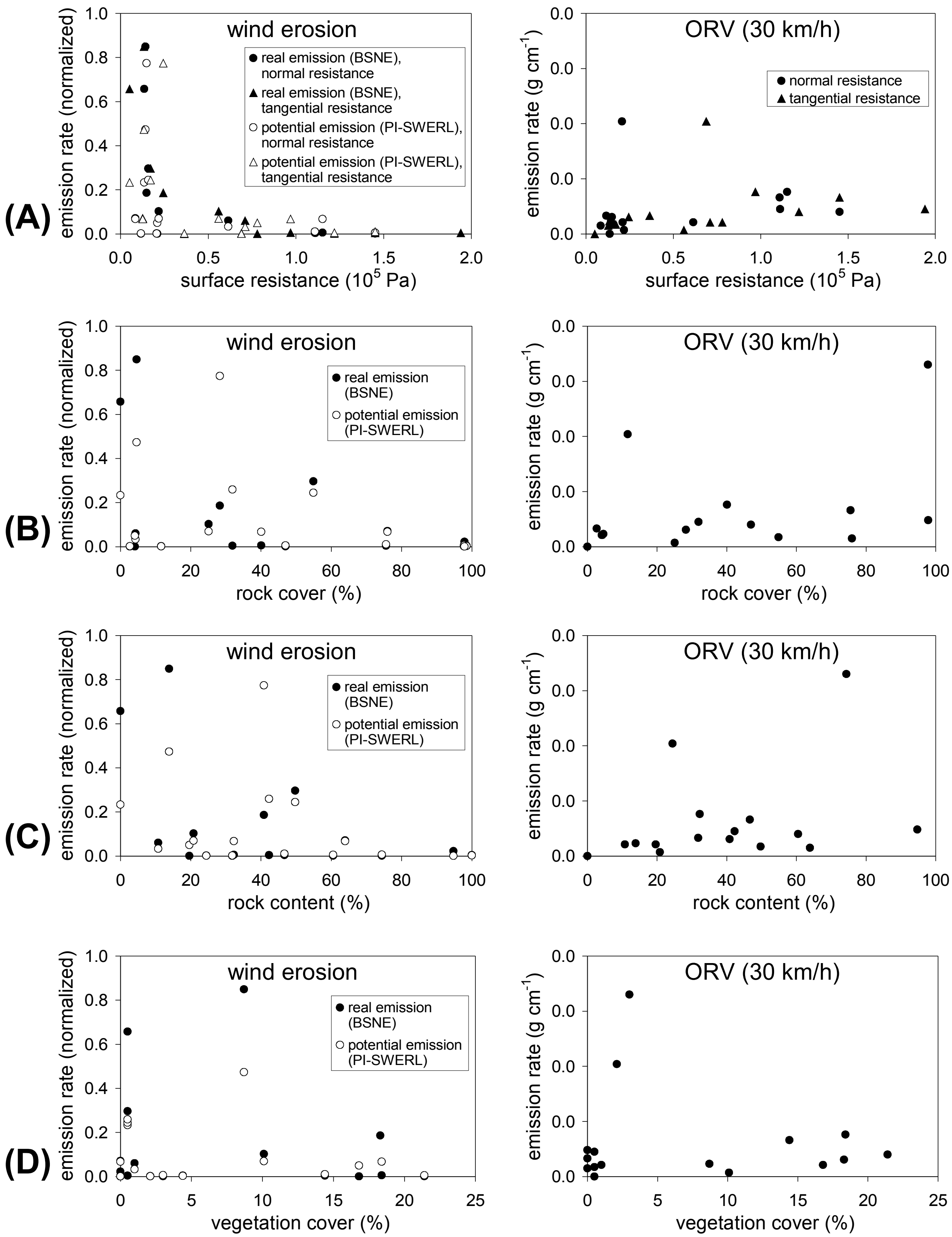

Fig. 10: Relationship between dust emission rate and (A) surface resistance; (B) rock cover; (C) rock content; (D) vegetation cover.

(fraction <20 μm), 935 ton (fraction 20-60 μm) and 8726 ton (fraction 60-100 μm). These numbers are for the year 2008, which was a "normal" meteorological year (Goossens and Buck, 2011). The annual amounts generated by off-road driving are calculated as 512 ton (fraction <20 μm), 1198 ton (fraction 20-60 μm) and 1503 ton (fraction 60-100 μm). These numbers are for an average vehicle (average of a dune buggy, a dirt bike and a 4-wheeler), for an average driving speed of 30 km h^{-1}, and for an average run length of 10 km. All numbers are representative averages for the Nellis Dunes area, where drivers are making many turns and topography is quite complex keeping the driving speed (and run length) relatively low compared to other ORV areas in the USA. For total suspendable dust, which has the capacity to leave the area and affect downwind regions, the numbers are 1794 ton for wind erosion and 1711 ton for ORV. These numbers are nearly identical.

Emission rates describe the susceptibility of the surface to dust emission. When comparing emission rates for wind erosion and ORV-activity the numbers are also comparable for the two suspendable fractions. For the fraction <20 μm the data are 0.36 t ha^{-1} yr^{-1} (wind erosion) and 0.20 t ha^{-1} yr^{-1} (ORV), respectively. For the fraction 20-60 μm the data are 0.44 t ha^{-1} yr^{-1} and 0.53 t ha^{-1} yr^{-1}. For the fraction 60-100 μm, which is largely transported in modified saltation, the numbers are 3.39 t ha^{-1} yr^{-1} and 0.57 t ha^{-1} yr^{-1}. Wind erosion is thus significantly more important than ORV for the coarsest dust particles, even at high driving speeds. For a driving speed of 50 km h^{-1}, for example, the emission rate for 60-100 μm dust is still only 1.42 t ha^{-1} yr^{-1}. In contrast, for suspendable dust, ORV is more important: at 50 km h^{-1} the emission rates for <20 μm and 20-60 μm dust are 0.63 t ha^{-1} yr^{-1} and 1.46 t ha^{-1} yr^{-1}, respectively.

There are large differences between the various types of surfaces. Wind erosion is the dominant dust-producing mechanism in sandy areas, for fine, medium-sized as well as coarse dust. Impact of saltating grains is the main mechanism responsible for the liberation of the particles. On surfaces poor in sand but rich in silt, wind erosion is limited due to the presence of surface crusts, the absence of large numbers of impacting saltating grains, and commonly a protective surficial cover of rock fragments. In contrast, ORV driving produces substantial dust emissions in areas rich in silt and poor in sand. ORV driving is very destructive, destroying any protective crust or rock cover, and exposing the large reservoir of dust in the silt fraction available for emission in the subsoil.

Total dust production in the Nellis Dunes area varies strongly as a function of surface type and driving speed. At low driving speeds nearly all dust is produced in the central sand dunes and the sandy areas in the northwest. When driving speed increases the silt and rock-covered silt zones in the north, east and southeast also become productive. However, the largest amounts of dust are still produced in the sand dunes. For high driving speeds some silt substrata in the north attain emission rates higher than those for the sand dunes, but their areal extent in NDRA is significantly smaller, resulting in much less overall production than in the sand dunes.

References

BLM, 2004. Las Vegas Valley Disposal Boundary, Final Environmental Impact Statement and Record of Decision, Chapter 3: Affected Environment. Las Vegas Bureau of Land Management, Las Vegas, NV, USA.

Fryrear, D.W., 1986. A field dust sampler. Journal of Soil and Water Conservation 41, 117-120.

Goossens, D., Buck, B., 2010. Gross erosion, net erosion and gross deposition of dust by wind: field data from 17 desert surfaces. Earth Surface Processes and Landforms, doi: 10.1002/esp.2080.

Goossens, D., Buck, B., 2011. Effects of wind erosion, off-road vehicular activity, atmospheric conditions and the proximity of a metropolitan area on PM10 characteristics in a recreational site. Atmospheric Environment 45, 94-107.

Pye, K., Tsoar, H., 1990. Aeolian Sand and Sand Dunes. Unwin Hyman, London.

Shao, Y., 2008. Physics and Modelling of Wind Erosion, 2nd edn. Springer Science + Business Media BV, Dordrecht.

Sylvester, J.T., 2009. Montana Off-Highway Vehicles 2008. Bureau of Business and Economic Research, University of Montana-Missoula.

Tiittanen, P., Timonen, K.L., Ruuskanen, J., Mirme, A., Pekkanen, J., 1999. Fine particulate air pollution, resuspended road dust and respiratory health among symptomatic children. European Respiratory Journal 13, 266-273.

Chapter 7

AMBIENT PM10 CONCENTRATIONS IN THE NELLIS DUNES RECREATION AREA

CONTRIBUTIONS OF WIND EROSION, OFF-ROAD VEHICULAR ACTIVITY, ATMOSPHERIC CONDITIONS AND THE PROXIMITY OF THE LAS VEGAS CONURBATION

Dirk Goossens and Brenda Buck

Department of Geoscience, University of Nevada Las Vegas

1. Description of the problem

Air quality is a special concern in the Las Vegas valley, southern Nevada, USA. Las Vegas is one of the fastest-growing metropolitan areas in the United States (Lazaro et al., 2004) with approximately 1.9 million people. Last year Las Vegas received a failing grade from the American Lung Association's (2010) annual "State of the Air" report. Of special concern is particulate matter, which is one of the largest problems with air quality not only in Las Vegas, but also in many other regions worldwide.

Apart from industrial or traffic-generated particles, dust generated from unvegetated land is a significant geological source of airborne particulate matter in desert cities such as Las Vegas. Research into the effects of PM10 (particulates <10 µm) and PM2.5 (particulates <2.5 µm) emissions on human health increasingly show a strong link to numerous diseases and mortality including asthma, heart disease, dementia, and cancer (Besancenot et al., 1997; Lambert et al., 1999; Korenyi-Both et al., 1992; Jinadu 1995; Athar et al 1998; Komatsu et al., 2003; Ichinose et al., 2005; Griffin and Kellogg 2004; Sultan et al., 2005; Wang et al., 2008). Epidemiological studies have demonstrated that daily mortality may be attributed to cardiopulmonary and respiratory damages caused by ambient particulate matter in the PM2.5 and PM10 range (Dockery et al., 1993; Peters et al., 1997; Laden et al., 2006). Furthermore, outdoor dust and soil are primary sources for indoor dust to which all infants to the elderly are exposed. In fact, studies have demonstrated a remarkable agreement between both house and outdoor dust (Fishbein 1991; Feng and Barratt 1993; Fergusson and Kim 1991; Akhter and Madany, 1993).

Adverse health effects have also been found to result from exposure to airborne cadmium, lead, arsenic and other chemical elements (Järup, 2003). These include cancer, hypertension, cardiovascular disease, kidney damage, diminished intellectual capacity in children, and skeletal damage (Järup, 2003). Naturally occurring minerals in numerous locations throughout southern Nevada contain significant quantities of these and other known hazardous elements (Castor and Ferdock, 2004). Therefore, dust from these sources may pose potential additional health risks beyond those induced by the particulates themselves. In addition, because the greatest concentration of many harmful chemical elements resides in the smallest particle sizes (PM10, PM2.5 or even smaller), and because these particulates are the most easily transported and also the most easily inhaled, the problem becomes even more significant.

PM10 concentrations in the Las Vegas valley are routinely monitored on an hourly basis by the Clark County Department of Air Quality and Environmental Management (DAQEM). Approximately 20 stations have been installed in Clark County. Some (but not all) of these stations also measure PM2.5. Most stations are located in the urban environments of Las Vegas, North Las Vegas, Henderson and Boulder City. The PM10 station closest to the Nellis Dunes Recreation Area (NDRA) is Apex, located 12 km north of NDRA and 32 km northeast of the center of Las Vegas. Because of its distance to NDRA, and also because of its location to the north, most dust emitted at NDRA is not recorded by this station. Only southern winds will bring NDRA dust to Apex; during southeastern or southwestern winds the Apex station does not receive NDRA dust. Analysis of wind data recorded at Nellis Air Force Base, which borders on NDRA, shows that on an annual basis the proportion of south winds is 21% (Goossens and Buck, 2010). Most of the dust emitted at NDRA is thus not recorded by the Apex station.

Dust emission at NDRA is very high due to both intense wind erosion and off-road vehicular activity, as shown in the Chapters 3, 5and 6 of this report. Because the Apex data cannot be used to quantify the concentrations at NDRA, a separate study measuring the concentrations at the site itself was carried out. The aim of the study was not only to quantify the airborne PM10 concentrations in the Nellis Dunes area, but also to compare the data to concentrations recorded in rural areas elsewhere in the Las Vegas valley that are not affected by off-road driving. The data were also used to investigate the diurnal and seasonal patterns of the PM10 concentration at NDRA. In addition, we analyzed the role of the following factors that can be expected to affect the PM10 concentrations at NDRA: local wind erosion, local off-road vehicular (ORV) activity, atmospheric conditions, and the proximity of the Las Vegas metropolis. The latter factor was studied because of the large amounts of PM10 that are produced in the metropolis daily, and that are tracking over the Nellis Dunes area during southwest wind conditions. This chapter reports the results of this study.

2. PM10 measurements: field procedure

2.1 Location

Due to budgetary restrictions, and also because of safety reasons (vandalism was extensive during the project), only a single dust concentration monitor could be installed on a permanent basis in the Nellis Dunes area. The objective of this specific study was to measure the overall combined effect of wind erosion and ORV activities on PM10 concentration. Since wind erosion and ORV activities are highly variable throughout the NDRA, the placement of the dust concentration monitor should be located on a surface very resistant to local wind erosion and removed from the areas with the greatest natural wind erosion and ORV emissions. Direct contributions of local sources to the dust load are thus eliminated and the dust collected can be considered sufficiently representative of the background dust at NDRA as a whole. The monitor was installed in the north-central portion of NDRA (Fig. 1), on surface unit 3.2 (rock-covered surface with silt and clay). This is the most abundant unit in the Nellis Dunes area, and its capacity to produce PM10 during wind erosion is very low. This unit has the third lowest value for wind erosion of all 17 surface units in NDRA, after units 3.5 (bedrock) and 2.1 (silt and clay with crust). The site is also located in a zone with only a couple rarely used ORV trails so that local dust production by ORV activity is minimal. Therefore, its location is very well suited for studying the overall airborne PM10 concentrations in the NDRA.

2.2 Instrumentation and methods

All PM10 concentrations were measured with a DustTrak 8520 aerosol monitor (TSI Inc., St. Paul, Michigan, USA). It is a portable, battery-operated laser photometer that measures the real-time concentration of aerosols (Fig. 2). It can measure PM10, PM2.5 and PM1.0 concentrations. For this study we used the PM10 inlet nozzle and measured PM10. Dust was collected at a height of 75 cm above the desert floor. Data were collected over one complete year, from December 19, 2007 to December 17, 2008. Concentrations were measured every second and stored as 20-min averages. Instrument calibration was performed every 14 days, but corrections were hardly necessary.

To get an idea of the variations in grain size of the dust, two vertical poles 2 m high and 2 cm in diameter were installed near the DustTrak (Fig. 3). Dust was collected with BSNE collectors (Fryrear, 1986) at four levels: 25 cm, 50 cm, 75 cm and 100 cm. For this study we analyzed the samples collected at 75 cm (same height as the DustTrak). All samples were analyzed with a Malvern Mastersizer 2000 laser particle size analyzer (Malvern Instruments Ltd., Malvern, UK) at the Environmental Soil Analytical Laboratory at

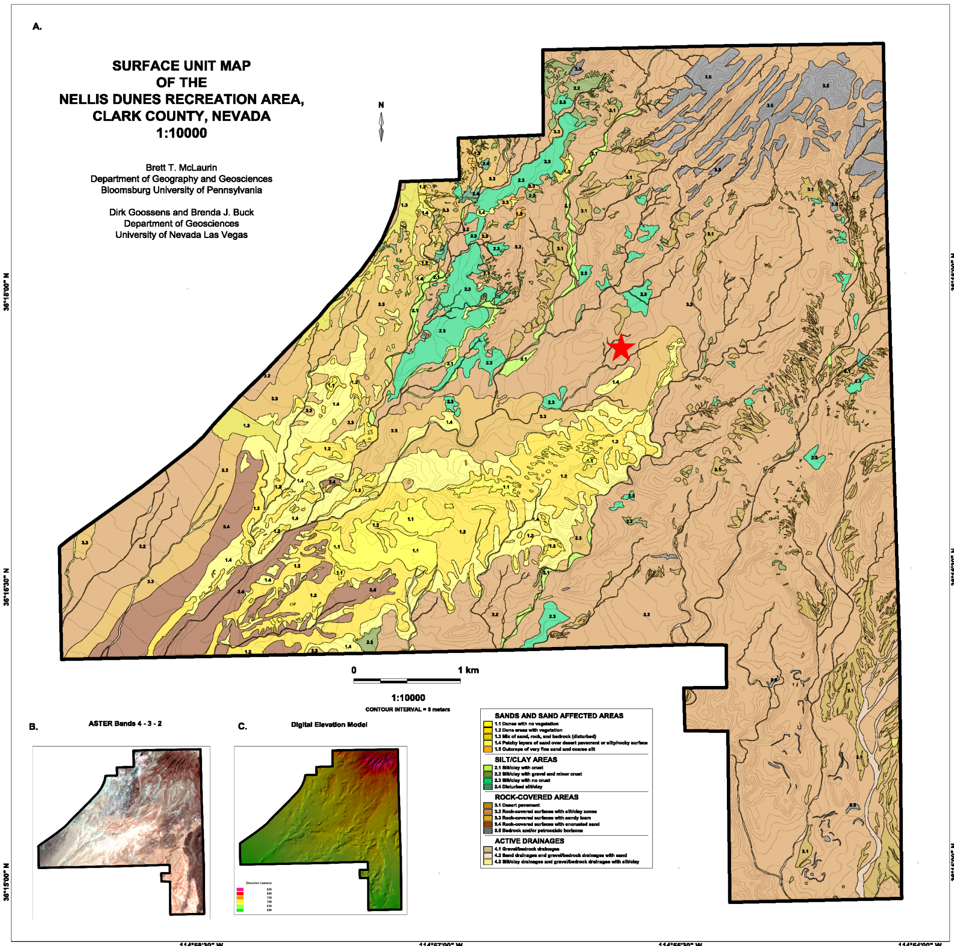

Fig. 1: Location of the PM10 measurement site

UNLV. Because the instrument measures many grain size classes in the range 0-10 µm it was possible to examine the PM10 fraction in detail. The minimum quantity of dust for these analyses required sampling periods of 14 days. Therefore, 26 periods of 14 days were analyzed.

Wind speed and direction were measured throughout the experiment using electronic cup anemometers and a wind vane. A 20-m wind tower was erected close to the DustTrak site and three supplementary towers (one 10m; two 20m) were also erected in other parts of NDRA for comparison. Fig. 4 shows one of the 20-m wind towers. Data from the nearby Nellis Air Force Base meteorological station, which borders on NDRA, were used to fill data gaps. Such gaps were filled only after careful calibration between the wind towers and the Nellis Air Force Base station.

Fig. 2: The DustTrak 8520 aerosol monitor (top) and its installation in an environmental enclosure (bottom)

Fig. 3: Poles with BSNE dust samplers

Fig. 4: 20-m wind tower with anemometer and wind vane

3. PM10 measurements: results

3.1 Wind regime

Data on wind speed and wind direction during the measuring period are shown in Figs. 5 and 6. Wind speed was highest in April, decreased systematically until December, and then stayed more or less constant until March. This pattern applies to both the day-time (8:00 - 20:00) and night-time (20:00 - 8:00) winds. Winds were stronger during the day hours, and the difference between day and night was more or less constant between January and August but decreased considerably from September to December. There were nearly no differences in monthly average wind speed between day and night in November and December. In March wind speeds by day were abnormally low (at least, in 2008).

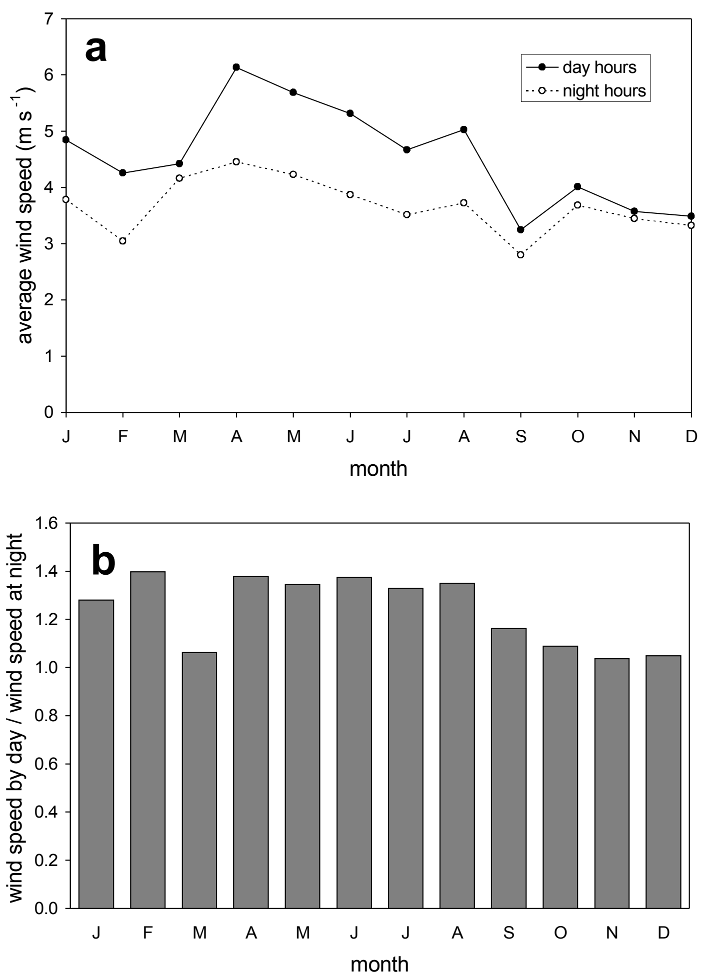

Fig. 5: Wind speed regime at NDRA. (a) average wind speed (at 20 m); (b) ratio of wind speed by day to wind speed at night.

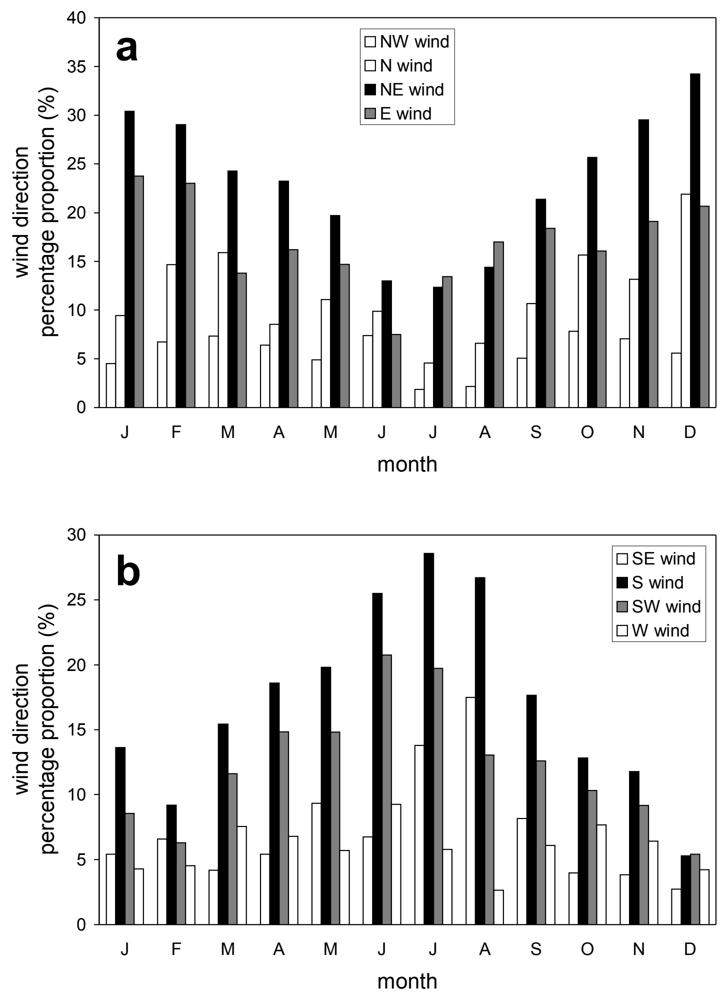

Fig. 6: Bi-seasonal regime of wind direction at NDRA. (a) N-NE sector; (b) S-SW sector. Percentages are based on 24-h data.

There is a distinct bi-modal regime of wind direction: in the late spring through early autumn, winds blow mainly from the S and SW whereas in the late autumn through early spring they blow opposite, predominantly from the NE-E (Fig. 6). However, they can blow from any direction at any time.

We compared our 2008 data to wind data collected at the nearby Nellis Air Force Base over the past decade (1998-2008) and found that the 2008 data can be considered "normal". The 2008 average wind speed is 3.1 m s^{-1} and average gust speed is 11.2 m s^{-1} compared to 1998-2008 averages of 3.3 m s^{-1} and 11.0 m s^{-1} respectfully. Also, 2008 precipitation (96 mm) and soil moisture (Palmer Drought Severity Index: -2.91) are not significantly different from the 1998-2008 average of 117 mm and -1.17.

3.2 Frequency distributions of the ambient PM10 concentrations in NDRA

At NDRA, PM10 concentrations measured at 20-min periods for the entire year 2008 show that 56 % of the time concentrations were <5 μg m^{-3}, and 80 % of the time they were <10 μg m^{-3} (Fig. 7a). Only 0.1 % of the time they were >100 μg m^{-3}. However, the distribution is less skewed when considering daily averages of PM10 concentrations (Fig. 7b). Most frequently, PM10 concentrations were 3 to 4 μg m^{-3}. Only 11 days in 2008 (3 %) had average PM10 concentrations >20 μg m^{-3}.

PM10 concentrations vary significantly between day and night (Fig 7c,d). Dust concentrations are greater during the day: averaging 8.90 μg m^{-3} as compared to 5.67 μg m^{-3} for the night. During the night, episodes of very low concentrations occur frequently; (Fig. 7d), whereas during the day, the distribution is much less skewed, with a mode between 4 and 5 μg m^{-3} (Fig. 7c).

3.3 Annual patterns

Average daily PM10 dust concentrations for 2008 show several individual events (Fig. 8). The dustiest day was January 27, when PM10 concentration peaked at 1297 μg m^{-3} around noon. This value suggests that total dust concentration should have been close to 26,000 μg m^{-3}, if we use the 2008 average at NDRA of a 5% PM10 content in total dust (TSP). This is very high but still realistic for intense dust storms (Hagen and Woodruff, 1973). Apart from rather short dust episodes, there are several events lasting longer than 24 hours such as April 20-22, September 30 to October 3, and November 27-28 (Fig. 8).

Both the number of individual dust events and the background PM 10 concentrations are higher in April through September as compared to October-March (Fig. 8). Most dusty periods occurred in mid-April to mid-May, mid-June to mid-July, and the end of September to the beginning of October. Low PM10 concentrations occurred from early February to mid-March, during the first part of November, and nearly the whole of December. Interestingly, there is substantial internal variability during periods of high PM10 emissions. During these times, many periods of low emissions can be found alternating with high dust events.

In order to more easily discern general trends, we grouped the data into monthly averages (Fig. 9). April through September show increased dust for the daily averages as well as for day and night periods separately. However, these monthly averages show that the annual cycle of PM10 concentration is more variable at night than during the day hours (Figs 9b,c). April was exceptionally dusty, mainly because of a very high number of high-magnitude dust events and very high background concentrations between April 15 and 30 (Fig. 8).

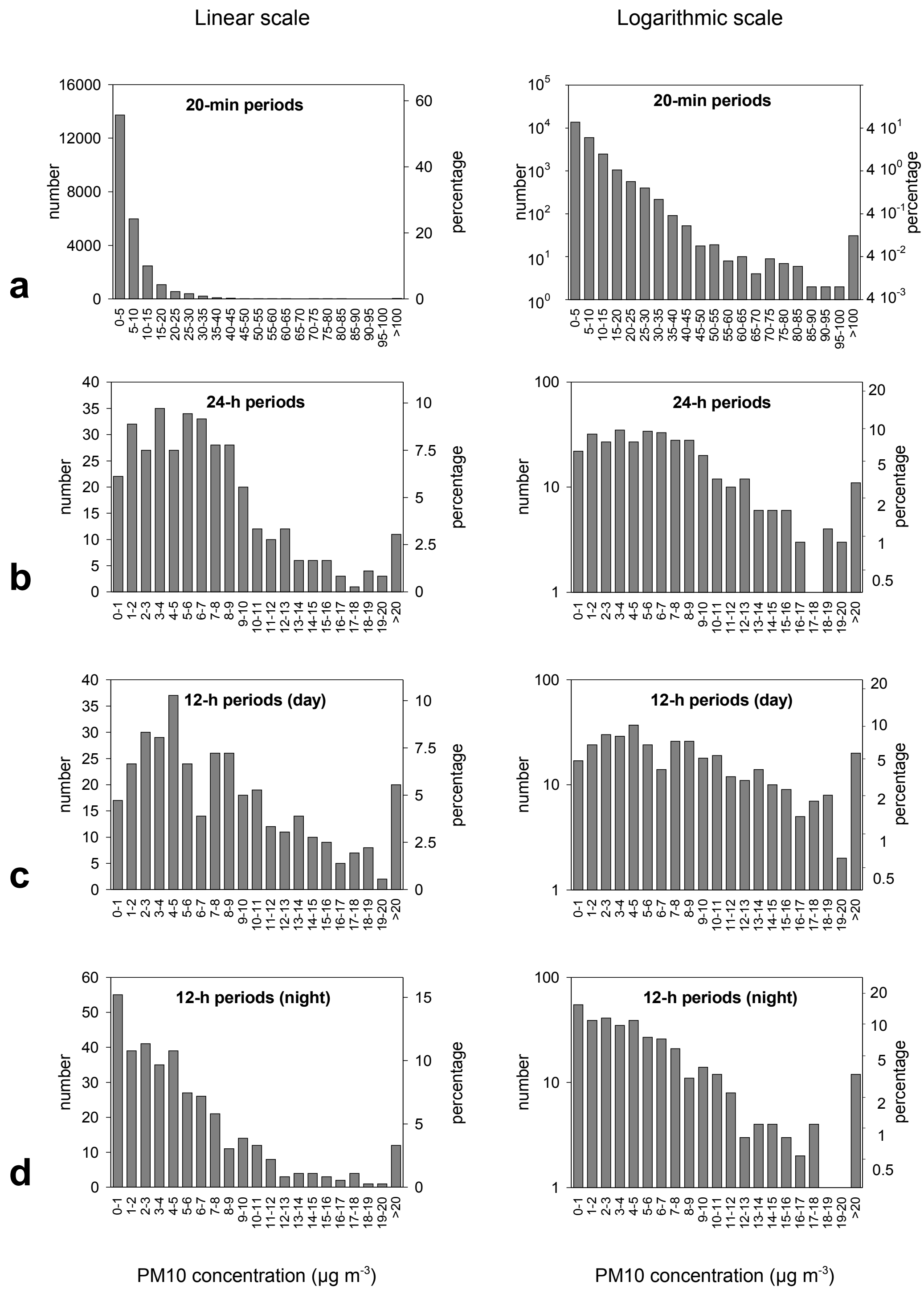

Fig. 7: Frequency distributions for PM10 concentrations measured over 1 year. Numbers and percentages are shown in both linear (left) and logarithmic (right) scales. (a) 20-min periods; (b) 24-h periods; (c) day hours; (d) night hours.

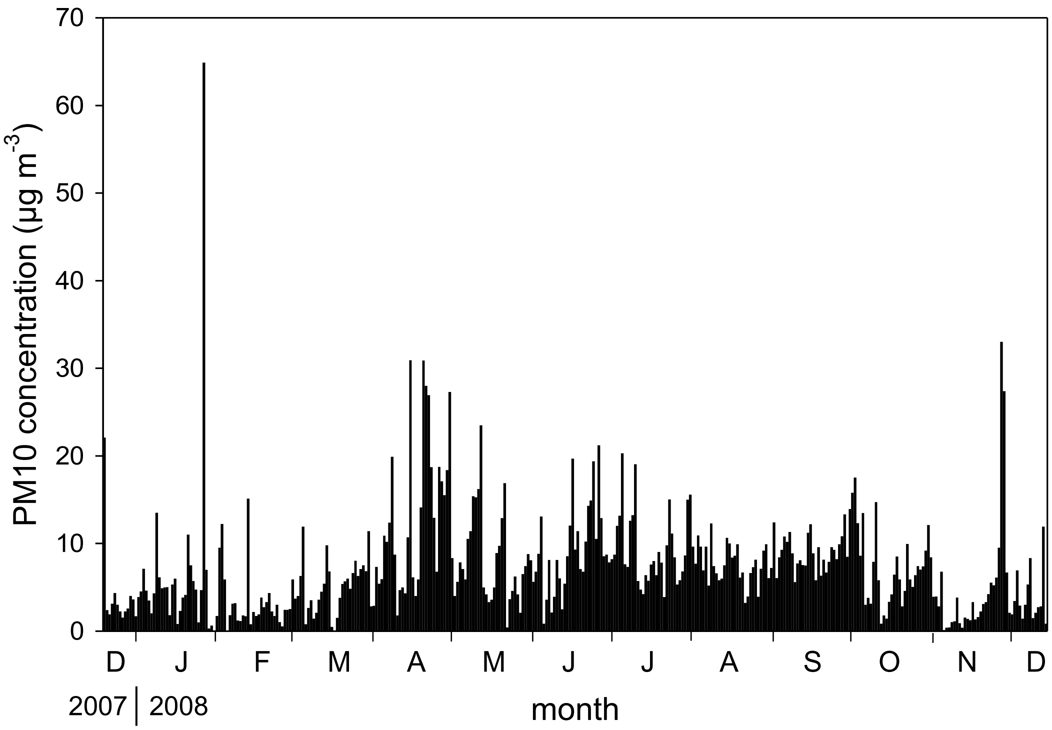

Fig. 8: Daily evolution of PM 10 dust concentration at NDRA based on 24-h averages (19 December 2007 - 17 December 2008)

The ratio of PM10 concentration at night to PM10 concentration by day is variable throughout the year (Fig. 10a). Several temporary high-magnitude events (HMEs) obscure the seasonal trends. To exclude these temporary events, we used N/D < 0.25 and N/D > 4 as criteria to define HMEs, where N = dust concentration at night and D = dust concentration by day. These criteria enable one to locate the 12-h periods during which HMEs (which are short, but intense events) occurred. When these HMEs are excluded, the monthly ratio of dust concentration at night to dust concentration by day is highest in October-May and lowest in June-September (Fig. 10b). Although the month of March has a lower ratio as compared to the other autumn-winter months, it does not substantially affect these trends. Therefore, PM10 concentrations at NDRA are lower at night than during the day, but the difference is more expressed in summer than in winter.

Similar trends have been reported for other deserts. For the Negev desert in Israel, Offer and Goossens (1990) and Goossens and Offer (1995) measured D/N ratios (the reciprocal of the ratio N/D studied here) during the years 1989-1992 and found patterns similar to those at NDRA. In those studies too, the seasonal trends became evident when excluding the HMEs.

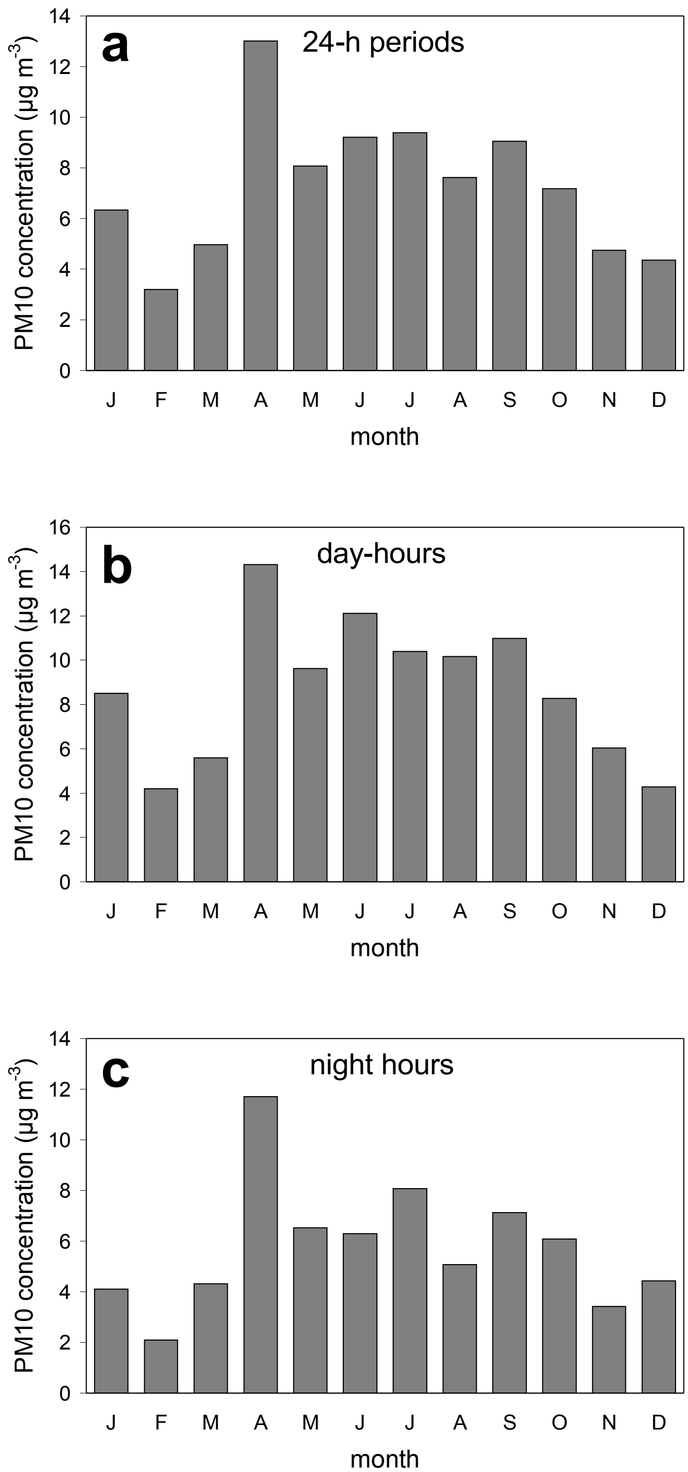

Fig. 9: Monthly evolution of dust concentration at NDRA. (a) 24-h periods; (b) day hours; (c) night hours.

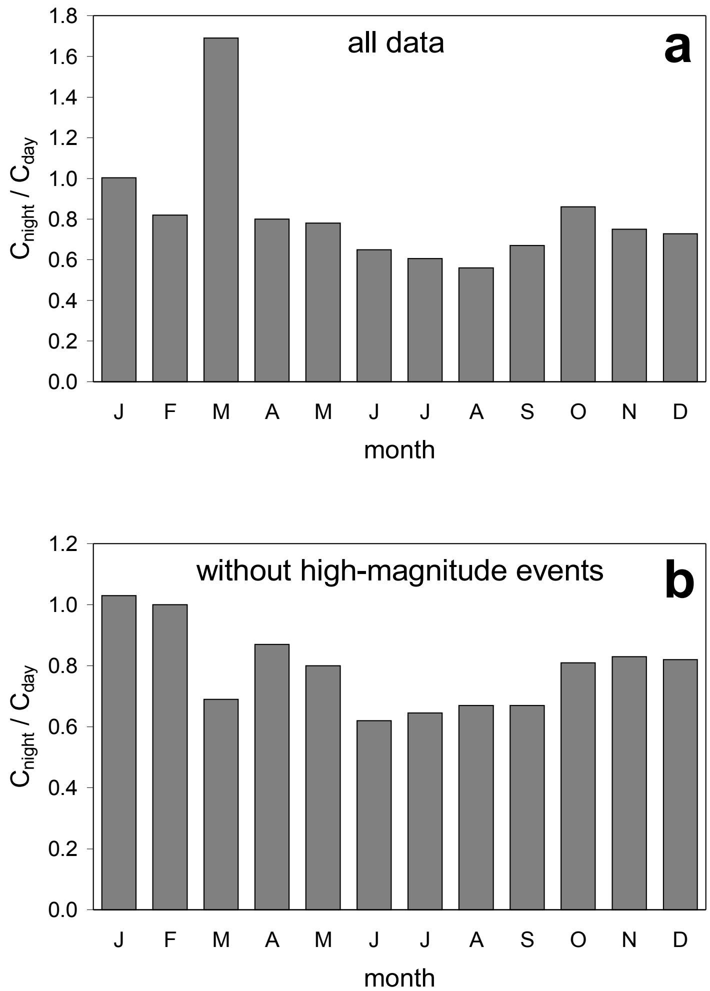

Fig. 10: Ratio of dust concentration at night (C_{night}) to dust concentration by day (C_{day}). (a) all data; (b) high-magnitude events excluded.

To evaluate seasonal variability in grain size for the PM10 fraction, we collected dust from BSNE samplers at NDRA. The median grain diameter of the PM10 fraction was calculated for all 12 months (Fig. 11). The finest dust occurs in summer and early autumn whereas the coarsest dust occurs in winter. Therefore, on an annual basis, the periods of highest dust concentration are associated with fine dust and those of lowest concentration with coarse dust. Higher airborne concentrations (expressed in mass per volume) are not related to a larger mass of individual particles but to a larger number of particles per volume. In other words, during the late spring, summer, and early autumn seasons, finer, and many more PM10 particles occur in the near-surface layer at NDRA than in winter.

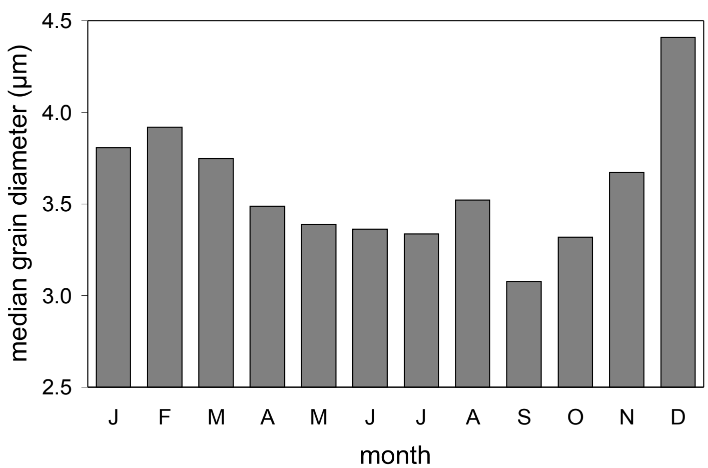

Fig. 11: Monthly evolution of median grain diameter of airborne PM10 dust at NDRA

3.4 Diurnal patterns

The diurnal variation of PM10 concentration at NDRA is shown in Fig. 12a for each month. The picture is complex because the baseline of the curve varies throughout the year: minimum concentrations are considerably higher in summer than in winter. Adjusting the curves to the same baseline (Fig. 12b) shows that during the summer months, monthly average diurnal PM10 concentrations are considerably higher, and also more variable as compared to the winter months. Notice also that PM10 concentrations peak more sharply in the hottest months (June-September) than during the coldest months (November-February).

When the results are normalized (Fig. 12c) we see that all months have increasing dust concentrations in the morning and a subsequent drop in the afternoon. In the morning, both the rate and uniformity of the increase in monthly average PM10 concentrations are highly variable. In the afternoon the drop in PM10 concentration is much more uniform and the rate of decrease is constant year-round. Presenting the curves separately for each month (Fig. 13) we see that, at night, several months show a secondary maximum. In summer (June-August) no secondary peak occurs at night. For the remaining months, there are two maxima, a major in the early afternoon and a minor (sometimes double) at night. The nocturnal maximum is most pronounced in the winter months (November-February) and then decreases until it has disappeared in June.

Monthly average diurnal PM10 concentrations can be grouped into two distinct periods: October-March and April-September (Fig. 14a). In the period October-March PM10 concentration peaks in the early afternoon and at night; in the period April-September there is only one peak, in the afternoon. Also, a small plateau is apparent in both curves

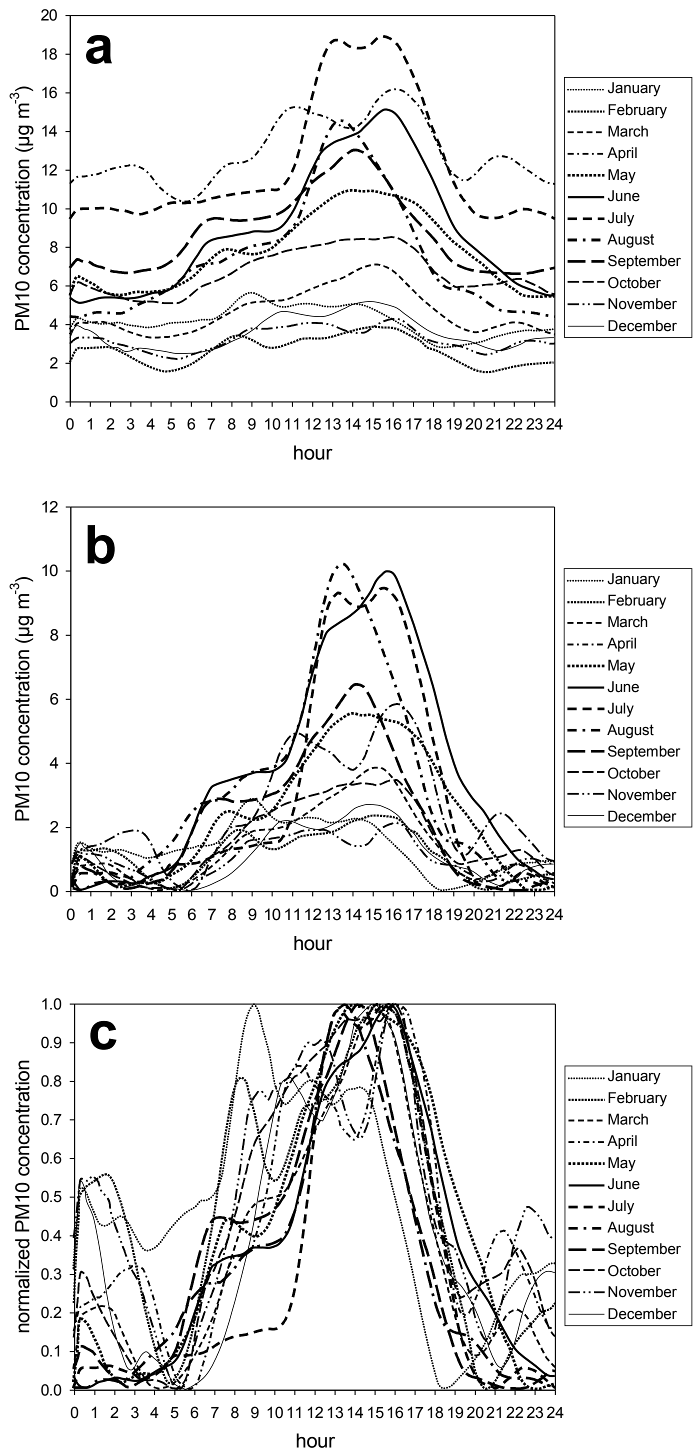

Fig. 12: Diurnal evolution of PM10 concentration grouped as monthly averages. Continuous curves are shown instead of individual data points to improve readability; each curve is based on 72 data points. (a) raw data; (b) baselines set to zero; (c) normalized curves.

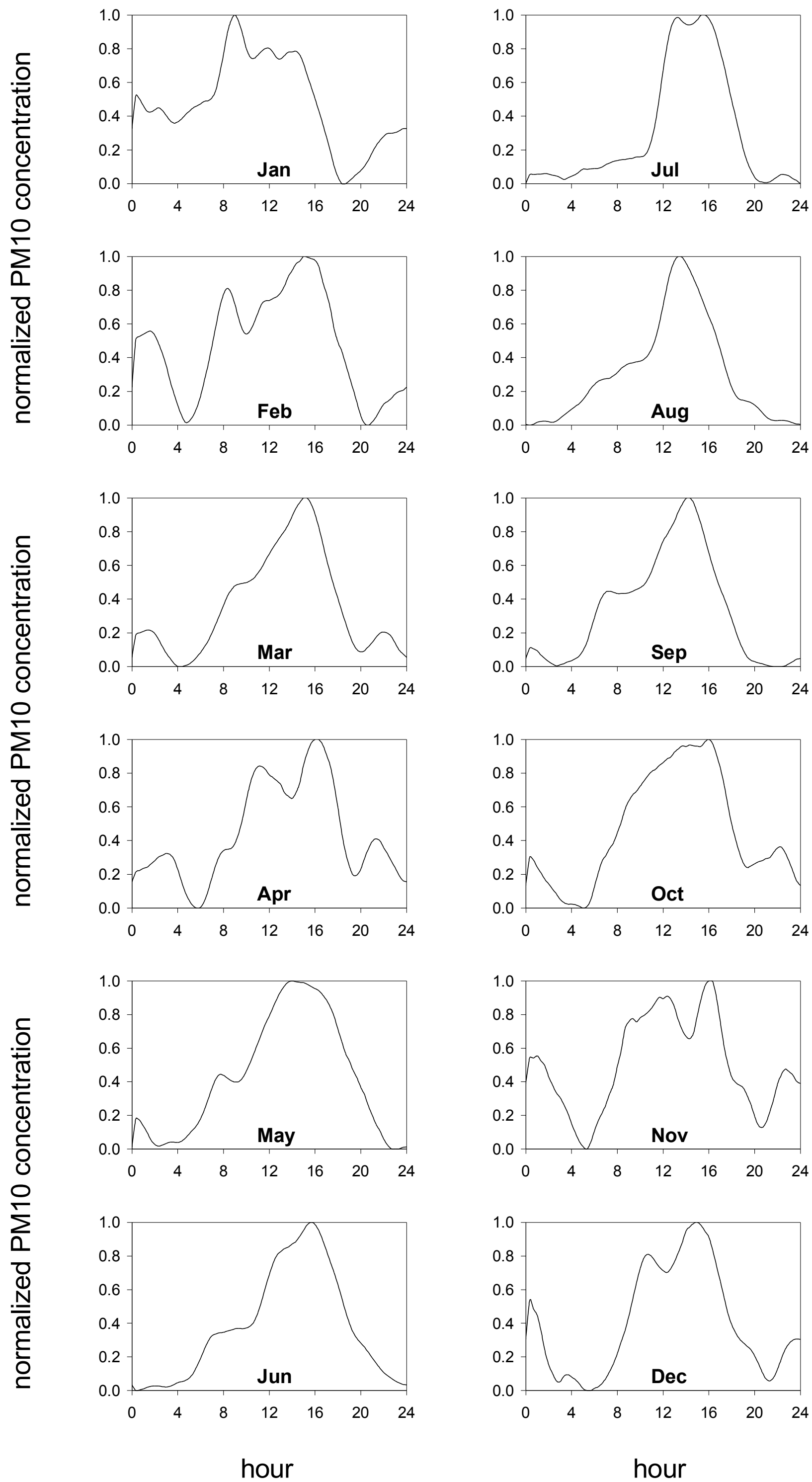

Fig. 13: Normalized monthly average diurnal PM10 concentration

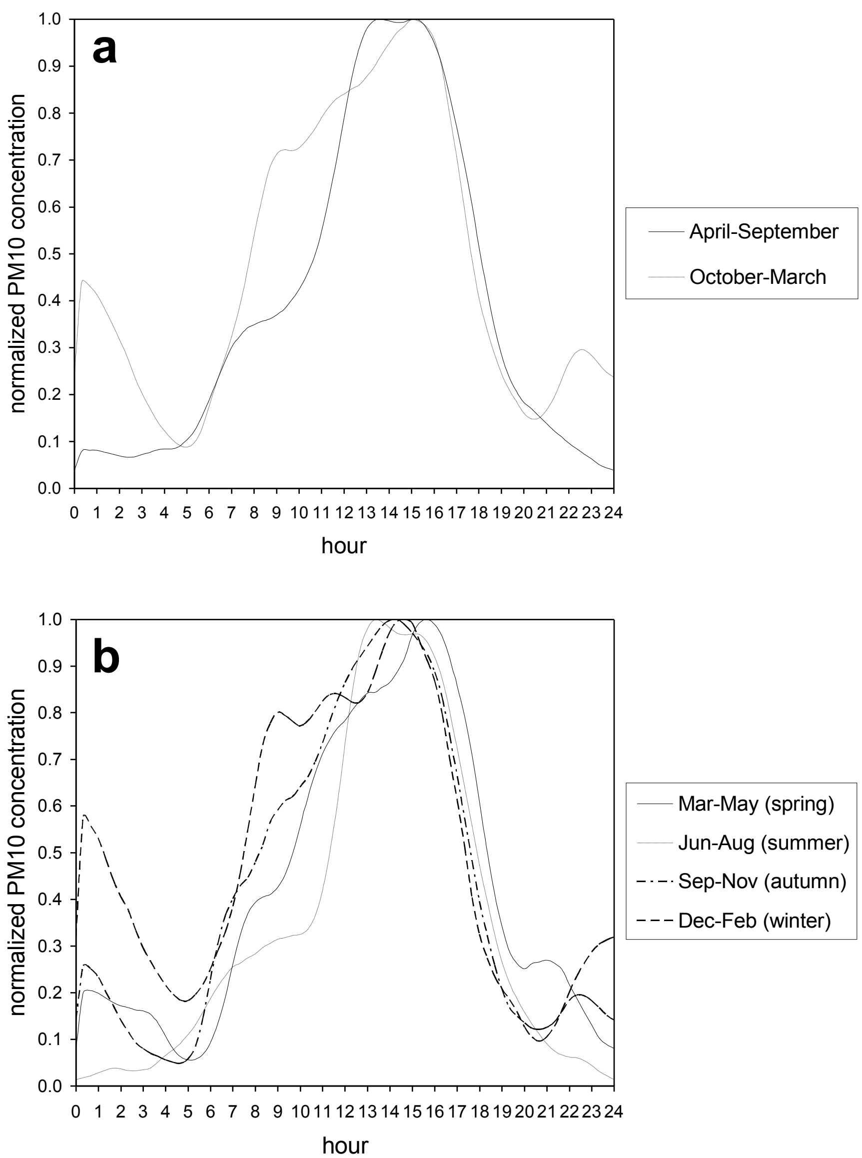

Fig. 14: Diurnal evolution of PM10 concentration throughout the year.
(a) April-September and October-March; (b) the 4 classic meteorological seasons.

in the morning, around 8:00 in the period April-September and somewhat later, around 9:00, in October-March. The 1-h difference and the sharper peak in April-September result in a substantial difference in shape of the curves in the morning; in the afternoon both time periods behave identically. To try and gauge any seasonal patterns, the monthly average diurnal PM10 concentrations were grouped according to the 4 meteorological seasons (Fig. 14b). The seasons show great variability in morning PM10 concentrations, but similar afternoon behaviors.

On a monthly basis, we compared the morning hours when the increase in PM10 concentration started (Fig 15a). In winter, the increase starts somewhere between 5:00 and 5:30 (November and December), changes to approximately 3:30 in January, and then increases to between 4:00 and 5:00 in February and March. From April onward the hour slides back to midnight (in June-August) and then moves forward again in autumn. Note that the data for April may not reflect the average long-term pattern because of the many HMEs that occurred in 2008.

No significant monthly variation is observed for the hour when dust concentration starts to decrease in the afternoon (Fig. 15b). Concentration thus reaches its maximum at more or less the same hour (between 14:00 and 16:00) all year round.

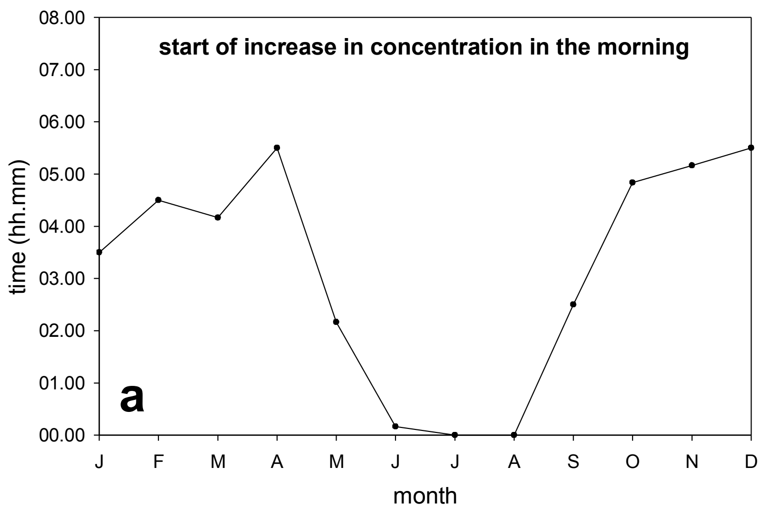

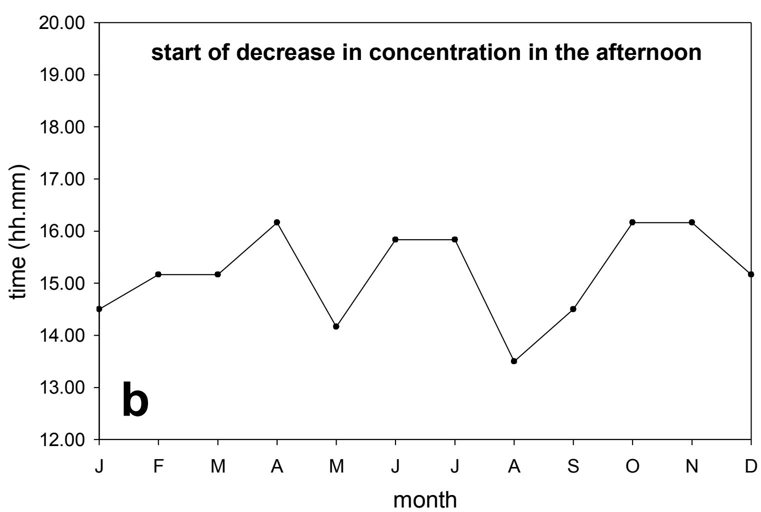

Fig. 15: Start (a) and end (b) of period of high dust concentration during the day hours

Lastly, PM10 concentration curves are shown for the two major wind directions in the Las Vegas region (Fig. 16). From April to September winds blow predominantly from the S-SW; from October to March they blow predominantly from the NE-E. Because of the difference in wind regime between these two periods, and also because the diurnal pattern of PM10 concentration is different, we split the data in Fig. 16 in two figures: one for October-March (Fig. 16a) and the other for April-September (Fig. 16b). The figures were constructed by selecting those days where the wind blew from the northeastern (or southwestern) sector during both the night hours and the day hours, i.e. there is very little risk that short-term variations in wind direction during a day have affected the result.

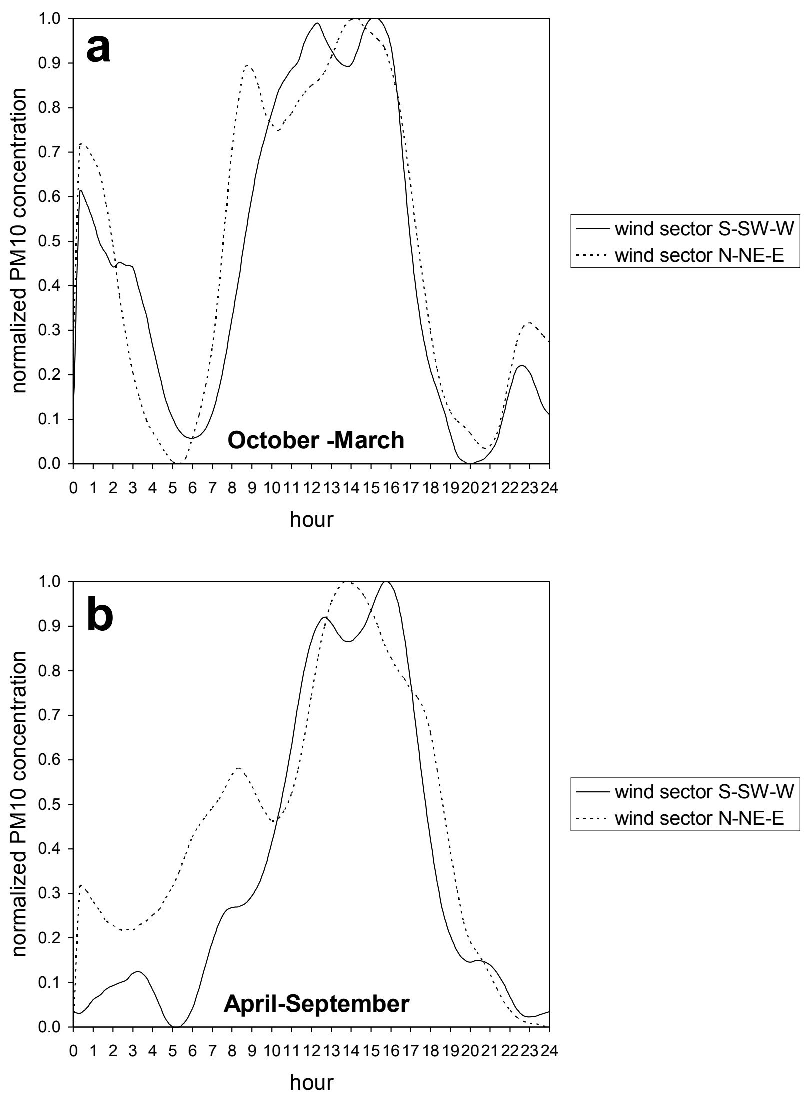

Fig. 16: Diurnal evolution of PM10 concentration for the 2 dominant wind directions at NDRA. (a) October-March; (b) April-September.

Looking at the period October-March (Fig. 16a) there are no substantial differences between the two wind directions, except that during NE-E winds an extra peak occurs between 8:00 and 9:00 in the morning. S-SW winds do not show this peak. The situation is similar during April-September (Fig. 16b). Here too the extra peak between 8:00 and 9:00 is very pronounced during NE-E winds whereas it is much less expressed during S-SW winds. Additionally, in the period April-September PM10 concentrations are much higher during the morning when wind blows from the NE-E.

4. PM10 measurements: discussion

Apart from emissions caused by wind erosion or human activity, dust concentration is expected to depend on atmospheric processes affecting transportation, concentration and/or dilution of airborne particles. For the NDRA the proximity of the Las Vegas metropolis requires special attention because of the huge amounts of PM10 produced in the city. In this section we investigate the effect of these factors on the PM10 characteristics at NDRA.

Diurnally, wind speeds and PM10 concentrations behave similarly throughout the year with a maximum in the early afternoon and a minimum in the morning (Fig. 17). However, they do not evolve in parallel. On average, dust concentration at NDRA runs 2 hours ahead compared to wind speed (Fig. 17a). This difference is greatest from April to September (Fig. 17b). In October to March the peaks in the afternoon coincide much closer, but the difference of 2 hours is still apparent in the morning (Fig. 17c). That dust concentration at NDRA is not predominantly related to local wind speed is further illustrated in Fig. 18. There is no correlation between the parameters, either during the day or night hours. Studies based on long-term series of observations (i.e., not focusing on stormy events) also show that high dust concentrations do not necessarily occur during periods of high wind speed, even when the topsoil is dry (Offer and Goossens, 1990; Goossens and Offer, 1995; Chow and Watson, 1997). In a recent study carried out near Delhi (India), Tandon et al. (2010) compared the diurnal cycles of dust concentration and wind speed and found no parallel evolutions for either coarse (>10 µm) or fine (< 10 µm) particle fractions.

We compared dust concentrations at NDRA with wind direction (Fig. 19). We used a wind speed below 3 m s^{-1} as a criterion for non-erosive periods, which is well below the wind erosion thresholds of 6-7 m s^{-1} for non-stabilized sand surfaces and 9-10 m s^{-1} for non-stabilized silt surfaces. During non-erosive periods dust concentration is close to uniform for all wind directions; only the N-NE sector shows (slightly) lower values (Fig. 19). During very windy periods (wind speeds above erosion threshold, i.e. local wind erosion is likely) the pattern becomes very asymmetric, with much higher concentrations during S, SW or W winds. These are also the directions where the most emissive zones in

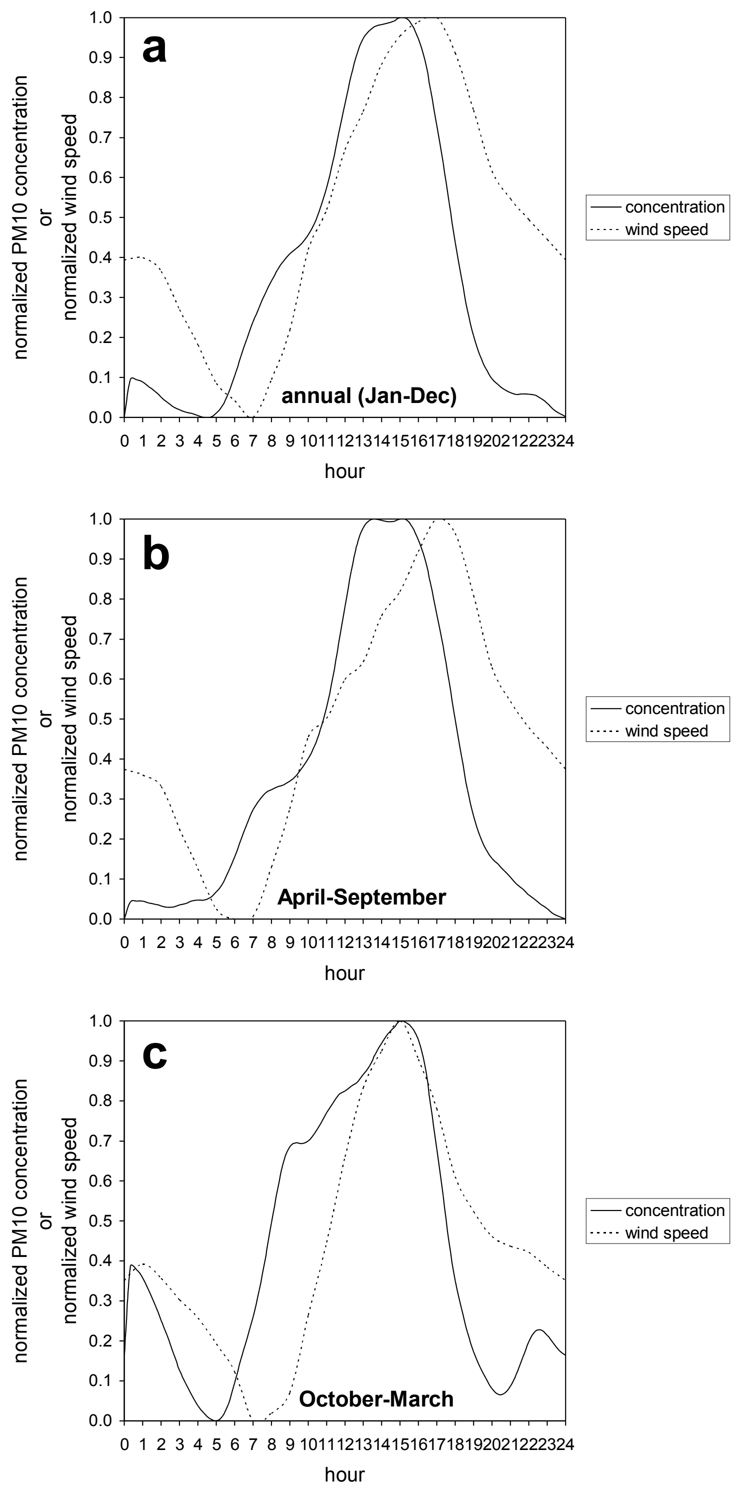

Fig. 17: Comparison of diurnal evolutions of PM10 concentration and wind speed. (a) annual pattern; (b) April-September; (c) October-March.

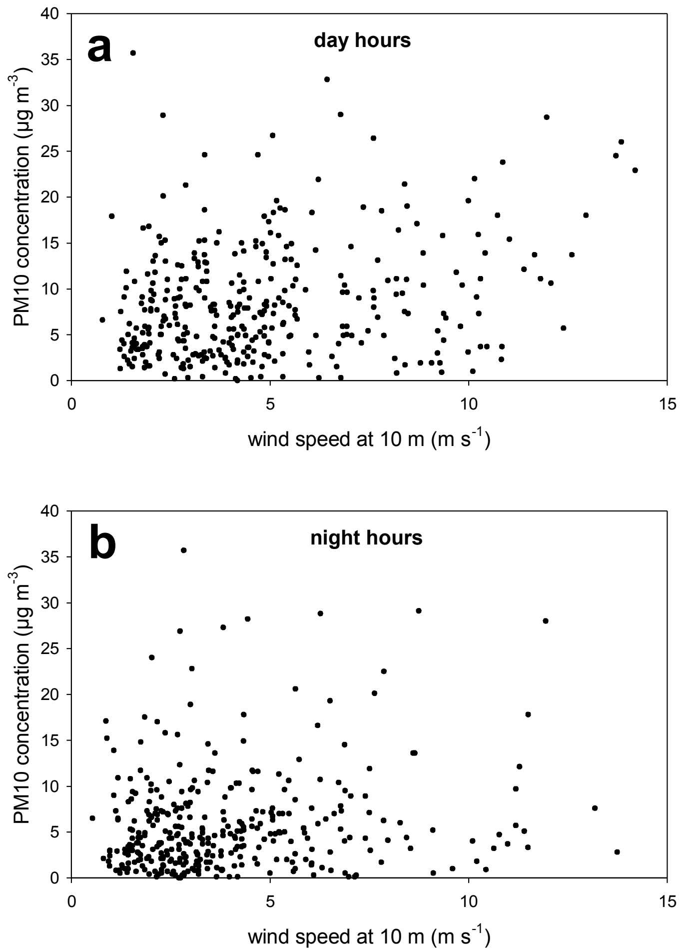

Fig. 18: Correlation diagram for PM10 concentration and wind speed.
(a) day hours; (b) night hours.

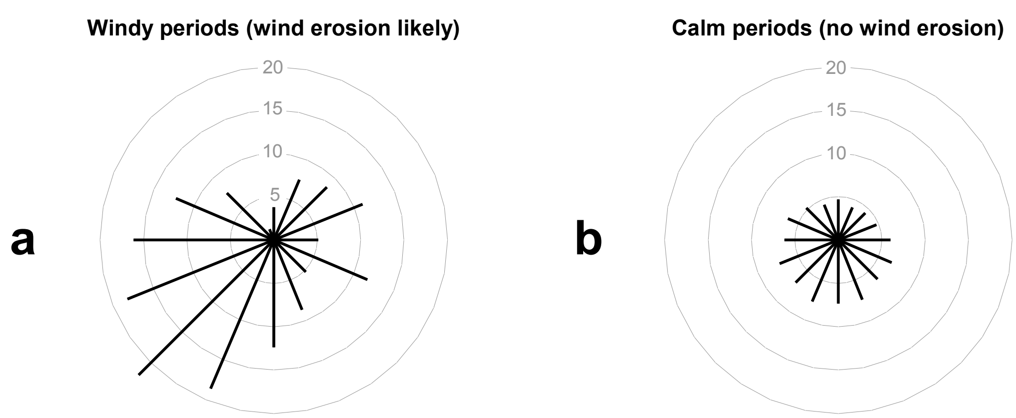

Fig. 19: Hourly average PM10 concentration (µg m^{-3}) as a function of wind direction. (a) windy periods (wind erosion likely); (b) calm periods (no wind erosion). See text for criteria.

NDRA are located relative to the spot where PM10 concentrations were measured. Does this mean that the PM10 concentrations in this study were mainly determined by wind erosion? To test this hypothesis we calculated the diurnal patterns of dust concentration for the stable and windy periods separately (Fig. 20). During stable periods (no wind erosion) the pattern is very similar to the average annual pattern (Fig. 17a). This result shows that wind erosion is not the dominant factor determining the afternoon PM10 peak at NDRA. On the contrary, during wind erosion, concentrations show a clear tendency to be highest at night (Fig. 20).

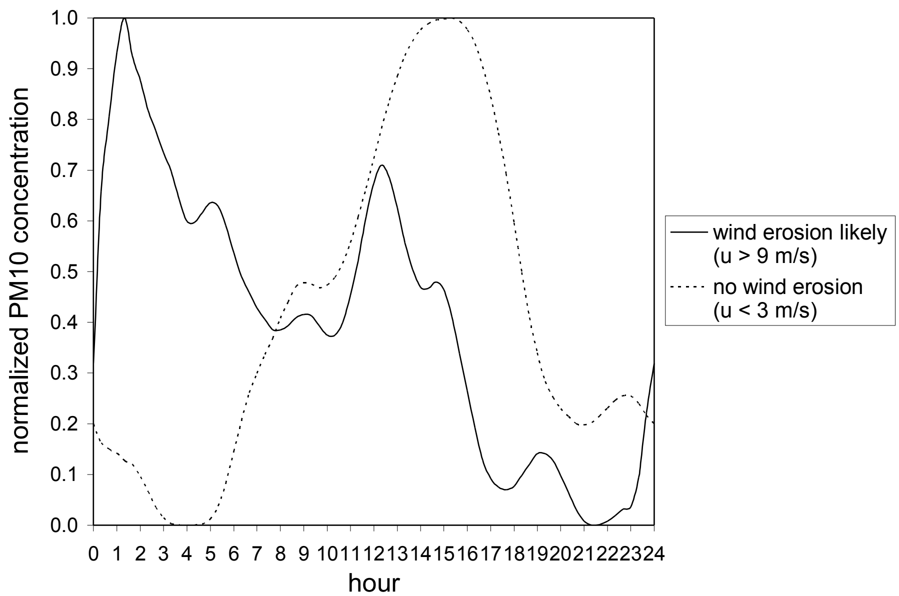

Fig. 20: PM10 concentration and probability of wind erosion in NDRA

An important atmospheric parameter affecting fine particulate concentration is atmospheric stability, which by itself is related to radiation (and, hence, temperature) and wind shear (i.e., wind speed). The literature states that PM10 concentrations are highest in stable atmospheres (usually at night) because of the reduced height of the mixing layer and limited ventilation (Choularton et al., 1982; Chow and Watson, 1997; Zhao et al, 2009). Vertical wind and temperature data were collected from the North Las Vegas Airport (NLVA) Integrated Upper-Air Monitoring Station, which is located only 20 km west of NDRA. This station records hourly values of wind speed up to 3 km altitude and hourly values of temperature and humidity up to 10 km altitude. NLVA started collecting data from September 11, 2009 onward. Although this NDRA study was carried out in 2008, reliable stability patterns can be calculated because the pattern of temperature is fairly constant from one year to another. Comparing atmospheric stability to PM10 concentration we find that the highest PM10 concentrations occur when atmosphere is unstable and lowest concentrations when atmosphere is stable (Fig. 21). Also, note that there is a lag of approximately 1.5 hours between the peak in PM10 concentration and the peak in atmospheric instabililty in the early and late afternoon. Therefore, diurnal evolution of PM10 at NDRA is not a result of changes in atmospheric stability.

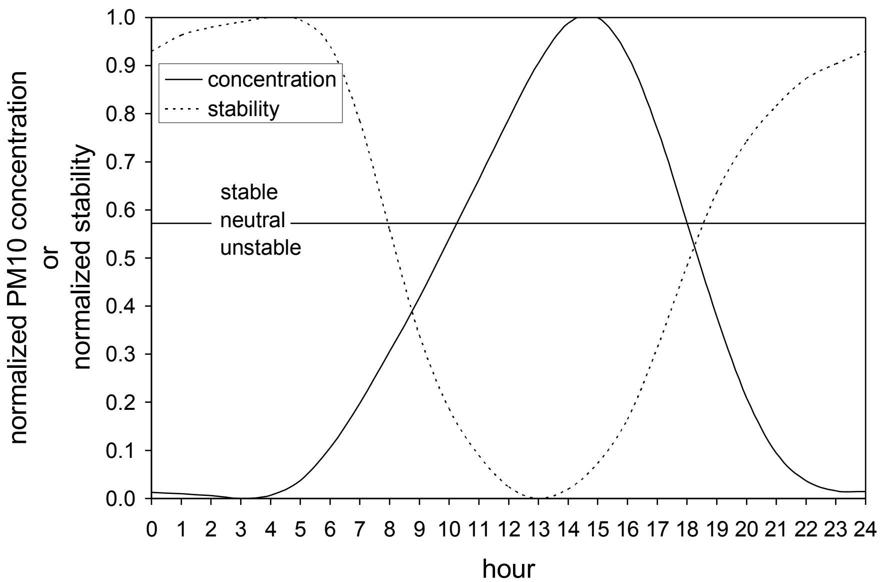

Fig. 21: PM10 concentration and atmospheric stability at NDRA. Stability was measured as T_{100} - T_0, where T_{100} = temperature at 100 m altitude and T_0 = temperature at ground level. Curves are based on hourly averages and were normalized to facilitate comparisons. The figure shows the annual average.

To investigate the potential effect of PM10 production in Las Vegas, data from various stations located in the Las Vegas valley were analyzed. Most stations are located within the conurbations of Las Vegas / North Las Vegas / Henderson, Boulder City and Mesquite, and are heavily affected by traffic and construction works. Therefore, these stations are not useful comparisons to explain PM10 patterns at NRDA. However, there are two rural stations that can be studied. Apex station is located 32 km northeast of the center of Las Vegas, 12 km north of NDRA. Jean station is located 50 km SW of the city center. A third station in the center (Sunrise Acres, in Las Vegas) was also selected for comparison. Hourly PM10 data were collected from these stations, for the period investigated in this study (19 Dec 2007 - 17 Dec 2008). The location of the stations is very fortunate for investigating the effect of Las Vegas on the PM10 patterns in NDRA. Because of the bimodal wind regime in the region one station will always be located upwind, the second downwind and the third in the center of Las Vegas.

The monthly averages of the ratio of PM10 concentration at night to PM10 concentration by day are similar for the rural stations of Apex and Jean (Fig. 22a,b). In general, the ratio is highest in summer and lowest in winter (note that the pattern is more irregular in Apex compared to Jean). In Sunrise Acres (Fig. 22c) seasonal effects no longer occur. This could be expected since there is human activity in the city all year round.

These patterns differ significantly from that found at NDRA (Fig. 22d). Monthly average PM10 concentrations are always higher during the day hours than at night (note the small difference in January). This differs from the two other rural stations, where at least several months during the year nocturnal concentrations are higher. In the city, concentrations are also highest at night (Fig. 22c). Secondly, the annual pattern is different. In NDRA the ratio of dust concentration at night to dust concentration by day is lowest in summer and highest in winter. In Jean and Apex the situation is reverse.

Comparing the annual average of diurnal PM10 concentrations for the two primary wind directions shows that NDRA differs from the other stations (Fig. 22e-h). Apex, Sunrise Acres, and SW winds at Jean show higher PM10 concentrations during the night hours than during the day. Chow and Watson (1997) attributed the high PM10 concentrations during the day at Jean during NE wind to inflow of dust from Las Vegas, especially during the rush hours. Rush hour effects in the city are substantial. PM10 curves for Sunrise Acres show a local peak in concentration in the morning (Fig. 22g). For S-SW winds it appears two hours earlier because these winds mainly occur in the spring and summer whereas the N-NE winds mainly occur in the autumn and winter. In summer, many people in Las Vegas start working very early in the morning to take advantage of the cooler temperatures. No extra peak in PM10 concentration is observed in the afternoon, most probably because the end of the working-day is much more flexible.

The PM10 curve for NE winds for Jean shows two peaks during the day hours. The first, around 9:00, may result from inflow of PM10 produced in Las Vegas during the morning rush hour (see Chow and Watson, 1997). The 3-h difference with Sunrise Acres, 6:00 in Sunrise Acres and 9:00 in Jean, can be explained by the distance between the stations (50 km, which fits well with the average wind speed of 4-5 m s^{-1}, see Fig. 5a). The second peak, around 16:00, is less well developed. A dry lake 5 km ENE of Jean is used as a place for off-road driving activities, though much less intense than the Nellis Dunes. These activities could contribute to the small peak in the afternoon during NE winds. There are no large urban or recreation areas south and southwest of Jean. For this sector, minimum PM10 concentrations occur during the day and maximum concentrations at night.

The Apex station also shows a (small) peak in PM10 concentrations for winds blowing from the city center (Fig. 22e). This peak occurs approximately at noon. However, it is questionable whether this peak is caused by urban rush hours because it occurs at least 6 hours later than the one at Sunrise Acres. The distance between the stations is 32 km. In order for the Apex mid-day peak to be a result of rush hour traffic, the average wind

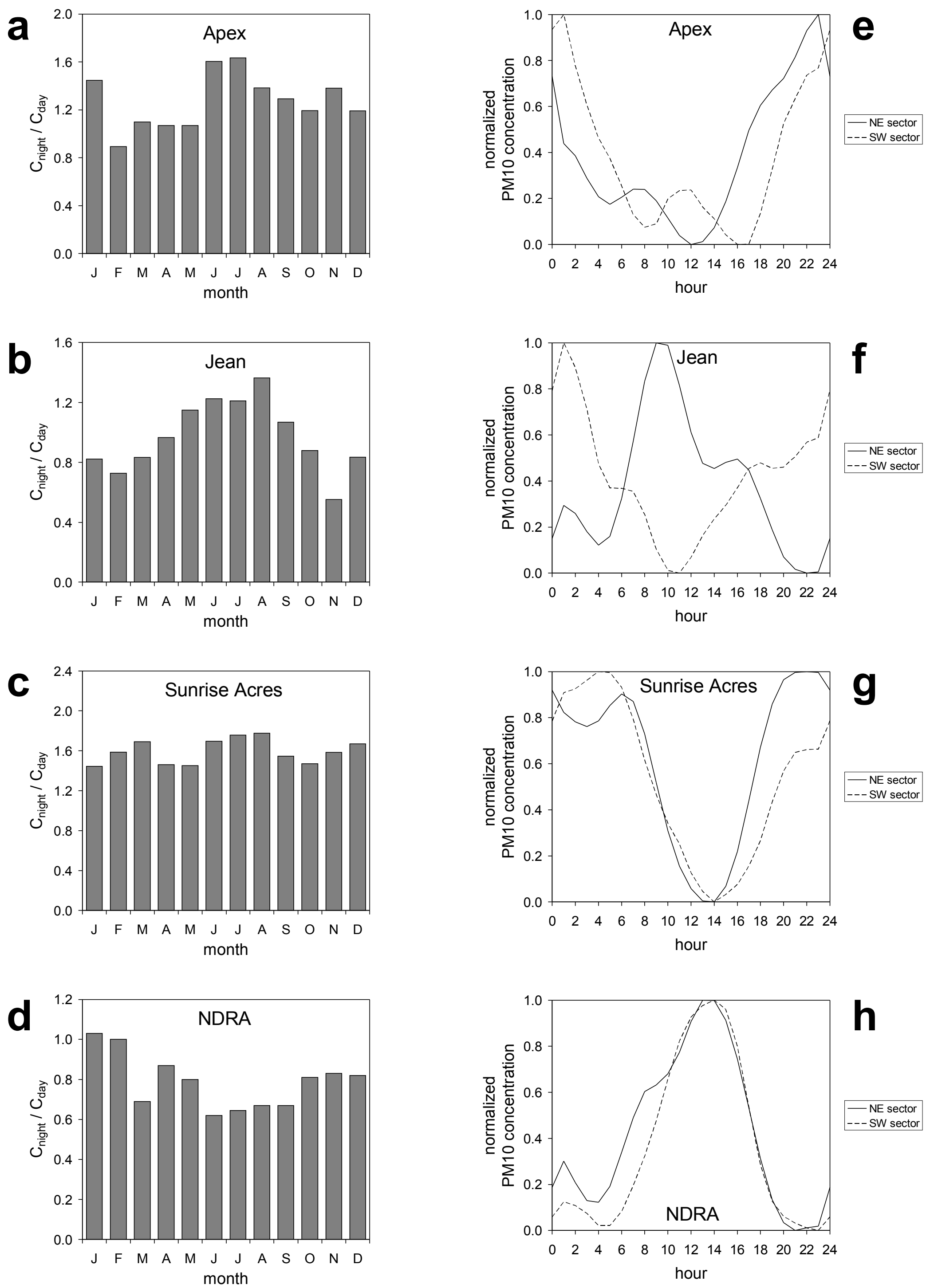

Fig. 22: Comparison of PM10 patterns for Apex, Jean, Sunrise Acres and NDRA. (a-d) monthly averages of the ratio of PM10 concentration at night to PM10 concentration by day; (e-h) diurnal pattern of PM10 concentration (curves are annual averages for the two wind directions shown).

speed must be as low as 1.5 m s^{-1}, which is much lower than the actual values (shown in Fig. 5a) even if the greater surface roughness of the city is considered. A similar, although smaller, peak in concentration occurs in the Nellis Dunes around 12:00 for S-SW winds (see Fig. 16, which is based on 20-min data instead of the 1-h data in Fig. 22). Therefore, for both Apex and NDRA the patterns of PM10 concentration cannot be explained by rush hour effects produced in the conurbation of Las Vegas.

This conclusion is further supported by two observations. First, the increase in PM10 concentration in the morning at NDRA begins while the winds are still blowing from the N-NE sector (the common situation at night, both in autumn-winter and in spring-summer); there is a difference of about 2 hours between the increase in dust concentration and the change in wind direction (Fig. 23). Also, in April-September, concentrations in the afternoon start to decrease well before the wind starts blowing from the eastern sector.

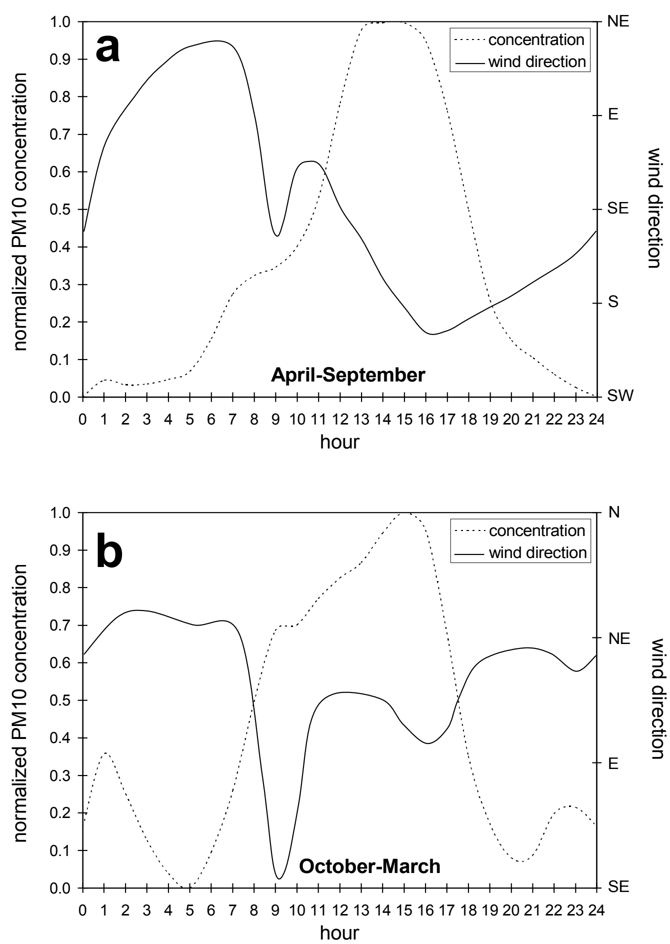

Fig. 23: Comparison of diurnal evolutions of PM10 concentration and wind direction. (a) April-September; (b) October-March.

Secondly, at NDRA PM10 concentration is always highest during the day hours, even when winds blow from the NE sector. This sector is much less dust productive than the SW sector. Apart from a power plant in Moapa 50 km to the northeast, the only substantial dust sources northeast of NDRA are Milford Flats and Sevier dry lake, both at a distance of 350 km, and Dugway Proving Grounds, about 450 km from NDRA. A quarry, a landfill and a (small) dry lake 7, 12 and 20 km north of NDRA respectively do not affect the area during NE wind conditions (dust from these sources does not flow over NDRA during NE winds). It is very unlikely that the more distant sources determine the diurnal PM10 pattern at NDRA because the dust plumes they generate are already significantly diluted upon arrival at NDRA. These sources could affect weekly, monthly, seasonal or annual PM10 curves by creating spikes of high concentration when active, but not diurnal curves. Variations in PM10 on a time scale of only hours or even less do not scale with the distance of these sources to NDRA. A further argument that distant sources do not explain the diurnal pattern of PM10 concentration is that the S-SW curve for Jean is not affected by S-SW located dust sources. Ft. Irwin tank training base is an important dust source 110 km SW of Jean, and several dry lake beds occur as close as 15-30 km S-SW of the Jean station. None of these appear to affect the diurnal PM10 pattern at Jean, although they may explain spikes of high dust concentration in weekly, monthly or annual PM10 curves.

Therefore, a local dust-producing mechanism must exist to explain the patterns of PM10 concentration at NDRA. It should preferentially be active during the day, and be more productive in summer than in winter. Off-road vehicular activity is the only realistic explanation. We recall that the number of ORV visitors at NDRA currently (2011) is close to half a million annually. Previous research (McLaurin et al., in press) showed that many surfaces in NDRA (especially the silty and silty rocky substrata) produce huge amounts of dust during ORV activity. ORV driving in NDRA occurs during the day hours only because of the absence of lighting and the rough and dangerous terrain. In addition there is much more dust production by ORV activities during the summer months compared to the winter months because the period of daylight is longer and the number of driving hours is higher. During our fieldwork, we observed that the intense heat during the summer months does not restrict the population from driving in the area. The data in Chapter 6 show that in NDRA the annual production of ORV-generated dust equals the production of wind-erosion generated dust. In addition, for the PM10 fraction only ORV-produced dust is even greater than wind-erosion produced dust. For all these reasons it is plausible that the diurnal pattern of PM10 concentration at NDRA is determined by the intense ORV activity in the area. The role of other factors such as inflow of PM10 from Las Vegas, local dust production by wind erosion, the effect of atmospheric stability, or the potential inflow of PM10 from distant sources, is subordinate to that of ORV activity. The effect of atmospheric stability, which usually is very dominant (see Figs. 22e-g), does not change the diurnal PM10 pattern at NDRA because nearly all PM10 produced by ORV during the day has already left the area well before midnight. The diameter of NDRA is only about 7 km; at an average wind speed of 4-5 m s^{-1} (see Fig. 5a) it takes less than 30 minutes to evacuate locally produced PM10 particles.

5. Summary of conclusions

At NDRA, PM10 concentrations measured at 20-min periods for the entire year 2008 show that 56 % of the time concentrations were <5 μg m^{-3}, and 80 % of the time they were <10 μg m^{-3}. Only 0.1 % of the time they were >100 μg m^{-3}. When daily averages are considered, the distribution is less skewed. Most frequently average daily concentrations were 3 to 4 μg m^{-3}. Only 11 days in 2008 (3 %) had average daily PM10 concentrations >20 μg m^{-3}.

Two mechanisms of dust production occur in NDRA. Wind erosion in the sand dunes and on loose, uncompacted silty substrata in the center and west produce dust during periods of strong wind. All year round, off-road vehicular activity adds additional dust to the atmosphere. On an annual basis, the amount of dust produced at NDRA by ORV activity equals the amount produced by wind erosion.

At NDRA PM10 concentrations are highest during April-September and lowest from October-March. They are also higher during the day hours than at night. Short-term high-magnitude wind erosion events may occur all year but are most abundant in spring. During such events PM10 concentrations can be very high, up to 1300 μg m^{-3} and more.

At NDRA PM10 is finest at the end of the summer and coarsest in winter. Median grain diameter in summer is around 3 μm compared to 4 μm in winter.

The diurnal pattern of PM10 concentration at NDRA shows a maximum in the early afternoon and a minimum in the morning. In winter, a secondary maximum occurs around midnight and two nighttime peaks occur in October-December and March-April. Summer months show only one maximum, in the afternoon. Also, the duration of high PM10 concentration is shorter in the summer: from 11:00 to 18:00 as compared to 7:00 to 18:00 in winter.

No correlation was found between PM10 concentration and wind speed. High concentrations were observed at all wind speeds, and high wind speeds did not necessarily result in high PM10 concentrations. Therefore, the higher concentrations during the day are not related to local wind erosion. They are also not explained by the diurnal pattern of atmospheric stability. Highest concentrations are observed in the early afternoon, when atmosphere is unstable and mixing height and ventilation are large. Lowest concentrations are observed at night, when atmosphere is stable and mixing height and ventilation are small. Importation of dust from the nearby conurbation of Las Vegas also does not explain the diurnal pattern of PM10 concentration at NDRA. No rush hour effects are present, and the increase in PM10 concentration in the morning occurs well before the wind starts blowing from the city. Also, peaks in PM10 concentration occur when winds are blowing from the much cleaner northeastern sector. Off-road vehicular activity in NDRA is the most plausible mechanism for generating the diurnal and other patterns of PM10 concentrations recognized in this study.

Although dust from NDRA is blowing towards Las Vegas from late autumn to early spring and also during most of the nights, no quantitative data is currently available on the impact NDRA-emitted dust may have on the PM10 concentrations in the city. More research is necessary to determine the degree of dilution as the dust blows towards the city, and how concentrations change with the increased surface roughness in town.

Acknowledgements

The DustTrak aerosol monitor was graciously provided by D. James, College of Engineering, University of Nevada Las Vegas, Las Vegas, NV, USA. Wind data were collected from four wind towers set up and managed by D. Pepper (College of Engineering, University of Nevada Las Vegas, Las Vegas, NV, USA) and X. Wang (Purdue University Calumet, Hammond, IN, USA). Additional wind data from the Nellis Air Force Base meteorological station were provided by M. EmelyPoynter (Nellis Air Force Base, Las Vegas, NV, USA). Vertical wind and temperature data were obtained from the North Las Vegas Airport Integrated Upper-Air Monitoring Station. R. Merle and P. Wiker (Department of Air Quality & Environmental Management, Las Vegas, NV, USA) provided assistance in collecting these data. L. Bangen assisted in setting up instrumentation in the field.

References

Akhter, M.S., Madany, I.M., 1993. Heavy metals in street and house dust in Bahrain. Water Air Soil Pollution 66, 111-119.

American Lung Association, 2010. The American Lung Association State of the Air 2010. American Lung Association National Headquarters, Washington DC, www.longusa.org.

Athar, M., Iqbal, M., Beg, M.U., Al-Ajmi, D., Al-Muzaini, S., 1998. Airborne dust collected from Kuwait in 1991-1992 augments peroxidation of cellular membrane lipids and enhances DNA damage. Environment International 24, 205-212.

Besancenot, J.P., Boko, M., Oke, P.C., 1997. Weather conditions and cerebrospinal meningitis in Benin (Gulf of Guinea, West Africa). European Journal of Epidemiology 13, 807-815.

Castor, S., Ferdock, G., 2004. Minerals of Nevada. University of Nevada Press, 512 pp.

Choularton, T.W., Fullarton, G., Gay, M.J., 1982. Some observations of the influence of meteorological variables on the size distribution of natural aerosol particles. Atmospheric Environment 16, 315-323.

Chow, J.C., Watson, J.G., 1997. Fugitive Dust and Other Source Contributions to PM10 in Nevada's Las Vegas Valley, Volume 2. Desert Research Institute, DRI Document No. 4039.2F1, Reno.

Dockery, D.W., Pope, C.A., Xu, X., Spengler, J.D., Ware, J.H., Fay, M.E., Ferris, B.G. Jr., Speizer, F.E., 1993. An association between air pollution and mortality in six U.S. cities. The New England Journal of Medicine 329, 1753-1759.

Feng, Y., Barratt, R., 1993. An assessment of data of trace elements in indoor and outdoor dusts. International Journal of Environmental. Health Research 3, 18-31.

Fergusson, J.E., Kim, N.D., 1991. Trace elements in street and house dusts: sources and speciation. Science of the Total Environment 100, 125-150.

Fishbein, L., 1991. Indoor environments: the role of metals. In: Merian, E. (Ed.), Metals and their Compounds in the Environment. VCH Verlagsgesellschaft mbH, Weinhelm, 287-309.

Fryrear, D.W., 1986. A field dust sampler. Journal of Soil and Water Conservation 41, 117–120.

Goossens, D., Buck, B., 2010. Effects of wind erosion, off-road vehicular activity, atmospheric conditions and the proximity of a metropolitan area on PM10 characteristics in a recreational site. Atmospheric Environment, doi: 10.1016/j.atmosenv.2010.09.046.

Goossens, D., Offer, Z.Y., 1995. Comparisons of day-time and night-time dust accumulation in a desert region. Journal of Arid Environments 31, 253-281.

Griffin, D.W., Kellogg, C.A., 2004. Dust storms and their impact on ocean and human health: Dust in Earth's atmosphere. EcoHealth 1, 284-295.

Hagen, L.J., Woodruff, N.P., 1973. Air pollution from dust storms in the Great Plains. Atmospheric Environment 7, 323-332.

Ichinose, T., Nishikawa, M., Takano, H., Sera, N., Sadakane, K., Mori, I., Yanagisawa, R., Odae, T., Tamura, H., Hiyoshi, K., Quan, H., Tomura, S., Shibamoto, T., 2005. Pulmonary toxicity induced by intratracheal instillation of Asian yellow dust (Kosa) in mice. Environmental Toxicology and Pharmacology 20, 48–56.

Järup, L., 2003. Impact of environmental pollution on heath: balancing risk. British Medical Bulletin 68, 167-182.

Jinadu, B.A., 1995. Valley Fever Task Force Report on the Control of Coccidioides imitis. Kern County Health Department, Bakersfield, CA.

Komatsu, K., Vaz, V., McRill, C., Colman, T., Comrie, A., Sigel, K., Clark, T., Phelan, M., Hajjeh, R., Park, B., 2003. Increase in coccidioidomycosis – Arizona, 1998-2001. Journal of the American Medical Association 289, 1500-1502.

Korenyi-Both,A.L., Korenyi-Both, A.L., Molnar, A.C., Fidelus-Gort, R., 1992. Al Eskan disease/ Desert Storm pneumonitis. Military Medicine 157, 452-462.

Laden, F., Schwartz, J., Speizer, F., Dockery, D., 2006. Reduction in fine particulate air pollution and mortality: extended follow-up of the Harvard six cities study. American Journal of Respiratory and Critical Care Medicine 173, 667-672.

Lambert, A.L., Dong, W., Winsett, D.W., Selgrade, M.K., Gilmour, M.I., 1999. Residual oil fly ash exposure enhances allergic sensitization to house dust mite. Toxicology and Applied Pharmacology 158, 269-277.

Lazaro, M.A., Chang, Y-S., Kuiper, J.A., Kotamarti, V.R., James, D.E., Brazao, R., Pulugurtha, S., 2004. Cumulative Las Vegas Valley Air Quality Modeling Assessment of Ongoing Bureau of Land Management (BLM) Federal Land Disposition Actions within the BLM Disposal Boundary. Report prepared for the Bureau of Land Management (BLM), University of Chicago and University of Nevada Las Vegas.

McLaurin, B., Goossens, D., Buck, B.J., in press. Combining surface mapping and process data to assess, predict, and manage dust emissions from natural and disturbed land surfaces. Geosphere.

Offer, Z.I., Goossens, D., 1990. Airborne dust in the Northern Negev Desert (January-December 1987): general occurrence and dust concentration measurements. Journal of Arid Environments 18, 1-19.

Peters, A., Wichmann, H., Tuch, T., Heinrich, J., Heyder, J., 1997. Respiratory effects are associated with the number of ultrafine particles. American Journal of Respiratory and Critical Care Medicine 155, 1376-1383.

Sultan, B., Labadi, K., Guegan, J.F., Janicot, S., 2005. Climate drives the meningitis epidemics onset in West Africa. PLoS Med 2, 43-49.

Tandon, A., Yadav, S., Attri, A.K., 2010. Coupling between meteorological factors and ambient aerosol load. Atmospheric Environment 44, 1237-1243.

Wang, K., You, D., Balakrishna, S., Ripple, M., Ahlert, T., Fahmy, B., Becnel1, D., Daly, M., Subra, W., McElduff, J.S., Lomax, L.G., Troxclair, D., Cormier, S.A., 2008. Sediment from hurricane Katrina: potential to produce pulmonary dysfunction in mice. International Journal of Clinical and Experimental Medicine 1, 130-144.

Zhao, X., Zhang, X., Xu, X., Xu, J., Meng, W., Pu, W., 2009. Seasonal and diurnal variations of ambient PM2.5 concentration in urban and rural environments in Beijing. Atmospheric Environment 43, 2893-2900.

Chapter 8

MINERALOGICAL COMPOSITION OF SOIL SAMPLES IN THE NELLIS DUNES RECREATION AREA

Deborah Soukup[1], Brenda Buck[1], Dirk Goossens[1], Yuanxin Teng[1] and Dirk Baron[2]

[1]*Department of Geoscience, University of Nevada Las Vegas*
[2]*Department of Physics and Geology, California State University*

1. Introduction

Natural dust is primarily composed of mineral grains. A mineral is a substance having a crystalline internal structure and characteristic chemical composition or a definite range of composition that has been formed naturally and occurs in the Earth's crust (Watt, 1982). Most minerals have a characteristic crystal form and physical properties. Characterizing the types of minerals present in dust is an extremely important, but often overlooked task (Guthrie, 1992). Determining the types of minerals present in dust is important because (1) many minerals are known to accumulate in lung tissue and adversely affect health (for example: quartz, mica, gypsum, apatite, talc, rutile, pyroxene, feldspar, numerous clay and zeolite minerals, and numerous serpentine and amphibole minerals, some of which are commonly referred to as 'asbestos') (Guthrie, 1992; Klein, 1993; Ross et al., 1993); and (2) some minerals are highly chemically reactive and can pose increased risk because known carcinogens may be absorbed onto them or they may be bioreactive (Nettesheim and Griesemer, 1978; Guthrie, 1997; Plumlee et al., 2006; Duzgoren-Aydin, 2008). In order to better understand the mineralogy of dusts derived from the surfaces at NDRA, we determined the mineralogy of soil samples from the 17 surface map units and 5 parking areas using x-ray diffraction (XRD)

2. Potential health effects of mineralogical components

The harmful effects of some minerals on human health have been recognized for centuries. Hippocrates (460-355 BC) referred to the metal digger as “a man who breathed with difficulty” (Carretero et al., 2006). Pliny the Elder (23-79 AD) described illnesses associated with exposure to mercury (Hg) sulfide dust. Health effects caused by exposure to mineral dusts were sufficiently known by the Middle Ages to be discussed by Agricola in De Re Metallica (1556). In this publication, Agricola noted: “…Some mines are so dry that they are entirely devoid of water and this dryness causes the workmen even greater harm, for the dust, which is stirred and beaten up by digging, penetrates into the windpipe and lungs and produces difficulty in breathing… It eats away the lungs and implants consumption in the body” (Carretero et al. 2006).

Historically, research into potential health effects associated with exposures to mineral dusts has focused on workplace settings, particularly in mining operations extracting or processing asbestos, crystalline silica, coal, and toxic metals including lead (Pb) and mercury (Hg). Recently, the focus has shifted to environmental exposures to asbestos, coal or heavy metal bearing dusts that have been linked to diseases such as asbestosis, silicosis, or coal miners pneumoconiosis, as well as other earth materials such as kaolinite (a clay mineral), soil dusts, cements and other materials containing elements such as calcium (Ca), manganese (Mn), and vanadium (V) whose toxicities are not well known (Duzgoren-Aydin, 2008). Research has demonstrated that mineral dusts primarily cause damage when inhaled, and rarely by ingestion, or penetration into the skin. Several minerals have been shown to produce a variety of pathologies within the lungs including lung cancer, mesothelioma (mesothelial cancer), and pneumoconiosis (the lung loses its capacity to function; Carretero, et al. 2006). Mineral toxicity may be determined in epidemiological studies (evaluating the relationships between human exposure to a hazardous substance and the potential health effects), in vivo studies in which animal models are used to study the effects of mineral dusts on exposed populations, and in vitro studies which focus on determining the biological activity of a mineral (Guthrie, 1992).

Several characteristics are important in determining the biological activity and potential toxicity of minerals. These include particle size and shape, surface properties, dissolution behavior, ion exchange and sorptive properties (Hochella, 1993; Guthrie, 1997; Carretero et al., 2006). Particles with diameters greater than approximately 10 microns (µm) impact the upper reaches of the respiratory tract, and move rapidly up the bronchioles by specially adapted cells that sweep the particles towards the throat. These particles are then cleared and coughed or spit up or swallowed. Particles with diameters of one to two µm are capable of penetrating the deepest regions of the lung. These particles tend to remain in the alveolar walls of the lung because the body’s natural clearance processes are not efficient in the deep lung.

Mineral dusts are removed from the lung by multiple mechanisms including exhalation of suspended particles, sequestration of particles by macrophages, relocation through the mucocilliary escalator and lymphatic system, in situ dissolution, or some combination of these mechanisms (Lehnert, 1993; Plumlee et al., 2006). Inflammation and other immune responses to mineral particles may also play a role in disease (Plumlee et al., 2006). Since macrophages are not able to completely engulf mineral fibers that are longer than the cells themselves, phagocytosis of fibers is incomplete and irreversible cell damage and death may result. Many researchers have found that fiber length is one of the most important carceinogenic properties of inhaled minerals (Rödelsperger et al., 1987) ADSTER, 2003). Stanton et al. (1981) developed the "Stanton hypothesis" which relates a fiber's morphology to its activity for the induction of tumors. These researchers stated that the optimum dimensions for the induction of tumors is a diameter $\leq$0.25 µm and a length >8 µm. Nolan and Langer (1993) subsequently reported that the "Stanton hypothesis" has some limitations. Other investigators have defined critical fiber dimensions for lung cancer and mesothelioma as <0.3 to 0.8 µm in diameter and >10 to 100 µm in length for lung cancer, and 0.1 µm in diameter and >5 to 10 µm in length for mesothelioma (Carretero et al. 2006). Pott (1989) reported that fiber pathogenicity depends not only on the fiber dimensions, but also on the persistence of the fiber in the lung.

The surface is the portion of a mineral that ultimately interacts with a fluid or cell. In some instances, the surface structure may differ significantly from the "bulk" structure. For example, a mineral undergoing dissolution often forms a precipitate at the surface with a composition and/or structure that differs from the bulk material. Differences in surface related factors relative to the bulk can result in changes in the active sites on the surface, affect binding and sorption processes, alter dissolution characteristics and impact a mineral's pathogenic potential (Guthrie, 1997).

Dissolution may play a significant role in particle clearance mechanisms and can result in the release of metals such as iron or other potentially toxic elements to the lung fluid. Dissolution characteristics are often used to differentiate nonhazardous minerals from potentially hazardous minerals. Nonhazardous minerals typically do not remain in the lung for long periods of time, whereas hazardous minerals may have long residence times in the lung (Guthrie, 1997). One of the ways in which a mineral can interact with a fluid is through exchange of an element or molecule. Most minerals have only a limited capacity for cation exchange because sorption occurs only at the surface. For these minerals, the cation exchange capacity is related to the amount of surface area, and complexation of ions or molecules with the surface may have a significant impact on the reactivity of the mineral (Guthrie, 1997). However, other minerals, including smectites and zeolites, have internal as well as external surface areas. As a result, these minerals are characterized by high cation exchange capacities (CECs) and ions can rapidly diffuse from the mineral surface to its interior.

In summary, the primary factors that influence the health hazards of minerals are: (1) point of entry into the body (skin, ingestion, inhalation); (2) type of response (irritation, fibrosis, cancer); (3) duration of exposure to the particles; (4) particle size; (5) morphology of fibers with diameters <0.25 μm and lengths >8.0 μm; (6) chemical composition, including high iron content; (7) low solubility at low pH; (8) surface potential; (9) hydrophobic character versus hydrophilic character; (10) in vitro activation of phagocytic leukocytes; and (11) production of hydroxyl radicals that can break the DNA strand which constitutes the first step in genotoxicity and cancer (Carretero et al. 2006; Plumlee et al., 2006). A classification scheme designating mineral particles as Category I (exceedingly dangerous) or Category II (dangerous after continuous and protracted exposure) was developed by van Oss et al. (1999) using factors (5), (7), and (10). For either category, the onset of disease in humans typically occurs after one to several decades. It is also important to note that mineral dust risks are closely associated with cigarette smoking. For the same time period of mineral dust exposure, smokers are more likely to be affected than non-smokers (Carretero et al., 2006).

Inhalation of minerals are the greatest cause of respiratory cancer after cigarette smoking (Omenn et al., 1986). Two well-known illnesses responsible for the majority of human deaths resulting from mineral dust exposure and inhalation are silicosis and asbestosis. Silicosis (a pneumoconiosis type), is caused by exposure to quartz particles and was prevalent during the Industrial Revolution when quartz was a major component of many materials used in a variety of manufacturing processes (Carretero et al., 2006). Asbestosis is a serious illness resulting from the inhalation of asbestos. “Asbestos” is the commercial name for fibrous minerals used in industry. The dust from asbestos minerals produces lung fibrosis than can result in lung cancer or mesothelioma (Lemaire et al. 1989; Guthrie, 1992). Currently six asbestos minerals are regulated in the USA: chrysotile (a serpentine mineral), and five amphibole minerals: crocidolite (riebeckite asbestos), amosite (cummingtonite-grunerite asbestos), anthophyllite asbestos, tremolite asbestos, and actinolite asbestos (Strohmeier et al., 2010).

There is an important difference between fibrous and asbestiform morphologies in minerals. A fibrous morphology describes long, thin crystals. The asbestiform morphology is a special type of fibrous morphology in which the fibers are extremely thin and flexible and occur in aggregates in which individual fibers are aligned in parallel and can easily separate (Strohmeier et al., 2010). Asbestiform crystals typically have a length to width ratio greater than 20:1 (Strohmeier et al., 2010). There are 394 minerals that are known to occur with a fibrous morphology (Skinner et al., 1988). Only a few of these occur with an asbestiform morphology (Strohmeier et al., 2010). Palygorskite is a commonly occurring mineral in desert soils (Brock and Buck, 2009) that almost exclusively occurs in an asbestiform habit (Huggins et al., 1962; Ross et al., 2008). The 5 amphibole minerals that are regulated as ‘asbestos’, may or may not occur in the asbestiform morphology – only when they have the asbestiform morphology are they regulated (Strohmeier et al., 2010). There is still much disagreement about the potential negative health affects of the non-asbestiform varieties, as well as non-regulated asbestiform minerals (e.g. Rödelsperger et al., 1987; Wylie and Verkouteren, 2000; ADSTR, 2003; Groppo et al., 2005; Turci et al., 2005; Plumlee et al., 2006; Addison and McConnell, 2008; Harper, 2008; Lee et al., 2008; Duncan et al., 2010).

3. Soil mineralogy at Nellis Dunes Recreation Area

3.1 Sampling locations

Soil samples were taken from 17 dust stations representing the 17 different surface types in the Nellis Dunes Recreation Area. Additional soil samples were collected from five parking areas. The location of the sampling spots is shown in Fig. 1. All samples were taken from the original desert surface (i.e., outside ORV trails) except for surface units 1.3 and 2.4 (disturbed sand and disturbed silt) and the parking areas, which can be classified as unit 1.3 (disturbed sand areas).

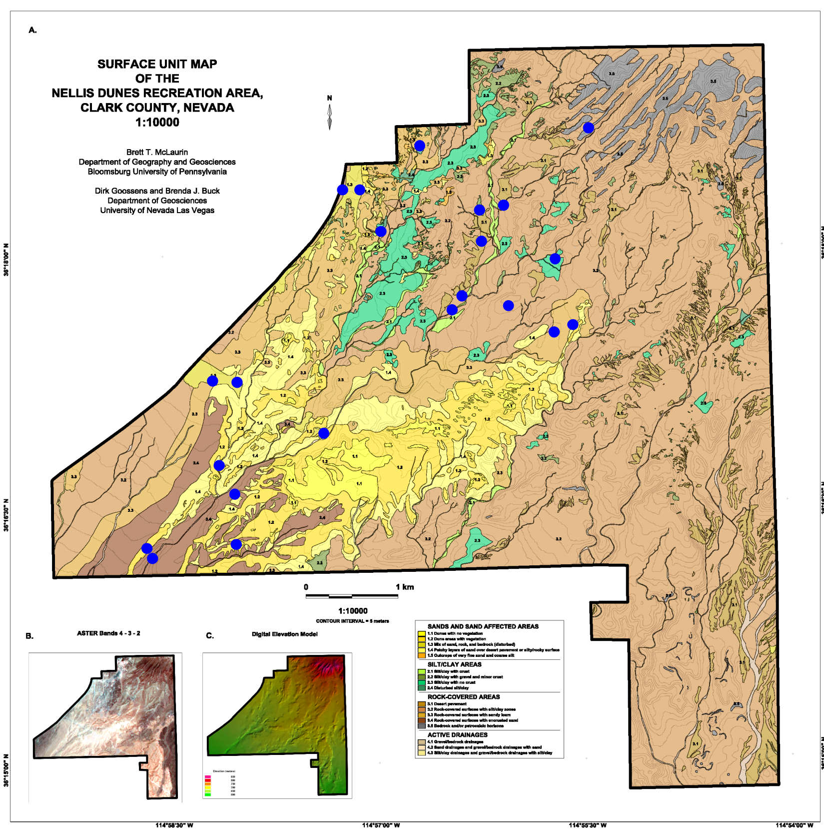

Fig. 1: Location of the sampling sites (blue dots)

3.2 Methodology

X-ray diffraction (XRD) analyses were made on all soil samples to determine the mineralogical composition. Four size fractions were investigated: <2 µm, 2-20 µm, 20-60 µm and 60-100 µm. These fractions were separated by centrifugation and sedimentation following rinsing with distilled water. The distilled water rinses were necessary to remove soluble salts from the soils in order to disperse the samples prior to fractionation.

Pastes of K- and Mg-saturated clay (<2 µm) and silt (2-20 µm) were smeared on glass slides (Theisen and Harward, 1962). The K-saturated sample slides were examined by XRD at 25°C and after heating at 350 and 550°C for two hours. The Mg-saturated samples were also analyzed at 25°C and after being placed in a desiccator containing a pool of ethylene glycol and heated at 65°C for two hours. The desiccator vent was closed upon removal from the oven and the slides stored in the desiccator at least 12 hours prior to XRD analysis. The 20-60 µm and 60-100 µm size fractions were dried from a water slurry onto glass slides. All samples were examined by XRD (CuKα radiation) using a PANalytical X'PERT Pro diffractometer, equipped with an X'Celerator detector. Additional descriptions of these methods can be found in Reid-Soukup and Ulery (2002) and Soukup et al., 2008.

3.3 Results

3.3.1 Mineralogical components

The mineralogical composition of the 20-60 µm and 60-100 µm fractions of the 17 dust station and 5 parking lot samples is relatively uniform, consisting mainly of quartz and calcite, with lesser amounts of plagioclase and alkali feldspars (Table 1). Over one-half of the samples contain palygorskite; palygorskite is more commonly observed in the finer fractions of the samples. Several of the samples also contain amphiboles and a few contain a trace of kaolinite, gypsum, and mica/illite. Most of the gypsum that may have been present in these samples would have been removed during the distilled water rinses prior to fractionation.

XRD analyses reveal that the mineralogical composition of the clay (<2 µm) and silt (2-20 µm) fractions of the soil samples at NDRA is dominated by smectite with lesser amounts of mica/illite, kaolinite, quartz, and calcite (Table 1). Nearly all of the samples also contain chlorite, palygorskite, and plagioclase and alkali feldspars. Three of the silt samples contain amphiboles and one sample contains a 1:1 interstratified illite/smectite within the clay and silt fractions. Gypsum was also identified in several samples, although it should be noted that most of the gypsum present would have been removed during the distilled water rinses prior to fractionation.

3.3.2 Distribution and occurrence of hazardous minerals

Potentially hazardous minerals in soils at Nellis Dunes include quartz, kaolinite, illite, smectite, and palygorskite. Quartz was identified in all of the particle size fractions analyzed, with only two exceptions (Table 1). Smectite was reported in all of the clay and

Table 1: Mineralogical components in the soil samples

Surface Unit	Particle Size (µm)	Minerals[1]										
		Sm	Mi/Ill	Chl	Kao	Paly	Qtz	Cal	Gyp	Fsp	Amph	1:1 Ill/Sm
Sand and Sand-Affected Areas												
1.1	<2	X	X	X	X	X	X		X			
	2 - 20	X	X	X	X	X		X	X			
	20 - 60						X	X	X		Tr[2]	
	60 - 100						X	X	X		Tr	
1.2	<2	X	X	X	X	X	X	X	X			
	2 - 20	X	X	X	X	X	X	X	X			
	20 - 60					X	X	X	X	X	X	
	60 - 100					Tr	X	X	X	X	X	
1.3	<2	X	X	X	X	X	X	X	X			
	2 - 20	X	X	X	X	X	X	X	X			
	20 - 60					X	X	X	X	X		
	60 - 100					Tr	X	X	X	X		
1.4	<2	X	X	X	X	X	X			X		X
	2 - 20	X	X	X	X	X	X	X		X	X	X
	20 - 60		Tr				X	X		X		
	60 - 100						X	X		X		
1.5	<2	X	Tr		X	X	X	X				
	2 - 20	X	Tr	X	X	X		X				
	20 - 60		Tr			Tr	X	X		X		
	60 - 100		Tr			Tr	X	X		X		
Silt/clay Areas												
2.1	<2	NS[3]	NS	NS	NS	NS	NS	NS	NS	NS	NS	NS
	2 - 20	X	X	X	X	X	X	X	X	X		
	20 - 60				Tr	X	X	X	X	X	X	
	60 - 100				Tr	X	X	X	X	X	X	
2.2	<2	X	X		X		X	X		X		
	2 - 20	X	X	Tr	X		X	X		X		
	20 - 60						X	X		X		
	60 - 100						X	X		X		
2.3	<2	X	X	Tr	X		X	X	X	X		
	2 - 20	X	X	X	X		X		X	X		
	20 - 60		Tr				X	X	Tr	X		
	60 - 100		Tr				X	X	Tr	X		
2.4	<2	X	X	X	X	X	X	X				
	2 - 20	X	X	Tr	X	X	Tr	X				
	20 - 60					X	X	X	X	X		
	60 - 100					Tr	X	X	X	X		

Notes:
(1) Sm = smectite; Mi/Ill = mica/illite; Chl = chlorite; Kao = kaolinite; Paly = palygorskite; Qtz = quartz; Cal = calcite; Gyp = gypsum; Fsp = feldspar; Amph = amphiboles; 1:1 Ill/Sm = 1:1 interstratified illite/smectite
(2) Tr = Trace amount of mineral detected by x-ray diffraction
(3) NS = no sample available

Table 1 (ctd.): Mineralogical components in the soil samples

Surface Unit	Particle Size (µm)	Minerals[1]										
		Sm	**Mi/Ill**	**Chl**	**Kao**	**Paly**	**Qtz**	**Cal**	**Gyp**	**Fsp**	**Amph**	**1:1 Ill/Sm**
Rock-covered Areas												
3.1	<2	X	X	X	X	X	X		Tr	X		
	2 - 20	X	X	X	X	X	X	X	X	X		
	20 - 60					Tr	X	X	X	X		
	60 - 100					Tr	X	X	X	X		
3.2	<2	X	X	X	X	X	X	X	X	X		X
	2 - 20	X	X	X	X	X	X	X	X	X		
	20 - 60					Tr	X	X	X	X	X	
	60 - 100					Tr	X	X	X	X		
3.3	<2	X	X	X	X	X	X		X	X		
	2 - 20	X	X	X	X	X	X	X	X	X	X	
	20 - 60		X		Tr		X	X	X	X		
	60 - 100				Tr		X	X	X	X		
3.4	<2	X	X	X	X	X	X	X				
	2 - 20	X	X	X	X	X	X	X				
	20 - 60						X	X	X	X	X	
	60 - 100						X	X	X	X		
3.5	<2	X	X	X	X	X	X	X	X	X	X	
	2 - 20	X	X	X	X	X	X	X	X	X		
	20 - 60		Tr	Tr		Tr	X	X	X	X	X	
	60 - 100		Tr	Tr			X	X	Tr	X		
Drainage Areas												
4.1	<2	NS	NS	NS	NS	NS	NS	NS	NS	NS	NS	
	2 - 20	X	X	X	X		X	X	Tr	X		
	20 - 60					Tr	X	X	X	X		
	60 - 100					Tr	X	X	X	X		
4.2	<2	X	X	X	X	Tr	X	X				
	2 - 20	X	X	X	X	Tr	X	X				
	20 - 60		Tr			Tr	X	X	Tr	X		
	60 - 100						X	X	Tr	X		
4.3	<2	X	X	Tr	X	Tr	X	X	X	X		
	2 - 20	X	X	X	X		X	X	Tr	X		
	20 - 60					Tr	X	X	X	X	X	
	60 - 100				Tr	Tr	X	X	X	X		
Parking Lot Areas												
NA[4]	<2	X	X	X	X	X	X	X	X	X		
	2 - 20	X	X	X	X	X	X	X	X	X		
	20 - 60						X	X	X	X	X	
	60 - 100						X	X	X	X		
NA	<2	X	X	X	X	X	X	X	X	X		
	2 - 20	X	X	X	X	X	X	X	X	X		
	20 - 60						X	X	X	X	X	
	60 - 100						X	X	X	X	X	
NA	<2	X	X	X	X	X	X	X	X	X		
	2 - 20	X	X	X	X	X	X	X	X	X		
	20 - 60					Tr	X	X	X	X		
	60 - 100					Tr	X	X	X	X		
NA	<2	X	X	X	X	X	X	X	X	X		
	2 - 20	X	X	X	X	X	X	X	X	X		
	20 - 60					Tr	X	X	X	X		
	60 - 100					Tr	X	X	Tr	X	X	
NA	<2	X	X	X	X	X	X	X	X	X		
	2 - 20	X	X	X	X	X	X	X	X	X		
	20 - 60						X	X	X	X		
	60 - 100						X	X	X	X		

Notes:
(1) Sm = smectite; Mi/Ill = mica/illite; Chl = chlorite; Kao = kaolinite; Paly = palygorskite; Qtz = quartz; Cal = calcite; Gyp = gypsum; Fsp = feldspar; Amph = amphiboles; 1:1 Ill/Sm = 1:1 interstratified illite/smectite
(2) Tr = Trace amount of mineral detected by x-ray diffraction
(3) NS = no sample available

silt-size samples that were analyzed; illite and kaolinite were also detected in most of the clay and silt-size samples (Table 1). Although palygorskite is widely distributed throughout NDRA, it is most prevalent the <2 μm and the 2-20 μm size fractions throughout the site.

Although XRD analysis is the standard method to identify the mineral species present, it cannot be used to measure the precise amounts of minerals present. Relative abundances among minerals can be estimated by comparing peak widths and intensities. The sharper and more intense peaks indicate either/both increased relative abundance and/or increased internal crystalline order.

Based on the relative size and sharpness of the peaks, for the grain sizes most likely to be inhaled (<2 μm and the 2-20 μm), palygorskite is more abundant in the sandy areas at NDRA (units 1.1, 1.2, and 1.3) and in four of the five parking areas (PLN#1, PLN#2, PLS#1, PLS#2). As discussed previously in Chapter 6, the sandy areas are the most emissive units at the site. The amount of palygorskite in surface units 1.4, 3.2, 3.3, 3.4, and 3.5 is reduced relative to units 1.1, 1.2, 1.3 and the four parking lots. The lowest amount of palygorskite in the two finest grain size fractions was detected in surface units 1.5, 2.1, 2.4, 3.1, 4.1, 4.2, 4.3, and in PLSE#1. Palygorskite was not detected in units 2.2 and 2.3.

4. Harmful effects of the different minerals identified at Nellis Dunes Recreation Area

Although quartz and asbestos are the most hazardous minerals to human health identified to date, other clay minerals may be dangerous because of their limited solubility in the lung, reactivity, small particle size, and fibrous morphology. The main harmful effects of the different minerals identified at NDRA are discussed below.

4.1 Kaolinite

The pathogenicity of kaolinite appears to be primarily related to the presence of quartz, because kaolinite-bearing rocks typically contain other minerals, including quartz (Carretero et al., 2006). Some workers who received heavy exposures to kaolinite dust have developed pneumoconiosis, although an increased risk of lung cancer was not reported (Ross et al., 1993). Guthrie (1992) reviewed several epidemiological studies and reported that exposure to kaolinite-bearing dust is fibrogenic only when dust

concentrations are very high or exposure is combined with another respiratory disease, such as tuberculosis.
The results of *in vivo* experiments regarding the fibrogenic potential of kaolinite-bearing dusts are not conclusive. Previous investigations have indicated that kaolinite did not induce tumors in Syrian hamsters, while others indicated that a slight fibrogenic response was observed (Carretero et al., 2006). However, Wastiaux and Daniel (1990) reported that prolonged exposure of rats to high concentrations of kaolinite (300 mg m-3) was lethal. Davis (1993) suggested that differences in the kaolin dust dosages used in the experimental inhalation studies may be responsible for the different results.

Kaolinite-bearing dusts have been shown to be cytotoxic to most cell types in several *in vitro* experiments. The capacity of kaolin dusts to damage cells may exhibit significant variation between samples, because of variations in mineralogical characteristics between deposits and the presence of other minerals in varying quantities, particularly silica (Carretero et al., 2006).

4.2 Illite and Smectites

There have only been a few epidemiological studies of respiratory disease resulting from exposure to illite and smectite containing dusts. The results of some of these studies indicated that these dusts may elicit a mild fibrogenic response at high exposure levels (Carretero et al., 2006). The results, however, are complicated because of the presence of other minerals such as silica and amphiboles in the dust. For example, the silica content (including quartz and cristobalite) of Wyoming bentonite, which is composed primarily of smectites, ranges from 0 to 24% (Ross et al., 1993).

In vivo studies indicate that dusts containing illite and smectite are slightly fibrogenic, and *in vitro* studies suggest that they may be slightly cytotoxic (Guthrie, 1992). The variability in cytotoxicity is apparently due to SiO2 polymorphs (i.e., quartx, cristobalite, tridymite). However, a 1980 study by Daniel and Le Bouffant concluded that most smectite containing dusts were very cytotoxic *in vitro* (Carretero et al., 2006).

Oscarson et al. (1986) studied lysis of red blood cells in bovine by several silicate minerals. These investigators reported that the hemolytic activity of these minerals decreased in the following order smectites > silica > palygorskite > sepiolite > chrysotile (asbestos) > kaolinite.

More recently, Kibanova et al. (2009) studied the ability of three smectites to induce oxidative stress, a primary indicator of cell damage and toxicity. Minerals can cause cell damage because of free radicals. The cell damage is often determined as the progress of lipid peroxidation, the oxidative degradation of lipids in cell membranes. These investigators concluded that smectites can induce oxidative stress via lipid peroxidation, and that the high concentrations of structural iron (Fe) impacts the ability of the minerals to induce this reaction. However, Kibanova et al. (2009) also indicated that there is still a lack of understanding regarding how smectites and other minerals impact processes such as proton exchange, metal complexation, and electron transfer in the body.

4.3 Palygorskite

Palygorskite (sometimes referred to as attapulgite) and its potential effects on human health have been studied fairly extensively, because of its fibrous morphology and use as a substitute for asbestos. The International Agency for Research on Cancer has concluded that palygorskite fibers greater than 5 microns in length are possibly carcinogenic to humans (CIR, 2003). Other studies indicate that the health risks from palygorskite are variable and depend primarily on the fiber length and diameter, and other physiochemical parameters which are controlled by the geological conditions in which it formed (Nolan et al. 1991; Galan, 1996; Carretero et al., 2006). Nolan et al. (1991) studied nine palygorskite specimens obtained from different geological locales that exhibited a range of surface characteristics and found a corresponding range in hemolytic activity. They concluded that experimental data may exhibit variable carcinogeneity for palygorskite depending on its geological origin. These investigators stated that mineral morphology is insufficient to determine a mineral's carcinogenic properties, and that fiber size distribution, surface adsorption characteristics, and stability *in vivo* must be considered when determining whether specific palygorskites will present an inhalation health hazard.

In vivo studies of palygorskite have shown that most palygorskite-containing dusts are mildly active in the lung, although some samples can be quite active (Guthrie, 1992). *In vitro* experiments have suggested that palygorskite is as hemolytic as chrysotile asbestos, but in other non-erythrocite cell types it is non-genotoxic, and only slightly cytotoxic (Carretero et al. 2006). Oscarson et al. (1986) studied the lysis of erythrocites by palygorskite and concluded that palygorskite was a lysing agent.

Wagner et al. (1987) performed intrapleural tests with sepiolite and palygorskite in rats, and found no increased incidence of tumors. These minerals produced an interstitial reaction similar to that caused from nuisance dust but did not produce fibrosis. However, these investigators reported mesothelioma in rats that had inhaled sepiolite and palygorskite dusts that contained a significant number of fibers more than 5 to 6 μm in length. Similarly, Davis (1993) suggested that fibers greater than 5 μm were harmful, whereas materials consisting primarily of short fibers were not.

Lemaire (1991) and Lemaire et al. (1989) studied the reactivity of rat lungs to palygorskite, chrysotile, xonotlite, and some man-made fibrous silicates. The palygorskite used was less than 1 µm in length. Lemaire (1991) found that single intratracheal administration of palygorskite in rates produced granulomas and multinucleated giant macrophages and enhanced IL-1-like activity. Lemaire et al., (1989) found that palygorskite induces some of the histologic and cellular features of asbestos-induced fibrosis. However, they cautioned that their results could not be extrapolated to human exposure conditions.

In desert environments such as NDRA, palygorskite most commonly forms as a pedogenic mineral in petrocalcic horizons, which are colloquially termed 'caliche' (Watts, 1980; Monger and Daugherty, 1991; Brock, 2007; Robins, 2010; Brock and Buck, 2009). It also commonly occurs in less well-developed soils containing calcic pendants (Brock and Buck, 2005; Singer et al., 1995). In arid climates, palygorskite can also precipitate in highly alkaline lake environments, some hydrothermal systems, and from alkaline groundwaters (Callen, 1984; Singer, 1989).

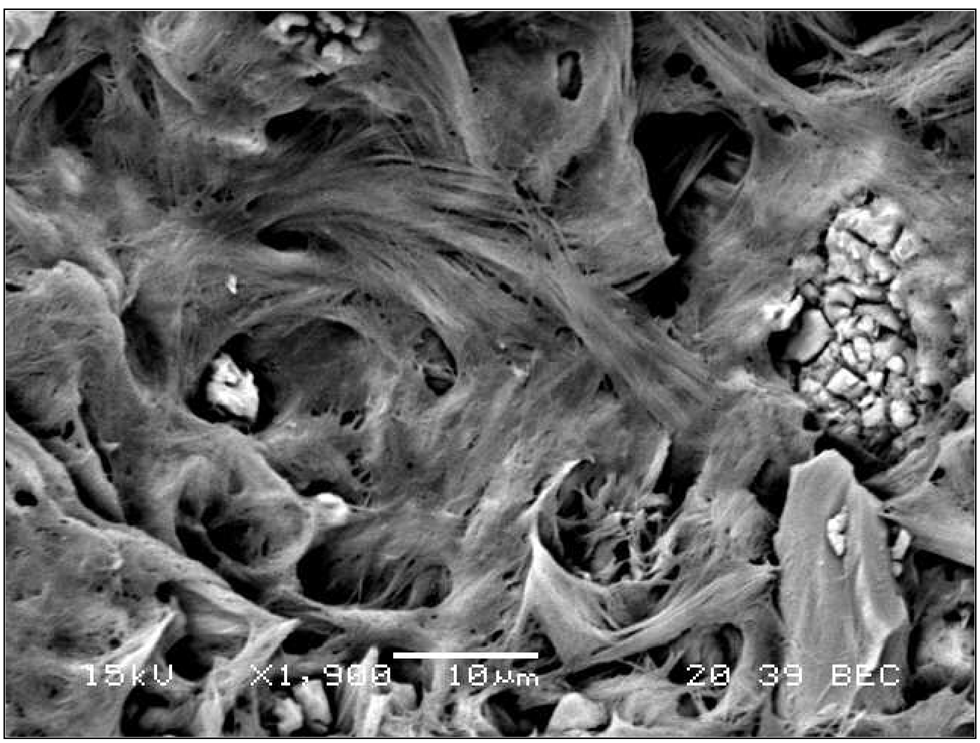

Fig. 2: SEM image of asbestiform palygorskite from Mormon Mesa, NV (from Brock, 2007).

SEM analyses of pedogenic palygorskite from areas near NDRA, show that it has an asbestiform habit, with crystals that often exceed 8 µm in length (Fig. 2) (Brock and Buck, 2005; Brock, 2007; Robins, 2010; and Buck, unpublished data). Because the geological and pedological conditions at NDRA are similar to those studied by Brock and

Buck (2005, 2009), Brock (2007) and Robins (2010), this suggests that the palygorskite at NDRA may pose a potential health risk if inhaled. However, determining the morphology and length of the palygorskite at NDRA was beyond the scope of this study. Future research, should characterize the palygorskite present in dusts at NDRA, including its concentration in air, the length to width ratio, and how these characteristics vary across the different map units.

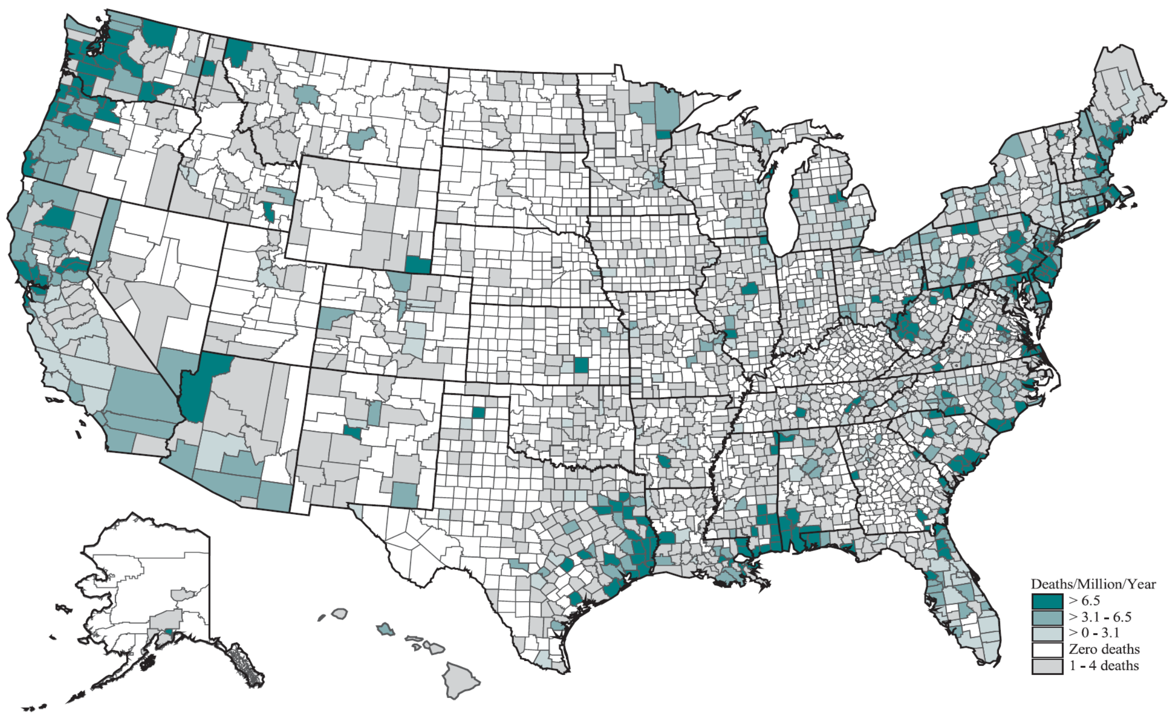

Fig. 3. Epidemiological map of national age-adjusted rates of asbestosis-related mortality by county for U.S. residents age 15+, 1970-1999. (From NIOSH WoRLD, 2006).

An epidemiological map showing age-adjusted rates of asbestosis-related mortality indicates that Clark County has one of the higher national rates (NIOSH WoRLD, 2006; see Fig. 3). There are no known asbestos mines or mineral resources in Clark County (Van Gosen, 2008), which suggests that our high rates of asbestosis-related mortalities may occur from (1) occupational exposures, (2) human exposures prior to people moving here, and/or (3) exposures to non-regulated asbestiform minerals that cause health effects similar to those by regulated asbestos minerals (i.e. Rom et al., 1983). Much more extensive research is needed to determine whether palygorskite plays a role in pulmonary disease in this region.

5. Summary of conclusions

Several minerals including quartz, kaolinite, illite, smectite, and palygorskite are present at NDRA, and are known to have adverse effects on human health when inhaled in large amounts or over a long time period. These minerals can result in different pathologies in the lung including cancer, mesothelioma, or pneumoconiosis. Of special concern at NDRA is the common occurrence of palygorskite, especially in the finest fractions. Because palygorskite is an asbestiform mineral, it has the potential to have health effects similar to the regulated asbestos minerals that are known to cause severe health problems. Future research is needed to determine the morphology of the palygorskite crystals (i.e. length:width ratios), and their airborne concentrations across the many different surface types at NDRA. This information needs to be combined with an assessment of the human exposure to palygorskite at NDRA during different activities (ORV and bystander), on different surface types, and under different wind conditions. Additionally, information concerning the toxicity of dust with mixed mineralogy such as that in the Nellis Dunes is not available. Future research to measure the toxicity of NDRA dust would require the use of animal models, human exposure, and/or epidemiology studies.

References

Addison, J., McConnell, E., 2008. A review of carcinogenicity studies of asbestos and non-asbestos tremolite and other amphiboles. Regulatory Toxicology and Pharmacology, 52:S187-S199.

Agency for Toxic Substances and Disease Registry, 2003. Report on the Expert Panel on Heath Effects of Asbestos and Synthetic Vitreous Fibers: The Influence of Fiber Length, AB24-COMM-110-3.

Brock, A.L., 2007. Characterization of stage VI petrocalcic horizons: S. Nevada and N.W. Arizona. Ph.D. Dissertation, University of Nevada Las Vegas, Department of Geoscience, 148 pp.

Brock, A.L., Buck, B.J., 2009. Polygenetic development of the Mormon Mesa, NV petrocalcic horizons: Geomorphic and paleoenvironmental interpretations. Catena 77, 65-75.

Brock, A.L., Buck, B.J., 2005. A new formation process for calcic pendants from Pahranagat Valley, Nevada: Implication for dating Quaternary landforms. Quaternary Research 63, 359-367.

Callen, 1984. Clays of the palygorskite-sepiolite group: Depositional environment, age and distribution. In: Singer, A., Galan, E. (eds). Palygorskite-Sepiolite: Occurrences, genesis, and uses. Developments in Sedimentology 37. New York, Elsevier, pp. 1-37.

Carretero, M.T., Gomex, C.S.F., Tateo, F., 2006. Clays and human health. In: Bergaya, F., Theng, B.K.G., Lagaly, G. (eds.). Handbook of Clay Science. Elsevier, Amsterdam, pp. 717-741.

Cosmetic Ingredient Review Expert Panel, 2003. Final report on the safety assessment of aluminum silicate, calcium silicate, magnesium aluminum silicate, magnesium silicate, magnesium trisilicate, sodium magnesium silicate, zirconium silicate, attapulgite, bentonite, fuller's earth, hectorite, kaolin, lithium magnesium silicate, lithium magnesium sodium silicate, montmorillonite, pyrophyllite, and zeolite. International Journal of Toxicology 22, 37-102

Davis, J.M.G., 1993. *In vivo* assays to evaluate the pathogenic effects of minerals in rodents. In: Guthrie, G.D., Mossman, B.T. (eds.). Health Effects of Mineral Dusts. Reviews in Mineralogy. Mineralogical Society of America, Washington, DC, 28, 471-487.

Duncan, K., Ghil, A., Dailey, L., Bern, A., Gibbs-Flournoy, E., Padilla-Carlin, D., Roggli, V., Devlin, R., 2010. Effect of size fractionation on the toxicity of amosite and Libby amphibole asbestos. Toxicological Sciences 118, 420-434.

Duzgoren-Aydin, N.S., 2008. Health effects of atmospheric particulates: A medical geology perspective. Journal of Environmental Science and Health Part C 26, 1-39.

Galan, E., 1996. Properties and applications of palygorskite-sepiolite clays. Clay Minerals 31, 443-453.

Groppo, C., Tomatis, M., Turci, F., Gazzano, E., Ghigo, D., Compagnoni, R., Fubini, B., 2005. Potential toxicity of nonregulated asbestiform minerals: balangeroite from the western Alps. Part 1: Identification and characterization. Journal of Toxicology and Environmental Health Part A, 68,1-19.

Guthrie, G.D., 1992. Biological effects of inhaled minerals. American Mineralogist 77, 225-243.

Guthrie, G.D., 1997. Mineral properties and their contributions to particle toxicity. Environmental Health Perspectives Supplements 105, 1003-1021.

Harper, M., 2008. 10th anniversary Critical Review: Naturally occurring asbestos. Journal of Environmental Monitoring 10, 1394-1408.

Hochella, M., 1993. Surface chemistry, structure, and reactivity of hazardous mineral dust. In: Guthrie, G.D., Mossman, B.T. (eds.). Health Effects of Mineral Dusts. Reviews in Mineralogy. Mineralogical Society of America, Washington, DC, 28:275-308.

Kibanova, D., Nieto-Camacho, A., Cervini-Silva, J., 2009. Lipid peroxidation induced by expandable clay minerals. Environmental Science and Technology 43, 7550-7555.

Klein, C., 1993. Rocks, minerals and a dusty world. In: Guthrie, G.D., Mossman, B.T. (eds.). Health Effects of Mineral Dusts. Reviews in Mineralogy. Mineralogical Society of America, Washington, DC, 28:7-59.

Lee, R., Strohmeier, B., Bunker, K., Van Orden, D., 2008. Naturally occurring asbestos – a recurring public policy challenge. Journal of Hazardous Materials 153,1-21.

Lehnert, B.E., 1993. Defense mechanisms against inhaled particles and associated particle-cell interactions. In: Guthrie, G.D., Mossman, B.T. (eds.). Health Effects of

Mineral Dusts. Reviews in Mineralogy. Mineralogical Society of America, Washington, DC, 28, 427-469.
Lemaire, I., Dionne, P.G., Nadeau, D., Dunnigan, J., 1989. Rat lung reactivity to natural and man-made fibrous silicates following short-term exposure. Environmental Research 48, 193-210.
Monger, H.C., Daugherty, L.A.., 1991. Neoformation of palygorskite in a southern New Mexico aridisol. Soil Science Society of America Journal 55, 1646-1650.
Nettesheim, P., Griesemer, R.A., 1978. Experimental models for studies of respiratory tract carcinogenesis. In: Harris, C.C. (ed). Pathogenesis and Therapy of Lung Cancer. Dekker, New York, pp. 75-188.
NIOSH WoRLD, 2006. Work-related lung disease (WoRLD) surveillance system. http://www2a.cdc.gov/drds/WorldReportData/FigureTableDetails.asp?FigureTableID=12
Nolan, R.P., Langer, A.M., 1993. Limitations of the Stanton hypothesis. In: Guthrie, G.D., Mossman, B.T. (eds.). Health Effects of Mineral Dusts. Reviews in Mineralogy. Mineralogical Society of America, Washington, DC, 28, 309-326.
Nolan, R.P., Langer, A.M., Herson, G.B., 1991. Characterisation of palygorskite specimens from different geological locales for health hazard evaluation. British Journal of Industrial Medicine 48, 463-475.
Omenn, G., Merchant, J., Boatman, E., Dement, J., Kuschner, M. Nicholoson, W., Peto, J., Rosenstock, L., 1986. Contribution of environmental fibers to respiratory cancer. Environmental Health Perspectives 70,51-56.
Oscarson, D.W., Van Scoyoc, G.E., Ahlrichs, J.L., 1986. Lysis of erythrocytes by silicate minerals. Clays and Clay Minerals 34, 74-80.
Plumlee, G., Morman, S., Ziegler, T., 2006. The toxicological geochemistry of earth materials: an overview of processes and the interdisciplinary methods used to understand them. Reviews in Mineralogy and Geochemistry 64, 5-57.
Pott, F., 1989. Carcinogenicity of fibers in experimental animals. Data and evaluation. In: Bates, D.V., Dungworth, D.L., Lee, P.N., McClellan, R.O., Roe, F.J.C. (eds.). Assessment of Inhalation Hazards. Springer, Berlin, pp. 243-253.
Robins, C.R., 2010. Phyllosilicate mineralogy, $^{40}Ar/^{39}Ar$ geochronology, and genesis of petrocalcic soils in the southwest U.S.A. Ph.D. dissertation, UNLV Department of Geoscience, Las Vegas, NV, 174 pp.
Rödelsperger, K., Brückel, B., Manke, J., Woitowitz, H-J., Pott, F., 1987. Potential health risks from the use of fibrous mineral absorption granulates. British Journal of Industrial Medicine 44, 337-343.
Rom, W., Casey, K., Parry, W., Mjaatvedt, C., Moatamed, F., 1983. Health implications of natural fibrous zeolites for the Intermountain West. Environmental Research 30, 1-8.
Ross, M., Nolan, R.P., Langer, A.M., Cooper, W.C., 1993. Health effects of mineral dusts other than asbestos. In: Guthrie, G.D., Mossman, B.T. (eds.). Health Effects of Mineral Dusts. Reviews in Mineralogy. Mineralogical Society of America, Washington, DC, 28, 361-409.

Singer, A., 1989. Palygorskite and sepiolite group minerals. In: Dixon, J.B., Weed, S.B. (eds). Minerals in Soil Environments (Second Edition). SSSA Book Series. Madison, Soil Science Society of America, pp. 829-872.

Singer, A., Kirsten, W., Bühman, C., 1995. Fibrous clay minerals in the soils of Namaqualand, South Africa: Characteristics and formation. Geoderma 66, 43-70.

Soukup, D.A., Buck, B.J., Harris, W., 2008. Preparing soils for mineralogical analyses. In: Ulery, A.L., Drees, L.R. (eds.). Methods of Soil Analysis, Part 5 - Mineralogical Methods. Soil Science Society of America, Madison, pp. 13-31.

Reid-Soukup, D.A., Ulery, A.L., 2002. Smectites. In: Dixon, J.B., Schulze, D.G. (eds.). Soil Mineralogy with Environmental Applications. Soil Science Society of America, Madison, pp.467-499.

Stanton, M.F., Layard, M., Tegeris, A., Miller, E., May, M., Morgan, E., Smith, A. 1981. Relation of particle dimension to carcinogenicity of amphibole asbestoses and other fibrous minerals. Journal of the National Cancer Institute 67, 965-975.

Theisen, A.A., Harward, M.E., 1962. A paste method for preparation of slides for clay mineral identification by x-ray diffraction. Soil Science Society of America Proceedings 26, 90-91.

Turci, F., Tomatis, M., Gazzano, E., Riganti, C., Martra, G., Bosia, A., Ghigo, D., Fubini, B., 2005. Potential toxicity of nonregulated asbestiform minerals: balangeroite from the western Alps. Part 2: Oxidant activity of the fibers. Journal of Toxicology and Environmental Health Part A, 68, 21-39.

Van Gosen, B., 2008. Reported historic asbestos mines, historic asbestos prospects, and natural asbestos occurrences in the southwestern United States (Arizona, Nevada, and Utah), USGS Open-File Report 2008-1095.

van Oss, C.J., Naim, J.O., Costanzo, P.M., Giese R.F. Jr., Wu, W., Sorling, A.F., 1999. Impact of different asbestos species and other miner particles on pulmonary pathogenesis. Clays and Clay Minerals 47, 697-707.

Wagner, J.C., Griffiths, D.M., Munday, D.E., 1987. Experimental studies with palygorskite dusts. British Journal of Industrial Medicine 44, 749-763.

Wastiaux, A., Daniel, H., 1990. Pulmonary toxicity of kaolin in rats exposed by inhalation. In: Bignon, J. (ed.). Health Related Effects of Phyllosilicates, NATO ASI Series, Springer, Berlin, G21.

Watt, A., 1982. Barnes & Noble Thesaurus of Geology. Harper & Row, New York, 44 pp.

Watts, N.L., 1980. Quaternary pedogenic calcretes from the Kalahari (southern Africa): mineralogy, genesis and diagenesis. Sedimentology 27, 661-686.

Wylie, A., Verkouteren, J., 2000. Amphibole asbestos from Libby, Montana: aspects of nomenclature. American Mineralogist 85, 1540-1542.

Chapter 9

TRACE ELEMENT CHEMISTRY OF SOIL AND DUST SAMPLES IN THE NELLIS DUNES RECREATION AREA

Deborah Soukup[1], Brenda Buck[1], Dirk Goossens[1], Yuanxin Teng[1] and Dirk Baron[2]

[1]Department of Geoscience, University of Nevada Las Vegas
[2]Department of Physics and Geology, California State University

1. Introduction

Many naturally occurring chemical elements are potentially hazardous to health when inhaled. In particular, the elements arsenic, lead, cadmium and mercury are known to cause multiple adverse health effects (Jarup, 2003; Plumlee et al., 2006). Naturally occurring mineral dusts such as those at NDRA, are composed of a mixture of minerals, sorbed chemical elements, and biological substances, each with differing biosolubility and bioreactivity (Plumlee et al., 2006). There is limited information about the effects from exposure to two or more substances and thus, it is not known whether their ultimate effects are synergistic (enhanced) or antagonistic (reduced). In instances where one or more hazardous elements are found, site-specific health risk assessments are necessary to evaluate the biological effects from inhalation of these complex mixtures of substances.

Because both ORV activity and natural wind conditions at NDRA were found to emit substantial amounts of dust, we wanted to determine the concentrations of trace elements in dust and whether these concentrations might pose a potential threat to ORV operators or other visitors at the site. To do this, we initially scanned soil samples for 66 different elements using inductively coupled plasma mass spectroscopy (ICP-MS). Based on those initial results we narrowed our focus to 18 elements, and analyzed several different grain size fractions of soils and airborne samples that were derived from specific map units at NDRA.

2. Materials and methods

2.1 Field procedures

Soil samples were collected from the upper 2-3 cm of the 17 different surface types in the Nellis Dunes area and from five unpaved areas used for parking. Dust samples were also collected from 16 of the 17 surface types and from five unpaved parking areas using a Portable In Situ Wind Erosion Laboratory (PI-SWERL). This instrument creates an increased wind shear near the ground producing wind erosion under controlled conditions, and allows collection of the emitted particles. A detailed description of the instrument can be found in Chapter 4 of this report. PI-SWERL samples were collected both on ORV trails and on undisturbed terrain. No samples were collected from areas of outcropping bedrock or outcropping petrocalcic horizons, which contain negligible emittable dust.

Fig. 1 shows the sampling locations. Note that the scale of the map does not allow a clear distinction between the PI-SWERL sampling spots on the trails and the corresponding spots on undisturbed terrain. Therefore, the number of sampling locations is substantially greater than the number shown on the map.

2.2 Laboratory procedures

The soil samples collected from each of the surface units were air dried and sieved to remove coarse fragments (>2 mm). The <2 mm fraction was then acid digested in accordance with EPA Method 3052 (USEPA, 1996). Following digestion, the soil samples were initially scanned for 66 different elements using inductively coupled plasma mass spectroscopy (ICP-MS). The purpose of the initial semi-quantitative scan was to identify potential elements of environmental concern in the samples. Based on the results of the semi-quantitative scan, the following elements were identified as elements of potential concern: arsenic (As), cobalt (Co), chromium (Cr), cesium (Cs), copper (Cu), cadmium (Cd), silver (Ag), nickel (Ni), lead (Pb), strontium (Sr), uranium (U), vanadium (V), thallium (Tl), boron (B), molybdenum (Mo), antimony (Sb), and mercury (Hg). The soil and unpaved parking area samples were then re-analyzed quantitatively for these elements using ICP-MS. The arsenic results are addressed in Chapter 10 in this report and are not discussed further in the current chapter.

Analyses for the elements of potential environmental concern were also made on dust samples collected using the PI-SWERL. These samples were dry sieved to 60 μm. The 60 μm limit was used as a cut-off for total suspendable particles (TSP), because it represents

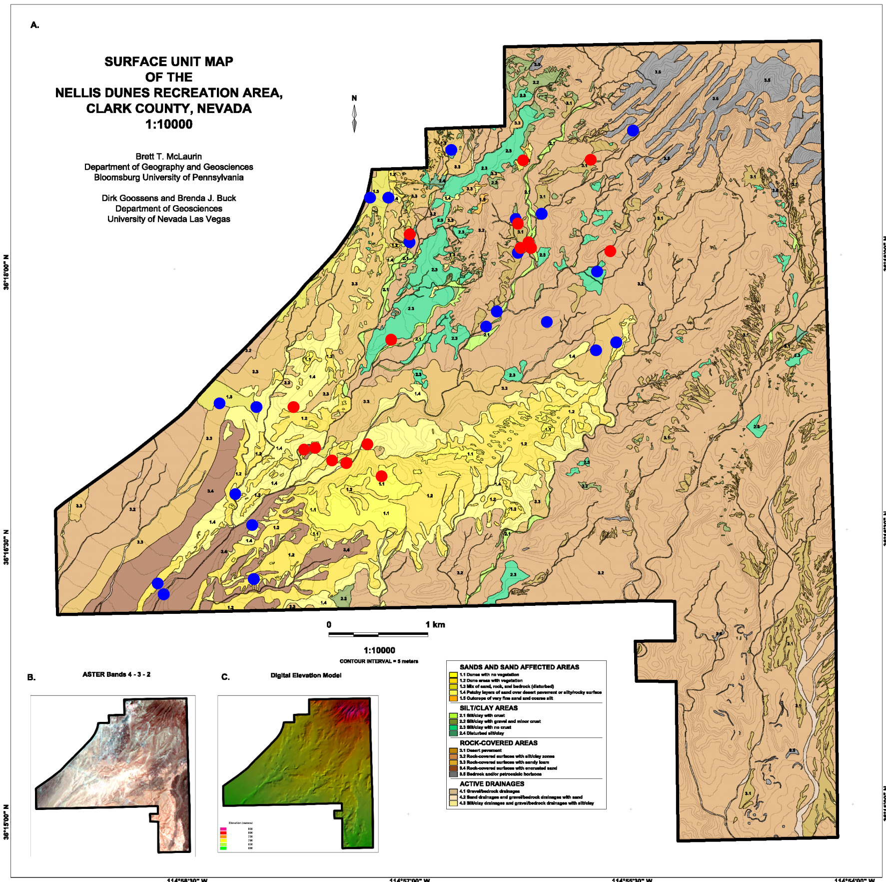

Fig. 1: Location of the sampling sites. More than one sample may have been taken from the locations indicated on the map (see text for details). Blue: soil samples; red: PI-SWERL samples.

the maximum size of grains that will still be transported in short-term suspension during average wind speed and turbulence (Pye and Tsoar, 1990). It also nearly coincides with the maximum diameter of silt (52 µm or 63 µm, depending on which criterion is used; Goossens and Buck, 2009). Coarser particles are unlikely to be transported very far or inhaled and therefore were excluded from this study.

To determine the water soluble constituents in the PI-SWERL samples, 1:10 soil:water extracts were prepared on the 0-60 µm size fraction. Finer size fractions could not be separated without the use of water, which would result in the loss of information regarding the concentrations of the water soluble components. The 1:10 extracts were used instead of a saturated paste because of limited sample sizes. These samples were allowed to sit overnight and were then filtered to obtain the supernatant. The supernatant solution was also analyzed by ICP-MS using similar instrument settings and quality control measures.

The remaining sample was then separated into <10 μm (PM10) and 10-60 μm size fractions by sedimentation and wet sieving and acid-digested in accordance with EPA Method 3052 prior to analysis.

3. Results

3.1 Soil and PI-SWERL samples

The concentrations of Cu, Cd, Ag, Ni, Pb, U, V, B, and Mo were typically lower, sometimes by as much as one order of magnitude, in the soil samples as compared to the PI-SWERL samples (Tables 1 and 2). These results are expected because of the larger particle size (<2 mm) of the soil samples as compared to the PI-SWERL samples (<10 μm and 10-60 μm). The x-ray diffraction (XRD) results (see Chapter 8) demonstrated that the finer fractions of the samples are dominated by smectite minerals, which are known to be major contributors to soil cation exchange capacity (CEC) and therefore, affect the retention of metals in the soil (Reid-Soukup and Ulery, 2002). The amount of smectite in the soil samples is “diluted” relative to that in the PI-SWERL samples, because smectite is only present in the finest portions of these samples.

The concentrations of Co, Cr, Cs, Tl, Sb, Sr, and Hg in the soil samples were generally similar to those in the PI-SWERL samples (Tables 1 and 2).

In general, the lowest elemental concentrations in the soil samples occurred in the sand areas, particularly in unit 1.2 (dunes with vegetation). These results are expected because the sand areas have the lowest proportion of clay and silt, and are thus less likely to have smectite or other highly chemically reactive minerals that will retain metals. The lowest reported concentrations of Pb, Sr, Mo, Sb, and Tl occurred in samples from the parking lots. The highest concentrations of most elements, as expected, occurred in samples from silt/clay areas, particularly in units 2.2 (silt/clay with gravel) and 2.3 (aggregated silt).

In contrast, the lowest elemental concentrations in the PI-SWERL samples occurred in various units, and not within the sand areas. This may be caused by variations in clay mineral composition as well as other minor mineralogical differences between samples. XRD analyses showed that the mineralogical composition of the clay (<2 μm) and silt (2-20 μm) fractions of the samples is relatively uniform, and dominated by smectite minerals. The highest elemental concentrations are primarily in unit 1.5, which consists of outcrops of very fine sand and coarse silt. The results of the XRD analyses showed that the <2 μm and 2 to 20 μm fractions of this sample are dominated by highly crystalline smectite. Therefore, combining the trace element results with the XRD results suggests that unit 1.5 smectite may have a lower layer charge than most of the other smectites present in the Nellis Dunes area. Smectites with lower layer charge have a greater shrink-swell capacity than smectites with higher layer charge resulting in greater amounts of water, hydrated metal cations and organic molecules being attracted to the interlayer region (Reid-Soukup and Ulery, 2002).

3.2 Soluble PI-SWERL extracts

The pH values of the soluble PI-SWERL extracts are near-neutral to alkaline, ranging from 6.58 to 9.11 (Table 3). Electrical conductivity (EC) values of the extracts range from 0.06 to 2.43 dS m^{-1} and document the salinity of most of the soils in the NDRA,

Table 1: Soil sample chemistry

Surface Unit	Trace Elements								Trace Elements							
	Co	Cr	Cs	Cu	Cd	Ag	Ni	Pb	Sr	U	V	Tl	B	Mo	Sb	Hg
	µg g^{-1}								µg g^{-1}							
	United States Environmental Protection Agency Regional Screening Levels[1]								United States Environmental Protection Agency Regional Screening Levels[1]							
Residential Soil	23	NP	NP	3,100	70	390	1,500	400	47,000	230	390	NP	16,000	390	31	5.6
Groundwater Protection	0.49	NP	NP	51	1.4	1.6	48	NP	770	49	180	NP	23	3.7	0.66	0.03
Unit 1: Sand Areas																
1.1	7.58	9.28	1.31	3.39	0.13	0.34	3.95	13.99	169.92	1.19	8.75	0.335	0.97	1.16	1.10	0.015
1.2	5.68	7.23	1.19	4.69	0.12	0.32	3.91	16.95	150.19	1.19	7.28	0.292	0.34	1.09	0.93	0.019
1.3	9.29	13.83	1.88	5.86	0.18	0.62	6.71	14.88	236.09	1.78	21.36	0.308	2.49	1.41	1.11	0.049
1.4	9.65	16.99	1.47	5.22	0.14	0.49	6.44	18.03	213.20	1.32	17.24	0.314	5.28	1.20	1.15	0.018
1.5	7.17	14.09	3.90	4.92	0.10	0.59	5.67	18.13	310.62	4.60	25.26	0.545	6.29	4.39	1.15	0.026
Unit 2: Silt/clay Areas																
2.1	10.35	20.18	1.83	8.06	0.18	0.78	8.96	26.66	277.08	3.01	32.86	0.50	8.05	1.87	1.35	0.032
2.2	7.02	9.11	6.34	5.63	0.09	0.25	6.00	13.53	199.55	7.44	38.97	1.05	6.53	8.01	1.15	0.036
2.3	13.93	43.50	0.54	22.23	0.50	0.90	20.98	29.69	206.45	4.81	90.71	0.80	34.78	2.42	1.76	0.038
2.4	8.60	16.06	3.15	6.65	0.15	0.52	6.94	19.63	205.57	2.17	26.11	0.43	5.60	1.49	1.20	0.023
Unit 3: Rock-covered Areas																
3.1	10.45	24.97	0.95	11.79	0.28	0.58	12.38	23.94	205.90	2.96	38.18	0.51	11.29	2.19	1.58	0.029
3.2	11.78	24.45	0.65	12.59	0.25	0.41	12.38	28.27	239.25	2.33	38.32	0.40	11.74	1.62	1.57	0.033
3.3	12.87	24.03	0.64	13.46	0.26	0.34	12.59	25.36	209.35	1.88	33.57	0.38	11.58	1.72	0.90	0.051
3.4	8.61	20.69	2.19	6.95	0.20	0.60	8.24	21.62	188.01	2.15	29.69	0.39	6.20	1.64	1.24	0.028
3.5	12.66	34.71	0.21	15.97	0.41	0.61	17.42	27.97	210.73	2.93	51.72	0.46	15.83	1.91	1.82	0.036
Unit 4: Drainage Areas																
4.1	13.98	19.73	2.96	11.21	0.32	0.62	10.70	26.70	630.01	3.60	38.70	0.70	9.23	4.56	1.70	0.036
4.2	8.08	10.53	3.48	7.50	0.24	0.26	6.72	20.58	132.04	3.07	19.04	0.54	4.00	3.16	1.31	0.039
4.3	16.14	22.11	1.62	9.39	0.69	0.72	12.38	18.23	821.05	3.46	40.75	0.59	10.15	4.47	1.50	0.031
Unpaved Parking Areas																
NA[2]	9.77	15.80	1.56	8.42	0.26	0.28	7.46	10.90	109.45	1.39	21.87	0.27	4.85	1.00	0.54	0.019
NA	9.97	16.39	1.47	7.30	0.29	0.35	8.17	12.15	120.01	1.59	20.86	0.26	4.26	1.18	0.53	0.026
NA	11.48	18.07	1.36	459.0	0.20	0.33	7.58	77.38	149.97	1.54	23.73	0.26	4.44	1.25	0.66	0.016
NA	12.13	14.20	1.99	7.36	0.23	0.25	7.11	21.44	128.79	2.12	22.70	0.50	5.02	2.53	0.83	0.020
Buffalo River Standard																
NA	16.9	118.7	0.8	70.1	2.9	1.4	36.0	245.0	144.7	3.2	81.4	1.0	45.2	4.8	4.3	0.6
	13-14	118-126	5.7-5.9	NP[3]	2.6-3.2	NP	39-47	133-167	NP	3.0-3.2	91-99	NP	NP	NP	2.8-3.4	NP
Bradford et al. 1996[4]																
	3-47	23-1579	1-9	9-96	0.1-1.7	0.1-8.3	9-509	12-97	20-271	1-21	39-288	0.2-1.1	1-74	0.1-9.6	0.2-2.0	0.1-0.9
	14.9	122	3.1	28.7	0.36	0.8	57	23.9	128	4.7	112	0.56	19	1.3	0.6	0.26
Shacklette & Boerngen, 1984[4]																
	<3-50	36586	NP	2-300	NP	NP	<5-700	<10-700		1-8	7-500	NP	<20-300	<3-7	NP	<0.01-4.6
	7.1	41	NP	21	NP	NP	15	17	200	2.5	70	NP	23	0.85	NP	0.046

NOTES:

1. The Screening Levels (SLs) are developed using risk assessment guidance from the EPA Superfund program and are used for site "screening" and as initial cleanup goals, if applicable. The groundwater protection concentrations shown are soil concentrations considered to be protective of groundwater resources.
2. NA = Not applicable
3. NP = Not provided.
4. Reported concentrations of trace elements in soil samples in these publications.

Table 2: Trace element concentrations in PI-SWERL samples

Surface Unit Sample	Particle Size (µm)	Co	Cr	Cs	Cu	Cd	Ag	Ni	Pb	Sr	U	V	Tl	B	Mo	Sb	Hg
			$\mu g\ g^{-1}$													$\mu g\ g^{-1}$	
							United States Environmental Protection Agency Regional Screening Levels(1)										
Residential Soil		23	NP	NP	3,100	70	390	1,500	400	47,000	230	390	NP	16,000	390	31	5.6
Groundwater Protection		0.49	NP	NP	51	1.4	1.6	48	NP	770	49	180	NP	23	3.7	0.66	0.03
Unit 1: Sand Areas																	
1.1R	<10	12.35	24.93	1.32	45.48	0.67	0.33	25.53	27.36	153.56	3.52	83.83	0.59	95.84	3.37	1.64	0.056
	10 to 60	9.54	23.65	2.15	24.78	0.45	0.29	17.47	21.26	162.62	3.49	55.80	0.50	41.72	3.92	1.36	0.140
1.1NR	<10	12.02	21.92	1.73	46.49	0.71	0.34	25.58	24.62	156.40	2.93	77.13	0.54	91.19	3.14	1.51	0.097
	10 to 60	8.52	21.50	1.72	43.77	0.41	0.27	15.31	16.54	121.86	3.10	49.45	0.48	30.09	3.16	1.06	0.102
1.2R	<10	12.07	34.14	1.39	29.71	0.46	4.73	25.60	19.78	159.84	3.80	100.48	0.54	93.01	2.05	1.17	0.044
	10 to 60	10.90	25.80	1.99	26.62	0.37	0.24	18.84	18.35	159.65	4.47	66.20	0.57	44.39	4.29	1.23	0.081
1.2NR	<10	11.79	40.83	3.16	36.22	0.63	1.54	27.30	21.12	100.24	3.11	101.43	0.53	109.29	2.19	1.24	0.046
	10 to 60	10.47	25.90	2.00	21.61	0.37	0.51	18.52	21.13	183.93	3.70	67.87	0.55	49.16	2.56	1.12	0.076
1.3R	<10	11.85	23.33	1.81	32.86	0.55	0.50	24.20	31.34	128.82	3.11	80.41	0.70	94.71	4.54	1.79	0.066
	10 to 60	11.04	23.89	1.90	28.83	0.90	0.28	18.74	30.93	99.62	3.92	61.40	0.73	46.34	4.79	1.57	0.070
1.3NR	<10	9.31	14.23	1.30	28.50	0.48	0.24	19.20	33.08	102.13	2.28	62.48	0.49	72.01	2.63	1.64	0.045
	10 to 60	9.26	23.59	1.67	28.96	0.42	0.23	18.93	27.79	123.12	2.86	55.36	0.54	41.30	2.97	1.52	0.062
1.4R	<10	10.12	20.68	1.41	39.30	0.77	0.22	22.77	32.36	110.93	2.25	67.20	0.44	75.79	2.28	1.68	0.046
	10 to 60	9.92	32.65	1.30	39.38	0.54	0.41	19.56	30.62	160.33	3.11	66.98	0.45	41.79	2.47	1.36	0.061
1.4NR	<10	12.98	26.84	1.94	40.88	0.78	0.36	26.83	28.46	128.92	2.55	80.68	0.52	76.88	4.26	1.46	0.069
	10 to 60	10.42	37.17	1.15	32.06	0.52	0.32	22.02	23.04	187.60	3.52	78.51	0.48	45.80	2.35	1.53	0.056
1.5R	<10	13.41	29.97	4.32	28.55	0.60	0.57	30.36	19.16	148.19	9.64	125.82	0.85	99.97	39.87	2.30	0.039
	10 to 60	15.40	30.55	2.15	21.59	0.69	0.31	26.39	18.69	144.06	10.36	76.08	0.99	67.09	42.17	2.73	0.078
1.5NR	<10	11.44	27.73	6.45	28.43	1.07	0.45	23.43	17.52	108.27	11.12	106.37	0.92	116.43	58.60	1.75	0.038
	10 to 60	14.44	32.19	5.38	26.71	1.41	0.63	23.43	20.68	193.07	15.03	88.47	1.20	91.81	74.77	1.82	0.051
Unit 2: Silt/clay Areas																	
2.1R	<10	10.14	24.79	2.41	27.15	0.49	0.32	22.14	19.25	161.73	3.29	83.98	0.80	62.71	12.11	1.30	0.034
	10 to 60	12.06	30.53	2.16	29.65	0.53	0.26	25.08	18.82	167.56	4.50	77.34	1.00	57.75	10.21	1.54	0.049
2.1NR	<10	10.88	25.41	2.13	35.27	0.58	0.53	24.94	19.16	141.14	3.37	91.66	0.87	90.62	9.92	1.43	0.043
	10 to 60	10.49	29.16	1.94	27.07	0.48	0.28	21.62	19.79	135.97	4.06	74.30	0.88	47.37	11.72	1.47	0.044
2.2R	<10	10.53	22.93	4.10	22.14	0.34	0.23	20.34	13.45	185.67	3.30	121.51	0.77	62.98	5.01	1.08	0.038
	10 to 60	12.33	33.22	2.59	24.89	0.32	0.38	22.58	17.81	167.40	3.92	115.24	0.96	57.10	5.22	1.28	0.048
2.2NR	<10	9.97	40.33	2.17	33.65	0.50	0.53	24.38	20.33	163.28	5.80	130.79	0.77	79.40	9.04	1.14	0.047
	10 to 60	10.71	33.54	1.85	29.59	0.52	0.30	22.26	22.49	249.34	6.09	105.57	0.82	61.72	8.20	1.44	0.052
2.3R	<10	11.06	34.36	4.41	30.06	0.57	0.54	25.04	15.43	106.85	3.24	108.04	0.69	90.11	1.62	0.93	0.020
	10 to 60	12.59	34.00	1.94	30.51	0.57	0.58	23.54	22.39	182.03	3.82	86.54	0.78	62.68	2.33	1.12	0.043
2.3NR	<10	11.90	40.44	2.42	36.30	0.68	0.61	27.07	18.24	171.22	3.95	115.59	0.73	87.37	2.08	1.17	0.033
	10 to 60	13.69	33.38	2.22	33.50	0.55	0.46	23.88	20.71	211.84	4.18	87.32	0.80	63.38	2.78	1.41	0.033
2.4R	<10	11.48	37.27	2.13	30.75	0.56	0.47	26.47	16.57	214.19	3.48	109.09	0.57	101.22	1.46	1.00	0.027
	10 to 60	11.00	29.05	1.57	26.56	0.48	0.37	23.08	18.33	215.23	3.48	88.04	0.54	71.59	1.70	1.08	0.035
2.4NR	<10	11.67	49.18	1.87	36.64	0.63	0.56	28.22	17.31	159.00	3.61	118.45	0.54	106.34	1.42	1.04	0.038
	10 to 60	11.65	37.83	1.36	29.33	0.50	0.68	25.05	18.67	210.61	4.16	100.95	0.62	87.75	1.85	1.17	0.037

NOTES:

1. The Screening Levels (SLs) are developed using risk assessment guidance from the EPA Superfund program and are used for site "screening" and as initial cleanup goals, if applicable. The groundwater protectionconcentrations shown are soil concentrations considered to be protective of groundwater.
2. NP = Not provided
3. Reported range of concentrations in wind-erodible Owens Lake playa crusts.
4. Reported range of concentrations in the <50 µm fractions of dust samples from the southwestern United States.
5. Concentrations shown are for one dust sample from the eastern Mojave Desert and one from southeastern Nevada. The concentrations are estimated from Figure 3 in the manuscript.

Table 2 (ctd.): Trace element concentrations in PI-SWERL samples

Surface Unit Sample	Particle Size (µm)	Co	Cr	Cs	Cu	Cd	Ag	Ni	Pb	Sr	U	V	Tl	B	Mo	Sb	Hg
		µg g^{-1}													µg g^{-1}		
		United States Environmental Protection Agency Regional Screening Levels(1)															
Residential Soil		23	NP	NP	3,100	70	390	1,500	400	47,000	230	390	NP	16,000	390	31	5.6
Groundwater Protection		0.49	NP	NP	51	1.4	1.6	48	NP	770	49	180	NP	23	3.7	0.66	0.03
Unit 3: Rock-covered Areas																	
3.1R	<10	11.81	42.70	1.86	31.29	0.38	0.43	29.49	14.14	140.42	2.19	77.39	0.52	66.71	2.96	1.25	0.026
	10 to 60	10.75	38.51	1.28	35.42	0.55	0.24	23.75	14.44	99.99	2.98	72.97	0.49	49.75	2.80	1.29	0.028
3.1NR	<10	10.44	37.77	1.65	27.68	0.34	0.38	26.08	12.50	124.19	1.93	68.45	0.46	59.00	2.62	1.11	0.023
	10 to 60	10.03	33.72	1.16	24.81	0.41	0.23	22.39	15.91	115.00	2.96	75.80	0.47	51.03	2.74	1.39	0.030
3.2R	<10	11.42	34.90	1.16	27.26	0.71	0.17	28.02	12.34	126.60	2.60	72.59	0.47	65.50	2.82	1.24	0.025
	10 to 60	10.23	42.39	0.82	22.38	0.45	0.27	23.10	13.31	158.78	3.02	73.38	0.46	52.24	2.47	1.20	0.027
3.2NR	<10	10.39	29.08	1.15	28.21	0.76	0.16	26.03	19.14	98.77	2.16	65.21	0.43	58.25	2.44	1.32	0.026
	10 to 60	10.93	41.21	0.86	26.95	0.43	0.32	23.64	19.02	111.66	3.11	80.28	0.41	51.56	2.44	1.50	0.024
3.3R	<10	12.99	34.44	1.43	32.55	0.54	0.24	31.92	15.59	161.80	2.35	77.65	0.66	67.14	3.39	1.33	0.033
	10 to 60	10.37	32.94	1.22	26.80	0.45	0.20	23.20	14.20	182.58	2.32	66.75	0.55	48.10	2.50	1.17	0.038
3.3NR	<10	11.42	29.60	2.02	34.37	0.62	0.26	26.03	25.51	174.88	2.23	73.17	0.58	69.28	2.99	1.35	0.050
	10 to 60	9.97	24.05	2.33	27.39	0.46	0.21	20.59	14.97	162.24	3.99	71.15	0.84	50.59	7.68	1.28	0.029
3.4R	<10	10.02	23.52	2.27	26.42	0.48	3.29	20.44	13.66	117.36	2.47	66.80	0.55	61.32	2.44	0.99	0.039
	10 to 60	9.50	21.85	2.59	27.68	0.46	0.21	17.41	16.14	75.98	3.40	59.75	0.62	40.15	4.41	1.34	0.022
3.4NR	<10	13.12	20.25	1.57	39.76	0.56	0.29	26.32	23.24	114.11	3.04	84.04	0.66	94.95	2.91	1.41	0.063
	10 to 60	8.54	19.55	2.37	26.00	0.37	0.17	17.23	18.15	90.81	3.04	62.70	0.54	51.38	4.61	1.61	0.027
Unit 4: Drainage Areas																	
4.1R	<10	11.35	24.07	1.64	29.36	0.62	0.20	24.50	15.81	112.33	3.51	79.86	0.72	69.40	5.65	1.23	0.035
	10 to 60	9.44	21.49	1.28	26.19	0.65	0.20	18.43	10.91	112.73	3.95	59.86	0.72	50.52	6.92	1.15	0.040
4.1NR	<10	11.70	22.86	1.47	46.79	0.64	0.21	26.26	18.75	152.31	4.08	87.67	0.83	80.63	7.57	1.44	0.032
	10 to 60	9.57	19.91	1.85	25.85	0.49	0.24	21.23	14.91	143.00	3.93	71.81	0.83	54.28	7.68	1.27	0.032
4.2R	<10	10.48	19.31	2.49	28.06	0.55	0.17	20.85	19.65	104.10	3.63	73.47	0.65	54.80	4.61	1.27	0.021
	10 to 60	7.20	12.18	1.76	21.56	0.35	0.17	13.97	11.72	55.69	2.74	50.12	0.49	40.05	10.00	2.41	0.023
4.2NR	<10	10.10	17.49	1.26	31.23	0.48	0.18	21.73	26.03	102.85	3.18	77.16	0.60	62.00	3.40	1.31	0.037
	10 to 60	7.97	16.61	1.84	25.44	0.36	0.16	16.87	24.93	81.65	2.96	61.54	0.51	52.82	3.59	1.36	0.028
4.3R	<10	11.46	24.62	1.17	28.18	0.63	0.17	27.24	19.71	164.03	3.51	83.98	0.61	68.63	4.93	1.36	0.040
	10 to 60	9.83	26.12	1.65	22.42	0.41	0.25	21.72	17.18	162.76	3.77	76.58	0.60	56.09	5.28	1.33	0.035
4.3NR	<10	9.11	20.92	1.36	25.28	0.53	0.38	22.75	20.25	207.84	4.12	80.87	0.58	72.88	6.37	1.34	0.037
	10 to 60	8.86	27.76	1.42	21.15	0.40	0.71	21.12	17.51	204.39	4.26	73.88	0.58	61.70	5.74	1.33	0.033
Parking Lot Areas																	
PLN#1	<10	9.33	17.57	0.81	25.91	0.76	0.23	21.87	18.01	74.37	1.97	55.71	0.45	46.19	2.25	1.11	0.102
	10 to 60	7.25	19.35	0.98	18.93	0.62	0.28	16.52	13.48	86.80	1.83	50.40	0.38	49.02	1.96	0.98	0.065
PLN#2	<10	10.75	25.63	0.87	27.54	0.53	0.23	24.10	18.06	114.39	2.21	67.78	0.52	49.33	2.30	1.21	0.050
	10 to 60	10.41	29.48	1.28	24.67	0.40	0.22	21.08	18.90	160.70	2.71	76.84	0.49	54.02	2.52	1.23	0.028
PLS#1	<10	11.07	25.19	0.73	65.16	0.43	0.33	25.43	19.31	153.63	2.32	69.85	0.49	63.15	2.86	1.21	0.030
	10 to 60	9.81	25.46	0.86	43.99	0.46	0.17	22.86	18.13	132.54	2.33	67.30	0.42	47.28	2.39	1.16	0.035
PLS#2	<10	10.54	13.14	0.95	59.15	1.51	0.23	23.76	44.21	71.68	2.09	61.77	0.44	50.24	2.38	1.51	0.042
	10 to 60	9.62	28.26	0.87	59.37	0.81	0.25	19.93	33.23	106.84	2.49	70.35	0.37	35.96	2.16	1.35	0.024
PLSE#1	<10	9.17	19.84	1.37	30.49	0.48	0.14	18.51	19.50	84.12	2.54	59.13	0.56	39.29	3.71	1.32	0.029
	10 to 60	9.25	20.59	2.08	25.19	0.38	0.18	17.38	20.25	89.90	2.75	56.11	0.60	37.91	3.76	1.28	0.023
Reference Samples																	
BRS 1		16.74	121.58	0.80	113.55	3.78	1.37	52.08	151.60	62.34	2.78	113.06	0.93	108.65	10.06	4.65	0.075
BRS 2		14.34	114.60	0.98	96.56	3.21	1.14	45.93	123.65	49.26	2.44	104.98	0.82	115.90	4.82	3.46	0.335
BRS 3		15.19	128.25	0.83	100.95	3.44	1.16	49.11	122.38	49.35	2.65	113.66	0.83	127.76	5.41	4.61	0.376
BRS 4		14.18	122.23	1.11	97.80	3.06	0.98	44.70	116.85	69.02	2.21	105.77	0.79	109.72	5.72	3.23	0.321
BRS5		14.40	115.55	1.39	102.31	3.22	1.11	47.33	128.65	55.28	2.02	107.79	0.81	114.15	4.71	3.30	0.308
Buffalo River Ref. Material 8704		13.14 - 14.00	18.1 - 125.7	71 - 5.95	NP(2)	55 - 3.23	NP	.2 - 46.6	33 - 167	NP	2.96 -3.22	90.6 - 98.6	NP	NP	NP	'5 - 3.39	NP
Gill et al. 2002(3)		NP	19.0-41.0	NP	1.0-36.0	NP	NP	9.0-19.0	17-32	50-1200	NP	22-127	NP	NP	NP	NP	NP
Reheis et al. 2002(4)		NP	26-90	7.2-11	NP	0.5-9.3	NP	28-60	170-360	280-960	3.4-4.7	NP	NP	NP	NP	2.0-11	NP
Reheis et al. 2009(5)		15, 12	80, 40	8, 6	100, 450	NP	NP	80, 30	90, 300	600, 600	4, 3	180, 100	1, 1	NP	2, 3	5, 6	NP

NOTES:

1. The Screening Levels (SLs) are developed using risk assessment guidance from the EPA Superfund program and are used for site "screening" and as initial cleanup goals, if applicable. The groundwater protectionconcentrations shown are soil concentrations considered to be protective of groundwater.
2. NP = Not provided
3. Reported range of concentrations in wind-erodible Owens Lake playa crusts.
4. Reported range of concentrations in the <50 µm fractions of dust samples from the southwestern United States.
5. Concentrations shown are for one dust sample from the eastern Mojave Desert and one from southeastern Nevada. The concentrations are estimated from Figure 3 in the manuscript.

Table 3: pH, electrical conductivity (EC) and water soluble trace element concentrations in PI-SWERL samples

Sample ID	pH	EC[1] dS m^{-1}	Co	Cr	Cs	Cu	Cd	Ag	Ni	Pb	Sr	U	V	Tl	B	Mo	Sb	Hg
						µg g-1								µg g^{-1}				
Unit 1: Sand Areas																		
1.1R[2]	8.23	2.43	0.084	0.109	0.005	0.52	0.021	0.004	1.84	0.013	343.73	0.051	1.07	0.004	12.35	0.42	0.064	0.010
1.1NR[3]	7.81	0.90	0.032	0.101	0.003	0.27	0.006	0.002	0.74	0.004	125.53	0.033	0.67	0.002	7.00	0.13	0.027	0.004
1.2R	7.83	0.76	0.049	0.253	0.004	0.49	0.003	0.001	0.54	0.005	132.86	0.118	2.00	0.003	13.37	0.39	0.041	0.011
1.2NR	8.18	0.18	0.012	0.148	0.001	0.39	0.001	ND[4]	0.12	0.002	34.83	0.026	1.72	0.001	3.97	0.09	0.021	0.004
1.3R	8.47	0.62	0.009	0.463	0.001	1.10	0.006	ND	0.13	0.018	17.90	0.114	3.12	0.002	26.62	1.00	0.154	0.009
1.3NR	8.15	0.28	0.065	0.171	0.002	0.68	0.013	0.001	0.92	0.005	142.22	0.025	0.44	0.002	7.18	0.26	0.063	0.004
1.4R	7.44	1.85	0.039	0.654	0.003	1.32	0.003	0.001	0.55	0.003	108.55	0.074	3.66	0.005	15.81	0.54	0.331	0.013
1.4NR	7.43	1.42	0.164	0.608	0.006	2.16	0.014	0.002	2.83	0.017	528.82	0.099	1.97	0.007	32.52	0.78	0.245	0.011
1.5R	7.86	2.87	0.116	0.150	0.034	0.44	0.035	0.001	2.02	0.006	539.43	0.696	0.81	0.012	115.77	8.75	0.028	0.003
1.5NR	7.55	2.31	0.104	0.285	0.03	0.65	0.059	0.003	1.69	0.005	392.40	1.168	0.30	0.021	174.42	13.53	0.024	0.003
Unit 2: Silt/clay Areas																		
2.1R	7.50	1.70	0.072	0.238	0.006	0.49	0.019	0.006	1.66	0.030	440.87	0.105	0.95	0.011	13.29	1.09	0.052	0.003
2.1NR	8.05	0.35	0.015	0.278	0.003	0.63	0.002	ND	0.25	0.002	124.79	0.052	1.61	0.006	8.00	0.40	0.050	0.004
2.2R	7.86	2.15	0.104	0.237	0.008	0.38	0.015	0.005	2.23	0.040	278.92	0.104	3.49	0.005	11.51	0.42	0.034	0.007
2.2NR	7.84	2.11	0.103	0.244	0.004	0.26	0.012	0.001	2.23	0.024	357.23	0.082	2.65	0.002	9.25	0.25	0.028	0.003
2.3R	7.74	1.78	0.216	0.288	0.021	3.05	0.035	0.011	4.39	0.046	1344.60	0.590	3.89	0.014	77.07	3.72	0.073	0.004
2.3NR	7.83	2.19	0.09	0.167	0.005	0.33	0.011	0.002	1.93	0.009	503.32	0.317	0.79	0.004	25.91	1.22	0.031	0.002
2.4R	7.63	2.08	0.174	0.221	0.008	0.99	0.013	0.003	3.77	0.010	959.26	0.338	10.80	0.006	46.05	0.67	0.081	0.006
2.4NR	7.76	1.46	0.052	0.230	0.004	0.51	0.009	0.005	0.84	0.005	213.50	0.067	2.19	0.003	14.93	0.22	0.025	0.004
Unit 3: Rock-covered Areas																		
3.1R	7.91	0.72	0.016	0.270	0.002	0.32	0.005	0.002	0.38	0.012	83.53	0.015	0.75	0.003	13.07	0.17	0.023	0.003
3.1NR	8.29	0.38	0.010	0.254	0.001	0.45	0.001	0.002	0.25	0.002	47.32	0.010	0.79	0.002	11.47	0.22	0.040	0.003
3.2R	8.06	0.42	0.010	0.282	0.001	0.32	0.005	ND	0.19	0.002	166.43	0.029	1.43	0.002	14.16	1.00	0.033	0.005
3.2NR	8.60	0.30	0.022	0.388	0.020	0.35	0.003	0.004	0.11	0.076	4.38	0.014	1.63	0.002	12.15	0.15	0.024	0.002
3.3R	8.21	0.30	0.014	2.425	0.001	0.44	0.002	ND	0.18	0.016	39.02	0.031	0.40	0.003	2.80	0.16	0.081	0.005
3.3NR	8.11	0.32	0.014	0.556	0.002	0.58	0.004	ND	0.25	0.003	52.38	0.035	0.78	0.003	6.71	0.24	0.097	0.006
3.4R	8.13	0.07	0.017	0.315	0.003	0.71	0.002	ND	0.26	0.003	47.76	0.036	1.00	0.003	6.61	0.23	0.106	0.007
3.4NR	6.58	0.06	0.008	0.152	0.001	0.14	ND	0.001	0.05	0.004	6.50	0.005	0.59	0.001	2.08	0.04	0.015	0.003
Unit 4: Drainage Areas																		
4.1R	7.87	2.26	0.127	0.278	0.004	0.54	0.010	0.004	2.47	0.010	583.80	0.208	0.83	0.009	24.99	1.22	0.056	0.006
4.1NR	8.39	0.48	0.131	0.323	0.004	0.59	0.010	0.001	2.57	0.005	617.38	0.154	0.90	0.008	20.24	1.27	0.056	0.003
4.2R	7.71	1.74	0.081	0.432	0.005	0.84	0.010	0.002	1.65	0.003	294.95	0.080	0.69	0.005	22.09	0.74	0.047	0.004
4.2NR	7.87	1.26	0.174	0.776	0.007	0.55	0.008	0.002	1.32	0.005	275.58	0.311	0.88	0.011	45.89	1.93	0.199	0.006
4.3R	8.07	0.40	0.013	0.343	0.002	0.26	0.002	ND	0.23	ND	73.05	0.025	1.27	0.003	10.74	0.35	0.051	0.004
4.3NR	8.56	0.12	0.017	0.387	0.003	0.49	0.002	0.001	0.33	ND	132.16	0.063	0.65	0.002	19.06	0.36	0.055	0.004
Parking Lot Areas																		
PLN#1	8.03	0.85	0.059	0.419	0.004	0.91	0.004	0.001	0.77	0.012	159.56	0.061	0.84	0.004	36.50	0.52	0.161	0.006
PLN#2	7.93	1.03	0.048	0.089	0.002	0.45	0.006	ND	0.53	0.005	121.20	0.077	0.72	0.002	26.99	0.30	0.111	0.004
PLS#1	9.11	1.96	0.031	1.248	0.003	2.75	0.007	0.050	0.25	0.020	9.54	0.212	5.80	0.002	114.04	1.70	0.265	0.023
PLS#2	8.31	0.50	0.022	0.355	0.001	1.12	0.014	ND	0.40	0.010	78.61	0.042	1.16	0.002	25.41	0.50	0.293	0.007
PLSE#1	8.28	0.44	0.022	0.50	0.004	0.73	0.004	0.002	0.29	0.004	89.81	0.091	2.36	0.004	35.57	1.07	0.197	0.01

NOTES:
1. EC = Electrical conductivity
2. R samples collected within tracks
3. NR samples collected in undisturbed areas
4. ND = Not detected

particularly considering the dilution factor of 10. The analytical results indicate that elevated concentrations of Sr, U, V, B, Mo, and Ni are present in some of the samples. Strontium concentrations range from 4.37 to 1,345 µg g^{-1}, U from 0.003 to 1.17 µg g^{-1}, V from 0.30 to 10.80 µg g^{-1}, B from 3.96 to 174 µg g^{-1}, Mo from 0.038 to 3.72 µg g^{-1}, and Ni from 0.05 to 4.39 µg g^{-1}.

Strontium is a relatively common trace element in the Earth's crust and is likely to be concentrated in intermediate magmatic rocks and in carbonate sediments. Strontium also behaves similarly to calcium (Ca) in the environment and is often associated with Ca in soil and sediments. Strontianite ($SrCO_3$) is easily solublized and its dissolution may be responsible for the elevated Sr concentrations (Kabata-Pendias, 2001). Under arid conditions, U forms compounds with varying solubility with oxides, carbonates, phosphates, vanates, and arsenates (Kabata-Pendias, 2001). The elevated concentrations of soluble B may result from the presence of soluble sodium borate salts, which commonly occur in alkaline soils in arid regions (McBride, 1994). Vanadium and Mo are also known to have high availability and bioavailability in oxidized soils that are neutral to alkaline.

3.3 Comparison of trace element concentrations with EPA screening levels

The concentrations of trace elements in the digested soil and PI-SWERL samples were initially compared with the USEPA Region 3, 6, and 9 screening levels (SLs) for chemical contaminants in residential soils and soil concentrations considered to be protective of groundwater resources (USEPA, 2010). The SLs are developed using risk assessment guidance from the EPA Superfund program and are used for site "screening" and as initial cleanup goals, if applicable. The risk-based SLs are considered by the EPA to be protective for humans (including sensitive groups) over a lifetime. However, it should be noted that the SLs may not be applicable at a particular site and they do not address non-human health endpoints, including ecological impacts.

None of the reported trace element concentrations in the soil, unpaved parking lot and PI-SWERL samples exceed the EPA's SLs for residential soil.

The reported concentrations of Co in all of the samples exceed the EPA SLs considered to be protective of groundwater (Tables 1 and 2). The SL for Sb is exceeded in all samples except for two of the unpaved parking lot soil samples. Ten of the soil samples and 53 of the PI-SWERL samples exceed the SL for Hg. Thirty-one of the PI-SWERL samples also exceed the SL for Mo, and all of the PI-SWERL samples and one soil sample exceed the SL for B. Three of the PI-SWERL and one of the soil samples collected in the unpaved parking lots exceed the SL for Cu, two PI-SWERL samples exceed the SL for Cd, and one PI-SWERL sample exceed the SL for Ag. None of the reported concentrations of Ni, Sr, U, and V in the samples exceeded the SLs for groundwater for these elements. The EPA has not established SLs for groundwater for Cr, Cs, Tl, and Pb.

Although the reported concentrations of some of the trace elements exceed the EPA SLs, the potential risk to groundwater resources from leaching of these elements is considered to be minimal in the Nellis Dunes area. This is because groundwater in the Nellis Dunes area is deep (>30 m below ground surface), and the arid climate minimizes leaching. However, the water-soluble concentrations of Sr, U, V, B, Mo, and Ni (see Table 3) may be of concern because of the potential for downstream contamination from runoff. Lake Mead, a major drinking water source for Las Vegas, is located hydrogeologically downgradient of the NDRA. In addition, if inhaled, these water-soluble elements may have an increased effect on health because of their solubility (Plumlee et al., 2006).

4. Comparison of trace element concentrations with reported regional concentrations of trace elements

In 1961, a sampling program was initiated by the United States Geological Survey (USGS) with the objective of providing estimates of the range of elemental abundances in surficial materials throughout the conterminous United States (Shacklette and Boerngen, 1984). The results of this study indicated that soils in the western United States generally had the highest average elemental concentrations when compared with soil samples from the eastern United States (Shacklette and Boerngen, 1984). The reported range of concentrations for each element and the average concentrations for samples collected in the western United States in this study are summarized in Table 1. More recently, total elemental analyses were performed on 50 soils collected throughout California. The reported concentration ranges and average concentrations of trace elements in these soils are also shown in Table 1 (Bradford et al., 1996).

The trace element concentrations in the Nellis Dunes soil samples generally fall within the ranges reported for the Shacklette and Boerngen (1984) and Bradford et al. (1996) studies with a few exceptions. The sample from one of the unpaved parking areas (PLS#2) had an anomalously high concentration of copper (459 $\mu g\ g^{-1}$). Copper concentrations in the other soil samples were within the ranges reported in the other studies, and ranged from 3.39 to 22.23 $\mu g\ g^{-1}$. Elevated concentrations of Sr, 630 and 821 $\mu g\ g^{-1}$, respectively, were also reported in two of the samples collected from the drainage areas (surface units 4.1 and 4.3). The high concentrations of Sr in these drainage areas may result from dissolution and transport of soluble Sr-containing minerals during rainfall events.

At least three regional studies have published the chemical composition of dust. Gill et al. (2002) studied the chemical composition of wind erodible crusts in playa sediments at Owens Lake, California. Reheis et al. (2002) studied the contribution of different local sources to dust in the southwestern United States by comparing elemental analyses of dust samples from potential source sediments, such as alluvial and playa deposits. Reheis et al. (2009) also conducted a compositional study of two dust samples collected in the desert southwest, United States. One of these samples was collected from the Cima Volcanic field approximately 130 km southwest of Las Vegas. The second sample was collected in Lower Kyle Canyon approximately 40 km northwest of Las Vegas. The reported concentrations of trace elements in these three studies are summarized in Table 2. It should be noted that not all three studies analyzed for the same elements. Additionally, the elemental concentrations were not reported in the Reheis et al. (2009) study. Rather, the concentrations were provided in a bar graph figure; the concentrations shown in Table 2 were estimated from this figure. Finally, only the Gill et al. (2002) study includes the concentrations of soluble constituents in the elemental analyses. However, soluble salts were removed prior to total elemental analyses in the Reheis et al. (2002) and Reheis et al. (2009) studies. In the following text we compare only the insoluble trace element results to the Gill et al. (2002) and Reheis et al., (2002, 2009) studies.

The concentrations of Co, Cr, Cs, Cu, Cd, Ni, Pb, U, V, Tl, Mo, and Sb in the Nellis Dunes PI-SWERL samples generally fall within the ranges reported for dust samples in one or more of the three studies cited above with a few exceptions. The Pb concentrations in the PI-SWERL samples range from 10.91 to 44.21 $\mu g\ g^{-1}$, and are within, or slightly higher, than the range of Pb concentrations (17 to 32 $\mu g\ g^{-1}$) reported by Gill et al. (2002). However, the Pb concentrations are one order of magnitude lower than those reported in the Reheis et al. (2002) and Reheis et al. (2009) studies (280-960 $\mu g\ g^{-1}$ and 90 and 300 $\mu g\ g^{-1}$), respectively. The Sr concentrations are also lower in all of the PI-SWERL samples, ranging from 55.69 to 208 $\mu g\ g^{-1}$. The reported range of Sr concentrations in the Gill et al. (2002) and Reheis et al. (2002) studies were 450 to 1200 $\mu g\ g^{-1}$, and 280 to 960 $\mu g\ g^{-1}$, respectively. The estimated concentration of Sr in the two dust samples analyzed in the Reheis et al. (2009) study was 600 $\mu g\ g^{-1}$. The Mo concentrations in the PI-SWERL samples are generally within the range of concentrations (2 to 11 $\mu g\ g^{-1}$) reported by Reheis et al. (2002), and the concentrations in the two dust samples (5 and 6 $\mu g\ g^{-1}$), reported in Reheis et al. (2009), except for the samples from surface unit 1.5. Molybdenum concentrations in the four samples from unit 1.5 are nearly one order of magnitude higher ranging from 39.9 to 74.8 $\mu g\ g^{-1}$. It is unclear why the Mo concentrations in the PI-SWERL samples from this unit are elevated.

5. Summary and conclusions

In summary, the concentrations of most of the trace elements analyzed were higher in the PI-SWERL samples than in the soil samples. These results are expected because of the larger particle size of the soil samples as compared to the PI-SWERL samples. The finer fractions of the samples are dominated by smectite minerals which are known to increase the retention of metals in the soil. Some of the highest concentrations of trace elements occurred in the PI-SWERL samples from surface unit 1.5. The reported concentrations of trace elements in the soil and PI-SWERL samples generally fall within the ranges reported previously by other investigators.

The reported concentrations of trace elements in the soil and PI-SWERL samples do not exceed the EPA's SLs for residential soil. However, the concentrations of some of the trace elements do exceed the EPA SLs considered to be protective of groundwater resources. The potential risk to groundwater resources from leaching of these elements is considered to be minimal in the Nellis Dunes area. This is because groundwater in the Nellis Dunes area is deep (>30 m below ground surface), and the arid climate minimizes leaching. The water-soluble concentrations of Sr, U, V, B, Mo, and Ni may be of potential concern if they are transported downstream in runoff. Lake Mead, a major drinking water source for Las Vegas, is located hydrogeologically downgradient of the NDRA. These water-soluble elements may also affect health if inhaled.

References

Bradford, G.R., Chang, A.C., Page, A.L., Bakhtar, D., Frampton, J.A., Wright, H., 1996. Background concentrations of trace and major elements in California soils. Kearney Foundation of Soil Science Special Report.

Gill, T.E., Gillette, D.A., Niemeyer, T., Winn, R.T., 2002. Elemental geochemistry of wind-erodible playa sediments, Owens Lake, California. Nuclear Instruments and Methods in Physics Research B 89, 209-213.

Goossens, D., Buck, B., 2009. Dust emission by off-road driving: Experiments on 17 arid soil types, Nevada, USA. Geomorphology 107, 118-138.

Järup, L., 2003. Hazards of heavy metal contamination. British Medical Bulletin 68, 167-182.

Kabata-Pendias, A. 2001. Trace Elements in Soils and Plants, 3rd ed. CRC Press, Boca Raton, pp. 126-128 and 199-201.

Matera, V., Le Hécho, I., 2001. Arsenic behavior in contaminated soils: Mobility and speciation. In: Selim, H.M., Sparks, D.L. (eds). Heavy Metals Release in Soils. CRC Press, Boca Raton, pp. 207-235.

McBride, M.B., 1994. Environmental Chemistry of Soils. Oxford University Press, New York, pp. 327-328.

Pye, K., Tsoar, H., 1990. Aeolian Sand and Sand Dunes. Unwin Hyman, London.

Reheis, M.C., Budahn, J.R., Lamothe, P.J., 2002. Geochemical evidence for diversity of dust sources in the southwestern United States. Geochimica et Cosmochimica Acta 66, 1569-1587.

Reheis, M.C., Budahn, J.R., Lamothe, P.J., Reynolds, R.L., 2009. Compositions of modern dust and surface sediments in the desert southwest, United States. Journal of Geophysical Research 114, FO1028.

Reid-Soukup, D.A., Ulery, A.L., 2002. Smectites. In: Dixon, J.B., Schulze, D.G. (eds.). Soil Mineralogy with Environmental Applications. Soil Science Society of America, Madison, WI, pp. 467-499.

Shacklette, H.T., Boerngen, J.G., 1984. Element Concentrations in Soils and Other Surficial Materials of the Conterminous United States. U.S. Geological Survey Professional Paper 1270, United States Govt. Printing Office, Washington DC.

United States Environmental Protection Agency, Office of Solid Waste, 1996. SW-846 test methods for evaluating solid waste, physical/chemical methods, method 3052. Microwave-assisted acid digestion of siliceous and organically based matrices. USEPA website, SW-846 on-line 3000 series methods. www.epa.gov/epaoswer/hazwaste/test/3_series.htm

United States Environmental Protection Agency Regions 3, 6, and 9 (April 10, 2010). Regional Screening Levels for Chemical Contaminants at Superfund Sites. http://www.epa.gov/reg3hwmd/risk/human/rb-concentration_table/index.htm

Chapter 10

ARSENIC CONCENTRATIONS IN THE NELLIS DUNES RECREATION AREA

Deborah Soukup[1], Brenda Buck[1], Dirk Goossens[1], April Ulery[2], Brett McLaurin[3], Dirk Baron[4] and Yuanxin Teng[1]

[1]*Department of Geoscience, University of Nevada Las Vegas*
[2]*Department of Plant and Environmental Sciences, New Mexico State University*
[3]*Department of Geography and Geosciences, Bloomsburg University of Pennsylvania*
[4]*Department of Physics and Geology, California State University*

1. Introduction

Chemical analyses were performed on soil and airborne sediment from all 17 surface units in the Nellis Dunes Recreation Area (NDRA). An overview of the results is provided in Chapter 9. However, one particular chemical element (arsenic) is of special concern because it occurs in exceptionally high concentrations in several surface units, much higher than reported in the scientific literature on arsenic in the western United States published to date. Exposure to arsenic constitutes an important health risk. Arsenic has been strongly linked to a long list of diseases such as heart disease, hypertension, peripheral vascular disease, diabetes, immune suppression, acute respiratory infections, intellectual impairment in children, and skin, lung, prostate, bladder, kidney and other cancers (Chen et al., 1992; Abernathy et al., 1999; Järup, 2003; Tseng et al., 2003; von Ehrenstein et al., 2006). Additionally, arsenic has been found to be uniquely harmful to lung tissue by inhibiting wound repair and altering genes associated with immune functions in lung tissue (Olsen et al., 2008; Kozul et al., 2009a; Kozul et al., 2009b). It is one of the most poisonous chemical elements naturally occurring on the Earth's surface.

The occurrence of high arsenic concentrations in the Nellis Dunes Recreation Area is of great concern for several reasons. First, arsenic is usually associated with, and attached to, the fine particle fraction of the soil (Chen et al., 1999; Van Pelt and Zobeck, 2007). It is this fraction in particular that is emitted by wind erosion or off-road vehicular (ORV) activity. Depending on the arsenic concentrations in the topsoil, the capacity of that topsoil to produce dust and the degree of disturbance of the top layer by either wind erosion or ORV activity, large to very large amounts of arsenic may be emitted from the soil. Secondly, once emitted the arsenic is transported downwind, it can settle to the ground and pollute other areas within the NDRA originally not characterized by high arsenic concentrations. Third, runoff and water erosion in the arsenic source areas bring substantial amounts of arsenic to the washes, where it is transported downstream. Several of the major washes in the NDRA are characterized by high concentrations of arsenic even at places several km downstream from the arsenic sources. These places behave as secondary sources when they dry and material is reemitted into the air. Finally, the number of visitors potentially exposed to arsenic emissions in NDRA is very high. A report published in 2004 (BLM, 2004) mentions a number of 285,000 visitors annually, but ORV activity in the region has quadrupled since then (Spivey, 2008).

For all these reasons a separate chapter on arsenic is provided in this report. It describes the occurrence, concentrations and emissions of arsenic in the NDRA, but does **NOT** consider the potential health impacts. A preliminary study was carried out using mice to model the impact NDRA dust might have on the human immune system (see Chapter 11). However, in order to more fully understand what the potential human health risks might be, a separate study is required. Such a study should include measurements of the actual amounts of arsenic and other chemicals and minerals contained within the dust inhaled by NDRA visitors during ORV activity and wind erosion, toxicological analysis of the impact of the inhaled dust to the human body, and a full risk analysis of all 17 surface units occurring in the NDRA. The original task agreement of the Nellis Dunes project did not include such a risk study because the high amounts of arsenic were only discovered during the project, and the budget did not allow adding a detailed risk analysis to the study. In addition, if needed, a second, separate study would be required to define the health risk the dust at NDRA might pose to the population in Clark County.

2. Sample collection

Soil samples were taken from all 17 surface units occurring in the NDRA. They included dust stations, locations where experiments with the off-road vehicles were carried out, and five supplementary sampling spots located on the major parking areas. All soil samples were taken from the upper 2-3 cm of the topsoil.

Additional airborne dust samples were collected from all ORV spots and from the five parking areas using the Portable In Situ Wind Erosion Laboratory or PI-SWERL (see Chapter 4 for a description of the instrument). The PI-SWERL was set to an RPM of 6000 and the dust emitted was collected by connecting a Dyson vacuum cleaner to the outlet of the PI-SWERL chamber. Samples were collected from the cyclone chamber of the vacuum cleaner after completion of the sampling. About 10 g of sediment was collected during each test. PI-SWERL samples were collected both on ORV trails and on undisturbed terrain. No samples were collected from areas of outcropping bedrock or outcropping petrocalcic horizons (unit 3.5, see Chapter 2 for a detailed description) because this unit contains negligible emittable dust.

The soil samples were sieved at 2 mm to exclude all gravel, which is not emitted during wind erosion. The arsenic in the remaining fractions represents the source of any arsenic distributed later over the NDRA, either by water, by wind or by human disturbance. The PI-SWERL samples only contain the emittable soil fractions and are thus representative for measuring the arsenic concentrations in the potential emissions. Fig. 1 shows the sampling locations. Note that the scale of the map does not allow a clear distinction between the PI-SWERL sampling spots on the trails and the corresponding spots on undisturbed terrain; the number of sampling locations is therefore substantially greater than the number shown on the map.

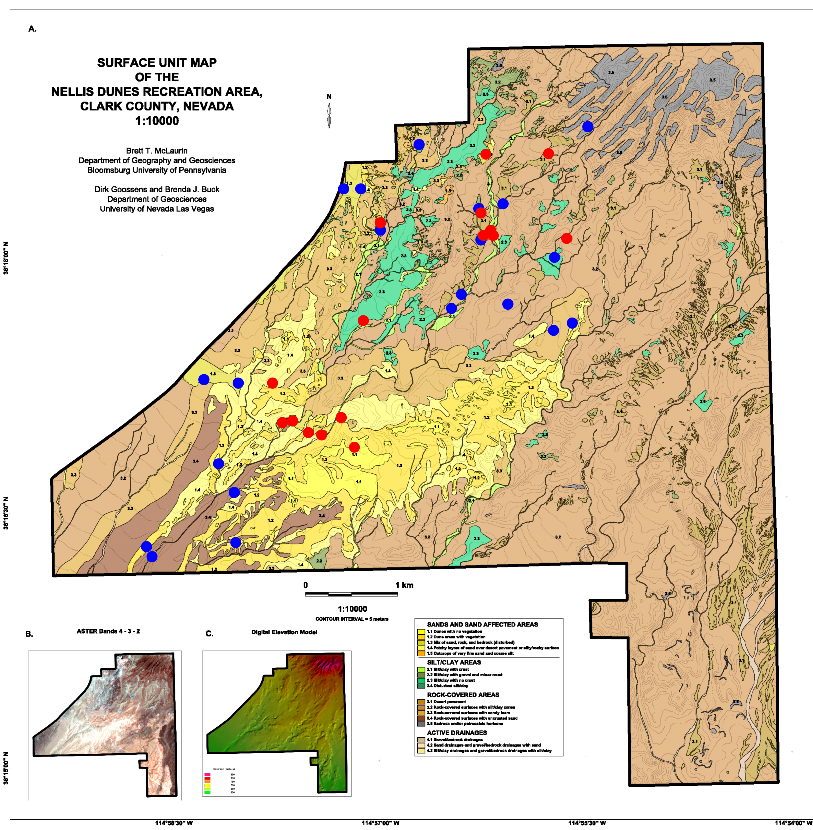

Fig. 1: Sample locations for arsenic. More than one sample may have been taken from the locations indicated on the map (see text for details). Blue: soil samples; red: PI-SWERL samples.

3. Laboratory procedure

The *soil samples* were air dried and sieved to remove coarse fragments (>2 mm). The <2 mm fraction was then digested in accordance with EPA Method 3052 (USEPA, 1996). The digested samples were initially scanned for 66 different elements using inductively coupled plasma mass spectroscopy (ICP-MS). The purpose of the initial semi-quantitative scan was to identify elements of potential environmental concern in the samples. Based on the results of the semi-quantitative scan, the following elements were identified as elements of potential concern: arsenic (As), cobalt (Co), chromium (Cr), cesium (Cs), copper (Cu), cadmium (Cd), silver (Ag), nickel (Ni), lead (Pb), strontium (Sr), uranium (U), vanadium (V), thallium (Tl), boron (B), molybdenum (Mo), antimony (Sb), and mercury (Hg). The samples were then re-analyzed quantitatively for these elements using ICP-MS.

To ensure quality control for the ICP-MS analyses, Buffalo River Sediment Reference Material 8704 was obtained from the National Institute of Standards and Technology (NIST), Gaithersburg, Maryland, USA. Samples of this material were digested in accordance with EPA Method 3052 and analyzed along with the NDRA samples. Satisfactory recoveries were found for the trace elements analyzed.

For the *PI-SWERL samples* a separate analysis was performed for the <10 µm (PM10) and 10-60 µm size fractions. The procedure was as follows. First, in order to not lose any soluble elements during wet sieving, 10:1 water:soil extracts were prepared to determine the water soluble constituents in the PI-SWERL samples. The 10:1 extracts were used instead of a saturated paste because of limited sample sizes. These samples were allowed to sit overnight and were then filtered to obtain the supernatant. The supernatant solution was analyzed by ICP-MS. Once this was completed, the <10 µm and 10-60 µm fractions were separated by sedimentation and wet sieving and digested in accordance with EPA Method 3052 prior to analysis. The 60 µm limit was used as a cut-off for total suspendable particles (TSP), because it represents the maximum size of grains that will still be transported in short-term suspension during average wind speed and turbulence (see Pye and Tsoar, 1990). It also nearly coincides with the maximum diameter of silt (52 µm or 63 µm, depending on which criterion is used; see Goossens and Buck, 2009 for more information). Although all of the samples were analyzed for the potential elements of environmental concern, this chapter focuses exclusively on the arsenic concentrations. The remaining elements were already addressed in Chapter 9.

4. Results

The reported concentrations of arsenic (As) in the surface unit and parking lot *soil samples* ranged from 3.49 to 83.02 µg g^{-1} or parts per million (ppm; Table 1). The highest concentrations of As in the soil samples occurred within the silt/clay areas (surface units 2.1 to 2.4), the drainages (surface units 4.1 to 4.3), and surface unit 1.5.

Table 1: Arsenic concentrations in the soil samples at NDRA. Particles coarser than 2 mm were removed from the samples prior to analysis.

Surface Unit Description	As ($\mu g\ g^{-1}$)
USEPA Regional Screening Levels(1)	
Residential Soil	0.39
Groundwater Protection	0.0013
Sand and Sand-Affected Areas	
1.1: Dunes with no vegetation	4.37
1.2: Dunes with vegetation	3.49
1.3: Disturbed sand surfaces	6.74
1.4: Patchy layers of sand over silty/rocky subsoil	4.92
1.5: Outcrops of very fine sand and coarse silt	46.06
Silt/clay Areas	
2.1: Silt/clay with crust	19.71
2.2: Silt/clay with gravel	83.02
2.3: Aggregated silt deposits	11.01
2.4: Disturbed silt surfaces	11.79
Rock-covered Areas	
3.1: Desert pavements	13.56
3.2: Rock-covered surfaces with silt/clay zones	7.89
3.3: Rock-covered surfaces with sandy loam	6.85
3.4: Rock-covered surfaces with encrusted sand	7.28
3.5: Bedrock and/or petrocalcic horizons	9.03
Drainage Areas	
4.1: Gravelly drainages	32.36
4.2: Gravel and sand drainages	23.39
4.3: Gravel and silt/clay drainages	31.45
Parking Lot Areas	
North Parking Lot #1	5.98
South Parking Lot #1	4.88
South Parking Lot #2	6.86
Southeast Parking Lot #1	17.62
Standard Samples	
BRS	14.64
Buffalo River Reference Material 8704	17

Notes:
(1) The Screening Levels (SLs) are developed using risk assessment guidance from the EPA Superfund program and are used for site "screening" and as initial cleanup goals, if applicable. The groundwater protection concentrations shown are soil concentrations considered to be protective of groundwater resources.
(2) NA = Not applicable

The As concentrations in the PM10 and 10-60 µm fractions in the *PI-SWERL samples* ranged from 18.56 to 290.01 and from 16.13 to 312.42 $\mu g\ g^{-1}$, respectively (Table 2). Note that these values only reflect arsenic that was not soluble in water. The highest As concentrations in both size fractions were reported in the samples collected from undisturbed terrain of surface unit 1.5; the lowest concentrations occurred in the undisturbed terrain samples from surface unit 3.2. Elevated As concentrations (41.13 to 161.32 µg g^{-1}; Table 2) also occurred in the ORV trails and undisturbed terrain samples from surface units 2.1, 2.2, 4.1, 4.2, and 4.3.

The *water-soluble As concentrations* in the 0-60 µm fractions of the PI-SWERL samples ranged from 0.42 to 14.71 µg g^{-1} (Table 3). The pH values of the soluble PI-SWERL extracts were near-neutral to slightly alkaline, ranging from 6.58 to 9.11 (Table 3). Electrical conductivity (EC) values of the extracts were from 0.06 to 2.43 dS m^{-1}. The EC values document the salinity of most of the soils in the NDRA, particularly when considering that the extracts were diluted by a factor of 10:1.

Table 2: Arsenic concentrations in airborne (PI-SWERL) samples. Surface unit 3.5 (bedrock) was not sampled.

Surface Unit Description	Particle Size (µm)	As (µg g^{-1})
USEPA Regional Screening Levels[1]		
Residential Soil		0.39
Groundwater Protection		0.0013
Sand and Sand-Affected Areas		
1.1R[2]: Dunes with no vegetation	<10	43.31
	10 to 60	30.40
1.1NR[3]	<10	46.56
	10-60	28.37
1.2R: Dunes with vegetation	<10	52.45
	10 to 60	42.14
1.2NR	<10	48.78
	10 to 60	36.55
1.3R: Disturbed sand surfaces	<10	54.14
	10 to 60	46.34
1.3NR	<10	37.96
	10-60	30.37
1.4R: Patchy layers of sand over silty/rocky subsoil	<10	26.32
	10 to 60	20.46
1.4NR	<10	27.21
	10 to 60	19.76
1.5R: Outcrops of very fine sand and coarse silt	<10	279.03
	10 to 60	248.31
1.5NR	<10	290.01
	10 to 60	312.42
Silt/clay Areas		
2.1R: Silt/clay with crust	<10	87.95
	10 to 60	79.68
2.1NR	<10	83.03
	10 to 60	79.30
2.2R: Silt/clay with gravel	<10	145.39
	10 to 60	130.61
2.2NR	<10	161.32
	10 to 60	138.50
2.3R: Aggregated silt deposits	<10	18.56
	10 to 60	24.87
2.3NR	<10	27.44
	10 to 60	33.46
2.4R: Disturbed silt surfaces	<10	25.10
	10 to 60	24.40
2.4NR	<10	23.54
	10 to 60	26.02

Table 2 (ctd): Arsenic concentrations in airborne (PI-SWERL) samples. Surface unit 3.5 (bedrock) was not sampled.

Surface Unit Description	Particle Size (µm)	As ($\mu g\ g^{-1}$)
USEPA Regional Screening Levels[(1)]		
Residential Soil		0.39
Groundwater Protection		0.0013
Rock-covered Areas		
3.1R: Desert pavements	<10	28.11
	10 to 60	26.46
3.1NR	<10	24.86
	10 to 60	22.34
3.2R: Rock-covered surfaces with silt/clay zones	<10	27.88
	10 to 60	21.85
3.2NR	<10	18.85
	10 to 60	16.13
3.3R: Rock-covered surfaces with sandy loam	<10	32.93
	10 to 60	25.84
3.3NR	<10	30.98
	10 to 60	70.64
3.4R: Rock-covered surfaces with encrusted sand	<10	44.03
	10 to 60	49.54
3.4NR	<10	41.74
	10 to 60	41.43
Drainage Areas		
4.1R: Gravelly drainages	<10	64.33
	10 to 60	70.59
4.1NR	<10	78.14
	10 to 60	70.24
4.2R: Gravel and sand drainages	<10	54.16
	10 to 60	45.35
4.2NR	<10	44.15
	10 to 60	41.27
4.3R: Gravel and silt/clay drainages	<10	65.13
	10 to 60	66.00
4.3NR	<10	94.09
	10 to 60	72.20
Parking Lot Areas		
North Parking Lot #1	<10	28.09
	10 to 60	20.03
North Parking Lot #2	<10	27.76
	10 to 60	23.99
South Parking Lot #1	<10	34.34
	10 to 60	19.25
South Parking Lot #2	<10	23.56
	10 to 60	17.10
Southeast Parking Lot #1	<10	45.24
	10 to 60	39.89
Standard Samples		
BRS1		21.08
BRS2		19.16
BRS3		20.33
BRS4		18.46
BRS5		18.64
Buffalo River Reference Material 8704		17

Notes:

(1) The Screening Levels (SLs) are developed using risk assessment guidance from the EPA Superfund program and are used for site "screening" and as initial cleanup goals, if applicable. The groundwater protection concentrations shown are soil concentrations considered to be protective of groundwater.

(2) R samples collected within ORV trails

(3) NR samples collected in undisturbed areas

Table 3: pH, electrical conductivity and soluble arsenic concentrations in airborne (PI-SWERL) dust extracts. Surface unit 3.5 (bedrock) was not sampled.

Surface Unit Description	pH	Electrical Conductivity (dS m^{-1})	As ($\mu g\ g^{-1}$)
Sand and Sand-Affected Areas			
1.1R[(1)]: Dunes with no vegetation	8.23	2.43	1.78
1.1NR[(2)]	7.81	0.90	0.55
1.2R: Dunes with vegetation	7.83	0.76	4.36
1.2NR	8.18	0.18	2.23
1.3R: Disturbed sand surfaces	8.47	0.62	6.82
1.3NR	8.15	0.28	0.61
1.4R: Patchy layers of sand over silty/rocky subsoil	7.44	1.85	6.05
1.4NR	7.43	1.42	2.80
1.5R: Outcrops of very fine sand and coarse silt	7.86	2.87	8.04
1.5NR	7.55	2.31	4.13
Silt/clay Areas			
2.1R: Silt/clay with crust	7.50	1.70	8.28
2.1NR	8.05	0.35	5.88
2.2R: Silt/clay with gravel	7.86	2.15	9.24
2.2NR	7.84	2.11	10.59
2.3R: Aggregated silt deposits	7.74	1.78	5.02
2.3NR	7.83	2.19	1.49
2.4R: Disturbed silt surfaces	7.63	2.08	9.58
2.4-NR	7.76	1.46	2.17
Rock-covered Areas			
3.1R: Desert pavements	7.91	0.72	0.81
3.1NR	8.29	0.38	1.04
3.2R: Rock-covered surfaces with silt/clay zones	8.06	0.42	0.87
3.2NR	8.60	0.30	0.65
3.3R: Rock-covered surfaces with sandy loam	8.21	0.30	1.91
3.3NR	8.11	0.32	1.40
3.4R: Rock-covered surfaces with encrusted sand	8.13	0.07	2.20
3.4NR	6.58	0.06	0.42
Drainage Areas			
4.1R: Gravelly drainages	7.87	2.26	3.11
4.1NR	8.39	0.48	3.47
4.2R: Gravel and sand drainages	7.71	1.74	2.17
4.2NR	7.87	1.26	14.71
4.3R: Gravel and silt/clay drainages	8.07	0.40	3.93
4.3NR	8.56	0.12	9.15
Parking Lot Areas			
North Parking Lot #1	8.03	0.85	1.38
North Parking Lot #2	7.93	1.03	1.04
South Parking Lot #1	9.11	1.96	7.78
South Parking Lot #2	8.31	0.50	1.32
Southeast Parking Lot #1	8.28	0.44	5.57

Notes:

(1) R samples collected within ORV trails
(2) NR samples collected in undisturbed areas
(3) NA = Not applicable

5. Discussion

5.1 Occurrence of arsenic at NDRA

The results indicate that arsenic is preferentially concentrated in the drainages that receive increased runoff and concentrate soluble arsenic (surface units 4.1 to 4.3), and/or in map units that contain increased clay content (surface units 2.1 to 2.4; and 4.3). The highest concentrations of As in *soil samples* occurred within the silt/clay areas (surface units 2.1 to 2.4), the drainages (surface units 4.1 to 4.3), and surface unit 1.5 (Table 1). The highest concentrations of As in *airborne sediment* (PI-SWERL samples) occurred in surface units 1.5, 2.1, 2.2 and all drainages (surface units 4.1 to 4.3). The highest concentrations of *soluble arsenic in airborne sediment* (PI-SWERL samples) occurred in two of the drainages (surface units 4.2 and 4.3), the silt/clay areas (2.1, 2.2, 2.4) and surface unit 1.5. For most of the airborne samples, the As concentrations were generally higher in the PM10 fraction than in the 10-60 µm fraction, and these fractions were significantly higher than the <2 mm bulk soil samples.

The high concentrations of As occurring in the drainage areas (surface units 4.1 to 4.3) combined with the water-soluble As results indicate that significant amounts of soluble arsenic is being dissolved and concentrated in the dry washes at NDRA during rainfall events. Much more detailed work is required to determine the specific mineral-As associations. However, studies in other regions have found that soluble arsenic minerals such as sodium arsentates occur in neutral to alkaline soils (McBride, 1994; Matera and LeHécho, 2001). Other studies have found arsenic to be either sorbed onto the surface of soluble calcite or gypsum; or present in their mineral structures due to isomorphic substitution (Roman-Ross et al., 2003; Di Benedetto et al., 2006; Fernández-Martínez et al., 2008). Additional mechanisms that can release As into solution include reductive dissolution of Fe-oxides and oxidative dissolution of sulfide minerals as well as redox cycling of As (Hering and Kneebone, 2002; Huerta-Diaz et al., 1998). Manganese may also play a role in controlling As mobility, as a result of redox reactions of manganese oxides with arsenite. More research is needed to identify the mineralogy of the soluble arsenic measured in this study (Table 3). However, the relatively high arsenic concentrations even in the coarse textured sandy drainages (unit 4.2) indicate significant re-mobilization of arsenic in these sediments.

The highest values of non-water-soluble arsenic in the PI-SWERL data are found in two units: 2.2 and 1.5. Interestingly both of these units have a distinct yellow color. Although XRD data (see Chapter 8) did not indicate any Fe-oxide minerals, the yellow color strongly suggests that one or more Fe-oxide-hydroxide substances may be present. Detection of well- to moderately well-crystalline Fe-oxide minerals by XRD analyses is generally possible when a given Fe-oxide mineral comprises 3 to 5% (w/w) of the sample

(Bigham et al., 2002). Identification of poorly crystalline Fe-oxide phases by XRD is more difficult, and amorphous Fe-oxides cannot be identified by XRD analyses. Therefore, the yellow color may result from Fe-oxide-hydroxide coatings on grains that were not abundant enough to be detected by XRD analyses, or from poorly crystalline or amorphous Fe-oxides. Because Fe-oxides have a high sorption affinity for trace elements (Bigham et al., 2002), including arsenic, this may explain the correlation between the yellow color and the high arsenic contents in these two units.

The increased As concentrations in the finer textured map units and in finer PI-SWERL fractions suggests retention of As on clay complexes or Fe-oxide-hydroxides and/or concentration of As within clay or other fine-grained mineral species. XRD analyses reveal that the mineralogical composition of the clay (<2 μm) and silt (2-20 μm) fractions of the soil samples at NDRA is dominated by smectite with lesser amounts of palygorskite, mica/illite, kaolinite, quartz, and calcite (see Chapter 8). Gypsum was also identified in several samples, although it should be noted that most of the gypsum present would have been removed during the distilled water rinses prior to fractionation and XRD analyses (see Chapter 8). Smectites are known to be major contributors to soil cation exchange capacity (CEC) and therefore, affect the retention of metals in the soil (Reid-Soukup and Ulery, 2002). Sorption of As onto the surface and isomorphic substitution within the structures of both calcite (Roman-Ross et al., 2003; Di Benedetto et al., 2006) and gypsum (Roman-Ross et al., 2003; Fernández-Martínez et al., 2008) have also been reported. Additionally, these fine-textured surface units (2.1 to 2.4; and 4.3) have decreased permeability that minimizes leaching of As during rainfall events.

Many other studies have shown that As is often preferentially concentrated in finer size fractions. Chen et al. (1999) reported that clay content and CEC were highly correlated with As concentrations in Florida surface soils. Van Pelt and Zobeck (2007) quantified the chemical constituents of fugitive dust in the Southern High Plains of Texas. These investigators also reported that the finer particles in the source soils contained higher concentrations of chemical constituents, including As. However, As concentrations in the source soils in Van Pelt and Zobeck's (2007) study were lower than those in the NDRA soils, ranging from 1.13 to 3.89 μg g^{-1}. Another possibility is that the As in the NDRA soil is associated with smectite minerals. Pascua et al. (2005) reported the occurrence of an As-rich smectite (1,500 to 4,000 ppm) in a geothermal field in Japan. These investigators found that minimal adsorption of As on smectite surfaces had occurred. Rather, the As was predominantly dissolved within the smectite or occurred within mineral occlusions. Additional studies are currently underway to determine the geological processes that lead to the concentration of As in these sediments.

In the Nellis Dunes Recreation Area there is not a clear relationship between As concentrations and location of disturbed (i.e., ORV trail) versus undisturbed surfaces. For the PM10 samples, As concentrations in 9 of the 16 ORV trail samples were higher (1.56 to 16.18 μg g^{-1}) than those measured in the associated undisturbed terrain samples, and approximately equal in one sample (Table 2). In the other six PM10 samples, the As concentrations in the undisturbed terrain samples ranged from 3.25 to 28.96 µg g^{-1} higher than those detected in the associated ORV trail samples. Arsenic concentrations in the 10-60 µm fraction were higher in 7 of the 16 ORV trail samples (2.03 to 8.11 µg g^{-1}) and approximately equal in three samples as compared to the associated undisturbed terrain samples (Table 2). The As concentrations in the other six ORV trail samples were from 1.62 to 64.11 µg g^{-1} lower than those reported in the corresponding undisturbed terrain samples.

5.2 Regional and national distribution of arsenic in soils

Naturally occurring background concentrations of arsenic vary regionally because of a combination of climatic, geologic, and anthropogenic factors. Sources of As in the environment include weathering of As-bearing rocks and minerals, volcanic eruptions, fly ash from coal burning plants, smelter fumes released during the treatment of As-containing metallic ores, mining wastes, and application of arsenical pesticides, herbicides and corrosion inhibitors. Because the only anthropogenic process occurring at NDRA is ORV activity, it is believed that the arsenic at NDRA is naturally occurring as a result of regional geologic processes.

The concentrations of As in some of the soil samples at NDRA are substantially higher (3.49 to 83.02 ppm) than in soils elsewhere in the United States, where the average ranges from 3.6 to 8.8 ppm; and throughout the world where averages range from 2.2 to 25 ppm (McBride, 1994). In a 1975 study of 21 soil samples collected in the western United States, As concentrations ranged from non-detectable to 97 ppm with an average concentration of 6.1 ppm (Connor and Shacklette, 1975). In another study, As analyses were performed on 50 soils collected throughout California. Arsenic concentrations in these soils ranged from 0.6 to 11 ppm, with an average concentration of 3.5 ppm (Bradford et al., 1996). Reheis et al. (2009) report median As concentrations of 10 ppm in surface soil samples in southern Nevada and California. However, five surface soil samples in that study contained As concentrations ranging from approximately 30 to 50 ppm.

Arsenic concentration data for the entire United States is also available from a soil inventory prepared by the United States Department of Agriculture Natural Resources Conservation Service (USDA-NRCS, 2010). This database includes information on As concentrations in more than 2,800 soil samples collected at over 480 different locations in the United States. Using this data, we constructed a figure showing the reported soil As concentrations (Fig. 2). Arsenic concentrations in the USDA-NRCS database are nearly always less than 20 ppm, and rarely above 30 ppm. Comparing this data shows that As concentrations for most surface units at NDRA are comparable with those measured elsewhere in the United States (Table 1). The exceptions are the drainage units (4.1, 4.2, and 4.3) and units 1.5 and 2.2, which have anomalously high As concentrations.

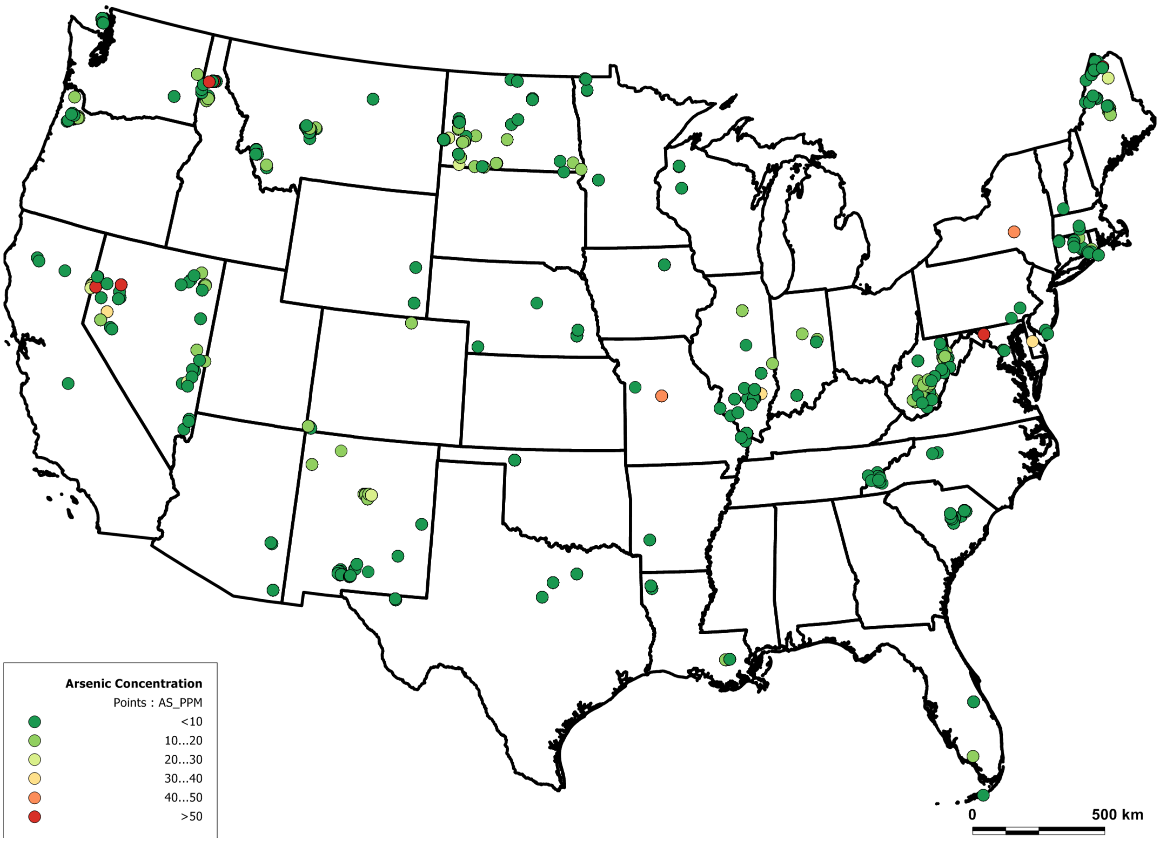

Fig. 2: Arsenic concentration in soil samples from the United States.
Source: UDSA-NRCS, 2010.

The reported As concentrations in soils for NDRA units 1.5 and 2.2 are among the highest documented in the United States to date. Breit et al. (2009) reported As concentrations in the water soluble soil fraction at Franklin Lake Playa (approximately 100 km southwest of NDRA) over 400 ppm, but these values were measured at a depth of more than 50 cm below the playa surface. Arsenic concentrations were much lower closer to the playa surface, <100 ppm at a depth of 20 cm and <50 ppm in the uppermost 10 cm. Reynolds et al. (2008) and Goldstein et al. (2008) reported water-soluble salts on the ground surface in Ash Meadows and Carson Slough, immediately north of Franklin Playa, had As concentrations as high as 600 ppm. The Reynolds et al. (2008) and Goldstein et al. (2008) studies are the only studies performed on non-mining sites in the western United States that we are aware of with reported As concentrations higher than those of NDRA unit 2.2.

5.3 Arsenic in dust

Few studies have analyzed As in airborne dust, and none have reported values as high as found in the current Nellis Dunes study. Reheis et al. (2002) studied the contributions of different local sources to dust in the southwestern United States by comparing elemental analyses of samples collected from dust traps to analyses of samples from potential source sediments, such as alluvial and playa deposits. The average concentration of As in the <50 µm fraction of dust samples ranged from 5 to 25 ppm. The results of the Reheis et al. (2002) study also showed that all dust samples were enriched in As relative to source samples, and that dusts in the Owens Valley have higher concentrations of As than dust samples from other areas. The highest concentrations of As occurred in Owens Valley alluvium and lake-marginal deposits away from the dry bed of Owens Lake. The average concentration of As in the <50 µm fraction from the Owens Valley lake bed samples was reported to be 40 ppm and 45 ppm in dust from elsewhere in Owens Valley (Reheis et al., 2002). More recently, Reheis et al. (2009) conducted a compositional study of modern dust and surface sediments in southern Nevada and California. These investigators reported median As concentrations of 20 ppm in airborne dust (collected at a height of 2 m above the surface) and 10 ppm in surface soil samples. One outlier airborne dust sample had an As concentration of 50 ppm.

5.4 Arsenic hazards to health

Exposure to arsenic has been strongly linked to heart disease, hypertension, peripheral vascular disease, diabetes, immune suppression, acute respiratory infections, intellectual impairment in children, and skin, lung, prostate, bladder, kidney and other cancers (Chen et al., 1992; Abernathy et al., 1999; Järup, 2003; Tseng et al., 2003; Smith et al., 2006; von Ehrenstein et al., 2006; Kozul et al., 2009). Additionally, arsenic has been found to be uniquely harmful to lung tissue by inhibiting wound repair and altering genes associated with immune functions in lung tissue (Olsen et al., 2008; Kozul et al., 2009a; Kozul et al., 2009b).

Because of this, the reported concentrations of As in the digested soil and PI-SWERL samples were initially compared with the USEPA Region 3, 6, and 9 screening levels (SLs) for chemical contaminants in residential soils and soil concentrations considered to be protective of groundwater resources (USEPA, 2010). The SLs are developed using risk assessment guidance from the EPA Superfund Program and are used for site "screening" and as initial cleanup goals, if applicable. The risk-based SLs are considered by the EPA to be protective for humans (including sensitive groups) over a lifetime. However, it should be noted that the SLs may not be applicable at a particular site and they do not address non-human health endpoints, including ecological impacts. The As concentrations in all of the NDRA samples analyzed exceed the EPA's SL of 0.39 $\mu g\ g^{-1}$ for As in residential soil by one to three orders of magnitude (Table 1).

The reported concentrations of As in all of the samples exceed the EPA SLs considered to be protective of groundwater. Although the reported As concentrations exceed the EPA SLs, the potential risk to groundwater resources from leaching of As is considered to be minimal in the Nellis Dunes area. This is because groundwater in the Nellis Dunes area is deep (>30 m below ground surface), and the arid climate minimizes leaching. However, the high soluble concentrations of As are of concern because of the potential for downstream contamination from runoff. Lake Mead, a major drinking water source for Las Vegas, is located hydrogeologically downgradient of the NDRA.

The most important potential health hazard in this area is human exposure to As through inhalation of dust. In order to better understand potential risks of As in dust emissions we calculated PM10 emission rates for As resulting from natural wind erosion in NDRA for each surface unit. We multiplied the emission rates for total PM10 dust (published in the study by Goossens and Buck, 2010) with the As content of the PM10 PI-SWERL samples. PI-SWERL samples are used in the calculation because they represent the sediment fractions prone to emission during wind erosion. For unit 3.5, where no PI-SWERL samples could be taken, we used a similar As content as for unit 3.1 because the rock cover is almost 100% for these units and because the dust in these units is not affected by the underlying geologic deposits but is entirely created by settling airborne background dust. Note that because water was necessary to fractionate the samples to <10 µm, the water-soluble As concentrations are not included in these calculations. Therefore the As emission rates presented here are minimum values. The As emission rates ranged from a low of 9.74 x 10^{-18} g cm^{-2} s^{-1} in surface unit 3.5 (bedrock and/or outcropping petrocalcic horizons) to a maximum of 3.67 x 10^{-14} g cm^{-2} s^{-1} in surface unit 1.5 (outcrops of very fine sand and coarse silt). Emission rates for As were also high in the other units containing sand (1.1, 1.2, 1.3, 1.4 and 3.4; see Fig. 3).

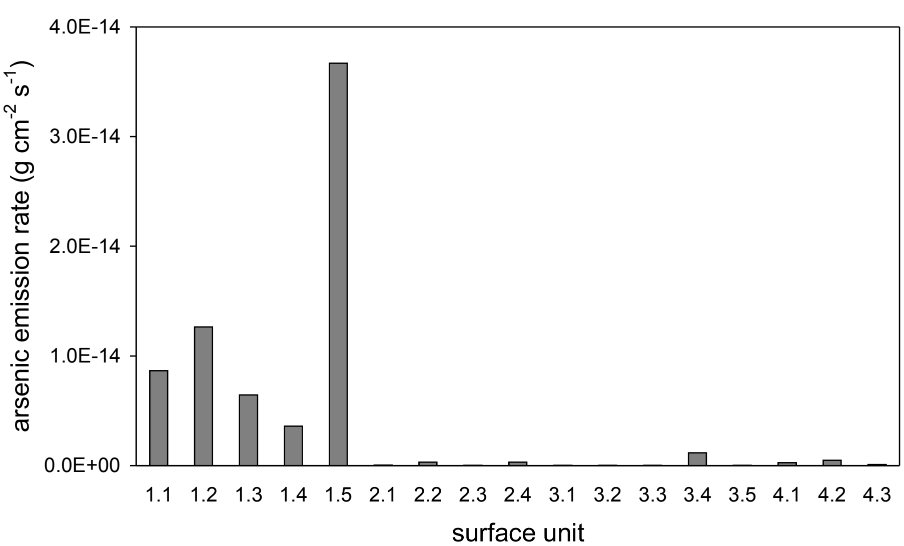

Fig. 3: Emission rate for arsenic during wind erosion. Data are for the fraction <10 µm (PM10).

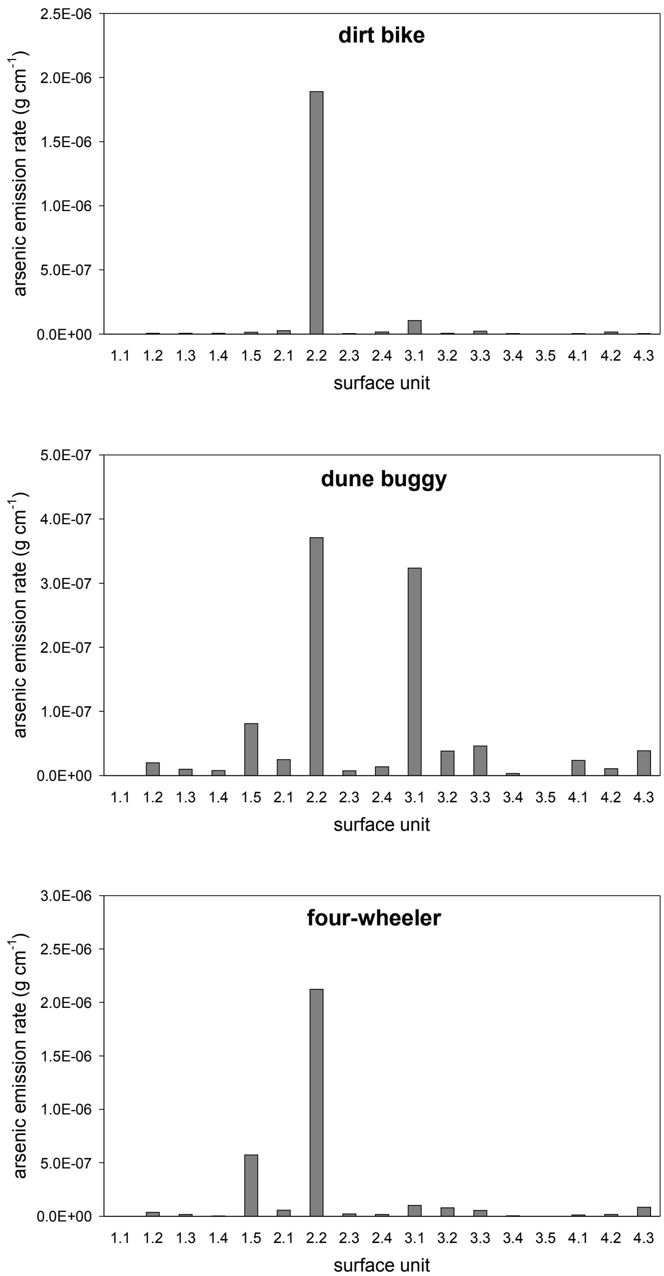

Fig. 4: Emission rate for arsenic during ORV activity: (a) Dirt bike; (b) Dune buggy; (c) Four-wheeler. Data are for the fraction <10 µm (PM10) and for an average driving speed of 30 km h^{-1}.

Similarly, we calculated PM10 emission rates for As resulting from ORV activities (Figs. 4a,b,c). These rates were calculated by multiplying the ORV emission rates for total PM10 dust (available from the study by Goossens and Buck, 2009) with the As concentration in the PM10 PI-SWERL samples. Again, water-soluble As concentrations are not included in these calculations and therefore the As emission rates are minimum values. The emission rates for each ORV activity were highest in surface units 2.2 (silt/clay with gravel) and 3.1 (desert pavements) and lowest in surface unit 3.4 (rock-covered surfaces with encrusted sand). High emission rates were also measured in surface unit 1.5 (mixture of fine sand and coarse silt) for the four-wheeler. The As emission rates ranged from 2.57×10^{-9} g cm^{-1} to 1.89×10^{-6} g cm^{-1} for dirt bikes, 3.08×10^{-9} g cm^{-1} to 3.71×10^{-7} g cm^{-1} for dune buggies, and 1.58×10^{-9} g cm^{-1} to 2.12×10^{-6} g cm^{-1} for four-wheelers. These rates are calculated for a driving speed of 30 km hr^{-1}, which is a conservative, but representative average for the NDRA. At higher driving speeds, emission rates are considerably higher. For example, for an average vehicle (average of a dirt bike, dune buggy, and four-wheeler), the emission rate nearly doubles at 40 km hr^{-1} (average rate of increase for all units together: 1.89 times), and at 50 km hr^{-1} more than triples (average rate of increase for all units together: 3.27 times).

The potential health effects of the dust generated during ORV use at the NDRA are not known because emissions vary greatly depending on what type of vehicle is used, how intensely an area is driven, and whether riders drive closely behind one another. Information regarding the exact number of drivers, the length of each drive and the specific routes followed is also unknown (Goossens and Buck, 2009). It is also important to note that the grain size distribution of the PI-SWERL released dust does not necessarily correspond to that of ambient dust. The PI-SWERL dust is locally eroded dust whereas ambient dust also contains particles that were eroded elsewhere and are in transport. Archived ambient dust samples that were previously collected at NDRA using BSNE samplers will be analyzed in the future to evaluate whether As concentrations are similar to those in the PI-SWERL samples. In order to determine the actual exposures, monitoring of personal dust exposure must be performed on ORV users under different driving conditions, and on other visitors at the site.

6. Conclusions

The concentrations of As in soil samples at NDRA are substantially higher (3.49 to 83.02 ppm) than in soils elsewhere in the United States (average ranges from 3.6 to 8.8 ppm); and throughout the world (averages range from 2.2 to 25 ppm) (McBride, 1994). There is no evidence to suggest that the As at NDRA is derived from anything other than natural geological processes. At NDRA, greater As concentrations are associated with finer grain-size fractions and areas that receive run-off. The As is likely being held on clay or Fe-oxide-hydroxide complexes, concentrated within soluble sodium and calcium arsenates, and/or other arsenic containing minerals including calcite and gypsum. High values of soluble As in some surface units explain the increased As concentration within dry arroyos. There is not a clear relationship between As concentrations and disturbed (i.e., ORV trails) versus undisturbed surfaces. It is hoped that future work will identify the mineral phases containing the As and further explain the geological history of As enrichment at the Nellis Dunes site.

Few studies have documented the As content in dust samples, and none have reported values as high as those reported in this study. Arsenic concentrations in emitted dust are much higher than As concentrations in the associated soil. For emitted PM10, the concentrations are, on average for all surface units, 4.5 times higher than in the soil. However, substantial differences occur between units. For sand units, the concentrations were 5 times or more greater for units 1.3, 1.4, and 1.5, and more than 10 times greater for units 1.1 and 1.2. Units rich in silt and poor in sand had the lowest enrichment rates of As compared to the associated soils (<2.5 times greater). Units dominated by rocks exhibited intermediate values. For coarser dust fractions (10-60 µm), the numbers are comparable, although the relationship with the type of unit is more subtle.

The highest concentrations of As measured in this study occurred in the samples from units 1.5 and 2.2. Arsenic concentrations in soil samples from these units were 46 and 83 ppm, respectively. Concentrations of As in PM10 emitted dust from these units were 290 and 161 ppm, respectively, and in the emitted 10-60 µm dust fraction, 312 and 139 ppm. Note that the actual As concentrations in the PM10 and 10-60 µm dust fractions are even higher because these values do not include the water-soluble As contents. These values are among the highest measured in the United States to date. These units are of special concern because unit 1.5 is highly susceptible to wind erosion and unit 2.2 is the unit with the highest dust production when subject to ORV driving.

Concentrations in all of the samples analyzed exceed the EPA's screening level (SL) of 0.39 $\mu g\ g^{-1}$ for As in residential soil by one to three orders of magnitude. The reported concentrations of As in all of the samples also exceed the EPA SLs considered to be protective of groundwater. Although the reported As concentrations exceed the EPA SLs, the potential risk to groundwater resources from leaching of As is considered to be minimal. This is because of the arid climate and groundwater in the Nellis Dunes area is deep (>30 m below ground surface). However, the high soluble concentrations of As are of potential concern because of the possible downstream contamination from runoff. Lake Mead, the source of drinking water for Las Vegas, is located hydrogeologically downgradient of the site.

The most important potential pathway for As exposure to humans at NDRA is through inhalation of dust. Arsenic has been strongly linked to a long list of diseases. Therefore, dust containing As will likely have increased health effects beyond those caused by PM10 size fractions alone. However, the potential for negative health effects to ORV operators, site visitors, and others exposed to emissions from NDRA is currently unknown because of several different factors. In order to accurately evaluate the potential health effects, monitoring of personal dust exposure must be performed on ORV users and other site visitors. The actual concentration of As in the air must also be quantified, since existing standards for As exposure in the workplace are based on the concentrations in air. Currently, there are no standards in the United States for As in recreational settings. There is also no information available regarding potential As concentrations in dust generated at the NDRA after it is transported downwind to Las Vegas and surrounding urban areas. Finally, toxicological analysis of the impact NDRA arsenic emissions exert on the human body, and a full risk analysis of all 17 surface units occurring in the NDRA, are required to define the health risk the arsenic at NDRA exposes to the population in Clark County

References

Abernathy, C.O., Liu, Y.P., Longfellow, D., Aposhian, H.V., Beck, B., Fowler, B., Goyer, R., Menzer, R., Rossman, T., Thompson, C., Waalkes, M., 1999. Arsenic: health effects, mechanisms of actions, and research issues. Environmental Health Perspectives 107, 593-597.

Bigham, J.M., Fitzpatrick, R.W., Schulze, D.G., 2002. Iron oxides. In: Dixon, J.B., Schulze, D.G. (eds):Soil Mineralogy with Environmental Applications. Soil Science Society of America, Madison, Wisconsin, 323-366.

BLM, 2004. Las Vegas Valley Disposal Boundary, Final Environmental Impact Statement and Record of Decision, Chapter 3: Affected Environment. Las Vegas Bureau of Land Management, Las Vegas, Nevada.

Bradford, G.R., Chang, A.C., Page, A.L., Bakhtar, D., Frampton, J.A., Wright, H., 1996. Background concentrations of trace and major elements in California soils. Kearney Foundation of Soil Science Special Report, p. 20.

Breit, G.N., Goldstein, H.L., Reynolds, R.L., Yount, J.C., 2009. Distribution of major anions and trace elements in the unsaturated zone at Franklin Lake Playa, California, USA. In: Oren, A., Naftz, D., Palacios, P., Wurtsbaugh, W.A. (eds.): Saline Lakes Around the World: Unique Systems with Unique Values. Natural Resources and Environmental Issues, vol. XV, S.J. and Jessie E. Quinney Natural Resources Research Library, Logan, Utah, USA, 93-103.

Chen, C.J., Chen, C.W., Wu, M.M., Kuo, T.L., 1992. Cancer potential in liver, lung, bladder, and kidney due to ingested inorganic arsenic in drinking water. British Journal of Cancer 66, 888-892.

Chen, M., Ma, L.Q., Harris, W.G., 1999. Baseline concentrations of 15 trace elements in Florida surface soils. Journal of Environmental Quality 28,1173-1181.

Connor, J.J., Shacklette, H.T., 1975. Background geochemistry of some rocks, soils, plants, and vegetables in the conterminous United States. Geological Survey Professional Paper 574-F, United States Government Printing Office, p. F27.

Di Benedetto, F., Costagliola, P., Benvenuti, M., Lattanzi, P., Romanelli, M., Tanelli, G., 2006. Arsenic incorporation in natural calcite lattice: Evidence from electron spin echo spectroscopy. Earth and Planetary Science Letters 246, 458-465.

Fernádez-Martínez, A., Cuello, G.J., Johnson, M.R., Bardelli, F., Román-Ross, G., Charlet, L., Turrillas, X., 2008. Arsenate incorporation in gypsum probed by neutron, x-ray scattering and density functional theory modeling. Journal of Physical Chemistry A 112, 5159-5166.

Goldstein, H.L., Reynolds, R.L., Reheis, M.C., Yount, J.C., Neff, J.C., 2008. Compositional trends in aeolian dust along a transect across the southwestern United States. Journal of Geophysical Research 113, F02S02. doi:10.1029/2007JF000751.

Goossens, D., Buck, B., 2009. Dust emission by off-road driving: Experiments on 17 arid soil types, Nevada, USA. Geomorphology 107, 118-138.

Goossens, D., Buck, B., 2010. Gross erosion, net erosion and gross deposition of dust by wind: field data from 17 desert surfaces. Earth Surface Processes and Landforms, doi: 10.1002/esp.2080.

Hering, J.G., Kneebone, P.E., 2002. Biogeochemical controls on arsenic occurrence and mobility in water supplies. In: Frankenberger, W.T. Jr. (ed): Environmental Chemistry of Arsenic. Marcel Dekker Inc., New York, 155-181.

Huerta-Diaz, M.A., Tessier, A., Carignan, R., 1998. Geochemistry of trace metals associated with reduced sulfur in freshwater sediments. Applied Geochemistry 13, 213-233.

Järup, L. 2003. Hazards of heavy metal contamination. British Medical Bulletin 68, 167-182.

Kozul, C.D., Hampton, T.H., Davey, J.C., Gosse, J., Nomikos, A., Eisenhauer, P., Weiss, D., Thorpe, J., Ihnat, M., Hamilton, J., 2009a. Chronic exposure to arsenic in the drinking water alters the expression of immune response genes in mouse lung. Environmental Health Perspectives 117, 1108-1115.

Kozul, C.D., Ely, K.H., Enelow, R.I., Hamilton, J.W., 2009b. Low-dose arsenic compromises the immune response to influenza A infection *in vivo*. Environmental Health Perspectives 117, 1441-1447.

Matera, V., Le Hécho, I., 2001. Arsenic Behavior in Contaminated Soils: Mobility and Speciation. In: Selim, H.M., Sparks, D.L. (eds): Heavy Metals Release in Soils. CRC Press, Boca Raton, Florida, 207-235.

McBride, M.B. 1994. Environmental Chemistry of Soils. Oxford University Press, New York, 327-328.

Olsen, C.E., Liguori, A.E., Zong, Y., Clark Lantz, R., Burgess, J.L., Boitano, S., 2008. Arsenic upregulates MMP-9 and inhibits wound repair in human airway epithelial cells. American Journal of Physiology - Lung Cellular and Molecular Physiology 295, L293-L302.

Pascua, C., Charnock, J., Polya, D.A., Sato, T., Yokoyama, S., Minato, M., 2005. Arsenic-bearing smectite from the geothermal environment. Mineralogical Magazine 69, 897-906.

Pye, K., Tsoar, H. 1990. Aeolian Sand and Sand Dunes. Unwin Hyman, London.

Reheis, M.C., Budahn, J.R., Lamothe, P.J., 2002. Geochemical evidence for diversity of dust sources in the southwestern United States. Geochimica et Cosmochimica Acta 66, 1569-1587.

Reheis, M.C., Budahn, J.R., Lamothe, P.J., Reynolds, R.L., 2009. Compositions of modern dust and surface sediments in the desert southwest, United States. Journal of Geophysical Research 114, FO1028.

Reid-Soukup, D.A., Ulery, A.L., 2002. Smectites. In: Dixon, J.B., Schulze, D.G. (eds.): Soil Mineralogy with Environmental Applications. Soil Science Society of America, Madison, WI., 467-499.

Reynolds, R., Breit, G., Goldstein, H.L., Yount, J., Morman, S.A., Reheis, M., Fulton, R., King, J., 2008. Dust from playas in the Mojave Desert, USA: Controls on metal contents and emission. Abstracts with Programs – Geological Society of America, Vol. 40, pp. 78, October 2008.

Román-Ross, G., Charlet, G., Cuello, G.J., Tisserand, D., 2003. Arsenic removal by gypsum and calcite in lacustrine environments. J. Phys. IV France 107, 1153-1156.

Spivey, S. 2008. Off-road fans, critics face off. Las Vegas Review-Journal 10B, Monday, March 17, 2008.

Tseng, C., Khim, C., Tseng, C., Hsueh, Y., Chiou, H., Tseng, C., Chen, C., 2003. Long-term arsenic exposure and ischemic heart disease in arseniasis-hyperendemic villages in Taiwan. Toxicology Letters 137,15-21.

USDA-NRCS, 2010. United States Department of Agriculture Natural Resources Conservation Service (USDA-NRCS), National Cooperative Soil Characterization Data. http://ssl.data.nrcs.usda.gov/

USEPA, 1996. United States Environmental Protection Agency, Office of Solid Waste, SW-846 test methods for evaluating solid waste, physical/chemical methods, method 3052: Microwave-assisted acid digestion of siliceous and organically based matrices. http://www.epa.gov/epaoswer/hazwaste/test/3_series.htm

USEPA, 2010. United States Environmental Protection Agency Regions 3, 6, and 9, April 10, 2010: Regional Screening Levels for Chemical Contaminants at Superfund Sites. http://www.epa.gov/reg3hwmd/risk/human/rb-concentration_table/index.htm

Van Pelt, R.S., Zobeck, T.M., 2007. Chemical constituents of fugitive dust. Environmental Monitoring and Assessment 130, 3-16.

von Ehrenstein, O., Mazumder, D., Hira-Smith, M., Ghosh, N., Yuan, Y., Windham, G., Ghosh, A., Haque, R., Lahiri, S., Kalman, D., Das, S., Smith, A., 2006. Pregnancy outcomes, infant mortality, and arsenic in drinking water in west Bengal, India. American Journal of Epidemiology 163, 662-669.

Chapter 11

EVALUATION OF IMMUNOTOXICITY FOLLOWING A 3-DAY EXPOSURE TO DUST SAMPLES COLLECTED FROM NELLIS DUNES RECREATION AREA

Deborah Keil[1] and Margie Peden-Adams[2]

[1]*Department of Pathology, University of Utah*
[2]*Harry Reid Center, University of Nevada Las Vegas*

1. Introduction

Epidemiologic studies have demonstrated an association between particulate matter (PM) and daily mortality (Dockery et al., 1994), increased emergency room visits and hospital admissions (Schwartz et al., 1993), or decreased pulmonary function (Boezen et al., 1998). In mouse models, repeated airway exposure of dust induces lung inflammation in the presence or the absence of allergen (Ichinose et al., 2005; Hiyoshi et al, 2005; Ichinose et al., 2006). Many of these studies have focused on urban sources of dust, where fine particles (aerodynamic diameters equal to or less than 2.5 µm; PM2.5) are the major type of dust exposure consisting of acid condensates, sulfate, and nitrate particles (Yang et al., 2005). However, few studies have examined the specific health risks associated with dust generated in non-urban areas, and even less is known about potential health risks to dust exposure while recreating in the desert.

Recent epidemiologic studies have shown that dust events are associated with an increase in daily mortality in Seoul, Korea, and Taipei, Taiwan (Kwon et al., 2002), and that these dust particles cause cardiovascular and respiratory dysfunction in Taipei (Chan, 2002). Furthermore, the PM2.5 and PM10 fractions of dust contains various metals (i.e., Pb, Cd, Zn, As, Mn, etc.). One study identified that ambient concentrations of PM2.5 and PM10 were not significantly associated with changes in peak expiratory lung flow rates, but that most of the metal concentrations bound to the particulates were significantly associated with decreases in pulmonary function (Hong et al., 2010). This study also reported similar potency in reduction of pulmonary function regardless of whether the source of metals on the dust particles was anthropogenic or natural occurring (Hong et al., 2010).

Understanding the chemical composition of PM exposure is key in determining health risks. In many cases, much is known about single metal toxicity, but little is known regarding exposure to complex metal mixtures. Although each metal exhibits unique toxicity, there are common toxic pathways to include mimicry, oxidative damage, and adduct formation with DNA or protein. Nonessential metals may mimic essential metals causing a disruption in cellular and enzymatic mechanisms. Examples include the replacement of essential zinc by cadmium, replacement of potassium by thallium, replacement of phosphates by arsenate, and mimicry of manganese in place of iron. Further, the generation of reactive oxidative species is often induced by metals in their ionic form, resulting in oxidative modification of DNA or proteins, including aberrant gene expression and carcinogenesis (Ballatori, 2002; Basalt, 2004).

Dust released from the Nellis Dunes Recreation Area (NDRA) consists of many metals at the parts per million level, adsorbed to PM10 or smaller particles (see Chapter 9). Therefore, an initial study was undertaken to examine the toxicological and histopathological effects following exposure to dust samples from NDRA.

2. Procedures

2.1 Dust collection and characterization

Samples were collected from 3 different surface units in the NDRA: unit 2.2 (silt and clay deposits with gravel), unit 3.1 (desert pavement with a silty Av horizon underneath), and unit 3.2 (rock-covered silt deposits). All dust was extracted from samples taken from the uppermost cm of the topsoil using a Soil Fine Particle Extractor (Goossens, 2011). This instrument enables one to select the finest fractions of the soil for analysis. Median diameter of the dust used in the tests was 4.2 µm (unit 2.2), 2.4 µm (unit 3.1), and 3.1 µm (unit 3.2).

Dust samples were acid-digested in the Environmental Soil Analytical Laboratory (UNLV) in accordance with EPA Method 3052 prior to total elemental analysis using inductively coupled plasma mass spectroscopy (ICP-MS) analysis. ICP-MS analyses were performed for the following elements: arsenic (As), cobalt (Co), chromium (Cr), cesium (Cs), copper (Cu), cadmium (Cd), nickel (Ni), lead (Pb), strontium (Sr), uranium (U), vanadium (V), thorium (Th), boron (B), molybdenum (Mo), selenium (Se), manganese (Mn), zinc (Zn), barium (Ba), titanium (Ti), iron (Fe), and aluminum (Al).

Concentrations of calcium (Ca), magnesium (Mg), potassium (K), and sodium (Na) were determined using atomic absorption spectroscopy (AAS). Phosphorus (P) concentrations were determined colorimetrically using molybdate-ascorbic acid method (Kuo 1996). To ensure quality control for the ICP-MS and AAS analyses, Buffalo River Sediment Reference Material 8704 was obtained from the National Institute of Standards and Technology (NIST), Gaithersburg, Maryland, USA. Samples of this material were digested in accordance with EPA Method 3052 and analyzed along with the NDRA samples. Satisfactory recoveries were found for the trace elements analyzed with the exception of Cs, Ba, Fe, and Al. Based on comparison with the Buffalo River standard, the concentrations of these elements were underestimated. It is likely that these results were underestimated because of interferences caused by high soluble salt concentrations in the samples and some insoluble mineral fluorides may have been formed during digestion (Kingston and Haswell, 1997). The analytical results are shown in Table 1.

2.2 Exposure route and dose

To learn about potential toxicological effects caused by acute exposure to NDRA dust, a standardized rodent exposure model and assays were utilized. B6C3F1 mice were exposed for 3 consecutive days to the dust extracted at 0, 0.1, 1.0, 100, or 1000 mg/kg/day. Intratracheal aspiration was the route of exposure used as it has several advantages over inhalation exposure (Driscoll et al, 2000). The small particle size, 4.3 micrometer in diameter or less (Table 1), is appropriate for the smaller size of the rodent while also relevant to human health concerns regarding exposure to small dust particles (i.e., PM2.5). Limitations of this type of exposure include that a bolus amount of dust is delivered as compared to smaller amounts over a period of hours or day.

As the level of dust exposure in humans is not known at NDRA, the exposures applied in this study ranged from a 0.1 to 1000 mg/kg/day to capture dose-responsive effects applicable to lower, reasonable levels that might be anticipated in human exposures at NDRA. This range was derived based on previous studies in the literature that have examined exposure to metal dust during welding activities (Anderson et al., 2007).

3. Results and discussion

3.1 Immunotoxicology

The plaque forming cell (PFC) assay and flow cytometric evaluation of lymphocytic subpopulations were assessed in this study. These two assays are recommended by the US Environmental Protection Agency (USEPA) when assessing risk of immunotoxicity

Table 1: Metal concentrations and median diameters for the dust extracts used in the mouse exposure study

	NDRA Samples			Buffalo River Sample (BRS)	
	Unit 2.2	Unit 3.1	Unit 3.2	BRS Value (µg/g)	BRS Reference Material 8704 (Provided value/range for SRM) (µg/g)
Median Diameter (µm)	4.30	2.40	3.10		
Metal Concentration (µg/g)					
As	142.48	24.89	23.19	16.64	17.000
Co	9.12	12.76	10.79	13.82	13.14 - 14.00
Cr	9.26	19.50	17.96	92.61	118.1 - 125.7
Cs	3.05	0.46	0.38	0.86	5.71 - 5.95
Cu	71.43	36.07	43.45	79.90	NP
Cd	0.34	0.46	0.65	3.90	2.65 - 3.23
Ni	17.97	29.21	27.09	40.92	39.2 - 46.6
Pb	23.52	23.04	18.26	159.47	133 - 167
Sr	182.76	125.60	106.39	51.74	NP
U	8.27	3.88	4.15	2.24	2.96 - 3.22
V	105.06	78.35	72.75	99.63	90.6 - 98.6
Th	2.18	3.15	0.49	3.83	8.91 - 9.23
B	41.19	51.50	50.04	73.19	NP
Mo	6.10	3.10	2.93	4.47	NP
Se	ND	ND	ND	ND	NP
Mn	274.52	428.12	419.21	482.70	523 - 565
Zn	68.20	92.13	86.18	323.74	393 - 423
Ba	641.75	296.86	72.34	152.69	400 -426
Ti	2411.07	3127.00	2647.99	4575.10	4370 - 4770
Fe	4949.43	9223.15	8865.79	26696.80	38700 - 40700
Al	8452.57	9745.57	6660.24	13538.97	59200 - 62800
Ca	40900.00	36020.00	100541.00	26400.00	25580 - 27240
Mg	40370.00	29620.00	45190.00	14450.00	11820 - 12180
K	22230.00	32000.00	28090.00	17730.00	19600 - 20420
Na	660.00	1130.00	1960.00	5880.00	5380 -5680
P	420.00	1280.00	1030.00	900.00	NP

Notes:
1. ND= Not Done
2. NP= Not Provided
3. SRM= Standard Reference Material

to humans. These two assays are known to be predictive of alterations in immune function (Luster et al., 1992, 1993). The standardized plaque forming cell (PFC) assay measures the ability to mount an IgM immune response to a foreign antigen, in this case, sheep red blood cells. The PFC response was dose-responsively suppressed beginning at 0.1 mg/kg/d exposure to map unit 2.2 and 1.0 mg/kg/d to exposure to map units 3.1 and

3.2 (Fig. 1). Flow cytometric studies identified dose-responsive decreases in splenic lymphocytic populations beginning at 0.1 mg/kg/d for map unit 2.2 and 1.0 mg/kg/d for map unit 3.1 (Fig. 2). No significant changes were detected with map unit 3.2 (Fig. 2). In these studies, the lowest observed adverse effect level (LOAEL) was determined to be 0.1 mg/kg/d for map unit 2.2 and 1.0 mg/kg/d for map units 3.1 and 3.2.

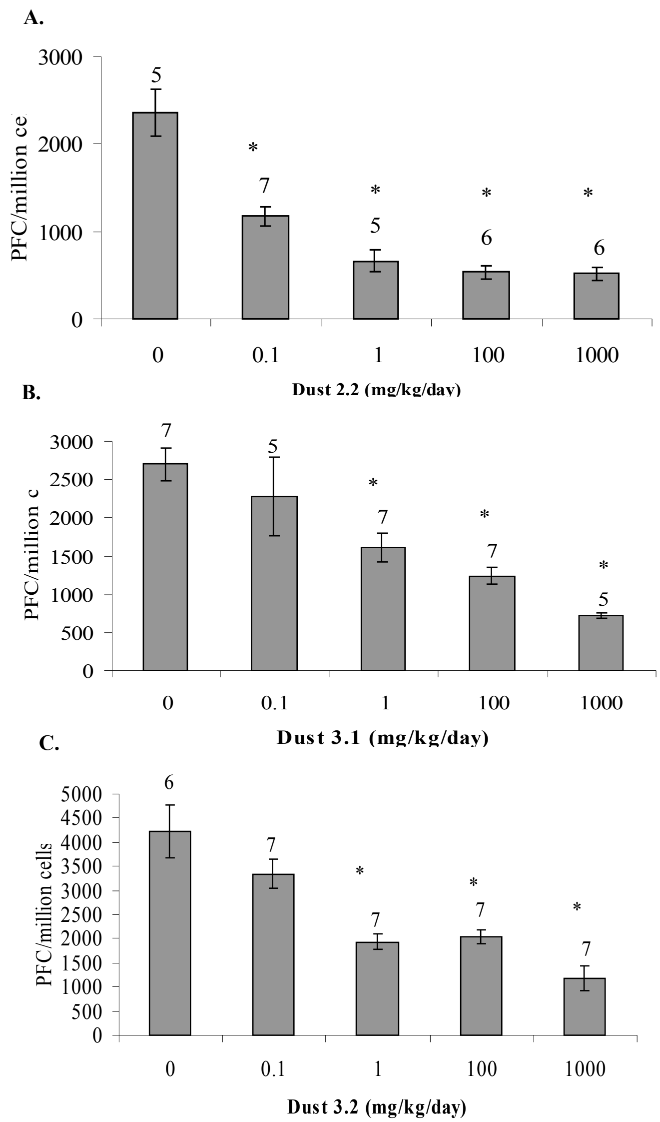

Fig. 1: Sheep red blood cell-specific-IgM antibody production in adult female B6C3F1 mice following intratracheal aspiration exposure to dust 2.2 (A), 3.1 (B), or 3.2 (C). Data are presented as mean ± SEM. Numbers above SEM bars indicate sample size. (*)Indicates significantly different from respective control ($p < 0.05$). Dust 2.2 = dust samples collected from unit 2.2. Dust 3.1 = dust samples collected from unit 3.1. Dust 3.2 = dust samples collected from unit 3.2.

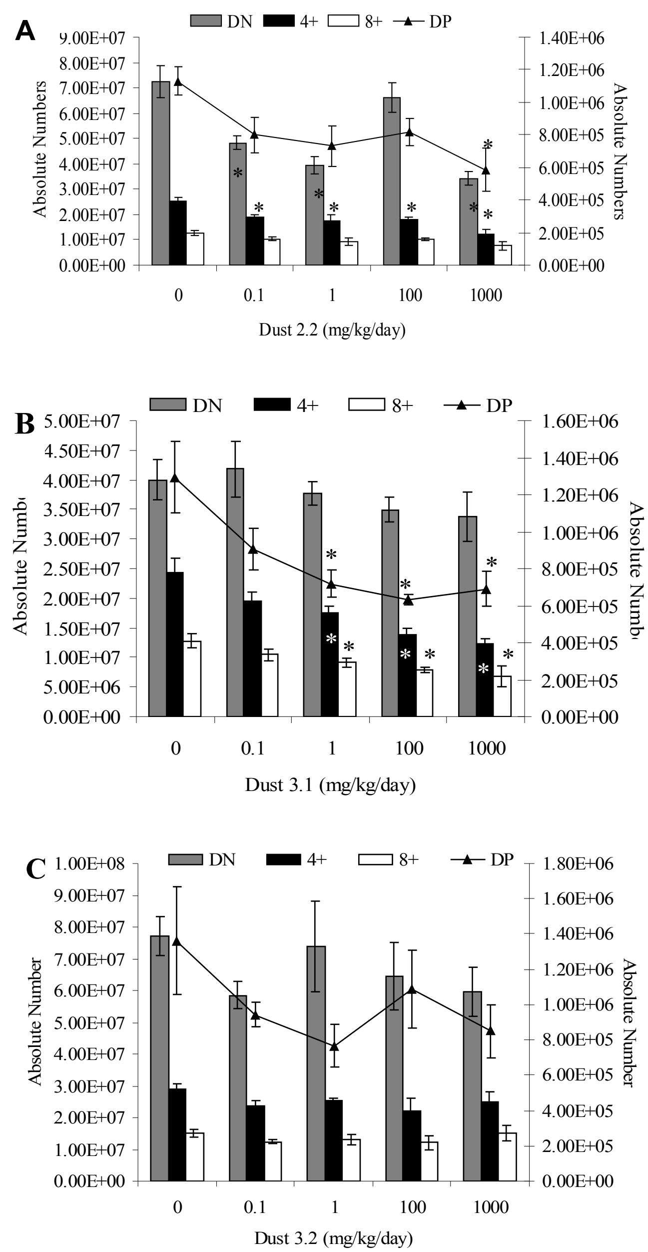

Fig. 2: Splenic T-cell populations (CD4CD8) in adult female B6C3F1 mice following intratracheal aspiration exposure to dust 2.2 (A), 3.1 (B), or 3.2 (C). Data are presented as mean ± SEM. Sample sizes for 0, 0.1, 1, 100, and 1000 mg/kg/day for dust 2.2 are 5, 7, 5, 6 and 6, respectively. Sample sizes for 0, 0.1, 1, 100, and 1000 mg/kg/day for dust 3.1 are 7, 5, 7, 7 and 5, respectively. Sample sizes for 0, 0.1, 1, 100, and 1000 mg/kg/day for dust 3.2 are 6, 7, 7, 7, and 7, respectively. (*)Indicates significantly different from respective control ($p < 0.05$). Double positive (DP; CD4+DC8+) cells are one the second axis. DN= Double negative cells (CD4-CD8-), 4+ = CD4+CD8-, 8+ =CD4-CD8+. Dust 2.2= dust samples collected from unit 2.2. Dust 3.1= dust samples collected from unit 3.1. Dust 3.2= dust samples collected from unit 3.2.

3.2 General toxicology

The most notable changes in body weight occurred at exposure levels of 100 or 1000 mg/kg/d (Fig. 3). Significant decreases in body weight occurred at the 1000 mg/kg/d exposure level for dust map units 2.2 and 3.1 (Fig. 3), while 100 and 1000 mg/kg/d exposure significantly decreased body weight following exposure to dust map unit 3.2. Significant changes in body weight suggest overt toxicity has occurred. It is important that overt toxicity is not present when defining a LOAEL. In this study, overt toxicity was not present at the LOAELs of 0.1 and 1.0 mg/kg/d established from the immunotoxicity data.

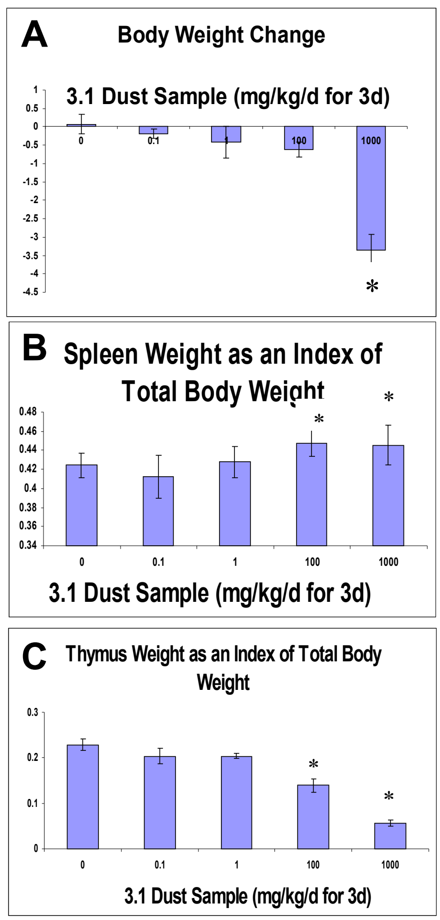

Fig. 3: Body (A), spleen (B) and thymus (C) weight in adult female B6C3F1 mice following intratracheal aspiration exposure to dust map unit 3.1 at levels of 0, 0.1, 1.0, 100 and 1000 mg/kg/d. Data are presented as mean $\pm$ SEM. (*)Indicates significantly different from respective control ($p < 0.05$). Spleen and thymus weight are represented an index to body weight (organ weight/body weight).

Thymus weight is often a sensitive target of environmental agents and in the current study, significant decreases in thymus weight were observed at 100 and 1000 mg/kg/d for dust map units 2.2 and 3.1 (Fig. 3), but only 1000 mg/kg/d for dust map unit 3.2 (data not shown). Thymus cellularity was consistent with changes in this organ weight in that the total cell counts were decreased at 100 and 1000 mg/kg/d for all map units tested.

Significant changes in liver weight (hepatic) were different for each of the map units examined in this study. For map unit 2.2, 100 mg/kg/d increased liver weight, while 1000 mg/kg/d decreased liver weight. For map unit 3.1, 1000 mg/kg/d exposure decreased liver weight (Fig. 4). Lastly, exposure to map unit 3.2 caused decreases in liver weight at 100 and 1000 mg/kg/d.

Kidney weight was unaffected following exposure to dust map units 2.2 and 3.2. However, dust exposure to map unit 3.1 caused significant increases in kidney weight at 100 and 1000 mg/kg/d (Fig. 4).

Overall, these data indicate that changes in body and organ weight occurred only in the 100 and 1000 mg/kg/d exposure groups. These changes were different for each map unit. As each map unit is a complex mixture with varying metal content, it is not surprising that alterations in organ weight also vary.

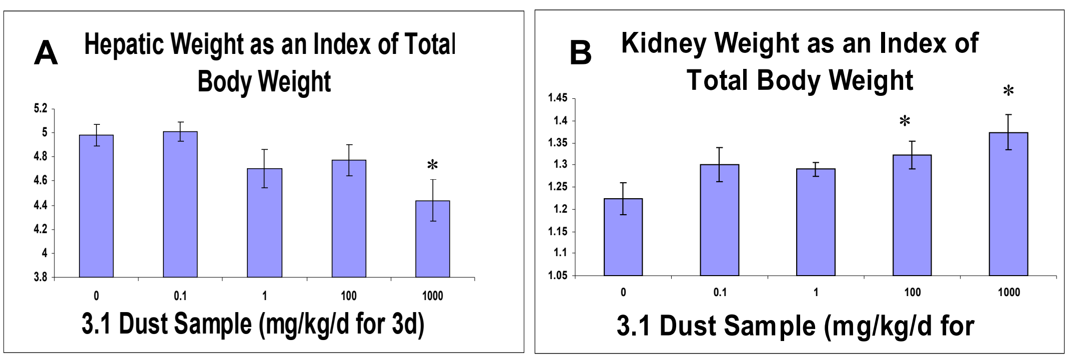

Fig. 4: Hepatic (A) and liver (B) weight in adult female B6C3F1 mice following intratracheal aspiration exposure to dust map unit 3.1 at levels of 0, 0.1, 1.0, 100 and 1000 mg/kg/d. Data are presented as mean $\pm$ SEM. (*)Indicates significantly different from respective control ($p < 0.05$). Organ weights are represented an index to body weight (organ weight/body weight).

3.3 Hematology

Peripheral white blood cell differentials were examined in the mice exposed to NDRA dust. No changes in distribution of cells were evident following exposure to dust map unit

3.2. Following exposure to map unit 2.2 and 3.1 (Fig. 5), changes were only evident at the highest exposure level, 1000 mg/kg/d. Due to minimal amounts of blood available for analysis, total white blood cell counts were not done.

3.4 Histopathology of lungs

Pulmonary histopathology was evident in mice that received dust from surface units 2.2, 3.1 or 3.2, but was restricted to the high dose groups (100 and 1000 mg/kg/d) from each site. The character of the lung lesions was similar among the different dust samples with greatest severity in the highest dose group. The principal morphologic lesion was a multifocal, centriacinar brochiolitis characterized by marked accumulation of dust-filled macrophages associated with interstitial fibrosis and a mixed inflammatory cell infiltrate of neutrophils, lymphocytes, and lesser numbers of eosinophils. Alveolar bronchiolarization and bronchiolitis obliterans were also common features of these lung lesions characteristic of pneumoconiosis.

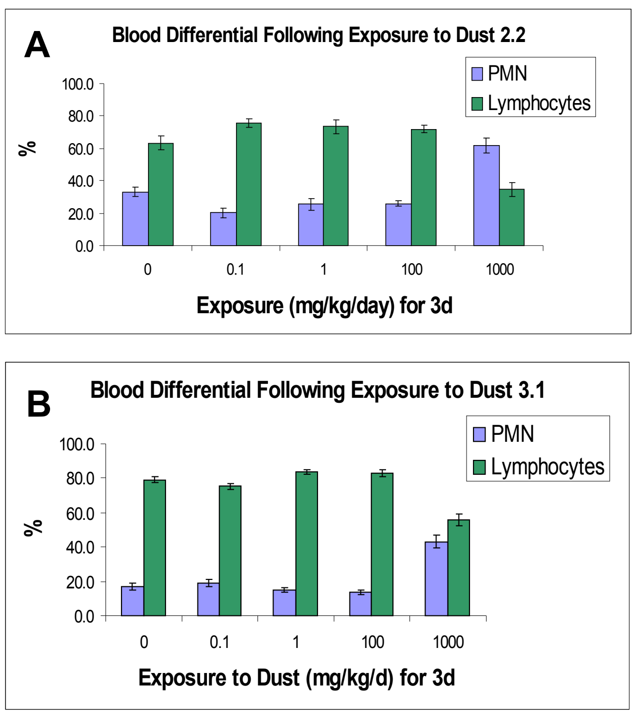

Fig. 5: Peripheral white blood cell differentials were performed on map units 2.2 (A), 3.1 (B) and 3.2 (data not shown). Significant changes were evident at the 1000 mg/kg/d exposure group only. Neutrophils (PMN) and lymphocytes are represented as these are the two primary cell population in the peripheral blood. No changes were observed following exposure to map unit 3.2 (data not shown).

4. Summary and conclusions

The level of human exposure to dust generated at the NDRA is not known. Therefore, a large dose-response range was utilized in these toxicology studies. Changes in immune function and suppression of humoral immunity were the most sensitive parameters affected by the surface units tested in this study. Immunotoxicity occurred at test exposures where no overt toxicity was indicated. The immunological parameters affected in this study are known to be predictive of increased disease susceptibility (Luster et al., 1992, 1993) and, therefore, are key to the maintenance of good health and disease resistance. The *LOAEL based on immunotoxicology parameters are 0.1 mg/kg/d for map unit 2.2 and 1.0 mg/kg/d for map units 3.1 and 3.2.* The present data indicate the need for further studies to characterize the potential risks to human health for exposure to dust from NDRA map units 2.2, 3.1, and 3.2.

Acknowledgements

We would like to acknowledge Nadia Ayala, Jennifer Berger-Ritchie, Stephanie LeBahn and Sharon Young for their assistance and expertise with this study.

References

Anderson, S., Meade, J., Butterworth, L.F., Munson, A., 2007. The humoral immune response of mice exposed to manual metal arc stainless steel-welding fumes. Journal of Immunotoxicology 4, 15-23.

Ballatori, N., 2002. Transport of toxic metals by molecular mimicry. Environmental Health Perspectives110, Supplement 5, 689-694.

Baselt, R.C., 2004. Disposition of Toxic Drugs and Chemicals in Man, 7th ed. Biomedical Publications, Foster City.

Boezen, M., Schouten, J., Rijcken, B., Vonk, J., Gerritsen, J., van der Zee, S., et al., 1998. Peak expiratory flow variability, bronchial responsiveness, and susceptibility to ambient air pollution in adults. American Journal of Respiratory and Critical Care Medicine 158, 1848-54.

Chan, C.C., 2002. Adverse health effects of China sandstorms in Taipei, Taiwan. Environmental Protection Administration, EPA-91-FA11-03-D036.

Dockery, D.W., Pope, C.A., 1994. Acute respiratory effects of particulate air pollution. Annual Review of Public Health 15, 107-132.

Driscoll, K.E., Costa, D.L., Hatch, G., Henderson, R., Oberdorster, G., Salem, H., Schlesinger, R.B., 2000. Intratracheal instillation as an exposure technique for the

evaluation of respiratory tract toxicity: Uses and limitations. Toxicological Sciences 55, 24-35.
Goossens, D., 2011. A method for dry extracting large volumes of fine particulate matter from bulk soil samples. Air Quality Atmosphere and Health, in press.
Hiyoshi, K., Ichinose, T., Sadakane, K., Takano, H., Nishikawa, M., Mori, I., Yanagisawa, R., Yoshida, S., Kumagai, Y., Tomura, S., Shibamoto, T., 2005. Asian sand dust enhances ovalbumin-induced eosinophil recruitment in the alveoli and airway of mice. Environmental Research 99, 361-368.
Hong, Y.C., Pan, X.C., Kim, S.Y., Park, K., Park, E.J., Jin, X, Yi, S.M., Kim, Y.H., Park, C.H., Song, S., Kim, H., 2010. Asian dust storm and pulmonary function of school children in Seoul. Science of the Total Environment 408, 754-759.
Ichinose, T., Nishikawa, M., Takano, H., Sera, N., Sadakane, K., Mori, I., Yanagisawa, R., Oda, T., Tamura, H., Hiyoshi, K., Quan, H., Tomura, S., Shibamoto, T., 2005. Pulmonary toxicity induced by intratracheal instillation of Asian yellow dust (Kosa) in mice. Environmental Toxicology and Pharmacology 20, 48-56.
Ichinose, T., Sadakane, K., Takano, H., Yanagisawa, R., Nishikawa, M., Mori, I., Kawazato, H., Yasuda, A., Hiyoshi, K., Shibamoto, T., 2006. Enhancement of mite allergen-induced eosinophil infiltration in the murine airway and local cytokine/chemokine expression by Asian sand dust. Journal of Toxicology and Environmental Health A 69, 1571-1585.
Kingston, H.M., (Skip), Haswell, S.J. (eds.), 1997. Microwave Enhanced Chemistry. Chapter 3: Environmental microwave sample preparation: fundamentals, methods and applications.American Chemical Society, Washington DC., 772 pp.
Kuo, S., 1996. In: Sparks, D.L. et al. (eds.). Methods of soil analysis. Part 3: Chemical Methods. SSSA Book Series 5, Soil Science Society of America, Inc. and America Society of Agronomy, Inc., Madison, 1390 pp.
Kwon, H.J., Cho, S.H., Chun, Y., Lagarde, .F, Pershagen, G., 2002. Effects of the Asian dust events on daily mortality in Seoul, Korea. Environmental Research 90, 1-5.
Luster, M.I., Portier, C., Pait, D.G., White, K.L., Gennings, C., Munson, A.E., Rosenthal, G.J., 1992. Risk assessment in immunotoxicology. I: Sensitivity and predictability of immune tests. Fundamental and Applied Toxicology 18, 200-210.
Luster, M.I., Munson, A.E., Thomas, P.T., Holsapple, M.P., Fenters, J.D., White, K.L. Jr, Lauer, L.D., Germolec, D.R., Rosenthal, G.J., Dean, J.H., 1988. Development of a testing battery to assess chemical induced immunotoxicity: National Toxicology Program's guidelines for immunotoxicity evaluation in mice. Fundamental and Applied Toxicology 10, 2-19.
Luster, M.I., Portier, C., Pait, D.G., Rosenthal, G.J., Germolec, D.R., Corsini, E., Blaylock, B.L., Pollock, P., Kouchi, Y., Craig, W., et al., 1993. Risk assessment in immunotoxicology. II:. Relationships between immune and host resistance tests. Fundamental and Applied Toxicology 21, 71-82.
Schwartz, J., Slater, D., Larson, T.V., Pierson, W.E., Koenig, J.Q., 1993. Particulate air pollution and hospital emergency room visits for asthma in Seattle. American Review of Respiratory Disease 147, 826-31.

Schwartz, J., Norris, G., Larson, T., Sheppard, L., Claiborne, C., Koenig, J., 1999. Episodes of high coarse particle concentrations are not associated with increased mortality. Environmental Health Perspectives 107, 339-342.

Yang, C.Y., Chen, Y.S., Chiu, H.F., Goggins, W.B., 2005. Effects of Asian dust storm events on daily stroke admissions in Taipei, Taiwan. Environmental Research 99, 79-84.

Chapter 12

LAND MANAGEMENT RECOMMENDATIONS FOR THE NELLIS DUNES RECREATION AREA

Dirk Goossens[1], Brenda Buck[1] and Brett McLaurin[2]

[1]*Department of Geoscience, University of Nevada Las Vegas*
[2]*Department of Geography and Geosciences, Bloomsburg University of Pennsylvania*

1. Introduction

This chapter summarizes the major results of the Nellis Dunes project and provides recommendations regarding dust emissions. Two types of processes contribute to dust emission in the Nellis Dunes area: wind erosion and off-road vehicular (ORV) activity. The amounts of dust produced annually by these two types of processes is almost identical, but in the Nellis Dunes area dust emission by wind erosion is much more difficult to control because these emissions are a natural phenomenon and because by far most of the emissions occur in the sand dunes, which are very active and extremely difficult to stabilize. Stabilization of the dunes is also ecologically not recommendable because it would result in the loss of a unique ecosystem near the city of Las Vegas. It would also result in the withdrawal of an area offering recreation to hundreds of thousands of people each year. Sand dunes are common landforms in a desert environment and it would be inappropriate to stop their natural development, except under exceptional circumstances in which they pose a hazard. If reductions in dust emissions at NDRA are desired, interventions should primarily focus on the off-road activities as these produce equal amounts of dust compared to wind erosion and are much easier to control. These interventions include measures related to the driving itself and measures related to restricting the geographic locations for ORV driving. This chapter discusses the interventions that are possible in the Nellis Dunes area. Interventions that may be practiced in other ORV areas but are not feasible in the Nellis Dunes area will not be discussed.

To provide a better background in understanding the significance and operation of the different measures proposed, an overview of the major results collected during the Nellis Dunes project is given below. This overview does not aim to provide the technical details but just summarizes the main facts. For a detailed discussion of each topic the reader is referred to the other chapters of this report.

2. Summary of major findings

2.1 Wind erosion

2.1.1 Emission balance

In the Nellis Dunes area all 17 surface units are net-emissive: i.e. there is always more emission than deposition. All units are therefore characterized by a negative sedimentation balance. However, large differences exist between the units. Table 1 shows the data for several grain size fractions.

Table 1: Net emission rates for dust emission by wind erosion for the 17 surface units, for sediment prone to long-term suspension (<20 μm), short-term suspension (20-60 μm) and modified saltation (60-100 μm).

surface unit	net emission rate by wind erosion (g m^{-2} year^{-1})		
	<20 μm (long-term suspension)	20-60 μm (short-term suspension)	60-100 μm (modified saltation)
1.1	118.32	193.44	2059.51
1.2	188.37	224.44	2169.64
1.3	92.94	92.90	506.17
1.4	85.32	22.83	484.21
1.5	81.84	92.75	184.79
2.1	0.23	1.52	2.56
2.2	1.03	4.23	3.34
2.3	0.60	1.70	1.21
2.4	7.96	21.19	24.33
3.1	0.60	3.54	3.98
3.2	0.31	3.09	4.28
3.3	0.48	3.03	7.85
3.4	23.58	36.10	242.02
3.5	0.17	1.56	1.50
4.1	1.70	8.66	6.76
4.2	5.74	29.22	57.53
4.3	0.48	2.74	3.46
sandy surfaces	113.36	125.27	1080.86
silty surfaces	2.46	7.16	7.86
rock-covered surfaces	5.03	9.46	51.93
drainages	2.64	13.54	22.59

2.1.2 Seasonal patterns

In NDRA most dust transport from natural wind processes takes place from mid April to mid May (Fig. 1). Dust transport is low from mid July to mid February, and intermediate in the remaining months. The evacuation rate is highest in spring (April-May) and in the fall (October), and lowest in summer (June-August) and in winter (January-February).

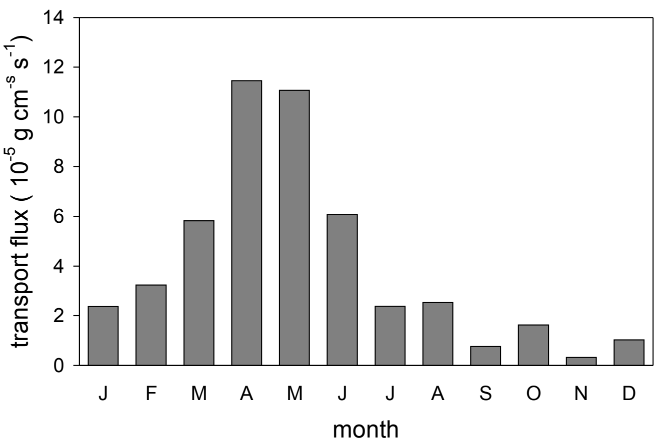

Fig. 1: Seasonal evolution of dust transport at NDRA. Data are for total suspendable dust (0-60 μm).

The silty, rocky and drainage surfaces produce most dust in the spring (April-May) and significantly less dust in summer (June-July). The sandy surfaces behave differently in that they are also highly emissive in the winter months (December-March) when the other surfaces are relatively stable. The contrast between winter-spring and summer-fall is much more pronounced for surfaces containing sand than for other surface types (Fig. 2).

2.1.3 Vulnerability of the surface units to dust emission

Under natural wind conditions, the units most vulnerable to dust emission (i.e., showing the highest emission rates) are the sandy substrata, followed by the rock-covered substrata and the drainages. Silty substrata with no, or only sparse rock fragments are the least naturally-emissive surfaces (Table 1).

The potential PM10 production by wind erosion is significantly higher in ORV trails than on undisturbed terrain (Fig. 3). ORV trails thus constitute a higher risk for wind erosion than undisturbed terrain. This is especially true for trails developed on silty surfaces, and less so for those in sand.

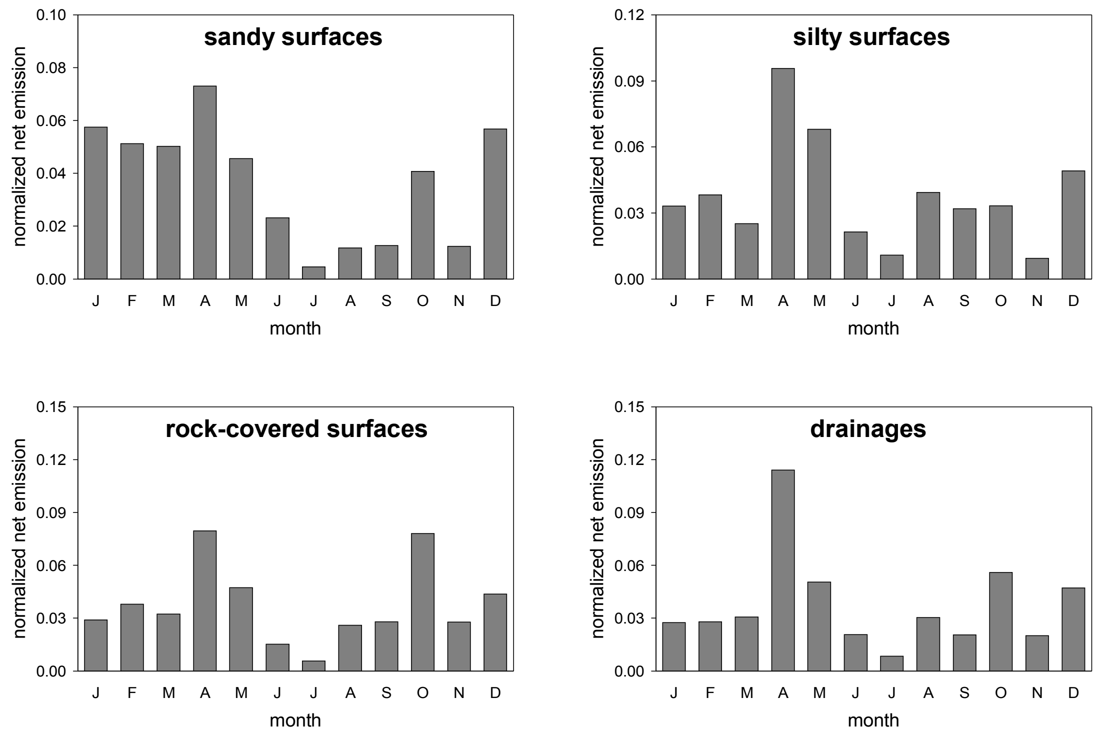

Fig. 2: Seasonal evolution of net emission in NDRA for the four categories of surfaces: sandy surfaces (units 1.1 to 1.5), silty surfaces (units 2.1 to 2.4), rock-covered surfaces (units 3.1 to 3.5), and drainages (units 4.1 to 4.3). Data are for total suspendable dust (0-60 µm).

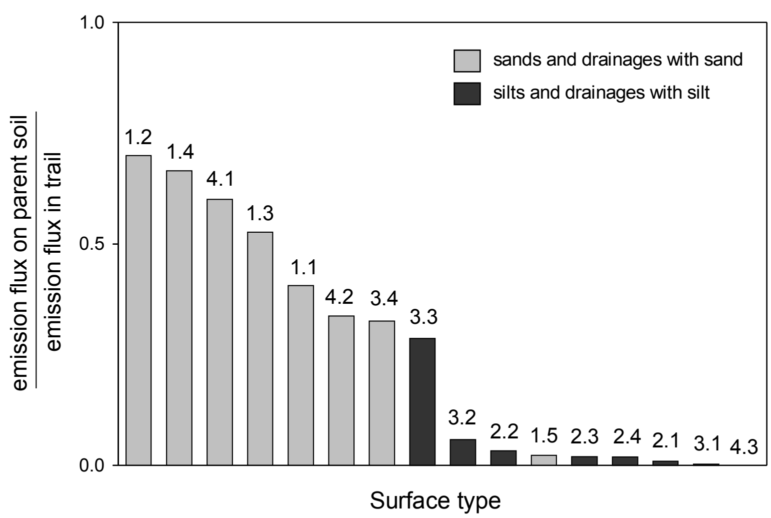

Fig. 3: Ratio of emission flux on undisturbed terrain to the emission flux in a trail, for the various surface units investigated

2.1.4 Initiation of emission: deflation threshold

In undisturbed surfaces, sandy substrata have a low deflation threshold (Fig. 4). They will start to erode and produce dust with rather low wind speeds, around 6 to 7 m s^{-1}. Undisturbed substrata composed of silt have higher deflation thresholds; they will only produce dust from wind speeds of 9-10 m s^{-1} or even higher, depending on whether they consist of pure silt or contain some minor sand. Undisturbed rock-covered surfaces may show high or low deflation thresholds depending on the textural composition of the underlying erodible fraction. Undisturbed drainages are characterized by higher deflation thresholds than their non-drainage equivalent because precipitated salts and carbonates cement and bind the particles.

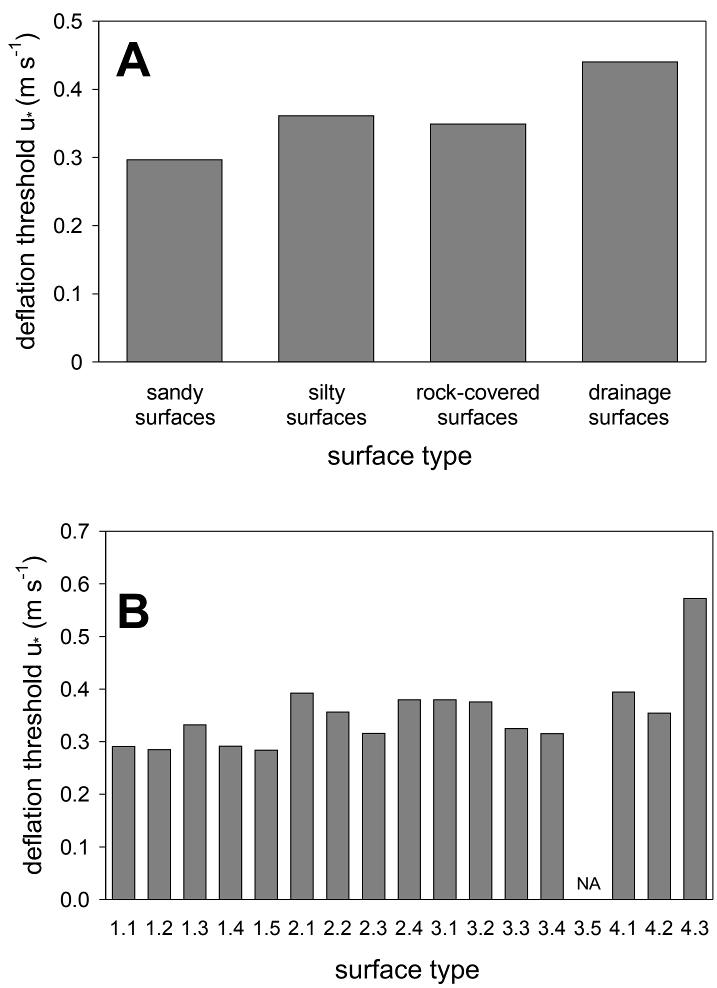

Fig. 4: Deflation threshold for (A) the 4 surface groups; (B) the individual surface units. Unit 3.5 was not measured because this unit consists of bedrock.

2.1.5 Productivity of the surface units

During wind erosion by far the most dust in NDRA is emitted in the loose, uncompacted sandy units 1.1 to 1.4 and in the rock-covered sands of unit 3.4 (Fig. 5). The most emissive areas are the partly vegetated sand dunes (unit 1.2). The unvegetated dunes (unit 1.1) produce significantly less dust. All undisturbed silty units, although very rich in dust, do not significantly contribute to net dust production in NDRA during wind erosion because their top layer is stabilized by surface crusts and/or rock cover. Unit 1.5 (mixture of sand and fine silt) is not an important supplier of dust in the NDRA because of its very limited occurrence and the presence of a physical surface crust. The relatively high production of unit 3.2 (rock-covered silt) is due to the high abundance (more than 56 % of the surface area) in NDRA.

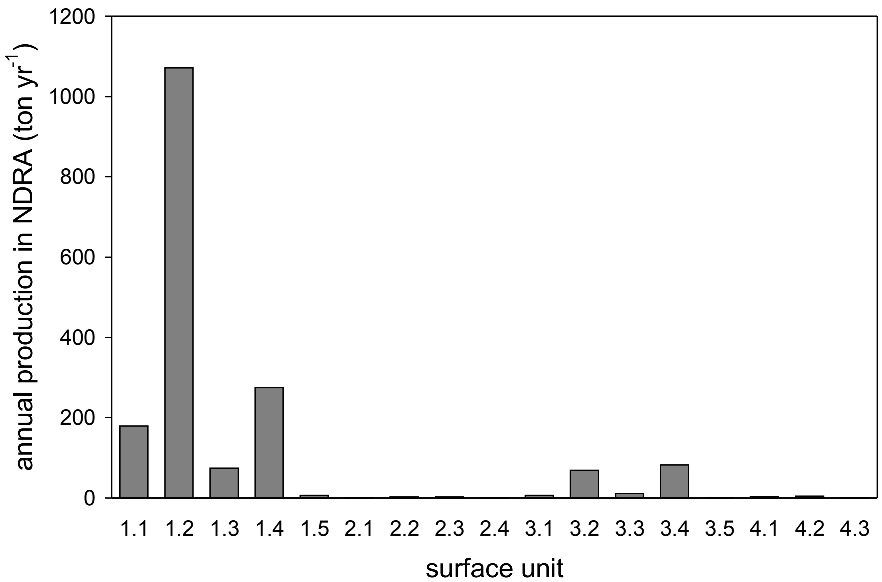

Fig. 5: Annual amounts of dust produced in NDRA by wind erosion for the 17 surface units. Data is for total suspendable dust (0-60 µm).

2.1.6 Grain size of the dust emitted

Airborne dust from wind erosion in NDRA is coarsest in winter (December-February) and gets finer until November. Dust emitted from sandy areas is considerably finer than dust emitted from silty areas, and even finer than dust emitted from rock-covered areas and drainages (Fig. 6).

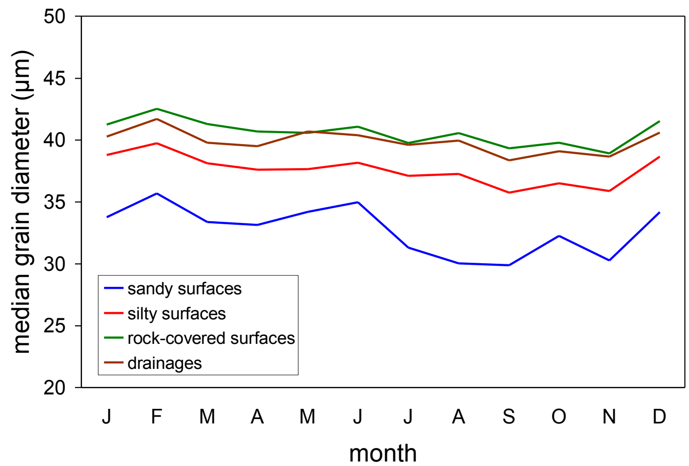

Fig. 6: Seasonal evolution of the median grain diameter of total suspendable airborne dust (0-60 µm). Average data for the four sampling heights of 25 cm, 50 cm, 75 cm and 100 cm.

2.1.7 Most easily eroded fractions

For non-sandy units in the Nellis Dunes area susceptibility to net erosion by wind is at a maximum for grains between 60 and 70 µm and decreases as particles become finer or coarser (Fig. 7). Undisturbed surfaces composed of sand show a continuous decrease in susceptibility with decreasing particle size down to approximately 30 µm. A diameter of maximum susceptibility to wind erosion around 70 µm no longer exists; instead, a narrow optimum occurs around 15 µm.

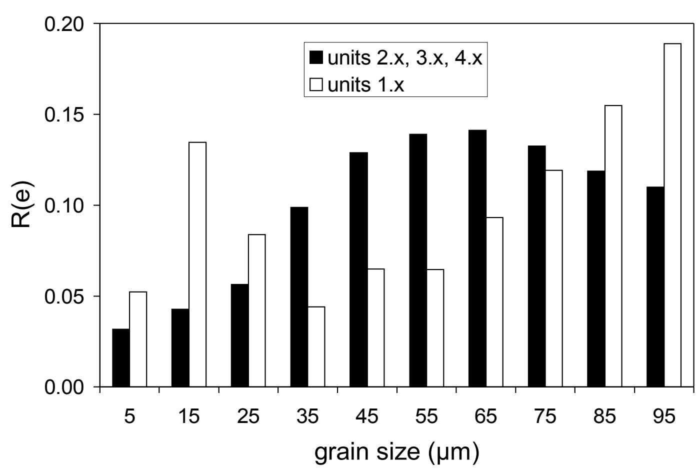

Fig. 7: Susceptibility of various grain size fractions to net erosion by wind, for the four categories of surfaces. The parameter *R(e)* in the ordinate is the ratio of the normalized number of grains net eroded to the normalized number of grains available in the top layer; the higher *R(e)*, the higher the susceptibility of the grains become.

2.2 Off-road driving

2.2.1 Dust production capacity

The areas with the highest capacity to produce dust during ORV driving are the silty and rock-covered silt substrata (Fig. 8), and especially units 2.2 (silt/clay with gravel) and 3.1 (desert pavements). The diagram in Fig. 8 shows the data for an average vehicle (average of a 4-wheeler, a dune buggy and a dirt bike), an average driving speed (30 km h^{-1}) and the total suspendable dust fraction (0-60 µm). This is a useful diagram because the surface units behave very similar for other combinations of the parameters. Sandy substrata and non-silt drainages produce much less dust during ORV activity. The units with the lowest capacities to produce ORV dust are 3.5 (bedrock) and 1.1 (unvegetated dunes). Note that vegetated dunes (unit 1.2) produce substantially more dust than unvegetated dunes (unit 1.1) when driven on by ORV vehicles.

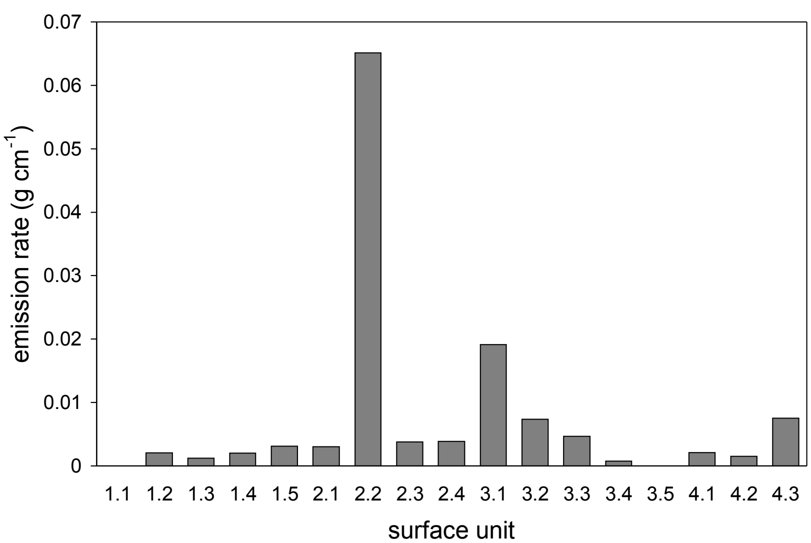

Fig. 8: Dust emission rate during off-road driving, for the 17 surface units in NDRA. Data is for total suspendable dust (0-60 µm) and refers to an average vehicle and an average driving speed of 30 km h^{-1}.

2.2.2 Comparison with wind erosion

Except for very coarse dust (>60 µm, which is not transported in suspension but in modified saltation) the annual amounts of dust produced in NDRA are comparable for off-road vehicular activity and wind erosion (Table 2). The data for wind erosion refer to the year 2008, which was a "normal" meteorological year (see Chapter 7); the numbers in

Table 2: Annual amounts of dust produced in NDRA by wind erosion and ORV activity

grain size fraction	dust produced by wind erosion (ton yr^{-1})	dust produced by ORV (ton yr^{-1})
0-10 µm (PM10)	394	372
0-20 µm (long-term suspension)	859	512
20-60 µm (short-term suspension)	935	1198
0-60 µm (total suspendable dust)	1794	1711
60-100 µm (modified saltation)	8726	1503

the table are therefore representative for the long-term situation at NDRA. The data for ORV are for an average vehicle (average of a dune buggy, a dirt bike and a 4-wheeler), for an average driving speed of 30 km h^{-1}, and for an average run length of 10 km. All these numbers are representative averages for the Nellis Dunes area, where drivers are making many turns and topography is quite complex keeping the driving speed and run length relatively low compared to other ORV areas in the USA.

2.2.3 Driving speed

Dust production by ORV vehicles increases considerably with the driving speed (Fig. 9). This result was found for all combinations of vehicle types and surface units. For most combinations the increase of emission was exponential; in a few cases the relationship was linear.

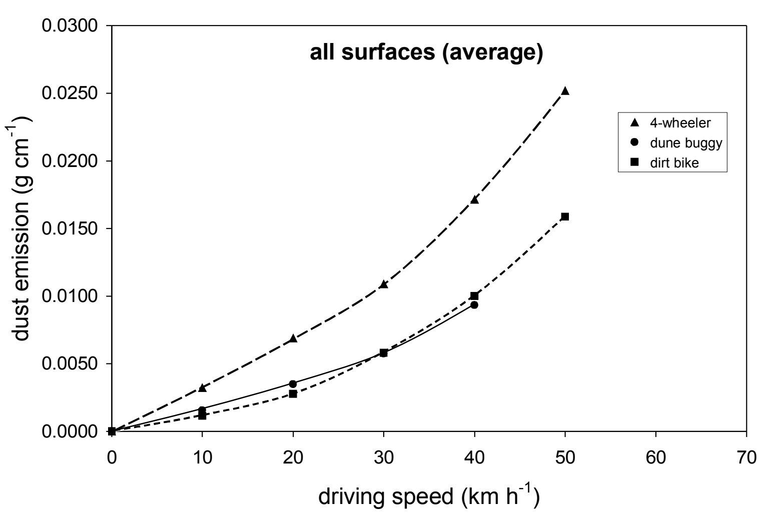

Fig. 9: Dust production by ORV vehicles as a function of driving speed. Data is for total suspendable dust (0-60 µm).

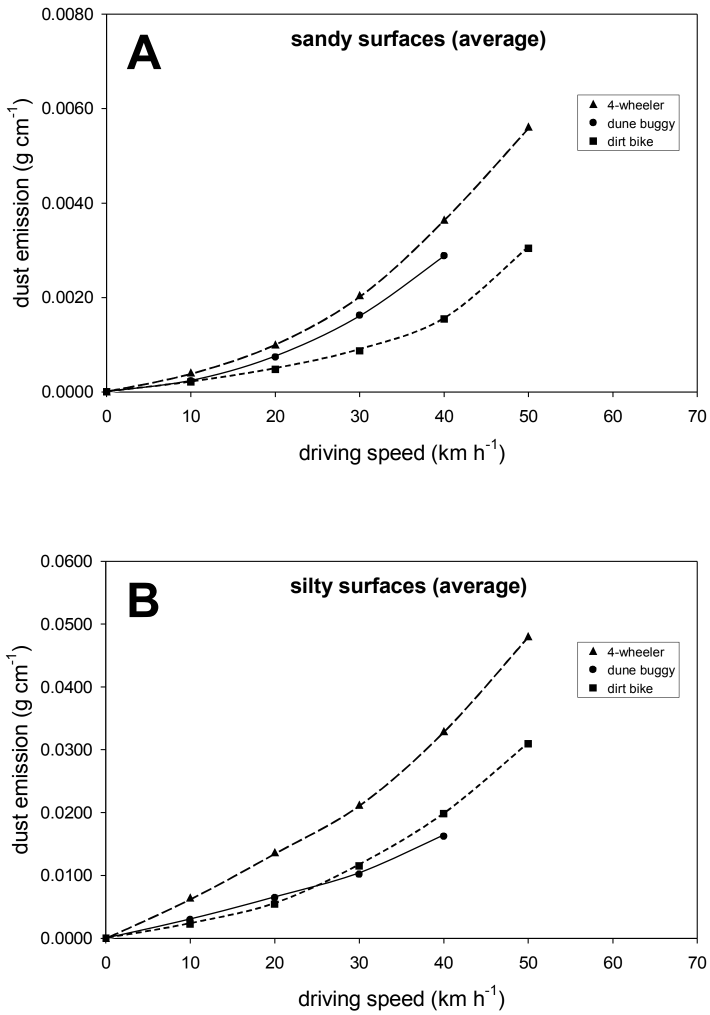

Fig. 10: Dust production by a 4-wheeler, a dune buggy and a dirt bike on (A) sandy surfaces; (B) silty surfaces. Data is for total suspendable dust (0-60 μm).

2.2.4 Type of vehicle

On all surfaces tested 4-wheelers produce the most dust. On sandy surfaces dune buggies produce more dust than dirt bikes (Fig. 10). The situation is the same for silty surfaces (with or without rock fragments) except for driving speeds below 25 km h^{-1} where dirt bikes are the second most emissive, and dune buggies are the least (Fig. 10). Because the average driving speed at NDRA is approximately 30 km h^{-1} for all surfaces, overall, the most dust-productive vehicle at the site is the 4-wheeler followed by the dune buggy and the dirt bike.

2.2.5 Deflation thresholds in ORV trails

ORV driving decreases the deflation threshold on silty surfaces and in drainages, but increases the threshold on sandy surfaces (Fig. 11). This means that it takes less wind to generate dust emissions after silty surfaces and drainages have been disturbed by ORV driving. In contrast, sandy surfaces require more wind to initiate dust emissions after ORV driving because the disturbance has increased compaction of the sand. However, local factors, especially irregularities in the local topography due to incisions in and by the trails, also affect the deflation threshold.

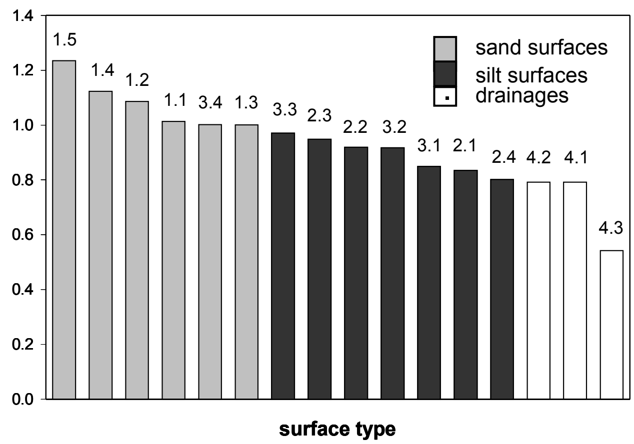

Fig. 11: Ratio of deflation threshold u_{*t} in a trail to the deflation threshold on undisturbed terrain, for the 17 surface units investigated

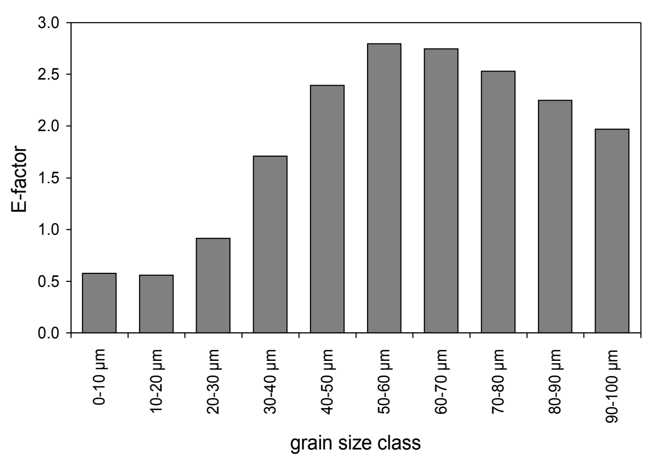

Fig. 12: Susceptibility of various grain size classes to dust production by off-road driving. The E-factor in the ordinate is the ratio of the proportion of a class in emitted dust to the proportion of that class in the top layer; the higher the E-factor, the higher the susceptibility of the grains become.

2.2.6 Most easily emitted fractions

During ORV driving the susceptibility to emission is greatest for grains between 60 and 70 µm (Fig. 12). These particles are the most easily emitted during ORV driving.

2.2.7 Effect of ORV driving on the grain size distribution in a trail

Continuous off-road driving in a trail leads to a progressive coarsening of the top layer in the trail (Fig. 13). Except for the aggregated silt deposits (unit 2.3) the sediment in the trails is consistently coarser than the one emitted, which means that the trails become coarser with time. However, the speed of coarsening depends on the type of surface. Trails in drainages coarsen the most rapidly, and trails on sandy surfaces coarsen faster than trails on silty surfaces. The deviant behavior of unit 2.3 is caused by the pulverization of the aggregates in this unit during ORV driving and is not representative for the other 16 surface units in NDRA.

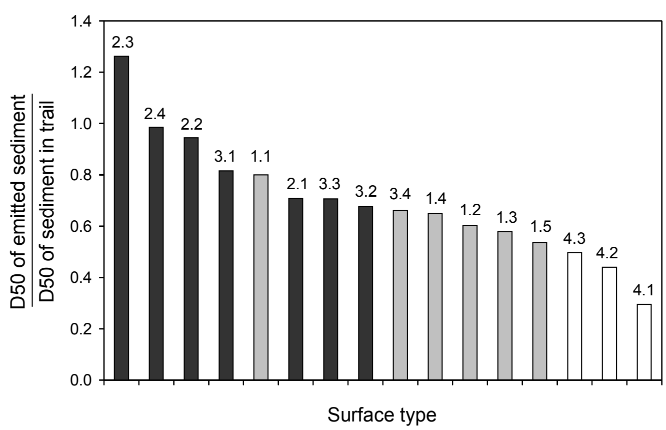

Fig. 13: Ratio of median grain diameter (D50) in ORV-emitted sediment to the median grain diameter in the trail, for the various surface units investigated

2.2.8 Surface characteristics affecting dust emissions by ORV

In contrast to wind erosion, where many surface characteristics such as texture (percentage silt, sand and clay), the presence of rock fragments (rock cover, rock content of the top layer) and the presence of surface crusts (either physical or biological crusts) strongly affect the emission of dust, for ORV-generated emission only texture plays an important role. The silt and clay content in the topsoil determines the size of the reservoir of dust available for emission. The other soil factors do not affect dust production by ORV activity because ORV driving is a very destructive process that neutralizes any protective effects these factors offer to the topsoil.

2.2.9 Creation of new trails

Creation of new ORV trails should be avoided in areas where the topsoil consists of silt or rock-covered silt. These surfaces produce only very small amounts of dust when undisturbed, but become great emitters once disturbed. By far the most vulnerable type of surface is the desert pavement (unit 3.1, see Fig. 14). Silty drainages (unit 4.3) also show significantly increased emissions once disturbed by ORV activity. In contrast, sandy surfaces do not increase emissions after disturbance by ORV activity. Therefore, when looking at the quantity of dust emissions alone, new ORV trails in sandy areas are acceptable but ORV activities should be avoided in silty areas, especially desert pavements, and in silty drainages.

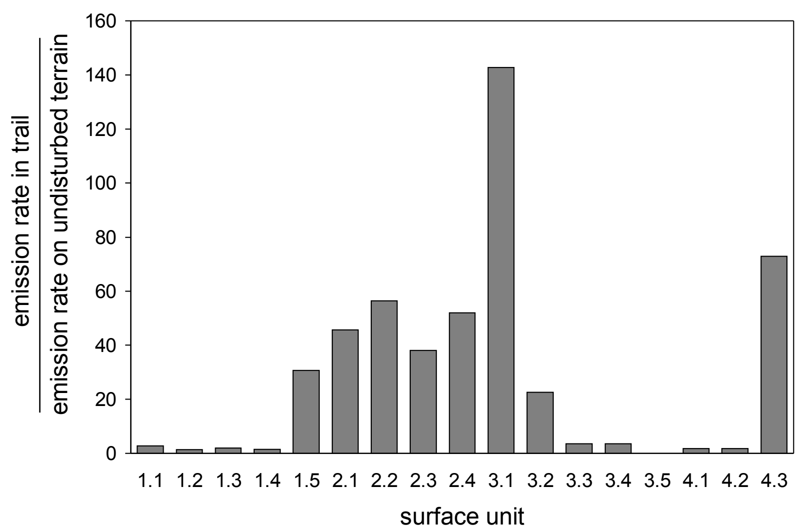

Fig. 14: Ratio of emission rate in an ORV trail to the emission rate on undisturbed land.

2.2.10 Distribution of ORV trails in NDRA

ORV trails occur in all parts of the Nellis Dunes Recreation Area, but are particularly abundant in the northwest and the center-west (Fig. 15). These zones are located near the two main entrances of the NDRA and are easily accessible to the public. The northwest zone of high trail density is located in an area of complex assemblage of surface units and topography. Nearly all surface units occur in this area. The zone in the center-west is predominantly sandy and includes the majority of the vegetated and unvegetated dunes.

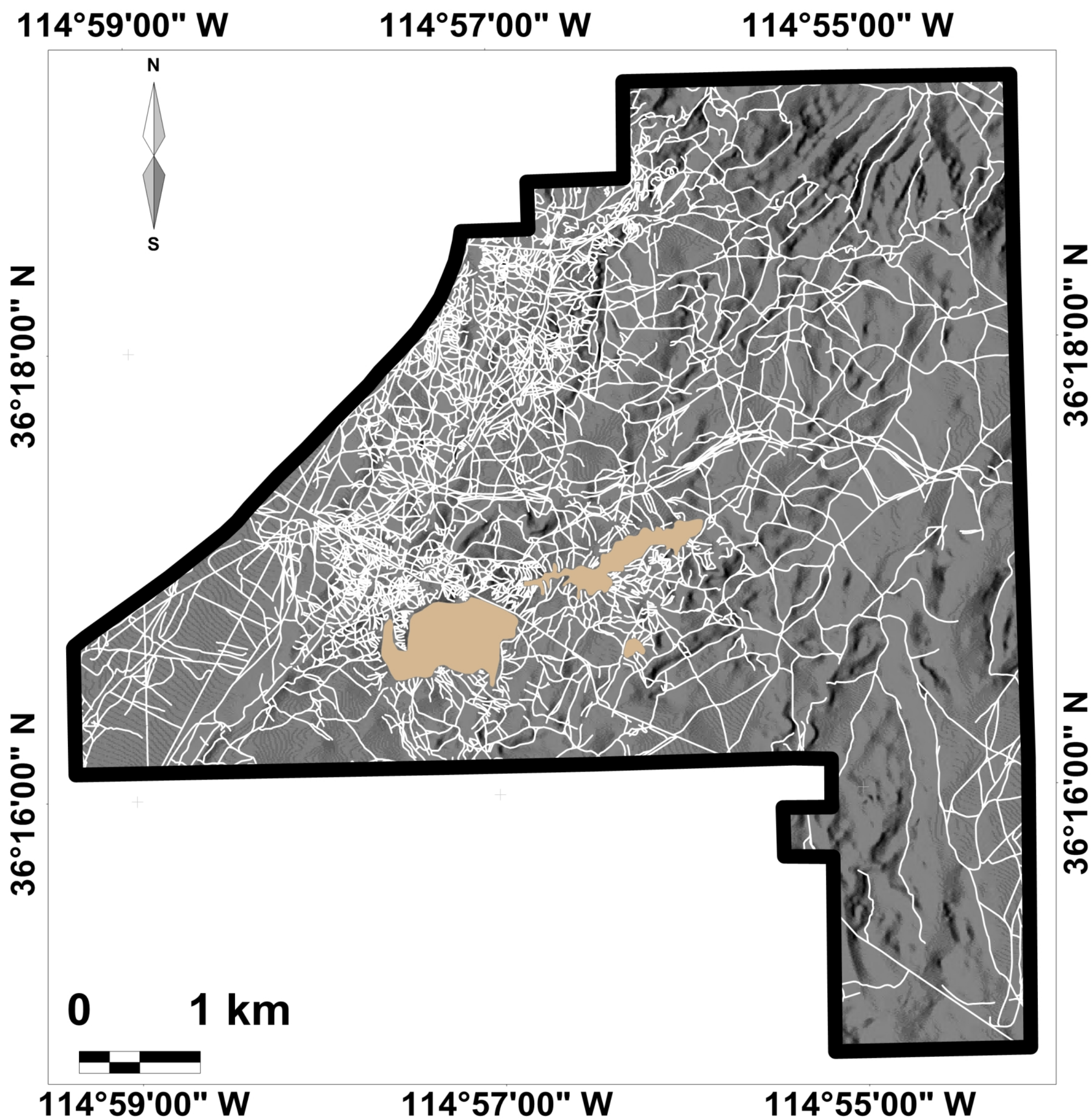

Fig. 15: Location of the ORV trails in the Nellis Dunes Recreation Area. Areas underlain by sandy units often show abrupt termination of trails, especially within the more active dunes (unit 1.1 and, to a lesser extent, unit 1.2). The movement of windblown sand buries any trails generated from off-road driving. These areas are delineated by the brown shading.

The unit with the longest length of trails in NDRA is unit 3.2 (rock-covered surfaces with silt and clay). More than 38 % of the trails are developed on these surfaces (Fig. 16). Trails are also abundant in the units 1.2 (vegetated dunes), 1.4 (patchy layers of thin sand), 3.3 (rock-covered surfaces with sandy loam), and unit 1.1 (unvegetated dunes) but in the latter the trails do not preserve well due to being quickly covered by windblown sand. Their actual length in this unit could thus not be determined from the satellite imagery but is likely comparable to units 1.2, 1.4 and 3.3.

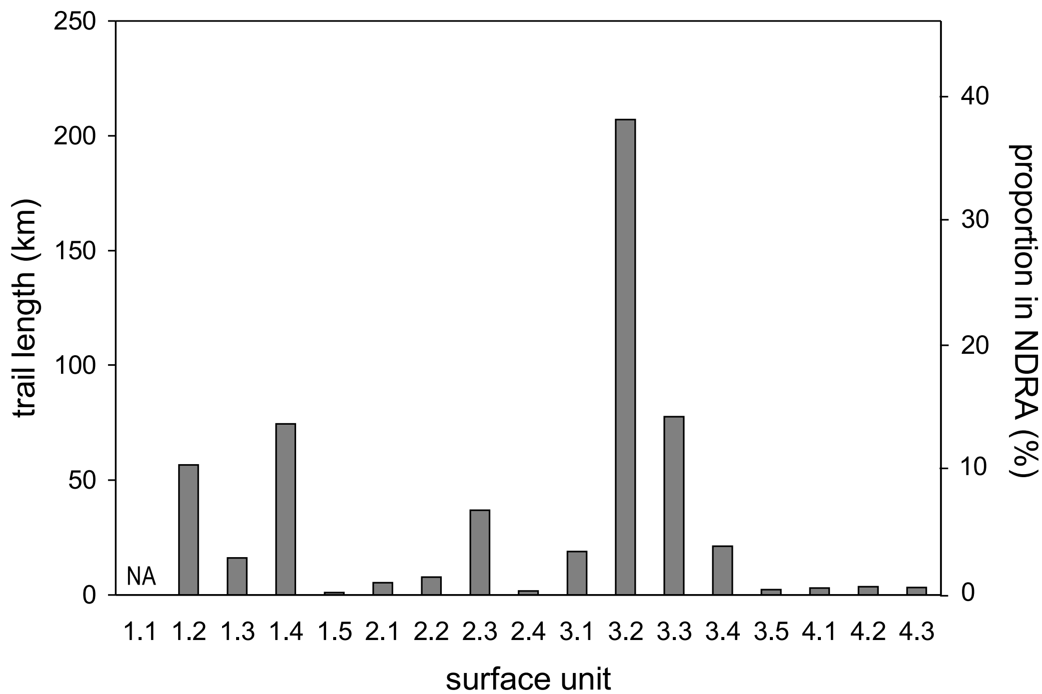

Fig. 16: Length of ORV trails in the 17 surface units in the Nellis Dunes area.

2.2.11 Total (wind erosion + ORV) dust production in NDRA

At low ORV driving speeds it is mainly the sandy substrata that produce most dust in NDRA, because emissions from natural winds dominate (Fig. 17). With increasing ORV driving speeds the silt and silt/rock areas become important sources. For the two suspension fractions (0-20 µm and 20-60 µm) the contributions to dust production of the silty areas are equal or exceed those of the sandy areas from a driving speed of approximately 30-40 km h^{-1} and greater. In contrast, for coarse dust (60-100 µm) the sandy areas supply the most dust for all speeds tested.

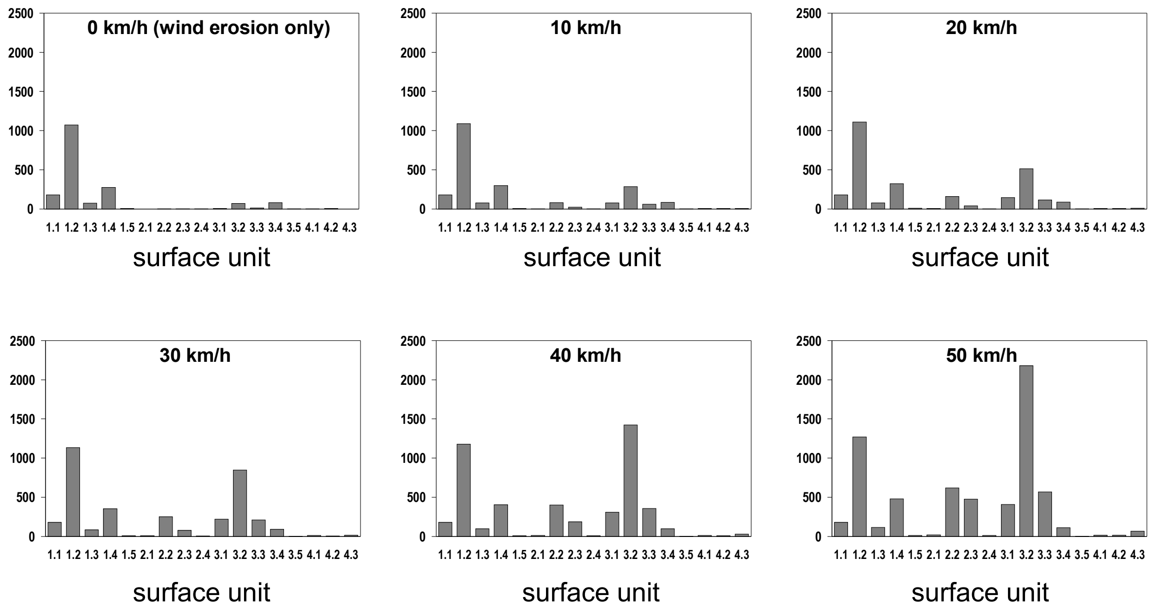

Fig. 17: Annual dust emission (wind erosion + ORV) at Nellis Dunes Recreation Area. Data are for total suspendable dust (0-60 µm).

2.3 Chemistry and mineralogy

Concentrations of most of the trace elements analyzed are higher in the finest fractions (PI-SWERL samples) as compared to the coarser fractions (soil samples). Highly reactive smectite minerals occur in the finest fractions and increase retention of metals there as compared to the coarser fractions.

Soils at NDRA contain minerals common to this region: quartz, calcite, plagioclase, kaolinite, smectite, gypsum, mica/illite, and palygorskite. Of these, the minerals that have been previously found to have health effects when inhaled include quartz, kaolinite, illite, smectite, and palygorskite. Palygorskite is of special concern because it commonly crystallizes in an asbestiform morphology. In the finest fractions, palygorskite is relatively more abundant in the sandy areas and parking lots, but is present in every unit except 2.2 and 2.3.

Except for arsenic, the concentrations of trace elements in the soil and PI-SWERL samples generally fall within normal ranges. The concentrations of As in soil samples at NDRA are substantially higher than in soils elsewhere in the United States and throughout the world. On average, arsenic concentrations in the airborne PM10 fraction are 4.5 times higher than in the soil. The highest concentrations of As measured in this study occurred in the samples from units 1.5 and 2.2. Arsenic concentrations in soil samples from these units were 46 and 83 ppm, respectively. Concentrations of As in PM10 emitted dust from these units were 290 and 161 ppm, respectively, and in the emitted 10-60 μm dust fraction, 312 and 139 ppm. These values are among the highest measured in the United States to date.

The highest concentrations of As in *PI-SWERL* samples occurred in surface units 1.5, 2.1, 2.2 and all drainages (surface units 4.1 to 4.3). The highest concentrations of *water-soluble arsenic in PI-SWERL* samples occurred in two of the drainages (surface units 4.2, 4.3), the silt/clay areas (2.1, 2.2, 2.4) and surface unit 1.5.

2.4 Toxicological results

A preliminary study was carried out to partially asses health risks on airborne samples derived from 3 map units: 2.2 (high arsenic and high ORV emissions), 3.1 (high ORV emissions and a measurement of 'background dust' because these desert pavements contain an Av horizon formed from thousands of years of dust accumulation), and 3.2 (map unit with the greatest surface area at NDRA). *In vivo* experiments were conducted in mice to examine the toxicological and histopathological effects following exposure to dust samples collected from the 3 map units tested. Changes in immune function and suppression of humoral immunity were the most sensitive parameters affected by the dust tested in this study. Immunotoxicity occurred at test exposures where no overt toxicity was indicated. The immune parameters' effects are known to be predictive of increased disease susceptibility and, therefore, are key to the maintenance of good health and disease resistance. The lowest adverse effect level (LOAEL) based on immunotoxicology parameters are 0.1 mg/kg/day for map unit 2.2 and 1.0 mg/kg/day for map units 3.1 and 3.2. As these values are lower than preliminary exposure estimates for humans, the present data indicate the need for further studies to characterize the potential risks to human health for exposure to dust from NDRA map units 2.2, 3.1, and 3.2.

3. Risk maps for the Nellis Dunes Recreation Area

Risk maps for the Nellis Dunes area were produced for a number of parameters relevant to dust emission. These maps were generated by combining numerical data collected during field or laboratory measurements with the areal data from the surface unit map. All patterns depicted on the risk maps are based on average numbers, collected from a large number of measurements. The maps related to dust emission by wind erosion are based on continuous measurements carried out during one complete, meteorologically "normal" year. At least 4 locations in the Nellis Dunes area were investigated for each surface unit, and the differences between these locations were usually very small. The maps related to ORV emissions are based on 3684 test runs with ORV vehicles. The patterns shown by the maps are therefore very reliable. The reliability is further increased because the data are grouped into classes. Working with classes makes it possible to remove any small, non-significant and non-representative small-scale spatial variations in the patterns so that the general picture is adequately displayed. What is essential in the maps is the qualitative picture; the quantitative picture is only of secondary importance and all risk maps were constructed with that goal in mind. The main aim of the maps is to display the ranking of the 17 surface units for the parameter shown, and the spatial pattern resulting from that ranking. This allows one to instantly distinguish between zones at NDRA that are of concern for the parameters shown by the maps and those that are not.

From what is explained above it directly follows that the numbers (values) used to delineate the risk classes on the map may vary according to the grain size fraction for which the risk is shown; numbers have been chosen such that the spatial patterns are optimally displayed.

The risk maps presented in this chapter only depict the risk for the parameter shown in the maps. They do not provide information on potential health risks associated to this parameter. For such information a separate study is required.

The risk maps produced during this project are presented and briefly discussed below. An electronic 1:10,000 version is available for each map and copies are available upon request.

3.1 Risk maps for dust emission caused by off-road vehicular activity

For ORV-generated emissions in NDRA, the following six risk classes were defined: highly emissive, very emissive, emissive, moderately emissive, slightly emissive and stable. Risk maps were constructed for 3 size classes of dust: <20 µm, 20-60 µm and 60-100 µm. These 3 classes were selected based on the mode of transport of the particles: long-term suspension (<20 µm; particles can travel tens to hundreds of km after being released), short-term suspension (20-60 µm; particles usually travel several km to several tens of km after being released), and modified saltation (60-100 µm; particles usually travel several tens to at maximum several hundreds of m before settling to the surface again). For a justification of the threshold values of 20, 60 and 100 µm we refer to Chapter 6 of this report. Particles >100 µm were not considered because most of these particles are transported in saltation, stay close to the surface, and are very unlikely to create specific health problems at NDRA.

To facilitate comparisons of the emission risk for the three dust classes we present the maps in a single figure (see Fig. 18).

There are nearly no differences between the two finest fractions whereas the pattern for 60-100 µm is substantially different, at least in the western part of the NDRA (Fig. 18). However, in all three maps, the most emissive units are always 2.2 (silt and clay surfaces with gravel) and 3.1 (desert pavements). The 2.2 units cover only a small portion of the land in NDRA and occur as patchy spots, especially in the east. However, they occur within some of the mostly heavily used areas for ORV activity. The desert pavements

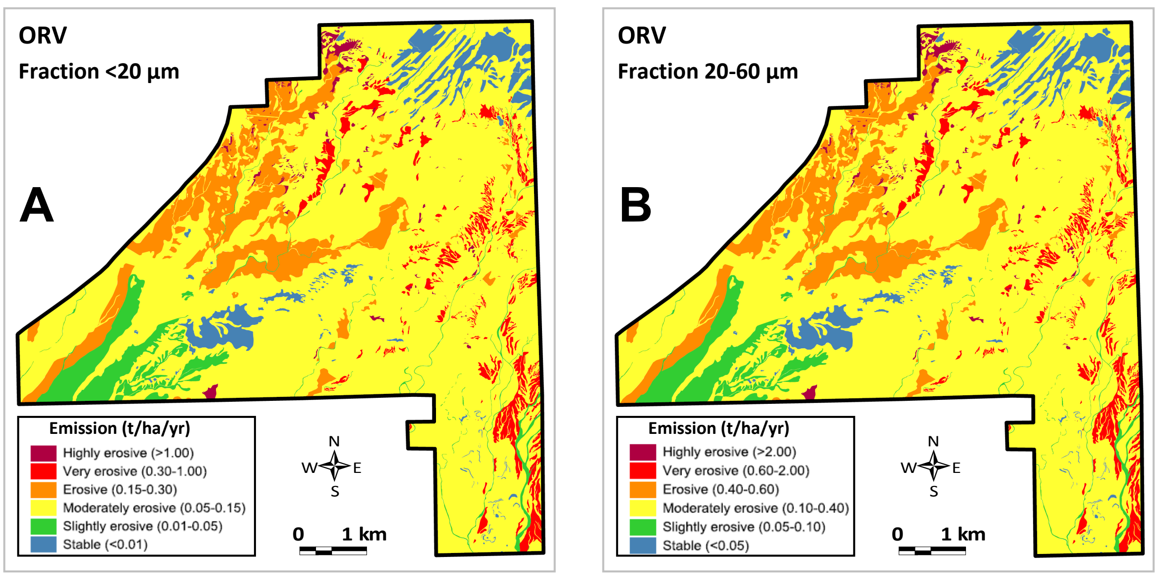

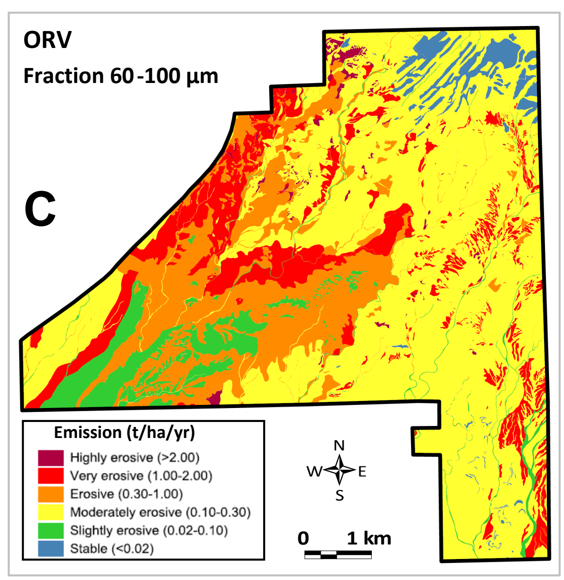

Fig. 18: Risk maps for dust emission caused by off-road vehicular activity.

(A) fraction <20 µm
(long-term suspension)

(B) fraction 20-60 µm
(short-term suspension)

(C) fraction 60-100 µm (modified saltation).

cover a larger area and are mainly located in the north and east. For the coarsest fraction, the areas of highest risk increase to include the 3.3 zones (rock-covered surfaces with sandy loam) north of the sand dunes and in the northwest. For all three size fractions, the least emissive units from ORV driving alone, are always 1.1 (unvegetated dunes), 3.4 (rock-covered surfaces with encrusted sand) and 3.5 (bedrock). They occur in the southwest and northeast corners of the NDRA. Note that the differences between fine (<60 µm) and coarse (>60 µm) dust are always in the medium productive units: classes "moderately emissive" and "emissive". These units are less emissive for fine dust compared to coarse dust: "moderately emissive" *versus* "emissive" (for units 1.2, 1.3 and 1.4), and "emissive" *versus* "very emissive" (for unit 3.3). Note also that unit 1.1 is less emissive in the finer fractions: "stable" *versus* "slightly emissive". ORV activity on bedrock (blue areas in the upper right corner of the maps) is uncommon and difficult because of the pronounced topography and highly irregular terrain.

Therefore, a management plan to decrease direct emission generated during ORV activity would need to encourage or instruct drivers to stay within the areas covered by unvegetated sand dunes (1.1) and the rock-covered surfaces with encrusted sand (3.4) and avoid or prohibit ORV activity on the silt areas, especially the silt and clay areas with gravel (2.2) and the desert pavements (3.1).

3.2 Risk maps for dust emission caused by wind erosion

The same six risk classes that were used in the ORV risk maps were used in the risk maps for dust emission caused by wind erosion: highly emissive, very emissive, emissive, moderately emissive, slightly emissive and stable. Here too, risk maps were constructed for the classes <20 µm, 20-60 µm and 60-100 µm (Fig. 19).

Unlike the ORV maps, the zones of medium wind erosion (moderately emissive, emissive) cover only a very small area in the NDRA. Most surfaces are characterized by either strong erosion (highly emissive, very emissive) or produce nearly no dust (slightly emissive, stable). The difference between the center-south (and a small zone in the northwest) and the entire north, east and southeast of NDRA is very pronounced (Fig. 19).

The patterns in the <20 µm and 60-100 µm maps are almost identical. The most emissive zones are the disturbed sands of unit 1.3 in the NW and W, and especially the dune area in the center (units 1.1 and 1.2) including the areas with a shallow layer of blown-in sand (unit 1.4). For the 20-60 µm fraction unit 1.4 (area of blown-in sand) is clearly less emissive; this unit behaves similarly to the encrusted sand of unit 3.4 in the SW (orange in the map). The difference is significant because the 1.4 areas are important in NDRA: they comprise 2546 ha, which is 41% of the total sand area. Another important difference can be seen in the SE, where the large drainage channels are more emissive for 20-60 µm dust than for <20 µm and 60-100 µm dust.

The least emissive zones are the bedrock areas in the northeast (for evident reasons), the encrusted silt zones of unit 2.1 (adjacent to the drainage channels in the north), and the aggregated silt deposits of unit 2.3 (in the northwest). The high stability of unit 2.1 is largely caused by a moderate to well-developed moss-lichen biological crust. This crust is more well-developed than the cyanobacterial crust on unit 3.4, which is much more emissive (see orange zones in the southwest of the maps). The high stability of unit 2.3 is

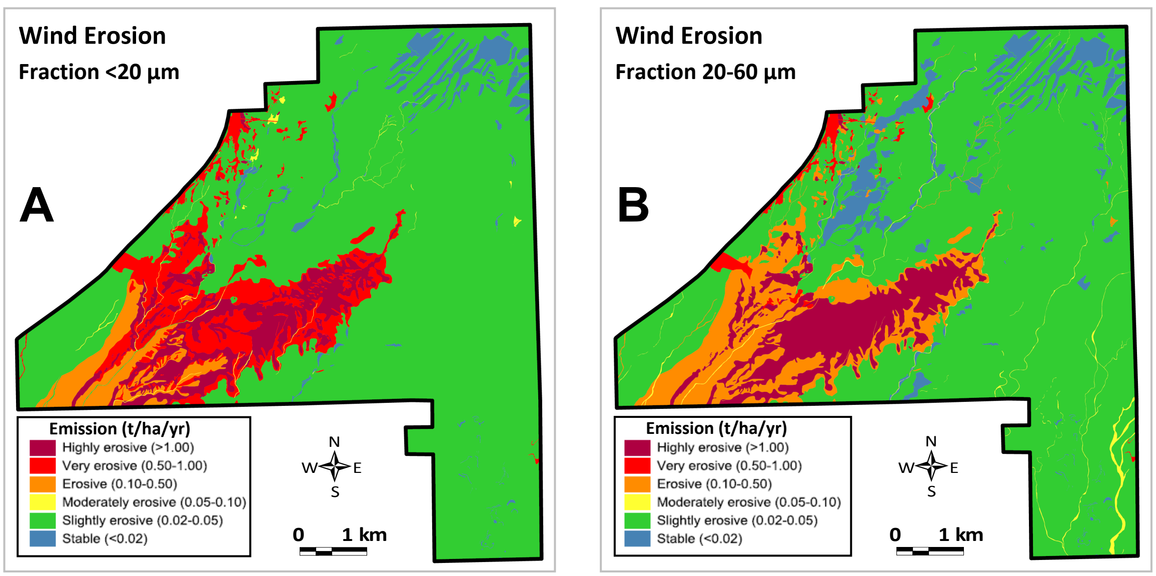

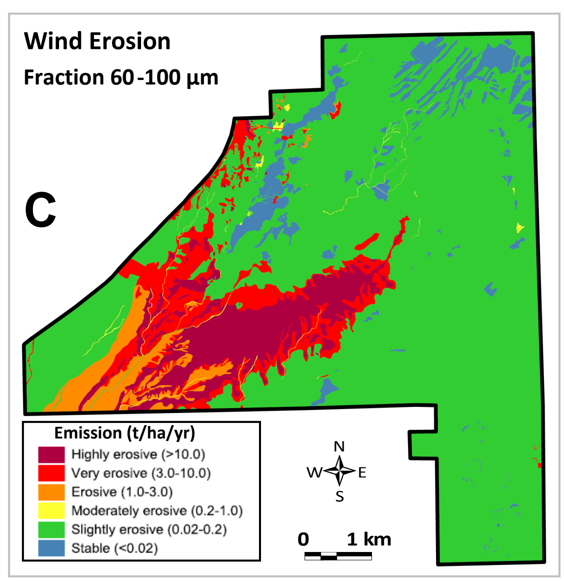

Fig. 19: Risk maps for dust emission caused by wind erosion.

(A) fraction <20 µm (long-term suspension)

(B) fraction 20-60 µm (short-term suspension)

(C) fraction 60-100 µm (modified saltation).

predominantly explained by a combination of a physical crust and the surface being covered by coarse aggregates of silt. The physical crust often develops many surface cracks that would produce dust if it were not protected by the surficial layer of coarse aggregates.

It is important to note that, except for the disturbed sand and silts of units 1.3 and 2.4, the maps in Fig. 19 display the patterns for dust production on ***undisturbed*** desert terrain. ***Once disturbed, all surfaces containing significant amounts of silt will produce dust during strong winds.*** This is especially important for the ORV trails, which are the only important zones in the east of NDRA where wind erosion is capable of emitting dust.

3.3 Risk maps showing the relative importance of wind erosion and off-road vehicular activity in dust production

To evaluate the role of wind erosion and off-road driving as suppliers of dust in the Nellis Dunes Recreation Area we calculated the ratio WE/ORV where WE is the emission rate for dust production by wind erosion and ORV the emission rate for dust production generated by off-road vehicular activity. These calculations were performed for each surface unit and for the three dust fractions investigated (<20 μm, 20-60 μm and 60-100 μm). To ensure reliable results we used average numbers for both parameters: annual average emission rates for wind erosion, and average driving conditions for off-road vehicular activity in the Nellis Dunes area (driving speed of 30 km h^{-1}, average vehicle). For ORV-generated emissions, we transformed the mass-per-length emission rates into mass-per-surface emission rates so that the physical units are identical for the two emission mechanisms and correct ratios can be calculated (for the procedure of this transformation the reader is referred to Chapter 6)). When ORV was larger than WE, the reciprocal of the ratio (i.e., ORV/WE) was calculated to allow direct comparisons. The data were then grouped in eight classes: four classes where the emission rate for wind-generated dust (WE) was larger than that for ORV-generated dust (ORV), and four classes where ORV was larger than WE. The same criteria (class boundaries) were used for each category when delineating the emission classes, allowing an objective comparison of the two dust-producing mechanisms.

Results are shown in the maps in Fig. 20. Areas in NDRA where wind erosion has a higher capacity to produce dust are displayed in blue; areas where ORV activity has a higher capacity to produce dust are depicted in red. It should be emphasized that the maps display the ratio of emission rates, not ratios of absolute amounts of dust emitted. They thus show the situation in each surface unit and the spatial pattern of that situation in the NDRA, but do not tell where in NDRA the largest amounts of dust are produced annually because for that information the areal extent of each surface unit should also be taken into account. *Therefore, what the maps show is which of the two dust-producing mechanisms* *dominates in which area, and how large the dominance is. The darker the color the more the prevailing mechanism dominates the subordinate mechanism; the lighter the color the more equal the role of both mechanisms becomes.*

The spatial patterns of wind-erosion-dominance and ORV-dominance are nearly identical for the three dust fractions investigated (Fig. 20) Wind erosion dominates as a dust production mechanism in all the units with sand, in the bedrock areas, and in the non-silty drainages (but not for 20-60 µm dust in the latter). ORV dominates in the areas with silt, rock-covered silt and silty drainages. The distinction between the areas with sand and the areas with silt (either rock-covered or largely rock-free) is very pronounced, for all three grain size classes.

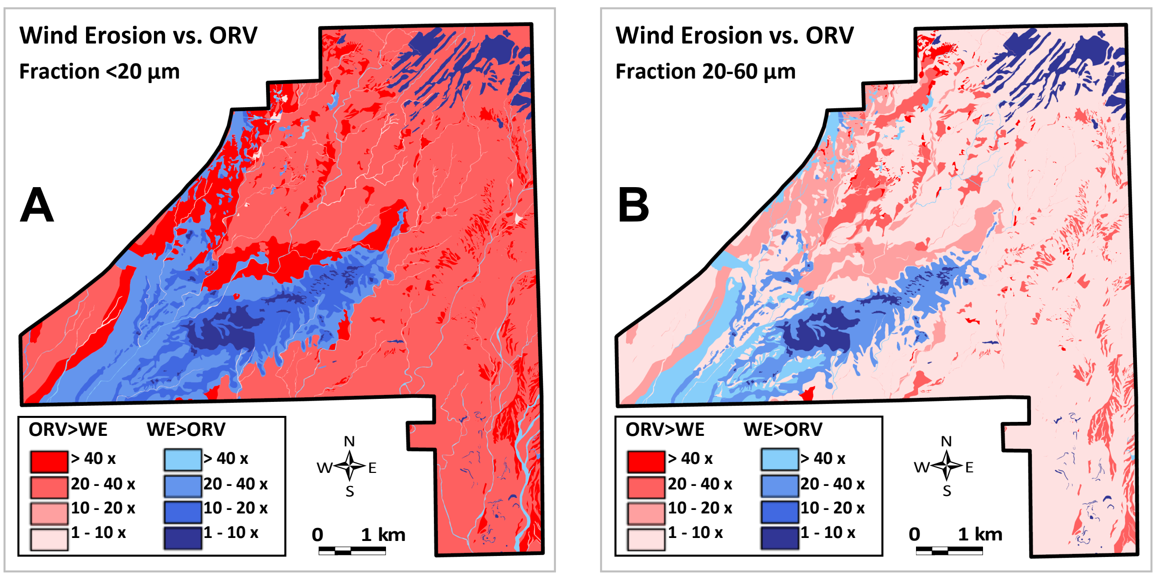

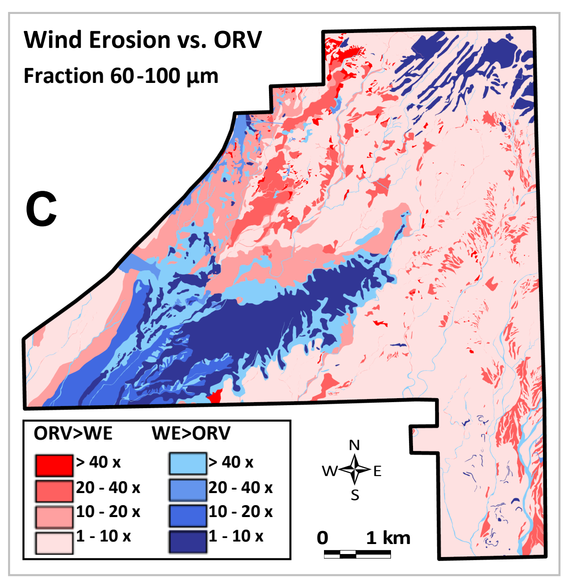

Fig. 20: Relative importance of dust production by wind erosion and dust production by off-road vehicular activity. The maps show the ratio WE/ORV (when wind erosion dominates) or ORV/WE (when off-road vehicular activity dominates).

WE = dust emission rate generated by wind erosion; ORV = dust emission rate generated by off-road vehicular activity.

(A) fraction <20 µm (long-term suspension)

(B) fraction 20-60 µm (short-term suspension)

(C) fraction 60-100 µm (modified saltation).

The maps for the two coarsest fractions (20-60 µm and 60-100 µm) are similar apart from a somewhat higher dominance of wind erosion in the wind-erosion-dominant areas for the coarsest fraction. However, there is a substantial difference between the two suspendable dust fractions. In the ORV-dominant areas the role of ORV in generating dust is much more dominant for fine dust. This is important because it demonstrates the significant role that off-road driving plays in releasing the finest dust in these areas. These particles are characterized by high deflation thresholds and are very resistant to wind erosion; ***only artificial disturbances such as off-road driving will bring these particles into suspension.*** In addition, these finest fractions are those that are the most harmful to health and have the greatest ability to be carried a significant distance downwind.

The delineation, within NDRA, of the zones where wind erosion is the dominant dust production mechanism and the zones where off-road driving is dominant is thus easy to predict: wind erosion dominates in the sandy areas and areas largely composed of bedrock, whereas off-road driving dominates in all areas with silt, either with or without a significant rock cover.

3.4 Risk maps for total emission (wind erosion + off-road vehicular activity)

Total dust production in NDRA is equal to the sum of wind-erosion-generated dust and ORV-generated dust, but the latter strongly depends on the intensity of the driving (number of vehicles, length of the trajectories followed), the location of the trajectories in NDRA, the type of vehicle, and on the driving style (predominantly the driving speed). For the first four factors we used the following criteria: (1) NDRA is visited by 300,000 visitors per year; (2) average length of a run is 10 km; (3) the proportion of a surface unit in a run equals the proportion of that unit in the total track length within NDRA; (4) visits are made with an "average" vehicle (average of a dirt bike, a dune buggy and a 4-wheeler, which altogether represent almost 99% of the vehicles used at NDRA). Criterion (1) is an adequate estimate based on a survey carried out by the Las Vegas office of the Bureau of Land Management in 2004 (see Chapter 6). The number in criterion (2) may look somewhat low when compared to other ORV areas, but at NDRA many tracks are very rough (resulting in low driving speeds), and the density of tracks also is very high (which means drivers make many turns, resulting in a limited daily average driving speed and, thus, in a limited number of km driven). The number of 10 km per run is a good average at NDRA. The assumption in criterion (3) is justified because it can be expected that the more popular a unit is to ORV drivers, the more tracks will be driven in that unit over time, and therefore the higher the track density will become within that unit. Criterion (4), finally, is a reasonable assumption as there is no real preference in type of vehicle used at NDRA.

To account for the fifth variable (driving speed), we calculated the total dust emission rates for 6 different driving speeds ranging from 0 km h^{-1} (= wind erosion only) to 50 km h^{-1}. Total emission maps were produced for the same 3 grain size classes as before: <20 µm, 20-60 µm and 60-100 µm (Figs. 21, 22 and 23). Each map contains 12 classes, which were chosen such that the areal differences that occur within NDRA are optimally displayed. Classes are thus different for the 3 fractions because the emission numbers differ, but they are identical for all 6 maps of each fraction. *What is important in the maps is not the intrinsic value (class) of each unit, but the changes in the pattern as the driving speed increases.*

The aim of the maps is (1) to show where in NDRA the most dust-emissive units are located, and (2) how the patterns change as a function of the driving speed. The effect of the driving speed is especially investigated because it is a parameter that can be easily handled by the driver to reduce dust emission without having to stay away from areas very attractive to ORV driving but characterized by a high dust emission potential.

Note that the maps display emission rates and not annual amounts. Therefore, they show the situation in each surface unit and the spatial pattern of that situation in the NDRA. These maps do not tell where in NDRA the largest amounts of dust are produced annually because for that information the areal extent of each surface unit should also be taken into account. The annual amounts produced by the 17 surface units are shown in Fig. 17 in this Chapter.

For all three grain size fractions investigated, when natural emissions are combined with ORV-generated emissions, the most emissive zones are located in the sandy areas, and especially in the sand dunes. This is true for all driving speeds, although for very high driving speeds the 2.2 areas (silt and clay surfaces with gravel) in the extreme north become very emissive – these become even more emissive than the sand dunes for the two suspendable fractions. The least emissive zones are the bedrock areas and secondly, most of the silty units. Within the large silty area in the eastern portion of the NDRA it is mainly the desert pavements (unit 3.1) that are most emissive.

Therefore, in NDRA, the patterns of the total dust emission rate are heavily dominated by wind erosion, except for unit 2.2 (silt and clay with gravel), which becomes very productive at high driving speeds; and unit 3.1 (desert pavements).

Driving in the central sand dunes has very little effect on total emission. For unit 1.1 (dunes with no vegetation) the emission class is stable over the entire ORV driving speed range of 0-50 km h^{-1} for all three grain-size fractions, and for the vegetated dunes (unit 1.2) the difference remains very small. These units produce only very little dust during ORV driving; almost all dust produced by these units comes from wind erosion. For unit 1.4 (patchy layers of blown-in dune sand) the differences are also small. In contrast, when ORV driving speeds increase, the most dramatic changes in dust emissions occur for unit 2.2 (silt and clay with gravel), followed by unit 3.1 (desert pavements) and, lastly, unit 2.3 (aggregated silt deposits).

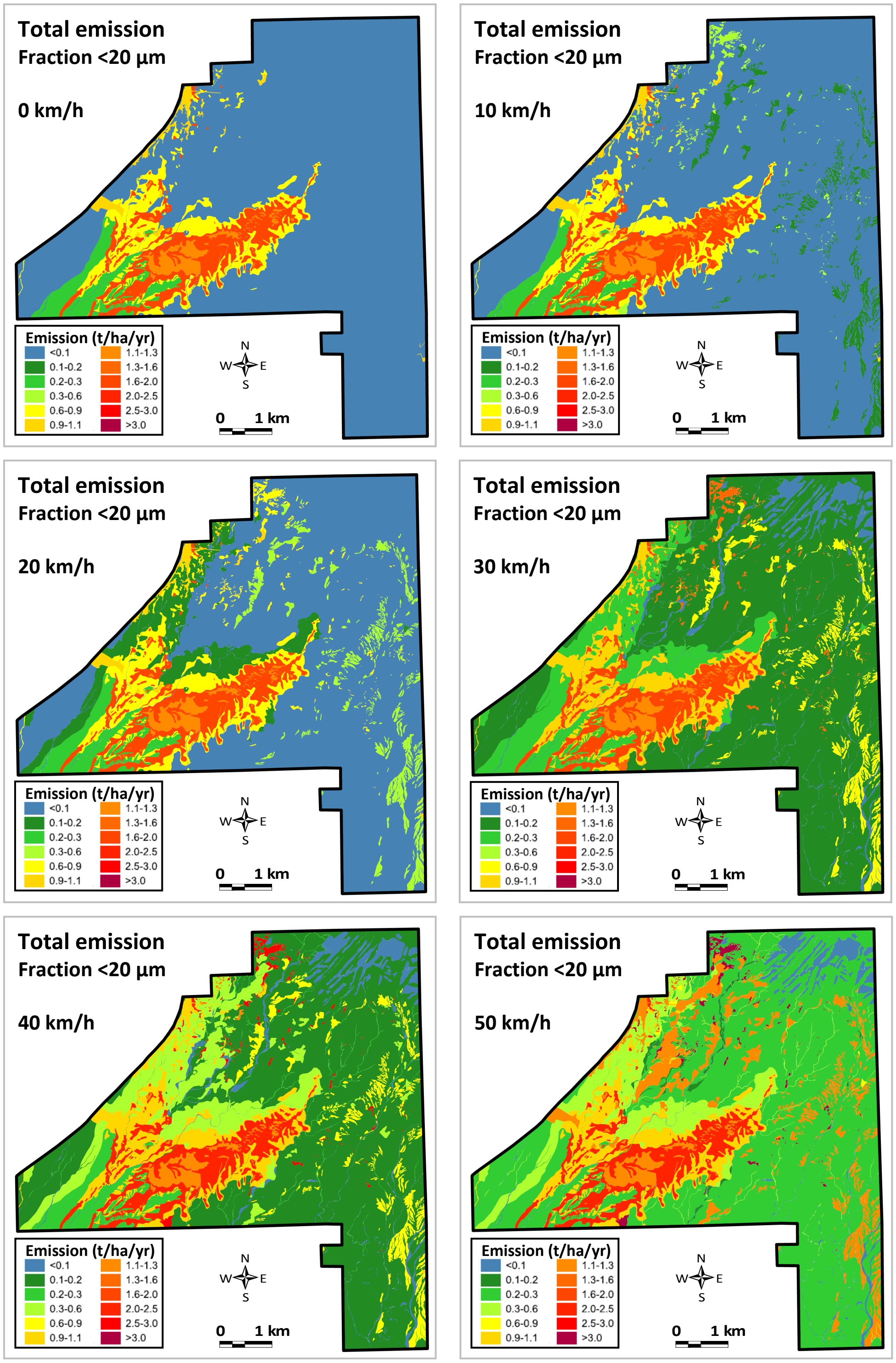

Fig. 21: Risk maps for total emission (wind erosion + ORV) for long-term suspendable dust (fraction < 20 µm), for 6 driving speeds. Data are for an average vehicle (average of a dirt bike, a dune buggy and a 4-wheeler).

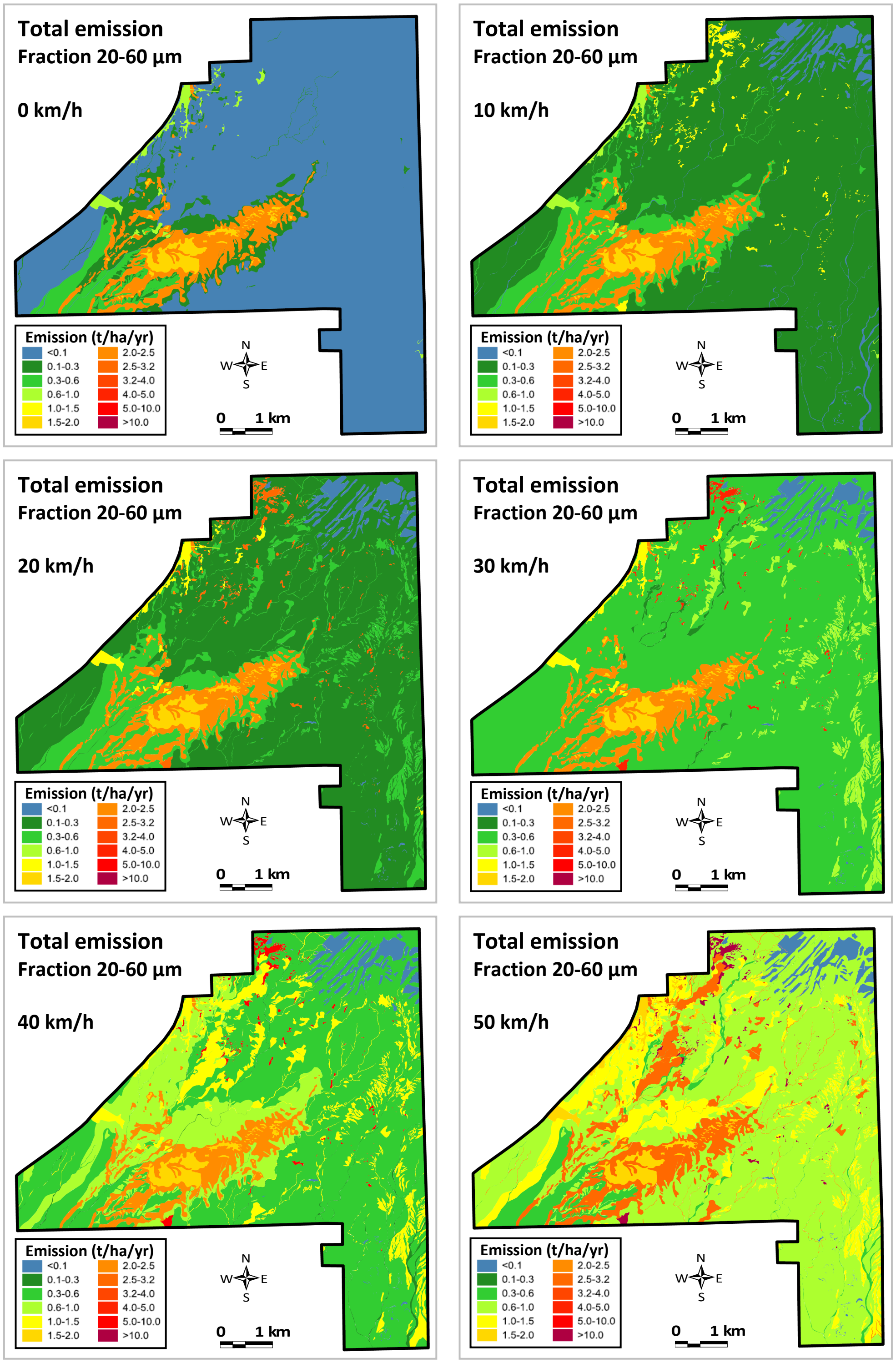

Fig. 22: Risk maps for total emission (wind erosion + ORV) for short-term suspendable dust (fraction 20-60 µm), for 6 driving speeds. Data are for an average vehicle (average of a dirt bike, a dune buggy and a 4-wheeler).

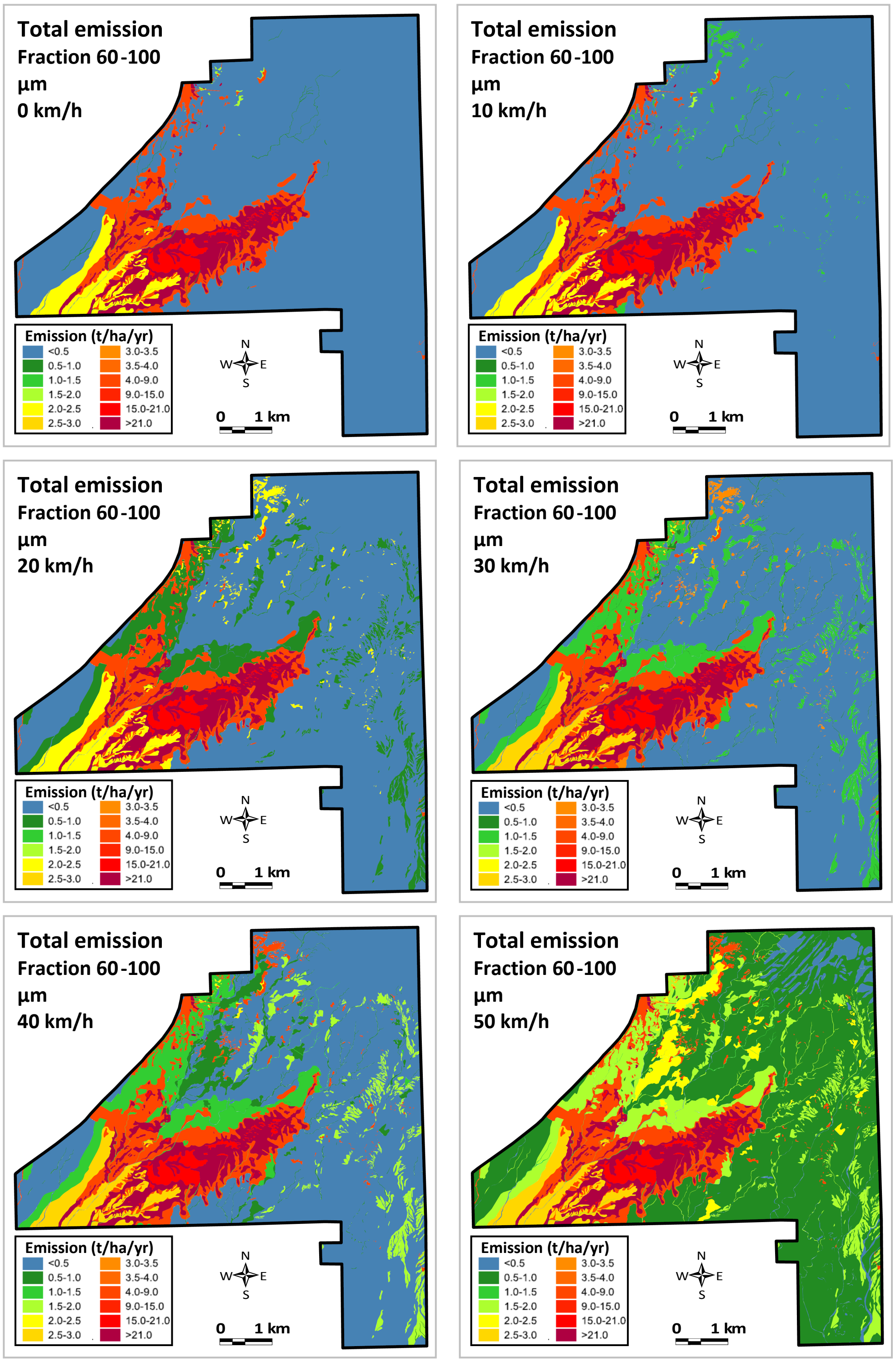

Fig. 23: Risk maps for total emission (wind erosion + ORV) for modified saltation dust (fraction 60-100 µm), for 6 driving speeds. Data are for an average vehicle (average of a dirt bike, a dune buggy and a 4-wheeler).

Probably the most prominent change that can be seen in these maps is when the silt, clay and rock-covered surfaces in the eastern half of the NDRA start to produce dust. For <20 μm dust this happens at a driving speed between 20 and 30 km h^{-1}. For 20-60 μm dust it happens much earlier: the eastern portion of NDRA is already emissive at a driving speed of 10 km h^{-1}, i.e. immediately after driving has started. For 60-100 μm dust a driving speed of at least 40 km h^{-1} is required.

The sandy areas, and especially the dunes of units 1.1 and 1.2, are the major dust sources in NDRA at low driving speeds. As driving speed increases the other units except the bedrock of unit 3.5 also start producing dust. Units that are especially vulnerable to ORV driving include 2.2 (silt and clay with gravel), 3.1 (desert pavements), and, to a lesser extent, unit 2.3 (aggregated silt deposits). However, due to their large areal extent the sand dunes remain the largest supplier of dust within NDRA (see Fig. 17) although for some of the fractions unit 2.2 has a higher intrinsic emission rate at high driving speeds.

3.5 Risk maps for arsenic emissions in the Nellis Dunes Recreation Area

Chemical analyses were performed on soil samples (upper 2 cm) and on airborne dust samples generated by the PI-SWERL. Eighteen chemical elements were measured in total. One element (arsenic) was of special concern because several units in NDRA contain extraordinarily high amounts of arsenic in the soil, up to more than 200 times the EPA's screening level for arsenic in residential soil. Exposure to arsenic has been strongly linked to a long list of diseases (see Chapter 10 of this report) and constitutes an important health risk if inhaled or ingested. In this section we present and discuss the risk maps for arsenic emissions in the Nellis Dunes area.

3.5.1 Risk maps for arsenic emission during wind erosion.

Emission rates for arsenic were calculated for all surface units by combining the emission rates for dust with the concentrations of arsenic in that dust. A map for the concentrations of arsenic in the soil is presented in Chapter 10. Because the risk maps aim to display the potential risk for exposure to airborne arsenic (not arsenic in the soil) we cannot use the data from the soil map but need to work with arsenic concentrations measured in airborne dust. PI-SWERL samples were used for this purpose because they only contain dust released from the surface unit under investigation. That the PI-SWERL only measures potential emissions does not preclude one from constructing reliable risk maps because a strong linear relationship exists between the potential emissions measured by the PI-SWERL and the real emissions generated by natural wind erosion (see Fig. 24). Constructing the risk map in a qualitative format (i.e., with qualitative risk classes) eliminates problems related to the quantitative concentrations and allows displaying correct spatial patterns. The aim of the maps shown here is to present these spatial risk patterns.

Note that the actual risk to humans cannot be determined from these data because airborne dust during any activity at NDRA contains both locally derived dust (i.e. PI-SWERL data) and dust eroded from distant sources. The chemical composition of such dust will vary with different activities and wind conditions. In addition, the risk to humans must also include a measurement of the amount of exposure (i.e. how much dust is inhaled and/or ingested), which is controlled by many other factors. These data were outside the scope of this project.

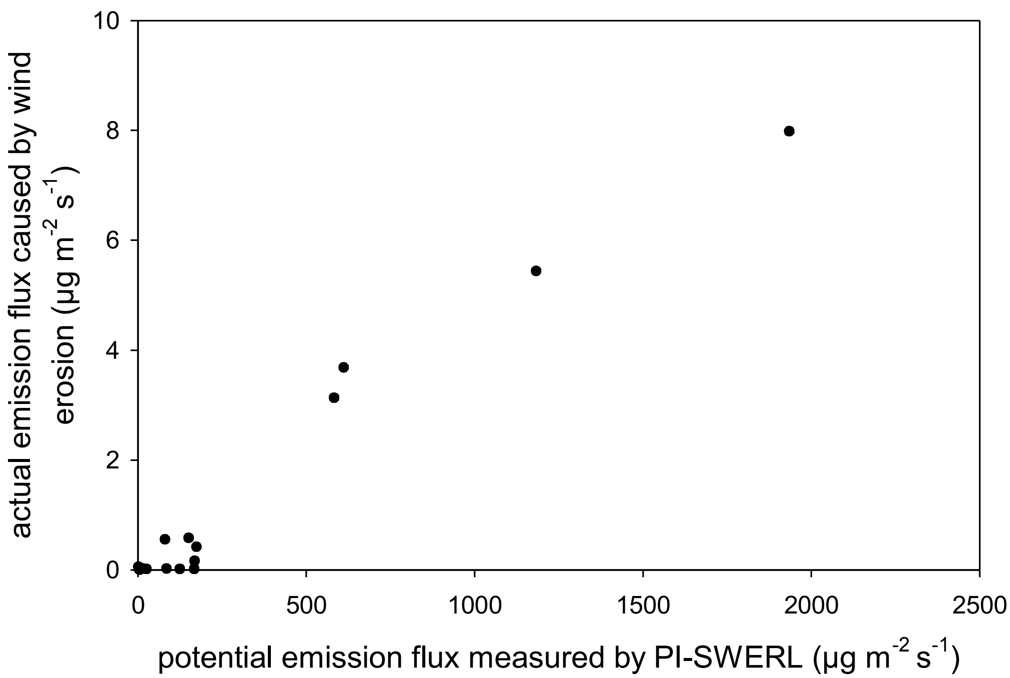

Fig. 24: Comparison of PI-SWERL-measured potential emissions and actual emissions caused by wind erosion. Paired measurements were done for all 17 surface units in Nellis Dunes Recreation Area; each dot in the figure represents one surface unit. Actual and potential emissions were measured during the same time period (2-16 May 2008). Since the soils stayed completely dry over the entire period, surface conditions were identical during all measurements. Actual emission flux (y-axis) is the average for the period 2-16 May 2008; potential emission flux (x-axis) is the flux for a 3000 rpm rotational speed of the PI-SWERL blade, corresponding to an aerodynamic friction velocity of 0.55 m s^{-1}. All data are for the particle fraction <10 µm (or PM10) because the PI-SWERL measures only that fraction.

The qualitative risk maps presented here show which areas in NDRA have the potential to emit the greatest amounts of dust containing arsenic under natural wind conditions or from ORV activities. Fig. 25 shows the risk map for wind-erosion-generated arsenic for two fractions: PM10 and total suspendable dust (PM60). Only these two fractions were considered because the arsenic concentrations in the PI-SWERL samples were determined for 0-10 µm and 10-60 µm dust only (see Chapter 10). The risk maps for the two fractions are very similar. The highest risk is map unit 1. 5 (mixture of fine sand and coarse silt), but this unit comprises only 0.1 % of the total surface in NDRA and only occurs in the northwest. However, although very small, nearly all of the unit 1.5 areas are located in a zone very intensely used by ORV drivers (see Fig. 15). Therefore, these areas are also of concern during periods of wind erosion. The large belt of sandy surfaces in the center and southwest of the NDRA also is a concern during wind erosion. The units of especially high risk are units 1.1 (unvegetated dunes), 1.2 (vegetated dunes) and 1.3 (disturbed sand surfaces, including the two parking lot areas). Unit 1.4 (thin layer of blown-in dune sand) also is of concern, especially for PM10. In the southwest, unit 3.4 (rock-covered sands with biologic crust) shows a high arsenic emission risk. In the remaining areas of NDRA, the risk for arsenic emission by wind erosion is really very low, and it is almost nothing in the bedrock areas in the northeast.

Therefore, until more is known about the human health risk from these dust sources, ORV drivers are strongly advised to stay away from the central sand dunes and unit 1.5 during periods of strong winds.

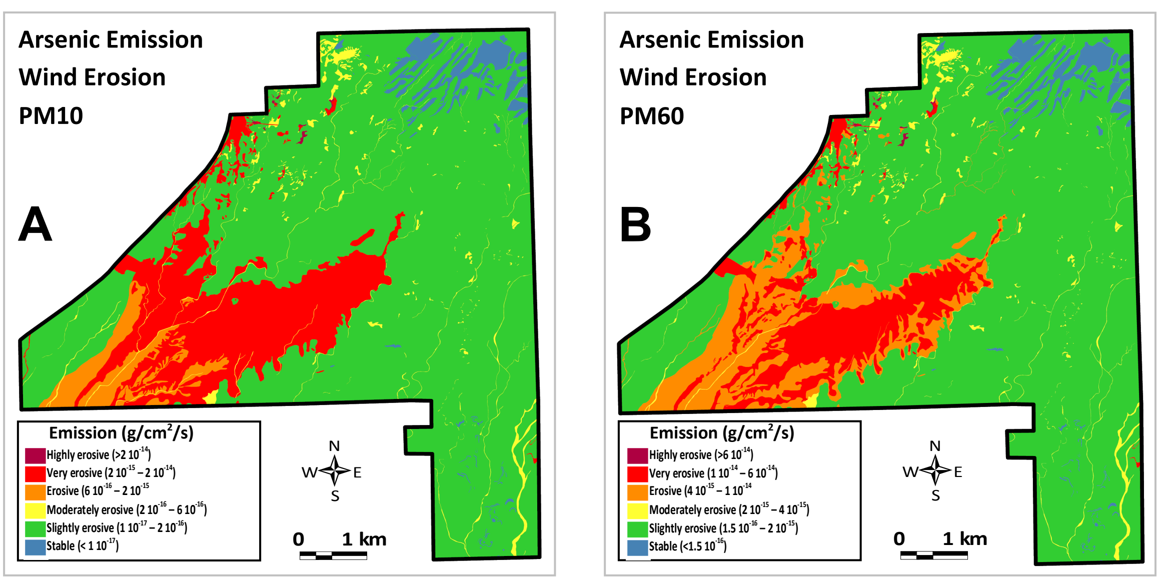

Fig. 25: Risk maps for wind-erosion generated arsenic emissions. (A) PM10 fraction; (B) total suspendable dust (PM60).

3.5.2 Risk maps for arsenic emission during ORV activity.

3.5.2.1 General pattern

Emission rates for ORV-generated dust were combined with the concentrations of arsenic in that dust. Here too we used the arsenic concentrations in the airborne PI-SWERL samples because they represent locally eroded dust.

The risk maps for arsenic emission during average ORV usage (average vehicle and average driving speed of 30 km h^{-1}) are displayed in Fig. 26 for PM10 and total suspendable dust (0-60 µm) respectively. Although the relative ranking of the units is very comparable for the two fractions there are differences for the surfaces with intermediate risk, especially unit 3.3 (rock-covered sandy loam) and unit 3.2 (rock-covered silt). These units show a higher emission risk in the PM10 size compared to total suspendable dust. Another difference in comparing the size fractions is unit 1.4 (patchy layers of blown-in sand), which is somewhat less emissive in the PM10 fraction compared to total suspendable dust. Apart from these three units the differences between the two maps are very minor. The map units that have the greatest risk in regards to ORV-generated arsenic emissions are 2.2 (silt and clay with gravel), 1.5 (mixture of fine

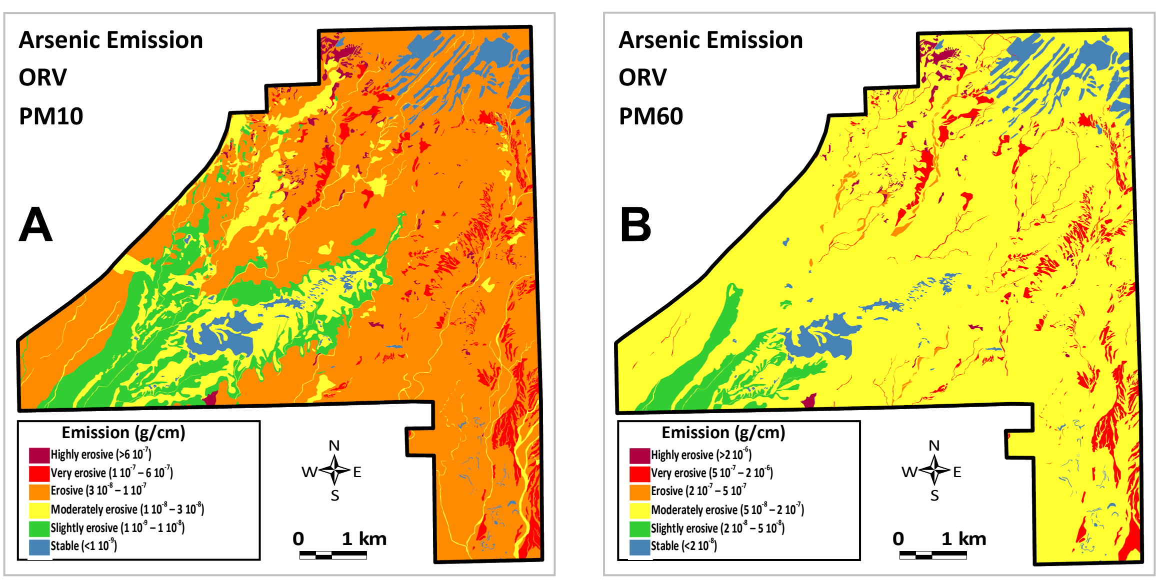

Fig. 26: Risk maps for arsenic emission generated during off-road vehicular activity. (A) PM10 fraction; (B) total suspendable dust (PM60). Data are for average ORV conditions (average vehicle and average driving speed of 30 km h^{-1}).

sand and coarse silt) and 3.1 (desert pavements). The map units with the least risk are 1.1 (unvegetated dunes), 3.4 (rock covered sand with biologic crusts) and 3.5 (bedrock). Driving in the sand dunes and the rock-covered sands with crust does not release much arsenic, at least when there is no wind erosion. On the other hand, driving on the arsenic-rich units 2.2 (silt and clay with gravel), 1.5 (mixture of fine sand and coarse silt), and on unit 3.1 (desert pavements), is strongly dissuaded as it generates dust with large amounts of arsenic.

Combining the risks for wind erosion and ORV driving, the most dangerous areas for arsenic emission in NDRA are the map units 1.5 (mixture of fine sand and coarse silt). These areas emit significant arsenic when being driven and also produce large amounts of arsenic during wind erosion. At this time, it is strongly recommended that ORV driving not occur on units 2.2 (silt and clay areas with gravel) and 3.1 (desert pavements). ORV driving on the sand dunes and their surroundings (including the two parking lot areas) should be avoided during wind erosion.

3.5.2.2 Effect of vehicle type

The data depicted in the maps in Fig. 26 is for an average vehicle (average of a dirt bike, a dune buggy and a 4-wheeler). To investigate the effect of the type of vehicle we calculated the emission rates for each vehicle type separately and constructed risk maps. The results for PM10 are presented in Fig. 27; for total suspendable dust the trends are very similar.

The patterns for the dune buggy and the 4-wheeler are nearly identical, but deviate strongly from that for the dirt bike (Fig 27). For arsenic emissions, driving a dirt bike emits less arsenic than driving a dune buggy or a 4-wheeler. More than 80% of the surfaces at NDRA can have significant arsenic emissions when driven on by a 4-wheeler or a dune buggy. The surfaces with the highest arsenic emissions resulting from the dirt bike are units 2.2 (silt and clay with gravel) and 3.1 (desert pavement).

3.6 Occurrence map for palygorskite

There are no methodologies available to quantitatively measure silicate clay mineral abundances in the complex mineral assemblages present at NRDA that were within the budget and time constraints of this project. Therefore, risk maps for mineral abundances could not be prepared as those presented for arsenic. However, relative abundances of minerals can be estimated from the XRD data (see explanation in Chapter 8). Currently of

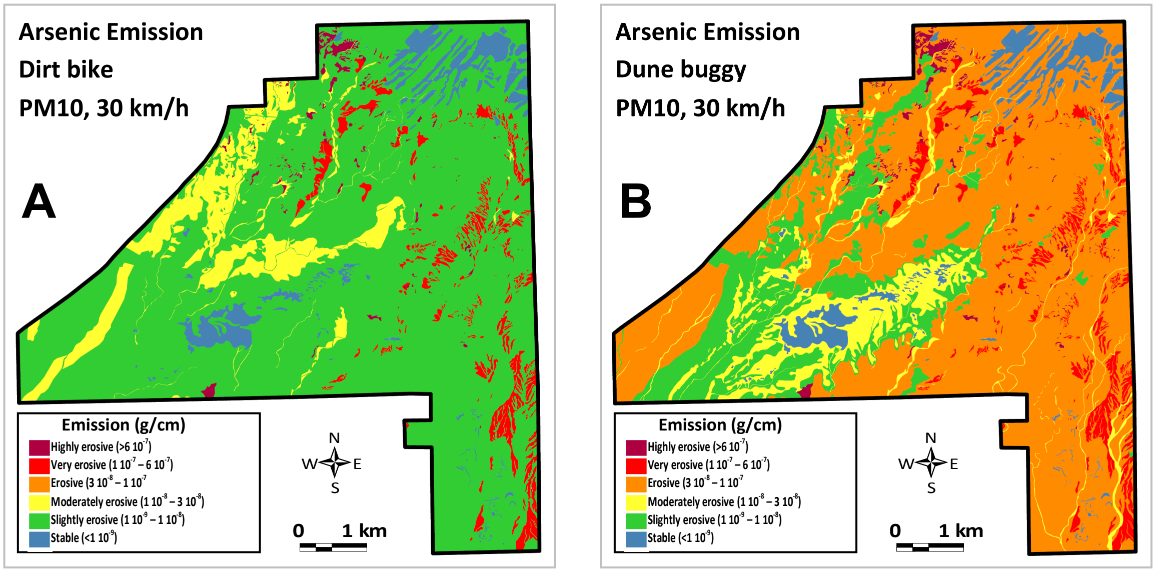

Fig. 27: Risk maps for arsenic emission generated during off-road vehicular activity.

(A) dirt bike

(B) dune buggy

(C) 4-wheeler

Data are for PM10 and for an average driving speed of 30 km h^{-1}

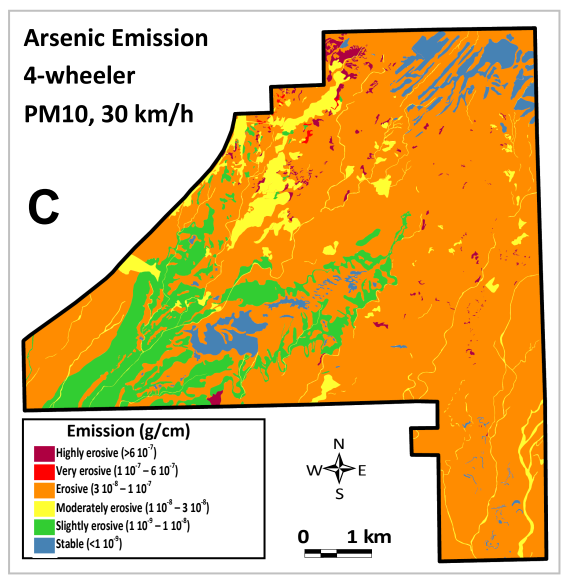

greatest concern is the presence of palygorskite, which is an asbestiform mineral that poses a potential health risk. The spatial occurrence of the relative abundances of palygorskite is shown in Fig. 28.

Palygorskite is most abundant in the fine grain-size fractions in the sand dunes, and in the sandy areas in the NW. These areas are highly emissive in windy conditions and are therefore potentially of concern. However, more research is needed to determine the health risks from palygorskite in the Nellis Dunes area.

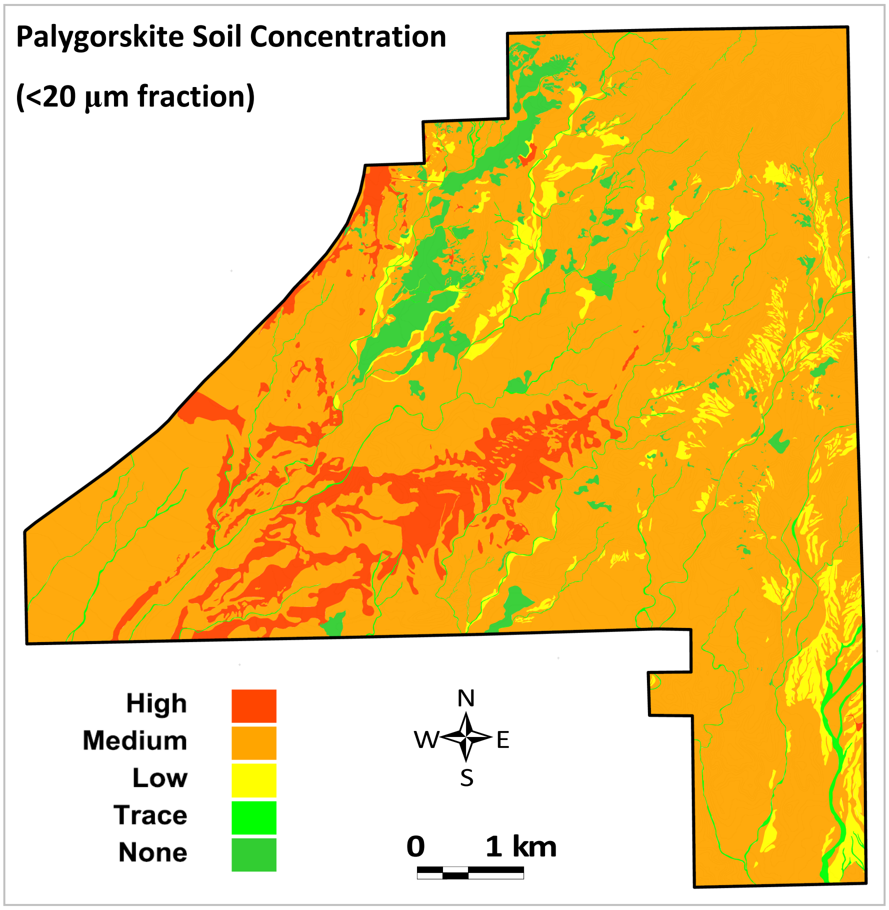

Fig. 28: Occurrence of palygorskite in the Nellis Dunes Recreation Area.

4. Analysis and recommendations

Adequate management of ORV designated areas requires maintaining a reasonable balance between social factors such as recreation, and environmental factors including ecology and health. Physical factors related to the nature of the surfaces also play a role and can significantly complicate the problem. NDRA is a good illustration because it includes a wide variety of soil and surface types, each of which responds differently to dust emission by natural wind conditions and/or ORV activities. In the sandy areas in the northwest and in the central sand dunes, wind erosion is the major initiator of dust emission. Due to the large extent of these surfaces, and also because of their high natural mobility, active intervention in these zones is very difficult and may also have a negative ecological impact. ORV limiting measures in these zones have little to no effect because these surfaces produce nearly no ORV-generated dust. In contrast, surfaces containing silt, with or without rock cover, are highly susceptible to ORV activities. ORV driving is by far the most important dust-generating mechanism in these zones, which means that active intervention is possible.

Management of ORV areas becomes significantly more complicated when considering potential health risks from dust inhalation. Dust, in itself, is known to be detrimental to human health (see Chapter 7). However at NDRA, the locally-derived dust contains high concentrations of arsenic – a known poison (see Chapter 10). In addition, palygorskite, an asbestiform mineral, is also present (see Chapter 8), as well as many other naturally-occurring elements (see Chapter 9) and radionuclides (see appendix A). It is beyond the scope of this project to determine what, if any potential human health risks may arise from activities at NDRA. However, this study can provide recommendations to reduce dust emissions at NDRA, and provide information regarding how wind and/or ORV activities generate dust emissions in specific areas within NDRA. Additionally, this study can combine concentrations of chemical elements with dust emissions to show which areas emit the greatest amounts of these substances.

4.1 Accessibility

One way to limit the exposure to airborne dust is to discourage, or even prohibit, public access to zones vulnerable to dust production. This is true for zones susceptible to ORV-generated emissions as well as for zones susceptible to wind-erosion-generated emissions.

4.1.1. ORV-generated emissions

The surfaces in NDRA that produce the most dust during ORV activities all contain considerable amounts of silt and are all low in sand: units 2.2, 2.3, 2.4, 3.1, 3.2, 3.3, and 4.3. By far the most emissive type of surface is unit 2.2 (silt and clay with gravel). Depending on the driving speed this unit produces from three to more than five times more dust than any other unit in NDRA. The second most productive units are 3.1 (desert pavements) and 2.3 (aggregated silt deposits), followed by 2.4 (disturbed silt), 4.3 (silty drainages), 3.3 (rock-covered sandy loam), and 3.2 (rock-covered silt). The two other units with silt do not produce much dust when being driven: 2.1 (silt and clay with crust), and 3.5 (bedrock, with sparse silt in the cracks). All other surfaces also produce very little dust when being driven. Therefore, a recommendation to lessen dust emissions that is based solely on the emission rates for ORV activities would be to encourage the ORV community to stay in the sand areas (especially the unvegetated sand dunes), and refrain from driving in the silt areas including the silty drainages.

4.1.2 Wind-erosion generated emissions

The surfaces at NDRA that generate dust emissions from natural wind conditions differ from those that generate emissions from ORV driving. The areas that produce significant dust during wind erosion are all sandy: units 1.1, 1.2, 1.3, 1.4, 1.5, 3.4, and 4.2. The most emissive units in NDRA are 1.1 and 1.2 (unvegetated and vegetated sand dunes), followed by unit 1.3 (disturbed sands), unit 1.5 (mixture of fine sand and coarse silt) and unit 1.4 (patchy layers of blown-in dune sand). Units 3.4 (rock-covered sands), 4.2 (sandy drainages) and 2.4 (disturbed silt) produce significantly less dust. The remaining surfaces produce almost no dust. Therefore, if ORV drivers wished to lessen their exposure to wind-generated dust only, drivers should be encouraged to avoid the sand units and stay in the silt or rock-covered units, or in the non-sandy drainages.

4.1.3 Recommendations

Based only on the data currently available, combining the risks for ORV emission and wind erosion emission, which show an opposite pattern, the following advice is given for the Nellis Dunes Recreation Area:

1. *During calm weather conditions (days with no wind erosion)* ORV driving in the Nellis Dunes could be suggested in unit 1.1 (the unvegetated sand dunes), unit 3.4 (the encrusted sand) and unit 4.1 (the gravelly drainages) because in these areas ORV-generated emissions are low. Driving in the other sand areas is also potentially acceptable, except for unit 1.5 (mixture of fine sand and coarse silt), which emits high amounts of arsenic and should be avoided. Driving in the silt and rock-covered areas is not recommended as ORV activities generate significant emissions here. If riding is performed in the silt and rock-covered areas the driving speed should be reduced, especially for 4-wheelers.

2. *During days with substantial wind erosion* ORV driving is strongly dissuaded in the central dunes (units 1.1, 1.2) including all surrounding areas (mostly units 1.4, 3.3 and 3.4) as well as all areas of NDRA located downwind of the dunes. Specific units included in the latter may vary according to the wind direction. Driving in these areas during windy days will expose ORV drivers and bystanders to significant amounts of dust.

3. *Driving should be avoided at all times on the following units*: 2.2 (silt and clay with gravel), 1.5 (mixture of fine sand and coarse silt) and 3.1 (desert pavements).

4. *Riders should stay on existing ORV trails*; driving outside existing trails is strongly dissuaded. The only exception is the loose, active sand of unit 1.1 (unvegetated dunes). These surfaces produce nearly no dust when subject to ORV driving, and any trails

created disappear soon because of burial with freshly deposited sand during the next episode of wind erosion. Under no circumstances should riders drive on pristine or even slightly disturbed desert pavements. Driving on existing trails in units 2.2 (silt and clay with gravel) and 1.5 (mixture of fine sand and coarse silt) is also strongly dissuaded. On units 1.3 and 2.4 (disturbed sands and disturbed silts) there are no preferential trails because the entire area has already been disturbed. If driving occurs in these areas, low driving speeds are strongly recommended.

5. *Units that are only slightly dust-productive year round* are 2.3 (aggregated silt), 3.5 (bedrock) and 4.1 (gravelly drainages).

4.2 Vehicle type and driving style

4.2.1 Vehicle type

Nearly all off-road vehicles used in the Nellis Dunes area belong to one of the following three types: dirt bikes (motorcycles), dune buggies, and 4-wheelers (quads). However, not all types are used in all areas. Dirt bikes and 4-wheelers are used anywhere in the NDRA, on all types of surfaces, although in the eastern parts dirt bikes are more abundant (probably because the two entrances are both located in the west?). Dune buggies, on the contrary, are widely used in the central sand dunes and surrounding areas. Therefore, there is currently no reason to provide recommendations regarding the use of dune buggies in the non-sand areas of NDRA.

In the sand areas the 4-wheeler always emits more dust than the dune buggy, and the dune buggy, more than the dirt bike (Fig. 29A). In the silt, rock-covered and drainage areas the same pattern applies (Fig. 29B): the 4-wheeler always emits more dust than the dirt bike. Therefore, in terms of dust emission, the dirt bike would be the most recommendable type of vehicle for off-road enjoyment in the Nellis Dunes area. Of course, the problem is more complicated because 4-wheelers and dune buggies are much easier to drive than a dirt bike and occasional or inexperienced riders will nearly always prefer 4-wheelers or dune buggies. Therefore, restricting 4-wheelers or dune buggies also restricts beginning or occasional ORV users. Another available option is to focus on the driving style, and especially the driving speed.

4.2.2 Driving speed

Limiting the driving speed is one of the most effective measures to reduce dust emissions in ORV areas. Emissions increase with increasing driving speed for any type of surface, whether sandy, silty or rock-covered. Even a limited reduction in speed is helpful because

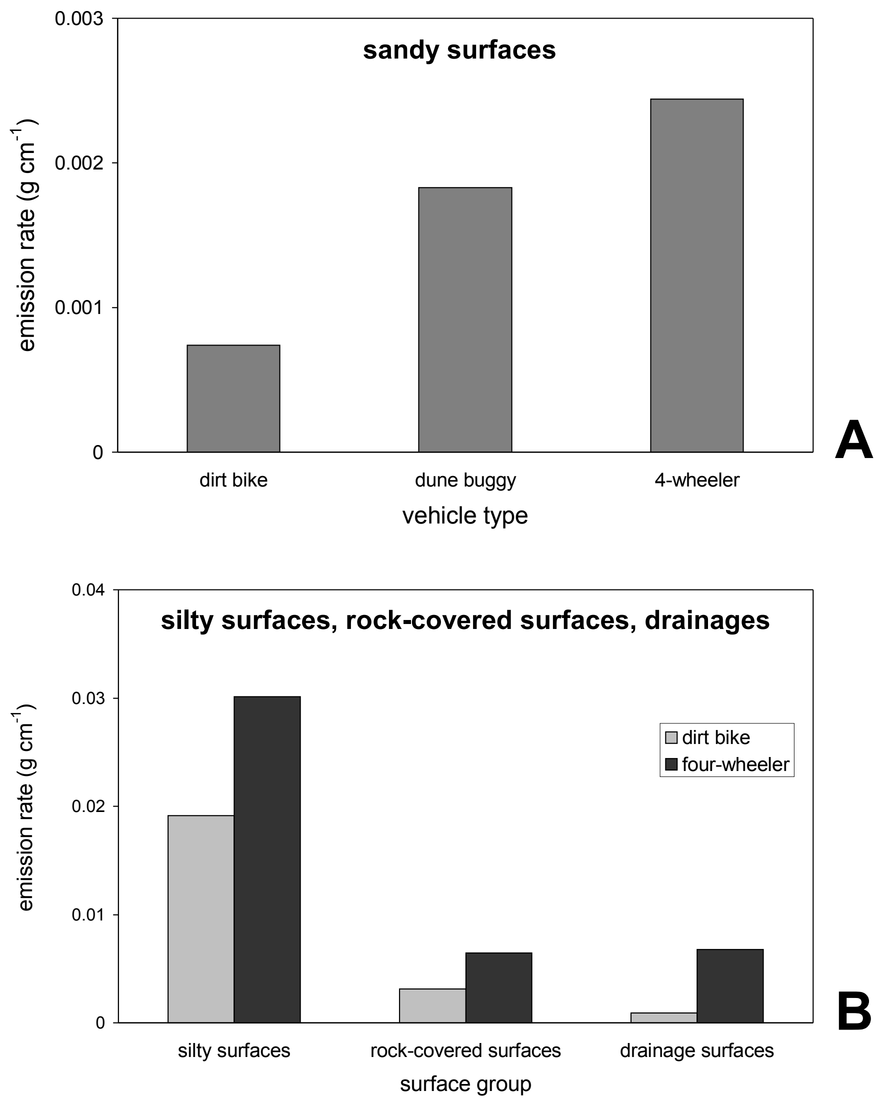

Fig. 29: Dust emission rates for the three types of vehicles used for off-road driving in the Nellis Dunes Recreation Area. (A) Emission rates on sandy surfaces; (B) Emission rates on silty surfaces, rock-covered surfaces, and in drainages. In NDRA there is no driving with the dune buggy on non-sandy surfaces.

the relationship between emission and driving speed is exponential for most types of surfaces. The results of this study show that emissions of medium-sized dust (20-60 μm), which is transported in short-term suspension, are especially reduced by limiting the driving speed. For fine dust (<20 μm) that is transported in long-term suspension, the effect is not as large, but still significant. For coarse dust (60-100 μm), which is mainly transported in modified saltation, limiting the driving speed is less efficient to reduce the emissions although low speeds are still recommendable.

Limiting the driving speed reduces dust emissions on all surfaces, but the reduction is greatest in drainages, followed by sandy surfaces and silty and rock-covered surfaces (Fig. 30A). In relative terms, limiting the driving speed would thus be more beneficial in the drainages and in the sand areas than in the silt and rock-covered areas. However, for our purposes it is the absolute emission rate that is important, and in that case reducing the driving speed is most beneficial in the silty areas (Fig, 30B), followed by the drainages, the sandy surfaces and the rock-covered surfaces. Drivers are especially

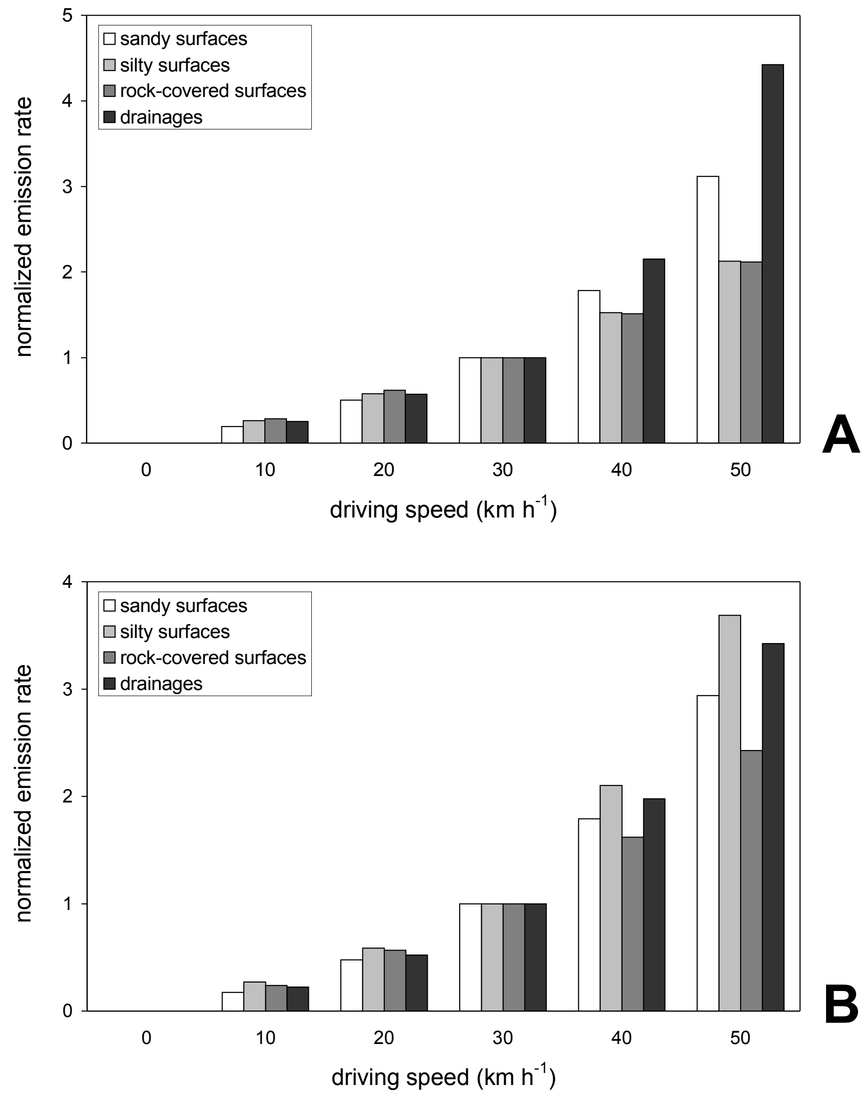

Fig. 30: Effect of driving speed. (A) Normalized dust emission rate as a function of the driving speed, for the 4 categories of surfaces. A speed of 30 km h^{-1} (a representative average for NDRA) was taken as the reference. (B) Same data as in part A, but combined with absolute emission amounts.

advised to reduce speed on surface unit 2.2 (silt and clay with gravel), which has by far the highest emission rate of all 17 surface units in the Nellis Dunes area. Reducing speed is also important on units 3.1 (desert pavements) and 4.3 (silty drainages). In the dunes, especially the unvegetated dunes (unit 1.1), reducing the driving speed is not required because these surfaces produce nearly no dust during ORV driving. Note that these recommendations are based solely on absolute emission rate and not on dust chemistry or mineralogy.

4.2.3 Keeping distance

The concentration of emitted dust decreases rapidly with the distance from the source due to natural dilution processes. Numerical modeling and experimental work have shown that this decrease usually occurs exponentially. To reduce the risk of inhaling high concentrations of dust, drivers should therefore keep sufficient distance to other vehicles especially when following another vehicle. Driving in a column of vehicles is strongly dissuaded. A distance of at least 50 m between vehicles is advised. Drivers should also observe the wind direction and drive accordingly to avoid the most intense dust clouds.

4.2.4 Refraining from creating unnecessary damage to the soil

Drivers should stay on existing trails and refrain from driving on undisturbed desert surfaces. This is especially important on all desert pavements (unit 3.1), which show the highest increase in dust emission potential when disturbed. The only unit where driving outside existing trails does not increase emissions and cause unnecessary damage to desert surfaces is unit 1.1 (unvegetated sand dunes).

Another activity that should be avoided is driving in small circles. Such circles occur on many spots in the Nellis Dunes area, especially close to the parking lots. Continuous driving in these circles results in significant incisions in the soil and emits much dust.

4.2.5 Recommendations

1. In terms of dust production, the *most recommendable type of vehicle* for off-road driving in the Nellis Dunes area is the dirt bike. This vehicle produces considerably less dust than the dune buggy and the 4-wheeler. The highest amounts of dust are produced by the 4-wheeler. The 4-wheeler also inflicts considerably more damage to the undisturbed desert soil than dirt bikes or dune buggies. Therefore, for lessening dust emissions and preventing soil destruction, the use of 4-wheelers in the Nellis Dunes area is not

recommended. If 4-wheelers are used, drivers should stay on the trails at all times except in the unvegetated dunes of unit 1.1 where driving does not increase dust emissions and does not disturb the soil.

2. *Limiting the driving speed* is an easy and very effective measure to reduce dust emissions in ORV areas. Even a limited reduction in speed is very helpful. Drivers are especially advised to reduce speed on surface unit 2.2 (silt and clay with gravel). Reducing speed is also important on units 3.1 (desert pavements) and 4.3 (silty drainages). When considering dust emissions generated by ORV use, it is not necessary to reduce the driving speed in the unvegetated dunes (unit 1.1) because that activity has little effect on dust emissions.

3. *Drivers should keep enough distance to other vehicles*, especially when following another vehicle. A distance of at least 50 m is advised. Driving in a column of vehicles is strongly dissuaded. Drivers should also observe the wind direction and drive accordingly to avoid the most intense dust clouds.

4. *Drivers should stay on existing trails* and refrain from driving on undisturbed desert surfaces. The only unit where driving outside existing trails does not increase dust emission or destroy fragile desert soils is unit 1.1 (unvegetated sand dunes).

4.3 Season of driving

Dust transport in the Nellis Dunes Recreation Area is highest in the spring months, and especially in April and May (Fig. 1). This is a direct result from wind erosion activity, which peaks during this period. During days with heavy wind erosion a blanket of fine dust can be often observed above the central dune area. This blanket dilutes as the dust is evacuating from the area, but is constantly renewed and the dunes remain covered by it as long as there is substantial wind erosion. This blanket of dust should be considered a concern, not only because of the high dust concentrations but also because the airborne dust generated from the dunes is finer than the dust emitted elsewhere in the Nellis Dunes area, even in the silt areas (Fig. 31). Also, this dust is likely to contain palygorskite and varying concentrations of arsenic. The units of greatest concern are the vegetated dunes (unit 1.2) and the areas with a thin layer of blown-in dune sand (unit 1.4). Due to dilution, concentrations diminish rapidly as the dust is transported away from the dunes, but local zones of high concentration do occur where wind erosion is important, for example in the sandy area in the northwestern portion of the NDRA.

These blankets of dust are most abundant in the spring and are rather sparse from July to February. As far as the season is concerned, driving in the Nellis Dunes area is most recommendable in summer, followed by the fall, and winter. Spring has the greatest

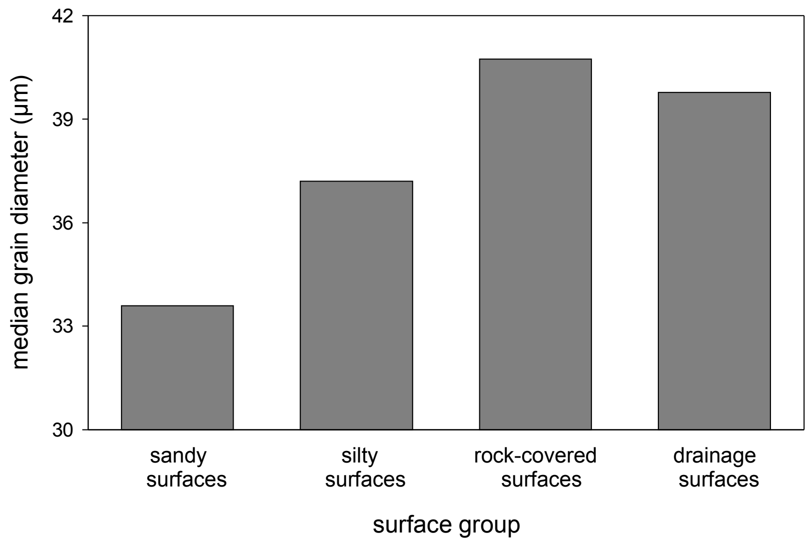

Fig. 31: Median grain diameter of the total suspendable dust fraction (0-60 µm) at NDRA. Numbers are annual averages and refer to the average diameter in the lowermost meter above the ground.

potential for windy days and is the least recommendable. However, temporary periods of high wind speed may occur at any time during the year and visits to the Nellis Dunes area should be avoided on such days.

Because NDRA is located in a desert the topsoil is dry during most of the year. Emission of dust, either by off-road driving or wind erosion, is very unlikely when the topsoil is wet. The days after a sufficient rainfall are thus the best periods to drive in the Nellis Dunes area when considering only dust emissions. Fine sediment dries much slower than coarse sediment and is thus much longer protected. Most of the surfaces covered by dune sand (units 1.1, 1.2 and 1.4) dry quickly and may already be fully emissive again after only a short time. The thunderstorms in July and August provide less protection than the rain showers in the fall and winter. The amounts of precipitation may be higher, but the temperatures and evaporation rates are also higher.

4.2.5 Recommendations

In the Nellis Dunes area dust concentrations are generally lowest in the summer and fall. In summer and the early fall the wind blows from the S-SW and brings polluted air from Las Vegas to the site; in the second part of the fall the wind blows primarily from the NE and the air is much cleaner. In general, therefore, air quality at the Nellis Dunes

Recreation Area is greatest at the end of the fall and in early winter. Periods after rainfall, when the topsoil is wet or moist, are also times with the best air quality.

4.4 Personal protection

Apart from the recommendations listed above, additional protection from inhaling dust can be obtained by wearing appropriate clothing or other gear. A helmet with a closable visor offers some protection especially if provided with a filter to trap the dust. Helmets are also elementary accessories for protection against accidents and should be worn by off-road drivers at all times. For passive visitors to the site, dust masks and other protective gear may provide adequate protection, especially during periods or in locations of high dust concentration.

5. Recommendations for continuing research

5.1 Personal dust exposure

The study described in this report measured airborne dust concentrations at 68 locations in the NDRA. These measurements, which were carried out with passive dust traps (BSNEs) as well as with an active dust sampler (DustTrak), yielded information on dust concentration over the 17 surfaces types identified in the area. In addition, estimates were made of dust concentrations close to off-road vehicles. The results indicate that, especially in the NDRA itself, dust production is important and that airborne concentration at locations intensively used for off-road vehicular activity can be high. The problem is complicated by significant wind erosion in the sand dunes and surrounding zones, which adds significant dust to that generated by the ORV vehicles. However, it was beyond the scope of this study to measure the amounts of dust people inhale while performing various activities at NDRA.

Dust concentrations measured by dust traps (active as well as passive ones) do not always give representative information on the actual amounts of dust people are inhaling. One reason is that efficiency of traps varies with the wind speed. Temporal variations in the wind speed, which is the natural situation, thus complicate accurate measurements. Of even more importance is the physical activity of a person. The total volume of air and, thus, dust that a person inhales depends on the tidal volume (volume inhaled during one breath) and the number of breaths per time unit. Both parameters vary considerably with the physical strain exercised during driving or other activities. They also differ between children and adults, and between males and females. Therefore, the only way to correctly measure the amounts of dust effectively inhaled during ORV driving (or, for passive visitors, when watching ORV activity) is to use personal dust monitors. Monitors powered by human breathing itself are preferred over active monitors, which use a constant flow rate while in operation and do not account for temporal variability in physical strain. If personal dust monitors cannot be used (for example, because of insufficient robustness during ORV driving), a good alternative is to combine airborne dust concentrations with measurements of the total volume of air inhaled by riders during the driving. The latter option will also provide the total amount of dust inhaled by the riders.

To assess the actual risk to human health of the dust emissions in the Nellis Dunes area, separate studies are necessary. These studies should measure, or use animal models to measure how the human body reacts to the inhalation of the dust. Because the NDRA dust contains several components that are either known poisons, or may be harmful to health, a site-specific study is recommended. Such studies use actual dust collected from specific site(s) in order to determine if the various mixtures of materials have any synergetic (enhanced) or antagonistic (reduced) health effects. Measurements are recommended for all types of surfaces intensely used for off-road driving in the NDRA, during various conditions of driving speeds, and preferentially also for the three types of vehicles used in the area. Parallel measurements on passive visitors would also be very useful. In addition, measurements during heavy wind erosion are also recommended to determine the role of this natural process.

5.2 Chemical composition of ambient airborne dust

During the project the chemical composition of the topsoil was determined for all 17 surface units, and in locally emitted dust collected with the PI-SWERL. The PI-SWERL was preferred over a portable wind tunnel because it allows collection on smaller locations. It also allows collecting the emitted particles more efficiently. The PI-SWERL samples consist exclusively of locally emitted dust, and as such are representative of sediment produced by local wind erosion or local ORV activity. However, the ambient dust inhaled by drivers or passive visitors is not just composed of locally produced dust but also contains dust produced elsewhere in the area and is in transport. Such dust from distant sources usually has a different chemical composition than locally eroded dust, not only because of the potential difference in composition of the sources, but also because it is finer than locally eroded dust. Many chemical elements harmful to the human body are concentrated in the finest particle fractions. Therefore, to get an accurate measurement of the chemical composition of the airborne dust over the NDRA it is insufficient to analyze only locally eroded dust. The actual ambient dust, collected by (for example) BSNEs, should also be examined. This is especially important when local dust production is small but intense production is taking place at other areas within the NDRA. Such conditions happen during intense wind erosion, especially when the wind blows from the SW. The central sand dunes produce much dust, which is then transported to the much more stable areas in the northeast and east. In these parts of the NDRA the ambient airborne dust does not originate from local sources but from the much more productive areas in the center and southwest. Analysis of samples containing only local dust would give incorrect information on the composition of the ambient dust (which is what people are inhaling) in these areas. Such analyses were not possible in this study due to funding limitations.

Chemical analyses of ambient dust collected at various parts of the NDRA are thus recommended in addition to the soil and PI-SWERL samples already investigated.

The contributions of local and distant sources to the ambient airborne dust in the region should also be determined. It is strongly recommended to collect this information for various size fractions of the dust since chemical and mineralogical composition, degree of inhalation and the transportation characteristics of dust depend on the size of the particles.

5.3 Total composition

A total of 17 chemical elements potentially harmful to the human body have been analyzed in the samples collected during this project. Arsenic received the most attention because of its numerous known health risks when inhaled and because of its extraordinarily high concentrations in several of the surface units in the NDRA. However, as previously mentioned, mixtures of elements can have a synergetic (enhanced) effect or can act in a protective role. Therefore, although the other elements measured in this study were not present in sufficiently high enough concentrations to warrant individual attention, when combined with the arsenic and other minerals present in the dust, they may play an important role in impacting human health. In-depth studies of the site specific risk that NDRA dust poses to human health are needed.

In addition to the chemical elements, mineralogical composition of the dust is also of concern. X-ray diffraction analyses of topsoil samples taken from the 17 surface units demonstrated the presence of minerals known to be harmful when inhaled. Currently of greatest concern is the presence of palygorskite, which is an asbestiform mineral that may pose a potential health risk. Future research is needed to determine the morphology (i.e. length:width ratios of crystals) and airborne concentrations of palygorskite for the various surface types at NDRA. To date, mineralogical analyses of Nellis Dunes sediment have been carried out for topsoil samples only. XRD analysis of clay mineralogy requires very large sample sizes. Therefore, no information is currently available for airborne dust, either locally eroded (during ORV or during wind erosion) or in ambient dust samples. However, the palygorskite at NDRA preferentially occurs in the dune environments, and in the smallest size fractions, and therefore is most likely to become airborne during windy conditions. Therefore, until more is known about the palygorskite at NDRA, it is recommended that the dune areas and areas downwind be avoided during windy days.

Biological analyses of the dust would also be very useful. Studies from other regions documented the occurrence of many types of organisms in airborne dust. For the Nellis Dunes area in particular the presence of *Coccidioides immitis,* a fungus causing valley fever, should be checked. NDRA is located within the area in which this organism is known to be endemic. Apart from *Coccidioides immitis* investigation of other potentially harmful organisms would also be very useful.

5.4 Effects of exposure on disease resistance

Using mice as a laboratory model for humans provided evidence that Nellis Dunes dust affects the immune system even when inhaled at very low concentrations. This project investigated the effect of exposure to NDRA dust on dose-responsive decreases in specific IgM B-cell responses and CD4/CD8 splenic lymphocytic subpopulations. Histopathological examination of lungs was also carried out. Dose-dependent presence of mixed immune cell infiltrates and fibrotic lesions containing particulates birefringent in polarized light were found, most consistent with centroacinar silicosis.

To date, only three of the seventeen types of surface units that occur in the NDRA were investigated (units 2.2, 3.1, and 3.2). Units very popular to the public, such as the central sand dunes, the race tracks in the north, the parking lots, and several other intensely driven zones, have not yet been tested. Considering the very low concentration levels at which the dust of the three units tested were shown to have a negative health impact, testing of the remaining areas is essential.

The current study examined the effects during an acute 3-day exposure only. Effects due to longer exposures (1 month or greater) have not been examined. Additional studies could include analysis of human blood samples for trace metals such as As, Pb, Sr, Mn and Cr before and after NDRA off-roading activity. This, and other studies could shed more light on the impact of NDRA dust exposure on respiratory health and disease resistance.

5.5 Dilution of locally produced dust

What is also yet unknown is to what extent dust from NDRA may be contributing to air quality downwind. In the summer and early fall, the wind blows NDRA dust away from population centers. However, in the later fall and winter months, the wind blows primarily from the NE such that dust from NDRA has the potential to blow into the conurbation of North Las Vegas/Las Vegas. This dust will be diluted the farther it travels and dust concentration will decrease. In most cases the decrease is exponential: concentrations drop rapidly in the first few hundreds of meters. It is the coarsest particles that will settle out most rapidly. Finer particles are carried by the turbulent velocity fluctuations of the wind, and will stay aloft much longer. There is, therefore, also a decrease in the grain size of airborne dust as it is transported away from the source.

The decrease in concentration and particle size results in a gradient of the risk the dust provides to human health. In general, the greater the distance from the source the lower the risk becomes. Areas located relatively far from a source are usually safer although the incoming dust is relatively fine. Close by the source the risk is much higher, mainly because of the higher concentrations.

If a future study is able to determine a significant human health risk exists from NDRA-sourced dust, then an additional study may be warranted to assess the extent to which NDRA dust may affect larger areas and populations. Estimates of the degree of dilution of NDRA-emitted dust would be best performed by means of atmospheric dispersion models, which yield a much better overall picture than field measurements close to the Earth's surface can provide.

5.6 Inventory of ORV data

This project collected a significant amount of information on dust production by wind erosion and off-road vehicular activity in the Nellis Dunes Recreation Area. Emission rates as well as annual emission amounts were calculated. While the data for wind erosion are based on an extensive field campaign with dust measurements carried out year-round, the data for ORV were measured during two short-term studies, one measuring the emission rates during experiments with ORV vehicles, and the other measuring the potential emissions and deflation thresholds (PI-SWERL study). All these studies, wind erosion as well as ORV, were performed using standard methodology and standard equipment and provided accurate data.

The only uncertainty in the data set is the exact number of off-road drivers that visit NDRA annually, the exact length and location of the trajectories they follow, and the variation of the visits throughout the year. The numbers used for these variables during calculation of the annual emission by ORV in NDRA were derived from previously published information (number of visitors) and from careful estimates based on our numerous visits to the area. Although we feel very comfortable with the values we used in the calculations, to confirm the results detailed quantitative information on these variables would be required. This would include accurate counts of the number of visitors during one complete year, interviewing riders, and measuring the occupation of the zones in NDRA most popular to off-road driving.

APPENDICES

Appendix A

Radionuclide Characterization of Nellis Dunes Recreation Area Soils

Appendix B

Gross Erosion, Net Erosion and Gross Deposition of Dust by Wind: Field Data from 17 Desert Surfaces

Radionuclide Characterization of Nellis Dunes Recreation Area Soils

R. Sudowe[1,2], A. Roman[2], B. Buck[3], D. Goossens[3] and Y. Teng[3]

[1]*Department of Health Physics and Diagnostic Sciences, & Radiochemistry Program, University of Nevada Las Vegas*
[2]*Radiochemistry Program, University of Nevada Las Vegas*
[3]*Department of Geoscience, University of Nevada Las Vegas*

Every soil contains a variety of naturally occurring and man-made radionuclides. The presence of shorter-lived man-made radionuclides in the soil is the result of fallout from atmospheric nuclear weapons tests conducted between 1945 and 1963. The resulting terrestrial radiation exposure to humans makes up for about 8% of the total average annual exposure of 360 mrem. This exposure is due to the radiation field caused by gamma-emitting radionuclides present in the soil. The alpha-emitting nuclides present in the soil have a higher energy deposition associated with their decay; however their range is so small that they cannot penetrate the outer layer of the skin. Their contribution to the external radiation exposure is therefore insignificant.

This situation changes drastically if radionuclides, in particular alpha emitters, are incorporated in the human body. Such incorporation can occur either through ingestion or, more likely, through inhalation. Radionuclides entering the body through inhalation will deposit either in the nasal passages, the tracheobronchial tree or the deep lung parenchyma. These three regions have very different characteristics for retention of aerosols that are introduced.

The penetration into these regions is determined entirely by the aerodynamic properties of the particles inhaled, in particular the particle diameter. Penetration into the deep lung parenchyma is the most important process to consider. As a result of this penetration the radioactive atom is placed in the immediate vicinity of a biologically sensitive target, such as the lung tissue. The energy resulting from the radioactive decay is completely absorbed by the tissue, which gives rise to an appreciable internal dose. In particular the high-energy deposition associated with the alpha decay of the radon daughters' polonium-218 and polonium-214 is of concern.

Off-road driving at NRDA will not only cause significant dust inhalation by the driver. It also has the potential to significantly increase the amount of dust generally present in the air. This will likely affect the air quality not only in the vicinity of NRDA but also in places that are downwind from the dunes. The goal of this preliminary study was to determine the concentration of radionuclides in soil samples from the NDRA to assess the potential health hazard associated with the dust inhalation.

A total of seventeen samples obtained from the NDRA were assayed to determine the concentration of gamma-emitting radionuclides. The samples were measured using a Canberra Model GR3519 high-purity germanium gamma detector with a relative efficiency of 35%. A certified soil reference standard in the same sample geometry was used to perform a multi-point energy and detection efficiency calibration on the detector. The calibration was carried out in accordance with ANSI Standard N42.14-1999. A certified reference material obtained by the National Institute for Standards and Technology was measured as an unknown sample to verify the calibration. Measurement and subsequent analysis of the soil samples was carried out using a modification of EPA Method 901.1. The samples, a blank and the detector background were all measured for 72 hours with the exception of one sample that was measured for 88 hours. All results were background corrected. The activities measured were corrected for sample mass to obtain the specific activity in picocurie per gram of soil.

The radioisotopes actinium-228 (Ac-228), lead-212 (Pb-212) and bismuth-212 (Bi-212) from the thorium decay series were found in all samples. The mother nuclide for this series, thorium-232 (Th-232) was found in seven samples. The members of the uranium decay series protactinium-234m (Pa-234m), lead-214 (Pb-214) and bismuth 214 (Bi-214) were also identified in all samples. Thorium-231 (Th-231) from the actinium decay series was found in all of the samples and protactinium-231 (Pa-231) from the same series was identified in five samples. The mother nuclide for this series, uranium-235 (U-235) was found in all samples except one. In addition the primordial isotope potassium-40 (K-40) was present in all samples. These radioisotopes are all naturally occurring and their presence is not unexpected. To understand the potential hazards to humans who inhale dust containing these radioisotopes, a separate study is required.

Cesium-137 (Cs-137) was also found in all samples. This isotope was deposited in the soil as a result of atmospheric testing of nuclear weapons. The Annual Limit of Intake for Inhalation of Cs-137 is 200 micro Curie. This is for a person designated as a radiation worker; for the general public this limit needs to be reduced to 4 micro Curie. The largest concentration of Cs-137 in the Nellis Dune soil samples analyzed was 2.1×10^{-7} micro Curie per gram of sample. The sample was taken at dust station 24, originating from soil type 3.3. Based on this concentration a person would have to inhale 19,046 kg (or 42,045 lbs) of soil to exceed the limit for the general public. *We can state with confidence that the Cs-137 content in these samples does not pose any health hazard.*

EARTH SURFACE PROCESSES AND LANDFORMS
Earth Surf. Process. Landforms (2010)

Published online in Wiley Online Library
(wileyonlinelibrary.com) DOI: 10.1002/esp.2080

Gross erosion, net erosion and gross deposition of dust by wind: field data from 17 desert surfaces

Dirk Goossens[1,2]* and Brenda Buck[1]
[1] Department of Geoscience, University of Nevada Las Vegas, 4505 S Maryland Parkway, Las Vegas, NV 89154-4010, USA
[2] Physical and Regional Geography Research Group, Department of Earth and Environmental Sciences, Katholieke Universiteit Leuven, Geo-Institute, Celestijnenlaan 200E, 3001 Heverlee, Belgium

Received 19 February 2010; Revised 12 July 2010; Accepted 19 July 2010

*Correspondence to: Dirk Goossens, Physical and Regional Geography Research Group, Department of Earth and Environmental Sciences, Katholieke Universiteit Leuven, Geo-Institute, Celestijnenlaan 200E, 3001 Heverlee, Belgium. Email: Dirk.Goossens@ees.kuleuven.be

ESPL
Earth Surface Processes and Landforms

ABSTRACT: Wind erosion measurements were carried out in Nellis Dunes Recreation Area, southern Nevada, USA. Gross erosion (the total mass of sediment effectively blown away from a surface), gross deposition (the total mass of sediment effectively depositing on a surface) and net erosion (the difference in sediment mass before and after an event) were measured for 1 year, on 17 different types of surfaces developed on loose dune sand, compacted sand, loose silt, compacted and/or aggregated silt, rock-covered sands and silts, mixtures of sand, silt and clay, exposed petrocalcic horizons, gravelly substrata and bedrock. Results showed that net erosion, which is the type of erosion measured in field and laboratory experiments, strongly differs from gross erosion. Activity on a surface is much higher than classic net erosion measurements suggest. Future studies on wind erosion should better acknowledge the distinction between the two types of process. Also, a grain diameter of maximum susceptibility to wind erosion ('optimum deflation diameter') near 70 μm as proposed by the aeolian literature only exists for net wind erosion. No such optimum diameter was found for gross wind erosion within the particle range 0–100 μm delineating the transport modes of suspension and modified saltation. In addition, desert surfaces predominantly composed of sand did not show an optimum deflation diameter (for net erosion) around 70 μm. Instead, there was a preferential grain size around 15 μm at which particles were most vulnerable to net emission. Desert surfaces poor in sand showed the classic value of 70 μm. This suggests that interactions exist between the type of surface and the susceptibility of particles to wind erosion. This study is solely based on field data. Although results are supported by two previous wind tunnel studies, more wind tunnel experiments documenting the interactions between gross erosion and gross deposition are necessary. Copyright © 2010 John Wiley & Sons, Ltd.

KEYWORDS: wind erosion; deposition; dust; particle size; deflation diameter

Introduction

Erosion, transportation and sedimentation (or deposition) are basic concepts in geomorphology. In the literature erosion has been described in different ways, but Thornbury's (1954) definition: 'the entrainment of loose weathered materials by a mobile agent' provides a good summary. Transportation is 'the movement of detached soil material across the land surface or through the air' (Websters Online Dictionary, 2009). Sedimentation can be defined as 'the settling of solids from suspension in a fluid' (Evans, 2004). Although these definitions themselves are clear, their interpretation often is incomplete, or even incorrect. What is measured – and described – as erosion in many cases is actually accumulation (another correct term is net erosion), i.e. the difference in grain mass, usually measured on a surface, before and after a time interval within which one or more geomorphic processes have occurred. Accumulation can be positive or negative. If it is positive the surface is nourished with new sediment and it will grow; the sediment layer thickens. If it is negative, a mass (of particles) is disappearing from the surface and the sediment layer becomes thinner. Because erosion and sedimentation are simultaneously occurring processes, every measurement, either in the field or in a laboratory, automatically measures accumulation. Real (or gross) erosion, representing the total mass of sediment effectively worn away from the surface, usually is much larger than net erosion because the latter also depends on deposition (Figure 1). Settling particles do not necessarily originate from the surface they are settling on; they may have been eroded substantially upstream, upwind or upslope from a different substratum, and are just settling during their transportation. Gross deposition includes *all* particles that settle on the surface, regardless of whether they will be retained or are subsequently entrained via rebound, through fluid dynamic forces, or as a result of impact of freshly depositing grains. Gross deposition takes place as long as sediment is present in the airflow (see Figure 1).

For geomorphic applications it usually is net erosion that is of concern for this is what we see and measure on the surface.

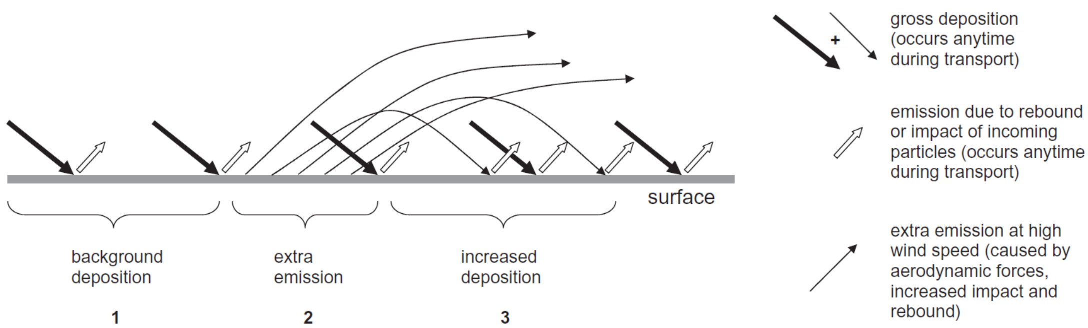

1: rebound-generated emission + impact-generated emission < deposition
net erosion < 0 (positive accumulation)

2: aerodynamic emission + rebound-generated emission + impact-generated emission > deposition
net erosion > 0 (negative accumulation)

3: rebound-generated emission + impact-generated emission < deposition
net erosion < 0 (positive accumulation)

Gross erosion = sum of all particles leaving the surface
Gross deposition = sum of all particles arriving at the surface
Net erosion = sum of all particles leaving the surface minus sum of all particles arriving at the surface
Total particle exchange = sum of all particles leaving the surface and all particles arriving at the surface

Figure 1. Concept of gross erosion, gross deposition, net erosion and total particle exchange.

Exceptions where gross erosion is of concern are, for instance, the deformation of the top layer, or the energy balance on a substratum.

Because laboratory and field measurements automatically measure net erosion, numerical relationships obtained (or derived) from such measurements specifically apply to this type of erosion. They do not necessarily apply to real (gross) erosion. A good example from the aeolian domain is the relationship between deflation threshold and grain size. Deflation threshold (for dry sediment) is minimum for grains somewhere between 40 and 80 µm, usually around 70 µm, and increases as the sediment becomes coarser or finer. This has been demonstrated abundantly in the literature (Bagnold, 1941; Horikawa and Shen, 1960; Iversen and White, 1982, Cornelis and Gabriëls, 2004). However, since wind tunnel and field measurements always measure net erosion the deflation threshold curve refers to this type of erosion. Does gross erosion also show a minimum deflation threshold, and if so, is it located near the same grain size of approximately 70 µm? The answer to this question can only be investigated indirectly, by measuring net erosion and gross deposition separately and combining both types of process. Similar examples exist for other geomorphic research fields.

This study attempts to provide more information on the importance of gross erosion, gross deposition and net erosion in aeolian processes. It aims to investigate the proportion of each subprocess in total aeolian activity, and to examine how that proportion varies as a function of particle size. Field measurements were carried out on 17 types of surfaces developed on various types of soils in the Mojave Desert (southwest USA). These soil and surface types are typical for most deserts on Earth, making the results of general and not just of local interest. Studying the processes on various substrata also allows examining whether the relationships are also affected by the type of surface. Substrata developed on identical sediment but with different surface characteristics (example: silt substrata with and silt substrata without rock cover) are expected to show different dynamics.

This study is entirely based on field data. Wind tunnel experiments with various types of sediment, and carried out with a set of aerodynamic conditions, would be the next logical step to evaluate these results and to better document the interactions between gross erosion and gross deposition.

Geographical and Sedimentological Settings

Situation

Field measurements were conducted for a total of 363 days (almost 1 year) at Nellis Dunes Recreation Area (NDRA), Nevada, USA (Figure 2). NDRA lies 6 km north-east of the city of Las Vegas in the north-eastern portion of the Las Vegas Valley referred to as the Nellis basin (Beard *et al.*, 2007).

Sediments and surface types

Seventeen surface types, which can be grouped into four major classes, appear in the Nellis Dunes area. These classes are:

1. *Sand and sand-affected areas*: active or stabilized sands, with or without rock fragments and/or vegetation.
2. *Silt/clay areas*: loose and slightly stabilized silt/clay deposits, with or without rock fragments.
3. *Rock-covered areas*: stabilized silty or sandy silty deposits with rock fragments on top, desert pavements over a silty sublayer, bedrock, and petrocalcic horizons.

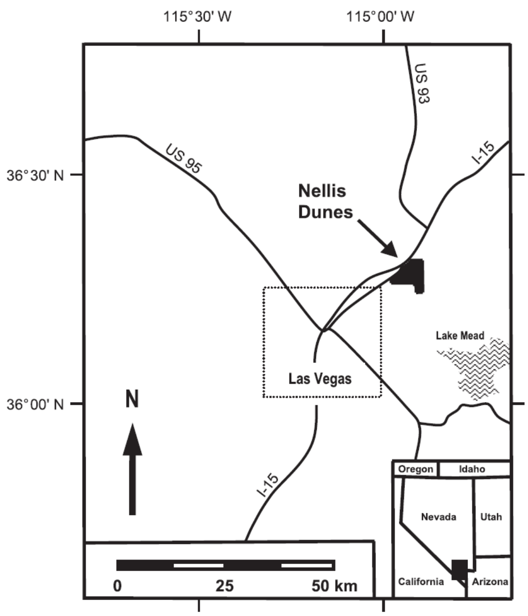

Figure 2. Location of Nellis Dunes Recreation Area, southern Nevada, USA.

4. *Drainage areas*: active drainages in sand and silt areas, and gravelly drainages.

In this study sand is defined as the fraction 63–2000 µm, silt as the fraction 2–63 µm, and clay as the fraction <2 µm.

Information on grain size, various soil and surface characteristics and vegetation cover is provided in Table I. Photographs of the units can be consulted in studies by Goossens and Buck (2009a, b) and McLaurin *et al.* (in press). The latter study also contains a detailed map of the study area with the exact location of all units. A short description of each surface type follows below.

Class 1: sand units

- *Surface unit 1.1: dunes with no vegetation.* Active dune sands and sand sheets with no vegetation. The median grain diameter is close to 210 µm and silt and clay particles occur only very sparsely (usually less than 3%). Sparse rock fragments and underlying petrocalcic horizons may locally outcrop where the sand layer is very shallow. Surface crusts are absent.
- *Surface unit 1.2: dunes with vegetation.* Dune sands with sparse and isolated shrubs (size: usually 30–70 cm; cover density: 5–10%). The sand is active and there is no surface crust. The median grain diameter is around 180 µm. Small coppice dunes may be present. Rock fragments may occur on the surface, but rock cover is low (<5%) and does not affect the deflation.
- *Surface unit 1.3: disturbed sand surfaces.* Mixture of loose and active sand, rock fragments and (eventually) bedrock. This unit typically occurs in areas where shallow (<2–3 cm) sands cover a substratum of petrocalcic horizons and/or bedrock and disturbance by human activity is high.
- *Surface unit 1.4: patchy layers of sand over silty/rocky subsoil.* These surfaces constitute a shallow layer of loose sand (depth usually 1–3 cm) covering the subsoil. Many underlying clasts are exposed at the surface. There is no surface crust; the sand is active and small dunes may locally occur.
- *Surface unit 1.5: outcrops of fine sand and coarse silt.* Mixture of fine sand (90%) and silt/clay (9% silt and 1% clay). The median grain diameter is about 150 µm. These units are almost free of vegetation but show a continuous and permanent silty sandy surface crust.

Class 2: silt/clay units

- *Surface unit 2.1: silt/clay with crust.* These units typically occur adjacent to drainage channels in silt areas. The sediment is predominantly composed of silt and commonly shows a continuous cyanobacterial crust. Some vegetation (isolated shrubs) is typical. A few rock fragments may occur, but they remain sparse (<3–4%).
- *Surface unit 2.2: silt/clay with gravel.* Mixture of silt and gravel, but with considerably more (>85% in weight) silt than gravel on the surface. A surface crust may be present although many areas are not encrusted. These surfaces do not occur in drainage areas but are typically located on hill slopes and plateau escarpments.
- *Surface unit 2.3: aggregated silt deposits.* Silt/clay surfaces where the particles are bound in aggregates up to 5 mm in diameter. The percentage of free particles is low. A surface crust is common but the crust may be disturbed or even absent. These surfaces are entirely devoid of vegetation and result in a badlands-style topography.
- *Surface unit 2.4: disturbed silt surfaces.* Mixture of noncrusted silt, rock fragments and (eventually) bedrock. They occur in areas where the surface has been disturbed by human activity and are the silt equivalent of surface unit 1.3.

Class 3: rock-covered units

- *Surface unit 3.1: desert pavements.* Well-developed mature desert pavements over silty subsoil (Av horizon). The rock fragments are partially embedded in the silt and rock cover density is close to 100%. Vegetation (shrubs) may locally occur, but most desert pavements are devoid of any vegetation.
- *Surface unit 3.2: rock-covered surfaces with silt/clay zones.* The top layer is composed of silt with some very fine sand and contains many rock fragments (cover percentage: 60–80%). Pavements are less-well developed than for unit 3.1. The areas in between the rock fragments show a continuous and permanent surface crust. Vegetation (shrubs) typically covers 10–15% of the surface.
- *Surface unit 3.3: rock-covered surfaces with sandy loam.* These surfaces resemble surface unit 3.2, but the top layer contains small amounts of sand. The sand has been blown in from nearby sand areas. In the Nellis Dunes field they typically occur in silt areas located close to the sand dunes.
- *Surface unit 3.4: rock-covered surfaces with encrusted sand.* This type of surface is similar to the 3.2 and 3.3 surfaces but is largely composed of sand, with small amounts of silt. It is covered by a continuous cyanobacterial crust. This crust is much weaker than the silt crusts of surface units 3.2 and 3.3. Vegetation (shrubs) is common and covers approximately 10% of the surface.
- *Surface unit 3.5: bedrock and/or petrocalcic horizons.* Outcropping bedrock and areas of outcropping petrocalcic horizons. The percentage of rock cover is close to 100%. Some sparse cracks may occur in the rock, and these accumulate fine atmospheric dust over time.

Class 4: active drainages

- *Surface unit 4.1: gravelly drainages.* Active drainages with almost pure gravel. In the Nellis Dunes area these surfaces

Table I. Texture, rock cover, surface crusting, surface resistance and vegetation cover of the 17 surface units. Texture is for the top soil (upper cm) and was derived from dry laser diffraction analysis. All numbers refer to the average of the dust stations located in the units; values in parenthesis indicate standard deviation

	Soil texture			Rock fragments			Surface crust	Surface resistance		Vegetation
				rock cover (on surface)						
Surface unit	sand (>63 µm) (%)	silt (2–63 µm) (%)	clay (<2 µm) (%)	total area (%)	non-vegetated area only (%)	rock content (>2 mm in upper 15 mm) (%)	presence	normal resistance (kg* cm^{-2})	tangential resistance (kg* cm^{-2})	vegetation cover (%)
Sands and sand-affected surfaces										
1.1	96·76	3·23	0·01	0·0	0·0	0·01	no	0·136	0·051	0·5
	(0·05)	*(0·05)*	*(0·00)*	*(0·0)*	*(0·0)*	*(0·00)*		*(0·001)*	*(0·010)*	*(0·7)*
1.2	95·03	4·95	0·02	4·3	4·6	13·86	no	0·143	0·134	8·7
	(1·19)	*(1·19)*	*(0·00)*	*(1·5)*	*(1·5)*	*(4·64)*		*(0·023)*	*(0·040)*	*(3·3)*
1.3	91·46	8·11	0·42	54·6	54·9	49·74	no	0·159	0·171	0·5
	(0·51)	*(0·54)*	*(0·03)*	*(0·2)*	*(0·6)*	*(1·41)*		*(0·021)*	*(0·042)*	*(0·7)*
1.4	92·71	7·23	0·05	23·6	28·3	40·84	no	0·149	0·244	18·3
	(0·08)	*(0·06)*	*(0·01)*	*(9·8)*	*(7·3)*	*(31·69)*		*(0·042)*	*(0·124)*	*(13·7)*
1.5	88·35	11·43	0·22	4·3	4·3	10·77	yes	0·615	0·710	1·0
	(0·95)	*(0·70)*	*(0·25)*	*(4·7)*	*(4·8)*	*(1·17)*		*(0·700)*	*(0·297)*	*(1·4)*
Silt/clay surfaces										
2.1	82·50	16·99	0·51	3·4	4·1	19·62	yes	0·210	0·780	16·8
	(2·74)	*(2·78)*	*(0·04)*	*(0·6)*	*(0·6)*	*(4·89)*		*(0·028)*	*(0·148)*	*(4·2)*
2.2	59·93	38·63	1·44	11·3	11·6	24·45	yes	0·207	0·689	2·1
	(7·28)	*(6·52)*	*(0·77)*	*(7·5)*	*(7·7)*	*(5·50)*		*(0·067)*	*(0·084)*	*(0·2)*
2.3	84·80	14·67	0·53	2·7	2·7	31·85[3]	yes	0·117	0·364	0·0
	(2·27)	*(2·19)*	*(0·09)*	*(3·7)*	*(3·7)*	*(2·48)*		*(0·016)*	*(0·181)*	*(0·0)*
2.4	89·27	10·29	0·44	31·7	31·9	42·31	yes	1·112	1·940	0·5
	(3·31)	*(2·73)*	*(0·57)*	*(18·2)*	*(18·5)*	*(21·84)*		*(0·334)*	*(0·577)*	*(0·7)*
Rock-covered surfaces										
3.1	53·74	40·18	6·08	94·9	97·8	74·40	no[1]	NA[1]	NA[1]	3·0
	(0·26)	*(0·13)*	*(0·39)*	*(3·7)*	*(2·0)*	*(6·69)*				*(1·8)*
3.2	74·21	23·22	2·58	64·4	75·6	46·68	yes	1·109	1·451	14·4
	(6·14)	*(4·68)*	*(1·46)*	*(6·4)*	*(12·7)*	*(6·52)*		*(0·409)*	*(0·270)*	*(5·8)*
3.3	91·20	8·41	0·39	32·6	40·1	32·29	yes	1·152	0·969	18·4
	(2·33)	*(1·84)*	*(0·49)*	*(4·2)*	*(6·6)*	*(5·33)*		*(0·314)*	*(0·086)*	*(3·0)*
3.4	91·44	8·11	0·45	22·6	25·1	20·81	yes	0·218	0·560	10·1
	(1·21)	*(1·19)*	*(0·03)*	*(3·0)*	*(2·5)*	*(13·12)*		*(0·003)*	*(0·167)*	*(2·7)*
3.5	45·36	49·07	5·56	94·3	98·5	99·99	no[2]	NA[2]	NA[2]	4·4
	(1·26)	*(1·12)*	*(0·14)*	*(1·1)*	*(0·0)*	*(0·00)*				*(1·1)*
Drainage surfaces										
4.1	91·49	8·18	0·34	97·9	97·9	94·77	no[1]	NA[1]	NA[1]	0·0
	(2·40)	*(2·35)*	*(0·05)*	*(1·3)*	*(1·3)*	*(6·82)*				*(0·0)*
4.2	92·25	7·46	0·30	76·0	76·0	63·93	no	0·085	0·127	0·0
	(0·50)	*(0·50)*	*(0·01)*	*(1·5)*	*(1·5)*	*(0·78)*		*(0·002)*	*(0·016)*	*(0·0)*
4.3	90·40	9·57	0·04	35·8	47·0	60·54	yes	1·452	1·219	21·4
	(7·58)	*(7·54)*	*(0·03)*	*(4·6)*	*(15·2)*	*(33·65)*		*(0·042)*	*(0·286)*	*(15·5)*

[1] Pavement.
[2] Bedrock.
[3] Particles >2 mm consist of aggregates of silt.

typically occur in the channels of the major drainages. The gravel is almost free of sand, silt and clay and its cover percentage is close to 100%.

- *Surface unit 4.2: gravel and sand drainages.* Active drainages with a mixture of sand and gravel. They occur in sand areas, more in particular in the smaller sized valleys, and also in the upstream zone of the larger drainages where there is insufficient water to wash the sand. Vegetation is usually absent.
- *Surface unit 4.3: gravel and silt/clay drainages.* Active drainages with a mixture of silt and gravel. They are the silt equivalent of surface unit 4.2 except that many of them have considerable vegetation, usually shrubs (size: 30–70 cm; cover density: 10–30%). Silt/gravel drainages without vegetation also occur, especially in first-order channels in badlands.

Methodology

Dust collection and analysis

Dust collections were performed on all 17 surface units. Four stations were installed on each unit, 68 stations in total. To ensure adequate sampling over the field and avoid potential interaction, measuring spots were located well away from each other, usually several hundreds of meters. Stations were also located well away from zones of intense recreational use.

Each station consisted of a 2 m long, 2 cm diameter metal pole to which four samplers were attached. Airborne sediment was collected at the following heights: 25 cm, 50 cm, 75 cm and 100 cm. No collections were performed at higher levels because the focus of the study was on erosion and deposition at or near ground level. BSNE samplers (Fryrear, 1986) were used because (1) this type of sampler is widely in use worldwide; (2) its efficiency for collecting particles has been determined over a wide particle range, from less than 10 µm up to 287 µm (Shao *et al.*, 1993; Goossens and Offer, 2000; Goossens *et al.*, 2000; Sharratt *et al.*, 2007). Samples were collected over periods of 2 weeks each, from 19 December 2007 to 16 December 2008. Twenty-six periods were thus sampled. Two-week samplings were the minimum to collect enough dust for subsequent grain size and chemical analysis.

After each period new, fresh samplers were installed and the used ones brought to the laboratory. Sediment was collected with a brush. Samples were weighed to a precision of 0·0001 g and subsequently analyzed for grain size distribution using a Malvern Mastersizer 2000 laser particle size analyzer (Malvern Instruments Ltd, Malvern, UK). Samples were initially analyzed in a water solution, but additional dry analyses were performed with a Malvern Mastersizer S instrument to determine the degree of dispersion during wet analysis. Some dispersion also occurred in a few samplers themselves during (rare) cases of rainfall during the measurements. All data were corrected for such dispersion using the information provided by the dry analyses.

Corrections for insplash of particles into the BSNEs during heavy rainfall were also performed. Comparisons of sediment mass collected at a same level and at identical airborne concentrations for splash and non-splash episodes showed that significant insplash only occurred in the lowermost two BSNEs; the uppermost two BSNEs were not significantly affected. Splash corrections were only necessary for a minority of collection periods.

Wind measurements

Three 20 m wind towers and one 10 m wind tower were erected in the Nellis Dunes area. Each cluster of dust stations contained at least one wind tower. Wind speed, wind direction and temperature data were collected as 1 h averages between 19 December 2007 and 16 October 2008 and as 10 min averages from 16 October 2008 to 16 December 2008. Data from the nearby Nellis Air Force Base meteorological station, which borders on the test field, were used to fill data gaps. Such gaps were filled only after careful calibration between the wind towers and the Nellis Air Force Base station.

Additional wind measurements were performed at all dust stations with a portable 3 m long wind tower containing four anemometers (heights: 56 cm, 121 cm, 202 cm and 259 cm) to determine the roughness length (z_0) and the wind profile near each pole. In total, 396 periods of 10 min each were sampled with the portable tower. Wind speeds at all catcher levels (25 cm, 50 cm, 75 cm and 100 cm) were then calculated and linked to the data collected from the four wind towers. From this information it is possible to calculate the wind speeds and friction velocities required to determine erosion, for wind erosion only occurs at winds strong enough to create a neutral atmospheric boundary layer in the lowermost meters near the ground (see Turner, 1994). Under such circumstances the wind profile is logarithmic and there is no need for stability corrections. Since there was at least one wind tower close by each dust station and wind speed was measured at relatively high altitudes from each tower, and because

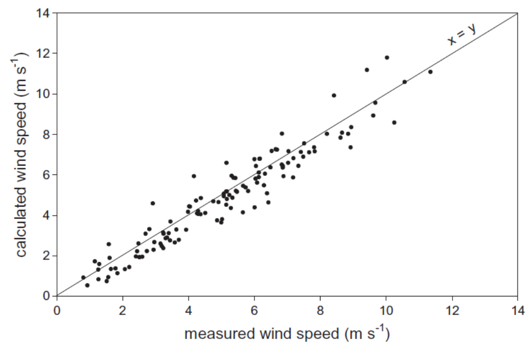

Figure 3. Calculated versus measured wind speeds. Duration of test periods varied from 20 to 40 min. Each test period consisted of individual intervals of 10 min; 396 intervals of 10 min were measured in total.

the roughness length is known at each station, wind data can be reconstructed at all stations using the wind profile (logarithmic, as explained above) and the tower data. Comparing data collected by the portable tower to those reconstructed by the method explained above (Figure 3) confirms the reliability of the technique.

Calculation of net erosion

Various methods exist to calculate net erosion of soil dust. A review is given in a recent book by Shao (2008). Emission calculations based on airborne dust concentration data generally are more reliable than calculations based on airborne dust transport data because they are more direct; therefore we selected the former option to calculate net erosion in the Nellis Dunes area.

Methods based on airborne concentration use vertical particle exchange to calculate vertical dust flux. Because this flux is affected by both the upward and downward movements of particles it always is an average flux; while in transport particles experience the effects of both velocity components. Also, they experience, simultaneously with the turbulent forces, the effect of gravity. Thus, numerical values of vertical dust flux collected from experiments always refer to net vertical flux; there is no need to add an extra term for deposition for the effect of deposition is already included in the experimentally recorded number.

Vertical dust flux can be calculated with Gillette's (1977) gradient method:

$$F = \frac{k \cdot u_* \cdot (C_1 - C_2)}{\ln(z_2/z_1)} \qquad (1)$$

where F = vertical dust flux, k = von Karman constant (0·4), u_* = friction velocity, and C_1 and C_2 = airborne dust concentrations at heights z_1 and z_2, respectively. This formula calculates the average vertical flux between heights z_1 and z_2; it does not calculate the erosion at ground level nor does it provide information on how the flux varies within the vertical layer bordered by z_1 and z_2. The latter problem can be solved by integrating the original exchange formula for neutral atmospheric conditions (neutral because we apply it to episodes with active wind erosion), $F = -k \cdot u_* \cdot z \cdot \frac{\partial C}{\partial z}$, accepting that C varies with z as a power function $C = a \cdot z^b$ (see Nickling, 1978;

Buschiazzo and Zobeck, 2005), where a and b are numerical constants. This leads to:

$$F = -k \cdot u_* \cdot a \cdot b \cdot z^b \tag{2}$$

This expression, which was first proposed by Goossens *et al.* (2001), allows calculating vertical dust flux at any arbitrary height z in the constant shear stress layer. For $b > 0$, F is negative and the flux is directed downward; for $b < 0$, F is positive and the flux is directed upward.

To calculate the flux at ground level, the best option is to construct the vertical flux profile and extrapolate it to zero level (Goossens *et al.*, 2001; Hoffmann *et al.*, 2008) for neither Gillette's gradient method nor Goossens *et al.*'s integration method provides a mathematical solution for $z = 0$. To do this, several options exist: (1) calculate the vertical flux for several separate layers using the gradient method, adjust each flux value to the average height of the corresponding layer, and extrapolate the profile to zero level (modified Gillette 1977 method); (2) use the gradient technique, but the vertical fluxes are calculated for layers bordered by the highest catcher (top) and each subsequent catcher underneath (bottom); the flux is then calculated as the average vertical flux for these layers (see Hoffmann *et al.*, 2008); (3) calculate the vertical flux at a large number of elevations using the integration method and extrapolating the profile to zero level (Goossens *et al.*, 2001); (4) calculate the vertical flux at only those elevations where the catchers are installed and extrapolate the profile to zero level. Comparative tests showed that the first and last option lead to similar results whereas those from the second option result in under-estimation and the third option results in an overestimation of the emission (Figure 4). The first option has the disadvantage that it sometimes results in negative erosion results and that small experimental error in the measurements (which is inevitable) has major effects on the final result. Option 4 does not suffer from these problems and also exclusively uses original data; therefore this option was selected to calculate net erosion in the Nellis Dunes experiment.

All extrapolations were done by fitting a third-order polynomial through the data points, which gave a variation coefficient $R^2 > 0{\cdot}99$ for all stations. Visual inspections of the profiles were made to confirm the extrapolations.

The airborne dust concentrations C_z, necessary to calculate erosion, were calculated by dividing the horizontal transport flux F_h measured by the BSNEs by the wind speed (at each appropriate elevation). Average values were used for each 2-week period because all horizontal flux data are 2-week averages. All data were corrected for the efficiency of the BSNE using information from the calibration studies by Shao *et al.* (1993) and Goossens and Offer (2000).

The value of u_* in Equation (2) refers to the average friction velocity of the episodes of wind erosion; not the average u_* of all 14 days in each 2-week period. To determine the episodes of wind erosion we measured the deflation threshold (critical friction velocity at which wind erosion starts) with a 'portable in situ wind erosion laboratory' (PI-SWERL, see Etyemezian *et al.*, 2007 for a description), at all dust stations. At least four measurements were made for each surface unit and the average deflation threshold was then calculated. The data can be consulted in the paper by Goossens and Buck (2009a). To calculate the value of u_* in Equation (2), all 1 h data from the 362 day long experiment were investigated and average friction velocities were calculated for each 2 week period by retaining only those u_* values that exceeded the deflation threshold. As 1 h periods are still quite long for averaging friction velocities for the purpose of erosion calculations, we

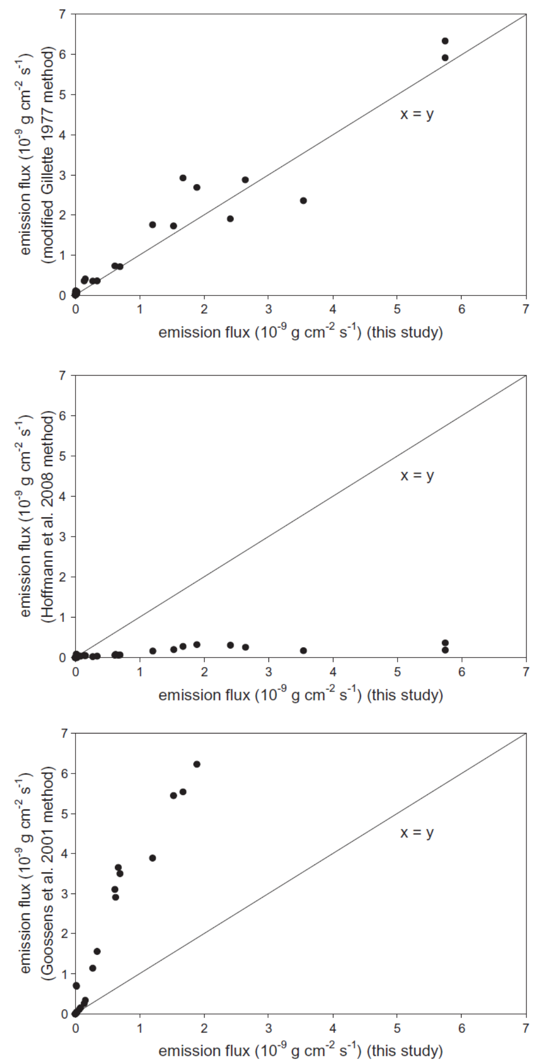

Figure 4. Comparison of methods for extrapolating vertical dust flux to ground level. See text for explanation of each method.

repeated the analysis for the period 16 October 2008 to 16 December 2008 for which 10 min data could be collected. Calculating the average friction velocities for 2 week intervals with these two options resulted in a difference of less than 3%, at all dust stations. Therefore, 1 h data could be used for calculating u_* in Equation (2).

Calculation of gross deposition

Various techniques exist to calculate gross deposition. An overview, including comparisons between techniques, can be found in the study by Goossens and Rajot (2008). No direct measurements of dust deposition were performed in NDRA because (1) direct measurements of deposition at ground level usually suffer from local disturbances; (2) the proportion of dust in sediment deposited in sand areas (for instance, the sand dune units 1.1 and 1.2 in NDRA) often is below the detection level of most grain size analyzers; and (3) the collection efficiency of dust deposition samplers heavily depends on wind speed and grain size, which affects the size distribution of collected dust (Goossens, 2007). Instead, dust deposition was calculated from the BSNE data using the inferential technique. This technique calculates deposition F_D as the product of airborne dust concentration C and the velocity of deposition v_d:

$$F_D = C \cdot v_d \tag{3}$$

In addition, comparative studies (Goossens and Rajot, 2008) showed that applying this technique to BSNE collections leads to deposition quantities identical to those measured with deposition catchers properly corrected for efficiency.

The velocity of deposition v_d, which is a function of particle size and shape and also depends on u_* and z_0, can be derived from standard graphs (see Sehmel, 1980), or it can be calculated from theoretical models (Sehmel and Hodgson, 1978; Slinn and Slinn, 1980; Slinn, 1983; Pleim *et al.*, 1984; Venkatram and Pleim, 1999). Because these models assume that particles are spherical, which is a too simplified presumption for natural dust (see Goossens, 2007 or Goossens and Rajot, 2008 for examples), we used Dietrich's (1982) formula to calculate v_d. This formula includes a term for flattening (*CSF*) and rounding (*P*) of grains and thus allows including particle shape in the calculations. For most types of soil-derived aeolian dust *CSF* and *P* are close to 0·70 and 3·45, respectively (Goossens, 2005); for the Nellis Dunes dust we used values of 0·69 and 3·47, which were derived from microscopic analysis of several dust samples. Strictly speaking Dietrich's formula does not calculate v_d but v_∞, the terminal settling velocity. For quartz grains in air and friction velocities below approximately 50 cm s^{-1} (typical values for the Nellis Dunes experiment reported here) the difference between v_d and v_∞ remains negligibly small once particles are coarser than 10 μm (see Sehmel, 1980). As the errors associated with particle shape are much larger than the difference between v_d and v_∞, Dietrich's approach was used. Comparisons of v_∞ and v_d calculated with Dietrich's (1982) and Slinn and Slinn's (1980) equations show that for (spherical, since Slinn and Slinn's formula applies to spheres) grains up to 50 μm the data are almost identical, and that for coarser grains the differences remain acceptable (Goossens and Rajot, 2008).

Velocities of deposition were calculated for 10 grain size fractions: 0–10 μm, 10–20 μm, 20–30 μm, 30–40 μm, 40–50 μm, 50–60 μm, 60–70 μm, 70–80 μm, 80–90 μm and 90–100 μm. Values for the mean particle size in each class (5 μm for the fraction 0–10 μm, 15 μm for the fraction 10–20 μm, etc.) were used when calculating deposition.

To obtain gross (i.e. real) deposition, all data need to be recalculated to a perfectly absorbent surface. For aeolian deposition, water most probably is the best option currently available (Breuning-Madsen and Awadzi, 2005; Gigliotti *et al.*, 2005; Goossens, 2005; Sow *et al.*, 2006); therefore all deposition fluxes were recalculated to a water surface using the conversion factors provided by Goossens' (2005) study. Field measurements on dust deposition in SW Niger by Goossens and Rajot (2008) showed that this approach leads to very reliable results.

Gross deposition values were calculated at all four levels where BSNEs were installed (25, 50, 75 and 100 cm). To determine gross deposition at ground level, vertical deposition profiles were calculated and extrapolated to zero level. As with net erosion, a third-order polynomial provided an excellent fit at all dust stations.

Note that the same dataset (concentrations measured with the BSNEs) is used for the calculations of gross deposition and net emission; this reduces the effect of experimental uncertainties when these two processes are compared.

Calculation of gross erosion

Because net erosion simply is the difference between gross erosion and gross deposition, gross erosion can be calculated as the sum of net erosion and gross deposition:

$$E = e + S \tag{4}$$

where E = gross erosion, e = net erosion and S = gross deposition. Note that, once sediment has been emitted, S can eventually become superior to E if sediment emitted upstream is settling at a rate higher than the local erosion rate. If this happens, e is negative, which simply means that the surface is accumulating sediment.

Calculation of evacuation rate

If E exceeds S, e is positive and the surface is losing sediment over time. The rate at which sediment is evacuated can be quantified by the ratio S/E. For example, if $S/E = 0{\cdot}90$ then 90% of the eroding particle mass is replaced with freshly settling grains eroded upwind; 10% of the mass is not replaced and will be evacuated from the spot in question. Especially the finest particle fractions, which are transported in long-term suspension and do not rapidly return to the surface, can be expected to be susceptible to evacuation. Note that, similar to E and S, evacuation can also be expressed in particle number instead of particle mass.

Calculation of total particle exchange

Total particle exchange can be calculated as $E + S$, the sum of gross erosion and gross deposition. It quantifies the total mass (or, alternatively, the total number) of particles impacting or leaving the surface. Note that it is not identical to total particle activity for it does not include those grains that are just being displaced over the surface without leaving it; however, it is proportional to total particle activity and in many cases it should give a good indication whether, and to what measure, a surface is characterized by high or low aeolian activity. Also, note that net erosion cannot be used for this purpose because highly active surfaces can be characterized by very low, even zero, net erosion. Because laboratory and field measurements always measure net erosion they do not necessarily provide correct information on how stable a surface is.

As far as the authors are aware, 'total particle exchange' has not been defined before in the aeolian literature to describe the sum of gross erosion and gross deposition and we propose to use that term in future studies.

Results and Discussion

The results of the Nellis Dunes experiment for annual average gross erosion (E), gross deposition (S), net erosion (e), evacuation rate (S/E) and total particle exchange ($E + S$) in terms of sediment mass are shown in Figure 5. Separate diagrams for the four surface groups are presented to illustrate the effect that each type of surface has on these data. Because the absolute values of E, S and e can strongly differ even within the same

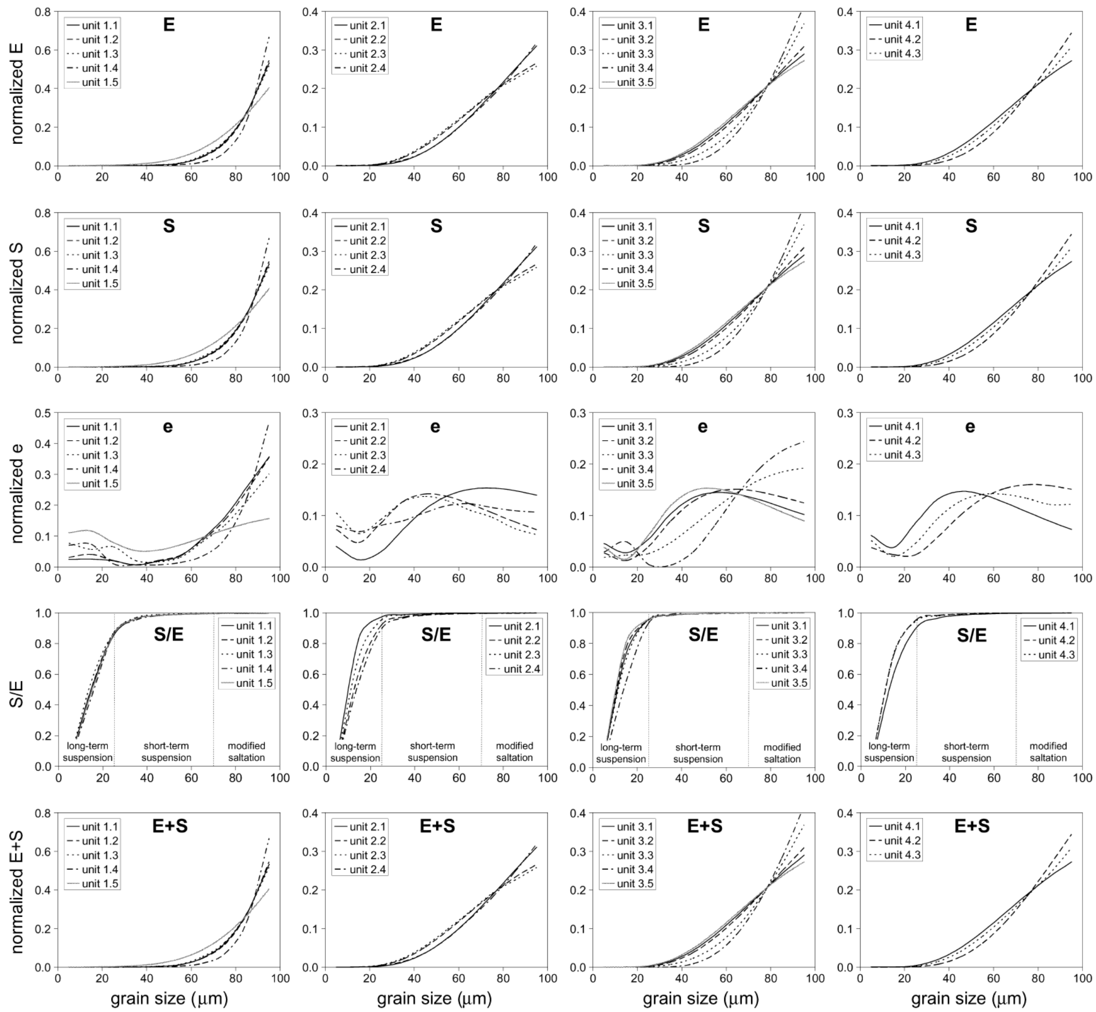

Figure 5. Gross erosion rate (*E*), gross deposition rate (*S*), net erosion rate (*e*), ratio of gross deposition to gross erosion (*S/E*), and total sediment exchange (*E* + *S*), as a function of grain size. All curves are for (normalized) particle mass.

surface group, it is necessary to normalize the data; otherwise the curves for the most active units would obscure those of the slightly active units. All data were normalized by setting the total mass of the entire sediment (0–100 μm) equal to unity. This does not affect the shape of the curves.

Gross emission (*E*) increases exponentially with the grain size, for all surface units (Figure 5). This is expected as all data are expressed in terms of mass, which is proportional to the third power of particle size. Also for the same reason, gross deposition (*S*) increases exponentially with the grain size (Figure 5). However, as shown by the diagrams for net emission (*e*), *E* and *S* are not identical. Annual average accumulation is negative for all units in the Nellis Dunes area. Therefore, all surfaces are experiencing net erosion and over time the area is emissive for all grain size fractions investigated. The diagrams also show a difference between the units composed of sand and those composed of silt or gravel. Apart from a local increase in the smallest particle fractions, the sand curves show a more or less monotonic increase from about 30–40 μm up to 100 μm (the upper size investigated in this study) whereas the silt/gravel curves all show a maximum somewhere in the range 50–70 μm. The effect of sand becomes clear in the curves of intermediate units 3.3 and 3.4, which contain substantially more sand than the other silty and rocky units.

The diagrams for evacuation rate (*S/E*) show that, from a grain size of approximately 40 μm, nearly all emitted dust settles down shortly after emission (Figure 5). The value of *S/E* was less than 0·01 (or 1 %) for the fractions 40–50 μm and coarser. A clear drop of the curves was only observed from the fraction 20–30 μm and finer.

The dashed vertical lines in the *S/E* diagrams show the boundaries between the aeolian transport modes as defined by Pye and Tsoar's (1990, p. 101) criteria. According to these criteria particles are transported in long-term suspension when $v_\infty/u_* < 0{\cdot}1$ (v_∞ = settling velocity of the grain and u_* = friction velocity), in short-term suspension when $0{\cdot}1 < v_\infty/u_* < 0{\cdot}7$, in modified saltation when $0{\cdot}7 < v_\infty/u_* < 1{\cdot}25$, and in saltation or creep when $v_\infty/u_* > 1{\cdot}25$. For the Nellis Dunes experiment u_* was 0·57 m s^{-1} (annual average for those periods that were effectively erosive; i.e. not total annual average). This number

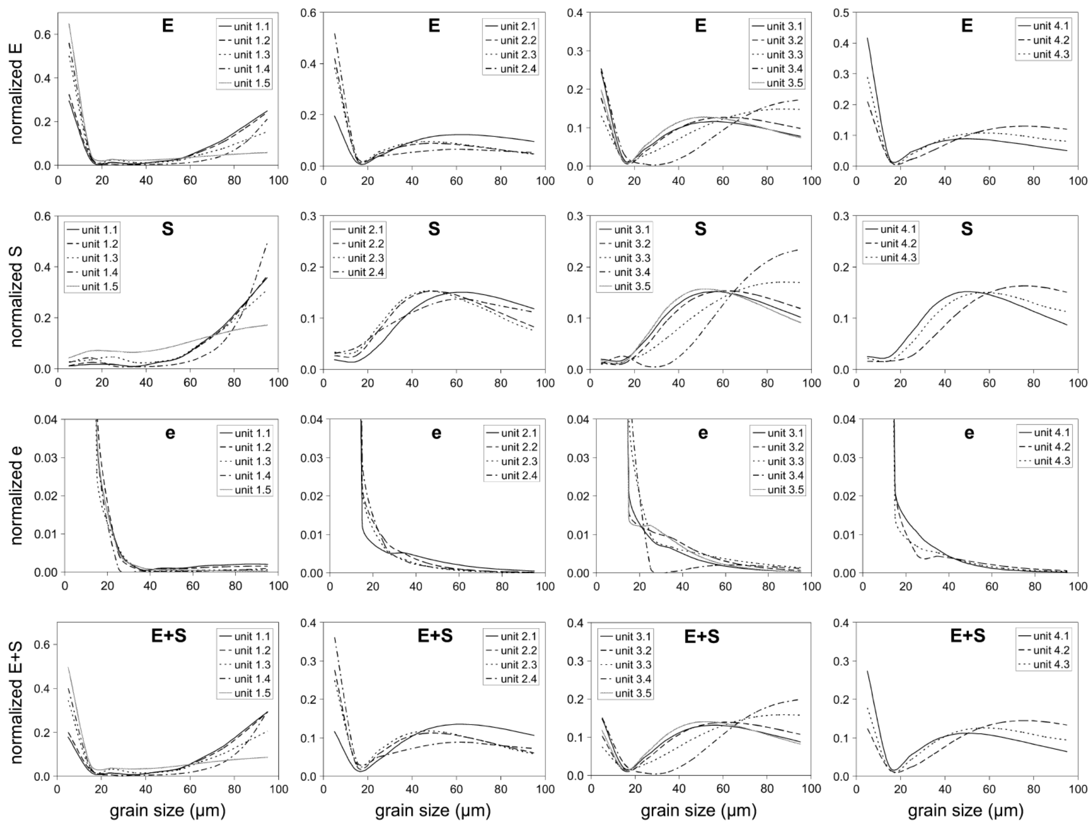

Figure 6. Gross erosion rate (*E*), gross deposition rate (*S*), net erosion rate (e), and total sediment exchange (*E* + *S*), as a function of grain size. All curves are for (normalized) number of particles.

refers to the average for all surface units. For quartz grains in air and $u_* = 0{\cdot}57$ m s^{-1} Pye and Tsoar's criteria demarcate the transition from long-term to short-term suspension at a grain size of 25 µm and that from short-term suspension to modified saltation at 70 µm. Figure 5 shows that 25 µm is where *S/E* curves start decreasing, which confirms Pye and Tsoar's approach. For evident reasons the 70 µm criterion is much more difficult to evaluate from these curves, but the average (for all units) *S/E* at 70 µm was 0·997 (minimum value: 0·995, for unit 1.1), which also confirms Pye and Tsoar's approach. For all 17 surface units as a whole, at least 91·5% of the Nellis Dunes dust transported in short-term suspension settles shortly after emission whereas the percentage is (very) much smaller for the dust transported in long-term suspension (how much smaller can be read from the diagrams in Figure 5, for each grain size).

Finally, the total particle exchange (*E* + *S*) diagrams in Figure 5 show similar trends to *E* and *S*: the coarser the grains, the more mass is exchanged on the surface.

Although the curves in Figure 5 are interesting, they should be interpreted with care because particle mass is heavily dominated by particle size (recall that the former is proportional to the third power of the latter), which may mask potentially existing trends. We therefore recalculated the data in terms of number of particles, an option that does not suffer from said inconvenience. First, the total number of particles eroding (*E*) or settling (*S*) is calculated for a unit area of surface (for example, 1 cm^2, or 1 m^2) by dividing the eroded (or deposited) mass flux through the mass of an individual particle (we used a particle density of 2·65 and approached the particles as spheres). Next, the data are normalized by setting the total number of particles within the range 0–100 µm equal to unity. As with Figure 5, this does not change the shape of the curves and allows comparison of several curves within the same diagram. Also, the effect of choice of unit area of surface for calculating particle number (1 cm^2, 1 m^2, etc.) is eliminated by the normalization.

Trends masked by the dependency of particle mass on particle size now become apparent in Figure 6. The curves for gross emission (*E*) show a very substantial difference between the sand substrata of units 1.x, the sand/silt mixture of unit 3.4 (transitional unit) and the silt and gravel substrata of units 2.x, 3.x and 4.x. For sand units, nearly no particles are emitted within the range 15–60 µm; the minimum is located from 15 to 20 µm. This is understandable because these units contain hardly any particles of these sizes. Therefore, to interpret these data more correctly, a correction for occurrence of particle size in the top layer is necessary. The silt (2.x; 3.x) and gravel (4.x) units also emit very few particles in the range of 15–20 µm, however, this cannot be explained by a limited occurrence of particles of this size in the top layer. On the contrary, all these units, and especially those of unit groups 2.x and 3.x, are very abundant in particles of this size. This paradox will be investigated later in this section.

The curves for gross deposition (*S*) are almost identical to those for gross erosion (E) except for the finest particles, which

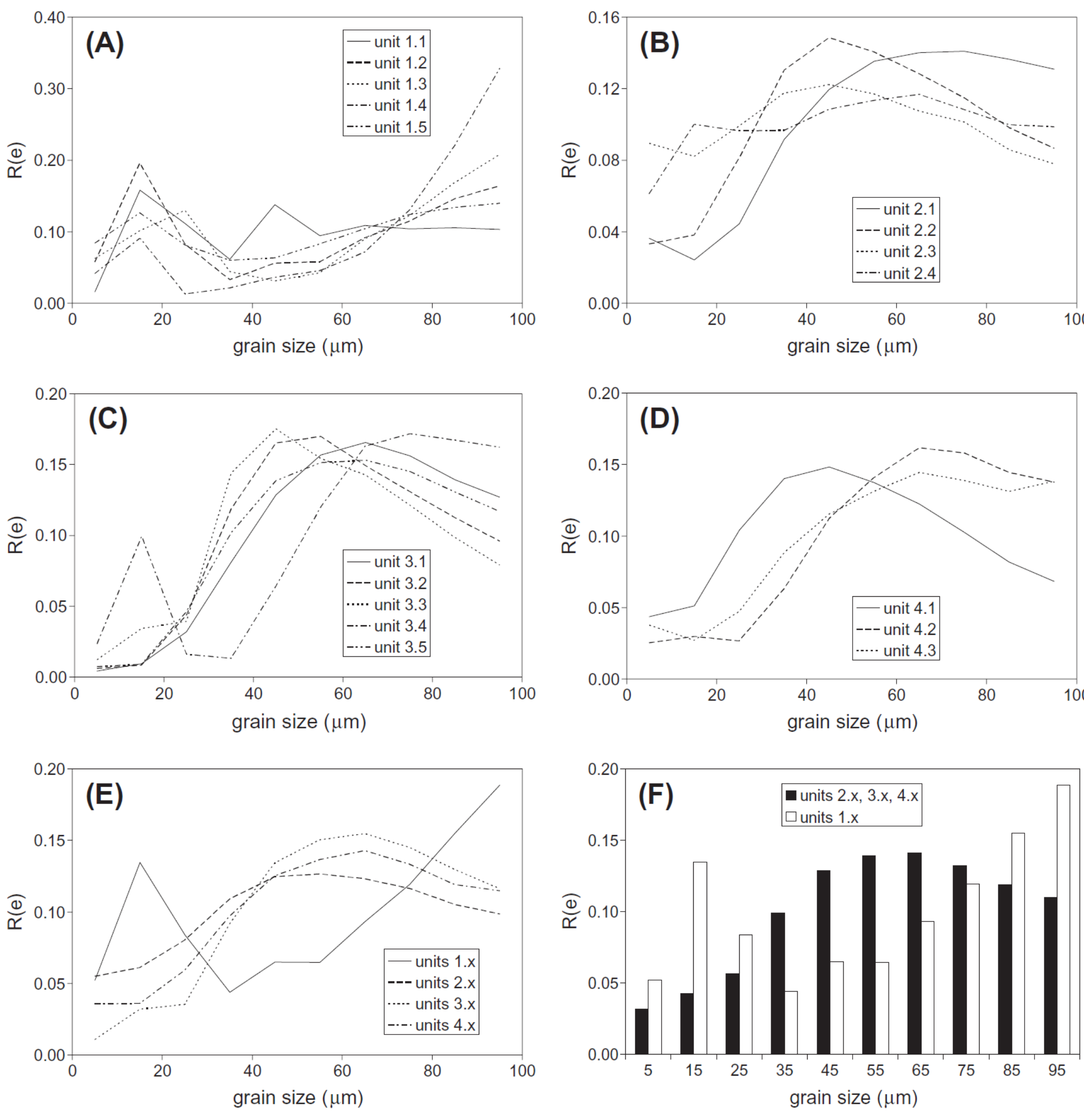

Figure 7. Ratio *R(e)* of normalized number of grains net eroded (*e*) to normalized number of grains available in the top layer.

do not settle soon after their emission. There is thus a very significant net loss of such particles, as can be clearly seen in the diagrams for net erosion (*e*). These diagrams also point to a significant difference between sand units (1.x) and the silt/gravel/drainage units (2.x, 3.x, 4.x): on sand, net emission of dust is limited to particles <40 μm; on other types of surfaces much coarser dust is prone to emission, up to at least 80 μm for units rich in rock fragments (3.x group). Note unit 3.4 (mixture of sand and silt) behaves very similarly to the sandy units. Again, to interpret these data more correctly, a correction for the occurrence of particle size in the top layer is necessary.

The diagrams for total particle exchange (*E* + *S*) show patterns similar to those of gross erosion (*E*). Minimum exchange is for particle sizes between 15 and 20 μm for all units; maximum exchange depends on the type of unit (90–100 μm for sand units, and between approximately 50 and 60 μm for most other units). Again, interpretation in relation to the grain size distribution of the top layer is necessary.

The net emission data, corrected for the grain size distribution of the top layer is shown in Figure 7. The procedure is as follows: first, the grain size distribution of the top layer is determined, for each surface unit. We sampled the uppermost cm of the top soil. Analysis was done using laser diffraction, as described in the methods. Next, since this study only investigates particles transportable in suspension and modified saltation (we used the size range 0–100 μm), the proportion of each grain size class (0–10 μm, 10–20 μm, etc.) in the size range 0–100 μm is calculated. Then the total number of grains present in each class per unit mass (we used 1 g) is calculated using the same procedure applied for Figure 6. The data are then normalized, whereby the total number of grains for the size range 0–100 μm is set equal to unity. The normalized number of net emitted grains, i.e. the data of Figure 6, is then divided by the normalized number of grains in the top layer. This ratio shows how large (or small) the proportion of each grain size class is in the emitted sediment compared to the original top layer (Figure 7). The larger the ratio, the higher the susceptibility of a grain size class to net emission. Because the numbers may differ substantially between surface units and we want to display the curves of homologous units in a single diagram, results are normalized a final time, setting the total for all grain size classes (i.e., the fraction 0–100 μm) equal to unity.

There is a clear and very systematic difference in the grain size of emitted sediment compared with the original top layer of soil between sand units (1.x) and non-sand units (2.x, 3.x and 4.x) (Figure 7). For non-sand units the curves show a maximum around 50–70 μm (varying slightly between units) and a rapid drop as the particles become finer. Sand units do not show a maximum around 50–70 μm: all curves drop continuously to a diameter of about 35 μm, show a local maximum at 15 μm, and then drop again for smaller sizes. The contrast can be even more clearly seen when all units in each type are averaged (Figure 7E).

The data for the two categories of surfaces (sand versus non-sand) are shown separately as histograms in Figure 7F. For non-sand units, susceptibility to net erosion by wind is at a maximum for grains between 60 and 70 μm and decreases as particles become finer or coarser. This behavior was already recognized by Bagnold as long as 70 years ago (Bagnold, 1941) and has since then been confirmed by a very large number of studies. It can be observed in the curves of fluid deflation threshold and impact deflation threshold (Pye and Tsoar, 1990). The increasing resistance to net erosion for fine particles has been explained as a result of increasing cohesion and decreasing aerodynamic forces, whereas for coarse particles gravity (weight of particles) is considered responsible for the increasing resistance (Shao, 2008). It is interesting to note that similar phenomena are observed for net emissions caused by human activity (not wind erosion). In reporting experiments on dust emissions created by off-road vehicular driving, for example, Goossens and Buck (2009b, p. 134) published a net emission diagram that is a nearly exact copy of the non-sand diagram in Figure 7F.

Natural, undisturbed surfaces composed of sand do not follow this trend (Figure 7F). All five surface units of group 1.x, as well as the transitional sand/silt substratum of unit 3.4, behave identically and show a continuous decrease, in susceptibility to net erosion, with decreasing particle size down to approximately 30 μm. A diameter of maximum susceptibility to wind erosion around 70 μm no longer exists; instead, a narrow optimum occurs around 15 μm. This alternative optimum appears in all sand curves (for unit 1.3, which is the human-disturbed sand, it is located near 25 μm).

As far as the authors are aware, such deviant behavior has not been reported before in the aeolian literature. The systematic occurrence in the curves in Figure 7 shows that it is not a result of experimental or calculation error. As a preliminary attempt to explain the phenomenon we hypothesize that this behavior might be a result of the impact of saltating grains. Fine dusty grains released by the impacts show a higher net emission than coarse dust grains because they weigh less, thus settling to the surface again less easily. We recognize that this mechanism does not explain why the highest susceptibility is not observed for the finest grains (PM10 fraction), unless we accept that those very fine particles are sticking very strongly to the other surface grains and will not release easily upon impact. The latter explanation sounds plausible, but more research is required to provide a final answer.

A 40-year-old study by Punjrath and Heldman (1972) reports entrainment experiments with substrata composed of glass beads in a wind tunnel. These authors claim that re-entrainment starts at the minimum Reynolds number, which in their experiments occurred at a particle size between 15 and 22·5 μm (note that the particle range in their experiments was smaller than in the present study: 0–40 μm). It is the only study we found suggesting an alternative particle diameter of maximum susceptibility to net wind erosion around 15 μm.

The ratio of the normalized number of grains gross eroded (E) to the normalized number of grains available in the top layer is shown in Figure 8. As with Figure 7, the sand units (1.x) behave differently compared to the other units (2.x, 3.x and 4.x). For all units the susceptibility to gross erosion increases with particle size up to at least 100 μm, but the rate of increase is different for the sand units compared to the other units. This difference becomes very apparent when the average curves are calculated (Figure 8E). Figure 8E also shows that there is no substantial difference in behavior between the non-sand units.

The most important conclusion that can be drawn from Figure 8 is that, contrary to net erosion, no grain diameter of maximum susceptibility to wind erosion ('optimum deflation diameter') exists for gross wind erosion within the particle range 0–100 μm covering the transport modes of suspension and modified saltation. The classic deflation curves in handbooks on wind erosion are applicable to net erosion only; they do not apply to gross erosion (which, in fact, describes the real number of particles, or sediment mass, leaving the surface). Susceptibility to gross wind erosion increases with particle size up to at least 100 μm, and the rate of increase is larger for surfaces containing sand compared with silty, silty/rocky or drainage surfaces.

Gravity is usually held responsible for the increase in resistance to net wind erosion for particles coarser than approximately 70 μm (Goudie and Middleton, 2006). However, the results of this study indicate that the effect of gravity is complex. Due to their larger mass, coarse particles weigh more than fine particles and gross deposition (S) thus increases with the particle size (at least, for particles >0·3 μm, which in the velocity of deposition diagram, are located right of the minimum; see Sehmel (1980) for examples). Because the increase of particle mass with particle size follows a third-power relationship, the pattern of gross erosion ($e + S$) will become dominated by S as the particles become coarser. This may explain why the susceptibility of gross wind erosion shows a continuous increase with particle size.

All results in this study are based on field measurements. Although results seem to be consistent and are backed by an extended set of 17 different types of sediments and surfaces, to fully verify these results wind tunnel experiments are needed. Two previous wind tunnel experiments do provide some support for our observations (Goossens, 2001, 2008). Goossens (2001) observed a positive accumulation (i.e. negative net erosion) within the friction velocity interval delineated by the deflation threshold and the accumulation threshold. This behavior can only be explained by gross deposition taking place above the deflation threshold. Also, the specific shape of the accumulation curve (see Figures 1 and 4 in Goossens, 2001), which was confirmed by wind tunnel experiments for a wind speed range between 0 and 13 m s^{-1}, shows that net erosion differs from gross erosion and can only be explained by the concept elaborated in the current paper. Similarly, Goossens (2008) found the ratio of the vertical sedimentation flux to the horizontal transport flux remained positive for friction velocities well above 0·33 m s^{-1} (see Figures 4–6 in Goossens, 2008), which also can only be explained by deposition taking place above the deflation threshold. However, more

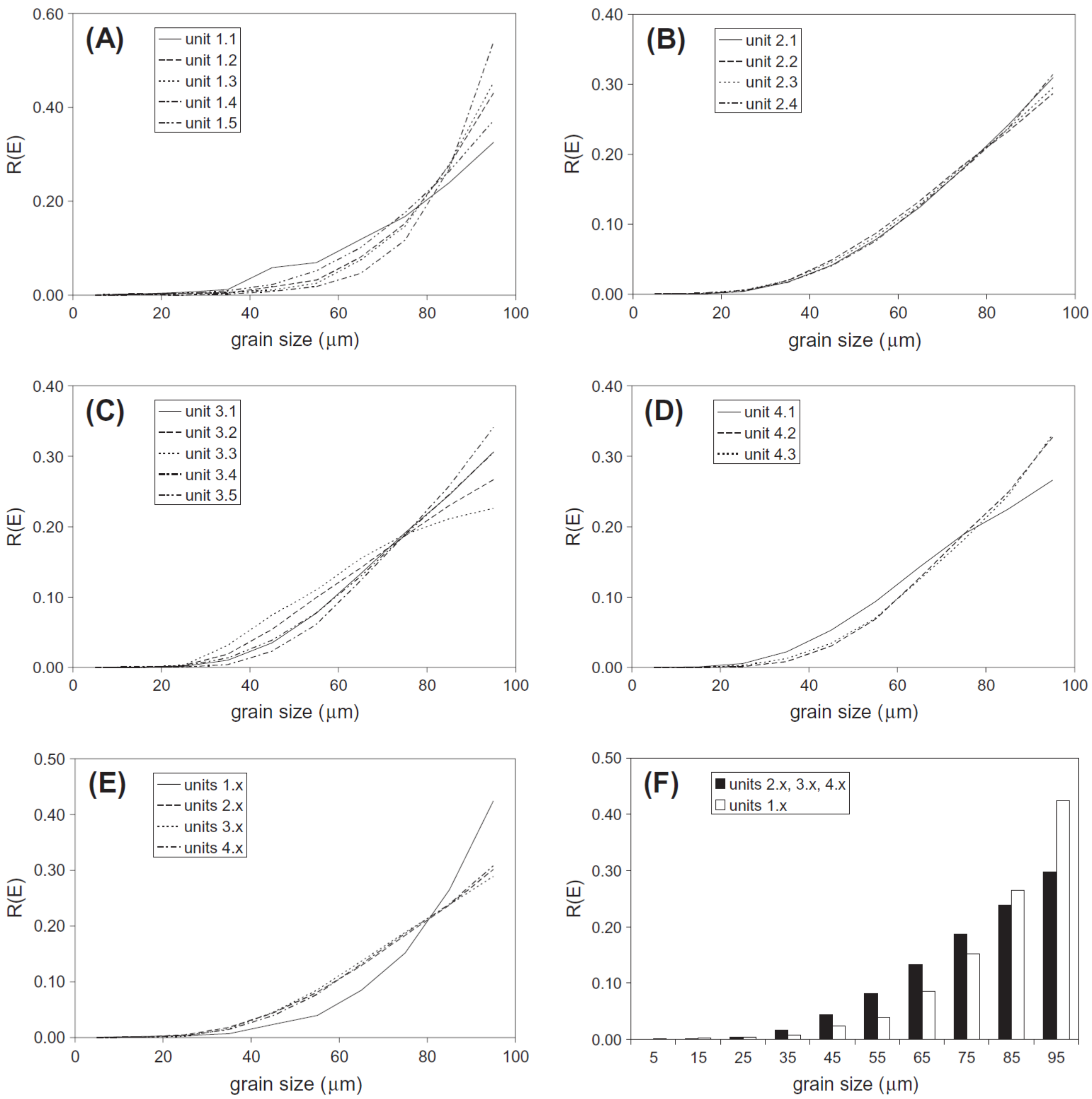

Figure 8. Ratio *R(E)* of normalized number of grains gross eroded (*E*) to normalized number of grains available in the top layer.

wind tunnel experiments are necessary to further test the concept elaborated in this paper. These experiments should also consider replications carried out under controlled aerodynamic and sediment conditions to better estimate the scale of error inevitably involved in field measurements. Therefore, the results of the current study should be seen as an invitation to the aeolian community, to further investigate the concept of gross erosion and net erosion and explore its consequences for aeolian research.

Conclusions

The Nellis Dunes experiment shows that it is necessary to distinguish between net erosion and gross erosion. Such distinction is insufficiently made in the literature, most probably because field and laboratory experiments always measure net erosion. Although, for most geomorphic applications, net erosion is of most concern the difference from gross erosion is fundamental and should receive better acknowledgement.

Both in terms of particle mass and particle number gross erosion heavily dominates over net erosion. On average for all 17 surface units examined in the Nellis Dunes study, gross erosion was 235 times larger than net erosion. However, the number strongly depends on the size of the grains: the coarser the particles, the more gross erosion dominates (Figure 9).

Gross deposition was of the same order of magnitude as gross erosion. In the Nellis Dunes experiment gross erosion was always larger than gross deposition. Thus, all surface units were net erosive.

Once eroded by wind, nearly all grains >40 μm settle down quickly. In the Nellis Dunes experiment the number was 0·99, or 99%. Accepting 25 μm as the boundary between long-term and short-term suspension, at least 91·5% of the sediment

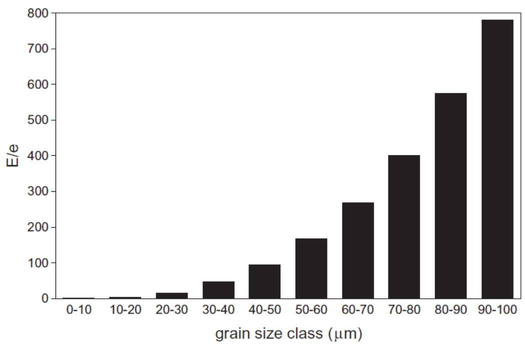

Figure 9. Ratio of gross erosion (*E*) to net erosion (*e*) as a function of grain size. Data represents the annual average for all 17 surface units investigated in this study and applies to particle mass as well as to particle number.

mass transported in short-term suspension (and modified saltation) settled shortly after emission.

In terms of mass, very little sediment <30 µm was gross emitted or deposited. For substrata containing significant sand, little net emission was observed for particles between 20 and 60 µm. In contrast, silt, silt/rock and drainage substrata showed net emissions for all particle sizes between 0 and 100 µm.

A grain diameter of maximum susceptibility to wind erosion around approximately 70 µm, as proposed by the aeolian literature, only exists for net erosion. There is no such diameter for gross erosion within the range 0–100 µm delineating airborne dust. Therefore, the classic deflation curves on wind erosion are only applicable to net erosion, not to gross erosion. Also, for sandy substrata a value of 15 µm instead of 70 µm was observed (for net erosion). For the human-disturbed sand, it was located near 25 µm. This may reflect impacts of saltating grains but further research is needed. Therefore, the type of surface affects the susceptibility of particles to wind erosion.

The results of this study are exclusively based on field measurements. Although some wind tunnel experiments preliminarily support the conclusions in this study, new wind tunnel experiments with various types of sediment, carried out under a range of aerodynamic conditions, are required to further document the interaction between gross erosion and gross deposition.

Implications

Although the results of this study may have only limited direct impacts on air quality research or aeolian landform development, they have important implications on theoretical and conceptual issues and on aeolian modeling. They show that the physical concept of erosion should be elaborated in a context wide enough to allow interactions of all mechanisms involved in it. In aeolian research, but also in other geomorphic disciplines, erosion usually has been interpreted (and studied) within the context of net erosion – which, in fact, is nothing else than negative accumulation. This study shows that net erosion, though of incredible importance in geomorphology, is only part of the story. Activity on a surface (exchange of particles) is much higher than net erosion suggests. The role of deposition, especially the usually unperceived continuous deposition during wind erosion events themselves or during aeolian transport, is largely underestimated or even neglected, particularly when particles are small (aeolian dust). Theoretical models of dust emission and dust transport should consider these continuous and simultaneous interactions between the airborne particles and the surface, otherwise they remain incomplete. Future verification of these results using extended wind tunnel experiments is necessary prior to initiating such extended theoretical models.

Acknowledgements—The Federal Bureau of Land Management (BLM) funded this project through a SNPLMA Conservation Initiative, and granted permission for executing the measurements in the Nellis Dunes area. D. Pepper and U. Rangegowda (College of Engineering, University of Nevada Las Vegas, Las Vegas, NV, USA) and X. Wang (Purdue University Calumet, Hammond, IN, USA) organized the collection of wind data from the wind towers and performed the initial processing of the wind records. V. Etyemezian and G. Nikolich (Desert Research Institute, Las Vegas, NV, USA) provided the portable wind tower and processed the raw data. Wind data from the Nellis Air Force Base meteorological station were provided by M. EmelyPoynter (Nellis Air Force Base, Las Vegas, NV, USA). B. McLaurin (Department of Geography and Geosciences, Bloomsburg University of Pennsylvania, Bloomsburg, PA, USA) collaborated on the mapping of the surface units used in this study. L. Christianson (Bureau of Land Management, Las Vegas, NV, USA) provided administrative assistance throughout the project. We also thank the following persons who assisted in the field experiments: L. Bangen, J. Carter, R. Davis, C. Griffing, J. Morton, R. Fairchild, and M. Stropky. Special thanks are expressed to two anonymous reviewers, who made many constructive comments and provided very useful suggestions to improve this paper.

References

Bagnold RA. 1941. *The Physics of Blown Sand and Desert Dunes*. Methuen: London.

Beard LS, Anderson RE, Block DL, Bohannon RG, Brady RJ, Castor SB, Duebendorfer EM, Faulds JE, Felger TJ, Howard KA, Kuntz MA, Williams VS. 2007. *Preliminary geologic map of the Lake Mead 30′ × 60′ quadrangle, Clark County, Nevada, and Mohave County, Arizona*. U.S. Geological Survey Open-File Report 2007-1010, scale 1:100,000, 3 sheets + text.

Breuning-Madsen H, Awadzi TW. 2005. Harmattan dust deposition and particle size in Ghana. *Catena* **63**: 23–38.

Buschiazzo DE, Zobeck TM. 2005. Airborne horizontal mass flux calculated with different equations. *Proceedings of 2005 ASAE Annual Meeting*, Tampa, Florida, USA, Paper No. 052049.

Cornelis WM, Gabriëls D. 2004. A simple model for the prediction of the deflation threshold shear velocity of dry loose particles. *Sedimentology* **51**: 39–51.

Dietrich WE. 1982. Settling velocity of natural particles. *Water Resources Research* **18**: 1615–1626.

Etyemezian V, Nikolich G, Ahonen S, Pitchford M, Sweeney M, Purcell R, Gillies J, Kuhns H. 2007. The Portable In Situ Wind Erosion Laboratory (PI-SWERL): a new method to measure PM10 windblown dust properties and potential for emissions. *Atmospheric Environment* **41**: 3789–3796.

Evans MG. 2004. Sedimentation. In *Encyclopedia of Geomorphology*, Goudie AS (ed). Routledge: London; 938–941.

Fryrear DW. 1986. A field dust sampler. *Journal of Soil and Water Conservation* **41**: 117–120.

Gigliotti CL, Totten LA, Offenberg JH, Dachs J, Nelson ED, Reinfelder J, Eisenreich SJ. 2005. Atmospheric concentrations and deposition of polycyclic aromatic hydrocarbons to the mid Atlantic east coast region. *Environmental Science and Technology* **39**: 5550–5559.

Gillette DA. 1977. Fine particulate emissions due to wind erosion. *Transactions of the ASAE* **20**: 890–897.

Goossens D. 2001. The aeolian dust accumulation curve. *Earth Surface Processes and Landforms* **26**: 1213–1219.

Goossens D. 2005. Quantification of the dry aeolian deposition of dust on horizontal surfaces: an experimental comparison of theory and measurements. *Sedimentology* **52**: 859–873.

Goossens D. 2007. Bias in grain size distribution of deposited atmospheric dust due to the collection of particles in sediment catchers. *Catena* **70**: 16–24.

Goossens D. 2008. Relationships between horizontal transport flux and vertical deposition flux during dry deposition of atmospheric dust particles. *Journal of Geophysical Research* **113**: F02S13. doi: 10.1029/2007JF000775.

Goossens D, Buck B. 2009a. Dust dynamics in off-road vehicle trails: measurements on 16 arid soil types, Nevada, USA. *Journal of Environmental Management* **90**: 3458–3469.

Goossens D, Buck B. 2009b. Dust emission by off-road driving: experiments on 17 arid soil types, Nevada, USA. *Geomorphology* **107**: 118–138.

Goossens D, Offer ZY. 2000. Wind tunnel and field calibration of six aeolian dust samplers. *Atmospheric Environment* **34**: 1043–1057.

Goossens D, Rajot JL. 2008. Techniques to measure the dry aeolian deposition of dust in arid and semi-arid landscapes: a comparative study in West Niger. *Earth Surface Processes and Landforms* **33**: 178–195.

Goossens D, Gross J, Spaan W. 2001. Aeolian dust dynamics in agricultural land areas in Lower Saxony, Germany. *Earth Surface Processes and Landforms* **26**: 701–720.

Goossens D, Offer ZY, London G. 2000. Wind tunnel and field calibration of five aeolian sand traps. *Geomorphology* **35**: 233–252.

Goudie AS, Middleton NJ. 2006. *Desert Dust in the Global System*. Springer: Berlin.

Hoffmann C, Funk R, Li Y, Sommer M. 2008. Effect of grazing on wind driven carbon and nitrogen ratios in the grasslands of Inner Mongolia. *Catena* **75**: 182–190.

Horikawa K, Shen HW. 1960. Sand Movement by Wind Action. US Army, Corps of Engineers, Beach Erosion Board, Tech. Memo 119.

Iversen JD, White BR. 1982. Saltation threshold on Earth, Mars and Venus. *Sedimentology* **29**: 111–119.

McLaurin B, Goossens D, Buck BJ. in press. Combining surface mapping and process data to assess, predict, and manage dust emissions from natural and disturbed land surfaces. Geosphere.

Nickling WG. 1978. Eolian sediment transport during dust storms: Slims River Valley, Yukon Territory. *Canadian Journal of Earth Sciences* **15**: 1069–1084.

Pleim JE, Venkatram A, Yamartino R. 1984. *ADOM/TADAP Model Development Program, vol. 4: The Dry Deposition Module*. Ontario Ministry of Environment: Rexdale.

Punjrath JS, Heldman DR. 1972. Influence of air turbulence on re-entrainment of small particles from flat surfaces. *Transactions of the ASAE* **15**: 559–562.

Pye K, Tsoar H. 1990. *Aeolian Sand and Sand Dunes*. Unwin Hyman: London.

Sehmel GA. 1980. Particle and gas dry deposition: a review. *Atmospheric Environment* **14**: 983–1011.

Sehmel GA, Hodgson WH. 1978. A Model for Predicting Dry Deposition of Particles and Gases to Environmental Surfaces, DOE Report PNL-SA-6721, Pacific Northwest Laboratories, Richland, WA.

Shao Y. 2008. *Physics and Modelling of Wind Erosion*, 2nd edn. Springer Science + Business Media BV: Dordrecht.

Shao Y, McTainsh GH, Leys JF, Raupach MR. 1993. Efficiencies of sediment samplers for wind erosion measurement. *Australian Journal of Soil Research* **31**: 519–532.

Sharratt B, Feng G, Wendling L. 2007. Loss of soil and PM10 from agricultural fields associated with high winds on the Columbia Plateau. *Earth Surface Processes and Landforms* **32**: 621–630.

Slinn WGN. 1983. Air-to-sea transfer of particles. In *Air–Sea Exchange of Gases and Particles*, NATO ASI Series, Liss PS, Slinn WGN (eds). Reidel: Dordrecht; 299–405.

Slinn SA, Slinn WGN. 1980. Predictions for particle deposition on natural waters. *Atmospheric Environment* **14**: 1013–1016.

Sow M, Goossens D, Rajot JL. 2006. Calibration of the MDCO dust collector and of four versions of the inverted frisbee dust deposition sampler. *Geomorphology* **82**: 360–375.

Thornbury WD. 1954. *Principles of Geomorphology*. Wiley: New York.

Turner DB. 1994. *Workbook of Atmospheric Dispersion Estimates: An Introduction to Dispersion Modeling*. Lewis Publishers: Boca Raton, FL.

Venkatram A, Pleim J. 1999. The electrical analogy does not apply to modeling dry deposition of particles. *Atmospheric Environment* **33**: 3075–3076.

Websters Online Dictionary 2009. http://www.websters-online-dictionary.org, accessed 26 January 2010.

